Complexity

Financial Networks 2019

Lead Guest Editor: Benjamin M. Tabak
Guest Editors: Thiago C. Silva and Ahmet Sensoy

Financial Networks 2019

Complexity

Financial Networks 2019

Lead Guest Editor: Benjamin M. Tabak
Guest Editors: Thiago C. Silva and Ahmet Sensoy

Contents

Systemic Risk in the Interbank Market with Overlapping Portfolios
Shanshan Jiang and Hong Fan
Research Article (12 pages), Article ID 5317819, Volume 2019 (2019)

Price Linkage Rumors in the Stock Market and Investor Risk Contagion on Bilayer-Coupled Networks
Yue Dong, Jiepeng Wang, and Tingqiang Chen
Research Article (21 pages), Article ID 4727868, Volume 2019 (2019)

EC-Structure: Establishing Consumption Structure through Mining E-Commerce Data to Discover Consumption Upgrade
Lin Guo and Dongliang Zhang
Research Article (8 pages), Article ID 6543590, Volume 2019 (2019)

Hindawi
Complexity
Volume 2019, Article ID 8257404, 2 pages
https://doi.org/10.1155/2019/8257404

Editorial

Financial Networks 2019

Benjamin Miranda Tabak,[1] **Thiago Christiano Silva**,[2,3] **and Ahmet Sensoy**[4]

[1]*Fundação Getúlio Vargas, Escola de Políticas Públicas e Governo (FGV/EPPG), Brasilia, Brazil*
[2]*Universidade Católica de Brasília, Brasília, DF, Brazil*
[3]*Universidade de São Paulo, Ribeirão Preto, SP, Brazil*
[4]*Bilkent University, Ankara, Turkey*

Correspondence should be addressed to Benjamin Miranda Tabak; benjaminm.tabak@gmail.com

Received 18 October 2019; Accepted 19 October 2019; Published 5 December 2019

This special issue on financial networks seeks to bring novel methods and discussions to improve our understanding of financial markets. The bulk of the literature studies, interbank markets, or stock markets networks. This literature has provided important insights for the development of portfolio and risk management and financial regulation.

Since the global financial crisis of 2008, many important aspects of how networks can amplify shocks have come to the debate in the academia and also for policymaking. For instance, the integration of other contagion transmission channels besides the traditional interbank and stock markets is an important step to take if one wants to really understand how interconnectedness drives loss amplification across different financial systems. Therefore, there are many areas that are at their early stages in terms of modeling and further research is necessary. In this special issue, we seek to fill some gaps in the literature and provide a relevant contribution to the discussion of these issues.

Some papers in our special issue estimate systemic risk (Systemic Risk in the Interbank Market with Overlapping Portfolios) and model contagion using an agent-based modeling approach combined with complex networks (Nonlinear Dynamics Characteristic of Risk Contagion in Financial Market Based on Agent Modeling and Complex Network) and risk investor contagion (Price Linkage Rumors in the Stock Market and Investor Risk Contagion on Bilayer-Coupled Networks).

We have papers that deal with stock price prediction using knowledge graphs (Anticipating Stock Markets of the Renowned Companies: A Knowledge Graph Approach), and also a paper that combines network decomposition with spatial econometrics (Analyzing Stockbrokers' Trading Patterns: A Network Decomposition and Spatial Econometrics Approach).

Some papers deal with stock market networks from a new methodological perspective (Thermodynamic Entropy in Quantum Statistics for Stock Market Networks) with mutual funds (Modeling Overlapped Mutual Funds' Portfolios: A Bipartite Network Approach) and with credit default swaps (Weight of the Default Component of CDS Spreads: Avoiding Procyclicality in Credit Loss Provisioning Framework).

Other papers deal with the effect of investor behavior on returns (Understanding How Short-Termism and a Dynamic Investor Network Affects Investor Returns: An Agent-Based Perspective), pairs-trading strategies (Optimizing the Pairs-Trading Strategy Using Deep Reinforcement Learning with Trading and Stop-Loss Boundaries), control strategies (P D^9 Control Strategy for a Fractional-Order Chaotic Financial Model), and EC-structure (EC-Structure: Establishing Consumption Structure through Mining E-Commerce Data to Discover Consumption Upgrade).

The set of papers in this issue contributes to enhancing our understanding of financial and complex networks and also to the application of new methods. We highlight the importance of the use of multilayer and multiplex networks to improve the modeling of real-world networks that may have distinct dimensions. We also highlight the relevance of agent-based modeling in providing new insights on

economic and financial behaviors of both investors' and consumers' financial products or services.

Several areas need further research. Financial networks comprised of commodities are still understudied and could provide important insights (see [1]). Their relationship with stock markets and other financial markets is also an important issue. The integration of new contagion transmission channels [2, 3] is also of utmost importance to avoid underestimating the ability of financial networks in amplifying losses. How to model efficiency and performance using information on network formation [4–6] is also an important task, as well as that of using dynamic efficiency tools to model the evolution of financial markets [7].

Conflicts of Interest

The editors declare that they have no conflicts of interest.

Benjamin Miranda Tabak
Thiago Christiano Silva
Ahmet Sensoy

References

[1] B. M. Tabak, T. R. Serra, and D. O. Cajueiro, "Topological properties of commodities networks," *The European Physical Journal B*, vol. 74, no. 2, pp. 243–249, 2010.

[2] T. C. Silva, M. A. da Silva, and B. M. Tabak, "Systemic risk in financial systems: a feedback approach," *Journal of Economic Behavior & Organization*, vol. 144, pp. 97–120, 2017.

[3] T. C. Silva, M. D. S. Alexandre, and B. M. Tabak, "Bank lending and systemic risk: a financial-real sector network approach with feedback," *Journal of Financial Stability*, vol. 38, pp. 98–118, 2018.

[4] T. C. Silva, S. M. Guerra, B. M. Tabak, and R. C. C. Miranda, "Financial networks, bank efficiency and risk-taking," *Journal of Financial Stability*, vol. 25, pp. 247–257, 2016.

[5] T. C. Silva, B. M. Tabak, D. O. Cajueiro, and M. V. B. Dias, "A comparison of DEA and SFA using micro- and macro-level perspectives: efficiency of Chinese local banks," *Physica A: Statistical Mechanics and its Applications*, vol. 469, pp. 216–223, 2017.

[6] T. C. Silva, B. M. Tabak, D. O. Cajueiro, and M. V. B. Dias, "Adequacy of deterministic and parametric frontiers to analyze the efficiency of Indian commercial banks," *Physica A: Statistical Mechanics and its Applications*, vol. 506, pp. 1016–1025, 2018.

[7] A. Sensoy and B. M. Tabak, "Dynamic spanning trees in stock market networks: the case of Asia-Pacific," *Physica A: Statistical Mechanics and its Applications*, vol. 414, pp. 387–402, 2014.

Hindawi
Complexity
Volume 2019, Article ID 3582516, 20 pages
https://doi.org/10.1155/2019/3582516

Research Article

Optimizing the Pairs-Trading Strategy Using Deep Reinforcement Learning with Trading and Stop-Loss Boundaries

Taewook Kim [1,2] **and Ha Young Kim** [3]

[1] *Qraft Technologies, Inc., Ttukseom-ro 1-gil, Sungdong-gu, Seoul 04778, Republic of Korea*
[2] *Department of Financial Engineering, Ajou University, Worldcupro 206, Yeongtong-gu, Suwon 16499, Republic of Korea*
[3] *Graduate School of Information, Yonsei University, 50 Yonsei-ro, Seodaemun-gu, Seoul, 03722, Republic of Korea*

Correspondence should be addressed to Ha Young Kim; haimkgetup@gmail.com

Received 6 February 2019; Revised 14 April 2019; Accepted 11 June 2019; Published 12 November 2019

Guest Editor: Benjamin M. Tabak

Many researchers have tried to optimize pairs trading as the numbers of opportunities for arbitrage profit have gradually decreased. Pairs trading is a market-neutral strategy; it profits if the given condition is satisfied within a given trading window, and if not, there is a risk of loss. In this study, we propose an optimized pairs-trading strategy using deep reinforcement learning—particularly with the deep Q-network—utilizing various trading and stop-loss boundaries. More specifically, if spreads hit trading thresholds and reverse to the mean, the agent receives a positive reward. However, if spreads hit stop-loss thresholds or fail to reverse to the mean after hitting the trading thresholds, the agent receives a negative reward. The agent is trained to select the optimum level of discretized trading and stop-loss boundaries given a spread to maximize the expected sum of discounted future profits. Pairs are selected from stocks on the S&P 500 Index using a cointegration test. We compared our proposed method with traditional pairs-trading strategies which use constant trading and stop-loss boundaries. We find that our proposed model is trained well and outperforms traditional pairs-trading strategies.

1. Introduction

Pairs trading is a method for obtaining arbitrage profit when there is a statistical difference between two stocks with similar characteristics that are cointegrated or highly correlated. This is possible because of the statistical reason that spreads made by two stocks have a mean reversion in the long run [1]. In the early days, pairs-trading methods were popular because of the opportunity to obtain arbitrage profit [1–4]. However, as many investors including hedge funds sought these arbitrage opportunities by executing the pairs-trading strategy, its profitability began to deteriorate [5, 6]. To overcome these shortcomings, significant research has been conducted to improve the pairs-trading strategy [7–10].

The mechanism of pairs trading is as follows. First, a pair of stocks with similar trends is identified. Second, regression analysis such as ordinary least squares (OLS), total least squares (TLS), and error correction models (ECM) is used to calculate the spread of these stocks. Finally, if the spread hits preset boundaries, investors will open a portfolio which takes a long position on the undervalued stock and shorts the overvalued stock. Subsequently, if the spread reverses to the mean, investors will close the portfolios which are opposite position to the open portfolio. In this case, the investor obtains an arbitrage profit by executing this strategy. However, there is a risk when the spread does not reverse to the mean. In such a situation, investors are at high risk because they cannot close the portfolio. By setting a stop-loss boundary, investors can hedge the risk [11–13].

Many researchers have applied various statistical methods to improve the efficiency and performance of pairs trading. In particular, they focused on using the spread as a trading signal. The study in [1] collected pairs of stocks based on minimizing the sum of squared deviations between the two stocks and then executed the trading strategy if the difference between the pairs is twice the standard deviation of the spread. They used normalized US stock price data from 1962 to 2002 to test the profitability of pairs trading. The

study in [14] used the cointegration approach to protect the pairs-trading strategy from severe losses. They applied an OLS method to create a spread and set various conditions that translated into trading actions. From these models, they achieved a trading strategy with a minimum level of profits protected from risk of loss. The results showed about an 11% annualized excess return over the entire period. The research in [15] compared the distance and cointegration approaches for each high-frequency and daily dataset to check whether it is profitable for Norwegian seafood companies. The performance is similar between two approaches. Reference [16] used a Kalman filter to calculate spread, which was then used as a high-frequency trading signal, on the shares constituting the KOSPI 100 Index. He found that the pairs-trading strategy's performance was significant on the KOSPI and was better during daily market conditions at market opening and closing. Moreover, [7] optimized a pairs-trading system as a stochastic control problem. They used the Ornstein-Uhlenbeck process to calculate spread as a trading signal and tested their model with simulated data; the results showed that their strategy performs well. In addition, [17] suggested the Ornstein-Uhlenbeck process to make a market microstructure noise used as a trading signal in pairs trading strategy. The performance is better under this method than in traditional estimators such as ARIMA(1,1) and maximum likelihood. Reference [18] applied a cointegration method to Chinese commodity futures from 2006 to 2016 to check whether pairs trading was suitable in that market. They used OLS regression to create spreads from the pairs. Furthermore, [10] applied a cointegration test to assorted pairs of stocks and a vector error-correction model to create a trading signal.

It is important to set a boundary to optimize the pairs-trading strategy. This boundary is a criterion for deciding whether to execute a pairs-trading strategy. If a low boundary is set, many strategies will be executed, but profits will be lower; if a high boundary is set, investors will get high returns when the strategy is executed. However, all this assumes that mean reversion occurs. If the spread does not return to the average in the specified trading window, losses will be incurred. If a low boundary is set, the loss will be small. However, if the strategy is executed with a high boundary, the loss will increase. Therefore, the performance of pair trading depends on how the boundary is set. Reference [14] suggested taking a minimum-profit condition, which could be efficient to reduce losses in a pairs-trading system. They set a trading rule with a diverse open condition: for example, if the spread is above 0.3, 0.5, 0.75, 1.0, and 1.5 standard deviations. They used the daily closing prices from January 2, 2001, to August 30, 2002, of two stocks, the Australia New Zealand Bank and the Adelaide Bank. The results showed that, as the open condition value decreases, the number of trades and profits increases. Also [19] suggested optimal preset boundaries calculated from estimated parameters for the average trade duration, intertrade interval, and number of trades and used them to maximize the minimum total profit. They used the daily closing price data from January 2, 2004, to June 30, 2005, of seven pairs of stocks on the Australian Stock Exchange. The results showed that their proposed method was efficient in making profits using the pairs-trading strategy. Reference [18] examined whether the pairs-trading strategy could be applied to the daily return of Chinese commodity futures from 2006 to 2016 using three methods: classical, closed-loop, and dynamic stop-loss. The closed-loop method takes only a stop-profit barrier which executes the strategy and does not consider the risk if spreads revert to the mean. The classical method adds stop-loss boundaries to the closed-loop method. The dynamic stop-loss method uses a variety of stop-profit and stop-loss barriers to fit the spreads if the spread is larger than the standard deviation, which is set using criteria based on the historical average of spreads. The results showed that these methods obtained an annualized return of over 15%, especially the closed-loop method, which yielded the highest profit of 26.94%. In addition, [20] experimented with fixed optimal threshold selection, conditional volatility, percentile, spectral analysis, and neural network thresholds in pairs-trading strategy. Of these, the neural network threshold has outperformed all other strategies.

Following the success of reinforcement learning, demonstrated by its successful performance at Atari games [21], many researchers have attempted to apply this algorithm to the financial trading system. Reference [22] proposed a deep Q-trading system using reinforcement learning methods. They applied Q-learning to a trading system to trade automatically. They set a delta price using data from the past 120 days, had three discrete action spaces (buy, hold, and sell), and used long-term profit as a reward. They used daily data from January 01, 2001, to December 31, 2015, of the Hang Seng Index and the S&P 500 Index. The experimental results showed that their proposed method outperformed buy-and-hold strategies and recurrent reinforcement learning methods. Reference [23] proposed three steps to apply reinforcement learning to the financial trading system. First, they reduced relative replay size to fit financial trading. Second, they proposed an action-augmentation technique that provides more feedback from the action to the agent. Third, they used long sequences as reinforcement data to conduct recurrent neural network training. The experimental data comprised tick-by-tick data of 12 forex currency pairs from January 2012 to December 2017. The results showed that the action-augmentation technique yielded more profit than an epsilon-greedy policy. Reference [10] used an N-armed bandit problem to optimize the pairs-trading strategy. They took the spread using an error-correction model and found the parameters using a grid-search algorithm. They compared their proposed model with a constant parameter model, which was similar to a traditional pairs-trading strategy. They used intraday one-minute data of some stocks in the FactSet database from June 2015 to January 2016. The performance of their proposed model was better than the constant-parameter model.

We investigate not only the dynamic boundary based on a spread in each trading window—which can achieve higher profit than the fixed boundary used in traditional pairs trading strategy—but also if it is possible to train deep reinforcement learning methods to follow this mechanism. To this end, we propose a new method to optimize the pairs trading strategy using deep reinforcement learning, especially deep Q-networks, since pairs trading strategy can

be thought of as a game. After opening a portfolio position, the profit can be set whether portfolio is closed, stop-loss position. Therefore, if we set this strategy as a game by setting boundaries which are optimized in spreads in trading window, we can achieve more profit than traditional pairs trading strategies. In particular, we set the pairs-trading system to be a kind of game and obtain the optimal boundaries, trading thresholds, and stop-loss thresholds according to the calculated spread. The reason for this construction is that if the portfolio is opened and closed in the trading window in the calculated spread, it will be unconditionally profitable if the portfolio is closed. If the portfolio reaches the stop-loss boundary or does not converge to the mean, losses may occur. We therefore set the DQN to learn by positively rewarding it if it takes a closed position and negatively rewarding it if it reaches the stop-loss or exit thresholds. We conducted the following experiments to verify that our proposed method is optimized compared to the conventional method. First, we used different spreads calculated using OLS and TLS to see how the results differ depending on the spread used for input. Second, depending on the formation window and trading window, the spread and hedge ratio will be varied. We therefore set a total of six window sizes for selecting the optimal window size which had the best performance. Finally, we compared the proposed method with the traditional pairs-trading strategy using the test data with the optimal window size. In this experiment, we use the daily adjusted closing prices from January 2, 1990, to July 31, 2018, of 50 stocks in the S&P 500 Index. Experimental results show that our proposed method outperforms the traditional pairs-trading strategy across all the pairs. In addition, we can confirm that the performance measure varies according to the spread.

The main contributions of this study are as follows. First, we propose a novel method to optimize pairs trading strategy using deep reinforcement learning, especially deep Q-networks with trading and stop-loss boundaries. The experimental results show that our method can be applied in the pairs trading system and also to various other fields, including finance and economics, when there is a need to optimize a rule-based strategy to be more efficient. Second, we propose an optimized dynamic boundary based on a spread in each trading window. Our proposed method outperforms traditional pairs trading strategy which set a fixed boundary. Last, we find that our method outperforms traditional pairs trading strategy in all pairs based on constituent stocks in S&P 500. Since our method selects optimal boundaries based on spreads, it can be applied to other stock markets such as KOSPI, Nikkei, and Hang Seng. It should be noted that the present work is a part of the Master thesis [24].

The rest of this paper is organized as follows. Section 2 explains the technical background. Section 3 describes the materials and methods. Section 4 shows the results and provides a discussion of the experiments. Section 5 provides our conclusions to this study.

2. Technical Background

2.1. The Traditional Pairs-Trading Strategy. Pairs trading is a representative market-neutral trading strategy which simultaneously longs an undervalued stock and shorts an overvalued stock. This strategy is a form of statistical arbitrage trading that assumes the movements of the prices of the two assets will be similar to previous trends [1]. It follows the assumption that asset prices will return to the long-term equilibrium. This strategy started from the idea that arbitrage opportunities exist when the price gap between two assets expands to or past a certain level. It is also based on the belief that historical price movements will not change significantly in the future.

In Figure 1, the graph drawn in blue is a spread made of two stocks that are cointegrated, the red lines are the trading boundaries, and the green lines are the stop-loss boundaries. When this spread reaches the trading boundaries, the portfolio is opened and only closed when the spread returns to the average. However, losses are incurred when prices reach the stop-loss boundaries after the portfolio is opened and do not return to the average. Furthermore, after the portfolio is opened, if the trading signal is not reversed to mean during the trading window, the portfolio is closed by force; this is called the exit position of the portfolio.

2.1.1. The Cointegration Test. There are many approaches for pair selection such as the discrete approach [11, 25–27], the cointegration approach [10, 16, 27], and the stochastic approach [7, 8]. In this study, we use the cointegration approach to choose pairs which have long-term equilibrium. Generally, a linear combination of nonstationary variables is also a nonstationary relationship. Assume that x_t and y_t have unit roots; as previously mentioned, the linear combination of these variables follows nonstationary conditions.

$$x_t \sim I(1), \quad y_t \sim I(1) \tag{1}$$

$$y_t = \alpha + \beta x_t + \varepsilon_t \tag{2}$$

However, it can be a stationary relationship if the nonstationary variables are cointegrated. In this case, this regression must be checked to determine whether it is a spurious regression or cointegrated. Johansen's method is widely used to test for cointegration [28]. In this method, the number of cointegration relations and the parameters of the model are estimated and tested using maximum likelihood estimation (MLE). Since all variables are regarded as endogenous variables, there is no need to select dependent variables and multiple cointegration relationships are identified. In addition, we use MLE to estimate the cointegration relation with the vector autoregression model and to determine the cointegration coefficient based on the likelihood-ratio test. There is therefore an advantage in performing various hypothesis tests related to the estimation of cointegration parameters and the setting of other models when there is cointegration, and not merely to test for cointegration.

2.2. Spread Calculation

2.2.1. Ordinary Least Squares. In regression analysis, OLS is widely used to estimate parameters by minimizing the sum

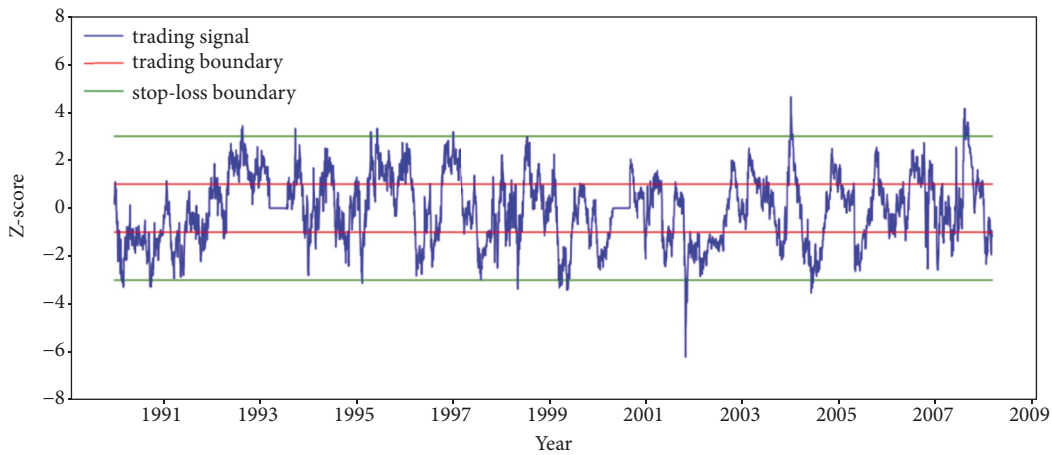

Figure 1: The traditional pairs-trading strategy.

of the squared errors [29]. Assume that x_i, y_i, and ε_i are an independent variable, a dependent variable, and an error term. We can estimate β from the following equation by taking a partial derivative:

$$y_i = \beta x_i + \varepsilon_i \sim N\left(0, \sigma_\varepsilon^2\right) \tag{3}$$

$$\sum_{i=1}^{n} \left(y_i - \beta x_i\right)^2 \tag{4}$$

$$\beta = \left(\sum_{i=1}^{n} x_i{}' x_i\right)^{-1} \sum_{i=1}^{n} x_i{}' y_i \tag{5}$$

The value obtained from equation (5) is used for the number of stock orders. The epsilon value is also used as a trading signal through Z-scoring, in the state composed of the formation-window size.

2.2.2. Total Least Squares. TLS estimates parameters to minimize the sum of the measured distance and the vertical distance between regression lines [30]. Since the vertical distance does not change when the X and Y coordinates are changed, the value of β is calculated consistently. In the TLS method, the observed values of X_i and Y_i have the following error terms:

$$Y_i = y_i + e_i \sim N\left(0, \sigma_e^2\right) \tag{6}$$

$$X_i = x_i + u_i \sim N\left(0, \sigma_u^2\right) \tag{7}$$

where x_i and y_i are true values and e_i and u_i are error terms following independent identical distributions. It is assumed that there is linear combination of true values. For convenience, we represent the error variance ratio in equation (10):

$$y_i = \beta_0 + \beta_1 x_i \tag{8}$$

$$Y_i = \beta_0 + \beta_1 x_i + e_i \sim N\left(0, \sigma_e^2\right) \tag{9}$$

$$\tau = \frac{\operatorname{var}\left(Y_i \mid x_i\right)}{\operatorname{var}\left(X_i \mid x_i\right)} = \frac{\sigma_e^2}{\sigma_u^2} \tag{10}$$

The orthogonal regression estimator is calculated by minimizing the sum of the measured distance and the vertical distance between regression lines in equation (11):

$$\sum_{i=1}^{n} \left\{ \frac{\left(Y_i - \beta_0 + \beta_1 x_i\right)^2}{\tau} + \left(X_i - x_i\right)^2 \right\} \tag{11}$$

$$\beta_1 = \frac{s_{YY}^2 - \tau s_{XX}^2 + \left\{\left(s_{YY}^2 - \tau s_{XX}^2\right)^2 + 4\tau s_{XY}^2\right\}^{1/2}}{2 s_{XY}} \tag{12}$$

The value obtained from equation (12) is used in the same way as that obtained from equation (5) and the epsilon value is also used as a trading signal through the Z-score in the state composed of the formation-window size.

2.3. Reinforcement Learning and the Deep Q-Network. The idea of reinforcement learning is to find an optimal policy which maximizes the expected sum of discounted future rewards [31]. These rewards come from selecting the optimal value of each action, called the optimal Q-value. Reinforcement learning basically solves the problem defined by the Markov decision process (MDP). It consists of a tuple (S, A, P, R, γ), where S is a finite set of states, A is a finite set of actions, P is a state transition probability matrix, R is a reward function, and γ is a discount factor. In environment ε, agent-observed state s_t at time t, action a_t is selected. From the results of these sequences, environmental feedback is provided to the agent in the form of reward r_t and next state s_{t+1}. An action is selected by the action-value function $Q_\pi(s, a)$ that represents the expected sum of discounted future rewards.

$$Q_\pi\left(s_t, a_t\right) = \mathbb{E}_\pi\left[\sum_{i=t}^{T} \gamma^{i-t} r_i \mid s_t, a_t, \pi\right] \tag{13}$$

In this action-value function $Q_\pi(s_t, a_t)$, we find an optimal action-value function $Q^*(s_t, a_t)$, following an optimal policy

which maximizes the expected sum of discounted future rewards.

$$Q^*(s_t, a_t) = \max_{\pi} Q_{\pi}(s_t, a_t) \tag{14}$$

This optimal action-value function can be formulated as the Bellman equation.

$$Q^*(s_t, a_t) = \max_{a_{t+1}} [r_t + \gamma Q(s_{t+1}, a_{t+1})] \tag{15}$$

The DQN uses a nonlinear function approximator to estimate the action value function. This network is trained by minimizing a sequence of loss functions $L_t(\theta_t)$, which changes with each sequence of t. The weight of θ_t is updated as the sequence progresses:

$$L_t(\theta_t) = \mathbb{E}_{(s,a)\sim\rho(\bullet)}\left[(y_t - Q(s_t, a_t; \theta_t))^2\right] \tag{16}$$

$$y_t = \max_{a_{t+1}} [r_t + \gamma Q(s_{t+1}, a_{t+1}; \theta_{t-1}) \mid s_t, a_t] \tag{17}$$

3. Materials and Methods

3.1. Data. In this study, 50 stocks from the S&P 500 Index were selected based on their trading volume and market capitalization. To carry out the experiment, the data must cover the same period. Therefore, corresponding stocks were selected, leaving a total of 25 stocks. Table 1 represents the dataset of stock names, abbreviations of those stocks, and their respective sectors. We collected the adjusted daily closing prices using Thomson Reuters' database. The period of the training dataset is from January 2, 1990, to December 31, 2008, comprising 4792 data points; the test dataset covers the period from January 2, 2009, to July 31, 2018, comprising 2411 data points. From these datasets, a pair of stocks will be selected during the training dataset period using the cointegration test.

3.2. Selecting Pairs Using the Cointegration Test. It is necessary to pair stocks which have long-run statistical relationships or similar price movements. It is possible to determine the degree to which two stocks have had similar price movements through the correlation value. Furthermore, the long-term equilibrium of a pair of stocks is an important characteristic for the execution of pairs trading. In this study, we used the cointegration approach to select pairs of stocks. Through Johansen's method, we selected 11 pairs of stocks that have long-run equilibria. Table 2 shows the resulting pairs of stocks that were identified based on t-statistics and Figure 2 shows price movements of the cointegrated stocks XOM and CVX. Using this dataset, we will verify whether our proposed method has better performance than the traditional pairs-trading method.

3.3. Trading Signal. After selecting the pairs, it is necessary to extract the signal for trading. To extract signals, we opt for the OLS or TLS methods. First, because the stock price follows a random walk [32], we need to ensure that it follows the $I(1)$ process through the augmented Dickey-Fuller test. Subsequently, the $I(0)$ process should be created using the logarithmic difference in stock prices which is then applied to the OLS and TLS methods. In equation (18), α_1 is a constant value, β_1 is a hedge ratio (which is used as trading size), ε_t is the error term, and $\log P_{A,t}$ and $\log P_{B,t}$ are the logarithmic differences in the stock prices A and B at time t. We convert values of ε_t into a Z-score used as a trading signal. For example, if the trading signal reaches the threshold, we short one share of the overvalued stock (represented as $\log P_{A,t}$) and long β_1 shares of the undervalued stock (represented as $\log P_{B,t}$). The hedge ratio is determined based on the window size. We set a total of six discrete window sizes to obtain the optimal window size for the experiment. Trading windows are constituted using half of the formation-window size. The spread obtained here is used as a state when applying reinforcement learning (i.e., as an input of the DQN).

$$\log P_{B,t} = \alpha_1 + \beta_1 \log P_{A,t} + \varepsilon_t \tag{18}$$

3.4. Proposed Method: Optimized Pairs-Trading Strategy Using the DQN Method. In this study, we optimize the pairs-trading strategy with a type of game using the DQN. We will attempt to implement an optimal pairs-trading strategy by taking optimal trading and stop-loss boundaries that correspond to the given spread, since performance depends on how trading and stop-loss boundaries are set in pairs trading [14]. Figure 3 shows the mechanism of our proposed pairs-trading strategy. Throughout the cointegration test, we identify pairs and, using regression analysis, obtain a hedge ratio used as trading volume and a spread used as a trading signal and state. In the case of the DQN, two hidden layers are set up and the number of neurons is optimized by taking half of input size through trial and error. Action values consist of the six discrete spaces in Table 3. Each value of a_t has values for trading and stop-loss boundaries.

A pairs-trading system can make a profit if the spread touches the threshold and returns to the average such that the portfolio is closed in each trading window. On the other hand, if the trading boundary is touched and the stop-loss boundary is reached, the system tries to minimize losses by stopping trades. If the spread touches the trading boundary but fails to return to the average, the strategy may end up with a profit or a loss. In this study, the pairs-trading strategy is therefore considered as a kind of game; closing a portfolio yields a positive reward and a portfolio that reaches its stop-loss threshold yields a negative reward. Although an exited portfolio may possibly generate a positive profit, there is also a possibility that losses will occur and it is therefore set to yield a negative reward. We set the other conditions (such as the maintenance of the portfolio or not to execute the portfolio) to zero so as to concentrate on the close, stop-loss, and exit positions.

$$W_t = \left| v_{A,t} \times \frac{S_{A,t'} - S_{A,t}}{S_{A,t}} + v_{B,t} \times \frac{S_{B,t'} - S_{B,t}}{S_{B,t}} \right| t < t' \tag{19}$$

$$R_t = \begin{cases} 1000 \times W_t & \text{if portfolio closed} \\ -1000 \times W_t & \text{if portfolio reaches stop-loss threshold} \\ -500 \times W_t & \text{if portfolio exited} \end{cases} \tag{20}$$

Table 1: The 25 stocks on the S&P 500 Index used in this study.

No.	Ticker	Stock	Sector
1	AAPL	Apple Inc.	Technology
2	MSFT	Microsoft Corporation	Technology
3	BRKa	Berkshire Hathaway Inc.	Financial Services
4	JPM	JPMorgan Chase & Co.	Financial Services
5	JNJ	Johnson & Johnson	Healthcare
6	XOM	Exxon Mobil Corporation	Energy
7	BAC	Bank of America Corporation	Financial Services
8	WFC	Wells Fargo & Company	Financial Services
9	WMT	Walmart Inc.	Consumer Defensive
10	UNH	UnitedHealth Group Incorporated	Healthcare
11	CVX	Chevron Corporation	Energy
12	T	AT&T Inc.	Communication Services
13	PFE	Pfizer Inc.	Healthcare
14	ADBE	Adobe Systems Incorporated	Technology
15	MCD	McDonald's Corporation	Consumer Cyclical
16	MDT	Medtronic plc	Healthcare
17	MMM	3M Company	Industrials
18	HON	Honeywell International Inc.	Industrials
19	GE	General Electric Company	Industrials
20	ABT	Abbott Laboratories	Healthcare
21	MO	Altria Group, Inc.	Consumer Defensive
22	UNP	Union Pacific Corporation	Industrials
23	TXN	Texas Instruments Incorporated	Technology
24	UTX	United Technologies Corporation	Industrials
25	LLY	Eli Lilly and Company	Healthcare

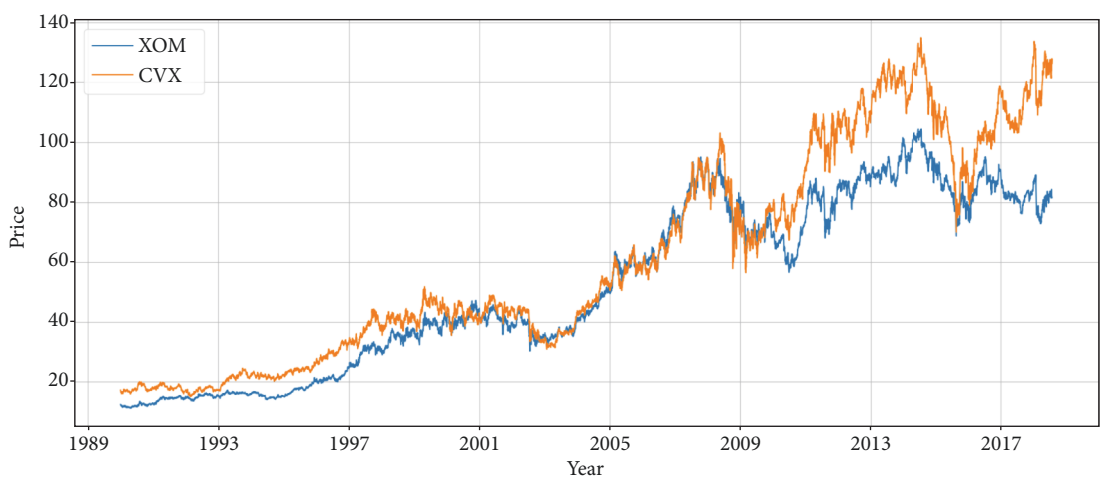

Figure 2: Cointegrated stock price movements.

We fix the values of portfolio close, stop-loss, and exit to +1000, −1000, and −500, respectively. When we update the Q-values, we must consider the reward as a significant component of efficiently training the DQN. We therefore set the reward value to have a range similar to that of the Q-value. Additionally, we included the corresponding profit or loss value to reflect that weight after the trading ended. In equation (19), $v_{A,t}$ and $v_{B,t}$ are the stock orders of stocks A and B at time t, $S_{A,t}$ and $S_{B,t}$ are the stock prices of A and B at time t, and $S_{A,t'}$ and $S_{B,t'}$ are the stock prices of A and B at time t'.

Algorithm 1 shows the process of our proposed method. Before we start our proposed method, we set a replay memory and batch size and select pairs using the cointegration test. At each epoch, we initialized total profit to 1.0. In the training scheme, we set a state which has spreads within the formation window and select actions which are used as

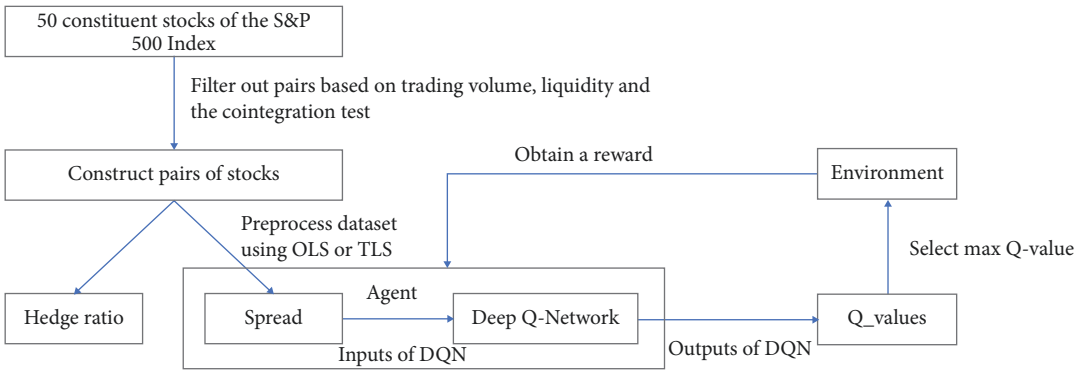

Figure 3: Steps for proposed pairs-trading strategy using the DQN method.

Initialize replay memory $\boldsymbol{D}$ and batch size $\boldsymbol{N}$
Initialize deep Q-network
Select pairs using cointegration test
(1) **For** each epoch **do**
(2) Profit = 1.0
(3) **For** steps t = 1, . . . until end of training data set **do**
(4) Calculate spreads using OLS or TLS methods
(5) Obtain initial state by converting spread to Z-score based on formation window $\boldsymbol{s_t}$
(6) Using epsilon-greedy method, select a random action $\boldsymbol{a_t}$
(7) Otherwise select $\boldsymbol{a_t} = \boldsymbol{argmax_a Q(s_t, a)}$
(8) Execute traditional pairs-trading strategy based on the action selected
(9) Obtain reward $\boldsymbol{r_t}$ by performing the pairs-trading strategy
(10) Set next state $\boldsymbol{s_{t+1}}$
(11) Store transition $(\boldsymbol{s_t}, \boldsymbol{a_t}, \boldsymbol{r_t}, \boldsymbol{s_{t+1}})$ in $\boldsymbol{D}$
(12) Sample minibatch of transition $(\boldsymbol{s_t}, \boldsymbol{a_t}, \boldsymbol{r_t}, \boldsymbol{s_{t+1}})$ from $\boldsymbol{D}$.
(13) $$\boldsymbol{y_t} = \begin{cases} \boldsymbol{r_t} & \boldsymbol{if\ s_{t+1} = terminal} \\ \boldsymbol{r_t + \gamma max_{a'} Q(s_{t+1}, a')} & \boldsymbol{if\ s_{t+1} = non-terminal} \end{cases}$$
(14) Update Q-network by performing a gradient descent step on $\{\boldsymbol{y_t} - \boldsymbol{Q(s_t, a)}\}^2$
(15) **End**
(16) **End**

Algorithm 1: Optimized pairs-trading system using DQN.

trading and stop-loss boundaries. Throughout the trading window, we executed a strategy similar to a traditional pairs-trading strategy using the action selected. After executing the strategy, we obtain a reward based on the results of the portfolio. Finally, for the Q-learning process, we update the Q-networks by performing a gradient descent step.

3.5. Performance Measure. We check our experiment results based on profit, maximum drawdown, and the Sharpe ratio. Profit is commonly used as a performance measure for trading strategies. It is calculated as the sum of returns taking into consideration trading cost. Since many trades can increase total profit, it is necessary to determine the total profit taking into consideration transaction costs depending on trading volume. In this study, we set a trading cost of 5 bp; equation (21) is almost the same as equation (19), but it does not include absolute value, and C is trading cost. Maximum drawdown represents the maximum cumulative loss from the highest to the lowest values of the portfolio during a given investment period where $P(t)$ is the value of the portfolio and T is the terminal time value. The Sharpe ratio is an indicator of the degree of excess profits from investing in risky assets used in evaluating portfolios [33]. In equation (23), R_p is the expected sum of portfolio returns and R_f is the risk-free rate; we set this value to 0 and σ_p is the standard deviation of portfolio returns.

$$Profit = \sum_{t=1}^{T} \left[\left(v_{1,t} * \frac{S_{1,t'} - S_{1,t}}{S_{1,t}} + v_{2,t} * \frac{S_{2,t'} - S_{2,t}}{S_{2,t}} \right) - C * \left(v_{1,t} + v_{2,t} \right) \right] \tag{21}$$

$$MDD(T) = \max_{\tau \in (0,T)} \left(\max_{t \in (0,\tau)} P(t) - p(\tau) \right) \tag{22}$$

Table 2: Summary statistics for pairs verified using cointegration tests.

No.	Pairs	t-statistic	Correlation
1	MSFT/JPM	−3.5423∗∗	0.9165
2	MSFT/TXN	−3.448∗∗	0.8641
3	BRKa/ABT	−3.5148∗∗	0.9493
4	BRKa/UTX	−3.3992∗∗	0.9609
5	JPM/T	−3.5882∗∗	0.8486
6	JPM/HON	−5.8209∗∗∗	0.9250
7	JPM/GE	−3.4494∗∗	0.9105
8	JNJ/WFC	−3.5696∗∗	0.9693
9	XOM/CVX	−4.05∗∗∗	0.9879
10	HON/TXN	−4.0625∗∗∗	0.7469
11	GE/TXN	−3.467∗∗	0.9148

Note: ∗∗∗ and ∗∗ denote a rejection of the null hypothesis at the 1% and 5% significance levels, respectively.

$$Sharpe\ ratio = \frac{R_p - R_f}{\sigma_p} \tag{23}$$

The Materials and Methods section should contain sufficient details so that all procedures can be repeated. It may be divided into headed subsections if several methods are described.

4. Results and Discussion

We use the stock pair XOM and CVX, which rejects the null hypothesis at the 1% significance level, to verify whether our proposed model is trained well. The lengths of the window sizes such as the formation window and trading window are selected from the performance results with the training dataset. From these results, we select an optimized window size and compare our proposed model with traditional pairs trading, which takes a constant set of actions with the test dataset.

4.1. Training Results. To find the optimum window size for the optimized pairs-trading system, we experimented with six cases. We performed the experiments based on six window sizes, and the results for each window size are calculated by averaging the top-5 results for a total of 11 pairs. From Tables 4 and 5, we can find that the best performance is obtained when the formation and training windows are 30 and 15, respectively, based on the profit generated by both the OLS and TLS methods. When we trained our networks, we set a positive reward for taking more closed positions and fewer stop-loss and exit positions. We can find the lowest ratio of portfolio closed positions based on the number of open positions, which in the formation and trading windows are for 30 and 15 days (0.68). Contrary to this result, the highest ratios of the number of closed positions in the formation and trading windows are for 120 and 60 days (0.73). However, the highest profits reported in the formation and trading windows are for 30 and 15 days. This can be explained when we check the ratio of the number of stop-loss portfolios. The formation and trading window sizes are 30 and 15 days and the ratio of portfolio stop-loss position is 0.13, but the formation and trading window sizes are 0.20. This result indicates that it is important to reduce the stop-loss position while increasing the closed position. In addition, we can see that the trading signals made with the TLS method are better than those made with the OLS method in all six of the discrete window sizes. The reason for this is based on the difference between the hedge ratios of the two methods. In OLS, when one side is the reference, the relative change of the other side is estimated. Since the assumption is that there is no error component on the reference side and there is an error only on the other side, the hedge ratio varies depending on the side used as the reference. However, in TLS, hedging ratios are the same regardless of which side is used as the reference. For this reason, the experimental results confirm that the TLS method is better able to determine when to execute the pairs-trading strategy. From these results, we take the optimum window size when we verify our proposed method in the test dataset. However, we first need to ensure that the model we proposed is well-trained.

It is important to check whether our reinforcement learning algorithm is trained well. Reference [21] suggested that a steadily increasing average of Q-values is evidence that the DQN is learning well. Figure 4(a) shows the average Q-values of HON and TXN as training progressed. We find that the average Q-values steadily increased, indicating that our proposed model is properly trained. In addition, we provide a positive reward when the portfolio closes and a negative reward when the portfolio reaches the stop-loss threshold or exits. Figure 4(b) shows the ratio of the number of portfolio positions as training progressed. The ratio of closed to open portfolio positions increased and the ratio of portfolios reaching their stop-loss thresholds to open portfolio positions decreased. We also find that the ratio of portfolio exits to open portfolio positions slightly increased. It is possible that the rewards given for an open portfolio position compared to those given for a closed portfolio position are relatively small. The DQN is therefore trained to prevent portfolios from reaching their stop-loss thresholds (the more important objective) over exiting them. This result can also serve as a basis for judging whether the proposed model is being trained properly.

Tables 6 and 7 represent the performance results of XOM and CVX in the training dataset. We call our proposed model pairs-trading DQN (PTDQN) and traditional pairs trading with constant action values as pairs trading with action 0 (PTA0) to pairs trading with action 5 (PTA5). From this result, we can confirm that our proposed method is more profitable than the constant pairs-trading strategies. In addition, we can see that the TLS method has a higher profitability compared to the OLS method. From PTA0 to PTA5, the trading boundary and the stop-loss boundary grew larger; the numbers of open and closed portfolios and portfolios that reached their stop-loss thresholds are reduced. In other words, there is less opportunity for profit, but the probability of loss is also reduced. It is important not only to take a lot of closed positions, but also to take the best action to open and close the portfolio. For example, if a portfolio is

Table 3: Setting a discrete action space.

	Action					
	A0	A1	A2	A3	A4	A5
Trading boundary	± 0.5	± 1.0	± 1.5	± 2.0	± 2.5	± 3.0
Stop-loss boundary	± 2.5	± 3.0	± 3.5	± 4.0	± 4.5	± 5.0

Table 4: Results of applying the DQN method to each window size using OLS.

Formation window	Trading window	MDD	Sharpe ratio	Profit	# of open portfolios	# of closed portfolios	# of stop-loss portfolios	# of portfolio exits
30	15	−0.3682	0.1197	2.7344	328	225	44	58
60	30	−0.3779	0.1327	2.5627	210	147	41	21
90	45	−0.4052	0.1409	2.4112	160	114	34	11
120	60	−0.4383	0.1165	2.0287	134	98	28	8
150	75	−0.4395	0.1244	2.0098	110	80	24	6
180	90	−0.5045	0.1180	1.9390	100	73	21	5

Table 5: Results of applying the DQN method to each window size using TLS.

Formation window	Trading window	MDD	Sharpe ratio	Profit	# of open portfolios	# of closed portfolios	# of stop-loss portfolios	# of exited portfolios
30	15	−0.4422	0.1061	2.9436	320	229	46	44
60	30	−0.5031	0.1143	2.5806	204	144	42	17
90	45	−0.5824	0.1072	2.4588	155	110	36	9
120	60	−0.5768	0.1181	2.4378	136	98	31	6
150	75	−0.5805	0.1245	2.4127	110	79	26	5
180	90	−0.5467	0.1209	2.3570	100	72	23	4

Table 6: Average top-5 performance results for XOM and CVX using OLS within the training period.

Model	MDD	Sharpe ratio	Profit	# of open portfolios	# of closed portfolios	# of stop-loss portfolios	# of exited portfolios
PTDQN	−0.0842	0.1835	3.4068	469	336	64	96
PTA0	−0.2014	0.1452	2.5934	565	382	132	50
PTA1	−0.1431	0.1773	2.7603	409	279	45	84
PTA2	−0.1234	0.1955	2.6307	325	191	16	118
PTA3	−0.2586	0.0861	1.3850	208	86	2	120
PTA4	−0.2591	0.0803	1.1933	124	39	2	83
PTA5	−0.2448	−0.0638	0.8588	47	11	0	36

Table 7: Average top-5 performance results for XOM and CVX using TLS within the training period.

Model	MDD	Sharpe ratio	Profit	# of open portfolios	# of closed portfolios	# of stop-loss portfolios	# of exited portfolios
PTDQN	−0.0944	0.2133	4.8760	541	399	104	63
PTA0	−0.1210	0.1522	4.1948	579	413	125	41
PTA1	−0.1015	0.1650	3.8834	430	310	50	70
PTA2	−0.1483	0.1722	3.3425	320	209	13	98
PTA3	−0.1386	0.1771	2.4385	217	101	3	113
PTA4	−0.1749	0.1602	1.6852	119	38	2	79
PTA5	−0.2862	0.0137	1.0362	55	10	0	45

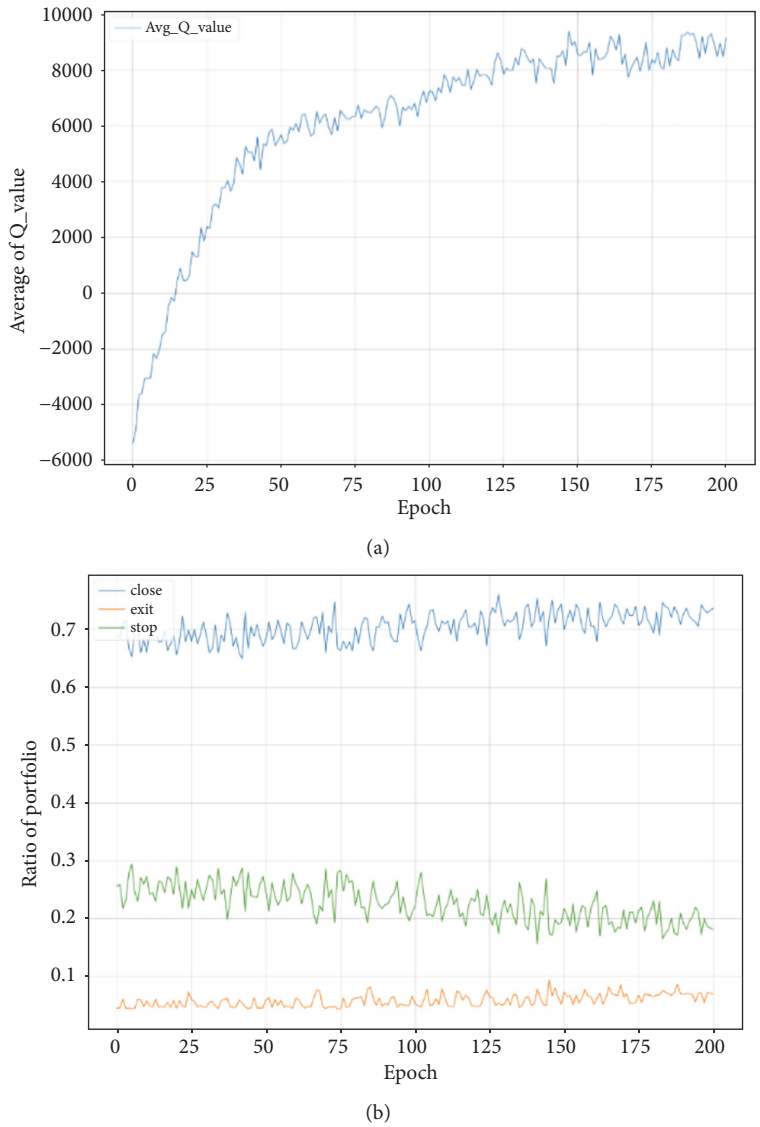

Figure 4: Verification that our proposed model is well-trained with HON and TXN using TLS. (a) Average of Q-values. (b) Ratio of portfolios.

opened and closed by a boundary corresponding to action 0 within the same spread and if a portfolio is opened and closed by a boundary corresponding to action 1, the corresponding profit is different. Assuming that the mean reversion is certain to occur, if we take the maximum boundary condition to open a portfolio, we will obtain a larger profit than when we take a smaller boundary condition. We can see that the PTDQN returns are higher than the strategy with the highest return among the traditional pairs trading strategies that take the constant action. Figures 5–8 show the changes in trading and stop-loss boundaries and the highest profit for constant action when applying the DQN method during the training period using OLS and TLS.

Figures 5 and 6 show comparisons of PTDQN and PTA1 using the TLS method. Figure 5 consists of the spread, trading, and stop-loss boundaries. We find that trading and stop-loss boundaries have different values in PTDQN, showing that it has learned to find the optimal boundary according to each spread. In contrast to PTDQN, PTA1 in Figure 6 has constant trading and stop-loss boundaries. Figures 7 and 8 exhibit the same features we see in Figures 5 and 6. The difference between these methods lies in the spreads: different results can be obtained depending on the spreads used. Making better spreads can therefore improve performance.

Figures 9 and 10 represent the profit corresponding to DQN and constant actions using TLS and OLS. Reference [34] suggested that an average value over multiple trials should be presented to show the reproducibility of deep reinforcement learning because there may be different results from high variances across trials and random seeds. We therefore conducted five trials with different random seeds. The profit graph of DQN represents the average profit of these trials and the filled region between the maximum and minimum profit values. We can see that PTDQN had a higher profit than the traditional pairs-trading strategies during

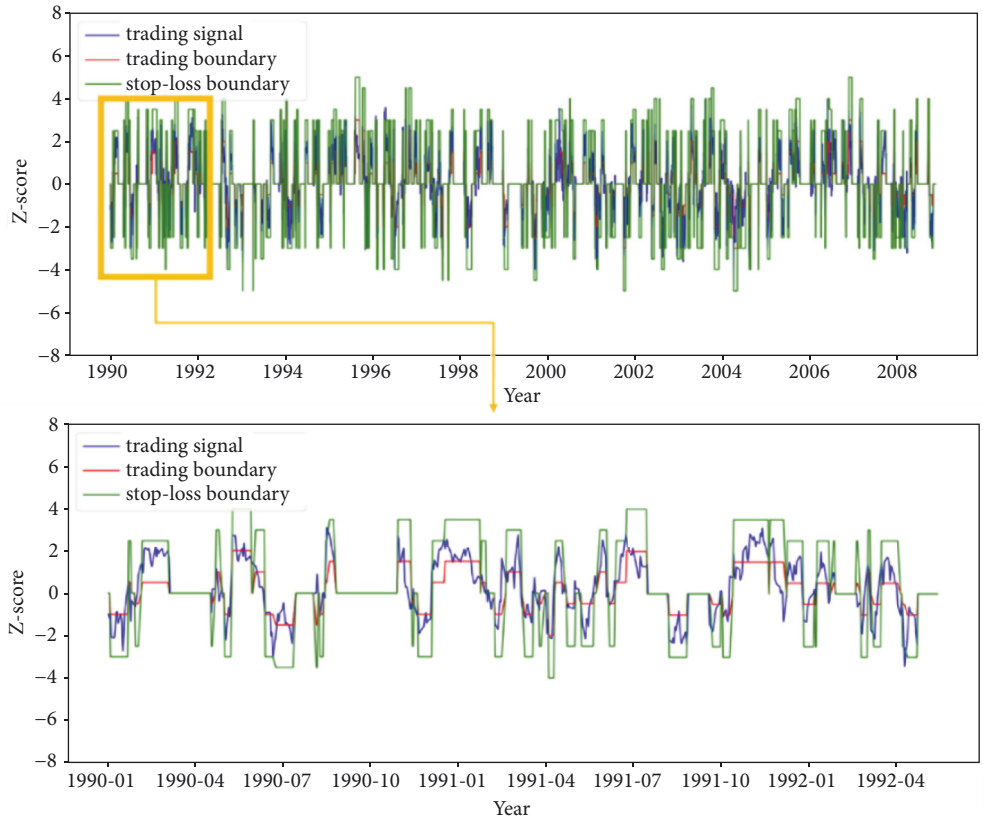

Figure 5: An example of optimizing pairs trading using PTDQN based on a training scheme using TLS.

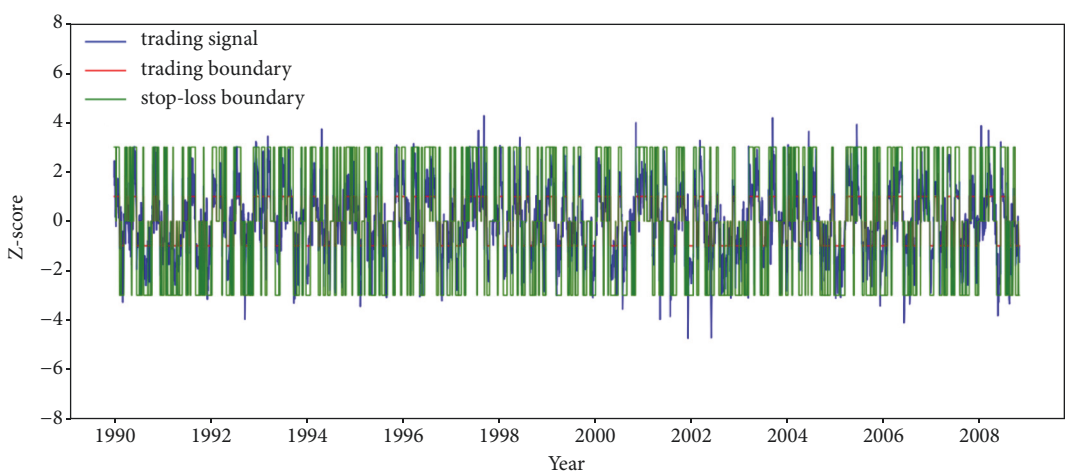

Figure 6: An example of PTA1 based on a training scheme using TLS.

the training period. This means that, even with the same spread, we can see how profit will change as the boundaries are changed. In other words, finding the optimal boundary for the spread is an important factor in optimizing the profitability of pairs trading.

4.2. Test Results. Tables 8 and 9 show the average performance measures of each pair tested by applying the top-5 trained models. We can see that the constant action with the highest returns for each pair is different, and the TLS method is higher in all pairs than the OLS method based on profit, as shown above. We also find that PTDQN has better performance than traditional pairs-trading strategies. The pair with the highest profit using the proposed method is HON and TXN (3.2755); it also shows the biggest difference between the DQN method and the optimal constant action (0.9377). We find that the proposed method has a higher Sharpe ratio in all pairs except for MO and UTX when the

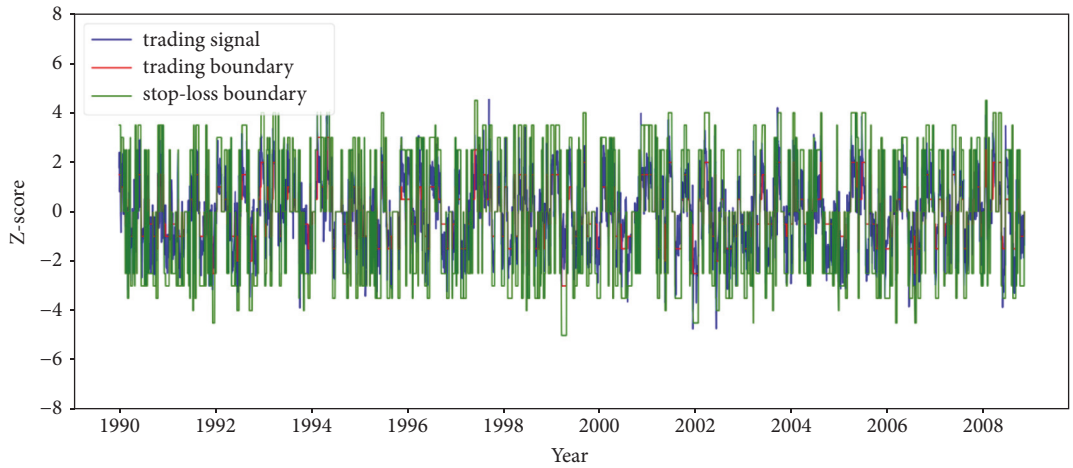

Figure 7: An example of optimizing PTDQN based on a training scheme using OLS.

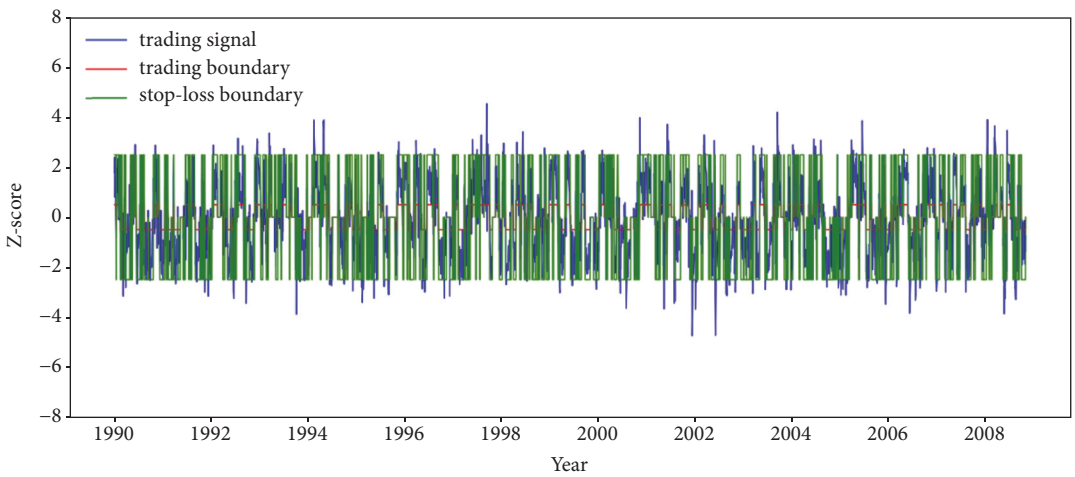

Figure 8: An example of PTA0 based on a training scheme using OLS.

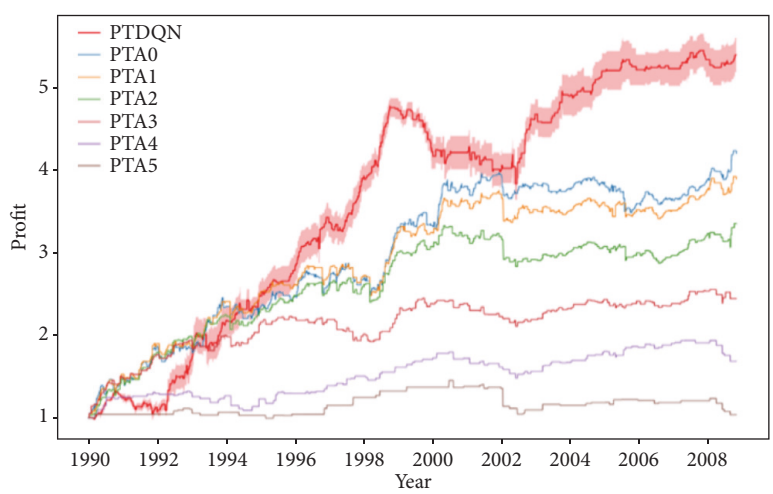

Figure 9: Average top-5 profits generated by PTDQN and traditional pairs-trading strategies using TLS in training periods.

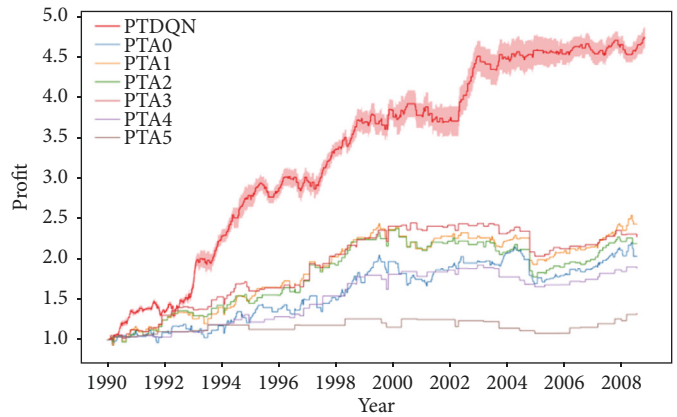

Figure 10: Average top-5 profits generated by PTDQN and traditional pairs-trading strategies using OLS in training periods.

TLS method is used. If we add the Sharpe ratio in addition to the total profit as an objective function, we can build a more optimized pairs-trading system. Based on these results, we can ensure the robustness of our proposed method for our dataset. The proposed method can be applied to other pairs of stocks found in other global markets.

In Figure 11, we can see that our proposed method, PTDQN, outperforms the traditional pairs trading strategies that have constant actions in test dataset. The crucial aspect of this method is the selection of optimal boundary in the spread that makes the highest profit in constant action, which is like a constant boundary. Therefore, the trend is the same as traditional pairs trading strategies; however, when the optimal boundaries which have the highest profit in the spread are combined, PTDQN is found to have higher profit than traditional pairs trading strategies. This method can therefore be applied in various fields when there is a need to optimize the efficiency of a rule-based strategy [35, 36]. In this study, we consider spread and boundaries to be the important factors of pairs trading strategy. Therefore, we tried to optimize pairs trading strategy with various trading and stop-loss boundaries using deep reinforcement learning and our method outperforms rule-based strategies. By optimizing key parameters in rule-based methods, it can improve the performances.

Pairs trading uses two types of stock which have the same trends. However, it can be broken due to various factors such as economic issues and company risk. In this situation, the spread between two stocks is extremely large. Although this situation cannot be avoided, we hedge this risk by taking a dynamic boundary. In this sense, taking the lowest stop-loss boundary is the best choice since it can be overcome with the least loss. By taking the dynamic boundary using the deep reinforcement learning method, we can see that not only profits are increased, but losses are also minimized as compared to taking a fixed boundary.

5. Conclusions

We propose a novel approach to optimize pairs trading strategy using a deep reinforcement learning method, especially deep Q-networks. There are two key research questions posed. First, if we set a dynamic boundary based on a spread in each trading window, can it achieve higher profit than traditional pairs trading strategy? Second, is it possible that deep reinforcement learning method can be trained to follow this mechanism? To investigate these questions, we collected pairs selected using the cointegration test. We experimented with how the results varied according to the spread and the method used. We therefore set different spreads using OLS and TLS methods as the input of the DQN and the trading signal. To conduct this experiment, we set up a formation window and a trading window. The hedge ratio, which is an important factor in determining how much stock to take, depends on this value. We therefore applied the OLS and TLS methods and experimented to find the optimal window size by varying the formation window and the trading window.

Tables 6 and 7 show the average performance values of the formation windows and trading windows in the training dataset. The results show that all six window sizes were higher when TLS spreads were used than in OLS spreads. In addition, we can see that profitability gradually increases as the estimation windows and trading windows of methods using TLS and OLS decreased. The reason is that although the ratio of closed position portfolio is the lowest in what we set formation and trading windows, the ratio of stop-loss position portfolio is also the lowest compared with other formation and trading windows. It means that reducing stop-loss position portfolio is important as well as increasing closed position portfolio to make a profit. Using the optimal window size, we then check whether our DQN is properly trained. At each epoch, we find that the average Q-value steadily increased, the ratio of closed portfolios increased, and the ratio of portfolios that reached their stop-loss thresholds decreased, confirming that our DQN is trained well. Based on these results, we find that our proposed model using the test dataset with a formation window of 30 and a trading window of 15 had results that were superior to those of traditional pairs-trading strategies in the out-of-sample dataset. In Figure 11, we can see that the profit path of PTDQN is similar PTA0 to PTA5, but better than that from

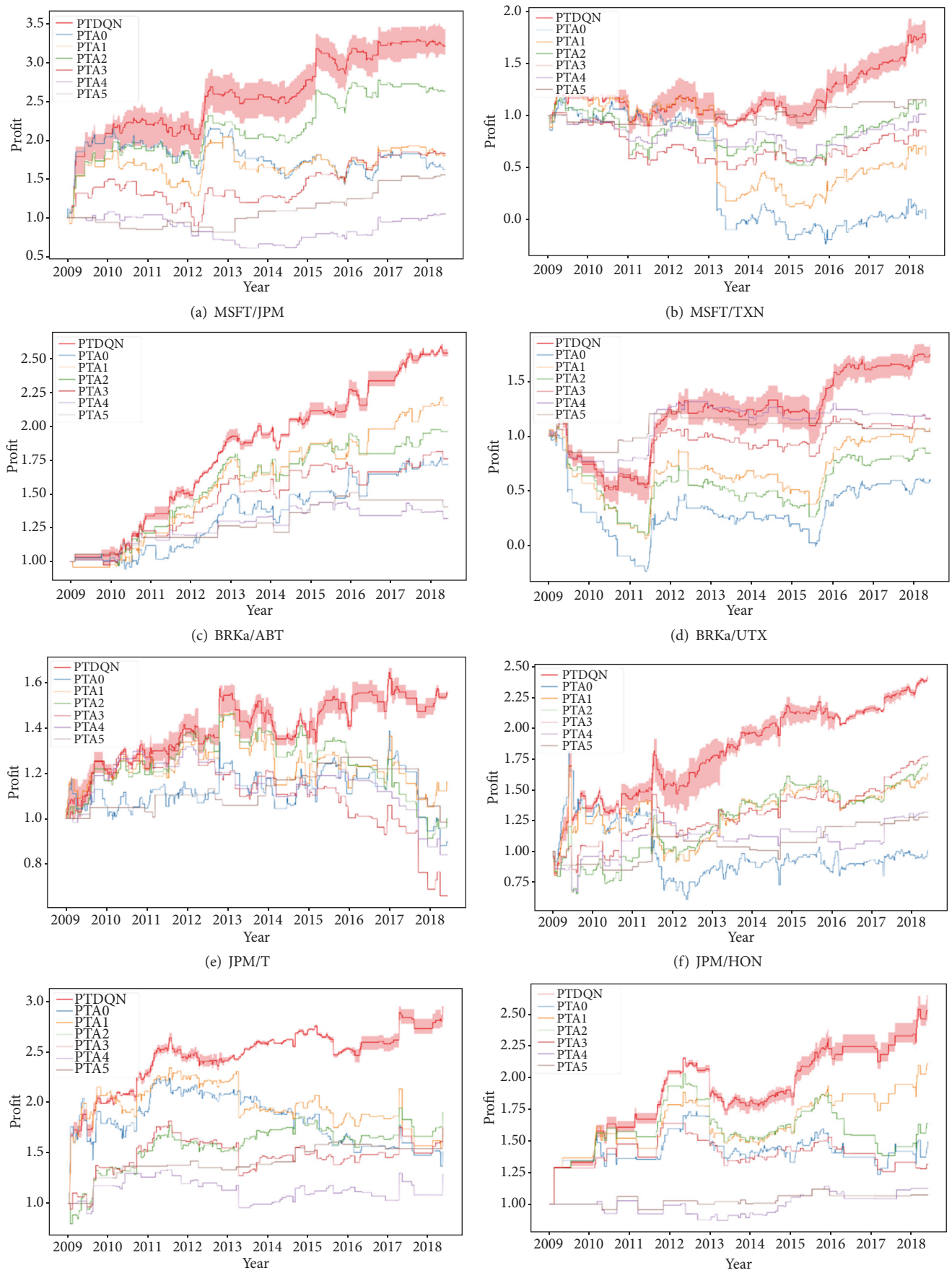

(a) MSFT/JPM

(b) MSFT/TXN

(c) BRKa/ABT

(d) BRKa/UTX

(e) JPM/T

(f) JPM/HON

(g) JPM/GE

(h) JNJ/WFC

Figure 11: Continued.

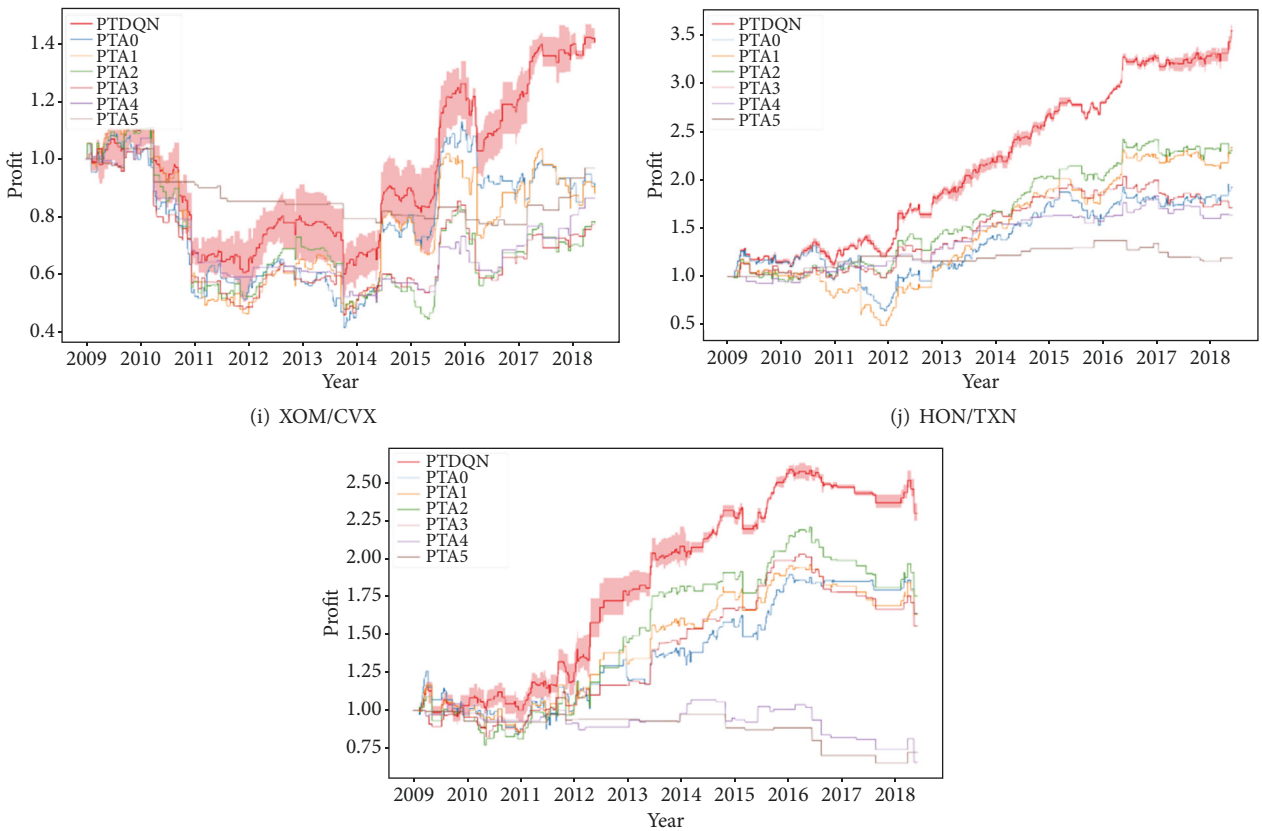

(i) XOM/CVX

(j) HON/TXN

(k) GE/TXN

Figure 11: Average top-5 profits of PTDQN and PTA0 to PTA5 using TLS with the test dataset.

other methods. This shows that taking dynamic boundaries based on our method is efficient in optimizing the pairs trading strategy. During economic issues uncertainties, it can be a risk to manage the pairs trading strategies including our proposed method. However, we set a reward function if spread is suddenly high, and our network is trained to prevent this situation by taking less stop-loss boundary since it is trained to maximize the expected sum of future rewards. Therefore, our proposed method can minimize the risk when the economic risks appeared compared with traditional pairs trading strategy with fixed boundary.

From the experimental results, we show that our method can be applied in the pairs trading system. It can be applied in various fields, including finance and economics, when there is a need to optimize the efficiency of a rule-based strategy. Furthermore, we find that our method outperforms the traditional pairs trading strategy in all pairs based on constituent stocks in S&P 500. If we select appropriate pairs which are cointegrated, we can apply our methods to other markets such as KOSPI, Nikkei, and Hang Seng. The study focused on only spreads made by two stocks, which have long-term equilibrium patterns. Since our method selects optimal boundaries based on spreads, it can be applied to other stock markets such as KOSPI, Nikkei, and Hang Seng.

In future works, we can develop our proposed model as follows. First, as profit was set as the objective function in this study, the performance of the model is lower than traditional pairs trading when based on other performance measures. It can therefore be possible to create a better-optimized pairs-trading strategy by including all these other performance indicators as part of the objective function. Second, we can use other statistical methods such as the Kalman filter and error-correction models to use diversified spreads. Finally, it is possible to create a more-optimized pairs-trading strategy by continuously changing the discrete set of window sizes and boundaries. We will solve these difficulties in future studies.

Data Availability

The data used to support the findings of this study have been deposited in the figshare repository (DOI: 10.6084/m9.figshare.7667645).

Disclosure

The funders had no role in the study design, data collection and analysis, decision to publish, or preparation of the manuscript. This work represents a part of the study

Table 8: Average top-5 performance results of the proposed method and the traditional pairs-trading strategy in the out-of-sample dataset using TLS.

Pairs	Model	MDD	Sharpe ratio	Profit	# of open portfolios	# of closed portfolios	# of stop-loss portfolios	# of exited portfolios
MSFT/JPM	PTDQN	−0.1122	0.2294	3.0446	186	126	38	62
	PTA0	−0.3411	0.0742	1.6236	211	136	57	18
	PTA1	−0.2907	0.0979	1.8001	162	104	26	32
	PTA2	−0.1507	0.1936	2.6303	131	64	7	60
	PTA3	−0.4032	0.1542	1.8282	97	39	1	57
	PTA4	−0.4340	0.0400	1.0480	55	13	0	42
	PTA5	−0.1836	0.3098	1.5524	30	7	0	23
MSFT/TXN	PTDQN	−0.3420	0.1001	1.5423	204	132	47	65
	PTA0	−1.2094	−0.0571	0.0013	244	152	76	16
	PTA1	−0.9225	−0.0177	0.6131	178	110	25	43
	PTA2	−0.5574	0.0351	1.0887	134	68	8	58
	PTA3	−0.5375	−0.0128	0.8326	97	34	1	62
	PTA4	−0.4485	0.0260	1.0118	66	15	1	50
	PTA5	−0.1048	0.1233	1.1502	32	5	0	27
BRKa/ABT	PTDQN	−0.0740	0.3159	2.3655	162	111	30	43
	PTA0	−0.1392	0.1554	1.7157	182	128	35	18
	PTA1	−0.1048	0.2464	2.1508	138	96	15	27
	PTA2	−0.1133	0.2538	1.9578	108	64	3	40
	PTA3	−0.1040	0.2480	1.7576	76	35	1	40
	PTA4	−0.0829	0.2087	1.3171	44	13	0	31
	PTA5	−0.0704	0.4366	1.4013	19	7	0	12
BRKa/UTX	PTDQN	−0.5401	0.1174	1.5744	167	105	35	58
	PTA0	−1.2143	−0.0199	0.5918	192	117	55	19
	PTA1	−0.9340	0.0346	1.0701	147	89	12	45
	PTA2	−0.9099	−0.0009	0.8435	122	60	5	57
	PTA3	−0.5673	0.0473	1.1520	89	32	1	56
	PTA4	−0.3641	0.0694	1.1628	53	9	0	44
	PTA5	−0.2309	0.0408	1.0405	18	3	0	15
JPM/T	PTDQN	−0.1384	0.1283	1.4653	175	113	42	53
	PTA0	−0.3630	0.0071	0.8968	205	129	60	15
	PTA1	−0.2801	0.0460	1.1595	144	94	17	32
	PTA2	−0.3750	0.0192	0.9987	119	62	5	51
	PTA3	−0.5241	−0.0717	0.6609	92	35	0	56
	PTA4	−0.3607	−0.0550	0.8411	56	18	0	38
	PTA5	−0.2235	0.0061	0.9851	22	6	0	16
JPM/HON	PTDQN	−0.1872	0.1523	2.2510	223	155	39	62
	PTA0	−0.6769	0.0190	1.0077	274	180	70	23
	PTA1	−0.4644	0.0622	1.6331	201	139	24	38
	PTA2	−0.4537	0.0840	1.7165	149	87	2	60
	PTA3	−0.2410	0.1414	1.7648	107	43	0	64
	PTA4	−0.3313	0.0879	1.3150	62	16	0	46
	PTA5	−0.1693	0.1803	1.2777	28	7	0	21

Table 8: Continued.

Pairs	Model	MDD	Sharpe ratio	Profit	# of open portfolios	# of closed portfolios	# of stop-loss portfolios	# of exited portfolios
JPM/GE	PTDQN	−0.1098	0.2123	2.8250	193	124	46	65
	PTA0	−0.3897	0.0507	1.5137	224	142	65	17
	PTA1	−0.3404	0.0640	1.6912	163	109	18	36
	PTA2	−0.1628	0.1284	1.9032	132	73	6	53
	PTA3	−0.2980	0.1142	1.7555	106	38	1	67
	PTA4	−0.2817	0.0790	1.2884	55	13	0	42
	PTA5	−0.0612	0.4776	1.7489	21	6	0	15
JNJ/WFC	PTDQN	−0.1576	0.2437	2.3741	143	100	28	38
	PTA0	−0.2872	0.0892	1.4932	164	115	37	12
	PTA1	−0.2219	0.1948	2.1147	127	90	15	21
	PTA2	−0.3188	0.1322	1.6362	99	55	5	38
	PTA3	−0.2324	0.1084	1.3141	68	27	0	41
	PTA4	−0.1532	0.1043	1.1228	40	14	0	26
	PTA5	−0.0970	0.1203	1.0734	16	6	0	10
XOM/CVX	PTDQN	−0.4265	0.0605	1.1924	218	135	45	77
	PTA0	−0.6189	0.0236	0.8812	256	161	67	28
	PTA1	−0.5999	0.0154	0.8809	197	118	25	54
	PTA2	−0.6034	−0.0073	0.7792	153	70	8	75
	PTA3	−0.5628	−0.0224	0.7734	114	38	2	74
	PTA4	−0.5311	−0.0200	0.8643	70	18	1	51
	PTA5	−0.2583	0.0060	0.9692	31	4	0	27
HON/TXN	PTDQN	−0.0874	0.2679	3.2755	233	164	49	63
	PTA0	−0.5108	0.1080	1.9219	276	186	66	23
	PTA1	−0.5841	0.1625	2.3378	207	140	28	38
	PTA2	−0.1926	0.2086	2.3096	158	92	4	62
	PTA3	−0.1611	0.1557	1.7100	114	49	2	63
	PTA4	−0.1254	0.2289	1.6374	69	23	0	46
	PTA5	−0.1578	0.1924	1.1925	28	9	0	19
GE/TXN	PTDQN	−0.1133	0.1871	2.1398	172	117	30	48
	PTA0	−0.3348	0.0967	1.6398	201	136	44	21
	PTA1	−0.1656	0.1070	1.6355	153	101	19	33
	PTA2	−0.2043	0.1388	1.7568	117	68	8	41
	PTA3	−0.2335	0.1591	1.5555	89	39	2	48
	PTA4	−0.3847	−0.1355	0.6570	45	7	0	38
	PTA5	−0.3489	−0.2730	0.7218	21	2	0	19
MO/UTX	PTDQN	−0.5264	0.0840	1.2940	150	88	35	58
	PTA0	−1.0950	−0.0272	0.6231	178	102	56	19
	PTA1	−0.7205	0.0286	1.0362	125	73	12	39
	PTA2	−0.8361	−0.0040	0.8658	105	51	3	50
	PTA3	−0.4311	0.0052	0.9323	79	24	0	54
	PTA4	−0.3916	0.1141	1.2129	48	12	0	36
	PTA5	−0.1311	0.2948	1.1276	14	3	0	11

Table 9: Average top-5 performance results of the proposed method and the traditional pairs-trading strategy in the out-of-sample dataset using OLS.

Pairs	Model	MDD	Sharpe ratio	Profit	# of open portfolios	# of closed portfolios	# of stop-loss portfolios	# of exited portfolios
MSFT/JPM	PTDQN	−0.2096	0.1228	1.9255	215	137	54	62
	PTA0	−0.3618	0.0492	1.3365	225	141	61	23
	PTA1	−0.5036	0.0188	1.0185	168	102	28	38
	PTA2	−0.4045	0.0611	1.3591	124	59	8	57
	PTA3	−0.5055	−0.0094	0.8636	97	33	3	61
	PTA4	−0.4195	−0.0009	0.9459	58	12	1	45
	PTA5	−0.2018	0.1236	1.1593	29	6	0	23
MSFT/TXN	PTDQN	−0.2878	0.0698	1.3466	244	153	65	68
	PTA0	−0.5271	0.0070	0.8489	252	156	72	24
	PTA1	−0.4721	0.0255	1.0286	187	117	26	44
	PTA2	−0.3816	0.0215	0.9912	145	71	10	64
	PTA3	−0.6553	−0.1015	0.5053	104	30	2	72
	PTA4	−0.2719	0.0422	1.0532	63	16	1	46
	PTA5	−0.1850	0.0068	0.9785	34	7	0	27
BRKa/ABT	PTDQN	−0.1282	0.1644	1.5076	180	109	48	57
	PTA0	−0.5073	−0.0265	0.7070	183	112	48	22
	PTA1	−0.2649	0.0453	1.0786	139	80	13	46
	PTA2	−0.2246	0.1056	1.2942	121	60	4	56
	PTA3	−0.1686	0.1241	1.2718	91	38	1	52
	PTA4	−0.1483	0.0176	0.9778	49	12	0	37
	PTA5	−0.1602	0.0004	0.9830	16	2	0	14
BRKa/UTX	PTDQN	−0.5231	0.0816	1.2976	215	132	57	69
	PTA0	−1.1928	−0.0647	0.3332	216	133	57	25
	PTA1	−0.8697	−0.0157	0.7445	167	100	15	51
	PTA2	−0.7815	−0.0071	0.8391	135	70	5	60
	PTA3	−0.3573	0.0315	1.0292	94	36	0	58
	PTA4	−0.2096	0.0684	1.0857	52	11	0	41
	PTA5	−0.1317	−0.1174	0.9312	16	2	0	14
JPM/T	PTDQN	−0.1338	0.1391	1.4547	205	127	60	50
	PTA0	−0.3588	0.0069	0.9054	208	130	61	16
	PTA1	−0.2535	0.0405	1.0902	151	96	19	35
	PTA2	−0.1872	0.0542	1.1198	119	66	5	48
	PTA3	−0.2574	0.0336	1.0502	94	39	0	55
	PTA4	−0.2212	0.0345	1.0312	57	20	0	37
	PTA5	−0.2348	−0.1922	0.8299	20	5	0	15
JPM/HON	PTDQN	−0.3869	0.1071	1.5175	250	162	57	68
	PTA0	−0.7141	0.0181	0.9444	256	166	59	30
	PTA1	−0.5065	0.0702	1.3071	198	127	22	49
	PTA2	−0.4649	0.1071	1.4260	152	84	3	65
	PTA3	−0.4871	0.0763	1.2098	102	44	0	58
	PTA4	−0.3503	−0.0694	0.8178	50	13	0	37
	PTA5	−0.2980	−0.1721	0.8040	23	6	0	17

Table 9: Continued.

Pairs	Model	MDD	Sharpe ratio	Profit	# of open portfolios	# of closed portfolios	# of stop-loss portfolios	# of exited portfolios
JPM/GE	PTDQN	−0.1195	0.1443	1.7682	226	133	64	69
	PTA0	−0.4379	0.0036	0.8549	232	137	66	29
	PTA1	−0.1523	0.0987	1.4814	165	98	16	51
	PTA2	−0.1738	0.1264	1.5661	134	62	5	67
	PTA3	−0.2680	0.0729	1.2026	93	29	0	64
	PTA4	−0.2104	0.1298	1.3242	51	12	0	39
	PTA5	−0.1461	−0.0423	0.9586	18	3	0	15
JNJ/WFC	PTDQN	−0.1890	0.1266	1.7194	202	130	47	56
	PTA0	−0.8705	−0.0326	0.4635	207	131	53	22
	PTA1	−0.6189	−0.0134	0.7318	150	91	19	39
	PTA2	−0.4763	0.0309	1.0563	124	57	4	62
	PTA3	−0.2318	0.1447	1.6072	97	33	2	62
	PTA4	−0.2415	0.0549	1.0632	50	13	0	37
	PTA5	−0.0880	0.2468	1.1886	20	4	0	16
XOM/CVX	PTDQN	−0.3316	0.0265	1.1517	141	81	23	43
	PTA0	−0.7629	−0.0547	0.4186	240	149	61	30
	PTA1	−0.5648	0.0132	0.8754	193	114	23	56
	PTA2	−0.6977	−0.0387	0.6655	154	70	7	77
	PTA3	−0.5235	0.0277	0.9865	117	38	1	78
	PTA4	−0.4781	−0.0577	0.8117	63	12	1	50
	PTA5	−0.3787	−0.1492	0.8090	29	3	0	26
HON/TXN	PTDQN	−0.1339	0.1534	1.8852	270	175	64	69
	PTA0	−0.4135	0.0212	0.9455	276	177	70	28
	PTA1	−0.2758	0.0666	1.3216	207	124	27	55
	PTA2	−0.2614	0.1054	1.5031	159	84	5	69
	PTA3	−0.1759	0.1413	1.5617	117	45	2	70
	PTA4	−0.0834	0.2650	1.7044	66	23	0	43
	PTA5	−0.0664	0.4606	1.6830	30	13	0	17
GE/TXN	PTDQN	−0.1676	0.1263	1.6411	206	140	43	62
	PTA0	−0.6133	0.0178	0.9742	211	144	44	23
	PTA1	−0.3085	0.0586	1.2743	166	109	19	38
	PTA2	−0.2402	0.0585	1.2216	128	68	5	55
	PTA3	−0.3190	−0.0013	0.9193	91	31	2	58
	PTA4	−0.2493	−0.0285	0.9117	49	8	0	41
	PTA5	−0.0862	0.1417	1.0936	23	4	0	19
MO/UTX	PTDQN	−0.3181	0.0524	1.1402	188	117	49	59
	PTA0	−0.4688	0.0041	0.8667	195	121	52	21
	PTA1	−0.6166	−0.0230	0.7470	144	84	13	46
	PTA2	−0.5034	−0.0076	0.8666	115	51	4	59
	PTA3	−0.2833	0.0457	1.0873	88	32	0	56
	PTA4	−0.2901	0.0356	1.0280	44	12	0	32
	PTA5	−0.1500	0.0992	1.0297	13	2	0	11

conducted as a Master Thesis in Financial Engineering during 2016 and 2018 at the University of Ajou, Republic of Korea.

Conflicts of Interest

The authors declare that there are no conflicts of interest regarding the publication of this paper.

Acknowledgments

This work was supported by the National Research Foundation of Korea (NRF) grant funded by the Korea Government (MSIT: Ministry of Science and ICT) (No. NRF-2017R1C1B5018038).

References

[1] E. Gatev, W. N. Goetzmann, and K. G. Rouwenhorst, "Pairs trading: performance of a relative-value arbitrage rule," *Yale ICF Working Paper No. 08-03*, 1998, https://ssrn.com/abstract=141615 or http://dx.doi.org/10.2139/ssrn.141615.

[2] R. J. Elliott, J. van der Hoek, and W. P. Malcolm, "Pairs trading," *Quantitative Finance*, vol. 5, no. 3, pp. 271–276, 2005.

[3] S. Andrade, V. Di Pietro, and M. Seasholes, "Understanding the profitability of pairs trading," 2005.

[4] G. Hong and R. Susmel, "Pairs-trading in the Asian ADR market," Univ. Houston, Unpubl. Manuscr., 2003.

[5] E. Gatev, W. N. Goetzmann, and K. G. Rouwenhorst, "Pairs trading: performance of a relative-value arbitrage rule," *Review of Financial Studies* , vol. 19, no. 3, pp. 797–827, 2006.

[6] B. Do and R. Faff, "Does simple pairs trading still work?" *Financial Analysts Journal*, vol. 66, no. 4, pp. 83–95, 2018.

[7] S. Mudchanatongsuk, J. A. Primbs, and W. Wong, "Optimal pairs trading: A stochastic control approach," in *Proceedings of the 2008 American Control Conference, ACC*, pp. 1035–1039, USA, June 2008.

[8] A. Tourin and R. Yan, "Dynamic pairs trading using the stochastic control approach," *Journal of Economic Dynamics & Control*, vol. 37, no. 10, pp. 1972–1981, 2013.

[9] Z. Zeng and C. Lee, "Pairs trading: optimal thresholds and profitability," *Quantitative Finance*, vol. 14, no. 11, pp. 1881–1893, 2014.

[10] S. Fallahpour, H. Hakimian, K. Taheri, and E. Ramezanifar, "Pairs trading strategy optimization using the reinforcement learning method: a cointegration approach," *Soft Computing*, vol. 20, no. 12, pp. 5051–5066, 2016.

[11] P. Nath, "High frequency pairs trading with U.S. treasury securities: risks and rewards for hedge funds," *SSRN Electronic Journal*, 2004.

[12] T. Leung and X. Li, "Optimal mean reversion trading with transaction costs and stop-loss exit," *International Journal of Theoretical and Applied Finance*, vol. 18, no. 3, 2013.

[13] E. Ekström, C. Lindberg, and J. Tysk, "Optimal liquidation of a pairs trade," in *Advanced Mathematical Methods for Finance*, pp. 247–255, Springer, Heidelberg, 2011.

[14] Y. Lin, M. McCrae, and C. Gulati, "Loss protection in pairs trading through minimum profit bounds: A cointegration approach," *Journal of Applied Mathematics and Decision Sciences*, vol. 2006, pp. 1–14, 2006.

[15] A. Mikkelsen, "Pairs trading: the case of Norwegian seafood companies," *Applied Economics*, vol. 50, no. 3, pp. 303–318, 2017.

[16] K. Kim, "Performance analysis of pairs trading strategy utilizing high frequency data with an application to KOSPI 100 Equities," *SSRN Electronic Journal*, p. 24, 2011.

[17] V. Holý and P. Tomanová, *Estimation of Ornstein-Uhlenbeck Process Using Ultra-High-Frequency Data with Application to Intraday Pairs Trading Strategy*, 2018.

[18] D. Chen, J. Cui, Y. Gao, and L. Wu, "Pairs trading in Chinese commodity futures markets: an adaptive cointegration approach," *Accounting & Finance*, vol. 57, no. 5, pp. 1237–1264, 2017.

[19] H. Puspaningrum, Y. Lin, and C. M. Gulati, "Finding the optimal pre-set boundaries for pairs trading strategy based on cointegration technique," *Journal of Statistical Theory and Practice*, vol. 4, no. 3, pp. 391–419, 2010.

[20] A. A. Roa, "Pairs trading: optimal thershold strategies," 2018.

[21] V. Mnih, K. Kavukcuoglu, D. Silver et al., "Playing atari with deep reinforcement learning," https://arxiv.org/abs/1312.5602, 2013.

[22] Y. Wang, D. Wang, S. Zhang, Y. Feng, S. Li, and Q. Zhou, "Deep Q-trading," 2017, http://cslt.riit.tsinghua.edu.cn/.

[23] C.-Y. Huang, "Financial trading as a game: a deep reinforcement learning approach," 2018, https://arxiv.org/abs/1807.02787.

[24] T. Kim, *Optimizing the pairs trading strategy using Deep reinforcement learning [M.S. thesis]*, Ajou University, Suwon, Republic of Korea, 2019.

[25] B. Do, R. Faff, and K. Hamza, "A new approach to modeling and estimation for pairs trading," in *Proceedings of the 2006 Financial Management Association European Conference*, 2006.

[26] R. D. Dittmar, C. J. Neely, and P. A. Weller, "Is technical analysis in the foreign exchange market profitable? A genetic programming approach," *Journal of Financial and Quantitative Analysis*, vol. 43, p. 43, 1997.

[27] H. Rad, R. K. Low, and R. Faff, "The profitability of pairs trading strategies: distance, cointegration and copula methods," *Quantitative Finance*, vol. 16, no. 10, pp. 1541–1558, 2016.

[28] S. Johansen, "Statistical analysis of cointegration vectors," *Journal of Economic Dynamics and Control*, vol. 12, no. 2-3, pp. 231–254, 1988.

[29] M. H. Kutner, C. J. Nachtsheim, J. Neter, and W. Li, "Applied linear statistical models," 1996.

[30] G. H. Golub and C. F. Van Loan, "An analysis of the total least squares problem," *SIAM Journal on Numerical Analysis*, vol. 17, no. 6, pp. 883–893, 1980.

[31] R. S. Sutton and A. G. Barto, "Introduction to reinforcement learning," *Learning*, 1998.

[32] E. F. Fama, "Random walks in stock market prices," *Financial Analysts Journal*, vol. 51, no. 1, pp. 75–80, 1995.

[33] W. F. Sharpe, "The sharpe ratio," *The Journal of Portfolio Management*, 1994.

[34] P. Henderson, R. Islam, P. Bachman, J. Pineau, D. Precup, and D. Meger, "Deep reinforcement learning that matters," in *Proceedings of the Thirthy-Second AAAI Conference On Artificial Intelligence (AAAI)*, 2018.

[35] Y. H. Li, X. M. Lu, and N. C. Kar, "Rule-based control strategy with novel parameters optimization using NSGA-II for power-split PHEV operation cost minimization," *IEEE Transactions on Vehicular Technology*, vol. 63, no. 7, pp. 3051–3061, 2014.

[36] L. Dymova, P. Sevastianov, and K. Kaczmarek, "A stock trading expert system based on the rule-base evidential reasoning using Level 2 Quotes," *Expert Systems with Applications*, vol. 39, no. 8, pp. 7150–7157, 2012.

Hindawi
Complexity
Volume 2019, Article ID 9202457, 15 pages
https://doi.org/10.1155/2019/9202457

Research Article

Anticipating Stock Market of the Renowned Companies: A Knowledge Graph Approach

Yang Liu,[1] **Qingguo Zeng**,[2] **Joaquín Ordieres Meré**,[1] **and Huanrui Yang**[3]

[1]*Department of Industrial Engineering, Business Administration and Statistics, Escuela Técnica Superior de Ingenieros Industriales, Universidad Politécnica de Madrid, Madrid 28006, Spain*
[2]*School of Mathematical Sciences, South China Normal University, Guangzhou 510631, China*
[3]*Electrical and Computer Engineering Department, Duke University, Durham 27708, USA*

Correspondence should be addressed to Yang Liu; yang.liu00@alumnos.upm.es

Received 26 March 2019; Accepted 18 July 2019; Published 7 August 2019

Guest Editor: Benjamin M. Tabak

An increasing number of the renowned company's investors are turning attention to stock prediction in the search for new efficient ways of hypothesizing about markets through the application of behavioral finance. Accordingly, research on stock prediction is becoming a popular direction in academia and industry. In this study, the goal is to establish a model for predicting stock price movement through knowledge graph from the financial news of the renowned companies. In contrast to traditional methods of stock prediction, our approach considers the effects of event tuple characteristics on stocks on the basis of knowledge graph and deep learning. The proposed model and other feature selection models were used to perform feature extraction on the websites of Thomson Reuters and Cable News Network. Numerous experiments were conducted to derive evidence of the effectiveness of knowledge graph embedding for classification tasks in stock prediction. A comparison of the average accuracy with which the same feature combinations were extracted over six stocks indicated that the proposed method achieves better performance than that exhibited by an approach that uses only stock data, a bag-of-words method, and convolutional neural network. Our work highlights the usefulness of knowledge graph in implementing business activities and helping practitioners and managers make business decisions.

1. Introduction

Research on stock market of company prediction has become popular with the introduction of Fama's efficient market hypothesis (EMH) [1], but in recent years, an increasing number of people have found that stock market of the renowned company changes is random, complex, and unstable given that they are affected by many factors. Stock market of company changes is affected by cultural aspects that fundamentally influence investor sentiment; traditional culture often determines people's investment psychology, which in turn, affects the inflow and outflow of stock market capital. Company-related issues, such as the effects of company operations on stock prices and market factors [2]. Using these factors as bases for accurately predicting stock price movement gives investors hope that the maximum profits will be achieved with the least stock investment. Correspondingly, analyzing stock market movements is both challenging and attractive to researchers and investors. Moreover, as the development of knowledge graph in natural language processing (NLP), researchers in the financial field began paying attention to text mining in financial news. As maintained by EMH and artificial intelligence technique, the best results are achieved when news information is used to forecast stock market movement, which can also control financial risk in business activities.

In May 2012, Google formally announced its knowledge graph project, which is aimed at improving the search engines effectiveness and search quality as well as user experience with the engine [3]. The development of knowledge graph promoted the extensive use of artificial intelligence technology in smart search, smart question-and-answer tasks, and intelligent finance. In finance, knowledge graph is designed to find relationships amongst entities, such as the management

of companies, news events, and user preferences. These entities can be used by investors to achieve efficient financial data-based decision-making and obtain business insights into predicting stock market [4]. For these reasons, the current research focused on how to use knowledge graph to improve the accuracy of stock price forecasts. Knowledge graph is databases that implement semantic searches by preserving relationships amongst multiple entities. Based on event tuples in knowledge graph [5], we can infer the definition of an event tuple as *(A, P, O)*, where *A* represents an agent, *P* denotes a predicate, and *O* represents an object [6]. In view of the objects converted by each event tuple are known, when they are converted to vectors, which loses more semantic information. Event tuples link relevant elements together and can be used as an efficient method of improving predictive accuracy. As a result, we propose a learning model of event tuples, which retains their semantic features at the maximum.

Knowledge graph embedding is a kind of representation learning in knowledge graph. Currently, several algorithms [3] explore the mapping relationship between entities and relationships in the translation distance model. The TransE model [7] is a computationally efficient predictive model that satisfactorily represents a one-to-one type of relationship. It has been used as a basis in the development of different translation distance models. The TransH model [8] maps the head and tail of a vector onto a hyperplane, after which these two components complete the translation process on the hyperplane. The TransR model [9], which is based on the TransE model, consists of entities and relationships that are located in different dimensions of space. For each relationship, the model defines a matrix that is used to convert entity vectors into space. The model is also dynamically determined by an entity relationship. The TransD model [10] is an improvement of the TransR model, which the former uses as a basis in considering a transformation matrix. In comparing these models, solving the head and tail of a news tuple for mapping in a single space necessitates the simple mapping of one-to-one entity extraction features. This functionality is found in the TransE model; this study is used to establish a feature combination model for news event metagroups.

This work selects six globally renowned companies to forecast their stock price movement, namely, Apple, Microsoft, Samsung, Boeing, Google, and Walmart as application scenarios. According to different data sources between Thomson Reuters and Cable News Network, we reveal the result of the case studies in some algorithms, which illustrates that the performance of combined feature outperforms that using only stock data, using a bag-of-words algorithm, and using convolutional neural network. Although there are already some examples of the powerful application of deep learning in NLP [11], such as speech recognition, text classification, and machine translation, most of the previous research in predicting stock price movement [12] is based on the semantic information news, which ignores the semantic features of structured events. The application of deep learning and knowledge graph on the renowned companies' stocks is rarely available. Thus, our work provides a viable application framework for financial markets, which can also be extended to other aspects of the financial filed.

For stock market prediction, we formulated a knowledge graph embedding-driven approach that involves four main phases (Figure 1). The first is data retrieval, which begins with searching keywords such as "Apple" or "Google" over the Thomson Reuters or Cable News Network (CNN), as shown in Figure 2. The yellow part is the headline of financial news and the orange part is the release time of the financial news. A web crawler is then used to obtain financial news from the sites and match them with corresponding stock data, combining all this information into one corpus. The second phase involves preprocessing, which encompasses corpus analysis, text normalization, word tokenization, label tagging, and word-to-vector transformation. The features derived from word embeddings and stock data layers are then selected for the computation of eigenvalues, after which a feature vector is generated using machine learning and knowledge graph embedding. The third phase is model creation, in which stock market prediction labels (increase or decrease) are assigned to financial news to training a classification model. Finally, the finance decision relies on the predictive performance of this framework. Specifically, a small improvement directly affects decision-making, which increases the renowned company's profits. The fourth phase involves model evaluation, wherein the results and the extraction of conclusions of each machine learning model are analyzed.

The remaining part of the paper is organized as follows. Section 2 is a review of existing studies on the use of machine learning in stock market prediction. Section 3 introduces the methodology adopted in this study, including the data description and feature selection approach. Section 4 presents the classification results, and Section 5 discusses the results and implications. Section 6 concludes with the summary.

2. Literature Review

In Table 1, the application of machine learning techniques to stock market prediction is an emerging research field. The advantage of machine learning models is their ability to facilitate the processing of large amounts of data. A procedure common to these models is the concatenation of features from different sources into a feature vector. For most machine learning models used, research is focused on predicting stock trends (increase or decrease).

Various feature extractions have already been proposed to predict the stock price of the renowned companies. In the early years, most of the company's stock prediction depends on the empirical analysis of the econometric model, namely, the feature extracted is the raw data of the company's stock. However, the previous work ignored the potential impact of unstructured data on company stocks. Since the bag-of-words is widely utilized in the task of document classification, the frequency of word appearance can be used as a feature of the classification. Hence, the bags of words model only calculate the frequency of words and do not consider the word order or word sparsity in the context, which directly impacts the prediction result. Furthermore, EMH had found that the emotional impulses of the renowned company investors often observe abnormal fluctuations in company stocks.

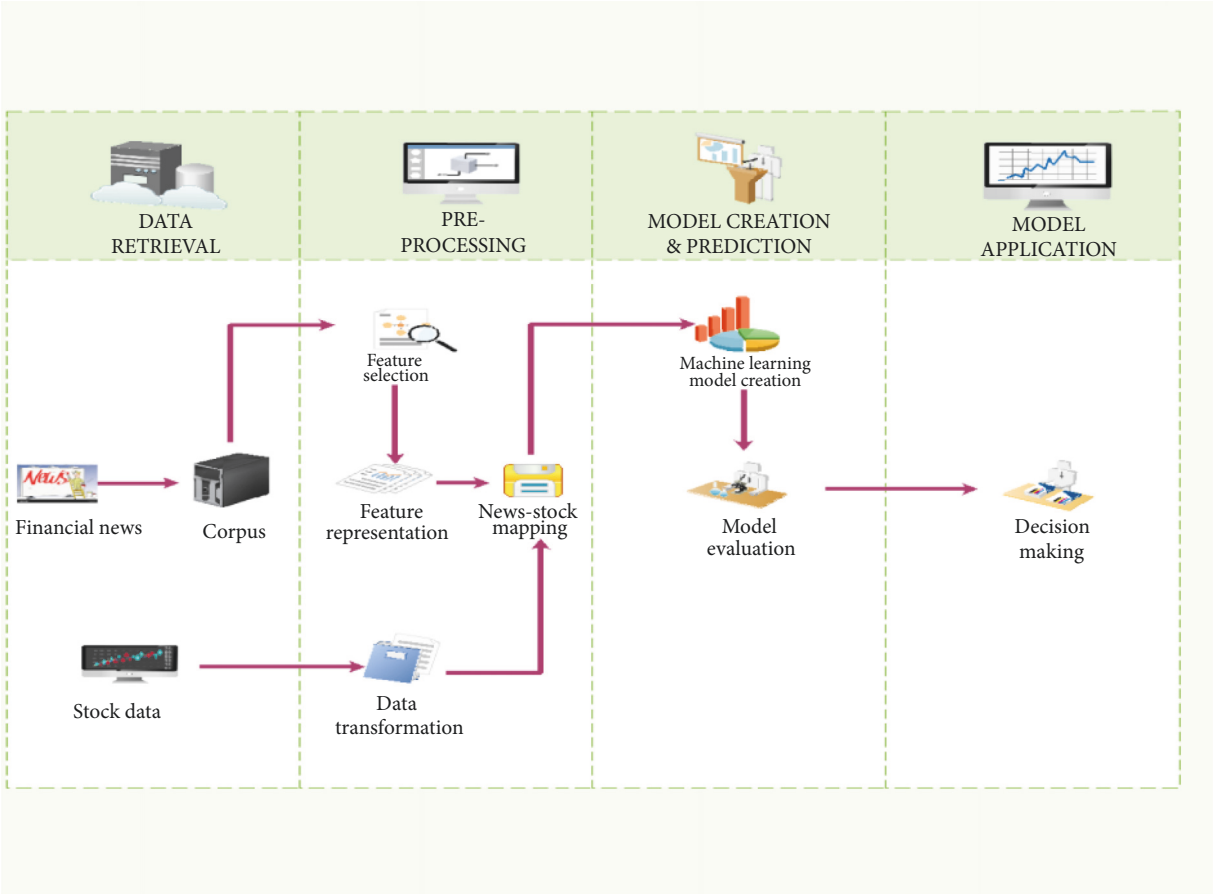

Figure 1: Research workflow for machine learning and knowledge graph.

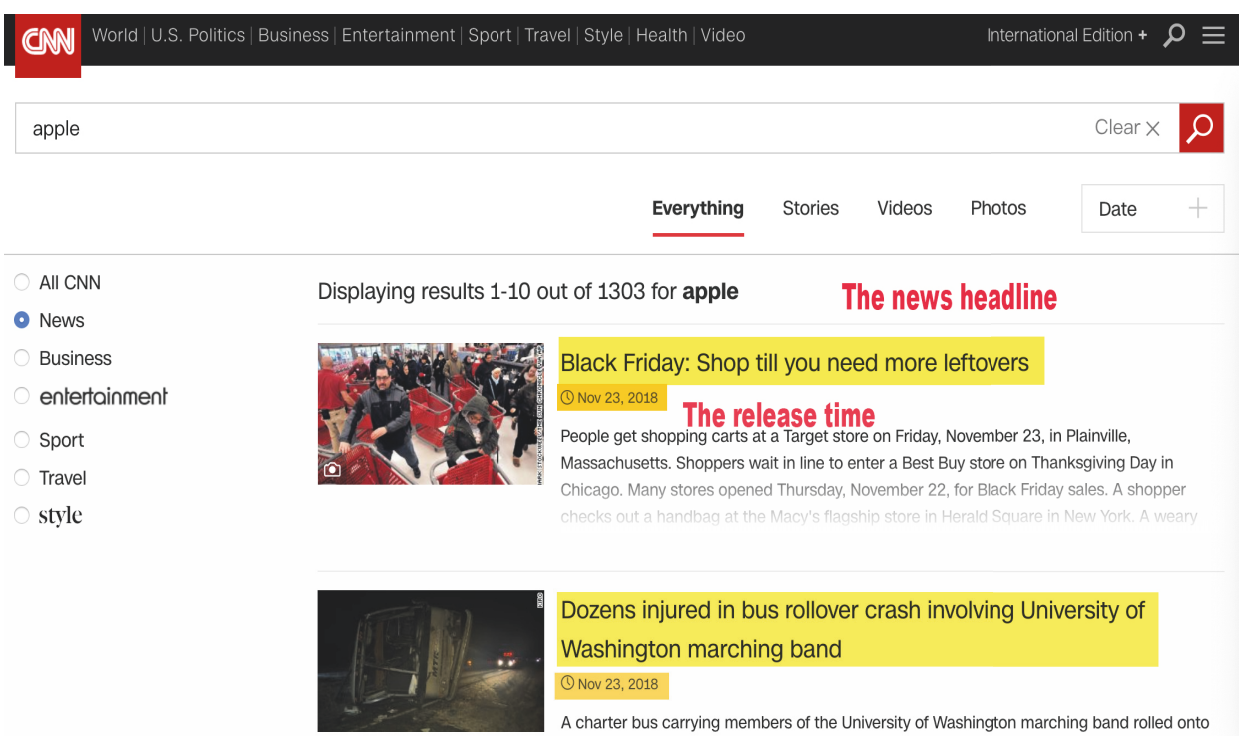

Figure 2: Example of collected financial news in CNN.

Table 1: A review of financial expert system. ANN, NB, KNN, SVM, DT and SVR stand for artificial neural network, naive Bayes, k nearest neighbors, support vector machine, decision tree, and support vector regression, respectively. Measure metrics: mean squared error (MSE); root mean square error (RMSE); area under the curve (AUC).

Paper	Text type	Feature extraction	Model type	Performance measure
[13]	Professional newspaper	Stock data	NB	Accuracy
[14]	Professional newspaper	Stock data	SVM	Accuracy
[15]	Message board	Stock data	Regression	Correlation coefficient
[16]	PRNewswire	Stock data	KNN, SVM	Accuracy, F1-score
[17]	Aggregate news	Stock data, bag-of-words	SVR	MSE, accuracy
[18]	Corporate disclosures	Stock data, bag-of-words	Multiple	Accuracy, recall, precision, F1-score
[19]	Financial news	Stock data, sentiment	DT	Accuracy, recall, precision, F1-score
[20]	Web media	Stock data, bag-of-words.	SVR	Accuracy, recall, precision, F1-score
[21]	Mixed type	Stock data, bag-of-words sentiment,	SVR	RMSE, accuracy, precision
[22]	Message board	Stock data, sentiment	SVM	Accuracy
[23]	Mixed type	Stock data, technical indicators, sentiment	ANN, SVM, DT	Accuracy, AUC, F1-score, precision
[24]	None	Stock data	Regression	Correlation coefficient
[25]	Media news	Stock data	Regression	Correlation coefficient
Our financial expert system	Financial news	Stock data, technical indicators, bag-of-words, syntax	Multiple	Accuracy, F1-score

Tetlock [26] adopted the popular news from the Wall Street Journal to find that news sentiment has predictive power on company stocks. Chen et al. [27] found information comentions have a significant influence on the stock return through sentiment analysis. Furthermore, the investors' sentiment trends after the positive news, which results in a buying trend, and higher stock market prices while after negative news stocks are sold result in a decrease of the price. However, sentiment analysis can only be employed in specific texts. If sentiment is implicit rather than direct emotional words, then the ability of using sentiment analysis for predicting the stock price of the renowned company is relatively limited. Mittermayer and Knolmayer [16] illustrated that news-CATS achieves a performance that is superior to that of other ATC prototypes used to forecast stock price trends. Li et al. [21] proposed a media-aware quantitative trading strategy by using sentiment information on web media. The simulation trading return was up to 166.11%. Nguyen et al. [22] proposed a feature topic sentiment to improve the performance of stock market prediction. Their method achieved an accuracy that is 9.83% better than that of the historical price method and 3.03% better than that of the human sentiment method.

We utilize the characteristics of syntax analysis as being proposed in [6, 12]; namely, a structured tuple is extracted from an unstructured text based on the semantic structure of each piece of news. Knowledge graph can enrich the structured representation of the news event and effectively retain feature vectors for the news event. The main feature extraction in the previous studies [28, 29] is sentiment analysis, which neglected the event characteristics in the text. Furthermore, the existing literature [23, 29] had proved the positive effect of technical indicators on stock market prediction. In summary, our research highlights syntax analysis in financial news, which also incorporates with other features extraction (stock data, technical indicators, and bag-of-words). Because of the variety of considered features, this research will deliver an improved prediction of the stock market value for renowned companies in at least 3.6%.

Previous research [30] was applied with the traditional machine learning algorithms, especially, since the powerful application ability of deep learning based on machine learning. Deep learning is utilized in several studies for predicting stock price movement. Kraus and Feuerriegel [31] forecasted the stock returns based on financial disclosures,

Table 2: Quotes and renowned company names.

Financial news dataset	Stocks	Company names	Time interval	Number of news headlines
Thomson Reuters	AAAL	Apple Inc.	3.10.2011- - -31.7.2017	6423
	MSFT	Microsoft Corporation	30.9.2011- - -29.11.2017	6623
	SSNLF	Samsung Electronics Co., Ltd.	30.9.2011- - -29.11.2017	6900
CNN	BA	The Boeing Company	8.9.1998- - -23.2.2017	2999
	GOOG	Google Inc.	25.5.2006- - -24.2.2017	5278
	WMT	Walmart Inc.	7.5.1997- - -24.2.2017	4913

Table 3: Samples extracted from the dataset.

Date	News headline	News headline event tuple
3/18/2012	Chinese writers' group sues Apple: state media	Chinese writers' group, sues, Apple
4/13/2012	German court upholds ban on Apple push email	German court, upholds ban on, Apple push email
4/4/2012	Apple, two publishers hold out against settlement-report	Apple- two publishers, hold out against, settlement-report
3/26/2012	Apple CEO Cook meets Chinese officials	Apple CEO Cook, meets, Chinese officials
4/25/2012	US STOCKS-Apple results put Nasdaq on track for best gain of year	Apple, results, Nasdaq on track for best gain

and their result demonstrated that a higher directional of deep learning surpasses traditional machine learning. Ding et al. [5] illustrated that deep learning also can forecast stock market of the renowned company. Sim et al. [32] proposed that technical indicators transform into images of the time series graph, which examines the applicability of deep learning in the stock market. Overall, we adopt the multiple models for prediction stock price of the renowned company, which proves the reliability of our proposed model as comparing different algorithms. This work applies deep learning incorporated with knowledge graph embedding for feature extraction, which examines the applicability of combined features methods in the renowned company stock price movement.

3. Materials and Methods

We developed a knowledge graph-based approach that consists of three steps, namely, data description, data preprocessing, and feature selection.

3.1. Dataset Description. Table 2 shows the custom financial news corpus built with headlines from two datasets. The first dataset contains news articles published by Thomson Reuters, including those regarding Apple Inc. (AAPL), Microsoft Corporation (MSFT), and Samsung Electronics Co., Ltd. (SSNLF). The second dataset comprises news reports published in CNN, including reports on the Boeing Company (BA), Google Inc. (GOOG), and Walmart Inc. (WMT). It also consists of financial news headlines published at specific time intervals, with each news report accompanied by a title and a release date. Titles are used for event embedding and feature extraction, and release dates are used as a reference in ensuring alignment between corresponding financial news and trading data from a time series. As shown in previous work [5, 31], using a headline to build corpora can help reduce noise in text mining as headlines concisely represent the content of a text. We used only the news headlines from Reuters and CNN for the prediction of stock price movement.

Daily stock data from index report in each company are collected by Yahoo Finance in the same period during stock data and financial news headlines. Daily trading data, which are common predictors of stock price [23, 33], and technical indicator features were used in our model. There are opening price, closing price, high price, low price, and volume and three technical indicators.

Table 3 shows some examples of filtered financial news headlines. To illustrate, 6423 headlines regarding Apple Inc. were extracted and then reduced to 2799 headlines after filtering via Reverb [34]. Let us take the article "*What is next for Apple's board*?", published on 6 October 2011, as a specific example. The title of the article cannot be transformed into an event tuple using Reverb. Because the sentence is in the interrogative form, there is no event tuple that constitutes a rule. After the matching of time-wise data and stock data, 941 headlines were left. Daily news and stock data were aligned to create input-output pairs, except the days when no news was released. In 9 January 2012, for instance, three news articles were reported, but we chose only one headline for alignment with stock market data. News events possibly happen several times within one day, but they do not happen every day, unlike stock trading, which happens daily, except on nontrading days falling on weekends or holidays.

Table 4 shows that the matches found are pairs between event tuples and stock data. From this complete dataset, we used 80% of the samples in training data and the remaining 20% for testing data. This selection method is the same as the previous literature [5, 24].

Table 4: Training and testing datasets.

Data source	Company	Training	Testing	Total
Reuters	Apple	780	161	941
	Microsoft	832	208	1040
	Samsung	855	214	1069
CNN	Boeing	528	132	660
	Google	1010	252	1262
	Walmart	798	200	998

Table 5: Number of event characteristic labels for each company.

	Companies					
Label	Apple	Microsoft	Samsung	Boeing	Google	Walmart
0	502	967	1433	133	661	206
1	537	432	379	200	245	287
2	661	557	378	152	389	233
3	692	707	724	233	683	438
4	407	228	193	147	196	180
Total	2799	2891	3107	865	2174	1344

Table 6: Features of the prediction model.

	Feature	Feature expression
1	Stock price yesterday + yesterday's trend (in Section 3.3.1)	$price_{t-1}$, $t\_indicator_{t-1}$
2	Same + bag-of-words (in Section 3.3.2)	$price_{t-1}$, $t\_indicator_{t-1}$, tf_idf_{t-1}
3	Same + some features inferred through a convolutional neural network (in Section 3.3.3)	$price_{t-1}$, $t\_indicator_{t-1}$, cnn_{t-1}
4	Same + some features inferred through feature combination (in Section 3.3.4)	$price_{t-1}$, $t\_indicator_{t-1}$, $f\_combine_{t-1}$

3.2. Data Preprocessing. The following three steps are for preprocessing, which prepares for feature extraction and model creation.

(1) Tagging the label for each news headline. Five possible labels are characterized by categorical values as follows: 0 for an extremely negative label, 1 for a negative label, 2 to signify a neutral label, 3 for a positive label, and 4 to denote an extremely positive label. According to the time characteristics of each news headline, an event is manually tagged with the label for each news headline. Table 5 shows the labeling applied for each company: Label 0 means that a company's competitor has happened in this event; label 1 means that the company lost something; label 2 means that it did not cause any impact on the company; label 3 means that this event enabled the company to obtain something; and label 4 means that the company increased its profits or created more value.

(2) Word vector transformation. We used the word2vec [35] algorithm to train word embedding and set the number of dimensions to 300. The word embedding was also trained using the Google News dataset, which contains 100 billion words that are characterized by a continuous bag-of-words structure.

(3) Technical indicators calculation. Three additional technical indicators that are calculated on the basis of daily trading data were used as follows:

(a) Stochastic oscillator (%K). This indicator is a momentum analysis method created by George C. Lane. When the price trend rises, the closing price tends to approach the highest price of the day. When the price trend declines, the closing price tends to approach the lowest price of the day [36].

(b) Larry Williamss %R indicator. This indicator is an oscillation indicator that measures the ratio of the highest price to the daily closing price. It indicates the proportion of stock price fluctuations in a certain period, thereby providing a signal out of the reversal of a stock market trend [37].

(c) Relative strength index (RSI). Buying and selling intentions in the market are analyzed by comparing the closing prices in a given period. Stocks that have had more or stronger positive changes have a higher RSI than do those that have had more or stronger negative changes. Strength indicators fall between 0 and 100; investors sell if this value is ≥ 80 and buy if it is ≤ 20 [23, 36].

3.3. Variable/ Feature Selection. To assess the effectiveness of applying the prediction model on the basis of financial news, we designed four sets of features for predicting stock price movement (Table 6). Features 3 and 4 are used for event characteristics. Each feature is explained in the succeeding subsections. The target output consists of a binary variable, for which a value of 1 indicates that the closing price at day $t + 1$ will be higher than that at day t, and a value of 0 indicates that the closing price at day $t + 1$ will be lower than that at day t.

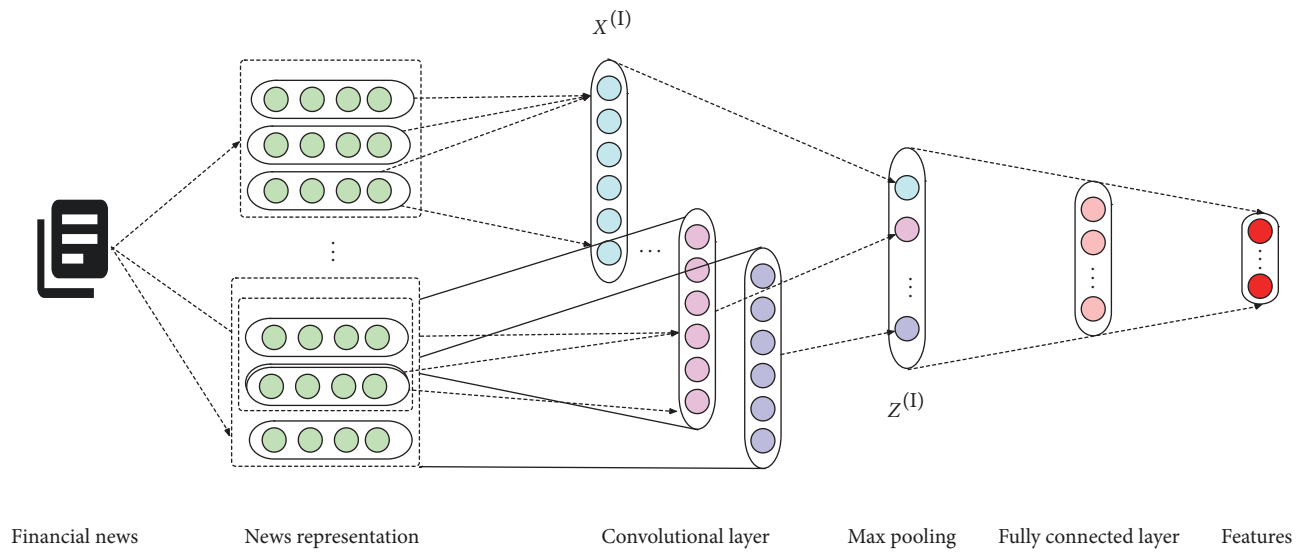

Figure 3: Convolutional neural network architecture proposed for feature selection.

3.3.1. Stock Data Only. We considered historical price as the input for predicting stock price movement and used it as a baseline for comparison with other sets of features. The features used to train the machine learning model that uses only stock data are $price_{t-1}$ and $t\_indicator_{t-1}$. The output is the indicator of price movement (increase or decrease) at each transaction date examined.

3.3.2. Bag of Words. The input feature set is based on a bag of words for the news and price trend for stock. Previous studies [18, 38, 39] have widely used and confirmed the feasibility of the bag-of-words algorithm, but this method disregards elements such as grammar and word order in the text. In the present study, we first prepared each headline for data preprocessing and then transformed the preprocessed headline into a feature vector using the term frequency-inverse document frequency (TF-IDF) algorithm [40], which assigns high weight to eigenvectors. The studies [41, 42] have strongly proven the effectiveness of the TF-IDF algorithm in feature extraction from news headlines. It estimates the frequency of a term in one document over the maximum in a collection of documents and assesses the importance of a word in one set of documents. Such importance increases proportionally with the number of word appearances in a document. The features used to train the bag-of-words machine learning model are $price_{t-1}$, $t\_indicator_{t-1}$, and tf_idf_{t-1}, which are the price movements (increase or decrease) at each transaction date examined.

3.3.3. Convolutional Neural Network. Given the sequence of words in a headline, the word2vec model [35] can be used to embed each of these words in a real valued-vector x. In this work, we set the dimension n of each word vector at 30 (i.e., $x \in \mathbb{R}^{30}$). We concatenated the word vectors of all the words in a headline sequentially to form a matrix $X = [x^{(1)}, x^{(2)}, x^{(3)}, \ldots, x^{(4)}]$ [35] as the input to a convolutional neural network model. For a headline with N words, the resultant input matrix has dimensions of $30 \times N$, and the dimension of news representation also is 30.

In Figure 3, this convolutional neural network model is made up of four consecutive layers: the first layer is the input, the second layer is convolutional, the third layer is a max-pooling, and the last layer is a fully connected layer. The convolutional and max-pooling layers were designed using the text-attentional convolutional neural network [43], which effectively carries out sentiment classification. In the convolutional layer, input matrix X convolves with a kernel $w \in \mathbb{R}^{n \times k}$, where n is the size of a word vector (30 in our work), and its dimension is 50. k denotes the size of a sliding window (k=3 in this study). The computation can be formulated as follows:

$$Z_i = \sigma\left(wX_{i:i+k-1} + b\right), \tag{1}$$

where $X_{i:i+k-1} = [x_i, x_{i+1}, \ldots, x_{i+k-1}]$ is the portion of input X falling within the sliding window, b denotes the optional offset, and $\sigma(\cdot)$ is the sigmoid function.

In the next step, we used the pooling layer to reduce the convolutional neural networks parameter space and consequently minimize information loss in the pooling processing and capture the most important features. The eigenvector of the filter in the pooling layer is cut into 3 chunks and a maximum value is taken in each chunk; we obtained 3 eigenvalues. Convolutional output vector Z was split into p windows, and only the maximum feature as 3 in each window was kept for passage onto the final fully connected layer. The fully connected layer is linear regression, and the output layer is the feature classification between 0 and 1.

Our convolutional neural network model is intended to extract a feature vector from the fully connected layer to describe the emotional characteristics of input headlines. Following the intuition that a good feature vector should lead to the accurate classification of the event characteristics of headlines, we attached a softmax layer after the fully

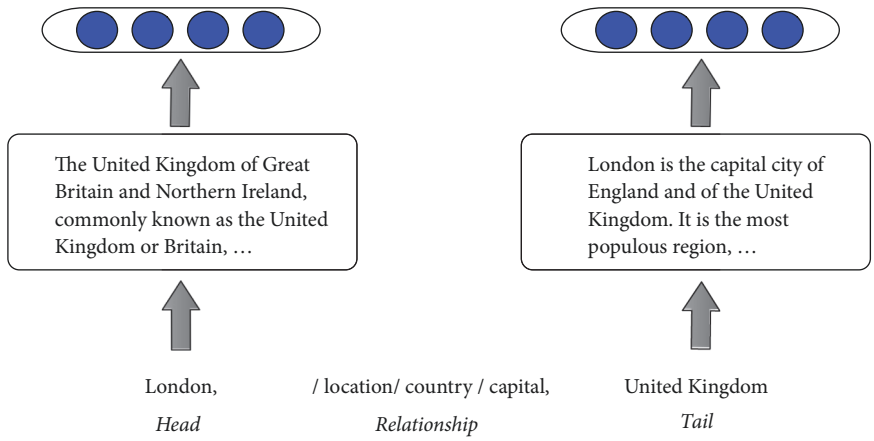

Figure 4: Text description of the entity.

connected layer when the convolutional neural network model was trained. The entire model was trained to classify the five emotional labels that describe event characteristics, and the resultant model will be able to provide a meaningful emotional feature vector for each inputted headline. Meanwhile, we define the loss function of the convolutional neural network model as E_d. The features used to train this machine learning model are $price_{t-1}$, $t\_indicator_{t-1}$, and cnn_{t-1}, which are the price movements (increase or decrease) at corresponding transaction date.

3.3.4. Combined Features. In the introduction section of this paper, we described various translation models. Because the TransE model represents a one-to-one relationship between two entities [7], the relationship amongst many entities must be continuously incorporated into texts and knowledge graph [44]. This model combines a convolutional neural network with textual information extraction, which fully exploits the semantic information in a knowledge graph and text [45, 46]. In Figure 4, knowledge graph contains rich semantics in entity description texts, but it is not fully utilized in feature extraction. Most of the existing text representation models simply train the text into word vectors through word2vec, which obtains the text representation by means of averaging, etc. Hence, these ways often lose more semantic information. We therefore proposed to extract feature vectors from news texts using a convolutional neural network model combined with the TransE model, which also fully integrates the two parts of the feature information.

In Figure 5, this architecture used in the feature combination model encompasses two parts, namely, a convolutional neural network (Section 3.3.3) and the TransE model. The feature combination sets are the average of each word vector in an entity and it was obtained using the word2vec model. The two entity vectors are mapped into the same relational space, and these entities using a trained low-rank weight matrix [47].

As assumed in the TransE model, relationship vector R should satisfy "$E + R \approx T$". The model can be represented as a parameter set $\emptyset = (L_r, R_r, \theta)$, where X, E, and R represent a word, an entity, and a relation, respectively. And r are the mapping matrices for entities in the structural model and represents the weights of the convolutional neural network. For instance, the sentence is "*Samsung sues Apple for infringement*", so "*Samsung* + *Apple* ≈ *sues*". The loss function E_s of this structural model is defined as follows:

$$E_s = \|h + r - t\|_2^2, \tag{2}$$

where h, r, and t represent head entity, relationship, and tail entity in event tuple, respectively [47].

And text representation E_d is consistent with Section 3.3.3, which denotes:

$$E_d = f_r(h_s, t_d) + f_r(h_d, t_s) + f_r(h_d, t_d), \tag{3}$$

where $f_r(h_d, t_d) = \|h_d + r - t_d\|_2^2$ represents the head entity and the tail entity is in text representation. $f_r(h_d, t_s) = \|h_d + r - t_s\|_2^2$ and $f_r(h_s, t_d) = \|h_s + r - t_d\|_2^2$ represent one of the head entity h and the tail entity t in text representation, another one is in structure representation.

Moreover, we combined two types of representation learning (convolutional neural network and feature combination) to map news titles; these vectors will be into feature vectors. The relationship vector R identical to the result of the feature extraction layer of the convolutional neural network in the structural model. Besides, we combined this loss with the classification loss of the convolutional neural network using $L2$ regularization, which obtains the overall loss function E for feature selection, that is,

$$E = E_s + \alpha E_d + \beta \|\emptyset\|^2, \tag{4}$$

where $\|\emptyset\|^2$ is a regular item. α and β are hyperparameters, which measure the loss of text information and the weight of the regular items, respectively. W denotes the convolutional kernels in the layer and T' is a negative sample set of T [7].

$$\begin{aligned} T' = &\left\{\left(h', r, t\right) \mid h' \in E\right\} \cup \left\{\left(h, r, t'\right) \mid t' \in E\right\} \\ &\cup \left\{\left(h, r', t\right) \mid r' \in R\right\}, \end{aligned} \tag{5}$$

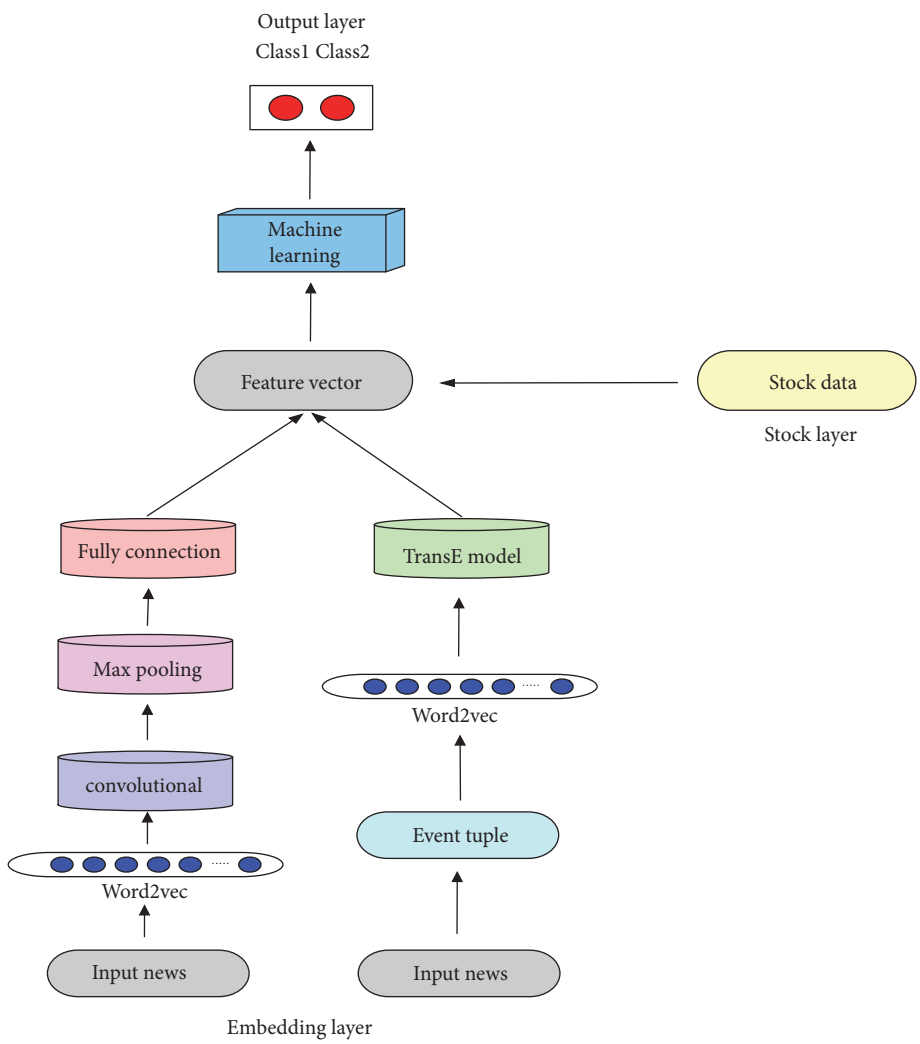

Figure 5: Proposed architecture for the feature combination model.

where the head entity and tail entity are randomly replaced by an entity or relationship in another tuple. In particular, if the replaced tuple is already in T, it would not be added to the negative sample. Since both h and t represent two types of entities, there are structure-based representations and text-based representations in interval-based loss functions. The stochastic gradient descent (SGD) is employed to minimize the above loss function.

In this structure, we choose the optimal parameters as followe: the learning rate of SGD $\lambda = 0.001$, the dimension of the representation vector of entities and relationships $k = 100$, the word vector dimension of the entity description text $n = 100$, and batch size during training is 1440. Convolution layer window size is $W \in \{1, 2, 3\}$. This experiment is performed in 1000 iterations of training and the optimal parameters are based on the testing set.

Hence, the features used for training the machine learning model are $price_{t-1}$, $t\_indicator_{t-1}$, and $f\_combine_{t-1}$, which are the price movement (increase or decrease) at corresponding transaction date.

4. Experiments and Results

4.1. Experimental Setting. This section compares the performance of different models in feature extraction from financial news expended with full sets of features. The evaluation was intended to obtain evidence that the proposed feature combination model is superior to other feature selection models in predicting the stock price movement. As shown in Table 7, we chose linear models, for instance, logistical regression and naive Bayes. Others are nonlinear models, for instance, the ensemble learning (random forest, adaboost, and gradient boosting) for the comparison. We constantly adjusted the parameters in the grid search and selected the optimal parameter value; their parameter value has proven to work well on machine learning method [29, 48].

We used a computer consisting of an Intel Core i5 processor with four cores running at 2.9 GHz and 8 GB RAM under the MacOS platform. We used the Scikit-learn library in Python in the experiments involving traditional machine learning algorithms and TensorFlow 1.4 in the

Table 7: List of machine learning methods.

Method	Classification	Parameter and their value
Traditional machine learning	Decision tree (DT)	Criterion= gini, splitter= best, max depth=None, min samples split=2, min samples leaf =1, min weight fraction leaf=0.0,
	Logistical regression (LR)	Random state=1
	Naive Bayes (NB)	No kernel estimator
	Stochastic gradient descent (SGD)	Loss=hinge, penalty=l2
	Support vector machine (SVM)	Polynomial kernel function with exponent = {1, 2}, RBF kernel function with gamma = 0.01
Ensemble learning	Random forest (RF)	Randomly sampled as candidates at each split = log2 + 1, max-depth=2, random state=0
	AdaBoost (AB)	Polynomial kernel function with exponent = {1, 2}, RBF kernel function with gamma = 0.01, n- estimators=100
	Gradient boosting (GB)	N-estimators =100, learning rate =1.0, max-depth=1, random state=0

Table 8: Abbreviations of the results for each algorithm considered.

Algorithms	Stock data (SD)	Bag of words (BOW)	Convolutional neural network	Feature combination model (FC)
DT	*DT_1*	*DT_2*	*DT_3*	*DT_4*
LR	*LR_1*	*LR_2*	*LR_3*	*LR_4*
NB	*NB_1*	*NB_2*	*NB_3*	*NB_4*
SGD	*SGD_1*	*SGD_2*	*SGD_3*	*SGD_4*
SVM	*SVM_1*	*SVM_2*	*SVM_3*	*SVM_4*
RF	*RF_1*	*RF_2*	*RF_3*	*RF_4*
AB	*AB_1*	*AB_2*	*AB_3*	*AB_4*
GB	*GB_1*	*GB_2*	*GB_3*	*GB_4*

experiments involving deep learning and the TransE model. The abbreviations used for comparing classification performance are presented in Table 8. During testing, 2-fold cross-validation is applied to evaluate the stability of the models. And we compared performance in predicting stock price movement for the next day with a test dataset and evaluated the performance of the models in terms of accuracy and F1-score [49].

4.2. Results

4.2.1. Thomson Reuters Case Study. Thomson Reuters is a multinational mass media and information firm. Three renowned companies on the website were selected for the analysis. The first is Apple Inc., which is an American multinational technology company that designs, develops, and sells consumer electronics, computer software, and online services. The second company selected is Microsoft, which is an American multinational technology company that develops, manufactures, supports, and sells computer software, personal computers, and other services. The last company chosen is Samsung, which is a South Korean multinational electronics company. We considered data from these three typical technology companies for our problem.

Measurements of average accuracy are shown in Table 9, and the results for each renowned company with respect to prediction based on different features are illustrated in Figure 6. We calculated the average of the four feature construction approaches for each model for comparison amongst the three companies. The proposed feature combination model generated the best results, achieving average accuracy levels of 61.63%, 59.18%, and 58.48% for Apple, Microsoft, and Samsung, respectively. These figures are consistent with the rates reported in previous research. However, many studies analyzed only one company or used only one algorithm. The current research probed into three companies on the basis of information from a common data source to build a prediction model with different feature selection functionalities and different algorithms. We used stock data, a bag-of-words algorithm, a convolutional neural network, and feature combination, together with eight algorithms. As indicated in Table 9, the proposed prediction model achieved 73.68% data extraction with the use of *LR_4* for Apple and 67.78% data extraction with the use of *SVM_4* for Microsoft. In particular, the LR algorithm used for Apple achieved accuracy and F1-score of 0.7326 and 0.7360, respectively, which highlights its powerful capability in a two-class classification.

Table 9: Results for data extracted from Thomson Reuters.

Algorithm	Company	Stock data (SD)	Bag of words (BOW)	Convolutional neural network	Feature combine model (FC)
		Accuracy/F1-score	Accuracy/F1-score	Accuracy/F1-score	Accuracy/F1-score
DT	Apple	0.4993/0.5079	0.4889/0.2460	0.6150/0.5814	0.6524/0.6486
	Microsoft	0.4868/0.1819	0.5065/0.5682	0.5817/0.5915	0.6587/0.6502
	Samsung	0.4707/0.4033	0.5654/0.5830	0.5529/0.6820	0.5680/0.6260
LR	Apple	0.5240/0.6727	0.5055/0.5083	0.6845/0.6911	0.7326/0.7368
	Microsoft	0.4757/0.1253	0.4430/0.4884	0.5274/0.5333	0.5467/0.5611
	Samsung	0.4947/0.3755	0.6054/0.6726	0.6541/0.6343	0.8053/0.7978
NB	Apple	0.5109/0.5123	0.4778/0.3896	0.5027/0.4497	0.5122/0.4030
	Microsoft	0.4840/0.0363	0.4557/0.4055	0.4599/0.2889	0.5000/0.5439
	Samsung	0.5293/0.5810	0.5144/0.6130	0.5048/0.6578	0.5117/0.6601
SGD	Apple	0.4672/0.1119	0.4778/0.4404	0.4974/0.6008	0.5366/0.2692
	Microsoft	0.5173/0.6819	0.4852/0.3222	0.6103/0.4231	0.6108/0.4193
	Samsung	0.5223/0.6541	0.4766/0.2000	0.5187/0.6751	0.5571/0.6548
SVM	Apple	0.5022/0.6121	0.5747/0.5542	0.6150/0.6129	0.6220/0.6173
	Microsoft	0.4784/0.1722	0.4439/0.4566	0.5232/0.5462	0.6875/0.6798
	Samsung	0.5008/0.3875	0.5047/0.5508	0.5135/0.6281	0.5352/0.6574
RF	Apple	0.5240/0.6554	0.5278/0.6083	0.5337/0.6232	0.6203/0.6243
	Microsoft	0.4840/0.2653	0.4177/0.1687	0.5325/0.2432	0.5721/0.5189
	Samsung	0.4872/0.3480	0.4485/0.1194	0.4766/0.3708	0.5052/0.5481
AB	Apple	0.5343/0.5384	0.4722/0.2963	0.4819/0.3333	0.6203/0.5420
	Microsoft	0.4687/0.2041	0.4768/0.0461	0.6147/0.6044	0.6202/0.6146
	Samsung	0.4857/0.3619	0.4579/0.2368	0.6010/0.6820	0.6338/0.6549
GB	Apple	0.5314/0.5129	0.4667/0,2941	0.6096/0.4748	0.6341/0.6591
	Microsoft	0.4743/0.2125	0.4728/0.1007	0.4557/0.4557	0.5385/0.2258
	Samsung	0.4872/0.4171	0.5192/0.6599	0.5337/0.6572	0.5622/0.6335

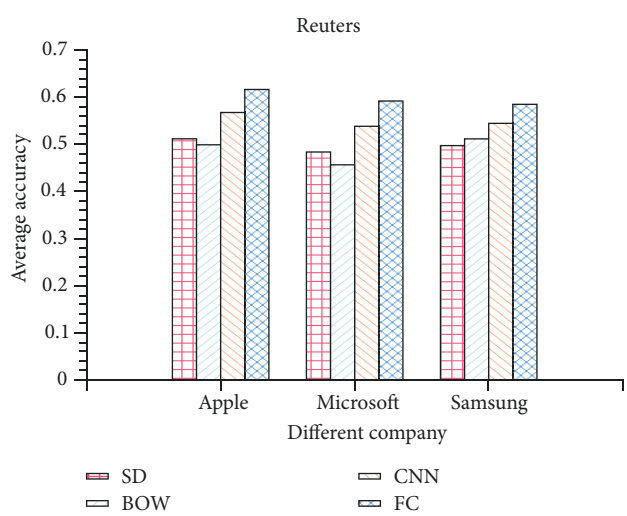

Figure 6: Average accuracy of prediction based on different feature sets for each company in Reuters.

To assess the effectiveness of our research, we compared the feature combination model that uses event tuples with the stock data approach and the bag-of-words algorithm. The results showed that the average accuracy of the event tuple-based model is better than that of the stock data approach and the bag-of-words algorithm by 10.01% and 10.87%, respectively. We also compared feature extraction using the stock data approach, the bag-of-words algorithm, and machine learning. The use of deep learning improved prediction accuracy by 5.25% and 6.11% over the levels achieved with stock data and bag of words, respectively. Therefore, we can conclude that using the proposed feature combination model and deep learning in feature extraction helps improve the accuracy with which stock price movement is predicted. These results also fully prove the effectiveness of embedding layer in feature extraction accuracy improvement.

4.2.2. CNN Case Study. CNN is an American basic cable and satellite television news channel owned by the Turner Broadcasting System. Three renowned companies on which these website reports were selected for the analysis. The first is Boeing, which is an American multinational corporation that designs, manufactures, and sells airplanes, rotorcraft, rockets, and satellites worldwide. The second company is Google, which is an American multinational technology

Table 10: Results for data extracted from CNN.

Algorithm	Company	Stock data (SD)	Bag of words (BOW)	Convolutional neural network	Feature combination model (FC)
		Accuracy/F1-score	Accuracy/F1-score	Accuracy/F1-score	Accuracy/F1-score
DT	Boeing	0.4950/0.3489	0.5413/0.6258	0.5414/0.6347	0.5591/0.5821
	Google	0.4858/0.5600	0.5182/0.3575	0.5692/0.4631	0.5491/0.5471
	Walmart	0.4996/0.4422	0.5300/0.4891	0.5088/0.4815	0.5722/0.5829
LR	Boeing	0.4923/0.2378	0.5113/0.4348	0.6923/0.6923	0.7596/0.5733
	Google	0.5041/0.6105	0.6235/0.6491	0.6250/0.6111	0.6563/0.6516
	Walmart	0.5290/0.5468	0.5412/0.5083	0.7320/0.7347	0.7719/0.7720
NB	Boeing	0.5162/0.6503	0.5489/0.5161	0.5197/0.6738	0.5564/0.7619
	Google	0.5112/0.6527	0.4899/0.5191	0.5587/0.5281	0.5344/0.4843
	Walmart	0.5044/0.3284	0.4794/0.5302	0.5206/0.5674	0.5300/0.6083
SGD	Boeing	0.4897/0.2407	0.5564/0.4870	0.5433/0.4727	0.5714/0.7220
	Google	0.5165/0.6769	0.5425/0.4375	0.5789/0.6364	0.5910/0.6327
	Walmart	0.5004/0.3804	0.5206/0.5280	0.5250/0.5581	0.5670/0.5922
SVM	Boeing	0.4897/0.3068	0.5714/0.6275	0.5385/0.6418	0.5940/0.7033
	Google	0.5077/0.6297	0.6032/0.6230	0.5749/0.5532	0.5789/0.5840
	Walmart	0.5118/0.4333	0.5000/0.5314	0.5200/0.5000	0.5614/0.5455
RF	Boeing	0.4906/0.1345	0.5113/0.3925	0.5096/0.5405	0.5276/0.5714
	Google	0.4923/0.1777	0.6032/0.6260	0.5223/0.5564	0.5951/0.5763
	Walmart	0.5118/0.5373	0.5300/0.3188	0.5300/0.4405	0.5000/0.5446
AB	Boeing	0.4945/0.3404	0.5197/0.5120	0.4961/0.5294	0.5673/0.5872
	Google	0.4876/0.3141	0.5101/0.6667	0.5893/0.5619	0.5951/0.6850
	Walmart	0.5073/0.5029	0.5150/0.5359	0.5497/0.5650	0.5619/0.5503
GB	Boeing	0.4899/0.3169	0.5118/0.4364	0.4409/0.4580	0.5000/0.5094
	Google	0.4912/0.3387	0.5870/0.5854	0.5625/0.5243	0.6032/0.6202
	Walmart	0.5003/0.4955	0.5050/0.5123	0.5361/0.5109	0.5497/0.5650

company that specializes in Internet-related services and products. The third is Walmart, an American multinational retail corporation that operates a chain of hypermarkets, discount department stores, and grocery stores.

The results on average accuracy are shown in Table 10 and Figure 7. These findings are very similar to those derived in the previous case study, and their comparison confirmed that the proposed feature combination model can outperform other feature selection models in stock price movement prediction. With regard to feature selection underlain by the bag-of-words algorithm, the CNN case study generated more robust results than did the Reuters case study. The average accuracy of the bag-of-words algorithm was lower than that of the stock data approach in the Reuters case study. In the CNN case study, the average accuracy levels of the proposed feature combination model were 57.94%, 58.79%, and 57.67% for Boeing, Google, and Walmart, respectively. In the case study on Reuters, an average accuracy that exceeds 60% was not achieved for any of the companies, illustrating that differences in data source directly affect stock price movement.

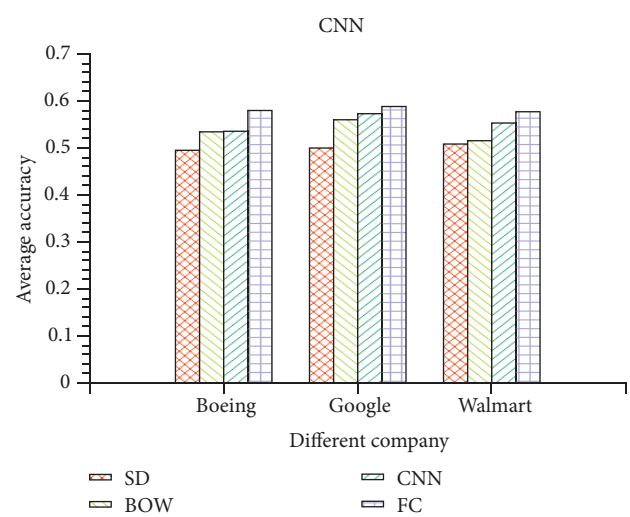

Figure 7: Average accuracy achieved on the basis of news from CNN and different feature set.

We chose a combination of deep learning and knowledge graph to build our feature selection model because this combination exhibited superior prediction performance in the comparison experiments involving other feature selection

strategies. The forecast results based on different features are shown in Table 10. We found that deep learning features are better than the use of bag-of-words and stock data. The correlation of event tuples with the stock market is relatively high in [5, 31], but the bag-of-words algorithm was relatively fragmented, and the correlation between event tuples and the stock market data was relatively weak. Combining event tuple features with deep learning significantly improves forecast results, indicating a close relationship between stock market movements and knowledge graph.

5. Discussion

5.1. Research Findings. We attempted to compare our prediction results with those made in previous studies wherein prediction was also based on the financial news of the renowned companies. However, the findings are incomparable because different studies use different datasets or algorithms, and these methods are difficult to investigate using financial news headlines. In the current research, we refrained from evaluating performance on one company dataset, this decision that enabled our knowledge graph method to exceed baseline predictions based only on the price by up to 3.6%. This also proves that feature extraction in deep learning is more effective than traditional machines. The combination of deep learning and knowledge graph fully integrates the semantic information in financial news, which effectively predicts the stock price movement of the renowned company.

This work demonstrated the application of deep learning and knowledge graph in finance. To the best of our knowledge, knowledge graph has been rarely applied in stock prediction. Because minimal financial training sets in knowledge graph are available, financial knowledge extraction is the main task for the organizational construction of a knowledge graph. Such extraction is critical for the understanding and processing of deep semantics in the event tuple, which also directly influences the feature extraction of financial news.

5.2. Implications for Business Activities. The utility of a feature combination model based on knowledge graph is not limited to financial analysis. Currently, knowledge graph data are available for medical diagnosis, speech recognition, precise marketing, and financial risk control [4]. Our model could also be applied in these areas.

Antifraud activities are an important part of finance. Applying our model on the basis of knowledge graph on customers helps organize all relevant knowledge fragments through deep semantic analysis and reasoning, which can be verified with a customer's bank information. Moreover, customers typically use keywords to search for products, and knowledge graph can provide relevant information to a customer. If a complete knowledge system of users is described and collected, a system would better understand and analyze user behaviors.

5.3. Limitations and Future Work. A deep learning model uses supervised learning and needs a dataset with sufficient labels, but our datasets do not work well with deep learning as a small number of financial news articles match stock data. At present, knowledge graph embedding inevitably produces a loss in news semantics, either because of a learning principle or the tokenization of knowledge representation for vectorization. Thus, continuous representation in a knowledge graph is still a huge challenge. We attempted to apply regression using the above-mentioned algorithms, but the results indicated poor performance. More specifically, the results for Apple validated our expectations.

The application of large-scale knowledge graph is still relatively limited, and knowledge graph for smart search, smart question-and-answer tasks, social media, and other areas are in their initial stages, with considerable room for improvement. The following advantages of knowledge graph should be considered: (a) the effective organization and expression of semistructured data, (b) knowledge reasoning, and (c) the expansion of cognitive ability for incorporating deep learning. Traditional knowledge elements (entities, relationship, attributes), extraction technologies, and methods have achieved good results in limited areas, but because of numerous constraints and poor scalability, knowledge graph is not fully functional for financial forecasting because of numerous constraints and poor scalability.

6. Conclusions

Stock movement prediction of the renowned company is a daunting task because stock prices are affected by many factors. This research presented a novel method for integrating knowledge graph embedding with stock market prediction. The contributions of this study can be summarized as follows. First, we developed a novel feature combination model that constructs a feature mapping vector for each tuple–news pair by simultaneously considering the diversity of entities and relationships. Second, the feature combination model was successfully applied to different types of companies and datasets and exhibited good performance in classification tasks.

Stock market prediction of the renowned company grounded in knowledge graph is an interesting topic for business activities. Given that the study of knowledge graph for feature set is still in its infancy, we expect it to be applied in a wide range of academic research. More companies will also earn profits and create more opportunities through the use of knowledge graph in the feature set.

Data Availability

The data used in this study can be accessed via https://github.com/linechany/knowledge-graph.

Conflicts of Interest

The author declares that there is no conflict of interest regarding the publication of this paper.

Acknowledgments

This work is supported by the China Scholarship Council (CSC) throughout the grant number: 201508390019. The

authors also want to thank the research program RFCS from the EU, which partially supported this research through the research project AutoSurveillance, with project ID 847202.

References

[1] B. G. Malkiel and E. F. Fama, "Efficient capital markets: a review of theory and empirical work," *The Journal of Finance*, vol. 25, no. 2, pp. 383–417, 1970.

[2] D. Galai and R. W. Masulis, "The option pricing model and the risk factor of stock," *Journal of Financial Economics*, vol. 3, no. 1-2, pp. 53–81, 1976.

[3] Q. Wang, Z. Mao, B. Wang, and L. Guo, "Knowledge graph embedding: A survey of approaches and applications," *IEEE Transactions on Knowledge and Data Engineering*, vol. 29, no. 12, pp. 2724–2743, 2017.

[4] H. Paulheim and P. Cimiano, "Knowledge graph refinement: A survey of approaches and evaluation methods," *Journal of Web Semantics: Science, Services and Agents on the World Wide Web*, vol. 8, no. 3, pp. 489–508, 2016.

[5] X. Ding, Y. Zhang, T. Liu, and J. Duan, "Deep learning for event-driven stock prediction," in *Proceedings of the 24th International Joint Conference on Artificial Intelligence, IJCAI 2015*, pp. 2327–2333, Argentina, July 2015.

[6] X. Ding, Y. Zhang, T. Liu, and J. Duan, "Knowledge-driven event embedding for stock prediction," in *Proceedings of the 26th International Conference on Computational Linguistics, COLING 2016*, pp. 2133–2142, Japan, December 2016.

[7] A. Bordes, N. Usunier, J. Weston, and O. Yakhnenko, "Translating embeddings for modeling multi-relational data," *Advances in NIPS*, vol. 26, pp. 2787–2795, 2013.

[8] H. Lin, Y. Liu, W. Wang, Y. Yue, and Z. Lin, "Learning entity and relation embeddings for knowledge resolution," *Procedia Computer Science*, vol. 108, pp. 345–354, 2017.

[9] G. Ji, K. Liu, S. He, and J. Zhao, "Knowledge graph completion with adaptive sparse transfer matrix," in *Proceedings of the 30th AAAI Conference on Artificial Intelligence, AAAI 2016*, pp. 985–991, USA, February 2016.

[10] G. Ji, S. He, L. Xu, K. Liu, and J. Zhao, "Knowledge graph embedding via dynamic mapping matrix," in *Proceedings of the 53rd Annual Meeting of the Association for Computational Linguistics and the 7th International Joint Conference on Natural Language Processing (Volume 1: Long Papers)*, pp. 687–696, Beijing, China, July 2015.

[11] Y. LeCun, Y. Bengio, and G. Hinton, "Deep learning," *Nature*, vol. 521, no. 7553, pp. 436–444, 2015.

[12] Q. Li, Y. Chen, J. Wang, and H. Chen, "Web media and stock markets: a survey and future directions from a big data perspective," *IEEE Transactions on Knowledge and Data Engineering*, vol. 4347, p. 1, 2017.

[13] B. Wuthrich, V. Cho, S. Leung, D. Permunetilleke, K. Sankaran, and J. Zhang, "Daily stock market forecast from textual Web data," in *Proceedings of the 1998 IEEE International Conference on Systems, Man, and Cybernetics (Cat. No.98CH36218), SMC'98*, vol. 3, pp. 2720–2725, October 1998.

[14] G. Pui Cheong Fung, J. Xu Yu, and W. Lam, "Stock prediction: integrating text mining approach using real-time news," in *Proceedings of the 2003 IEEE International Conference on Computational Intelligence for Financial Engineering, CIFEr 2003*, vol. 2003, pp. 395–402, China, March 2003.

[15] W. Antweiler and M. Z. Frank, "Is all that talk just noise? the information content of internet stock message boards," *SSRN Electronic Journal*, 2001.

[16] M.-A. Mittermayer and G. F. Knolmayer, "NewsCATS: A news categorization and trading system," in *Proceedings of the 6th International Conference on Data Mining, ICDM 2006*, pp. 1002–1007, China, December 2006.

[17] R. P. Schumaker and H. Chen, "Textual analysis of stock market prediction using breaking financial news: the AZFin text system," *ACM Transactions on Information and Systems*, pp. 1–29, 2009.

[18] S. S. Groth and J. Muntermann, "An intraday market risk management approach based on textual analysis," *Decision Support Systems*, vol. 50, no. 4, pp. 680–691, 2011.

[19] T. Vu, S. Chang, Q. Ha, and N. Collier, "An experiment in integrating sentiment features for tech stock prediction in twitter," in *Proceedings of the Workshop on Information Extraction And Entity Analytics on Social Media Data*, vol. 3, pp. 23–38, 2012.

[20] B. Wang, H. Huang, and X. Wang, "A novel text mining approach to financial time series forecasting," *Neurocomputing*, vol. 83, pp. 136–145, 2012.

[21] Q. Li, T. Wang, P. Li, L. Liu, Q. Gong, and Y. Chen, "The effect of news and public mood on stock movements," *Information Sciences*, vol. 278, pp. 826–840, 2014.

[22] T. H. Nguyen, K. Shirai, and J. Velcin, "Sentiment analysis on social media for stock movement prediction," *Expert Systems with Applications*, vol. 42, no. 24, pp. 9603–9611, 2015.

[23] B. Weng, M. A. Ahmed, and F. M. Megahed, "Stock market one-day ahead movement prediction using disparate data sources," *Expert Systems with Applications*, vol. 79, pp. 153–163, 2017.

[24] J. Eberhard, J. F. Lavin, and A. Montecinos-Pearce, "A network-based dynamic analysis in an equity stock market," *Complexity*, vol. 2017, Article ID 3979836, 16 pages, 2017.

[25] Z. Zhang, Y. Zhang, D. Shen, and W. Zhang, "The dynamic cross-correlations between mass media news, new media news, and stock returns," *Complexity*, vol. 2018, 11 pages, 2018.

[26] P. C. Tetlock, "Giving content to investor sentiment: The role of media in the stock market," *Journal of Finance*, vol. 62, no. 3, pp. 1139–1168, 2007.

[27] K. Chen, P. Luo, L. Liu, and W. Zhang, "News, search and stock co-movement: Investigating information diffusion in the financial market," *Electronic Commerce Research and Applications*, vol. 28, pp. 159–171, 2018.

[28] F. Z. Xing, E. Cambria, and Y. Zhang, "Sentiment-aware volatility forecasting," *Knowledge-Based Systems*, vol. 176, pp. 68–76, 2019.

[29] A. Picasso, S. Merello, Y. Ma, L. Oneto, and E. Cambria, "Technical analysis and sentiment embeddings for market trend prediction," *Expert Systems with Applications*, vol. 135, pp. 60–70, 2019.

[30] A. Khadjeh Nassirtoussi, S. Aghabozorgi, T. Ying Wah, and D. C. L. Ngo, "Text mining for market prediction: a systematic review," *Expert Systems with Applications*, vol. 41, no. 16, pp. 7653–7670, 2014.

[31] M. Kraus and S. Feuerriegel, "Decision support from financial disclosures with deep neural networks and transfer learning," *Decision Support Systems*, vol. 104, pp. 38–48, 2017.

[32] H. S. Sim, H. I. Kim, and J. J. Ahn, "Is deep learning for image recognition applicable to stock market prediction?" *Complexity*, vol. 2019, 10 pages, 2019.

[33] M. Jasemi, A. M. Kimiagari, and A. Memariani, "A modern neural network model to do stock market timing on the basis of the ancient investment technique of Japanese candlestick," *Expert Systems with Applications*, vol. 38, no. 4, pp. 3884–3890, 2011.

[34] A. Fader, S. Soderland, and O. Etzioni, "Identifying relations for open information extraction," in *Proceedings of the Conference on Empirical Methods in Natural Language Processing, EMNLP 2011*, pp. 1535–1545, Association for Computational Linguistics, UK, July 2011.

[35] T. Mikolov, K. Chen, G. Corrado, and J. Dean, "Efficient estimation of word representations in vector space," pp. 1–12, 2013, https://arxiv.org/abs/1301.3781.

[36] X. Lin, Z. Yang, and Y. Song, "Intelligent stock trading system based on improved technical analysis and Echo State Network," *Expert Systems with Applications*, vol. 38, no. 9, pp. 11347–11354, 2011.

[37] K.-J. Kim and I. Han, "Genetic algorithms approach to feature discretization in artificial neural networks for the prediction of stock price index," *Expert Systems with Applications*, vol. 19, no. 2, pp. 125–132, 2000.

[38] Y. Yu, W. Duan, and Q. Cao, "The impact of social and conventional media on firm equity value: A sentiment analysis approach," *Decision Support Systems*, vol. 55, no. 4, pp. 919–926, 2013.

[39] M. Hagenau, M. Liebmann, and D. Neumann, "Automated news reading: Stock price prediction based on financial news using context-capturing features," *Decision Support Systems*, vol. 55, no. 3, pp. 685–697, 2013.

[40] A. Aizawa, "An information-theoretic perspective of tf-idf measures," *Information Processing & Management*, vol. 39, no. 1, pp. 45–65, 2003.

[41] A. Khadjeh Nassirtoussi, S. Aghabozorgi, T. Ying Wah, and D. C. Ngo, "Text mining of news-headlines for FOREX market prediction: a Multi-layer dimension reduction algorithm with semantics and sentiment," *Expert Systems with Applications*, vol. 42, no. 1, pp. 306–324, 2015.

[42] D. Peramunetilleke and R. K. Wong, "Currency exchange rate forecasting from news headlines," *Australian Computer Science Communications*, vol. 24, no. 2, pp. 131–139, 2002.

[43] Y. Kim, "Convolutional neural networks for sentence classification," 2014, https://arxiv.org/abs/1408.5882.

[44] Z. Wang, J. Zhang, J. Feng, and Z. Chen, "Knowledge graph and text jointly embedding," in *Proceedings of the 2014 Conference on Empirical Methods in Natural Language Processing, EMNLP 2014*, pp. 1591–1601, Qatar, October 2014.

[45] J. Xu, X. Qiu, K. Chen, and X. Huang, "Knowledge graph representation with jointly structural and textual encoding," in *Proceedings of the 26th International Joint Conference on Artificial Intelligence, IJCAI 2017*, pp. 1318–1324, Australia, August 2017.

[46] R. Xie, Z. Liu, J. Jia, H. Luan, and M. Sun, "Representation learning of knowledge graphs with entity descriptions," in *Proceedings of the 30th AAAI Conference on Artificial Intelligence, AAAI '16*, pp. 2659–2665, February 2016.

[47] F. Tian, B. Gao, E. Chen, and T. Liu, "Learning better word embedding by asymmetric low-rank projection of knowledge graph," *Journal of Computer Science and Technology*, vol. 31, no. 3, pp. 624–634, 2016.

[48] F. Z. Xing, E. Cambria, and R. E. Welsch, "Natural language based financial forecasting: a survey," *Artificial Intelligence Review*, vol. 50, no. 1, pp. 49–73, 2018.

[49] C. Goutte and E. Gaussier, "A probabilistic interpretation of precision, recall and *F*-score, with implication for evaluation," in *Advances in Information Retrieval*, D. E. Losada and J. M. Fernández-Luna, Eds., vol. 3408 of *Lecture Notes in Computer Science*, pp. 345–359, Springer, Berlin, Germany, 2005.

Hindawi
Complexity
Volume 2019, Article ID 7490640, 18 pages
https://doi.org/10.1155/2019/7490640

Research Article

Analyzing Stock Brokers' Trading Patterns: A Network Decomposition and Spatial Econometrics Approach

Juan Eberhard,[1] Jaime F. Lavín,[2] Alejandro Montecinos-Pearce,[1] and José Arenas[1]

[1]*Escuela de Negocios, Universidad Adolfo Ibáñez, Padre Hurtado 750, Viña del Mar, Chile*
[2]*Escuela de Negocios, Universidad Adolfo Ibáñez, Diagonal Las Torres 2640, Peñalolén, Santiago, Chile*

Correspondence should be addressed to Alejandro Montecinos-Pearce; amontecinospascal@gmail.com

Received 22 February 2019; Revised 10 June 2019; Accepted 23 June 2019; Published 25 July 2019

Guest Editor: Ahmet Sensoy

Using a unique data set with all the daily transactions from the Santiago Stock Exchange, we develop a novel methodology that combines a network decomposition with a spatial econometrics technique to study how brokers' characteristics and trading decisions may affect the stock market return. We present suggestive evidence of a mechanism by which structural changes of the transaction network between brokers affect the aggregate returns of the stock market. We find that brokers tend to trade with counterparties with dissimilar intraday selling volume when market return significantly increases. Moreover, brokers with a research department tend to sell to brokers without a research department when the market experiences a considerable increase of its return. From the financial perspective, these results highlight new ways in which intermediaries may affect market equilibrium and the efficiency of the market.

1. Introduction

Financial institutions are relevant to the performance of capital markets. Every day companies and investors interact with financial intermediaries (FIs) such as banks, insurance companies, pension funds, mutual funds, and brokerage firms. The financial management of investors involves the existence of FIs [1], which form transaction networks while exercising their functions. It is possible that the dynamic behavior of these networks, studied by Sensoy and Tabak [2] and Guerra and others [3], affects market returns through the specific trading matches between different types of brokers. The behavior of some FIs such as banks [4–7] and mutual and pension funds [8] have been studied extensively in the financial literature.[1] However, the role of brokerage firms on stock market performance has been scarcely analyzed. This knowledge gap is particularly relevant in the context of the undergoing demutualization process of stock markets in developing economies.[2] The increase of the heterogeneity across brokerage firms, generated by the latter process, is likely to increase the complexity of the trading interactions within the stock markets of emerging economies. Thus, from a policy perspective, advancing our knowledge about these market interplays is critical in keeping regulation up to date, and consequently, from a financial point of view, it enhances the stock markets' efficiency.[3]

In this paper, we contribute to improve the understanding of the role of brokerage firms in a context of underdeveloped stock markets. Namely, we study the correlation between the patterns of the transaction network of brokers with specific typologies in an emerging economy during considerable increases of the market's return. The Santiago Stock Exchange (SSE) provides adequate conditions to study how the complexity of the trading interactions between FIs affects the market's efficiency. This occurs for several reasons. First, the data from the SSE allows the construction and studying a subset of financial transaction networks through time, mostly ignored by the literature. Second, the SSE is one of the most important markets of the Integrated Latin American Market agreement (*Mercado Integrado Latinoamericano*; MILA) [9]. Third, the SSE is the leader in the Chilean stock market with 92.9% of the total market share. Fourth, the SSE broker transaction network captures the bulk of stock purchase and sale decisions of institutional investors and the main

family offices and retail investors in Chile. Finally, Chile is a developing country with medium-level financial development. Thus, we expect our findings to provide a helpful guide for private stakeholders, policymakers, regulators, and market participants in stocks markets belonging to emerging economies.

In this emerging market context, brokers may face liquidity constraints generated by capital restrictions that prevent them from executing all the transaction orders they receive [10–12], and since there is a positive relationship between volumes traded and price changes [13–16], we should expect that, during relevant variations in market prices, there would be a positive assortative matching in traded volume between selling and buying brokers. That is, brokers that receive large orders look for matches with brokers that can absorb these transactions. In this sense, the latter pattern raises the question of whether positive assortative matching in selling volumes between brokers affects the probability of a large increase in the stock market's return.

Therefore, the main hypothesis of our paper (H1) is that brokers tend to trade with counterparties with similar selling volume per trading counterparty when the return of the market significantly increases. The recent literature on brokerage firms suggests the existence of frictions in the stock market associated with brokers' typologies and induced actions, which contribute to the formation of the brokers' transaction network. In particular, the latter literature suggests that having analysts organized in a research department, possessing large or small equity (size), and holding various complementary services (economies of scope) are important broker (brokerage firm) typologies that can affect the performance of a stock market.

Thus, we focus our analysis on the relation between these typologies and the aggregate return of an emerging economy's stock market. More specifically, we test whether there exists evidence of (H2.a), a negative correlation between positive assortative matching of intraday mean volume in the transaction subnetwork of brokers with a specific type "A", and a significant increase of the IPSA return; whether there exists evidence of (H2.b), a positive correlation between negative assortative matching of intraday mean volume in the transaction subnetwork of brokers with specific type "A", and a significant increase of the IPSA return; and whether there exists evidence of (H2.c), a positive correlation between positive (and negative) assortative matching of intraday mean volume in the transaction subnetwork between brokers with and without specific type "A", and a significant increase of the IPSA return[4] (see Section 5 for a detailed explanation of the difference between H2.a and H2.b).

To study the above, we compare the results from the whole transaction network with results associated with specific subnetworks defined by relevant brokers' types. Our methodology is flexible to accommodate the study of how the presence of organized analysts, the presence of brokers' size, and the presence of economies of scope or whether brokerage firms do proprietary trading may affect the election among trading counterparties, producing specific patterns in the brokers' transaction network.[5] Using methods that combine a network decomposition and spatial statistical analysis, we isolate the effect of exogenous brokers' characteristics on the selection of trading counterparties in the brokers' transaction network. For interpretational purposes we represent the brokers' transaction network in terms of sales.[6] We construct these networks using data provided by the SSE that covers every daily stock transaction from 2006 until 2015. In addition, we completed our dataset with public information provided by the Financial Market Commission (www.cmfchile.cl, is the Chilean equivalent of the SEC for the USA) and Bloomberg (www.bloomberg.com). Based on the latter information, we used the SSE IPSA price index to compute significant rises of the market return considering various magnitudes of increase as thresholds.

The social networks literature refers to the presence of positive assortative matching, i.e. positive spatial dependence, as *homophily* [17]. This phenomenon refers to the aggregate behavior in which individuals have a tendency to establish relations with those who have a similar type. However, brokers may tend to sell their volume to brokers who are *opposite* to them. We refer to this tendency to trade with the complement or opposite of oneself as *heterophily.* This latter pattern would emerge if brokers tend to sell to other brokers that strongly differ from themselves. For instance, when the typology is dichotomic, heterophily means that a broker of type "A" tends to sell to individuals of type "not-A".

To study the presence of homophily or heterophily in average volume traded by brokers in their daily transaction network, we use the Moran's I test for spatial dependence [18], where the individual broker's intraday average trading volume is the dependent variable in the test.[7] However, the brokerage literature suggest that a broker's intraday average selling volume may not be solely determined by her preference to trade with brokers sharing similar selling volume. Thus, stock market brokers may have two possible sources of average selling volume associated homophily (heterophily): First, the tendency to sell to brokers who sell similar intraday average volume. Second, the tendency to sell to brokers that share a common exogenous type, such as providing investment banking services or having analysts organized in a research department. We denote the first category of homophilic pattern as *endogenous homophily*, and the second variety of homophily as *exogenous homophily*, because the brokers' types are not affected by daily trading decisions. Thus, positive spatial dependency signals endogenous homophily and negative spatial dependency signals endogenous heterophily.

Because we represent the brokers' transaction network in terms of sales, a homophilic pattern implies that large volumes of shares tend to be bought by brokers that are prone to selling behavior. Thus, intraday positive spatial dependency (endogenous homophily) in large volume transaction networks suggests that in the market most of the drivers are brokers with a selling attitude, then the intraday market return would fall. In this situation, stocks at an aggregate level resemble a *hot potato* that only a few brokers are asked to buy and which the majority of brokers continue to sell.[8] On the contrary, a negative spatial dependence in a large volume transaction network indicates that brokers are consistently

selling to brokers who tend to sell smaller average volumes, i.e., brokers who tend to keep most of their buys.

Following several authors [10, 11, 19], we use four exogenous typologies to define the aforementioned set of subnetworks: (a) proprietary trading activity, (b) having a research department, (c) providing investment banking services, and (d) having large equity.[9] Thus, to study the mechanism that generates endogenous homophily, we partition the whole brokers' transaction network into specific nonoverlapping subnetworks to analyze the presence of spatial dependency (also using Moran's I). To study the relation between homophily/heterophily (endogenous or exogenous) and significant increases of the market return, we use a Probit estimation.

Our distinction between homophily and heterophily plays a key role in our analysis because the absence of one does not imply the other. Thus, we study the aforementioned Probit models independently for both an indicator of positive and negative spatial dependency. This methodology enables us to study whether, during episodes of a significant increase of the IPSA return (IPSA jumps), brokers exhibit homophilic or heterophilic trading patterns and how the latter occurs. Namely, we distinguish endogenous homophilic patterns from exogenous homophilic patterns. The latter allows us to circumscribe the subset of exogenous brokers' typologies that may initiate the trading mechanism which provokes a significant increase of the IPSA return.

Our main results indicate that the presence of endogenous homophily is negatively associated with episodes of significant increases of the IPSA return. When partitioning the brokers into groups, as previously explained, we find that the aggregated pattern mostly persists when the set of brokers is partitioned considering whether a broker has a research department, but is not present for the other partitions considered by the literature. More interestingly, the *research department* typology suggests the presence of exogenous heterophily during events of large increases of the IPSA return. That is, brokers with research departments tend to sell to brokers without research departments when an episode of a significant increase in the IPSA return occurs.

The rest of this paper is structured as follows. In Section 2 we discuss the related literature, and in Section 3 we describe our data. Then, the fourth section characterizes the Chilean brokerage industry. In Section 5, we present the methodology in depth. In Section 6, we present the results of our analysis, and finally, in the seventh section, we provide our conclusions and extensions.

2. Related Literature

Acting as facilitators for the trading of financial assets, brokerage firms can carry out a range of different activities, including underwriting new securities, making markets for seasoned securities and providing services to customers in their financing and investment activities [20]. The current literature on the implications of the FIs' and brokers' actions has solely focused on developed financial markets; however, in both developing and emerging markets, a deeper understanding of the impact of brokers on the operation of these markets is still required. This need stems from the fact that underdeveloped markets present a level of market efficiency that is lower than in developed countries [21]. Eberhard, Lavín, and Montecinos-Pearce [22] find evidence that structural changes in the brokers' transaction network are associated with positive increases of the stock market return in an emerging economy.

The standard analysis of financial markets assumes that, regardless of their types, the FIs' actions do not affect the value of financial assets. The latter occurs because asset valuation models focus exclusively on the risk and return relationship of the assets made by investors, and not on the process of financial intermediation [1]. Nevertheless and regardless of whether investors use their money to buy assets directly or acquire mutual funds to invest indirectly in the stock market, the final transaction of the purchase and sale of the asset is delegated to a broker. More specifically, in capital markets, there is a financial intermediation process in which assets are not transformed as in the case of banking. Namely, a deposit is transformed into a credit, but their ownership is transferred between an investor that buys and another investor that sells in transactions executed by brokers [23]. Thus, it appears that transactions between brokers should not affect the return of the capital assets they trade. In contrast to the latter approach, the financial market microstructure literature indicates that the structure of financial markets generates frictions that influence the returns of financial assets. Easley and O'Hara [13] argue that these frictions affect transaction costs and returns. Moreover, the causes of these frictions can be traced back to the brokers executing the transactions. These frictions are associated with fixed costs, size, fees, and factors that stem from the characteristics of the traded assets such as payment, liquidity, and volatility, among others. Traditionally, when a firm decides to raise external financing by issuing shares or bonds, it contracts a broker, who, in exchange for her services, receives a fee for placing the instrument in the market. However, brokers provide a wider and more complex scope of services than just executing orders from investors. More recently, these FIs are dedicated to traditional activities such as trade orders execution, but also perform economic analysis and business recommendations and investment banking tasks.[10]

Moreover, the business context in which brokers perform these tasks has changed in recent years. One source of this change is the profound technological transformations of the financial markets. This massive change has produced a dramatic evolution in the way trading is conducted, thereby inducing greater competitive pressure on the incumbent brokers in the industry [24]. Boehmer, Jennings, and Wei [25] found that clients' buying and selling order decisions are associated with execution quality. Namely, those brokers with low costs and fast execution receive more orders. Consequently, the brokerage industry faces pressures for lower fees and high-quality trade execution. Similarly, the urgency for increasing the brokerage firms' profitability exerts greater pressure on brokers to sustain revenues by fostering investment banking activities and increasing their own capital in proprietary trading [26].[11] These changes in conjunction

with the frictions mentioned above prompt optimizing agents in financial markets to exhibit specific behavioral patterns. We argue that the existence of these patterns strongly suggests mechanisms through which financial frictions affect the markets' returns.

The increasing complexity of the financial markets documented by Goldstein and others [26], suggests that specific broker's typologies play a role in the emergence of the aforementioned behavioral patterns. For example, Hagerty and McDonald [10] indicate that, in a market with asymmetric information, informed traders earn a profit at the expense of uninformed traders, and they face an incentive to serve as counterparty to the trade rather than just as a brokerage conduit. There is also evidence of frictions related to the existence of how different types of brokers affect the equilibrium of the stock market [27].

Recent studies on individual brokerage firms have not only analyzed the role of analysts on brokerage firms' profits, but also, the existence and effects of economies of scale and scope, and the effects of size on the efficiency of these FIs. Regarding trade execution, brokers face restrictions in accepting unlimited numbers of orders since, on the one hand, they face capital requirements, and on the other hand, they have limited capital [10]. In this regard, Demirbag and others [11] explore the efficiency of securities firms in Turkey. They indicate that knowledge, assets, and financial capabilities are relevant factors on the viability of these intermediaries. They find that bank affiliation, foreign ownership, and size positively influence the efficiency of brokers. In the same spirit, Lee and others [12] find that larger brokers in Korea enjoy economies of scale and scope. In particular, greater economies of scale are present in larger firms.

Consequently and according to several authors [10, 11, 19], the exogenous typologies of brokers that we consider in our analysis are brokerage firms with (a) proprietary trading activity, (b) a research department, (c) investment banking services, and (d) large equity.

3. Main Data Sources

We use all of the available data from the daily stock transactions conducted by stock brokers at the SSE for the period 2006-2015. The dataset provided in anonymized form, with no association between the broker's name and their transactions, includes the following information: day of transaction, instrument traded, type of operation, units exchanged, purchase price, and the identification of brokers involved in buying and selling. We use the latter data to construct the daily directed transaction network based on sales for the Chilean equity market following Eberhard and others [22].[12] We consider this brokers' transaction network, henceforth transaction network, as the space in which we apply a spatial econometrics technique to detect spatial dependence. Following the latter authors, we also consider standard financial variables to capture possible factors that may affect the IPSA return. Finally, we construct the time series of significant positive increases in the IPSA return; henceforth IPSA jumps, considering moving annual periods.

4. The Chilean Stock Market Brokerage Industry

In Chile, stock brokerage focuses on the intermediation of stocks, money market, and fixed income instruments, representing 80.8% of the total traded during 2015. The stock transactions averaged MMUSD 50,641 per year from 2006-2015. These transactions were conducted by an average of 32 brokers per year, who traded on average MMUSD 1,594 per broker.

There are four types of brokers in this industry: subsidiaries of commercial banks, subsidiaries of investment banks, those related to insurance companies, and traditional brokers. According to figures published by the SSE, as of December 2015, brokers linked to investment and commercial banks represented 87.5% of the total amount traded and 75.4% of the industry's total equity. In terms of equity, commercial bank brokers are the most important (54.9% of total equity). In terms of volume traded, investment bank brokers are the largest brokers (51% of the total volume). The largest number of brokers in the market consists of traditional brokers and those belonging to commercial banks with 63% joint market share.

In 2015, there were 2,695,141 stock purchase/sale transactions for an average value of MMUSD 21,932. These transactions include those transactions conducted on behalf of third parties (88% of the total) and on their proprietary accounts and related transactions (12% of the total). Despite the changes experienced in this market in recent years, the previous figures have stabilized around 10% for transactions on their proprietary accounts and 90% for third party operations. Moreover, according to SSE figures, 71.5% of the total traded is done by local investors.

The structure of the stock brokerage industry in Chile is stable over time, which is similar to stock markets in developed countries as found by Hayes and others [28] and Anand and Galetovic [29]. Table 1 shows the market share of the Top 10 brokers and the remaining 90%. Between 2006 and 2015, 80.2% of the total traded was executed by only 10 stockbrokers, which on average represent 32.1% of the total brokers operating in Chile in that same period.[13]

5. Methodology

As indicated previously, our objective is to study the possible correlation between the tendency to trade with brokers that sell similar volumes as their counterparts (endogenous homophily) and significant increases of the IPSA return (jumps). Our first step is to study the spatial dependence of the average volume sold by each broker in the daily transaction network in the SSE. Then, we isolate the effect of exogenous homophily on the trading counterparty decision of brokers, i.e., endogenous homophily (heterophily), on large increases of the market return. For this, we define three subnetworks of the transaction network that do not overlap. These subnetworks are the subnetwork of nodes of type "A"[14] and the subnetwork of nodes with type "not-A" and the

Table 1: Summary of stockbrokers (2006-2015).

Year	Top 10 Stockbrokers		Non-Top 10 Stockbrokers	
	% Traded	% Repr.	% Traded	% Repr.
2006	83.5%	29.4%	16.5%	70.6%
2007	77.7%	30.3%	22.3%	69.7%
2008	82.0%	32.3%	18.0%	67.7%
2009	80.7%	32.3%	19.3%	67.7%
2010	81.9%	32.3%	18.1%	67.7%
2011	83.6%	31.3%	16.4%	68.8%
2012	77.3%	30.3%	22.7%	69.7%
2013	75.9%	32.3%	24.1%	67.7%
2014	78.9%	33.3%	21.1%	66.7%
2015	80.3%	37.0%	19.7%	63.0%
Average	*80.2%*	*32.1%*	*19.8%*	*67.9%*

[1]Own elaboration based on public information.

bipartite subnetwork of transactions between the brokers of the two opposite types.[15]

It should be noted that the IPSA jumps are sparse in time. For this reason and because the occurrence of an IPSA jump is a dichotomous event, we estimate a Probit to study if changes in the network's matching patterns are correlated with the IPSA jumps. Specifically, we studied the correlations for 11 different magnitudes of IPSA jumps: increases that range from 1 standard deviation with increments of 0.1 standard deviations to reach increases of the IPSA return of 2 standard deviations.[16] That is, the Probit for the first case is estimated for the series that contains a 1 on the days where the IPSA returns exceed 1 standard deviation, and 0 if the IPSA returns do not exceed it. Similarly, in the second case, the series takes on values 1 when the changes in the IPSA return exceed 1.1 standard deviations, and so forth. In the latter class of models, the indicator of a significant increase of the market return is the dependent variable, and an indicator of spatial dependency (positive for endogenous homophily and negative for endogenous heterophily) is the independent variable of interest.

Another important element to consider is the transactions considered to build the networks in study. As in Eberhard and others [22], we study the correlation for networks constructed for different thresholds of the total amounts traded between brokers (volume deciles are used as thresholds). Decile 10 corresponds to 100% of the transactions, while decile 1 only contains the top 10% of the transaction volume. In this way, we analyze our hypotheses for different magnitudes of transactions: from smaller to larger and for different intensities of the increase in the IPSA return. This allows us to evaluate how considering smaller transaction flows, which potentially incorporate more volatility with respect to financial market movements, affects the correlation between jumps in the IPSA return with spatial dependence. At the same time, we can study whether the correlation between IPSA jumps and spatial dependence is stronger depending on the intensity of the IPSA jump.

Following Eberhard and others [22], the Probit estimation will be controlled by financial variables that may affect the IPSA returns. In particular, we control for the variation of the following variables: oil price, dollar price, VIX index, emerging markets index, copper price, 5-year credit default swaps, and the S&P 500 stock index. Additionally, controls are included by month and year to isolate seasonal effects in specific months and years. In order to simplify the presentation of results and to facilitate the visualization of the patterns that emerge when comparing the previous regressions, the results of the regressions for the controls are not presented; however, they are available for interested readers. Accordingly, figures of the results will focus on showing the significance of the spatial dependence variable for the aforementioned Probit models. Once the existence of positive and negative spatial dependence is assessed using the Moran I test, we generate an indicator variable for positive spatial dependence or *homophily* and an indicator variable for negative dependence correlation or *heterophily*. These variables are constructed for the networks defined for the 10 different jump thresholds in the IPSA return.

In order to study (H1), i.e., brokers that tend to trade with counterparties with similar selling volume per trading counterparty when the return of the market significantly increases, we first consider the entire transaction network as the space over which we conduct the Moran I test. Second, we study the Probit model previously described. A statistically significant coefficient on the indicator for spatial dependency may indicate that a potential homophilic (or heterophilic) behavior may influence the aggregate stock market returns.

Accordingly, the presence of positive spatial dependence in the transaction network indicates that brokers with a large sold average volume within the day tend to trade with other brokers that sell large average volumes within the day.[17] That is, when there is positive spatial dependence, brokers sell to similar counterparts, in terms of sold intraday average volume. Because the brokers' transaction network identifies which brokers sell to which, a homophilic pattern in large

volume transaction networks (deciles 1, 2, or 3) is consistent with the tendency to have large volumes being sold to brokers that intend to sell those volumes as well. If the latter is the case, then endogenous homophily would reduce the likelihood of an IPSA jump. The latter occurs, because if most brokers receive sell order that involve large volumes (transaction networks for the deciles 1 through 4), then only a minority of brokers are on the other side of the market, i.e., buying large volumes of stocks. In such a market context, the stocks resemble a *hot potato*. The opposite case emerges when the brokers' transactions follow an endogenous heterophilic pattern. Such a pattern suggests that brokers that sell large volumes tend to do so to brokers that *do not sell* large volumes, but could eventually *buy* large volumes. This suggests that the stocks are not a *hot potato*, but on the contrary, they are assets acquired to obtain an economic benefit. Thus, it should be more likely to observe an IPSA jump. Therefore, it is necessary to ask: what causes the brokers' tendency to trade with similar/dissimilar counterparties? That is to say, can one delve into understanding the possible mechanism through which the matching pattern between brokers arises in the presence of an IPSA jump. We address this question in considering the exogenous typologies found in the literature: (a) proprietary trading activity, (b) having a research department, (c) providing investment banking services, and (d) having large equity.[18] Accordingly, the analysis necessary to study the possible causes of endogenous homophily (heterophily) requires two key steps: decompose the set of brokers according to the mentioned criteria, and then calculate the spatial dependence indicators and run the Probit models.

First, we decompose the transaction network based on the brokers' exogenous typologies in order to capture the effect of exogenous homophily or heterophily on the spatial dependency of the average volume traded in each transaction subnetwork.[19] The classification of brokers according to an exogenous typology allows us to study the brokers' choice under two dimensions simultaneously: one endogenous (volume traded) and one exogenous (e.g., investment banking services). Second, we calculate the spatial correlation indicators previously described in each of the subnetworks defined by the aforementioned attributes;[20] and analogously in studying the complete network, we use the Probit model previously described to study the correlation between IPSA jumps and pattern of matches of trading counterparties in each subnetwork. That is, we will study if, for example, within the group of brokers with a research department, we observe that they trade with brokers with similar volume traded or not. These Probit models allow us to study the following hypotheses according to a specific type:[21]

(1) H2.a The coefficient of the positive spatial dependence indicator of the daily average volume sold in the type "A" broker subnetwork is negative and significant.

(2) H2.b The coefficient of the negative spatial dependence indicator of the daily volume traded in the type "A" broker subnetwork is positive and significant.

(3) H2.c The coefficient of the negative spatial dependence indicator of the daily volume traded in the subnetwork between type "A" and type "not-A" brokers is positive and significant.

In the presence of an IPSA jump, the absence of systematic positive assortative matching in daily average volume sold does not imply that there is systematic negative assortative matching in the same variable because there is not a necessity of any matching pattern. Thus, we need to test both hypotheses H2.a and H2.b. In addition, our working hypotheses do not have any implications regarding the way in which brokers, for example, without a research department trade among each other. Thus, we do not focus on studying specific patterns in the type "not-A" subnetworks.[22]

6. Results

Figure 1 shows the Probit model regression results for IPSA jumps of different intensities (columns 2-12) and for different total volume thresholds traded daily between brokers (rows 2-11). Each cell in Figure 1 contains the coefficient associated with the spatial dependence indicator for positive spatial dependence[23] and the corresponding *p-value*. A yellow cell indicates that the estimator of the coefficient in the Probit is negative, while a blue cell indicates that the coefficient is positive. Additionally, if the cell color is lighter, that is light yellow or light blue, then the coefficient is not significant, while darker colored cells are reserved for significant coefficients.[24] This color coding allows us to easily identify patterns across the many regressions presented. In Figure 1, the vast majority of coefficients are negative and not significant. This suggests that the presence of positive spatial dependence does not affect the likelihood of an IPSA jump for most thresholds. That is, apparently there is no evidence of a specific pattern when intermediaries decide to whom they will sell. This fact would be consistent with the notion derived from the efficient market theory that FIs do not matter as pointed out by Allen [1]. However, Figure 1 reveals the presence of a pattern when we focus on (daily) networks built exclusively with large aggregate volumes traded between brokers, particularly the first, second, and third deciles.[25] In these cases, most coefficients are significant and they show a clear tendency to increase in absolute value when the intensity of the IPSA jumps increases. This is evidence that the importance of positive spatial dependence grows with the size of the increase in the IPSA return.

The coefficients' negative sign and their significance indicate that when brokers sell to intermediaries with similar average daily sold volume, that is, when there is endogenous homophily (positive spatial dependence), the probability of an IPSA jump decreases. Therefore, if we focus on large volume transaction networks, this correlation between endogenous homophily and IPSA jumps is consistent with most brokers executing orders to sell stocks. This behavior is consistent with a bear market. The preceding leads us to ask the following question to circumscribe the nature of the relation between an endogenous homophilic trading pattern between brokers and the stock market's return: Does

	Size of the IPSA jump used in the Probit Regression										
Threshold for the construction of the network	1 s.d	1.1 s.d	1.2 s.d	1.3 s.d	1.4 s.d	1.5 s.d	1.6 s.d	1.7 s.d	1.8 s.d	1.9 s.d	2 s.d.
First Decile	**-0.257∗∗∗**	**-0.261∗∗∗**	**-0.206∗∗**	**-0.245∗∗**	**-0.330∗∗∗**	**-0.290∗∗**	**-0.292∗∗**	-0.209	**-0.372∗∗∗**	**-0.451∗∗∗**	**-0.507∗∗∗**
	0.00528	0.00581	0.0371	0.018	0.00238	0.0111	0.0139	0.102	0.00716	0.00165	0.00107
Second Decile	**-0.173∗∗**	-0.0883	-0.0299	-0.111	-0.149	**-0.177∗**	**-0.193∗**	**-0.206∗**	**-0.247∗∗**	**-0.289∗∗**	**-0.229∗**
	0.0378	0.305	0.739	0.234	0.132	0.092	0.0823	0.0762	0.0478	0.0254	0.0949
Third Decile	**-0.275∗∗∗**	**-0.235∗∗**	**-0.206∗∗**	**-0.207∗∗**	**-0.204∗∗**	-0.14	-0.156	**-0.217∗**	-0.181	**-0.291∗∗**	-0.131
	0.00179	0.0103	0.0304	0.0355	0.0486	0.203	0.179	0.0811	0.173	0.0359	0.351
Fourth Decile	-0.108	-0.0609	-0.039	-0.00912	-0.0222	0.0274	-0.012	-0.0808	0.0426	-0.0471	0.0456
	0.25	0.527	0.697	0.929	0.838	0.812	0.922	0.528	0.753	0.733	0.753
Fifth Decile	-0.171	-0.145	-0.14	-0.0943	-0.146	-0.138	-0.112	-0.0978	0.0182	-0.226	-0.244
	0.134	0.209	0.241	0.445	0.272	0.328	0.452	0.536	0.913	0.227	0.208
Sixth Decile	-0.0701	-0.018	-0.0612	-0.103	-0.216	**-0.296∗**	**-0.380∗∗**	**-0.456∗∗**	-0.361	-0.301	-0.18
	0.583	0.89	0.655	0.477	0.167	0.0882	0.0491	0.0364	0.121	0.187	0.421
Seventh Decile	-0.0863	-0.0724	-0.0726	-0.0664	-0.208	-0.177	-0.358	-0.242	-0.107	-0.0565	0.047
	0.56	0.638	0.651	0.691	0.254	0.349	0.111	0.283	0.65	0.81	0.841
Eighth Decile	-0.314	-0.266	-0.239	-0.249	-0.406	-0.303	**-0.594∗**	-0.475	-0.379	-0.349	-0.273
	0.111	0.188	0.278	0.283	0.111	0.228	0.0762	0.151	0.278	0.31	0.42
Ninth Decile	-0.22	-0.2	-0.099	-0.134	-0.183	-0.107	-0.387	-0.285	-0.203	-0.183	-0.103
	0.315	0.375	0.658	0.575	0.461	0.671	0.242	0.393	0.583	0.619	0.776
All transactions	-0.0642	-0.0306	0.0645	0.0327	-0.144	-0.0778	-0.373	-0.276	-0.234	-0.203	-0.124
	0.761	0.889	0.766	0.887	0.568	0.763	0.27	0.418	0.533	0.588	0.738

Figure 1: Estimated coefficients associated with the positive spatial dependence variable in Probit regressions with different thresholds defining the transaction network and different sizes of the IPSA shock used as the dependent variable in the Probit. Each regression controls for the variation of oil prices, dollar prices, VIX index, emerging market index, copper prices, 5-year credit default swaps S&P 500 stock index, month, and year. The size of the IPSA jump is measured in standard deviations (s.d.).

endogenous heterophily correlate positively with an IPSA jump?

We study the latter question based on the results presented in Figure 2, which are organized in the analogously as in Figure 1. The sole difference between Figures 1 and 2 is that Figure 2 uses the negative spatial dependence indicator as the independent variable in the Probit model. The calculations shown in Figure 2 suggest that heterophily increases the probability of an IPSA jump for the third, fourth, fifth, sixth, and seventh deciles. That is, when brokers with large sold average daily volume, trade with brokers with low sold average daily volume, the probability rises that the IPSA return will increase significantly. In the case of the large volume transaction networks (third and fourth deciles), this relation is consistent with observing a more balanced number of brokers on each side of the market. This condition is to be expected in a more bullish market. This pattern is the opposite of that observed when endogenous homophily occurs. The evidence suggests that this effect becomes more pronounced for larger shocks, especially on the third decile of transactions.

In short, for relatively large transactions (third decile) in which brokers tend towards endogenous heterophily, the likelihood of a positive shock to the IPSA return increases; on the contrary, when brokers tend towards homophily, the probability of an IPSA jump decreases. The latter pattern contradicts the notion suggested by Stoll [23]; transactions between brokers should not affect the return of the capital assets they trade. Moreover, the correlation between the probability of an IPSA jump and endogenous heterophily (or homophily) narrows down the sources of the frictions that affect the assets' returns, as Easley and O'Hara [13] argue.

Linnainmaa and Saar [27] trace these frictions back to how different types of brokers affect equilibrium returns. Thus, to further reduce the potential sources of market return affecting frictions, we study how the exogenous typologies of brokers, considered by the literature [10, 11, 19], correlate to their matching patterns in the transaction network. That is, we study potential mechanisms associated with *exogenous* homophily and heterophily, which can explain why this association between endogenous homophily/heterophily and IPSA jumps occurs.

Among all the exogenous typologies considered by the literature, only the possession of a research department emerges as a consistent explanation for the correlation between endogenous homophily (heterophily) and significant increases in the SEE market return measured by the IPSA return. Figures 3(a) and 3(b) show the results for Probit models considering positive spatial dependence of the subnetwork of brokers with a research department (Figure 3(a)) and of the bipartite subnetwork of brokers with and without a research department (Figure 3(b)).[26] In Figure 3(a), we observe a pattern very similar to that present in Figure 1. That is, endogenous homophily in intraday volume sold between brokers with a research department decreases the probability of occurrence of an IPSA jump. As before, the latter pattern is more apparent for large volume transaction networks (first, second, and third deciles). Additionally, this

	Size of the IPSA jump used in the Probit Regression										
Threshold for the construction of the network	1 s.d	1.1 s.d	1.2 s.d	1.3 s.d	1.4 s.d	1.5 s.d	1.6 s.d	1.7 s.d	1.8 s.d	1.9 s.d	2 s.d.
First Decile	--	--	--	--	--	--	--	--	--	--	--
	--	--	--	--	--	--	--	--	--	--	--
Second Decile	-0.108	-0.371	-0.275	-0.155	-0.0365	0.120	0.210	0.271	0.478	0.582	0.436
	0.787	0.420	0.543	0.727	0.934	0.784	0.612	0.521	0.260	0.167	0.395
Third Decile	**0.461∗∗∗**	**0.440∗∗**	**0.311∗∗**	**0.423∗∗**	**0.478∗∗**	**0.553∗∗∗**	**0.654∗∗∗**	**0.661∗∗∗**	**0.682∗∗∗**	**0.761∗∗∗**	**0.819∗∗∗**
	0.0091	0.0134	0.0917	0.0216	0.0115	0.0050	0.0007	0.0011	0.0035	0.0013	0.0007
Fourth Decile	**0.308∗∗**	0.221	0.173	0.232	0.229	**0.285∗**	**0.271∗**	**0.294∗**	**0.318∗**	**0.394∗∗**	**0.366∗**
	0.205	0.106	0.225	0.109	0.130	0.0723	0.0976	0.0751	0.0903	0.0375	0.0725
Fifth Decile	**0.257∗∗**	**0.194∗**	0.163	0.158	0.157	0.0574	0.00006	0.101	0.215	0.193	0.222
	0.0225	0.0938	0.170	0.201	0.229	0.686	1.000	0.501	0.175	0.230	0.184
Sixth Decile	**0.265∗∗∗**	**0.203∗∗**	**0.214∗∗**	**0.257∗∗**	**0.279∗∗**	**0.261∗∗**	**0.258∗∗**	**0.322∗∗**	**0.279∗∗**	**0.347∗∗**	**0.331∗∗**
	0.0059	0.0399	0.0364	0.0148	0.0118	0.0270	0.0354	0.0103	0.0492	0.0162	0.0286
Seventh Decile	**0.218∗∗**	**0.212∗∗**	**0.241∗∗**	**0.248∗∗**	**0.257∗∗**	0.138	0.101	0.0870	0.115	0.142	0.0369
	0.0142	0.0189	0.0101	0.0111	0.0129	0.206	0.380	0.476	0.391	0.302	0.805
Eighth Decile	0.134	0.0688	0.0615	0.0611	0.0076	-0.0578	-0.0503	-0.0646	-0.114	-0.115	-0.128
	0.116	0.438	0.495	0.518	0.939	0.588	0.650	0.582	0.371	0.383	0.365
Ninth Decile	0.111	0.115	0.127	0.0921	0.0783	0.0597	0.0351	0.0496	-0.0320	-0.0423	-0.113
	0.185	0.185	0.155	0.323	0.428	0.575	0.750	0.674	0.801	0.748	0.421
All transactions	**0.216∗∗**	**0.185∗∗**	**0.213∗∗**	**0.222∗∗**	**0.275∗∗∗**	**0.196∗**	**0.223∗**	**0.205∗**	0.223	0.185	0.186
	0.120	0.0359	0.0209	0.0222	0.0074	0.0710	0.0528	0.0958	0.101	0.178	0.207

Figure 2: Estimated coefficients associated with the negative spatial dependence variable in Probit regressions with different thresholds defining the transaction network and different sizes of the IPSA shock used as the dependent variable in the Probit. Each regression controls for the variation of oil prices, dollar prices, VIX index, emerging market index, copper prices, 5-year credit default swaps S&P 500 stock index, month, and year. The size of the IPSA jump is measured in standard deviations (s.d.).

correlation becomes greater in absolute value for larger IPSA jumps. The interpretation of this result is analogous to that provided for the results in Figure 1. The latter implies that the results presented in Figure 3(a) support H2.a.

The results in Figure 3(b) allow us to evaluate the behavior among brokers in different groups. That is, we study the possible effect of endogenous homophily in a network constructed on the basis of exogenous heterophily. Surprisingly, Figure 3(b) shows that, for relatively large transactions (third and fourth deciles) and for IPSA jumps of moderate size (smaller than 1.3 standard deviations), endogenous homophily decreases the probability of an IPSA jump. That is, within the bipartite network, trading with brokers of similar average sold volume decreases the probability that the IPSA return will increase considerably.

To complete the study of the relation between the matching patterns between brokers based on the organization of analysts in a research department and significant increases in the stock market return, now we present the results of the Probit models considering negative spatial dependence. Figure 4(a) presents the relation between endogenous heterophily in the subnetwork of brokers with research department. Analogously to the results presented in Figure 2, in Figure 4(a) clear patterns emerge in large volume transaction networks. First, the correlation between negative spatial dependence and the probability of an IPSA jump tends to increase with the aggregate volume traded by two brokers; and second, the latter correlation increases in absolute value with the intensity of the IPSA jump. Thus, when a heterophilic pattern of matching between brokers emerges is more likely the occurrence of a bull market, even for the subset of traders with research department. Hence, the information contained in Figure 4(a) support H2.b.

On the other hand, Figure 4(b) allows the evaluation of the relation between the likelihood of an IPSA jump when endogenous and exogenous heterophily occurs. Figure 4(b) shows two distinctive patterns. There is some evidence in very large volume transaction networks, and for very significant IPSA jumps, the conjunction of endogenous and exogenous heterophily reduces the probability of an IPSA jump. However, this incipient pattern overwhelmingly reverses when we admit relatively smaller aggregate trades between brokers (fifth trough ninth deciles and all transactions). In other words, in more than a third of the possible combinations of IPSA jumps, and transaction networks, the endogenous heterophily between traders with and without research department may increase the likelihood of a sizeable jump on IPSA return. That is, Figure 4(b) provides evidence that supports H2.c.

The presence of these patterns suggests that having a research department plays a relevant role in the matching process of counterparts in large volume transaction networks on the probability of an IPSA jumps. This regularity is different from the endogenous homophily/heterophily that can be associated, for example, to restrictions imposed by

Threshold for the construction of the network	Size of the IPSA jump used in the Probit Regression										
	1 s.d	1.1 s.d	1.2 s.d	1.3 s.d	1.4 s.d	1.5 s.d	1.6 s.d	1.7 s.d	1.8 s.d	1.9 s.d	2 s.d.
First Decile	**-0.251∗∗∗**	**-0.26∗∗∗**	**-0.218∗∗**	**-0.230∗∗**	**-0.306∗∗∗**	**-0.243∗∗**	**-0.24∗∗**	-0.165	**-0.329∗∗**	**-0.407∗∗∗**	**-0.458∗∗∗**
	0.00617	0.00540	0.0276	0.0277	0.00508	0.0343	0.0374	0.196	0.0180	0.00460	0.00302
Second Decile	**-0.206∗∗**	-0.124	-0.0571	-0.135	-0.161	**-0.195∗**	-0.172	-0.187	**-0.231∗**	**-0.274∗∗**	-0.215
	0.0137	0.151	0.526	0.149	0.106	0.0645	0.121	0.106	0.0651	0.0345	0.118
Third Decile	**-0.235∗∗∗**	**-0.214∗∗**	**-0.192∗∗**	**-0.175∗**	**-0.197∗**	-0.134	-0.150	**-0.213∗**	-0.178	**-0.286∗∗**	-0.126
	0.00800	0.0198	0.0433	0.0744	0.0575	0.225	0.194	0.0866	0.181	0.0383	0.368
Fourth Decile	-0.109	-0.0939	-0.0680	-0.0624	-0.0950	-0.0568	-0.0959	-0.168	-0.0513	-0.142	-0.0449
	0.246	0.348	0.509	0.560	0.398	0.635	0.453	0.214	0.718	0.328	0.765
Fifth Decile	-0.160	-0.131	-0.123	-0.0745	-0.154	-0.148	-0.119	-0.106	0.00907	-0.233	-0.246
	0.156	0.253	0.299	0.542	0.245	0.295	0.419	0.501	0.957	0.211	0.204
Sixth Decile	-0.0951	-0.0419	-0.0514	-0.0939	-0.207	**-0.287∗**	**-0.369∗**	**-0.444∗∗**	-0.358	-0.302	-0.185
	0.456	0.747	0.699	0.508	0.178	0.0935	0.0530	0.0394	0.125	0.188	0.416
Seventh Decile	-0.0627	-0.0409	-0.0372	-0.0858	-0.225	-0.196	**-0.374∗**	-0.260	-0.126	-0.0725	0.0357
	0.668	0.787	0.813	0.604	0.214	0.297	0.0945	0.246	0.591	0.757	0.878
Eighth Decile	-0.302	-0.245	-0.208	-0.306	**-0.458∗**	-0.353	**-0.636∗**	-0.520	-0.423	-0.394	-0.320
	0.106	0.202	0.314	0.181	0.0675	0.153	0.0532	0.110	0.217	0.243	0.336
Ninth Decile	-0.220	-0.188	-0.0769	-0.0816	-0.103	-0.0189	-0.445	-0.350	-0.275	-0.255	-0.178
	0.282	0.368	0.712	0.714	0.650	0.935	0.166	0.281	0.443	0.474	0.614
All transactions	-0.0229	0.0172	0.119	0.113	-0.0155	0.0515	-0.399	-0.306	-0.264	-0.237	-0.155
	0.910	0.934	0.567	0.605	0.947	0.830	0.231	0.363	0.476	0.523	0.672

(a) Estimated coefficients associated with the positive spatial dependence variable in Probit regressions using only the network of traders with research department. The regressions are estimated with different thresholds defining the transaction network and different sizes of the IPSA shock used as the dependent variable in the Probit. Each regression controls for the variation of oil prices, dollar prices, VIX index, emerging market index, copper prices, 5-year credit default swaps S&P 500 stock index, month, and year. The size of the IPSA jump is measured in standard deviations (s.d.)

Threshold for the construction of the network	Size of the IPSA jump used in the Probit Regression										
	1 s.d	1.1 s.d	1.2 s.d	1.3 s.d	1.4 s.d	1.5 s.d	1.6 s.d	1.7 s.d	1.8 s.d	1.9 s.d	2 s.d.
First Decile	-0.358	-0.394	**-0.476∗**	-0.374	-0.265	-0.114	-0.445	**-0.792∗∗**	-0.657	-0.555	-
	0.121	0.114	0.0509	0.124	0.274	0.635	0.160	0.0484	0.116	0.186	-
Second Decile	-0.194	-0.220	-0.258	-0.327	-0.309	-0.350	-0.352	-0.279	-0.184	-0.268	-0.175
	0.307	0.258	0.239	0.169	0.210	0.166	0.205	0.303	0.507	0.398	0.577
Third Decile	**-0.415∗∗**	**-0.489∗∗**	**-0.416∗**	-0.379	-0.206	-0.0661	-0.169	-0.0488	-0.117	-0.235	-0.420
	0.0300	0.0397	0.0845	0.125	0.382	0.778	0.532	0.851	0.679	0.456	0.249
Fourth Decile	**-0.353∗**	-0.376	**-0.645∗∗**	**-0.513∗**	-0.385	-0.227	-0.144	-0.225	-0.594	-0.573	-0.493
	0.0852	0.106	0.0263	0.0747	0.187	0.438	0.611	0.507	0.151	0.168	0.244
Fifth Decile	-0.238	-0.0959	-0.191	-0.164	-0.0158	-0.0138	0.0547	-0.0141	0.142	-0.0667	0.0105
	0.291	0.672	0.459	0.543	0.953	0.961	0.845	0.964	0.660	0.853	0.978
Sixth Decile	**-0.488∗**	-0.297	-0.657	-0.502	-0.347	-0.552	-0.489	-	-	-	-
	0.0962	0.316	0.116	0.216	0.383	0.276	0.337	-	-	-	-
Seventh Decile	-0.136	0.0339	-0.397	-0.738	-0.605	-	-	-	-	-	-
	0.675	0.918	0.403	0.214	0.286	-	-	-	-	-	-
Eighth Decile	-0.420	-0.258	-0.601	-	-	-	-	-	-	-	-
	0.378	0.579	0.416	-	-	-	-	-	-	-	-
Ninth Decile	-0.111	0.0598	0.172	-	-	-	-	-	-	-	-
	0.841	0.913	0.753	-	-	-	-	-	-	-	-
All transactions	-	-	-	-	-	-	-	-	-	-	-
	-	-	-	-	-	-	-	-	-	-	-

(b) Estimated coefficients associated with the positive spatial dependence variable in Probit regressions using the bipartite network of traders with and without research department. The regressions are estimated with different thresholds defining the transaction network and different sizes of the IPSA shock used as the dependent variable in the Probit. Each regression controls for the variation of oil prices, dollar prices, VIX index, emerging market index, copper prices, 5-year credit default swaps S&P 500 stock index, month, and year. The size of the IPSA jump is measured in standard deviations (s.d.)

Figure 3

	Size of the IPSA jump used in the Probit Regression										
Threshold for the construction of the network	1 s.d	1.1 s.d	1.2 s.d	1.3 s.d	1.4 s.d	1.5 s.d	1.6 s.d	1.7 s.d	1.8 s.d	1.9 s.d	2 s.d.
First Decile	-	-	-	-	-	-	-	-	-	-	-
	-	-	-	-	-	-	-	-	-	-	-
Second Decile	-0.198	-0.623	-0.544	-0.461	-0.358	-0.286	-0.177	-0.173	-0.130	-0.134	-0.0858
	0.625	0.172	0.235	0.307	0.439	0.538	0.696	0.695	0.775	0.766	0.848
Third Decile	**0.488∗∗∗**	**0.598∗∗∗**	**0.512∗∗∗**	**0.579∗∗**	**0.707∗∗∗**	**0.638∗∗∗**	**0.714∗∗∗**	**0.644∗∗∗**	**0.843∗∗∗**	**0.876∗∗∗**	**0.953∗∗∗**
	0.0063	0.0007	0.0062	0.0023	0.0002	0.0020	0.0004	0.0036	0.0002	0.0001	0.00003
Fourth Decile	**0.303∗∗**	0.245	0.150	0.228	0.232	**0.322∗**	**0.359∗**	**0.358∗**	**0.548∗∗∗**	**0.594∗∗∗**	**0.708∗∗∗**
	0.0438	0.115	0.372	0.185	0.190	0.0773	0.0525	0.0660	0.0071	0.0037	0.0006
Fifth Decile	**0.269∗∗**	**0.304∗∗**	**0.236∗∗**	**0.255∗**	**0.319∗∗**	**0.264∗**	0.255	**0.290∗**	**0.442∗∗**	**0.430∗∗**	**0.452∗∗**
	0.0403	0.0210	0.0855	0.0749	0.0289	0.0893	0.115	0.0798	0.0121	0.0158	0.0142
Sixth Decile	**0.226∗∗**	**0.200∗**	**0.210∗**	**0.220∗**	**0.242∗**	0.145	0.167	0.185	**0.290∗**	**0.296∗**	0.264
	0.0485	0.0877	0.0795	0.0796	0.0668	0.306	0.257	0.225	0.0801	0.0801	0.141
Seventh Decile	**0.235∗∗**	**0.234∗∗**	**0.207∗**	**0.235∗∗**	**0.320∗∗∗**	0.153	0.130	0.141	**0.259∗**	0.223	0.193
	0.0315	0.0331	0.0671	0.0460	0.0089	0.251	0.353	0.323	0.0962	0.166	0.254
Eighth Decile	0.0652	0.0374	0.0491	0.102	0.121	0.0204	0.0465	0.0589	0.0973	0.0724	0.0340
	0.540	0.732	0.661	0.376	0.323	0.877	0.734	0.675	0.535	0.658	0.847
Ninth Decile	-0.0982	-0.0487	-0.0224	0.0637	0.0803	-0.0270	-0.483	-0.104	-0.0221	0.0436	-0.0055
	0.360	0.651	0.840	0.578	0.510	0.838	0.728	0.467	0.886	0.777	0.973
All transactions	-0.0410	0.0119	0.0416	0.0817	0.0944	0.104	0.148	0.0340	0.0720	0.158	0.220
	0.708	0.914	0.712	0.482	0.444	0.428	0.277	0.817	0.661	0.338	0.211

(a) Estimated coefficients associated with the negative spatial dependence variable in Probit regressions using only the network of traders with research department. The regressions are estimated with different thresholds defining the transaction network and different sizes of the IPSA shock used as the dependent variable in the Probit. Each regression controls for the variation of oil prices, dollar prices, VIX index, emerging market index, copper prices, 5-year credit default swaps S&P 500 stock index, month, and year. The size of the IPSA jump is measured in standard deviations (s.d.)

	Size of the IPSA jump used in the Probit Regression										
Threshold for the construction of the network	1 s.d	1.1 s.d	1.2 s.d	1.3 s.d	1.4 s.d	1.5 s.d	1.6 s.d	1.7 s.d	1.8 s.d	1.9 s.d	2 s.d.
First Decile	-0.163	-0.108	-0.109	-0.239	-0.325	-0.312	**-0.64∗∗∗**	**-0.592∗∗**	**-0.445∗**	**-0.668∗∗**	**-0.480∗**
	0.351	0.54	0.542	0.218	0.123	0.166	0.00566	0.0118	0.0638	0.0181	0.0817
Second Decile	-0.0117	-0.0872	-0.0999	-0.12	-0.108	-0.23	-0.144	-0.0439	0.0032	-0.108	-0.323
	0.945	0.627	0.596	0.559	0.607	0.308	0.507	0.841	0.99	0.697	0.262
Third Decile	0.133	0.107	0.123	0.0557	0.035	-0.0368	-0.0633	-0.103	-0.117	-0.0384	-0.453
	0.407	0.525	0.488	0.761	0.859	0.861	0.774	0.661	0.669	0.889	0.272
Fourth Decile	0.13	0.158	0.156	0.173	0.171	0.168	0.207	0.216	0.15	0.261	0.0478
	0.262	0.194	0.217	0.181	0.213	0.251	0.17	0.161	0.376	0.121	0.802
Fifth Decile	**0.242∗**	**0.270∗**	**0.267∗**	**0.264∗**	**0.234∗**	0.162	0.18	0.137	0.151	0.183	0.117
	0.012	0.0059	0.0086	0.0115	0.0344	0.175	0.146	0.292	0.294	0.221	0.489
Sixth Decile	**0.268∗**	**0.280∗**	**0.327∗**	**0.331∗**	**0.305∗**	**0.242∗**	**0.231∗∗**	**0.237∗∗**	0.13	0.12	0.107
	0.0017	0.0014	0.0003	0.0004	0.0026	0.0263	0.0421	0.0491	0.324	0.378	0.465
Seventh Decile	**0.222∗**	**0.243∗**	**0.288∗**	**0.312∗**	**0.332∗**	**0.270∗**	**0.221∗**	**0.281∗∗**	0.185	0.183	0.236
	0.0093	0.0065	0.0022	0.0015	0.0013	0.0149	0.0554	0.0219	0.161	0.185	0.117
Eighth Decile	0.113	0.118	0.149	0.152	0.199∗	0.138	0.181	**0.224∗**	0.0905	0.0627	0.0872
	0.192	0.199	0.115	0.121	0.0588	0.214	0.119	0.0661	0.473	0.631	0.54
Ninth Decile	**0.230∗**	**0.181∗**	**0.243∗**	**0.233∗**	**0.282∗**	**0.210∗**	**0.204∗**	0.2	0.0819	-0.0007	0.0768
	0.0117	0.0566	0.0146	0.0257	0.0107	0.0738	0.0951	0.126	0.559	0.996	0.617
All transactions	**0.202∗**	0.13	0.166	**0.279∗**	**0.371∗**	**0.311∗**	**0.310∗∗**	**0.262∗**	0.171	0.11	0.201
	0.0343	0.189	0.107	0.0128	0.0016	0.0128	0.0173	0.0556	0.246	0.456	0.225

(b) Estimated coefficients associated with the negative spatial dependence variable in Probit regressions using the bipartite network of traders with and without research department. The regressions are estimated with different thresholds defining the transaction network and different sizes of the IPSA shock used as the dependent variable in the Probit. Each regression controls for the variation of oil prices, dollar prices, VIX index, emerging market index, copper prices, 5-year credit default swaps S&P 500 stock index, month, and year. The size of the IPSA jump is measured in standard deviations (s.d.)

Figure 4

other typologies studied by the literature such as the size of brokers.[27] The aggregate pattern that emerges from the analysis of Figures 3(a)–4(b) suggests that an informational motive connects matching patterns in the trading network and market returns, as suggested by Hagerty and McDonald [10].

We find no evidence which supports that the proprietary trading activity typology (suggested by Goldstein and others [26]), the investment banking services typology (suggested by Demirbag and others [11]), and the large equity typology (suggested by Hagerty and McDonald [10]) affect the correlation between matching patterns in the trading network and market returns. As a representative example of what happens with the other subnetwork partitions based on alternative typologies, we present below the results analogous to those presented in Figures 3(a) and 3(b) for the typology that divides brokers between those with and those without investment banking services, in Figures 5(a) and 5(b). Appendix shows analogous figures to 5(a) and 5(b) for the other criteria used in the literature to classify brokers exogenously: size, proprietary trading, and nationality. Nonetheless, many of the results we present for the investment banking criterion may be extended to these other classifications. More importantly, the conclusions of these analyses are the same.

In the case of the partition of brokers based on the criterion of providing investment banking services (Figure 5(a)), a similar result is observed as in the case of the subnetwork of brokers with a research department. That is, for relatively large transactions, endogenous homophily correlates with a decrease in the probability of an IPSA jump; however, this correlation is only observed for small jumps (increments of less than 1.5 standard deviations of the IPSA return).

At the same time, it appears that for transactions of intermediate size (deciles 5 and 6), endogenous homophily increases the probability of an IPSA jump. In the absence of a consistent pattern between the correlations presented in Figure 5(a), it is not possible to conjecture what the role of this exogenous characteristic is with respect to the decision made by brokers when it comes time to trade. On the other hand, Figure 5(b) shows the bipartite network results that capture the correlation between the conjunction of endogenous homophily and exogenous heterophily and the IPSA jumps. In this case, significance is only observed in 4 cells. This is interpreted as the presence of noise since no association is observed between spatial dependence with the probability of an IPSA jump in this bipartite network in the vast majority of decile-intensity pairs of the jump. In other words, exogenous homophily or heterophily associated with investment banking does not show a systemic correlation with the market return as a whole.

In conclusion, the evidence suggests that investment banking services is not an appropriate typology to understand the endogenous homophily and heterophily, presented in Figures 1 and 2, and that affects the stock market. These results differ from the analysis that considered the research department typology.

7. Discussion and Conclusion

The demutualization process experienced by most of the stock markets of developed and emerging countries in recent years responded to the internationalization of financial markets, regulatory reforms, new financial products, and ultimately, changes in the business environment that made the survival of the stock markets under a mutual structure scheme unfeasible.

This process, accelerated by technological advances, reduced the entry barriers for new participants in the brokerage industry but also compressed the sources of revenue for brokers. In this new environment, it is worth asking about the effects of the demutualization process on the structure of the industry, competition, and, ultimately, the market efficiency levels.

As the market microstructure literature points out, the presence of frictions at the level of brokers has an effect on market efficiency, by affecting the prices of financial assets. Characteristics of brokers, such as their size, financial capabilities, affiliation, and research department, among others, have been mentioned as relevant factors.

Our research shows that there are matching trading patterns among stock brokers that may affect the stock market performance in an emerging market context. First, we present a novel methodology that combines a simple network decomposition and spatial econometrics to study how the exogenous types of the brokers affect their matching choices and the correlation between those matches and the stock market return. Second, we find that considering whether brokers organize their analysts in a research department plays a role in how selling counterparty matches between stock brokers influence the occurrence of a significant increase in the return of a stock market in a developing economy. More precisely, our methodology unveils that when trade tends to occur between brokers with and without research department that have dissimilar intraday average aggregate selling volume, the probability of observing a bull market raises. Simultaneously, we observe that, under the consideration of the research department typology, the presence of endogenous and exogenous homophily reduces the probability of a significant increase of the stock market return. Finally, by studying the Chilean case, we provide evidence of the existence of a relation between homophilic (heterophilic) trading patterns among stock brokers and stock market return. The SSE case provides valuable insights to understand the stock market efficiency in an emerging market context.

Our empirical analysis suggests that brokers' exogenous types, i.e., having a research department, and trading matches may affect the efficiency of the market. As financial literature indicates, prices equal fundamental value in an efficient market. For this, the market is required to be liquid, competitive, and perfect. The latter condition includes absence of frictions and equal access to market prices and information. As our findings suggest the activities of research departments, such as the generation of valuable information about the current and future performance of a company, an industry, or the economic and financial perspective of a country,

Threshold for the construction of the network	Size of the IPSA jump used in the Probit Regression										
	1 s.d	1.1 s.d	1.2 s.d	1.3 s.d	1.4 s.d	1.5 s.d	1.6 s.d	1.7 s.d	1.8 s.d	1.9 s.d	2 s.d.
First Decile	0.000425	-0.0795	-0.0938	**-0.193***	**-0.234****	-0.162	-0.177	-0.13	-0.151	-0.199	-0.216
	0.996	0.392	0.333	0.0547	0.0263	0.148	0.129	0.29	0.262	0.152	0.146
Second Decile	**-0.137***	-0.125	-0.0463	-0.0979	-0.0885	-0.0608	-0.117	-0.149	-0.141	**-0.209***	-0.129
	0.0963	0.144	0.602	0.291	0.37	0.563	0.28	0.192	0.249	0.096	0.332
Third Decile	**-0.156***	**-0.162***	**-0.151***	**-0.167***	**-0.169***	-0.0905	-0.0561	-0.065	-0.0952	-0.0853	-0.059
	0.0561	0.0543	0.0853	0.073	0.084	0.371	0.597	0.565	0.438	0.498	0.657
Fourth Decile	0.0456	0.00113	-0.00476	-0.0362	-0.0906	-0.0373	-0.00609	-0.0181	0.115	0.112	0.123
	0.578	0.989	0.958	0.7	0.358	0.722	0.955	0.873	0.35	0.363	0.352
Fifth Decile	0.0845	0.0234	0.0859	0.115	0.107	**0.192***	0.182	**0.269****	**0.343*****	**0.315****	**0.246***
	0.305	0.789	0.343	0.231	0.291	0.0757	0.105	0.0218	0.00784	0.0175	0.0804
Sixth Decile	**0.167****	**0.160***	**0.169***	0.137	0.104	0.159	0.166	**0.213***	**0.235***	**0.296****	**0.279****
	0.044	0.0663	0.0604	0.152	0.308	0.139	0.136	0.0646	0.0643	0.0216	0.0461
Seventh Decile	0.0924	0.108	0.0804	0.0373	0.0132	0.0642	0.0651	0.129	0.213	0.186	0.193
	0.275	0.22	0.388	0.707	0.901	0.567	0.573	0.277	0.1	0.17	0.184
Eighth Decile	0.0552	0.0734	0.061	0.0818	0.0574	0.0855	0.00283	0.0693	0.157	0.11	0.152
	0.513	0.402	0.505	0.399	0.576	0.425	0.98	0.557	0.224	0.413	0.287
Ninth Decile	**0.149***	0.133	0.112	0.0909	0.0118	0.0471	0.0167	0.0871	**0.229***	**0.237***	**0.277***
	0.0841	0.14	0.233	0.356	0.912	0.67	0.884	0.459	0.0736	0.0757	0.0505
All transactions	0.05	-0.0207	-0.0189	-0.0218	-0.0286	0.0111	-0.00104	0.0812	0.113	0.214	**0.275***
	0.576	0.827	0.846	0.833	0.794	0.923	0.993	0.516	0.413	0.115	0.0552

(a) Estimated coefficients associated with the positive spatial dependence variable in Probit regressions using only the network of traders with investment banking services. The regressions are estimated with different thresholds defining the transaction network and different sizes of the IPSA shock used as the dependent variable in the Probit. Each regression controls for the variation of oil prices, dollar prices, VIX index, emerging market index, copper prices, 5-year credit default swaps S&P 500 stock index, month, and year. The size of the IPSA jump is measured in standard deviations (s.d.)

Threshold for the construction of the network	Size of the IPSA jump used in the Probit Regression										
	1 s.d	1.1 s.d	1.2 s.d	1.3 s.d	1.4 s.d	1.5 s.d	1.6 s.d	1.7 s.d	1.8 s.d	1.9 s.d	2 s.d.
First Decile	-0.26	-0.155	-0.0261	-0.29	-0.154	-0.0188	-0.0454	0.0182	-0.135	-0.296	-0.211
	0.268	0.506	0.91	0.252	0.539	0.942	0.871	0.948	0.655	0.408	0.55
Second Decile	**-0.402****	-0.267	-0.144	-0.115	0.0085	0.0489	0.0337	-0.0107	-0.118	-0.106	-0.0319
	0.0427	0.178	0.459	0.563	0.966	0.819	0.878	0.961	0.616	0.653	0.893
Third Decile	**-0.492***	-0.359	-0.228	-0.0938	0.0464	0.184	0.148	0.0628	-0.0212	-0.00693	0.0952
	0.0526	0.158	0.359	0.702	0.851	0.465	0.567	0.817	0.946	0.983	0.771
Fourth Decile	**-0.600***	-0.469	-0.585	-0.453	-0.345	-0.19	-0.0922	-0.361	-0.271	-0.229	-0.124
	0.0632	0.149	0.102	0.203	0.334	0.598	0.792	0.427	0.562	0.626	0.795
Fifth Decile	-0.105	0.0161	-0.187	-0.0705	0.059	0.23	0.294	0.00287	0.129	0.119	0.159
	0.733	0.958	0.578	0.836	0.86	0.497	0.385	0.995	0.772	0.792	0.731
Sixth Decile	0.251	0.368	0.272	0.34	0.198	0.329	0.166	-0.144	-0.132	-0.12	-0.0403
	0.418	0.235	0.395	0.286	0.543	0.324	0.667	0.769	0.796	0.812	0.935
Seventh Decile	0.0409	0.137	0.204	0.247	-0.155	-	--	--	--	--	--
	0.931	0.772	0.66	0.589	0.767	0.891					
Eighth Decile	0.345	0.434	0.536	0.299	-	-	--	--	--	--	--
	0.375	0.277	0.171	0.498	0.846	0.971					
Ninth Decile	0.528	0.633	0.715	0.748	0.266	0.306	--	--	--	--	--
	0.285	0.203	0.146	0.125	0.635	0.597					
All transactions	0.65	0.762	**0.877***	0.563	0.103	0.164	--	--	--	--	--
	0.189	0.125	0.0754	0.299	0.858	0.776					

(b) Estimated coefficients associated with the positive spatial dependence variable in Probit regressions using the bipartite network of traders with and without investment banking services. The regressions are estimated with different thresholds defining the transaction network and different sizes of the IPSA shock used as the dependent variable in the Probit. Each regression controls for the variation of oil prices, dollar prices, VIX index, emerging market index, copper prices, 5-year credit default swaps S&P 500 stock index, month, and year. The size of the IPSA jump is measured in standard deviations (s.d.)

Figure 5

may play an important role in the markets' returns. For example, they could help to improve efficiency by reducing the probability of the formation of assets bubbles. At the same time, the coexistence of significant endogenous heterophily in subnetworks constructed under the research department typology and an IPSA jump may indicate that the information generated by the research department enhances the sustainability of the stock market, since they help that prices tend to reflect fundamentals when they deviate from their intrinsic values.

Therefore, from a policy perspective, our study also provides a contribution in evaluating the importance of entry barriers to the brokerage industry and its composition. Thus, from market efficiency perspective, in markets undergoing a demutualization process, there may exist a tradeoff between increasing the number of incumbent brokers and the composition of the brokerage industry. A direct implication of the latter is that having a fixed number of brokers, the greater the proportion of brokers with research department, the better the efficiency in the market. In this sense, it is worth asking what would happen if the market was dominated by brokers without research capabilities? We conjecture that in a context of an emerging economy it may even amplify the impact of these brokers' typologies on the stock market, as the lesser efficiency of financial markets in developing economies suggests [21]. Accordingly, as the level of financial literacy of brokers and customers improves, together with accessible information regarding the brokerage participants in the market, it will let investors to make better-informed elections among different kinds of brokerages services and trade execution practices.

Therefore, our study proposes some directions for extensions. The first obvious extension is to clarify the mechanism that links research departments with stock market returns. A second extension is to improve the understanding of how research departments affect the aggregate stock market's efficiency. One possible conjecture that would explain the latter is that institutional and retail investors usually base their buying/selling decisions on the research emitted by sell-side analysts, reports which help investors to respond to the new information.

Appendix

See Figures 6, 7, and 8.

Data Availability

The data used to support the findings of this study are available from the corresponding author upon request.

Conflicts of Interest

The authors declare that they have no conflicts of interest regarding the publication of this paper.

Acknowledgments

The authors would like to thank the Santiago Stock Exchange for their help providing the data to elaborate on this research. We also thank an anonymous referee for her comments.

Endnotes

1. Diamond and Dybvig [4], Allen and Gale [5], Brealey and others [6], and Diamond [7] studied banking in its roles of delegated monitoring, asset transformation, production of information, and reduction of transaction costs. Stracca [8] studies mutual and pension funds in their capacity as delegated portfolio managers by providing asset transformation services, research, administration and custody of securities, portfolio management, and diversification of investment portfolios.
2. A demutualization process consists in the process of reducing the entry barriers to become a stock broker. Namely, the requirement of ownership of a stock market stock is eliminated.
3. The stock market promotes the acquisition and dissemination of information, reducing the transaction costs and facilitating the investment process. Additionally, it reduces agency problems among investors and firms and lessens the cost of capital of issuing companies [30].
4. For instance, suppose the type of a broker is defined by having investment banking services. Then, H2.a tests when brokers with investment banking services and low intraday average selling volume tend to sell to other with investment banking services and low intraday average selling volume, the probability of a large return of the IPSA decreases. On the other hand, hypothesis H2.b tests if brokers with investment banking services and low intraday average selling volume tend to sell to other with investment banking services and high intraday average selling volume, the probability of a large return of the IPSA increases.
5. For interpretation purposes we characterize the brokers' transaction network as a directed network which indicates the volume sold by one broker to another.
6. We follow Eberhard and others [22] in the construction of the transaction network.
7. We construct the same transaction network studied by Eberhard and others [22].
8. Our analysis of the behavior of the broker market is focused on an aggregate level and not on a specific level of certain shares.
9. These attributes are exogenous to the intraday decision to sell a specific volume of stock to a specific counterparty. It is also worth mentioning that we partitioned the set of brokers by using the average of the broker's average equity from 2006 to 2015.
10. Investment banking activities usually refer to issuance of an initial public offering of shares (IPO) and a

Threshold for the construction of the network	Size of the IPSA jump used in the Probit Regression										
	1 s.d	1.1 s.d	1.2 s.d	1.3 s.d	1.4 s.d	1.5 s.d	1.6 s.d	1.7 s.d	1.8 s.d	1.9 s.d	2 s.d.
First Decile	**-0.167***	**-0.157***	-0.0742	-0.104	**-0.205***	**-0.199***	**-0.214***	**-0.169**	**-0.299****	**-0.379*****	**-0.297****
	0.0547	0.0819	0.436	0.296	0.0507	0.0739	0.0639	0.168	0.0262	0.00650	0.0500
Second Decile	**-0.251*****	**-0.213****	**-0.154***	-0.136	-0.125	-0.129	-0.151	**-0.215***	**-0.255***	**-0.284****	-0.210
	0.00278	0.0140	0.0861	0.152	0.215	0.231	0.181	0.0737	0.0505	0.0342	0.136
Third Decile	**-0.247*****	**-0.190****	**-0.207****	-0.148	-0.170	-0.103	-0.126	**-0.220***	-0.204	**-0.236***	-0.0922
	0.00706	0.0447	0.0354	0.148	0.116	0.370	0.294	0.0920	0.139	0.0947	0.520
Fourth Decile	**-0.203****	-0.165	-0.117	-0.0649	-0.0363	0.0239	-0.0871	-0.191	-0.0885	-0.145	-0.0106
	0.0478	0.125	0.282	0.564	0.757	0.846	0.515	0.181	0.555	0.348	0.947
Fifth Decile	**-0.273****	**-0.213***	-0.165	-0.124	-0.148	-0.0535	-0.125	-0.111	-0.0722	-0.183	-0.204
	0.0236	0.0852	0.187	0.327	0.275	0.703	0.414	0.492	0.678	0.326	0.294
Sixth Decile	-0.0793	-0.0258	-0.0278	0.0947	0.0586	0.142	0.0568	-0.0308	0.0155	-0.0389	-0.0688
	0.536	0.844	0.835	0.486	0.685	0.342	0.728	0.862	0.935	0.847	0.747
Seventh Decile	-0.152	-0.168	-0.144	-0.177	**-0.308***	**-0.330***	**-0.884*****	**-0.774*****	**-0.722****	**-0.687****	**-0.584****
	0.334	0.309	0.376	0.304	0.0990	0.0869	0.000912	0.00442	0.0107	0.0141	0.0381
Eighth Decile	-0.213	-0.207	-0.108	-0.185	-0.304	-0.212	**-0.578***	-0.473	**-0.971****	**-0.931****	**-0.840****
	0.233	0.282	0.575	0.379	0.178	0.349	0.0831	0.162	0.0128	0.0149	0.0279
Ninth Decile	-0.204	-0.167	-0.0581	-0.0656	-0.0805	0.0116	-0.270	-0.410	-0.373	-0.319	-0.239
	0.298	0.406	0.772	0.755	0.705	0.957	0.351	0.227	0.310	0.384	0.508
All transactions	-0.142	-0.0929	0.0207	-0.0774	-0.240	-0.165	-0.445	-0.336	-0.298	-0.231	-0.138
	0.471	0.645	0.918	0.727	0.332	0.513	0.176	0.311	0.407	0.523	0.701

(a) Estimated coefficients associated with the negative spatial dependence variable in Probit regressions using only the network of traders with proprietary trading activities. The regressions are estimated with different thresholds defining the transaction network and different sizes of the IPSA shock used as the dependent variable in the Probit. Each regression controls for the variation of oil prices, dollar prices, VIX index, emerging market index, copper prices, 5-year credit default swaps S&P 500 stock index, month, and year. The size of the IPSA jump is measured in standard deviations (s.d.)

Threshold for the construction of the network	Size of the IPSA jump used in the Probit Regression										
	1 s.d	1.1 s.d	1.2 s.d	1.3 s.d	1.4 s.d	1.5 s.d	1.6 s.d	1.7 s.d	1.8 s.d	1.9 s.d	2 s.d.
First Decile	-0.107	-0.379	-0.284	-0.178	-0.322	-0.585	-0.450	-0.378	-0.346	-0.298	-0.229
	0.665	0.220	0.354	0.562	0.339	0.152	0.261	0.343	0.378	0.446	0.549
Second Decile	-0.0107	-0.0598	0.0454	0.104	0.0950	0.126	0.130	0.212	**0.343***	0.207	0.311
	0.949	0.738	0.796	0.559	0.616	0.517	0.514	0.290	0.0950	0.369	0.174
Third Decile	-0.290	-0.334	-0.331	-0.218	-0.0947	-0.0516	0.0460	-0.109	-0.0298	-0.148	-0.317
	0.123	0.100	0.110	0.292	0.648	0.815	0.833	0.675	0.914	0.632	0.343
Fourth Decile	-0.315	**-0.428***	**-0.534****	**-0.507***	-0.351	-0.211	-0.0880	-0.105	-0.254	-0.188	-0.0523
	0.113	0.0626	0.0325	0.0578	0.180	0.418	0.727	0.714	0.434	0.557	0.868
Fifth Decile	0.113	0.0020	-0.0956	0.0443	0.186	0.212	0.185	0.341	0.230	-0.0362	0.0623
	0.592	0.993	0.710	0.862	0.469	0.442	0.527	0.251	0.487	0.917	0.861
Sixth Decile	**-0.712****	**-0.525***	**-0.693****	**-0.895***	-0.722	-1.141	-0.911	-0.797	-0.715	-0.609	-0.479
	0.0145	0.0782	0.0300	0.0704	0.106	0.149	0.183	0.205	0.283	0.323	0.403
Seventh Decile	-0.391	-0.201	-0.414	-0.308	-0.218	-0.481	-0.342	-0.247	-0.157	-0.113	-0.0393
	0.216	0.536	0.247	0.388	0.543	0.293	0.458	0.586	0.744	0.818	0.936
Eighth Decile	-	-	-	-	-	-	-	-	-	-	-
	-	-	-	-	-	-	-	-	-	-	-
Ninth Decile	-	-	-	-	-	-	-	-	-	-	-
	-	-	-	-	-	-	-	-	-	-	-
All transactions	-	-	-	-	-	-	-	-	-	-	-
	-	-	-	-	-	-	-	-	-	-	-

(b) Estimated coefficients associated with the negative spatial dependence variable in Probit regressions using the bipartite network of traders with and without proprietary trading activities. The regressions are estimated with different thresholds defining the transaction network and different sizes of the IPSA shock used as the dependent variable in the Probit. Each regression controls for the variation of oil prices, dollar prices, VIX index, emerging market index, copper prices, 5-year credit default swaps S&P 500 stock index, month, and year. The size of the IPSA jump is measured in standard deviations (s.d.)

Figure 6

	Size of the IPSA jump used in the Probit Regression										
Threshold for the construction of the network	1 s.d	1.1 s.d	1.2 s.d	1.3 s.d	1.4 s.d	1.5 s.d	1.6 s.d	1.7 s.d	1.8 s.d	1.9 s.d	2 s.d.
First Decile	-0.131	-0.146	-0.135	**-0.246****	**-0.220****	**-0.222****	**-0.275****	**-0.279****	**-0.342****	**-0.403*****	**-0.325****
	0.134	0.106	0.154	0.0121	0.0354	0.0425	0.0142	0.0186	0.0110	0.00427	0.0317
Second Decile	**-0.342*****	**-0.293*****	**-0.217****	**-0.202****	**-0.255****	**-0.205***	-	**-0.33*****	**-0.273****	**-0.340*****	**-0.303****
	3.88e-05	0.000613	0.0146	0.0312	0.0116	0.0549	0.00727	0.00455	0.0325	0.00960	0.0305
Third Decile	**-0.249*****	**-0.201****	-0.150	-0.138	**-0.183***	**-0.206***	**-0.222***	**-0.275****	**-0.235***	**-0.260***	-0.149
	0.00509	0.0304	0.120	0.168	0.0836	0.0674	0.0634	0.0273	0.0767	0.0546	0.288
Fourth Decile	-0.151	-0.0973	-0.0616	-0.00400	-0.0265	-0.0167	-0.0548	-0.0989	-0.0846	-0.164	-0.0344
	0.101	0.312	0.531	0.969	0.805	0.884	0.648	0.436	0.532	0.234	0.811
Fifth Decile	-0.0553	-0.0165	-0.0609	0.0598	0.0772	0.0856	0.0263	-0.0500	-0.105	-0.171	-0.144
	0.572	0.869	0.556	0.575	0.491	0.469	0.832	0.711	0.488	0.273	0.388
Sixth Decile	-0.0347	0.00764	-0.0562	0.0216	0.0185	0.0398	-0.00722	-0.100	-0.117	-0.184	-0.139
	0.728	0.941	0.603	0.843	0.873	0.746	0.956	0.474	0.448	0.256	0.408
Seventh Decile	-0.161	-0.106	**-0.201***	-0.167	**-0.240***	-0.234	**-0.305****	**-0.402****	**-0.447****	**-0.387****	-0.275
	0.132	0.340	0.0959	0.178	0.0709	0.102	0.0485	0.0176	0.0140	0.0328	0.134
Eighth Decile	**-0.272****	**-0.263****	**-0.262****	-0.163	**-0.273****	**-0.325****	**-0.406****	**-0.359****	**-0.491****	**-0.419****	-0.284
	0.0130	0.0291	0.0371	0.201	0.0490	0.0349	0.0174	0.0427	0.0160	0.0377	0.157
Ninth Decile	**-0.174***	-0.124	**-0.179***	-0.130	-0.170	-0.198	**-0.293****	**-0.303***	**-0.355****	**-0.307***	-0.248
	0.0859	0.230	0.0976	0.248	0.164	0.138	0.0477	0.0525	0.0385	0.0737	0.171
All transactions	**-0.169***	-0.122	-0.164	**-0.210****	**-0.233****	**-0.202***	-0.209	-0.166	-0.180	-0.204	-0.168
	0.0752	0.212	0.109	0.0490	0.0434	0.0978	0.104	0.212	0.214	0.171	0.287

(a) Estimated coefficients associated with the negative spatial dependence variable in Probit regressions using only the network of traders with large equity. The regressions are estimated with different thresholds defining the transaction network and different sizes of the IPSA shock used as the dependent variable in the Probit. Each regression controls for the variation of oil prices, dollar prices, VIX index, emerging market index, copper prices, 5-year credit default swaps S&P 500 stock index, month, and year. The size of the IPSA jump is measured in standard deviations (s.d.)

	Size of the IPSA jump used in the Probit Regression										
Threshold for the construction of the network	1 s.d	1.1 s.d	1.2 s.d	1.3 s.d	1.4 s.d	1.5 s.d	1.6 s.d	1.7 s.d	1.8 s.d	1.9 s.d	2 s.d.
First Decile	**-0.425***	**-0.430***	**-0.488***	**-0.548****	**-0.743****	**-0.649****	**-0.938*****	**-0.835****	**-0.862****	**-0.807****	**-0.750****
	0.0604	0.0753	0.0536	0.0461	0.0179	0.0388	0.00851	0.0206	0.0211	0.0284	0.0468
Second Decile	-0.124	-0.0709	0.0410	0.0479	0.0216	0.0757	0.186	0.181	-0.109	-0.234	-0.112
	0.473	0.692	0.817	0.790	0.912	0.710	0.357	0.402	0.677	0.439	0.708
Third Decile	**-0.474****	-0.359	-0.234	-0.220	-0.244	-0.0998	0.00790	0.0905	0.0599	0.118	0.239
	0.0412	0.124	0.300	0.349	0.327	0.694	0.975	0.717	0.832	0.677	0.409
Fourth Decile	-0.250	-0.131	-0.00531	0.153	0.121	0.248	0.356	0.469	**0.689****	0.491	0.436
	0.349	0.627	0.984	0.561	0.672	0.391	0.208	0.112	0.0276	0.110	0.222
Fifth Decile	0.114	0.224	0.305	0.449	**0.590***	0.261	0.357	0.461	0.609	0.230	0.398
	0.711	0.463	0.318	0.153	0.0660	0.524	0.370	0.260	0.143	0.627	0.384
Sixth Decile	-0.405	-0.234	-0.153	0.0311	0.195	0.326	0.493	0.547	0.839	**0.949***	**1.128***
	0.409	0.638	0.753	0.950	0.697	0.525	0.328	0.273	0.118	0.0848	0.0454
Seventh Decile	-0.354	-0.204	-0.124	0.0488	0.200	0.324	0.453	0.512	0.806	0.967	**1.214***
	0.473	0.685	0.800	0.924	0.700	0.543	0.400	0.341	0.191	0.116	0.0691
Eighth Decile	-0.363	-0.217	-0.108	--	--	--	--	--	--	--	--
	0.492	0.685	0.840								
Ninth Decile	0.246	0.371	0.456	0.149	0.266	0.416	0.457	0.566	0.844	0.860	0.917
	0.536	0.357	0.264	0.775	0.611	0.428	0.377	0.277	0.114	0.104	0.113
All transactions	0.408	0.538	0.631	0.291	0.399	0.538	0.586	0.714	**1.032***	**1.060***	**1.179****
	0.359	0.232	0.166	0.606	0.480	0.337	0.294	0.203	0.0641	0.0503	0.0477

(b) Estimated coefficients associated with the negative spatial dependence variable in Probit regressions using the bipartite network of traders with and without proprietary trading activities. The regressions are estimated with different thresholds defining the transaction network and different sizes of the IPSA shock used as the dependent variable in the Probit. Each regression controls for the variation of oil prices, dollar prices, VIX index, emerging market index, copper prices, 5-year credit default swaps S&P 500 stock index, month, and year. The size of the IPSA jump is measured in standard deviations (s.d.)

Figure 7

Threshold for the construction of the network	Size of the IPSA jump used in the Probit Regression										
	1 s.d	1.1 s.d	1.2 s.d	1.3 s.d	1.4 s.d	1.5 s.d	1.6 s.d	1.7 s.d	1.8 s.d	1.9 s.d	2 s.d.
First Decile	-0.0481	-0.00119	0.00882	-0.0275	-0.0364	-0.0451	-0.0269	-0.0345	-0.0297	-0.0743	**-0.235***
	0.607	0.990	0.930	0.793	0.743	0.699	0.825	0.787	0.826	0.592	0.0966
Second Decile	**-0.288*****	**-0.228*****	**-0.208****	**-0.219****	**-0.238****	**-0.178***	**-0.215***	-0.128	-0.0770	-0.0749	-0.0750
	0.000479	0.00780	0.0198	0.0190	0.0176	0.0943	0.0513	0.274	0.543	0.569	0.573
Third Decile	-0.0351	-0.0809	-0.0590	-0.137	-0.140	-0.170	-0.114	-0.0876	-0.140	-0.0808	-0.0905
	0.663	0.338	0.503	0.141	0.149	0.103	0.286	0.432	0.252	0.522	0.491
Fourth Decile	-0.0424	-0.0586	-0.0866	-0.0910	-0.0891	-0.0953	-0.0292	-0.0170	-0.00998	0.0666	0.163
	0.604	0.487	0.323	0.324	0.358	0.349	0.780	0.877	0.932	0.584	0.186
Fifth Decile	-0.0689	-0.0767	-0.0628	-0.0971	-0.110	-0.0993	-0.0467	-0.0305	0.0445	0.00245	-0.0399
	0.405	0.379	0.488	0.306	0.273	0.350	0.671	0.791	0.724	0.985	0.776
Sixth Decile	-0.0407	-0.0545	-0.0460	-0.110	-0.0809	-0.0524	-0.0327	0.0374	-0.0555	-0.0471	-0.113
	0.631	0.533	0.611	0.258	0.426	0.621	0.763	0.735	0.648	0.710	0.398
Seventh Decile	-0.0598	-0.00673	-0.0737	-0.134	-0.167	-	**-0.248****	-0.167	-0.101	-0.0316	-0.114
	0.496	0.940	0.428	0.178	0.119	0.0247	0.0433	0.185	0.455	0.818	0.431
Eighth Decile	-0.124	-0.0630	-0.0972	-0.169	-0.165	-0.205	-0.213	-0.214	-0.114	-0.118	-0.153
	0.180	0.508	0.334	0.120	0.151	0.103	0.109	0.119	0.434	0.435	0.357
Ninth Decile	-0.0599	-0.00145	0.0190	0.0427	-0.0442	-0.0330	-0.0259	-0.136	-0.0469	-0.0494	-0.159
	0.534	0.988	0.852	0.690	0.705	0.790	0.841	0.326	0.755	0.748	0.361
All transactions	**-0.212****	-0.165	-0.129	-0.0561	-0.0477	-0.0218	-0.0130	-0.110	-0.0167	-0.0706	-0.129
	0.0298	0.103	0.214	0.602	0.681	0.858	0.919	0.430	0.909	0.647	0.446

(a) Estimated coefficients associated with the negative spatial dependence variable in Probit regressions using only the network of foreign traders. The regressions are estimated with different thresholds defining the transaction network and different sizes of the IPSA shock used as the dependent variable in the Probit. Each regression controls for the variation of oil prices, dollar prices, VIX index, emerging market index, copper prices, 5-year credit default swaps S&P 500 stock index, month, and year. The size of the IPSA jump is measured in standard deviations (s.d.)

Threshold for the construction of the network	Size of the IPSA jump used in the Probit Regression										
	1 s.d	1.1 s.d	1.2 s.d	1.3 s.d	1.4 s.d	1.5 s.d	1.6 s.d	1.7 s.d	1.8 s.d	1.9 s.d	2 s.d.
First Decile	-	-	-	-	-	-	-	-	-	-	-
	-	-	-	-	-	-	-	-	-	-	-
Second Decile	-0.0367	0.0956	0.210	**0.272***	**0.279***	**0.315****	**0.303***	**0.344***	0.266	**0.336***	**0.345***
	0.793	0.498	0.134	0.0590	0.0675	0.0489	0.0712	0.0502	0.176	0.0889	0.0956
Third Decile	**-0.499****	-0.369*	-0.281	-0.134	-0.297	-0.295	-0.221	-0.154	-0.257	-0.207	-0.143
	0.0256	0.0999	0.204	0.544	0.218	0.271	0.408	0.562	0.413	0.517	0.661
Fourth Decile	-0.289	-0.227	-0.255	-0.0766	-0.0928	-0.104	-0.0218	0.0670	-0.00826	0.0658	0.174
	0.188	0.338	0.305	0.757	0.718	0.714	0.939	0.814	0.980	0.843	0.604
Fifth Decile	-0.149	-0.145	-0.0356	-0.0479	-0.147	-0.208	-0.134	-0.388	-0.296	-0.267	-0.215
	0.553	0.597	0.894	0.864	0.615	0.541	0.693	0.383	0.519	0.568	0.650
Sixth Decile	**0.477****	0.370	**0.489***	0.332	0.237	0.187	0.256	0.116	0.280	0.329	0.453
	0.0447	0.178	0.0637	0.229	0.396	0.554	0.420	0.743	0.436	0.357	0.224
Seventh Decile	-0.662	-0.483	-0.387	-0.248	-0.143	-	-	-	-	-	-
	0.160	0.321	0.424	0.603	0.766	-	-	-	-	-	-
Eighth Decile	-	-	-	-	-	-	-	-	-	-	-
	-	-	-	-	-	-	-	-	-	-	-
Ninth Decile	-0.354	-0.215	-0.108	0.0605	0.130	-	-	-	-	-	-
	0.476	0.677	0.833	0.903	0.795	-	-	-	-	-	-
All transactions	-	-	-	-	-	-	-	-	-	-	-
	-	-	-	-	-	-	-	-	-	-	-

(b) Estimated coefficients associated with the negative spatial dependence variable in Probit regressions using the bipartite network of traders with and without proprietary trading activities. The regressions are estimated with different thresholds defining the transaction network and different sizes of the IPSA shock used as the dependent variable in the Probit. Each regression controls for the variation of oil prices, dollar prices, VIX index, emerging market index, copper prices, 5-year credit default swaps S&P 500 stock index, month, and year. The size of the IPSA jump is measured in standard deviations (s.d.)

Figure 8

seasoned equity offering (SEO), debt securities, mergers and acquisitions (M&A), and financial advice [31].

11. The latter trend also generates a source of conflict of interest because brokers' proprietary trading activities conflict with their fiduciary responsibility to obtain "best execution" and "independent" trades for clients.
12. A link between two brokers indicates the total volume sold by one broker to the other above a threshold. See Eberhard and others [22] for a detailed description on how to construct the broker's transaction network.
13. As mentioned in the financial literature, in Chile as in other markets, technological changes, competition, the emergence of professional investors, and the need to establish long-term relationships with customers have generated a concentrated market with a pyramidal type structure, consequently, affecting the brokerage services offered by brokers. Following Goldstein and others [26], there are also full-service and low-cost brokers in Chile. The former offers a full range of high-cost and high-quality brokerage services, while the latter focuses on the execution of low-cost purchase/sale transactions.
14. A criterium generates a partition of the set of brokers into two disjoint sets of brokers, a set of brokers that meet the criterium to be categorized as type "A" and a set of brokers that do not meet the criterium to be labeled as type "A".
15. We follow the same definitions for the network objects as in Eberhard and others [22]. If link ij exists in the transaction subnetwork g^A, then ij does not exist in g^B.
16. The calculation for the standard deviation of the IPSA return is made considering the last 360 days; that is, we use a "moving year."
17. Eberhard and others [22] find that the structure of transaction network between brokers correlates only with IPSA jumps and not with significant drops in this indicator.
18. We compared the average equity of each broker from 2006 to 2015 with respect to the entire industry average in the same period.
19. For example, the brokers' transaction subnetwork with a research department, the brokers' transaction subnetwork without a research department, or the bipartite subnetwork between both types of brokers.
20. Studying spatial dependence within respective groups allows us to analyze whether the choice of selling to a specific broker is just an endogenous choice to the financial market or if it is also a choice associated with the intermediaries' own characteristics
21. Thus, a statistically significant coefficient on the spatial dependency indicator in the subnetworks provides valuable information about the mechanism that would explain the presence of homophily/heterophily in the entire daily transaction network.
22. The interested reader can request the tests for spatial dependency (positive and negative) to the authors.
23. All analogous results for negative spatial dependence are available upon request.
24. Additionally, the standard nomenclature is included, where *, **, and *** represent significance at 10%, 5%, and 1%, respectively, and the coefficients are in bold font.
25. We consider the transaction networks built considering the first, second, third, and fourth deciles of the aggregate traded volume between two brokers as large volume transaction networks.
26. There are no testable hypotheses for the subnetwork of brokers with type "no-A", however the results of those analysis are available upon request.
27. The analogous figures for all the subnetworks based on the exogenous criteria mentioned in this paper (size, investment banking services, and proprietary trading) are also available upon request.

References

[1] F. Allen, "Do financial institutions matter?" *Journal of Finance*, vol. 56, no. 4, pp. 1165–1175, 2001.

[2] A. Sensoy and B. M. Tabak, "Dynamic spanning trees in stock market networks: the case of Asia-Pacific," *Physica A: Statistical Mechanics and its Applications*, vol. 414, pp. 387–402, 2014.

[3] S. M. Guerra, T. C. Silva, B. M. Tabak, R. A. de Souza Penaloza, and R. C. de Castro Miranda, "Systemic risk measures," *Physica A: Statistical Mechanics and its Applications*, vol. 442, Article ID 16392, pp. 329–342, 2016.

[4] D. W. Diamond and P. H. Dybvig, "Bank runs, deposit insurance, and liquidity," *Journal of Political Economy*, vol. 91, no. 3, pp. 401–419, 1983.

[5] F. Allen and D. Gale, "Financial markets, intermediaries, and intertemporal smoothing," *Journal of Political Economy*, vol. 105, no. 3, pp. 523–546, 1997.

[6] R. Brealey, H. E. Leland, and D. H. Pyle, "Informational asymmetries, financial structure, and financial intermediation," *The Journal of Finance*, vol. 32, no. 2, pp. 371–387, 1977.

[7] D. W. Diamond, "Financial intermediation and delegated monitoring," *The Review of Economic Studies*, vol. 51, no. 3, pp. 393–414, 1984.

[8] L. Stracca, "Delegated portfolio management: a survey of the theoretical literature," *Journal of Economic Surveys*, vol. 20, no. 5, pp. 823–848, 2006.

[9] N. Hardy, N. S. Magner, J. Lavin, R. A. Cardenas, and M. Jara-Bertin, "Small consequences of a major agreement: the MILA case," *Academia Revista Latinoamericana de Administración*, vol. 31, no. 3, pp. 486–518, 2018.

[10] K. Hagerty and R. McDonald, "Brokerage, market fragmentation, and securities market regulation," in *The Industrial Organization and Regulation of the Securities Industry*, pp. 35–62, University of Chicago Press, 1996.

[11] M. Demirbag, M. McGuinness, A. Akin, N. Bayyurt, and E. Basti, "The professional service firm (PSF) in a globalised economy: A study of the efficiency of securities firms in an emerging market," *International Business Review*, vol. 25, no. 5, pp. 1089–1102, 2016.

[12] D. Lee, J. Kim, and H. Kang, "Do larger brokerage firms enjoy larger economies of scale and scope?" *Seoul Journal of Economics*, vol. 27, pp. 445–467, 2014.

[13] D. Easley and M. O'Hara, "Microstructure and asset pricing," *Handbook of the Economics of Finance*, vol. 1, pp. 1021–1051, 2003.

[14] L. Blume, D. Easley, and M. O'hara, "Market statistics and technical analysis: the role of volume," *The Journal of Finance*, vol. 49, no. 1, pp. 153–181, 1994.

[15] J. Y. Campbell, S. J. Grossman, and J. Wang, "Trading volume and serial correlation in stock returns," *The Quarterly Journal of Economics*, vol. 108, no. 4, pp. 905–939, 1993.

[16] C. M. C. Lee and B. Swaminathan, "Price momentum and trading volume," *Journal of Finance*, vol. 55, no. 5, pp. 2017–2069, 2000.

[17] M. McPherson, L. Smith-Lovin, and J. M. Cook, "Birds of a feather: homophily in social networks," *Annual Review of Sociology*, vol. 27, pp. 415–444, 2001.

[18] L. Anselin, *Spatial Econometrics: Methods and Models*, Kluwer Academic Publishers, Dordrecht, Nederlands, 2001.

[19] H. S. Choi, J. Clarke, S. P. Ferris, and N. Jayaraman, "The effects of regulation on industry structure and trade generation in the US securities industry," *Journal of Banking & Finance*, vol. 33, no. 8, pp. 1434–1445, 2009.

[20] S. Liu, "Commission deregulation and performance of securities firms: Further evidence from Japan," *Journal of Economics and Business*, vol. 60, no. 4, pp. 355–368, 2008.

[21] C. Kearney, "Emerging markets research: Trends, issues and future directions," *Emerging Markets Review*, vol. 13, no. 2, pp. 159–183, 2012.

[22] J. Eberhard, J. F. Lavin, and A. Montecinos-Pearce, "A network-based dynamic analysis in an equity stock market," *Complexity*, vol. 2017, Article ID 3979836, 16 pages, 2017.

[23] H. R. Stoll, "Market microstructure," *Handbook of the Economics of Finance*, vol. 1, pp. 553–604, 2003.

[24] J. Hasbrouck and G. Saar, "Low-latency trading," *Journal of Financial Markets*, vol. 16, no. 4, pp. 646–679, 2013.

[25] E. Boehmer, R. Jennings, and L. Wei, "Public disclosure and private decisions: equity market execution quality and order routing," *Review of Financial Studies*, vol. 20, no. 2, pp. 315–358, 2007.

[26] M. A. Goldstein, P. Irvine, E. Kandel, and Z. Wiener, "Brokerage commissions and institutional trading patterns," *Review of Financial Studies*, vol. 22, no. 12, pp. 5175–5212, 2009.

[27] J. T. Linnainmaa and G. Saar, "Lack of anonymity and the inference from order flow," *Review of Financial Studies*, vol. 25, no. 5, pp. 1414–1456, 2012.

[28] S. Hayes, A. Spence, and D. Marks, *Competition in the Investment Banking Industry*, Harvard University Press, 1983.

[29] B. N. Anand and A. Galetovic, "Relationships, competition and the structure of investment banking markets," *The Journal of Industrial Economics*, vol. 54, no. 2, pp. 151–199, 2006.

[30] P. Arestis, P. O. Demetriades, and K. B. Luintel, "Financial development and economic growth: the role of stock markets," *Journal of Money, Credit and Banking*, vol. 33, no. 1, pp. 16–41, 2001.

[31] J. R. Ritter, "Investment banking and securities issuance," *Handbook of the Economics of Finance*, vol. 1, pp. 255–306, 2003.

Hindawi
Complexity
Volume 2019, Article ID 7820618, 19 pages
https://doi.org/10.1155/2019/7820618

Research Article

Weight of the Default Component of CDS Spreads: Avoiding Procyclicality in Credit Loss Provisioning Framework

Mariya Gubareva [1,2]

[1] *ISCAL–Lisbon Accounting and Business School, Instituto Politécnico de Lisboa, Av. Miguel Bombarda, 20, 1069-035 Lisbon, Portugal*
[2] *SOCIUS–Research Centre in Economic and Organizational Sociology, CSG-Research in Social Sciences and Management, Rua Miguel Lupi, 20, 1249-078 Lisbon, Portugal*

Correspondence should be addressed to Mariya Gubareva; mgubareva@iscal.ipl.pt

Received 21 February 2019; Revised 26 May 2019; Accepted 9 June 2019; Published 4 July 2019

Guest Editor: Thiago C. Silva

The current expected loss calculations have recently attracted considerable attention in the research on credit risk modeling, impairment provisioning, and financial networks' stability. A new CDS-based approach to estimate current expected credit loss is proposed for low default portfolios, containing credit exposures to corporate issuers covered by publicly traded CDS contracts. First, a fraction of CDS spread related to a pure default compensation for different CDS maturities is assessed. Our results contrast with previous research. Second, based on the obtained historical weights of the default risk premium, a forward-looking term structure of the probabilities of default implied by the current CDS quotes is derived. The proposed approach covers both investment and noninvestment grade debt. The resulting framework is applied to a sample of corporate bonds. The developed methodology provides a useful tool, on one hand, for credit risk managers and balance-sheet preparers and, on the other hand, for regulators of financial markets as it sheds light on how procyclicality could be avoided in provisions.

1. Introduction

Financial systems, being complex networks in their nature, evolve continuously and their features undergo a never-ending process of substantial changes (see, e.g., Tabak et al. [1]). There is a vast body of recent literatures on systemic financial risk arising from interconnectedness of institutions, targeting financial systems' stability (see, e.g., Aymann et al. [2]; Souza et al. [3]; Silva et al. [4]). One of the important domains analyzed in literature is the case of financial networks primarily linked through different types of credit contracts, portfolio contagion, or credit guarantees, (see, e.g., Li and Wen [5], Anagnostou et al. [6], and Jiang and Fan [7]).

However, the major part of the studies considers interconnectedness of institutions, which is mostly due to one certain mechanism of interactions, being either credit relationship, or derivatives-linked connectivity, or foreign exchange driven linkages, or other one-dimensional factors (Li and Wen [7] and Poledna et al. [8]). Still, agents of real financial systems interact in diverse manners and through several channels. Such a situation could be duly modeled by bipartite (Huang et al. [9]) and/or by multiplex, that is, multilayer (Li and Wen [5] and Poledna et al. [8]) networks.

With respect to the credit risk interconnectedness, it occurs at least at two different layers. The first one is the level of prudential regulation, at which the minimal capital requirements are established as obligatory for diverse financial institutions. The main objective to oblige financial institutions to hold capital buffers is to create resilience in the financial system by allowing banks and other lenders to withstand unexpected losses under eventuality of adverse future scenarios. The second layer is the level of impairment provisioning framework, related to the new accounting standards, recently issued by the Financial Accounting Standard Board (FASB) and by the International Accounting Standard Board (IASB), known, respectively, as CECL framework and IFRS 9 [10, 11]. Both the CECL model and IFRS 9 framework require financial institutions to abandon the solely incurred losses based accounting and estimate expected losses over the lifetime of credit exposures.

On one hand, the idea of these new standards is to address some issues revealed by the global financial crisis, including

those related to the incurred credit loss model. But if accounting, previously, was focused only on registering facts of the past, now a component of futurology, regarding expected credit losses, is entering into the domain of accounting, augmenting its interconnectedness with capital allocation framework and, hence, in a certain sense, potentially leading to systemic risks of other kinds, especially related to eventual procyclicality in the credit loss provisions, making both capital and provisioning frameworks interlinked [12, 13].

Both CECL and IFRS 9 standards allow the use of market sensitive parameters and, henceforth, are expected to cause cyclicality in provisions. However, what represents a potentially dangerous systemic handicap is an eventual unintended procyclicality, that is, amplified cycle-related fluctuations of impairment allowances, driven by the new accounting standards implementation.

Additionally, the systemic risk in the global financial system is interlinked even at a higher degree than one may perceive at the first sight, as both the capital allocation and the credit loss provisioning frameworks employ usually the same parameters of the credit risk, namely, probability of default (PD), loss given default (LGD), and exposure at default (EAD). It is worth noticing that the assessment of PDs for low default portfolios is one of the greatest hurdles for satisfying CECL and IFRS 9 requirements. Hence, financial institutions try to employ PD, derived from the same data for both capital requirements calculation, which must have through-the-cycle (T-t-C) features, and for expected loss provisioning, which must be based on the current forward-looking PDs. The perils of use of the unique risk measure across the financial system are evidenced, using the VaR metrics example by Aymann et al. [2].

Hence, from the point of view of financial networks' stability, it becomes highly desirable to use different sources of critical credit risk parameters, at least for PD. Such possibility will allow disentangling the capital requirements and the loss provisioning levels in the multiplex credit-related financial network, thus permitting diminishing procyclicality and potentially reducing overall systemic risks of the global financial system. The methodological approach presented herein is based on the use of CDS spreads as a starting point to estimate PDs and hence represents an alternative source with respect to PDs usually used by financial institutions to dimension their capital allocation processes.

Apart from our aspiration to shed light on possible ways to reduce procyclicality in provisions and diminish the systemic risk related to credit exposures, our motivation resides in our goal to propose a robust approach to deal with credit risk of low default portfolios. One needs to bear in mind that rare default events characterize some sectors like sovereign, banking, insurance, and so on. In this regard, the use of market-based metrics allows us to develop and calibrate PD models. Forward-looking PDs can easily be derived from publicly traded single-name CDS as spread quotes are usually available on a daily basis. A wide literature (see, e.g., Choudhry, [14]) describes how to move from CDS spreads to PD estimates.

Another feature facilitating the use of CDS spreads is their low correlation with interest rates. This circumstance makes them naturally suitable for credit impairment computation, which, at least in a pure theory, should not be affected by interest rate movements. For advanced reading on the interrelation between the credit spread and interest rates, see Gubareva and Borges [15]. While using yields and/or bond prices, they get influenced by the interest rates, as interest rates affect the time value of money but not necessarily impact the credit quality of the exposures. The use of CDS spreads makes, hence, the PD calculation sort of immune to interest rate trends as herein we are focused on creditworthiness of issuers.

It is worth noting that CDS spreads are commonly used in the literature to proxy credit risk. For additional reading, related to the use of CDS quotes for economic capital management, see Gubareva and Borges [16] and the references therein. Another case for CDS use is that CDS is also a very efficient and sensitive instrument to measure credit risk. For example, Sensoy et al. [17], studying dynamics of CDS contracts in emerging markets, demonstrate that CDS can be efficient even in the crisis episodes.

In accordance with the CECL and IFRS 9 accounting standards, robust and sound credit risk methodologies should not rely only on subjective, biased overly optimistic/pessimistic assumptions, or be based on purely hypothetic wishful-thinking considerations. The use of CDS spreads diminishes the importance of generating scenarios for ECL estimation, as they already reflect a certain set of market scenarios properly discounted by market participants. That is why the above-mentioned regulatory bodies, FASB and IASB, consider CDS spreads as valid market indicators of future debt performance: market price clears the battle of market participants' perspectives.

In this regard, we would like to point out that loss provisioning under CECL and IFRS 9 usually relies on a link function with macroeconomic scenarios, as PDs used by a vast majority of financial institutions for the origination, pricing, and capital adequacy assessment purposes are T-t-C measures, which lack point-in-timeliness and forward-looking aspects. To overcome these deficiencies, usually such financial institutions employ macroeconomic scenarios to transform their otherwise T-t-C PDs into current forward-looking estimates. That is why subjective scenario analysis usually becomes crucial for the entire ECL modeling.

The robustness of our approach vis-à-vis competing methods is its objectivity, as no subjective assumptions are needed to be made for expected credit loss (ECL) estimation, as our PDs are derived from CDS spread data currently observed in the market. Within the proposed CDS-based methodology, at any reporting date, PDs estimates are derived from CDS spreads term structure, which represents current forward-looking measures, as the macro- and microeconomic scenarios are already properly weighted by the market, which clears the respective CDS spreads for several maturities.

In order to further enhance our methodology, later on, it also could be linked to macroeconomic scenarios. Nevertheless, this topic remains outside of the scope of the current research paper. Our approach is also in line with the real economic value (REV) methodology applied by

the European Commission to evaluate impaired portfolios, which is based on a long-term average risk premium; see, for instance, Heynderickx et al. [18].

With respect to advancement of knowledge frontier in the domain of financial networks complexity, ECL calculation, and impairment provisioning, our paper contributes to the literature in the two following dimensions. First, we elaborate an effective approach for banks and financial institutions to optimize their modeling capacities complying with CECL and IFRS frameworks. Our approach allows estimating a truly forward-looking CECL which is free of subjective scenario analyses and thus enhances objectivity and reliability of the impairment allowances.

Second, to enable unbiased estimates of forward-looking PDs, we split the CDS spread into two, default and nondefault, components by assessing default risk premium for each forward term. This allows us to go beyond the actual frontier in CDS area. To the best of our knowledge, a somewhat similar study is performed by Huang and Huang [19] for the bond markets for 1973-1998. Authors attempt to calculate the weight of credit risk observed in corporate-Treasury yield spreads.

Additionally, the research paper by Arakelyan and Serrano [20], analyzing relatively recent data, assesses the fraction of the default component in CDS spreads within the period of 2004-2011. Still the main focus of this study is the liquidity component of CDS spreads. Thus, the quantification of the default-risk part of CDS spreads represents a by-product analysis of the main subject of this research, being assessed as a difference between the CDS spread and the liquidity component. However, our proposed CDS-based calibration approach to estimate the weight of the default component (WDC) is more robust and covers more recent period of 2007-2017, which is more relevant for CECL methodologies elaboration.

The rest of the paper is organized as follows. In the next section, we discuss conceptual remarks of the proposed approach aimed at deriving unbiased forward-looking PDs from CDS spreads. In the third section, we detail our PD calibration methodology and introduce the technique for distilling the WDC of CDS spreads. In the fourth section, we perform the calibration of our model and calculate the WDCs for BBB+, BBB, BBB-, BB+, BB, BB-, and lower than BB- ratings ranges of corporate debt for each point in the CDS spread term structure. In the fifth section, we illustrate an application of the calibrated PD term structure to the CECL-compliant ECL calculations for a set of Investment Grade (IG) and High Yield (HY) bond positions. The sixth and final section presents our conclusions and discusses their implications.

2. Model Set-Up: Forward-Looking PD Projection Based on CDS Spreads

2.1. Conceptual Remarks. Under CECL and IFRS 9 frameworks, the use of PD/LGD DCF method in the ECL calculations implies a necessity of the forward-looking projections of PD and LGD parameters. However, estimation of forward-looking PDs is in fact a major hurdle, especially for low-default portfolios. However, CECL and IFRS 9 frameworks are principal-based and impose only few specific requirements on methodology. They do not provide a particular methodology for calculating allowances, stating just that the loss allowances must reflect ECL based on past loss experiences, current economic situations, and "reasonable and supportable" forecasts of future economic conditions. Therefore, the modeling choices may generate variations in impairment allowances across institutions.

Hence, employing current CDS spreads for deduction of default term structure potentially helps to address the challenge of estimation of forward-looking PDs, because such market data incorporate both current information and forward-looking perspective. So, on one hand, CDS spreads contain information regarding credit quality of obligors available at the current point in the economic cycle. On the other hand, the term structure of CDS spreads permits deriving the respective term structure of spread-implied cumulative and then marginal PDs.

ECL methodologies and their implementation issues have recently attracted great attention of the academia researchers and practitioners; see McPhail and McPhail [21], Chawla et al. [22], Skoglund [23], and Zhang [24], among others. However, to the best of our knowledge, no methodology for credit loss impairment provisioning based on CDS spread quotes has been presented until now. Our paper fills this gap.

In addition, there are no sufficient internal data on low-default fixed-income portfolios to be used for the development of accurate internal models for ECL calculation. This could be explained by the rarity of the observed default events. At the same time, a considerable amount of external information on bonds, credit-linked notes, and alike instruments, including CDS, is available by many providers through the Bloomberg, Thomson-Reuters DataStream, and other data platforms. Therefore, we become motivated to design an easy-to-implement and easy-to-use methodology for ECL calculation in low-default bond portfolios based on public, readily available market data.

In line with the "guidelines on credit risk and accounting for expected credit losses" by the Basel Committee on Banking Supervision [25], sound credit risk methodologies should not merely rely on subjective, inherently biased assumptions or on purely hypothetic scenario constructions. Employing CDS spreads allows dedicating fewer efforts to scenario analyses, as traded CDS spreads by their proper nature represent an outcome of a set of scenarios properly discounted by market players.

Thus, CDS-based methodology allows preserving point-in-timeliness and forward-looking features of risk parameters as it relies on current projections of forward-looking PDs in a form of a PD term structure. Nevertheless, a methodological adjustment is needed as resulting PDs are inflated due to the nondefault component present in CDS spreads. We need to purge it out to allow for accurate PDs and, therefore, ECL estimates.

Note that a neutral character of ECL estimations is a goal of CECL framework, meaning that neither PDs nor ECL must be overoptimistic or overprudential. They just need to be precise and accurate to the maximum extent possible.

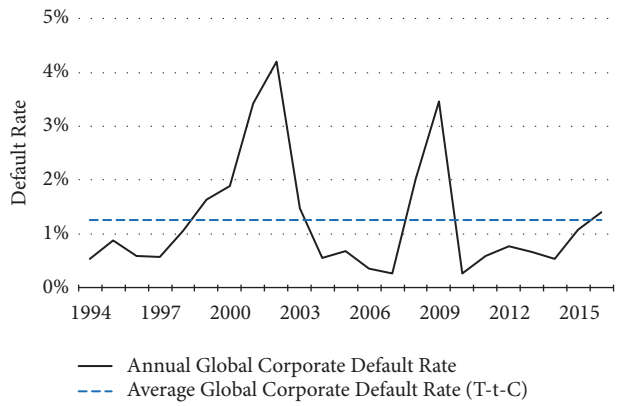

Figure 1: Global Corporate Default Rates (1994–2016).

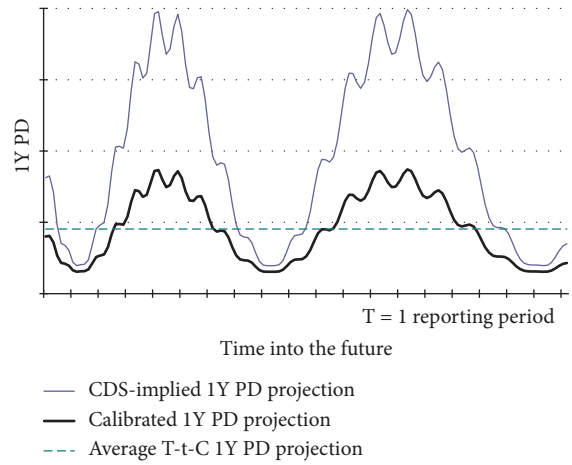

Figure 2: Illustrative 1Y PD projections.

2.2. Through-the-Cycle Observed Default Rates versus Forward-Looking PD Projections. Two different but complementary P-i-T and T-t-C concepts are usually employed by financial entities to describe the behavior of the PD. No exact definitions exist, but normally it is assumed that P-i-T PD is mostly based on current micro- and macroeconomic situations, while the T-t-C metrics PD is almost unaffected by economic conditions. It is also worth noting that many hybrid approaches are developed and used by lenders, rating agencies, and other institutions.

Alternatively, one can say that P-i-T measures seek to incorporate all the information available up to the current date and, hence, these measures change with the fluctuation of economic conjuncture. On the contrary, T-t-C measures are constant throughout the business cycle.

Figure 1 illustrates this dichotomy in the case of historical global corporate default studies. Figure 1 depicts the global corporate default rate, calculated as the average between the observed default rates (ODR) reported by the two major rating agencies; see S&P Global [26] and Moody's Investors Services [27]. The data incorporate the totality of default occurring across all the rating categories of the rated universes along the calendar years.

As can be seen from Figure 1, the annual default rate changes with time, climbing above and dropping below its average T-t-C level according to either good or bad shape of global economy. This is well evidenced looking backward, as this is what the ODR measure is all about.

The PD projection considerations differ from this mindset, as now we need to look forward into the future from the current point in the economic cycle. As the global corporate default rate changes along the time, it is reasonable to assume that such changes will be present in forward-looking PD projections, too. It is also expectable that the forward-looking PD for a chosen corporate entity may vary with fluctuations in micro- and macroeconomic conditions. The CDS spread quotes for any chosen reference entity and for any maturity point will not remain constant as time advances, indicating uninterrupted changes in its creditworthiness. So the future PD will also fluctuate around its average T-t-C value.

Figure 2 schematically visualizes the projected future behavior of the selected default related metrics for a hypothetical corporate entity. This figure does not pretend to suggest any concrete shape of a time dynamics of the parameters, but it is somehow inspired by the historically observed trends as per Figure 1.

Although the sole purpose of Figure 2 is to serve as a visual aid for a better comprehension of conceptual foundation of the proposed methodology, it is important to underline that the proportions of the chart correctly represent the relative values of the calibrated 1Y PD projections and the average T-t-C 1Y PD, as the latter is but the time average of the former.

In this way, Figure 2 allows perceiving the basic principal of the proposed approach. We project forward-looking PDs into the future in such a manner that the mean PD value of a sample, composed by the entities of the similar creditworthiness and averaged along the projection horizon, becomes equal to the historical ODR corresponding to the credit quality of the sample. In fact, the historically observed ODR is somewhat extrapolated into the future in a form of the average T-t-C PD. In other words, the projected forward-looking PDs become anchored to the historical ODRs.

Figure 2 shows what happens for just one point in the forward-looking PD term structure, namely, 1Y point. The same rational is also applied to cumulative PDs for diverse future horizons. Figure 3 schematically represents how the shape of a hypothetical PD term structure would vary in accordance with changes in the economic scenario.

Figure 3 shows that, under the T-t-C approach, a projected cumulative PD term structure does not vary with the cycle, since the T-t-C PDs are but the long-run ODRs. However, the corporate creditworthiness depends upon the state of economy and is expected to fluctuate in the years subjacent to projection horizon. Hence, a realistic projected cumulative PD term structure must be adjusted to reflect current and future economic conditions subjacent to a chosen macroeconomic scenario.

As a borrower default risk moves up or down through the economic cycle, the conditions-sensitive PD projection models are supposed to incorporate currently available information on the state of economy and assess default risk at

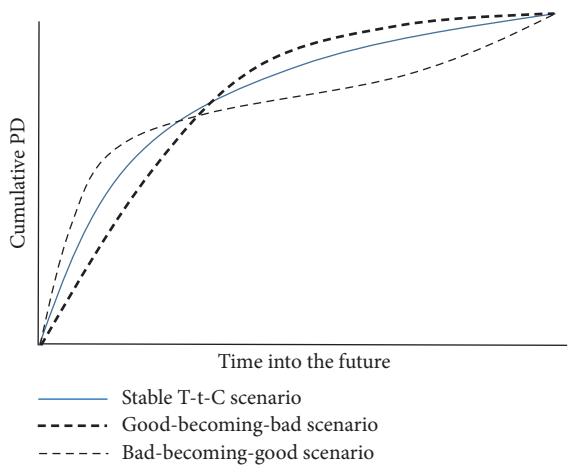

Figure 3: Schematic projections of a scenario-dependent PD term structure.

each point within the cycle. So realistic moment-sensitive projections of a chosen PD term structure ought to be used as a base for ECL allowance calculations under CECL framework.

In addition, when estimating lifetime ECL, the conditions-sensitive PD term structure must cover the entire loss projection horizon up to the contractual maturity of a financial instrument. A realistic forecast of the forward-looking PD term structure projects the cash flows and calculates the ECL allowance, among other metrics.

At this point, it is worth making a special comment, back regarding Exhibit 2. It is easy to see that the depicted CDS-implied PDs are inflated relative to the calibrated PD projection, anchored to the T-t-C PD, or the ODR. The next subsection discusses this issue in a major detail and focuses on the default and nondefault components present in CDS spreads.

2.3. Default versus Nondefault Spread Component. Default risk is only one of the factors contributing towards the CDS spread. Other factors include protection seller premium related to the future uncertainty, compensations for eventual illiquidity of CDS instruments, and political and disaster risk among many other aspects of nondefault origin.

That is why the average historically observed default rates (ODRs) for corporate obligors are typically much smaller in comparison to the average would-be hypothetical default rates as implied by nonadjusted CDS spreads. The default component hence is only a fraction of CDS spreads for the whole specter of corporate credit ratings.

Still, this fact alone does not allow making a conclusion regarding fairness of the total width of CDS spread, because, even in absence of other risks, the default component is meant to be only a part of the total CDS spread as the other part is a premium demanded by credit protection seller.

Protection sellers require such premium because the uncertainty of default presents systematic features, as default losses are more likely to negatively affect protection seller precisely when economy is in bad shape. It is worth noting that exactly because of the tendency for default events to cluster around economy downturns, the credit protection seller premium can be potentially very large.

To assure an unbiased estimation of PDs, we calibrate the spread-implied PDs by anchoring them to the long-run ODRs. Such calibration guarantees that our final P-i-T PDs estimates are commensurate in scale with historically verified ODRs.

In recent times, the process of deriving PDs and ratings from CDS spreads has been widely discussed in the literature; see Heynderickx et al. [18] and Jansen and Fabozzi [28] and references therein. Another research by Gubareva and Borges [16] is also related to our work, where CDS spreads are used as a proxy for credit risk metrics while addressing economic capital optimization strategies.

Herein we discuss the conceptual aspects of the above-mentioned PD calibration aimed at distilling the pure default compensation part from CDS spread, as CDS spreads contain considerable nondefault component. We recommend for additional reading papers by Longstaff et al. [29], Tang and Yan [30], Bongaerts et al. [31], and Arakelyan and Serrano [20], which provide liquidity studies focused on the CDS market.

An uncertainty-related risk premium of CDS spreads is also worth mentioning; that is, CDS spreads contain an additional premium demanded by credit protection sellers, which is related to the unpredictable distress changes in the default risk environment. See Berndt et al. [32] and references therein.

Furthermore, the paper by Bekaert et al. [33] alerts on another nondefault risk component present in CDS spreads, which has its origins in political risk.

In addition to the above-mentioned components of CDS spreads, one needs to also consider a component destined to compensate the cost of capital, allocated for CDS instruments. These CDS instruments, even though recognized off balance sheet, still result in capital consumption incurred by financial institutions. Consequently, the necessity to hold a capital affects CDS prices and spreads; see Gubareva and Borges [16].

Thus, if CDS spreads are employed unadjusted to derive the implied PD metrics, the nondefault component in spreads would result in an inflationary bias during the assessment of PDs, due to the presence of the nondefault component of CDS spreads.

Therefore, although CDS spread quotes are frequently available in the market for many corporate reference entities, they must undergo a process of adjustment as diverse nondefault risks explain a relevant part of CDS spreads.

The question is how to calibrate inflated P-i-T PDs, implied by unadjusted CDS-spread, in order to receive unbiased PDs, commensurate in scale with historically verified ODRs, while preserving specific individual entity information incorporated in CDS spread quotes.

It is not a simple issue as a P-i-T forward-looking PD is an individual measure, while the long-run through-the-cycle (T-t-C) ODRs are by their nature the aggregate measures. It is like comparing apple to oranges. Thus, to allow for meaningful comparison between P-i-T PDs and T-t-C

ODRs, the P-i-T forward-looking individual PDs ought to be subjected to a two-fold averaging procedure: over the long run and across the sample of the obligors characterized by a credit quality similar to the analyzed obligor. This will allow comparing comparable measures, that is, to have a sort of oranges-to-oranges comparison.

3. Calibration Methodology

In this section, we present a new calibration approach for forward-looking PD projections, which anchors the projected means of PDs to the T-t-C ODRs, reported by the major rating agencies for different ratings and time horizons.

The proposed method is based on historical default data. It is capable of providing consistent estimates of the default component of CDS spreads. We examine in detail the relationship between the average historical levels of CDS spreads, based on daily quotes data series, and the historically observed long-run ODRs. This methodological feature guarantees a neutral character of the resulting forward-looking PD projections.

To obtain our results, we separately work with seven large samples, consisting of reference entities, grouped according to similarity in the credit quality of sample constituents, in our case, BBB+, BBB, BBB-, BB+, BB, BB-, and those with credit ratings below BB-. For each sample and for each time horizon, we calculate the long-run historical average of the sample's mean "would-be" cumulative PD derived from single-name CDS spreads of the sample's constituents. Then we calibrate these cumulative PDs by normalizing them to the levels consistent with data on the respective historical ODR.

For a chosen sample, to reach the calibration target, we gauge the WDC of CDS spreads for each time horizon of the analyzed PD term structure. The debt seniority of the analyzed CDS contracts is of senior unsecured type. Additionally, we use an assumption that each reference entity has a senior unsecured bond outstanding and that the bonds issued by our reference entities have, on average, across the sample and along the time, the same probability of default as the historical ODRs for bonds of the same seniority and credit rating. The LGD parameter for the senior unsecured debt is assumed to be equal to the market consensus figure of 60%, which is close to the historical LGD values for such type of bonds.

The mechanics of our calibration is based on the widely used formula, which establishes relationship between CDS spread, maturity, and loss given default (see, e.g., Choudhry [14], page 155):

$$PD_{cum}(T) = \frac{\{1 - \exp(-Spread \times T)\}}{LGD} \tag{1}$$

where $PD_{cum}(T)$ stands for cumulative PD, *Spread* represents CDS spread for the maturity T, and LGD stands for loss given default.

Hence, having a CDS spread for a maturity T, we can calculate the implied cumulative $PD_{cum}(T)$ for the respective time horizon, and vice versa. But this is in theory, as (1) is valid only if *Spread* is a pure default spread or the default component of CDS spread. Now, the main question we need to answer is how to distill solely the default component of CDS spreads.

At this stage, we need a help of the reverse financial engineering. The long-run average of the mean default frequency observed for a chosen sample of issuers with similar creditworthiness defines the average default spread or the default component of across-the-sample mean CDS spread, averaged along the corresponding data history. Henceforth, the expression for long-run average of mean, hypothetical exclusively default-compensating spread of a selected sample of obligors, is

$$Spread_{LR\_D}(T) = -\frac{\ln\{1 - ODR_{cum}(T) \times OLGD\}}{T} \tag{2}$$

where spread $Spread_{LR\_D}$ stands for a would-be long-run default spread, $ODR_{cum}(T)$ stands for T-years cumulative long-run ODR, and *OLGD* stands for the time-average of the observed LGDs.

On the other hand, the long-run average of mean observed credit spread for a sample of obligors may be found by double averaging procedure: across-the-sample and along the analyzed long-run interval. That is,

$$\begin{aligned} &Spread_{LR\_AVG}(T) \\ &\quad = AVERAGE_{LR}\left[AVERAGE_{Sample}\{Spread_i(d, T)\}\right] \end{aligned} \tag{3}$$

where $Spread_{LR\_AVG}$ stands for long-run across-the-sample average of individual credit spreads ($Spread_i(d, T)$) for maturity T historically observed at each available date d within the long-run interval. But, as already discussed, this $Spread_{LR\_AVG}$ represents a sum of the components, being the default and the nondefault parts.

Now we arrive at the corner stone of the proposed methodology and can empirically filter out the nondefault component of CDS spreads and stay with the pure default compensation part. On average, for the ratio $WDC_{Sample}(T)$ of CDS spread, we can write the following expression:

$$WDC_{Sample}(T) = \frac{Spread_{LR\_D}(T)}{Spread_{LR\_AVG}(T)} \tag{4}$$

Thus, we are able to perform calibration of a current value of CDS spread in order to distil solely the default component. We just need to multiply a forward-looking current CDS $Spread_i$ (*current date*, T) of an issuer i from a chosen sample by $WDC_{Sample}(T)$ calculated for the sample to which the selected issuer belongs. Thus, at any current date for the pure default compensation $Spread_{i\_D}$ (*current date*, T), we have

$$\begin{aligned} &Spread_{i\_D}(current\ date, T) \\ &\quad = Spread_i(current\ date, T)\ \text{x}\ WDC_{Sample}(T) \end{aligned} \tag{5}$$

This default component, $Spread_{i\_D}$ (*current date*, T), ought to be used for projecting forward-looking cumulative $\mathrm{PD}_{\mathrm{cum}}(T)$ by means of (1).

The next section presents the result of our analyses in a form of the term structures of $WDC_{Sample}(T)$ for diverse categories of credit quality of corporate entities.

Table 1: Term structures of CDS WDCs for selected rating categories.

Credit Rating Grade	Number of entities in the sample	Maturity (years)				
		1	3	5	7	10
BBB+	76	11.0%	12.0%	10.9%	10.9%	10.9%
BBB	86	20.7%	18.0%	16.1%	15.0%	14.7%
BBB-	54	24.0%	23.8%	20.9%	19.2%	17.9%
BB+	38	20.2%	27.9%	25.3%	23.3%	21.0%
BB	17	34.3%	35.2%	28.7%	24.9%	23.1%
BB-	20	53.3%	53.0%	43.1%	38.7%	34.8%
below BB-	16	57.0%	56.6%	46.1%	41.3%	37.2%

4. Results: Weights of the Default Component of CDS Spreads

It is worth recalling that the proposed approach is based on the two-dimensional time-ensemble average of daily historical CDS market data observed through the complete economic cycle, to the T-t-C metrics of *ODR*, derived from the observed default frequencies reported by the credit rating agencies. Hence, it is possible to determine the WDC in market-quoted CDS spreads for all points of the CDS spread term structure.

Our extensive decade-long data panel on 250 IG names and 75 HY entities comprises the end-of-the-day mid-spread single-name CDS spread quotes as per CMAN provider (New York office of CMA Datavision) on a daily basis, for 1-, 3-, 5-, 7-, and 10-year tenors. We exclude sovereign reference entities from our analysis in order to have the panel data compatible with the reports on corporate issuers' T-t-C ODRs published by Standard & Poor's and Moody's rating agencies; see S&P Global [26] and Moody's Investors Service [27]. Our ODR master scale is constructed as a mean value of the respective S&P and Moody's ODR figures. For S&P default rates, we use Table 26, from S&P Global [26], presenting Global Corporate Average Cumulative Default Rates by Rating Modifier (1981-2016). For Moody's default rates, we operate with the data from Exhibit 35 providing Average Cumulative Issuer-Weighted Global Default Rates by Alphanumeric Rating, 1983-2016.

The time history of the CDS spread data series employed for averaging of historically observed daily quotes covers the 10-year period, from July 2007 to June 2017.

As already mentioned, to estimate the WDCs of CDS spreads, we separately work with seven large samples, consisting of reference entities, grouped according to similarity in the credit quality of sample constituents, in our case, BBB+, BBB, BBB-, BB+, BB, BB-, and those with credit ratings below BB-. The selection of the sample is automatically defined by the two main criteria, which restrict eligibility of constituents for a sample of a chosen rating quality, with exception of the below BB- sample for which a different methodology, explained later, is used.

First, for each eligible reference entity to be a part of a sample, the CDS quotes history must cover all the analyzed 10-year period.

Second, we also eliminate from the sample all those names, whose Basel rating, the second best, fluctuated more than within one notch up and one notch down with respect to the targeted credit rating of the sample within the considered 10-year-long observation window.

Such double data cleansing has the purpose of averaging only spreads corresponding to a chosen credit quality, for which the historical ODR data were computed by the rating agencies.

The lists of the companies considered for BBB+, BBB, BBB-, BB+, BB, and BB- samples in order to assess the WDCs are presented in Appendices A–F, respectively. The details of calculations involved are detailed in Appendix G. The methodology based on a second-degree calibration, developed for below BB- rating, is explained in Appendix H, which also provides details of the considered corporate entities and their securities.

Table 1 presents the term structures of the WDCs of CDS spreads for several different categories of the credit quality of the CDS reference entities.

Table 1 shows that the default risk for IG BBB range represents only a small part, varying between 10% and 24%. For HY BBB range, it remains within 21% to 54% interval, while for ratings below BB- it varies from 37% to 57% depending on the considered maturity, representing on average roughly a half of a CDS spread.

For all the maturities, the WDC grows as credit quality drops, with the only exception observed for BB+ rating at 1Y point, perhaps due to liquidity related chock at the crossover from IG to HY range.

For all the considered rating categories, from 3Y point towards the long end of the term structure, the WDC diminishes reflecting augmenting uncertainty concerns. For longer than 5Y maturities, such behavior is further enforced by the diminishing liquidity of the CDS instruments, as the most liquid point, at which a major part of trading occurs around 5-year maturity contracts.

From qualitative point of view, our results are in line with outcomes of other researches on CDS spread components (Longstaff et al. [29], Lin et al. [34], Chen H. et al., and Arakelyan and Serrano [20]).

On the quantitative side, our findings contrast the outcomes of Arakelyan and Serrano [20] for the period of 2004-2011, as authors find that, on average, the default risk premium

accounts for 40% of CDS spreads. Our empirical data suggests that the default risk premium for BBB entities, on average, is below 20% of CDS spreads, as per the three top rows of Table 1.

From a quantitative point of view, our numerical results represent a fundamental contribution to the existing literature on this subject. They reach beyond the current frontier in the empirical research on the matter in a sense that our figures are based on daily empirical data subjacent to a decade-long time window from 2007 to 2017, comprising distinct phases of the business cycle. The fact that the analyzed data history spreads over both distress and normal economic conditions assures robustness of the outcomes, especially for being employed in calculating life-long ECL.

In the next chapter, we provide several examples shedding light on how the *WDC*s could be used to calibrate PDs, implied by CDS spread quotes. We exemplify an application of our ready-to-use methodology to calculate CECL-compliant ECL for a selected set of IG and HY exposures.

5. Application: Examples of WDC Use in CDS-Based ECL Calculations

In order to illustrate the applicability of our approach to low default portfolios, we select five different investments in corporate bonds. The chosen debt issues are the following: CBS Corp bond with maturity, February 15, 2023 (ISIN US124857AS26); Goodyear Tire & Rubber company bond with maturity, November 15, 2023 (ISIN US382550BE09); and Windstream Services LLC bond with maturity, August 01, 2023 (ISIN US97381WAZ77). The end date of the reporting period, used as a reference date for ECL calculation, is chosen to be March 30, 2018.

In accordance with CECL framework, see FABS (2016), if an entity estimates expected credit losses using methods that project future principal and interest cash flows, that is, DCF–PD/LGD method, the entity shall discount expected cash flows at the financial asset's effective interest rate. When a discounted cash flow method is applied, the allowance for credit losses shall reflect the difference between the amortized cost basis and the net present value of the expected cash flows. Hence, we calculate the ECL as follows for the requirements established by IFRS 9:

$$ECL = \sum_{t=1}^{T} \frac{PD(t) \times LGD \times EAD(t)}{(1 + EIR)^t} \tag{6}$$

where $PD(t)$ is a marginal forward-looking PD, subjacent to the current point in the economic cycle, $EAD(t)$ is an exposure at default relative to a time interval t, LGD is a loss given default, and EIR stands for original effective interest rate when the asset was first recognized.

In the considered examples herein, for simplicity reasons, we use LGD value of 60%, which is a market consensus for senior unsecured debt. We also assume that the bond assets were purchased at their issue date, allowing us to use the initial yield at issue as a proxy for EIR. As our work is not focused on the finest details of the accounting algorithms of CECL-compliant EAD calculations, we employ an assumption that the assets used in our examples were originally recognized at par, and hence we calculate EAD as a sum of the nominal value of the position and the coupon due to be paid during the period t.

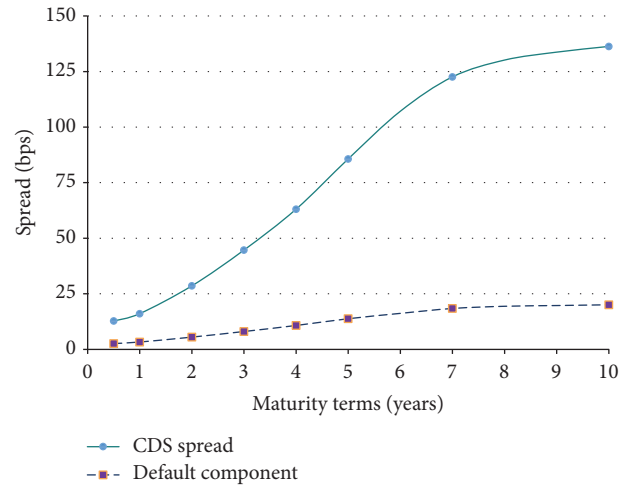

Figure 4: CBS Corp term structures: CDS spread and default component.

5.1. IG BBB-Rated Exposure to CBS Corp. As of March 30, 2018, the major credit rating agencies, namely, S&P, Fitch, and Moody's, rate the senior unsecured debt of the CBS Corp as BBB/BBB/Baa2, respectively. Hence, in our ECL calculations, we use the WDC for BBB rating category, as per Table 1. Our results are compiled in Table 2.

For the presented calculations in Table 2 we use the CDS spread quotes of March 30, 2018, and calibrate them by using the WDC from Table 1. For 0.5-year maturity point, we apply the 1-year WDC. The spreads and the WDC for the maturity point are obtained by the linear interpolation of 4-year and 5-year tenor figures. The purely default compensation parts of the CDS spreads are transformed in current marginal forward-looking PD projections. The coupon of 2,50% results in EAD per half-year period of 101,25 and for yearly periods of 102,50. Finally, summing marginal ECL we arrive at lifetime ECL of 0,61 percentage points.

In Figures 4 and 5 we present two charts, which shed further light on the method to project forward-looking PDs, as implied by CDS market information. Figure 4 presents the term structure of the CBS Corp CDS spreads along with the default spread component for each point of the term structure, as of March 30, 2018.

As per Figure 4, we conclude that the default component grows with time up to the 7-year point and then further remains almost constant although it continues to slightly increase with time. In Figure 4, the presented term structure of the default component is used to derive, by means of (1), the term structures of current cumulative and marginal PD projections, depicted in Figure 5.

In Figure 5, we see that the current forward-looking PD projections augment up to the 7-year point and then moderately decay forward into the future. While an exact

Table 2: Lifetime ECL for the bond of CBS Corp as of March 30, 2018.

Lifetime ECL for CBS Corp exposure as of March 30, 2018						
Date (mm.yyyy)	09.2018	03.2019	03.2020	03.2021	03.2022	02.2023
Maturity horizon (years) (A)	0.5	1	2	3	4	4.9
Spread quotes (bps)	12.8	16.1	28.6	44.7	63.1	83.0
WDC of BBB-rated CDS	20.7%	20.7%	19.4%	18.0%	17.1%	16.2%
Default component (bps)	2.7	3.3	5.5	8.1	10.8	13.5
Current cumulative PD projection (see (1))	0.02%	0.06%	0.18%	0.40%	0.72%	1.09%
Current marginal PD projection (B)	0.02%	0.03%	0.13%	0.22%	0.31%	0.37%
Coupon	2.50%	2.50%	2.50%	2.50%	2.50%	2.50%
Initial Yield (C)	2.50%	2.50%	2.50%	2.50%	2.50%	2.50%
LGD (D)	60%	60%	60%	60%	60%	60%
EAD/Nominal (p.p.) (E)	101.25	101.25	102.50	102.50	102.50	102.20
Marginal ECL (p.p.) ($F = B \times D \times E / (1+C)$ ^A)	0.01	0.02	0.08	0.12	0.17	0.20
ECL lifetime (p.p.)			0.61			

Table 3: Lifetime ECL for the bond of the Goodyear Company as of March 30, 2018.

Lifetime ECL for Goodyear Company exposure as of March 30, 2018							
Date (mm.yyyy)	09.2018	03.2019	03.2020	03.2021	03.2022	03.2023	11.2023
Maturity horizon (years) (A)	0.5	1	2	3	4	5	5.6
Spread quotes (bps)	20.7	31.5	45.4	68.9	103.9	141.3	161.5
WDC of BB-rated CDS	34.3%	34.3%	34.8%	35.2%	32.0%	28.7%	27.5%
Default component (bps)	7.1	10.8	15.8	24.3	33.2	40.6	44.4
Current cumulative PD projection (see (1))	0.06%	0.18%	0.53%	1.21%	2.20%	3.35%	4.12%
Current marginal PD projection (B)	0.06%	0.12%	0.35%	0.68%	0.99%	1.15%	0.77%
Coupon	5.125%	5.125%	5.125%	5.125%	5.125%	5.125%	5.125%
Initial Yield (C)	5.125%	5.125%	5.125%	5.125%	5.125%	5.125%	5.125%
LGD (D)	60%	60%	60%	60%	60%	60%	60%
EAD/Nominal (p.p.) (E)	102.56	102.56	105.13	105.13	105.13	105.13	103.22
Marginal ECL ($F = B \times D \times E / (1+C)$ ^A)	0.04	0.07	0.20	0.37	0.51	0.56	0.36
ECL lifetime (p.p.)				2.11			

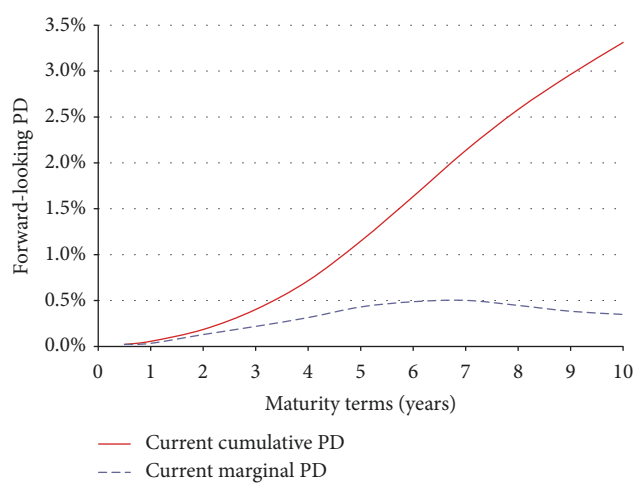

Figure 5: CBS Corp default risk structure: current PD projections.

interpretation of the factors behind the depicted dynamics of annual marginal PD is rather difficult, the chart supports the following insight. The market, through the CDS quotes, implicitly considers that the most difficult years for CBS Corp. to cope with its liabilities will be from the 6th to the 8th year into the future. Seemingly, as of March 30, 2018, market participants do not envisage any other significant stress for the long end of the term structure. Hence, we find the description of future creditworthiness of CBS Corp. presented by the term structure of the annual marginal forward-looking PD as plausible and convincing to be used in ECL calculations.

As could be seen in this example, the ECL calculations were performed using the points of the PD term structure, located within the positive slope of the curve, which means that the issuer, although somewhat stressed, is not at an imminence of default.

5.2. Lifetime ECL for a HY BB-Rated Exposure to Goodyear Company. As of March 30, 2018, the senior unsecured bond issued by Goodyear Tire & Rubber Company with maturity date November 15, 2023, is rated BB by S&P and by Fitch, and Ba3 by Moody's, though the company long-term rating is Ba2. Hence, in our ECL calculations, we use the WDC for BB rating category, as per Table 1. Our results are compiled in Table 3.

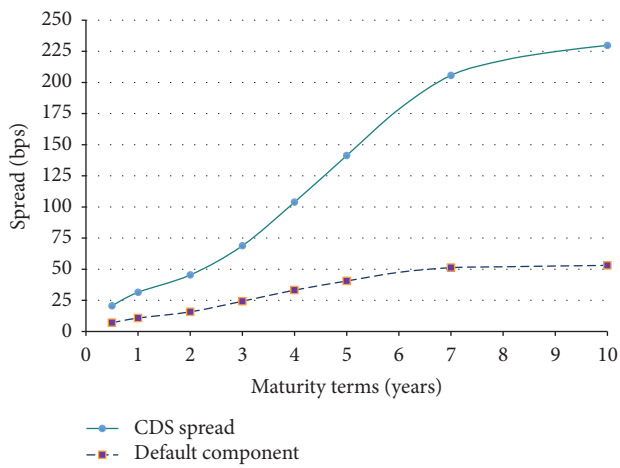

Figure 6: Goodyear Company term structures: CDS spread and default component.

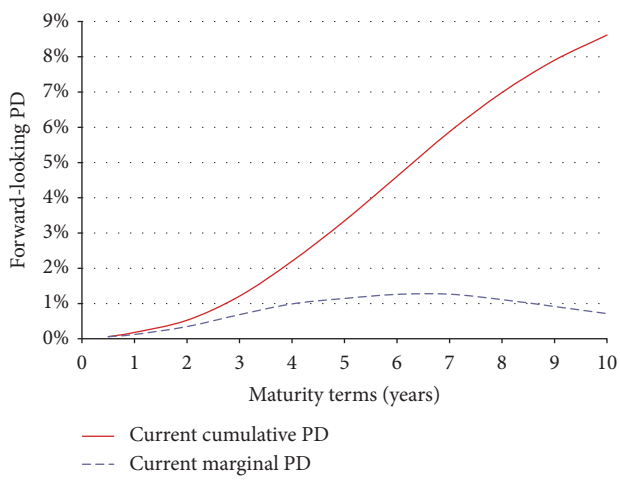

Figure 7: Goodyear Company default risk structure: current PD projections.

In Table 3, for the presented calculations, we use the CDS spread quotes of March 30, 2018, and calibrate them by using the WDC from Table 1. The spreads and the WDC for the maturity point are obtained by the linear interpolation of 5-year and 7-year tenor figures. The purely default compensation parts of the CDS spreads are transformed in current marginal forward-looking PD projections. Finally, summing marginal ECL until maturity, we arrive at lifetime ECL of 2,11 percentage points.

In Figures 6 and 7 we present two charts, which shed additional light on the method to project forward-looking PDs, as implied by CDS market information. Figure 6 presents the term structure of the Nabors Industries Inc. CDS spreads along with the default spread component for each point of the term structure, as of March 30, 2018.

As per Figure 6, our calculations show that, for Goodyear Company, the default component grows with time up to the 7-year point and then further on remains almost perfectly constant. In Figure 6 , the presented term structure of the default component is used to derive, by means of (1), the term structures of current cumulative and marginal PD projections, depicted in Figure 7.

In Figure 7, we see that the current forward-looking PD projections augment up to the 7-year point and then moderately decay forward into the future. Seemingly, as of March 30, 2018, market participants do not envisage any increase in credit-related stress for the long end of the term structure. We find the description of future creditworthiness of Goodyear Company presented by the term structure of the annual marginal forward-looking PD as plausible and convincing to be used in ECL calculations.

As could be seen in this example, the ECL calculations were performed using the points of the PD term structure, located within the positive slope of the curve, which means that the issuer, although somewhat stressed, is not at an imminence of default.

5.3. Lifetime ECL for a HY below BB- Exposure to Windstream Services LLC. Next, we apply our methodology to calculate ECL for exposure to Windstream Services debt, rated B- by SP, B by Fitch, and Caa1 by Moody's, as of March 30, 2018. We select the Windstream Services bond with maturity date August 01, 2023, on purpose to demonstrate a capacity of our approach to treat ECL of names under financial stress. In our ECL calculations, we use the WDCs for the below BB- rating category, as per Table 1. Our results are compiled in Table 4.

For the presented calculations in Table 4 we use the CDS spread quotes of March 30, 2018, and calibrate them by using the WDC from Table 1. The spreads and the WDC for the maturity point are obtained by the linear interpolation of 5-year and 7-year tenor figures. The purely default compensation parts of the CDS spreads are transformed in current marginal forward-looking PD projections. Finally, summing marginal ECL until maturity, we arrive at lifetime ECL of 46,61 percentage points.

In Figures 8 and 9 we present two charts, which shed further light on the method to project forward-looking PDs, as implied by CDS market information. Figure 8 presents the term structure of the Windstream Services CDS spreads along with the default spread component for each point of the term structure, as of March 30, 2018.

The inverted, at the short end, term structure of CDS spreads is considered to be an indication of an eventually approaching default or debt restructuring. As per Figure 8, we conclude that the default component decays from the level of 2200 bps at 0.5-year point to the 2-year point below 1500 bps and then remains almost constant until the 5-year point and then continues to gradually decay towards the long end of the term structure. In Figure 8 , the presented term structure of the default component is used to derive, by means of (1), the term structures of current cumulative and marginal PD projections, depicted in Figure 9.

In Figure 9, we see that the annual marginal forward-looking P-i-T PD within the 1st year exhibits a negative slope, reaching its local minima at 1-year point. Then it starts growing and reaches its local maximum around the end of the 3rd year into the future and then exhibits a decay tendency though quite inhomogeneous.

Table 4: Lifetime ECL for the bond of the Windstream Services as of March 30, 2018.

Lifetime ECL for Windstream Services LLC exposure as of March 30, 2018							
Date (mm.yyyy)	09.2018	03.2019	03.2020	03.2021	03.2022	03.2023	08.2023
Maturity horizon (years) (A)	0.5	1	2	3	4	5	5.3
Spread quotes (bps)	3808.2	2980.9	2428.9	2459.5	2692.2	3035.8	3036.7
WDC of BB-rated CDS	57.0%	57.0%	56.8%	56.6%	51.4%	46.1%	45.3%
Default component (bps)	2169.6	1698.2	1379.3	1392.1	1382.5	1399.7	1375.4
Current cumulative PD projection (see (1))	17.13%	26.03%	40.18%	56.90%	70.80%	83.89%	86.70%
Current marginal PD projection (B)	17.13%	8.90%	14.15%	16.72%	13.90%	13.09%	2.81%
Coupon	6.375%	6.375%	6.375%	6.375%	6.375%	6.375%	6.375%
Initial Yield (C)	6.375%	6.375%	6.375%	6.375%	6.375%	6.375%	6.375%
LGD (D)	60%	60%	60%	60%	60%	60%	60%
EAD/Nominal (p.p.) (E)	103.19	103.19	106.38	106.38	106.38	106.38	102.17
Marginal ECL ($F = B \times D \times E / (1+C)$ ^A)	10.29	5.18	7.98	8.87	6.93	6.13	1.24
ECL lifetime (p.p.)				46.61			

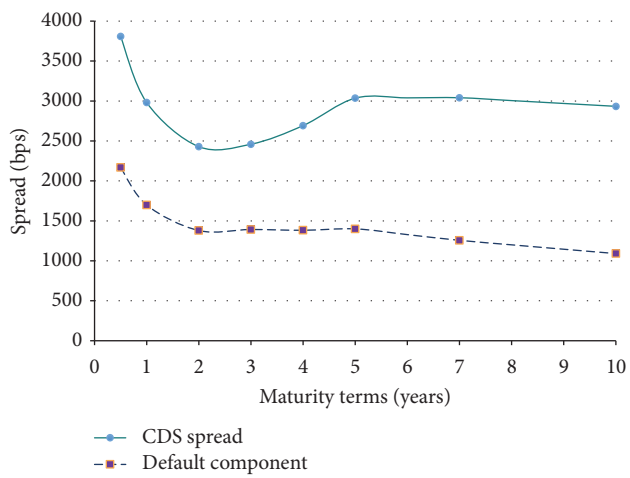

Figure 8: Windstream Services term structures: CDS spread and the default component.

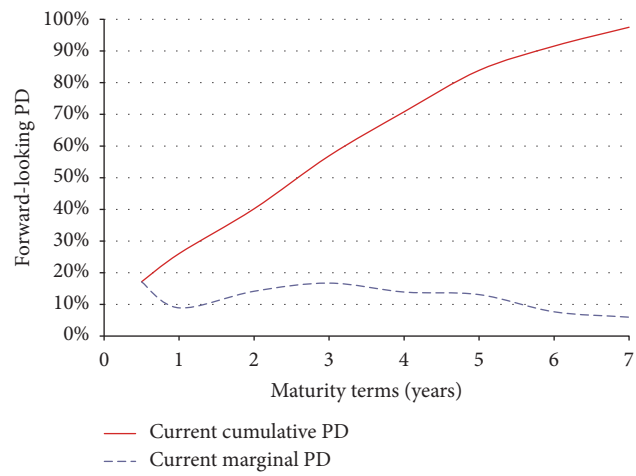

Figure 9: Windstream Services term structure of default risk: current PD projections.

While an exact interpretation of the factors behind the depicted dynamics of annual marginal PD is rather difficult, the chart corroborates the following explanation. The market through the CDS quotes implicitly considers that the most difficult moment for Windstream Services to cope with its liabilities lays within the next half a year. Seemingly, as of March 30, 2018, market participants also envisage another significant stress for the entity along the 2nd and the 3rd years in the term structure.

We consider the description of future creditworthiness of Windstream Services presented by the term structure of the annual marginal PD to be plausible, convincing, and, hence, applicable to ECL calculations.

Such a complex PD term structure results from the current March 30, 2018, CDS spread quotes for diverse points in the CDS term structure, which are representative of prices at which market had cleared on March 18, 2018. In our approach, we consider that these CDS represent all future scenarios duly weighted and discounted by market participants. The more reliable and the less speculative are the quotes, the more accurate is the result of the proposed ECL calculation methodology.

5.4. Additional Considerations. In is worth mentioning that an alternative approach to assessment of default risk profile, which is widely employed by financial industry players, is a transformation of the T-t-C PDs into forward-looking PD measures sensitive to the current point in the cycle by means of hypothetic scenarios. Still it is rather impossible for the T-t-C to current forward-looking PD conversion approach to result in such a detailed description of forward-looking marginal PDs, similar to those provided by our approach.

Differently from the commonly employed T-t-C to current PD conversion procedure, which starts with the T-t-C default rates and then converts them by means of scenario analyses into the forward-looking PD projections, our methodology incorporates the point-in-timeliness from the very beginning as it commences with the forward-looking term structure of quoted CDS spreads. Then, we calibrate the otherwise inflated PDs by duly treating the

spread components structure and distilling solely the default compensation part.

In addition, our methodology could be coupled with scenario analyses and macroeconomic considerations in order to see how ECL will behave under increased or diminished stress. However, these issues overcome the frame of the present paper and will be addressed in the future research.

Although there is a vast universe of single-name CDS curves and also of CDS indices (see Gubareva [35]), it does not cover the whole specter of the bond issuers. It is worth pointing out that the herein exemplified methodology can be also applied in the case of obligors without CDS spread curves; alternatively, instead of the CDS spread, the credit spread of the individual BVAL curves over the respective risk-free rates could be employed.

The applicability of the proposed approach could also be extended to the entities, for which there exists neither single-name CDS nor individual BVAL curves, as there is a wide range of generic BVAL curves for diverse economy sectors arranged according to letter rating grades. These generic BVAL yield curves are accessible through the Bloomberg terminal.

In such case, the term structure of the sector BVAL curve could be employed to proxy the default risk term structure. In addition, the adjustment procedure must be performed. The ratio of the obligor's yield to the sector's BVAL yield to maturity should be employed as a scaling factor to rescale the BVAL curve yield at each point of the term structure. Then, the proposed methodology, exemplified in our study for obligors with the single-name CDS spread curves, becomes fully applicable for BVAL-less obligors too.

Such methodology extension potentially allows for almost complete and highly accurate coverage of the entire bond domain of the fixed-income universe.

6. Conclusion

We develop CECL-compliant original methodology to calibrate forward-looking PDs estimates, based on CDS market information, thus making such PDs projections employable for the ECL calculations. Our approach is based on an innovative technique suitable for distilling the pure default component in CDS spreads.

To enable economic adjustment of PDs, we consider seven homogeneous samples corresponding to BBB+, BBB, BBB-, BB+, BB, BB-, and below-BB rating ranges, assuring in this manner a similarity in issuers' creditworthiness across each sample. Then, we analyze the relationship between a long-run average of the across-the-sample mean value of the CDS spreads of a chosen maturity, on one hand, and, on the other hand, the spread, implied by the long-run average of the respective cumulative ODR.

In this manner, we solve the problem of calibrating of an issuer's current forward-looking PD, which is an individual metrics, to the cumulative default rate, which is an aggregate measure relative to the cohort-like sample of individual issuers.

We provide the empirical results regarding the average WDC for each point in the CDS spread term structures derived for the seven different ranges of issuers' creditworthiness and empirically evidence that for BBB and BB rating categories nondefault risks are responsible for a major part of a CDS spread.

We evidence that the average value of the WDC for BBB reference entities represents only a small fraction, on average below 20% of CDS spread, while for BB entities this fraction is somewhat bigger, but still it predominantly remains below 40% of CDS spreads for all the tenors. Being qualitatively in line with previous research on nondefault drivers of CDS spreads, our results contrast with the quantitative findings of Arakelyan and Serrano [20], reporting that, on average, the default risk premium accounts for 40% of CDS spreads. In addition, it is important to stress that differently to previous research we provide WDC for each forward term and for several ranges of credit ratings.

To overcome the limited data on the below-BB sample, we develop a second-degree calibration procedure, which allows us to obtain the WDC for this low credit quality group of reference entities. We find that the WDC for this category varies between 57% and 37%, decaying for the long end of the term structure.

The performed assessment of the WDC allows for objective, that is, unconditional projections of multiperiod PDs to be used in ECL calculations. Our PDs are truly point-dependent current measures incorporating forward-looking information, as they are based on current CDS quotes, which provide a current market forecast on default risk of reference entities.

Differently from commonly employed approaches, which use the T-t-C default rates and then transform them by means of scenario analyses into the forward-looking PDs, our approach incorporates the point-in-timeliness from the very beginning as it starts with current quotes of CDS spreads, which contain forward-looking information. As a next step we calibrate these CDS spreads, by distilling the pure default component.

In this manner, the developed approach permits optimizing modeling efforts and avoiding waste of time, spent by financial institutions analyzing multiple scenarios in order to incorporate point-in-timeliness and forward-looking aspects into their otherwise T-t-C PDs. Another important drawdown of the scenario-based approaches is an inherent subjectivity related to scenario construction activities. Avoidance of subjective assumptions and forecasts in our methodology potentially enhances objectivity, robustness, and replicability of ECL calculations as well as their comparability among the field players.

CECL framework envisages the use of market sensitive parameters and, henceforth, is expected to cause cyclicality in provisions. However, what represents a potentially dangerous systemic handicap is an eventual unintended procyclicality, that is, amplified cycle-related fluctuations of impairment allowances, driven by CECL implementation. Our approach based on PDs calibration, which anchors them to the long-run T-t-C ODRs, assures that fluctuations in provisions are hold controlled by construction.

The employment of T-t-C ODRs for calibrating forward-looking PDs in our methodology marks the initial step

Table 5: Companies used for the IG BBB+ sample.

#	CDS COMPANY NAME	CDS CORP TICKER	#	CDS COMPANY NAME	CDS CORP TICKER
1	Aetna Inc.	AET	39	Humana Inc.	HUM
2	Akzo Nobel NV	AKZANA	40	Husky Energy Inc.	HSECN
3	Alltel Corp	VZ	41	Hyundai Motor Co	HYNMOT
4	American Electric Power Co Inc.	AEP	42	Ingersoll-Rand Co	IR
5	Anthem Inc.	ANTM	43	International Paper Co	IP
6	AstraZeneca PLC	AZN	44	Johnson Controls International	JCI
7	AT&T Corp	T	45	Kellogg Co	K
8	Atlantia S.p.A.	ATLIM	46	Kinder Morgan Energy Partner	KMI
9	Auchan Holding SA	AUCHAN	47	Kohl's Corp	KSS
10	Baxter International Inc.	BAX	48	Kraft Heinz Foods Co	KHC
11	Bertelsmann SE & Co KGaA	BERTEL	49	Kroger Co/The	KR
12	BorgWarner Inc.	BWA	50	Lockheed Martin Corp	LMT
13	Bouygues SA	ENFP	51	Omnicom Group Inc.	OMC
14	British Telecommunications PLC	BRITEL	52	ONEOK Inc.	OKE
15	Campbell Soup Co	CPB	53	Packaging Corp of America	PKG
16	Carrefour SA	CAFP	54	Pepco Holdings LLC	EXC
17	Centrica PLC	CNALN	55	Pioneer Natural Resources Co	PXD
18	Cigna Corp	CI	56	POSCO	POHANG
19	Clorox Co/The	CLX	57	Potash Corp of Saskatchewan	POTCN
20	Coca-Cola Amatil Ltd	CCLAU	58	Progress Energy Inc.	DUK
21	ConocoPhillips	COP	59	PSEG Power LLC	PEG
22	Continental AG	CONGR	60	Qantas Airways Ltd	QANAU
23	Corning Inc.	GLW	61	Quest Diagnostics Inc.	DGX
24	CSR Ltd	CSRAU	62	Reliance Industries Ltd	RILIN
25	CSX Corp	CSX	63	Repsol Oil & Gas Canada Inc.	TLMCN
26	CVS Health Corp	CVS	64	Republic Services Inc.	RSG
27	Eaton Corp	ETN	65	Reynolds American Inc.	RAI
28	Enbridge Energy Partners LP	EEP	66	RPM International Inc.	RPM
29	Enbridge Inc.	ENBCN	67	Ryder System Inc.	R
30	Energy Transfer LP	ETP	68	Sempra Energy	SRE
31	Entergy Corp	ETR	69	Shaw Communications Inc.	SJRCN
32	FedEx Corp	FDX	70	Sherwin-Williams Co/The	SHW
33	GATX Corp	GMT	71	Southern Co/The	SO
34	General Mills Inc.	GIS	72	Southwest Airlines Co	LUV
35	GS Caltex Corp	GSCCOR	73	Spectra Energy Capital LLC	SE
36	Halliburton Co	HAL	74	Starwood Hotels & Resorts Wo	HOT
37	Hasbro Inc.	HAS	75	Suncor Energy Inc.	SUCN
38	HP Inc.	HPQ	76	TE Connectivity Ltd	TEL

towards better convergence between capital quantifications under Basel III/IV accord, usually tied to T-t-C metrics, and CECL-compliant accounting treatment incorporating volatility of current economic conditions through the credit risk parameters, changing with the cycle. The herein presented framework allows for better comprehension of complex ongoing interactions, on one hand, between the impairment and economic capital requirements in relation to credit losses, and, on the other hand, between credit risk management and accounting.

We expect that our research will serve practical needs of many financial institutions, being at the same time of theoretical value for practitioners, regulators, and members of scientific community during and after the implementation of CECL requirements.

Appendix

A.

See Table 5.

B.

See Table 6.

Table 6: Companies used for the IG BBB sample.

#	CDS COMPANY NAME	CDS CORP TICKER	#	CDS COMPANY NAME	CDS CORP TICKER
1	Amcor Ltd/Australia	AMCAU	44	Martin Marietta Materials Inc.	MLM
2	AutoZone Inc.	AZO	45	McKesson Corp	MCK
3	BAE Systems PLC	BALN	46	Medco Health Solutions Inc.	ESRX
4	BCE Inc.	BCECN	47	Metso OYJ	METSO
5	British American Tobacco PLC	BATSLN	48	Mondelez International Inc.	MDLZ
6	CA Inc.	CA	49	Newmont Mining Corp	NEM
7	Canadian Natural Resources LP	CNQCN	50	Next PLC	NXTLN
8	Canadian Pacific Railway Co	CP	51	NiSource Inc.	NI
9	Capgemini SE	CAPFP	52	Packaging Corp of America	PKG
10	Cardinal Health Inc.	CAH	53	Pearson PLC	PSON
11	Carlsberg Breweries A/S	CARLB	54	Pioneer Natural Resources Co	PXD
12	CBS Corp	CBS	55	PostNL NV	PNLNA
13	CenterPoint Energy Inc.	CNP	56	Publicis Groupe SA	PUBFP
14	Cie de Saint-Gobain	SGOFP	57	Reliance Industries Ltd	RILIN
15	CMS Energy Corp	CMS	58	Rentokil Initial PLC	RTOLN
16	Computer Sciences Corp	COMPSC	59	Republic Services Inc.	RSG
17	Cox Communications Inc.	COXENT	60	Rohm & Haas Co	DOW
18	Delhaize America LLC	ADNA	61	RWE AG	RWE
19	Dominion Energy Inc.	D	62	Securitas AB	SECUSS
20	Dow Chemical Co/The	DOW	63	SES SA	SESGFP
21	DTE Energy Co	DTE	64	Sky PLC	SKYLN
22	E.ON SE	EOANGR	65	Smiths Group PLC	SMINLN
23	Eastman Chemical Co	EMN	66	Solvay SA	SOLBBB
24	Enbridge Inc.	ENBCN	67	Spectra Energy Capital LLC	SE
25	Endesa SA	ELESM	68	Starwood Hotels & Resorts	HOT
26	Enel S.p.A.	ENELIM	69	Swedish Match AB	SWEMAT
27	Entergy Corp	ETR	70	Tate & Lyle PLC	TATELN
28	Exelon Generation Co LLC	EXC	71	TECO Energy Inc.	TE
29	FedEx Corp	FDX	72	Telekom Austria AG	TKAAV
30	Gas Natural SDG SA	GASSM	73	Textron Inc.	TXT
31	GATX Corp	GMT	74	Time Warner Inc.	TWX
32	Glencore International AG	GLENLN	75	Tyson Foods Inc.	TSN
33	GS Caltex Corp	GSCCOR	76	Valeo SA	FRFP
34	Hasbro Inc.	HAS	77	Valero Energy Corp	VLO
35	Hillshire Brands Co/The	HSH	78	Veolia Environnement SA	VIEFP
36	International Paper Co	IP	79	Vivendi SA	VIVFP
37	ISS Global A/S	ISSDC	80	Waste Management Inc.	WM
38	Kering	KERFP	81	Western Union Co/The	WU
39	Kingfisher PLC	KGFLN	82	WestRock MWV LLC	WRK
40	Koninklijke Ahold Delhaize N	ADNA	83	Whirlpool Corp	WHR
41	Kroger Co/The	KR	84	Woolworths Ltd	WOWAU
42	Lafarge SA	LGFP	85	WPP 2005 Ltd	WPPLN
43	Marriott International Inc.	MAR	86	Xstrata Ltd	XTALN

C.

See Table 7.

D.

See Table 8.

E.

See Table 9.

F.

See Table 10.

Table 7: Companies used for the IG BBB- sample.

#	CDS COMPANY NAME	CDS CORP TICKER	#	CDS COMPANY NAME	CDS CORP TICKER
1	Allergan Inc./United States	AGN	28	Koninklijke KPN NV	KPN
2	Altadis SA	NA	29	Kraft Heinz Foods Co	KHC
3	Anadarko Petroleum Corp	APC	30	LANXESS AG	LXSGR
4	Anglo American PLC	AALLN	31	Macy's Inc.	M
5	Apache Corp	APA	32	Marathon Oil Corp	MRO
6	Arrow Electronics Inc.	ARW	33	Marks & Spencer PLC	MARSPE
7	Avnet Inc.	AVT	34	Masco Corp	MAS
8	Barrick Gold Corp	ABXCN	35	Mattel Inc.	MAT
9	Boston Scientific Corp	BSX	36	METRO AG	CECGR
10	Carlton Communications Ltd	ITVLN	37	Motorola Solutions Inc.	MSI
11	Clariant AG	CLNVX	38	Newell Brands Inc.	NWL
12	Conagra Brands Inc.	CAG	39	Noble Energy Inc.	NBL
13	Constellation Brands Inc.	STZ	40	Pernod Ricard SA	RIFP
14	Darden Restaurants Inc.	DRI	41	Renault SA	RENAUL
15	Deutsche Lufthansa AG	LHAGR	42	Repsol Oil & Gas Canada Inc.	TLMCN
16	Devon Energy Corp	DVN	43	Repsol SA	REPSM
17	Domtar Corp	UFS	44	SKF AB	SKFBSS
18	DR Horton Inc.	DHI	45	STMicroelectronics NV	STM
19	EDP - Energias de Portugal S	EDPPL	46	TDC A/S	TDCDC
20	Enbridge Energy Partners LP	EEP	47	Telefonica SA	TELEFO
21	Energy Transfer LP	ETP	48	Tesoro Corp	TSO
22	Exelon Corp	EXC	49	UBM PLC	UBMLN
23	Fresenius SE & Co KGaA	FREGR	50	Universal Corp/VA	UVV
24	GKN Holdings PLC	GKNLN	51	UPM-Kymmene OYJ	UPMFH
25	Imperial Brands PLC	IMBLN	52	Viacom Inc.	VIA
26	ITV PLC	ITVLN	53	Wendel SA	MWDP
27	Kohl's Corp	KSS	54	Xerox Corp	XRX

Table 8: Companies used for the HY BB+ sample.

#	CDS COMPANY NAME	CDS CORP TICKER	#	CDS COMPANY NAME	CDS CORP TICKER
1	Alstom SA	ALOFP	20	MDC Holdings Inc.	MDC
2	ArcelorMittal Finance SCA	MTNA	21	Metsa Board OYJ	METSA
3	Arconic Inc.	ARNC	22	Nielsen Co BV/The	NLSN
4	Belo Corp	TGNA	23	Nokia OYJ	NOKIA
5	British Airways PLC	IAGLN	24	NOVA Chemicals Corp	NCX
6	Casino Guichard Perrachon SA	COFP	25	Peugeot SA	PEUGOT
7	Centex LLC	PHM	26	Pitney Bowes Inc.	PBI
8	Edison S.p.A.	EDFFP	27	Plains All American Pipeline	PAA
9	Embarq Corp	EQ	28	PulteGroup Inc.	PHM
10	Encana Corp	ECACN	29	Qwest Corp	CTL
11	Expedia Inc.	EXPE	30	Smurfit Kappa Funding DAC	SKGID
12	FirstEnergy Corp	FE	31	Tata Motors Ltd	TTMTIN
13	Gap Inc./The	GPS	32	TEGNA Inc.	TGNA
14	Gazprom PJSC	GAZPRU	33	Telecom Italia S.p.A./Milano	TITIM
15	Hanson Ltd	HEIGR	34	Telefonaktiebolaget LM Ericsson	ERICB
16	Hess Corp	HES	35	Tesco PLC	TSCOLN
17	L Brands Inc.	LB	36	Toll Brothers Inc.	TOL
18	Lennar Corp	LEN	37	TransAlta Corp	TACN
19	Leonardo S.p.A.	LDOIM	38	Universal Health Services Inc.	UHS

Table 9: Companies used for the HY BB sample.

#	CDS COMPANY NAME	CDS CORP TICKER	#	CDS COMPANY NAME	CDS CORP TICKER
1	AES Corp/VA	AES	10	Nabors Industries Inc.	NBR
2	Aramark Services Inc.	ARMK	11	Norbord Inc.	OSBCN
3	CenturyLink Inc.	CTL	12	Olin Corp	OLN
4	Colt Group SA	COLTLN	13	Qwest Capital Funding Inc.	CTL
5	Commercial Metals Co	CMC	14	Stora Enso OYJ	STERV
6	Ladbrokes Coral Group PLC	LADLN	15	Thyssenkrupp AG	TKAGR
7	Levi Strauss & Co	LEVI	16	TUI AG	TUIGR
8	Louisiana-Pacific Corp	LPX	17	Williams Cos Inc./The	WMB
9	Murphy Oil Corp	MUR		---	

Table 10: Companies used for the HY BB- sample.

#	CDS COMPANY NAME	CDS CORP TICKER	#	CDS COMPANY NAME	CDS CORP TICKER
1	Amkor Technology Inc.	AMKR	11	PolyOne Corp	POL
2	Ashland LLC	ASH	12	Pride International LLC	ESV
3	Cooper Tire & Rubber Co	CTBUS	13	Sealed Air Corp	SEE
4	Dell Inc.	DELL	14	Staples Inc.	SPLS
5	Diamond Offshore Drilling In	DO	15	Teck Resources Ltd	TCKBCN
6	Fiat Chrysler Automobiles NV	FCAIM	16	United Rentals North America	URI
7	Freeport-McMoRan Corp	FCX	17	Unitymedia GmbH	UNITY
8	Freeport-McMoRan Inc.	FCX	18	UPC Holding BV	UPCB
9	Goodyear Tire & Rubber Co/The	GT	19	Virgin Media Finance PLC	VMED
10	Liberty Interactive LLC	LINTA	20	Wind AF SA	WINDIM

G. Details of WDC Calculations by Rating Grades

See Table 11.

H. WDC Calculations for below-BB- Sample

While trying to compose the below-BB sample, we just do not see enough entities with the stable but low ratings, with 10-year-long CDS spread history. So, the qualitatively new methodology for this rating range is necessary and we construct a reasonable short-cut approach, based on an additional second-degree calibration procedure.

As an initial trial set of the WDCs for the below-BB- sample, we start using the term structure of the WDCs for the BB- sample; see Exhibit 1. Then, for a chosen low credit quality exposure, we calculate what would be the ECL allowance and consequently obtain the would-be price metrics based on the CDS quotes at the end date of a chosen reporting period and the trial WDCs. In parallel, we extract the price benchmark for the same date using the Bloomberg Valuation service provider, that is, a BVAL price.

By comparing the would-be price, implied by the WDC-calibrated CDS spread, to BVAL price we find what should be the adjustment coefficient to be applied to the trial set WDCs, used as inputs. By repeating this algorithm for several below-BB- exposures and diverse reporting dates, our second-degree calibration procedure becomes more reliable and more robust. That is, the bigger the number of the positions and the number of the trial reporting dates are, the higher the precision of the final WDC figures would be.

We use a sample, consisting of 4 bonds and 4 reporting dates, that is, 16 calibrations. The retained securities are Frontier Corporation Corp bond with maturity on April 15, 2024 (ISIN US35906AAN81), Astaldi S.p.A. bond with maturity on June 21, 2024 (ISIN XS1634544248), Sears Holding Corp bond with maturity on December 15, 2019 (ISIN US812350AF31), and Windstream Services LLC bond with maturity on August 01, 2023 (ISIN US97381WAZ77), all of which are classified as Stage 2. The lifetime ECL is calculated as exemplified in Sections 5.1 and 5.2 (See Table 12).

Data Availability

The data could be provided on demand.

Disclosure

This article is part of the IPL/2018/MacroViews/ISCAL and IPL/2019/MacroVirtu/ISCAL projects and the FCT Strategic Project: UID/SOC/04521/2019.

Conflicts of Interest

The author declares that there are no conflicts of interest regarding the publication of this paper.

Table 11

(a) WDC term structure calculation for BBB+ sample

Selected debt metrics: BBB+ sample					
Maturity (years)	1	3	5	7	10
Avg. (2007-2017) BBB+ sample's CDS spread (bps) (A)	35.1	57.3	81.0	96.0	107.5
SP-Moody's average T-t-C sample's cumulative ODR	0.1%	0.3%	0.7%	1.2%	1.9%
ODR implied average BBB+ sample's spread (bps) (B)	3.8	6.9	8.9	10.5	11.7
Weight of the Default Component (WDC = B/A)	11.0%	12.0%	10.9%	10.9%	10.9%

(b) WDC term structure calculation for BBB sample

Selected debt metrics: BBB sample					
Maturity (years)	1	3	5	7	10
Avg. (2007-2017) BBB sample's CDS spread (bps) (A)	50.4	80.6	112.3	131.2	144.4
SP-Moody's average T-t-C sample's cumulative ODR	0.2%	0.7%	1.5%	2.3%	3.5%
ODR implied average BBB sample's spread (bps) (B)	10.4	14.5	18.1	19.7	21.3
Weight of the Default Component (WDC = B/A)	20.7%	18.0%	16.1%	15.0%	14.7%

(c) WDC term structure calculation for BBB- sample

Selected debt metrics: BBB- sample					
Maturity (years)	1	3	5	7	10
Avg. (2007-2017) BBB- sample's CDS spread (bps) (A)	65.5	108.6	152.0	175.7	190.4
SP-Moody's average T-t-C sample's cumulative ODR	0.3%	1.3%	2.6%	3.9%	5.6%
ODR implied average BBB- sample's spread (bps) (B)	15.7	25.9	31.8	33.7	34.1
Weight of the Default Component (WDC = B/A)	24.0%	23.8%	20.9%	19.2%	17.9%

(d) WDC term structure calculation for BB+ sample

Selected debt metrics: BB+ sample					
Maturity (years)	1	3	5	7	10
Avg. (2007-2017) BB+ sample's CDS spread (bps) (A)	123.6	179.0	230.0	255.3	266.9
SP-Moody's average T-t-C sample's cumulative ODR	0.4%	2.5%	4.8%	6.8%	9.1%
ODR implied average BB+ sample's spread (bps) (B)	24.9	50.0	58.1	59.6	56.0
Weight of the Default Component (WDC = B/A)	20.2%	27.9%	25.3%	23.3%	21.0%

(e) WDC term structure calculation for BB sample

Selected debt metrics: BB sample					
Maturity (years)	1	3	5	7	10
Avg. (2007-2017) BB sample's CDS spread (bps) (A)	118.0	201.9	281.4	314.3	329.6
SP-Moody's average T-t-C sample's cumulative ODR	0.7%	3.5%	6.6%	8.9%	12.2%
ODR implied average BB sample's spread (bps) (B)	40.4	71.2	80.8	78.3	76.1
Weight of the Default Component (WDC = B/A)	34.3%	35.2%	28.7%	24.9%	23.1%

(f) WDC term structure calculation for BB- sample

Selected debt metrics: BB- sample					
Maturity (years)	1	3	5	7	10
Avg. (2007-2017) BB- sample's CDS spread (bps) (A)	142.5	247.5	339.3	376.9	392.7
SP-Moody's average T-t-C sample's cumulative ODR	1.3%	6.4%	11.8%	16.2%	21.3%
ODR implied average BB- sample's spread (bps) (B)	75.9	131.1	146.3	145.7	136.6
Weight of the Default Component (WDC = B/A)	53.3%	53.0%	43.1%	38.7%	34.8%

Table 12: Adjustment coefficient for below BB- grade to be applied to BB- WDCs: CDS-based ECL versus BVAL price calibration.

Credit Metrics	Reporting Date			
Frontier Communication bond: FTR 7.625 04/15/24	29/12/2017	31/1/2018	28/2/2018	30/3/2018
BVAL mid price (Px)	63.16	66.23	63.55	62.62
Lifetime ECL based on BVAL (ECL_BVAL = 1 - Px)	36.84	33.77	36.46	37.38
Lifetime ECL based on CDS spreads and BB- WDCs	34.50	30.48	29.21	31.35
Adjustment coefficient to WDCs equating the ECLs	1.09	1.14	1.33	1.26
Average adjustment coefficient to the BB- WDC	1.20			
Astaldi S.p.A. bond: ASTIM 4.875 06/21/24	29/12/2017	31/1/2018	28/2/2018	30/3/2018
BVAL mid price (Px)	53.12	66.90	61.52	59.72
Lifetime ECL based on BVAL (ECL_BVAL = 1 - Px)	46.88	33.10	38.48	40.28
Lifetime ECL based on CDS spreads and BB- WDCs	50.61	34.13	62.26	37.46
Adjustment coefficient to WDCs equating the ECLs	0.89	0.96	0.49	1.10
Average adjustment coefficient to the BB- WDC	0.86			
Sears Holding Corp bond: SHLD 8 12/15/19	29/12/2017	31/1/2018	28/2/2018	30/3/2018
BVAL mid price (Px)	50.94	48.00	42.75	33.75
Lifetime ECL based on BVAL (ECL_BVAL = 1 - Px)	49.06	52.00	57.25	66.25
Lifetime ECL based on CDS spreads and BB- WDCs	43.45	46.70	53.44	54.42
Adjustment coefficient to WDCs equating the ECLs	1.17	1.15	1.10	1.34
Average adjustment coefficient to the BB- WDC	1.19			
Windstream Services bond: WIN 6.375 08/01/23	29/12/2017	31/1/2018	28/2/2018	30/3/2018
BVAL mid price (Px)	61.88	58.89	60.22	57.61
Lifetime ECL based on BVAL (ECL_BVAL = 1 - Px)	38.12	41.11	39.78	42.39
Lifetime ECL based on CDS spreads and BB- WDCs	36.23	37.73	41.10	44.47
Adjustment coefficient to WDCs equating the ECLs	1.07	1.12	0.96	0.94
Average adjustment coefficient to the BB- WDC	1.02			
Mean value of adjustment coefficient to the BB- WDC	1.07			

Acknowledgments

Financial support from national funds by IPL (Instituto Politécnico de Lisboa) and by FCT (Fundação para a Ciência e a Tecnologia) is gratefully acknowledged.

References

[1] B. M. Tabak, T. C. Silva, and A. Sensoy, "Financial networks," *Complexity*, vol. 2018, Article ID 7802590, 2 pages, 2018.

[2] C. Aymanns, F. Caccioli, J. D. Farmer, and V. W. C. Tan, "Taming the Basel leverage cycle," *Journal of Financial Stability*, vol. 27, pp. 263–277, 2016.

[3] S. R. de Souza, T. C. Silva, B. M. Tabak, and S. M. Guerra, "Evaluating systemic risk using bank default probabilities in financial networks," *Journal of Economic Dynamics & Control*, vol. 66, pp. 54–75, 2016.

[4] T. C. Silva, M. D. S. Alexandre, and B. M. Tabak, "Bank lending and systemic risk: A financial-real sector network approach with feedback," *Journal of Financial Stability*, vol. 38, pp. 98–118, 2018.

[5] S. Li and S. Wen, "Multiplex networks of the guarantee market: evidence from Chnia," *Complexity*, vol. 2017, Article ID 9781890, pp. 1–7, 2017.

[6] I. Anagnostou, S. Sourabh, and D. Kandhai, "Incorporating contagion in portfolio credit risk models using network theory," *Complexity*, vol. 2018, Article ID 6076173, 15 pages, 2018.

[7] S. Jiang and H. Fan, "Systemic risk in the interbank market with overlapping portfolios," *Complexity*, vol. 2019, Article ID 5317819, 12 pages, 2019.

[8] S. Poledna, J. L. Molina-Borboa, S. Martínez-Jaramillo, M. van der Leij, and S. Thurner, "The multi-layer network nature of systemic risk and its implications for the costs of financial crises," *Journal of Financial Stability*, vol. 20, pp. 70–81, 2015.

[9] X. Huang, I. Vodenska, S. Havlin, and H. E. Stanley, "Cascading failures in Bi-partite graphs: model for systemic risk propagation," *Scientific Reports*, vol. 3, no. 1219, pp. 1–8, 2013.

[10] FASB - Financial Accounting Standards Board, Measurement of Credit Losses on Financial Instruments. Financial Instruments — Credit losses (Topic 326), 2016.

[11] IASB - International Accounting Standards Board, IFRS 9 Financial Instruments, 2014.

[12] J. Abad and J. Suarez, "The procyclicality of expected credit loss provisions," CEPR Discussion Paper DP13135, 2018.

[13] ESRB – European Systemic Risk Board, *Expected Credit Loss Approaches in Europe and the United States: Differences from a Financial Stability Perspective*, 2019.

[14] M. Choudhry, *The Credit Default Swap Basis*, Bloomberg Press, New York, NY, USA, 2006.

[15] M. Gubareva and M. R. Borges, "Switching interest rate sensitivity regimes of U.S. corporates," *The North American Journal of Economics and Finance*, 2018.

[16] M. Gubareva and M. R. Borges, "Rethinking economic capital management through the integrated derivative-based treatment

of interest rate and credit risk," *Annals of Operations Research*, vol. 266, no. 1-2, pp. 71–100, 2018.

[17] A. Sensoy, F. J. Fabozzi, and V. Eraslan, "Predictability dynamics of emerging sovereign CDS markets," *Economics Letters*, vol. 161, pp. 5–9, 2017.

[18] W. Heynderickx, J. Cariboni, W. Schoutens, and B. Smits, "The relationship between risk-neutral and actual default probabilities: the credit risk premium," *Applied Economics*, vol. 48, no. 42, pp. 4066–4081, 2016.

[19] J. Huang and M. Huang, "How much of the corporate-treasury yield spread is due to credit risk?" *Review of Asset Pricing Studies*, vol. 2, no. 2, pp. 153–202, 2012.

[20] A. Arakelyan and P. Serrano, "Liquidity in credit default swap markets," *Journal of Multinational Financial Management*, vol. 37-38, pp. 139–157, 2016.

[21] J. McPhail and L. McPhail, "Forecasting lifetime credit losses: modeling considerations for complying with the new FASB and IASB current expected loss models," *Journal of Risk Management in Financial Institutions*, vol. 7, no. 4, pp. 375–388, 2014.

[22] G. Chawla, L. Forest Jr., and S. Aguais, "Point-in-time loss-given default rates and exposures at default models for IFRS 9/CECL and stress testing," *Journal of Risk Management in Financial Institutions*, vol. 9, no. 3, pp. 249–263, 2016.

[23] J. Skoglund, "Credit risk term-structures for lifetime impairment forecasting: a practical guide," *Journal of Risk Management in Financial Institutions*, vol. 10, no. 2, pp. 177–195, 2017.

[24] J. Zhang, Ed., *The New Impairment Model under IFRS 9 and CECL*, Risk Books, London, UK, 2018.

[25] Basel Committee on Banking Supervision, *Guidance on Credit Risk and Accounting for Expected Credit Losses*, 2015.

[26] Standard & Poor's Global, *Default, Transition, and Recovery: 2016 Annual Global Corporate Default Study and Rating Transitions*, 2017.

[27] Moody's Investors Service, *Default Research: Annual Default Study: Corporate Default and Recovery Rates, 1920-2016*, 2017.

[28] J. Jansen and F. J. Fabozzi, "CDS implied credit ratings," *Journal of Fixed Income*, vol. 26, no. 4, pp. 25–52, 2017.

[29] F. A. Longstaff, S. Mithal, and E. Neis, "Corporate yield spreads: Default risk or liquidity? New evidence from the credit default swap market," *Journal of Finance*, vol. 60, no. 5, pp. 2213–2253, 2005.

[30] D. Y. Tang and H. Yan, "Market conditions, default risk and credit spreads," *Journal of Banking & Finance*, vol. 34, no. 4, pp. 743–753, 2010.

[31] D. Bongaerts, F. De Jong, and J. Driessen, "Derivative pricing with liquidity risk: theory and evidence from the credit default swap market," *Journal of Finance*, vol. 66, no. 1, pp. 203–240, 2011.

[32] A. Berndt, R. Douglas, D. Duffie, M. Ferguson, and D. Schranz, "Measuring default risk premia from default swap rates and EDFs," Working Paper - Tepper School of Business, 2008.

[33] G. Bekaert, C. Harvey, C. Lundblad, and S. Siegel, "Political risk spreads," ERIM Working Paper, 2013.

[34] H. Lin, S. Liu, and C. Wu, "Dissecting corporate bond and CDS spreads," *Journal of Fixed Income*, vol. 20, no. 3, pp. 7–39, 2011.

[35] M. Gubareva, "Excess liquidity premia of single-name CDS vs. iTraxx/CDX spreads: 2007-2017," *Studies in Economics and Finance*, 2019.

Hindawi
Complexity
Volume 2019, Article ID 1715624, 21 pages
https://doi.org/10.1155/2019/1715624

Research Article

Understanding How Short-Termism and a Dynamic Investor Network Affects Investor Returns: An Agent-Based Perspective

Matthew Oldham

Department of Computational and Data Sciences, George Mason University, Fairfax, VA 22124, USA

Correspondence should be addressed to Matthew Oldham; oldhamma@gmail.com

Received 8 February 2019; Revised 30 May 2019; Accepted 12 June 2019; Published 3 July 2019

Guest Editor: Ahmet Sensoy

The unexplained and inconsistent behavior of financial markets provides the motivation to engage interdisciplinary approaches to understand its intricacies better. A proven approach is to consider investors as heterogeneous interacting agents who form information networks to inform their investment decisions. The rationale is that the topology of these networks has contributed to a better understanding of the erratic behavior of financial markets. Introducing investor heterogeneity also allows researchers to identify the characteristics of higher performing investors and the implications of investors exhibiting short-termism, a feature recognized by some as detrimental to the performance of the economy. To address these topics, an agent-based artificial stock market is implemented, where investors utilize various information sources, including advice from investors in their network, to inform their investment decisions. Over time investors update their trust in their information sources and evolve their network by connecting to outperforming investors—Oracles—and discarding poor advisers, thereby simulating the evolution of an investor network. The model's most significant finding is uncovering how the market's behavior is materially affected by the time-horizon of investors, with short-term behavior resulting in greater volatility in the market. Another finding is the reason why short-term investors generally outperform their long-term counterparts, particularly in more volatile environments. By providing significant insights into the formation of an investor network and its ramifications for market volatility and wealth creation (destruction), this paper provides crucial clues regarding the empirical data that needs to be collected, assessed, and tracked to ensure policymakers and investors better understand the dynamics of financial markets.

1. Introduction

Since the inception of equity markets, investors have attempted to enhance their wealth by investing their capital into these markets. However, the inconsistent behavior of equity markets has meant that most investors have failed to master them and achieve their investment goals. The dominant theory, at least until the 2000s, was that investors should accept that financial markets behave in an efficient manner, resulting in asset returns matching a Gaussian distribution as a consequence of a random-walk process ([1, 2]). The basis of the efficient market approach, as encapsulated in the Efficient Market Hypothesis (EMH) [3], is that a representative rational agent has timely access to all necessary information, correctly evaluates that information, and makes the optimal investment decisions, thereby ensuring that prices reflect the most recent and relevant information. However, the financial pricing models related to the principle of efficient markets have been found to provide only a rough approximation of financial returns and have failed to explain outlying events [4]. Further, two critical implications stem from the EMH: prices are always right, and no investor can outperform the market over the long-term on a risk-adjusted basis [5].

While there is some supporting evidence that on average investors have been unable to outperform the market ([6–8]), evidence does exist that some investors (represented in this paper as Oracles) have achieved and maintained a material positive performance differential over the market ([9, 10]). Two possible determinants of investment performance considered in this paper are the tendency of investors to trade and the investment horizon of investors. Barber and Odean [11] highlight opposing explanations regarding the observed levels of trading, with the theory most relevant to this paper being that excess trading occurs because investors have a

short-term focus and this leads to excessive speculative trading [12] which, in turn, results in inferior wealth generation [11]. Alternatively, when faced with volatile markets, it has been found that it is optimal for investors to employ short-term trading strategies [13].

Regarding the return characteristics of financial markets, these have been found to demonstrate a specific set of stylized facts that contradict the EMH-based Gaussian models. Kaldor [14] originally defined stylized facts as stable patterns that emerge from multiple empirical data sources after abstracting from the minutia of the evidence. The utility of stylized facts is that they enable the researcher to build a model capable of identifying, explaining, and communicating critical observations that require a scientific explanation without having the burden of explaining all the variations in the empirical evidence [15]. The vital stylized facts related to financial markets are excess volatility, the existence of large movements not supported by the arrival of new news; heavy tails, returns that exhibit heavy tails or fat tails; volatility clustering, large changes accompany further large changes; and volume/volatility clustering, trading volumes and volatility showing the same type of extended memory ([16, 17]). As expanded upon later, the utilization of these stylized facts has been instrumental in proving the utility of agent-based artificial stock markets.

Another vital characteristic of asset returns is that they have been found to match a power-law distribution over extended time intervals [18]. The existence of power-law returns provides the crucial insight that financial markets may operate as a complex adaptive system (CAS). Utilizing a CAS framework has become increasingly popular and relevant in attempting to understand the behavior of financial markets (for example, see [17, 19, 20]). Dependencies and the interaction between the various individual component of a CAS are deemed responsible for creating the macrolevel emergent outcomes [21], including extreme market movements. Allowing investors to interact with and receive information from other investors enables them to form an information network. The critical consequences of this process are that investor networks and financial networks in general have been found to be capable of affecting the behavior of the market ([22–24]), and they explain trading volumes and the performance of investors ([25, 26]). Critically, this analysis has not been, nor can it be, considered in the models underwritten by a representative agent approach.

The evidence on investment performance, trading volumes, and the non-Gaussian distribution of asset returns opens several compelling research questions. Specifically, issues arise regarding what makes high-performing investors unique, including how do they utilize various information sources to determine their investment decisions; how often do they trade; and what are the consequences of other investors attempting to replicate their strategies? These questions are addressed in this paper, by linking heterogeneous interacting investors with different investment horizons across a dynamic network, with trading information flowing across the network.

Unlike the return profile of financial markets, there is yet to emerge a definitive agreed-upon set of empirically grounded theories regarding the role of investor networks. This issue is most likely due to the rapid development of the research field and the initial and ongoing difficulty in accessing timely data to assess both the static and dynamic characteristics of these networks. The findings of Ozsoylev and Walden [25] are utilized to establish a level of empirical validation for the model presented in Section 2. Of most significance is that the investors with the highest connectedness will earn the largest profits from trading more aggressively, and the market's price volatility will be highest in an environment where the investor network exhibits an intermediate level of connectedness and lowest in markets with higher or lower levels of connectedness. The latter suggests that a scale-free topology will exhibit the highest volatility, a theory confirmed in various agent-based models (ABMs) (see [22, 27, 28]).

The standard analytical tools that underlie much of the conventional financial market analysis become redundant in the realm of a CAS [29]. ABMs are a possible solution as they allow researchers to build simulations from a bottom-up perspective, with the agents interacting with and adapting to their environment. Another justification for utilizing agent-based modeling, even in the absence of empirical data, is that ABMs can guide data collection and illuminate core dynamics [30]. Alternatively, ABMs can uncover the dynamics responsible for generating the stylized facts of financial markets [31], as evidenced by the substantial insights achieved via agent-based artificial stock markets (as reviewed in [32, 33]). Notably, the original models explained a great deal without the use of networks [34]. Despite this, the inclusion of networks within this framework is becoming an established field of research because by introducing structural heterogeneity—which manifests itself as a network between investors [34]—new dynamics regarding the stylized behavior of financial markets have been uncovered (recent examples include [22, 28, 35–37]). The common theme of these network models is that they utilize exogenously imposed, static, stylized networks. Therefore, the research gains in this area have occurred without empirically supported network structures.

A downside to the previously mentioned network modeling approach is that it limits the analysis to assessing the behavior of investors across a predefined static network, thereby providing no insight into how the network evolves. However, research is now expanding toward explaining the dynamics responsible for influencing how a network's structure evolves. ABMs have proven to be a successful tool for understanding the dynamics of network formation [38], with this paper making a further contribution to the research field. Within the artificial stock market literature, there is a body of work, which forms the foundation for this paper, that implements models that endogenously evolve networks between investors (see [31, 39]). The central theme of these papers was to include dynamic learning, with investors attempting to connect with investment "gurus" (defined as agents with superior investment performance) to improve their investment performance. This dynamic resulted in the expectations of the general population becoming aligned with those of the gurus. An essential finding of the models

was that the networks formed by the investors became highly interconnected through their shared connection to gurus, and matched a scale-free topology. This paper utilizes Oracles in a similar but not identical manner to gurus, hence the change of title for a superior investor.

This paper reports on the implementation of an agent-based artificial stock market model where investors determine their optimal information sources, including information coming from a dynamic investor network. The investor network evolves as investors adjust, at fixed intervals, the agents (advisers) from whom they receive advice. Agents also continually update the trust in their various information sources. In choosing their new advisers, investors seek out the better performing investors, known as Oracles. The intention of the process is for investors to enhance their investment performance by receiving the highest quality of information. Additionally, investors are divided into short- and long-term investors, to test the implications of considering more or less information and a differing decision threshold.

The intention of the paper is to assess the consequences, if any, at the market and agent level of connecting investors in a dynamic investor network and allowing them to utilize differing investment horizons. The specific research questions to be addressed at the market level are what are the implications of providing agents with the flexibility to select advisers; what form does the resulting investor network topology take; how long does it take the network to become stable, if at all; and what are the effects of allowing investors to take a myopic approach. At the agent level, the critical question relates to establishing whether specific agents are more successful in generating excess returns than others, and if so, what are their defining characteristics? In short, what are the attributes of an Oracle? The intention is to see if it is possible to grow a Warren Buffett (the Oracle of Omaha) in silico. The paper is structured as follows: Section 2 summarizes the implemented model with its results presented in Section 3, Section 4 provides a discussion of the results, and Section 5 concludes the paper.

2. Approach and Model Design

The contribution of this paper comes from two material changes to the model of Harras and Sornette [37] (H&S hereafter). This model has investors initiated with a unit of a risky and a risk-free asset and connected via a static lattice network. Investors are then continually provided with three sources of information: public, private, and trading intentions, that is, to buy, hold, or sell the risky asset, of their advisers (network links) to aid their own investment decision. Investors then adjust their trust in the various information sources based on its ability to correctly (or incorrectly) predict the movement of the risky asset's price. The trust updating and the new rewiring process provide the potential mechanism to feed a positive feedback loop which creates an asset bubble. The loop becomes more relevant as investors become aligned (herd) with one another as the trust in specific advisers grows. The justification for utilizing the H&S model as a foundation was that it provided a framework where information that affected investment decisions flowed across a network; considered the processes of adaptation and evolution adjusting trust in each of their information sources; showed that price movements were affected by how strongly neighbors influence an agent's investment decision; and generated asset returns that matched the stylized fact of fat-tailed returns.

Table 1: Agent decision thresholds.

Scenario	Action	Variable
$\omega_{ij}(t) > \overline{\omega}_j$	Buy	$a_{ij}(t) = +1$
$\omega_{ij}(t) < \overline{\omega}_j * -1$	Sell	$a_{ij}(t) = -1$
Otherwise	Hold	$a_{ji}(t) = 0$

Of the various changes, the most significant was allow investors, at varying intervals, to adjust their information network via a rewiring process. Via this process, the investors can select a higher quality adviser(s) (Oracles) as the simulation evolves. The work of Markose et al. [39] and Tedeschi et al. [31] motivated this functionality, with Section 2.2.1 detailing the modifications. The other alteration was to divide investors into two classes: long- and short-term investors. Section 2.2.2 provides the full details of this process: briefly stated, the extension relates to how investors assess the performance of their peers, update their trust in the various information sources, and make decisions. The intention is that a short-term investor will adjust trust more rapidly and be more reactionary in making trading decisions.

Sections 2.2 and 2.3 provide a brief description of the model and detail of the crucial changes. The model and an overview, design, and details (ODD) document [40], which details the model, is retrievable from http://tidy.ws/28jdyT. The rationale for providing both the model and ODD is that it allows for the replication of the results and dissemination of the model to motivate additional extensions. NetLogo 5.3 [41] was selected as the programming language to implement the model.

2.1. Model Background

Equation (1): The Precise Decision-Making Equation Used by Agents

$$\omega_{ij} = c_{1ij}\left(\sum_{k=1}^{K} nt_{jk}(t-1)\, E_{ij}\left[a_{ik}(t)\right]\right) + c_{2ij}\, pt_i(t-1)\, pi_i(t) + c_{3ij}\epsilon_{ij}(t) \tag{1}$$

Equation (1) is how investor j combines the three sources of information to determine the decision metric (ω_{ij}) for asset i. The decision metric, when compared against the investor's decision threshold ($\overline{\omega}_j$), determines whether the agents buy more, hold, or sell a proportion of their holding in the risky asset per Table 1. The information sources are the expected actions of their neighbors ($E_{ij}[a_{ik}(t)]$), public information ($pi_i(t)$), and private information ($\epsilon_{ij}(t)$). The public and private information sources are normally distributed stochastic variables with a mean of 0. Also, (1) details how additional variables weight the influence of each information

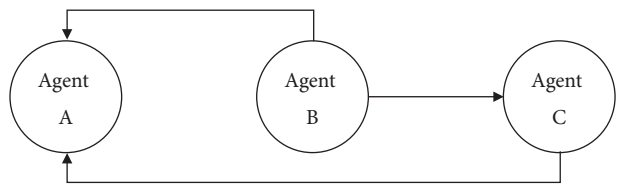

Figure 1: Stylized directed investor network.

source. For the public and network information, one set of the variables—the initial bias coefficients—remain fixed while the other variables—the trust coefficients—are updated to reflect the trust the investor has in each information source as they react to the market and the quality of the information. The fixed values are given by c_{1ij}, c_{2ij}, and c_{3ij}, while the variable coefficients are network trust (nt_{jk}) and public trust (pt_i). The fixed variables are uniformly distributed at initiation among the investors, with the lower limit being 0 and the upper limit determined by the user. By altering the upper limit of the initial bias (simplified to be read as c_1, c_2, and c_3) different model dynamics transpire. The parameter sweep of the implemented model includes values of c_1 ranging from 1 to 4, while the others remain fixed at 1. Once investors make their decision, trading occurs, with a new price endogenously determined for the risky asset. Investors utilize the pricing outcome to update various beliefs, including trust in their advisers (outbound network links).

2.2. Agent Classes

2.2.1. The Network. At initiation, the network is created by investors forming directed links to their nearest neighbors, thereby creating a lattice network. The user sets the number of immediate neighbors with the *Ring_M* parameter, with the number of advisers at initiation being double the setting for the *Ring_M* parameter. With directed links investors utilize outbound links to connect to the investors whom they wish to receive information from; therein, a chosen investor becomes an adviser, whom may ultimately be an Oracle. The information in this instance is the investment action (buy, hold, or sell) that the adviser intends to implement in the current time step (see (1)). Advisers will not seek information from those investors who connect to them. Figure 1 summarizes the various relationships where: Agent A (an Oracle) has two followers (Agent B and C) but does not seek information from any investors; Agent B has two advisers (Agent A and C) but has no followers; and Agent C has one adviser (Agent A) and one follower (Agent B).

The justification for this functionality is that investors (followers) become disciplines of Oracles and that Oracles maintain a disciplined investment approach. This point is illustrated by how the attendance at the annual Berkshire Hathaway—Warren Buffett's investment vehicle—annual meeting grew as his investment performance grew in status [42], while his investment style remained predicated on a concentrated value style [43]. In general, per Gergaud & Ziemba [43], there is no suggestion that their followers influence the investment decisions of star performers.

The more critical element of the model is how the rewiring process alters the advice network of the investors. The rewiring process occurs at intervals decided by the users, via the *rewire* variable. When the rewiring procedure is called, investors assess the trust they have formed in each of their advisers (their outbound directed links); their performance relative to the market; and their aggregate trust in the information they receive from their advisers. Table 2 summarizes the possible actions of an investor and the rationale for each behavior. The basis for the response is that investors are assessing their environment and then deciding the best course for improving their investment performance. Performance relates to the way an investor allocates their wealth between the risky asset and the risk-free asset. While the rewiring process occurs at discrete intervals, investors are updating their trust in their public and network information at each step. Therefore, investors may have little, or negative, trust in an individual adviser at the time of the rewiring process.

The implemented model has several differentiated network formation characteristics of the models of Markose et al. [39] and Tedeschi et al. [31]. The first is the use of a lattice network at initiation, as opposed to a random network. Crucially, this approach is consistent with Watts and Strogatz [44], who demonstrated how the critical elements of a small-world network (a network considered representative of most real-world networks [[45]])—a high clustering coefficient yet short average path length—evolved from lattice network. Utilizing a lattice network also allows for more accurate verification against the H&S framework. Additionally, the model rewires the network at discrete intervals while in the other models this process occurs in each period. The justification for this change is that investors do update their trust at each step so investors can essentially "cut" a link by not assigning weight to the available information from their advisers. The implemented model also allows for multiple outbound links from an investor, whereas Tedeschi et al. [31] have a single link per investor.

2.2.2. The Investors. To facilitate the introduction of two investor classes, the user sets the proportion allocated to the short- or long-term investor class. The introduction of the *%_longterm* variable facilitates this process. The investor's class has two effects: the amount of history the investor considers, and the distribution of the decision threshold value ($\overline{\omega}_j$). Utilizing past information, and how much of it, is a vital component in building artificial financial markets [46].

Table 2: Investor network behavior rationale.

Outperformed the market?	Positive Network Trust?	Action	The Rationale for the Behavior
Yes	Yes	Keep all advisers and add an Oracle	These investors judge that their advisers are a significant overall source of outperformance. Therefore, they are willing to overlook the individual performance of their advisers (noting that they already adjust their trust) in the rewiring process and merely look to add an Oracle in the expectation of improving their incoming information.
Yes	No	Do nothing	These investors are attributing their outperformance to the other information sources. That is, there is not a strong belief that advisers can aid performance. They have already adjusted the trust in each neighbor; thereby, they would be already ignoring the advice, so do not see the need for change.
No	Yes	Cut bad advisers and add an equivalent number of Oracles	These investors have underperformed but given the positive level of trust in their network information assume that removing poor advisers and adding Oracles will reverse their underperformance. This mechanism contrasts to outperformers who are prepared to forgive poor advisers.
No	No	Cut bad advisers without adding new advisers	These investors are effectively attributing their underperformance to their network information and to turn around their performance will cut ties with their advisers and not seek new advisers. In the extreme, these investors will only use public and private information.

The rationale is that short-term investors are deemed myopic in assessing all elements of the market ecosystem. Kay's [12] identification of the "hyperactivity" of the short-term investor provides the foundation for this approach.

The introduction of the *short_term_diff* variable accommodates the two investor classes, with (2) illustrating how the variable affects the amount of history that an investor considers. Section 2.3.4 provides the details through (3) and (4) as to how investor i considers history through the memory weight variable α_i. With the time-scale by which past information continues to influence various metrics given by $1/|\ln(\alpha_j)|$, any positive value for *short_term_diff* reduces the length of time that past performance affects current decision-making. For example, in the experiments reported in Section 3, the difference was set at .05, which is equivalent to 10 periods.

Equation (2): Determining an Investors' Memory Weight

$$\alpha_j = memory\_weight - short\_term\_diff \tag{2}$$

The next modification was the utilization of an exponential distribution, bounded between 0 and 2, to allocate the decision threshold variable ($\overline{\omega}_j$) from (1). For long-term investors, the distribution is 2 minus the value from the exponential distribution. Alternatively, short-term investors take the value generated by the exponential distribution, noting a value of 0 increased to 0.1. Therefore, short-term investors possess a lower trading threshold, due to the assumption that they have a higher propensity to act on the most recent information. A prima facie argument exists that this assumption will see short-term investors trade more. However, this result might not necessarily arise because short-term investors may struggle to maintain sufficient trust in any of their information sources, so they will become indifferent to trading.

2.2.3. The Risky Asset. The risky asset class encompasses a single asset i. The asset has a passive role, with its price movements being the primary variable of interest. Investors receive private and public information ($\epsilon_{ij}(t)$ and $p_i(t)$ respectively from (2)) about the asset at each step of the model. This information is in turn utilized to inform their decision-making process. Therefore, the information is broader than, yet not as specific as an earnings stream. This approach is consistent with the H&S framework, with the rationale of the method being that it will ensure that the dynamics reported in Section 3 relate solely to the behavior of the investors.

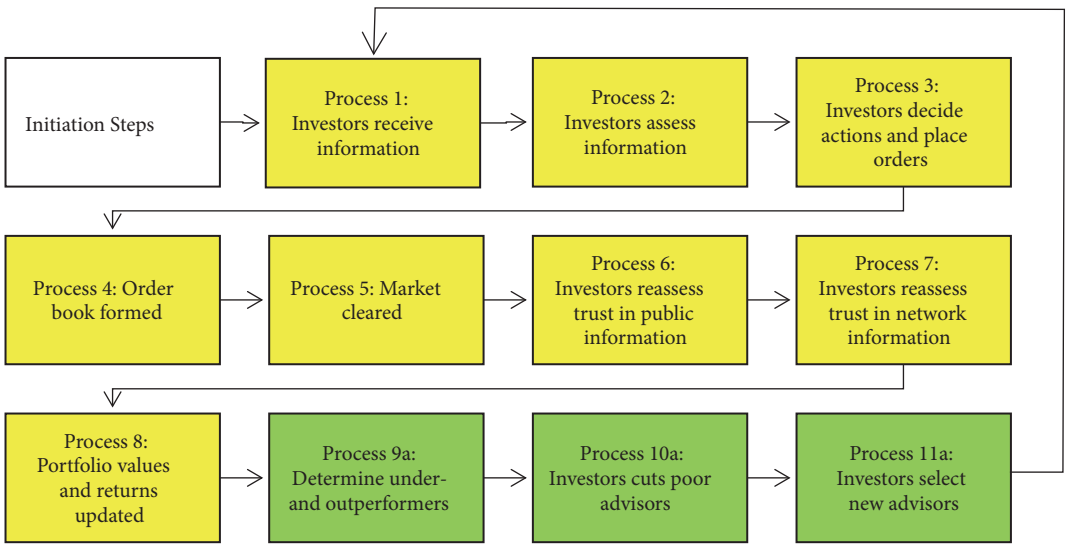

Figure 2: Representation of the model steps. Steps 9a to 11a only occur at the rewiring intervals.

2.3. Model Steps. Figure 2 details processes and the order of execution of various processes contained within a step of the model. A step in the model is assumed to be a day with some new material information arriving at each step, and daily price movements and trading decisions are a closer approximation of actual financial markets. Within a step, Process 1 to Process 7 (color-coded in yellow) are performed in a manner consistent with the model H&S. Processes 8a through 10a (color-coded in green) only occur when the step number matches, or is divisible by the *rewire* variable (set by the user); for example, if the *rewire* variable equals 500, the model will call the rewire procedure at steps 500, 1000, 1500, etc.

2.3.1. Receiving Information and Assessing Information (Processes 1 and 2). The first repeated process has investors receive information. Then they combine the information to decide their action for the step. Regarding private information (ϵ_{ij}), each investor's information comes from a normally distributed random-float with a mean of 0 and a finite variance (1 in this case). Equation (1) implies that a positive (negative) value provides an impetus to the investor to buy (sell) with a higher value, *ceteris paribus*, having a more material effect on the investment decision. Given the random nature of the private information, there should be no serial correlation between the private information of the investors. Public information for asset i (pi_i) at time t is generated in the same manner, except the population shares the same value. Investors will have varying inclinations toward following the data due to their independent trust (pt_i) in the source and their specific influence parameter (c_{2ij}).

To gather their network information, investors poll the intended actions of their advisers. The $E_{ij}[a_{ik}(t)]$ variable from (1) captures the expected actions of an investor's neighbors. The justification for following the actions of an adviser is that when an investor can only employ bounded rationality, it may become optimal to follow neighbors [46]. The information received from advisers is not weighted equally, with an investor consideration based on the trust in the given adviser (nt_{jk}) generated in the prior period *(t-1)*. Finally, each investor sum the weighted actions of their advisers before multiplying the value by their fixed influence term (c_{1ij}). Note that connecting with more advisers will increase the given investor's tendency to follow their network's behavior. In a similar vein to Markose et al. [39], by measuring the accumulated actions of the population, the herding tendency can be assessed, as reported in Figure 6.

2.3.2. Finalizing the Investment Decision (Processes 3 and 4). After determining their investment action, investors check they have the required resources to undertake the desired action and decide how much to trade. The need for the former comes from the assumption that there is no leverage or short-selling. Therefore, investors must have a positive balance of the risk-free asset at time t ($rf_j(t)$) to buy more of the risky asset and must hold a positive quantity of the risky asset ($holding_{ij}(t)$) if they intend to sell. If investors meet the requirements, they trade per Table 1. If an investor does not meet the trading requirements, the investor must sit out of the market. To determine the actual trading volume ($v_{ij}(t)$) of asset i at time t, the model utilizes the transaction ratio variable (tr). The user sets the *transaction_ratio* parameter at initiation, which is fixed and shared by all investors. Finally, to form the market book the orders of all the investors are accumulated.

2.3.3. Market Clearing (Process 5). This procedure clears the market and determines the risky asset's new price by processing the previously calculated market book. Within the agent-based artificial stock market literature, two alternate market-clearing processes exist, a market-maker and an auction market. In line with the H&S model, a market-maker model is employed. Tedeschi et al. [31] in contrast utilized an

auction market, but their model implemented 150 investors in comparison to the 2,500 implemented in the H&S model. Farmer [47] provides a detailed rationale for the market-maker model, with the chief support being that the process ensures the market is not frozen due to gaps in the order book yet it can still accurately determine an appropriate price change based on the surplus (deficit) demand for the asset.

2.3.4. Trust and Portfolio Updating (Processes 6 - 8). Once investors become aware of their returns, they utilize the information to adjust the level of trust they have in the information provided by their network (nt_{jk}) and public sources (pt_j). With trust initiated 0, investors begin to build trust in a source if it provides the correct advice; that is, if the agent receives a buy (sell) signal from the information source and the price subsequently increases (decreases), then the weight (trust) increases. This updating process is the point at which the difference in the short- and long-term investors manifests itself.

Equation (3) is the process that investors utilize to update their public trust, while (4) is the mechanism by which investors revise their network trust. The essence of the two equations is the same, with the first term in the equation discounting the previous trust value variable by the variable α_i. However, per (2) this variable differs for the two investor classes. The second part of the equation adds the assessment of the immediately preceding information, which has been discounted by (1- α_i) after the $r_i(t)/\sigma_{ir(t)}$ term multiples it. From these equations, a lower value of α_i increases the influence of the most recent history. Crucially, the $r_i(t)/\sigma_{ir(t)}$ term normalizes the past return of an asset ($r_i(t)$) by the standard deviation of its past returns $\sigma_{ir}(t)$. H&S [37] provide the rationale: a more substantial change scaled by its volatility enhances trust to a higher degree.

Equation (3): Public Trust Updating Process

$$pt_i(t) = \alpha_i pt_i(t-1) + (1-\alpha_i)\, pi_i(t-1) * \frac{r_i(t)}{\sigma_{ir}(t)} \tag{3}$$

Equation (4): Network Trust Updating Process

$$nt_{jk}(t) = \sum_{i=1}^{I} \alpha_i nt_{jk}(t-1) + (1-\alpha_i)\, E_{ij}\left[a_{ik}(t-1)\right] * \frac{r_i(t)}{\sigma_{ir}(t)} \tag{4}$$

The final process is for the model to update the portfolios of the investors to reflect the outcome of the market-clearing process. This process sees just the balance of the investors' holdings in the risky and risk-free assets adjusted.

2.3.5. Determining Under- and Outperformers (Process 9a). When the rewire procedure is called, investors undertake a detailed assessment of their performance. First, investors determine the value of the portfolio and calculate their return between the rewiring steps. Next, investors determine whether they have out-or underperformed their benchmark. The long-term investors compare the growth of their portfolio value to that of the markets since inception. In contrast, the short-term investors compare their most recent portfolio return against the return of the market since the last rewiring process. Investors consider themselves out (under) performers if they have exceeded or underperformed their relevant benchmark.

Next, the model selects the best-performed investors (Oracles) for each investor class. Given the difference in the performance criteria for the long- and short-term investors, there is a list of investors with the largest portfolio values and one with the largest returns since the last rewiring process. The user dictates the number of Oracles via the *Oracle_options* variable, with the identification details of the Oracles stored in a global list. It may be the case that the same investors are on both lists, but they are there on different criteria. The investors stored in these lists may be selected as advisers, as described in Section 2.3.6.

2.3.6. Cutting Poor Advisers and Selecting New Advisers (Steps 10a–11a). From Table 2 it is seen that underperformers (identified in Section 2.3.5) will cut poor advisers, defined as an adviser for whom the agent's trust level is negative. Once identified, the poor adviser is added to a list, named *stayorgo*. After reviewing all their advisers, the length of the *stayorgo* list is utilized to update the *p_new_ad* variable, whose purpose is to record the number of new advisers the investors may select in the next step. Having identified their poor advisers, the investor will cut the links to those advisers and remove them and their trust record from the relevant lists.

The initial process for investors to select a new adviser is to access the list of outperformers (Oracles) relevant to their subclass and choose at random the required number. An outperformer with overall positive trust in their network information will select one additional Oracle. For an underperformer with a combined positive level of trust in their network information, the number of Oracles selected comes from the value of their *p_new_ad* variable. Having selected an Oracle(s), the investors form a directed link to the Oracle, thus rewiring the network. New advisers have an initial trust level of 0.

3. Results and Findings

3.1. Experimental Settings and Result Summary. Table 3 provides a summary of the baseline settings and parameter changes utilized for the various experiments. The settings were chosen to ensure a level of consistency against Harras & Sornette [37] and Oldham ([23, 27]). These papers reported that as the variable that determines the inclination of the investor to be influenced by their network increases—denoted by c_1 (see (1))—the price series begins to experience increased periods of volatility. An elevated level of network influence ultimately results in a positive feedback loop between investors generating sufficient weight for "herding" to occur; that is, following the actions of their most trusted adviser becomes common practice within the

Table 3: Baseline parameter settings.

Variable	Settings
Time steps per run	2,999
Runs per setting	60
Number of investors (J)	2,500
Market depth (λ)	0.25
Transaction ratio (tr)	0.02
Memory for long-term investors (α)	0.95
Memory differentiation	0.05
Potential Oracles	10
Number of original neighbors	4
Network influence (the c_1 variable)	1,2,3,4
Percentage of short-term investors	0%, 25%, 50%, 75% & 100%
Rewiring intervals (time step)	250, 500, 1000, 1500

populations, and the price of the risky asset no longer moves randomly, per the arrival of private and public information. Asset bubbles also appear, noting that the catalyst for their collapse is that investors have insufficient funds to maintain their buying momentum. This loss of momentum impairs the positive feedback loop, and investors begin to lose trust in their neighbors' investment advice, meaning the population's investment strategies become less synchronized.

The research questions informed the design of the experiments presented in this section, with the essence of the analysis to understand how the system varies from the baseline results of Harras & Sornette [37]. Table 4 provides an overview of the main components of the two classes of experiments and a summary of the findings. In combination with Table 3, the reader should note that as each model run was 2,999 steps a final rewiring of the network did not occur; that is, for a rewiring set of 1,500 (250) the final rewiring occurred at step 1500 (2750). The rationale for this decision was to allow an analysis of the network and agent characteristics without the interference of a final rewiring process. The methodology put forward by Lee et al. [48] was utilized to decide the number of runs. The approach suggests that the number of runs should be such that the coefficient of variation for selected variables should demonstrate sufficient stability.

Time-series plots and summary statistics plots are utilized to present findings. The time-series plots provide a stylized temporal interpretation by using a LOESS smoothing technique. The benefit of this process is that clearly illustrates how each combination of parameters affects a given variable and removes unnecessary noise. Summary statistics plots—range plots or bar graphs—are utilized to illustrate the variation within a given set of parameters. Figure 3 through Figure 10 apply the same color-coding for the percentage of short-term investors in the ecosystem, with the variable of interest plotted on the y-axis. The facets for Figure 3 reflect the different levels of the network influence variable (c_1). Figures 4 through 10 utilize a facet grid, with the setting for network influence variable (c_1) described by the vertical facet and the rewiring setting represented by the horizontal facet. Additionally, the network influence variable facets have the prefix of (1) through (4), while the rewiring facets have the prefix of (a) through (e). Therefore, when referenced, a facet will be described by its coordinates; for example, facet b3 refers to a rewiring setting of 500 and a level of network influence equal to 3. Regarding the time-series plots, the x-axis indicates the time step of the simulation, and the y-axis is the variable of interest. Therefore, within a figure, each facet shares the same axes and is scaled consistently.

3.2. Detailed Results

3.2.1. Introducing Short-Term Investors. Figure 3 presents the stylized price dynamics of the various settings across time that are the result of introducing short-term investors without rewiring. The y-axis represents the range between the maximum and minimum price of the risky asset at each step from the multiple runs (60) of each experimental combination. Regarding validation, the ex-ante expectation was that a 50:50 mixture of short- and long-term investors would produce similar results to the original model. The results of facet 1 and facet 2 provide a level of confirmation for this hypothesis. However, from facet 3 and facet 4, it appears that a 25:75 mix of short- and long-term investors produces a comparable result.

The introduction of short-term investors produces several new dynamics, with the magnitude of these dynamics dependent on the composition of the ecosystem. The first observation, as illustrated in Figure 3 facet 1, is that it is only when the level of network influence exceeds 1 that there is any material change in the price dynamics. Next, when there is a high proportion of short-term investors, the system does not require the level of network influence to be as high for the system to show extreme price movements; Figure 3 facet 2 demonstrates this point. From Figure 3 facet 3 and facet 4 it is seen that a higher proportion of short-term investors leads to a more rapid expansion and deflation of the risky asset's price because it takes less time for the investors to form herds. Even a 25:75 combination is sufficient to increase price volatility as the long-term investors enter a buying herd. The final point of the initial analysis is the behavior of a population comprised entirely of long-term investors. From Figure 3, it is seen that under no circumstances does the price series become excitable. The conclusion drawn from this is that considering more price points and not being able to change advisers are sufficient to restrict the behavior of investors.

3.2.2. The Combination of Short-Term Investors and Rewiring. With the introduction of the dynamic network, there is the need to assess the dynamics of both the financial market and the investor network, more specifically, if, and in what form the investors evolve the topology of their network. The relevance of this outcome is that the topology of investor networks has been found to affect the behavior of the market materially [35]. The first stage of the analysis (Section 3.2.2.(1)) presents an assessment of the system's response to the conduct of the risky asset's price and the dynamic variables driving it. The second component

Table 4: Experimental design and result summary.

Model Setting	Key Components	Summary of Findings
Varying network influence (c_1) and short-term investors	The initial network for the investors is a lattice network. The parameters varied in the following manner: (i) network influence (c_1) [1, 2, 3 and 4]; (ii) percentage of short-term investors [0%, 25%, 50%, 75%, 100%]	The introduction of the short-term investors resulted in greater volatility, and the earlier synchronization of investor strategies, meaning the system tipped into bubble territory earlier. Also, bubbles appeared under conditions that did not previously result in a bubble. Of note was that only a small percentage of short-term investors was required to increase the activity in the system.
Varying network influence (c_1), short-term investors, rewiring	As above with the exception that the investor network rewiring occurs in the following increments: (i) [250, 500, 1000, 1500] steps, meaning rewiring occur: [11, 5, 2, 1] times.	The rewiring process resulted in even more significant variations in the behavior of the system. This conclusion comes from previously dormant markets, those that contained only long-term investors, producing volatile behavior; thereby identifying the fact that the presence of Oracles can destabilize the market The wealth distribution was extremely skewed under the conditions responsible for severe price movements, with short-term investors gaining off long-term investors.

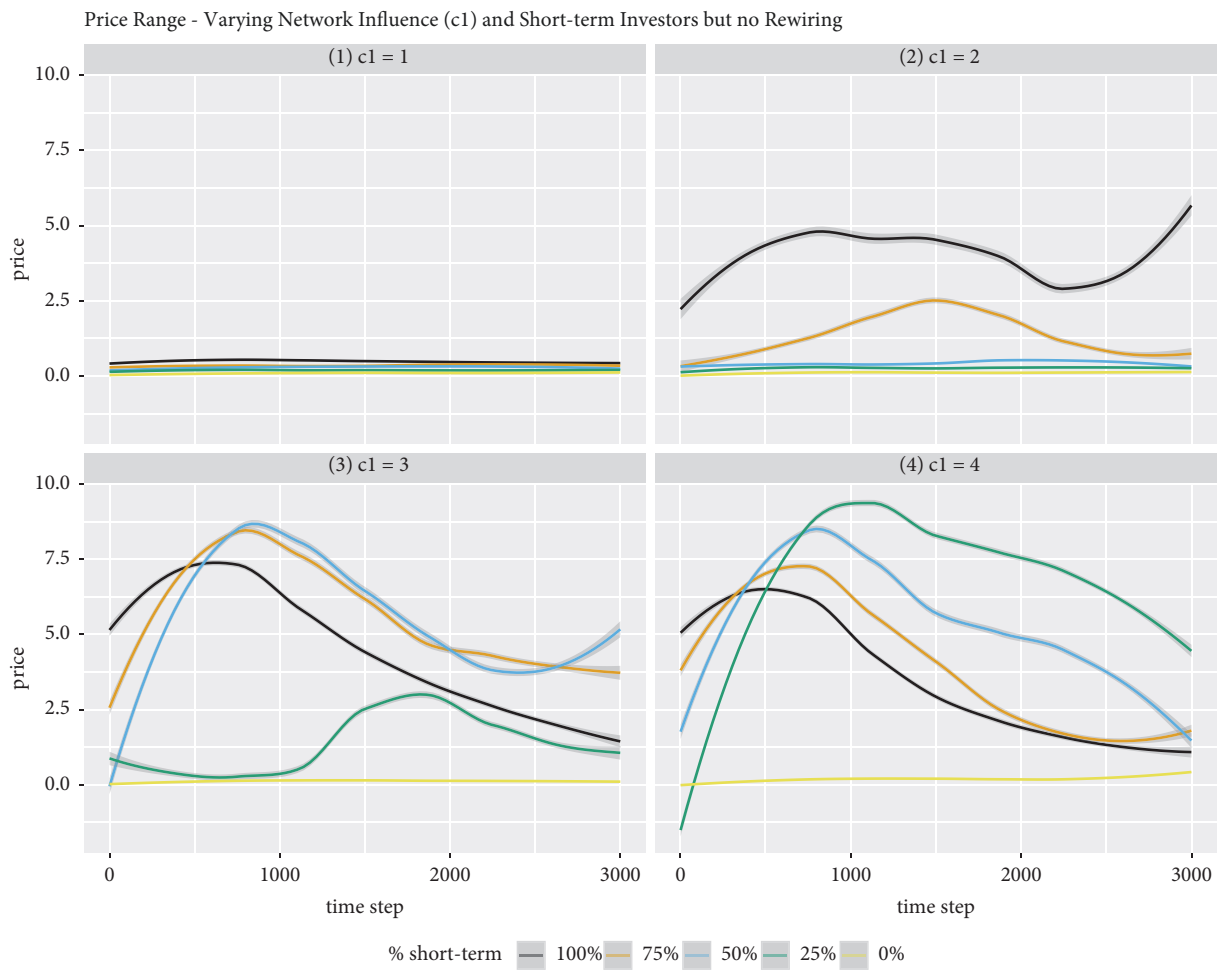

Figure 3: Temporal price behavior of the risky asset with no rewiring. The lines are prepared by applying a LOESS and represent the temporal evolution of the risky asset's price for the various combination of short- and long-term investors.

(Section 3.2.2.(2)) then assesses how investors rearrange themselves in their network.

(1) The Behavior of the Risky Asset's Price. Figure 4, which provides a facet grid of the price behavior of the risky asset, provides sufficient evidence that rewiring does have a positive effect on the price movements of the risky asset. The only condition to this statement is that the initial setting for the network influence parameter is greater than 1. This fact can be seen by the lack of activity in the price series in facets a1 through e1 when compared to the remainder of Figure 4. Therefore, short-termism may well be an irrelevant concern if investors can maintain a balanced perspective regarding where and how they assess the information. However, if investors are inclined to favor the information coming from advisers—seen with a c_1 variable setting higher than 1—and can select their advisers, many implications arise. The first implication is that a previously "nonvolatile" market environment—that is, where extreme price movements do not occur—becomes volatile. Facets a3 through e3 are clear indications of this, with the most obvious example being where there are no short-term investors. Facet e3 shows that with no rewiring and no short-term investors, the price series is dormant. In contrast, the remaining facets record material movements in the price immediately following the rewiring set, noting that the LOESS smoothing will spread the action before and after the actual rewiring step. More generally, when comparing the facets in column e to those of a through d, the effect that the rewire interval has on bringing forward the upward trajectory of the risky asset's price is evident.

Figure 5 provides a more specific illustration of the risky asset's price movement characteristics by illustrating the maximum draw-down and -up metrics. The draw-down (up) is calculated as the value of each consecutive uninterrupted downward (upward) streak of price reductions (increases) and represents the potential gains (losses) an investor can experience. The maximum is then the longest upward and downward streak. The advantage of these metrics is that the number of time steps in the simulation does not influence the magnitudes of these variables as they represent a specific subset of the data: that is, an uninterrupted streak of a price movement. Figure 5 plots the median maximum draw-down or -up with the standard deviation illustrated by the bars.

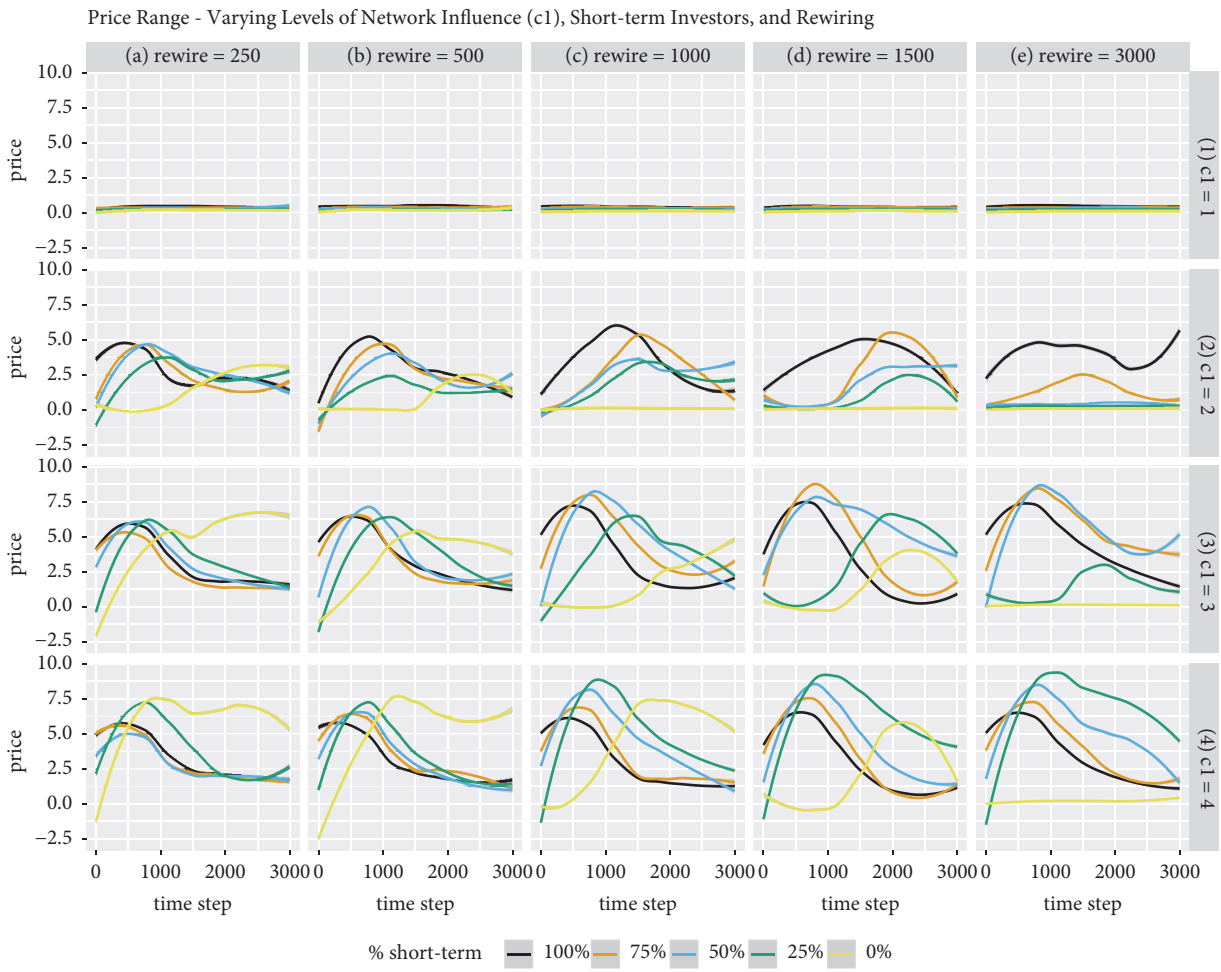

FIGURE 4: Temporal behavior of the risky asset's price with rewiring introduced. Facets now differentiate for the rewire and c_1 variables. The lines are prepared by applying a LOESS and represent the progression of the asset's price for the various combination of short- and long-term investors.

Consistent with the other findings, the rewiring interval and the network influence have a noticeable effect. This point can be seen with the points "jawing" open; that is, the gap between the maximum draw-down and -up increases as the interval decreases, with a scenario of no short-term investors being the anchor point. However, given the muted activity in facet 1, the results show that a higher initial level of network influence is required to instigate the positive feedback loop that results in the more extreme price movements.

The combined effects on the draw-down or -up variable of a shorter rewiring interval and a higher proportion of short-term investors are seen in facet rows 3 and 4. The first observation is that the jaws open farther, including some instances with no short-term investors experiencing material drawdowns and drawups (for example, facet a4 and b4), thus supporting the concept that even long-term investors can herd when given the ability to change advisers. The second observation is that jaws open in a linear fashion in facet row 3, while in facet row 4 the width of jaws is constant, except for when the rewiring process does not occur. This finding implies that the inclination of investors following neighbors, given by the c_1 variable, has a more significant effect than do the rewiring intervals.

Figure 6 provides an insight into how herding, instigated across the investor network, affects the pricing behavior of a risky asset. The herding coefficient—the proportion of the population undertaking the most common trading activity, thus excluding holding—captures both the inflation and deflation of an asset bubble. The main observation regarding the herding coefficient is that the collective behavior grows in the early stages of the simulation, peaks and then decline for the remainder of the simulation, thus mirroring the stages of an asset bubble. The mechanism that explains this process is that the positive feedback loop grows in influence as investors herd, before losing momentum as investors exhaust their investable funds. As the price momentum slows, investors begin to lose trust in their advisers, which eventually leads to some investors starting to leave the buying herd and decrease their holding in the risky asset. This dynamic ultimately creates a selling herd, thus extending the collective behavior, before the loss of any synchronized behavior in the population.

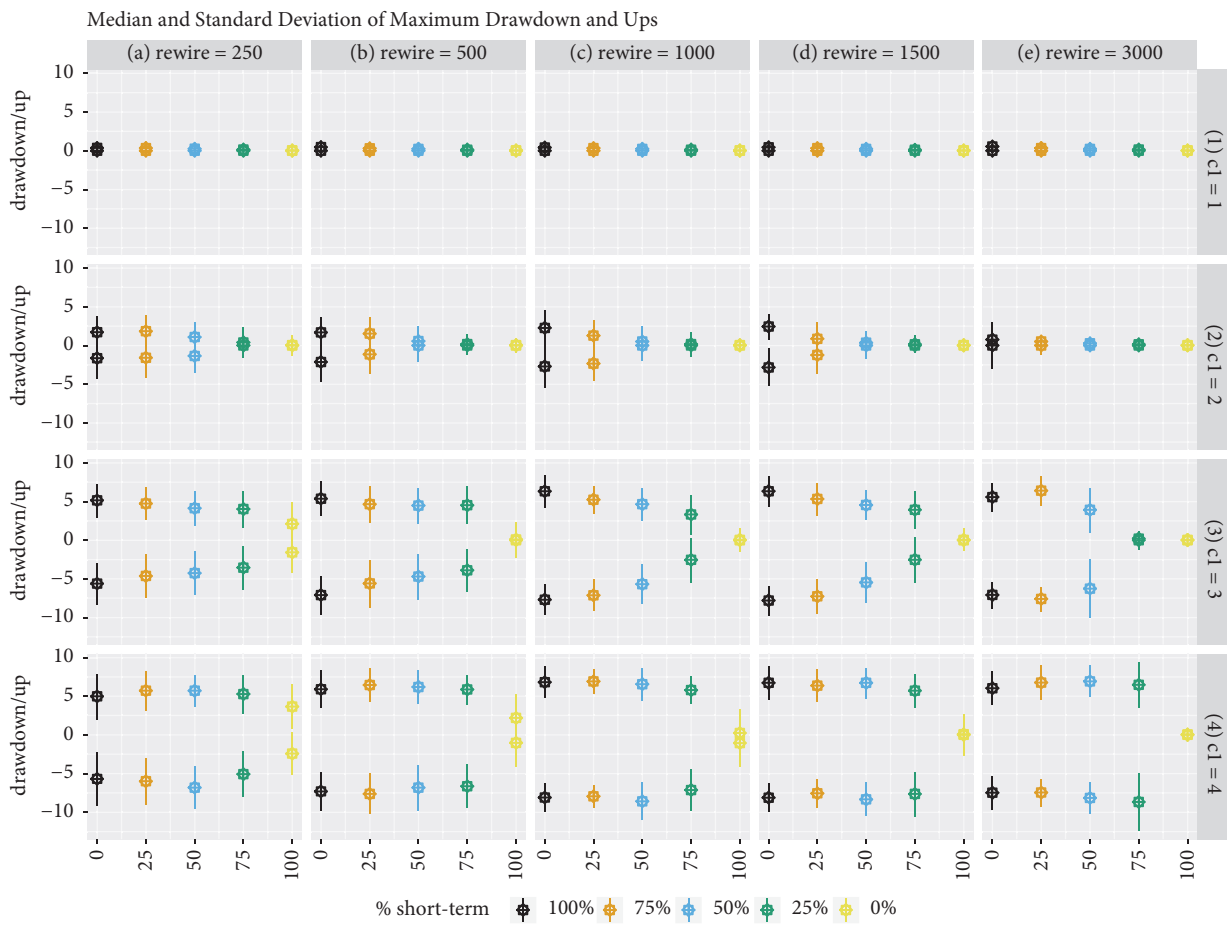

Figure 5: The maximum drawdowns and drawups recorded in the market across the various settings with rewiring. The boxes represent the median, while the lines represent the upper and lower maximums recorded for each combination.

Multiple implications arise from the analysis of how the interaction of investors of varying characteristics affects the behavior of the artificial stock market. The first is that a higher proportion of short-term investors will increase the volatility of the market because these investors are more reactionary and built trust in their advisers at an enhanced rate. The second is that by allowing investors to choose from whom they receive information hastens the building of trust and ultimately accelerates the realization of extreme price movements. The size and timing of these movements are also affected by the investors' preference for following advisers (the network influence variable). If investors do not prefer any information source, that is, $c_1 = c_2 = c_3 = 1$, these interactions become irrelevant.

(2) The Behavior of the Investor Network. This section establishes how the characteristics of the investors and the environment affect the evolution of the investor network topology. Ozsoylev and Walden [25] propose a theory regarding the importance of the topology of the network by explaining that markets would record higher volatility when there was an intermediate level of connectedness between investors, yet lower in markets with higher or lower connectedness. Therefore, if investors form a scale-free network, the volatility of the market should be higher. The rationale for this dynamic is straightforward, in that many investors would tend to follow the decisions of a few Oracles, resulting in a higher prevalence of herding and more substantial price changes.

A vital component in assessing the evolution of the network topology is the investment performance of the investors because as detailed in Section 2.2.1, it is essential to the rewiring process. Figure 11 splits the short and long-term investor results and represents the evolution of the median number of outperformers within each subclass. An observation is that long-term investors have difficulty outperforming over the entirety of the simulation, despite having some success in the early portion of the simulation. Additionally, a higher proportion of short-term investors accentuates the poor performance of long-term investors. The rationale for these points is that the short-term investors are early to join(leave) a significant price upswing(downswing) and first to exit(join) the downward(upward) correction. The opposite holds for long-term investors, who are "left without a chair when the music stops." These results imply that long-term investors will be less inclined to utilize their information network.

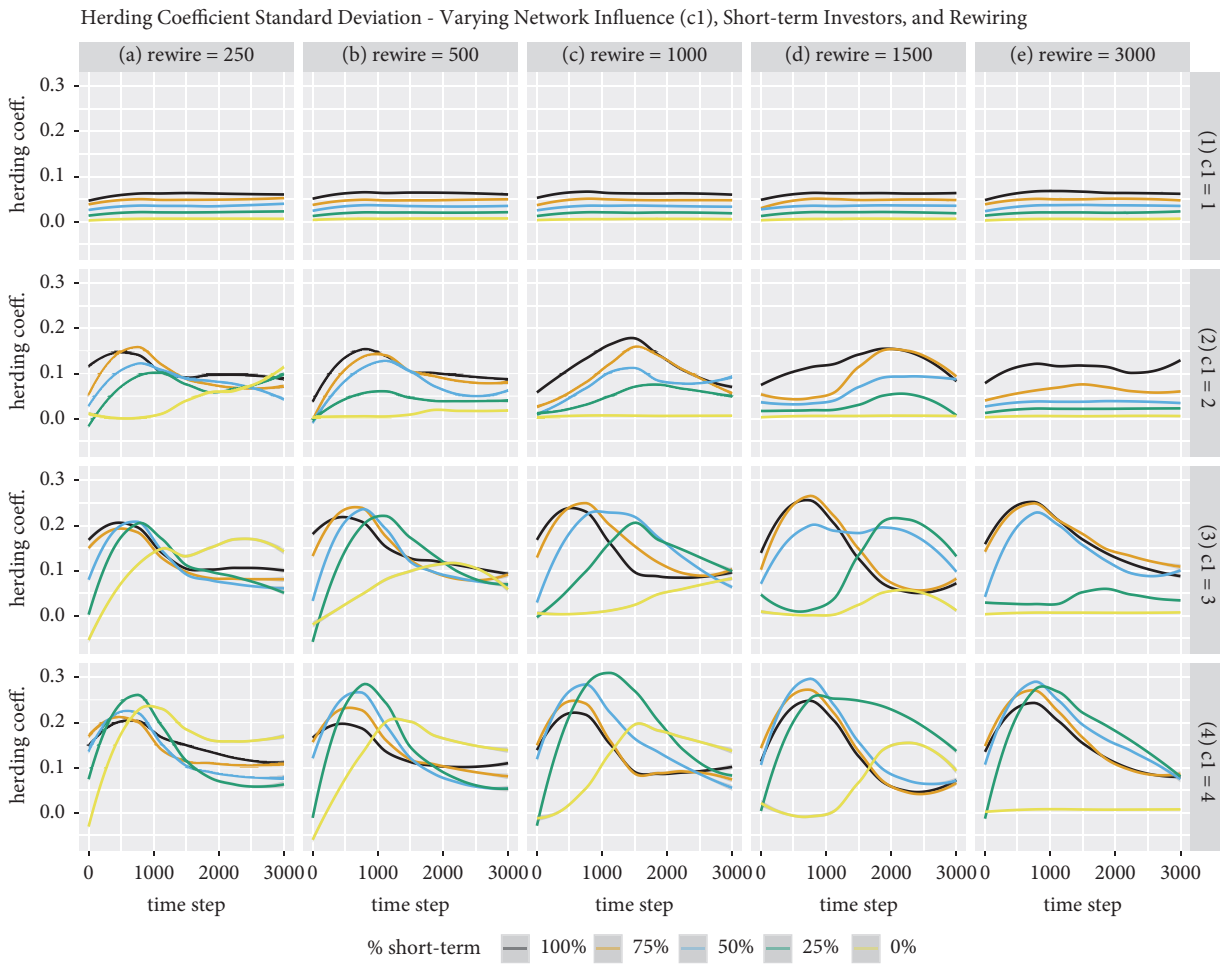

FIGURE 6: The evolution of the herding coefficient with rewiring. The lines come from applying a LOESS process to the standard deviation of the herding coefficient determined at each step from the runs of a specific experimental setting.

The short-term investors, in general, appear better equipped to match or exceed their benchmark. Crucially, the ability to match or exceed the market appears dependent on shorter intervals between reassessing and selecting advisers and the proportion of long-term investors. The implication from this observation is that without long-term investors to "feast" off, short-term investors struggle to outperform. They can correct this situation by rewiring their investor network, a process which may involve ignoring the advice from other investors. These results all provide strong support for the need to assess a market ecosystem.

Figure 7 illustrates the evolution of the median number of links in the network. The rationale for assessing the number of links is that it provides evidence of whether investors, on average, are inclined to add or reduce the number of advisers, remembering that this process is highly dependent on their investment performance. More links are indicative of a denser network, with investors on average utilizing a higher number of advisers and having higher trust in their network information. The first general observation is that the number of links declines through time. A notable exception is when there are no short-term investors (see facet row 1 and 2). A decline in links occurs because investors cut and do not replace advisers because their aggregate level of trust in their advisers becomes negative and they are underperforming the market. The second observation is that the rate of decline becomes progressively faster the higher the proportion of short-term investors. This finding is in step with higher and more volatile prices associated with an increased percentage of short-term investors.

The question arising from Figure 7 is: which investor class is disregarding the information available from their neighbors and thereby, causing the collapse of the network? Why this occurs comes from an assessment of the distribution of out-degree of the investors that is the number of advisers an investor utilizes and the performance of the investor subclasses. The rationale for this analysis is that it will provide evidence for the conditions responsible for investors having a higher inclination, or otherwise, for seeking advice. Investors increase their number of advisers when they are outperforming the market and have positive trust in the network information and cut advisers when they have negative trust in their network information and underperform.

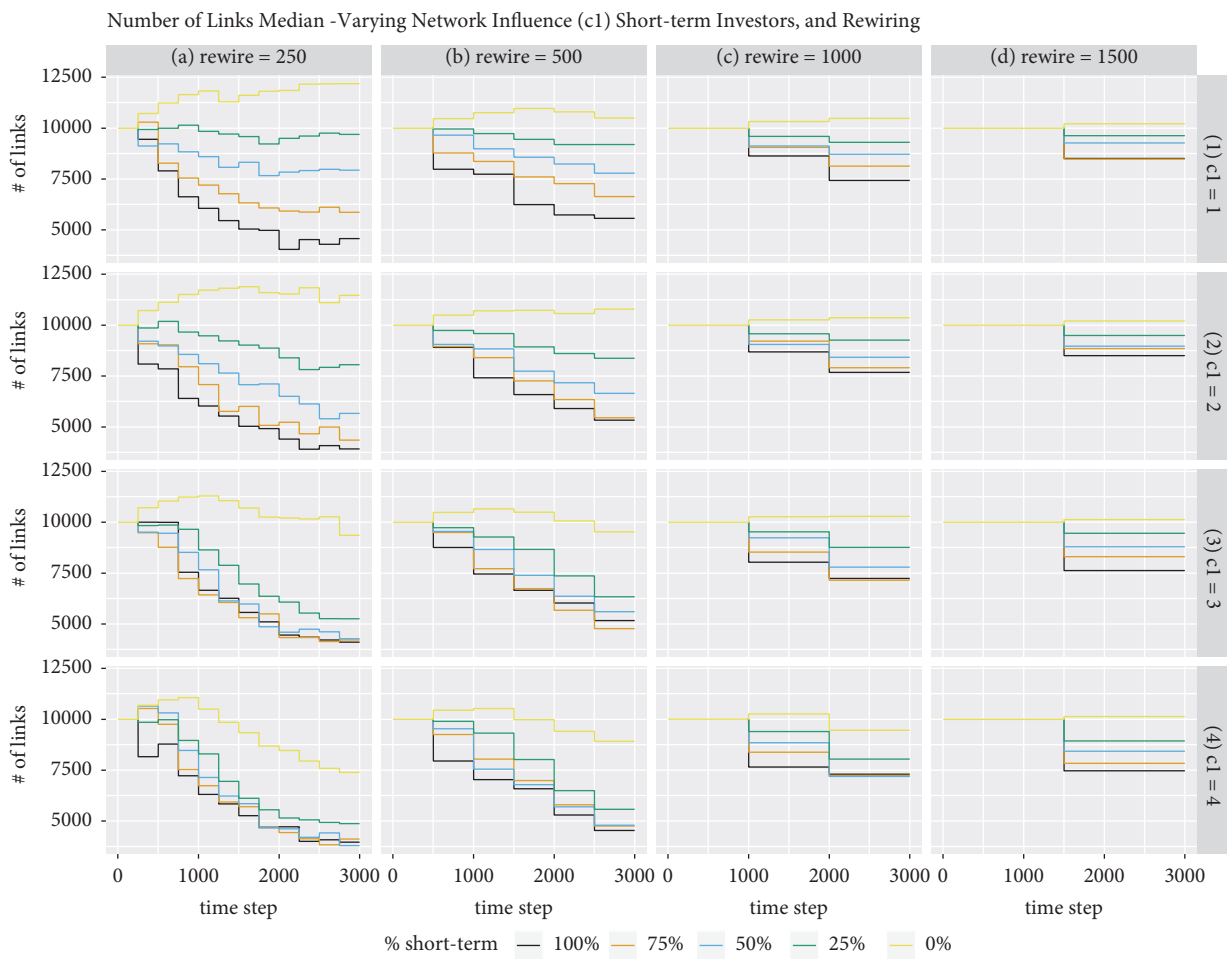

Figure 7: Temporal evolution of the variation in the median number of links maintained in the network after rewiring. Rewiring occurs at discrete steps; hence, the "jagged" appearance in the evolution of the metric. A higher frequency of rewiring is responsible for impairing the network.

Figure 8 shows the dynamics of the median out-degree of the various investor classes. The dynamics appear to strongly parallel those that were evident when assessing the pricing dynamic. The central dynamic is that when long-term investors are forced to compete in an environment rich with short-term investors, they suffer poor performance. This outcome, in turn, leads to an accelerated loss of trust and a more significant decline in the number of advisers they maintain. A critical condition for this process, as seen in facet rows 2ii through 4ii, is that the level of network influence must be higher than 1, a setting that has proven to generate excess price volatility. Otherwise, long-term investors are capable of outperforming under the right conditions, namely when there is a higher proportion of long-term investors. Under these conditions, long-term investors are less inclined to reduce advisers and are even inclined on average to add them.

Alternatively, short-term investors appear generally less inclined to disregard advisers, with the composition of the investor population being less influential. An important observation is that when there is a less volatile environment, that is, when the network influence variable equals 1, short-term investors generally do not perform as well and tend to reduce their adviser numbers (see facet a1i). This finding compounds the evidence that the behavior of the market and the ability of certain classes of investors to outperform is highly conditional on the composition of the investor ecosystem and inclinations that influence their investment decisions.

It is also vital to understand how the rewiring process creates perpetual Oracles, that is, advisers who retain a disproportionate number of followers. Figure 9 explores this aspect by illustrating the median and the upper and lower range for the number of followers for each investor, which are the investors in-links, and represents how many people are seeking advice from a given investor. The expectation is due to the processes involved with investors seeking Oracles the distribution will be highly skewed. However, it is imperative to understand to what extent the distribution is skewed, because investors only search for Oracles under certain circumstances, as defined in Table 2, and may not retain their faith in their Oracles.

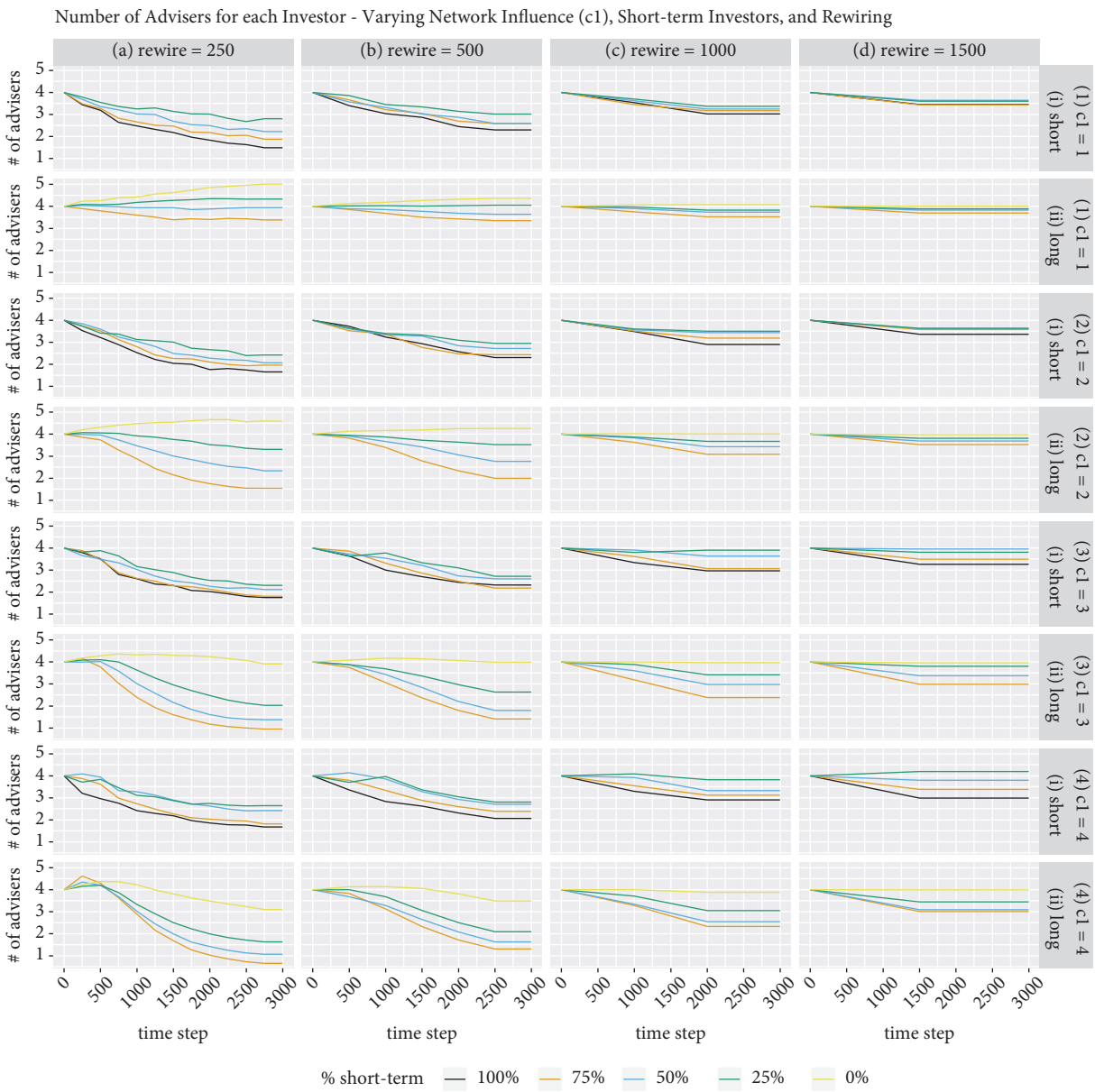

Figure 8: The development of the median number of advisers the investor population maintains. The investor subclasses split the facets and along with the other settings highlight the different behavior of the two classes, with the lines representing the median.

The immediate impression from Figure 9 is, as expected, evidence of a highly skewed distribution. More critically, meaningful differences across the various settings appear. From facet column a, the first difference of note appears with the skewness increasing as the proportion of short-term investors decreases. The other point from facet column a is that when comparing facet a4 to the others, it appears that the upper range peaks before declining in the latter portion of the simulation. Noting the similar extreme price characteristic for facet a4 and the ability of investors to rewire on a more regular basis, this suggests that investors tend to lose faith in taking advice from other investors.

The next question relates to how to classify the evolved network topology. Given the rewiring process, namely, the ability to select Oracles, it was expected that the model would evolve into a scale-free network. This finding would be consistent with Tedeschi et al. [31]. Alternatively, the network may be unable to maintain its structure; that is, it will match a random network with little structure as the volatility of the market will result in investors losing faith in the information coming from their network. The difference in the two processes would see the scale-free network maintain an intermediate level of clustering and a highly skewed in-degree as investors connect to Oracles, while the random network would have a low level of clustering as investors either do not connect or Oracles consistently change. From Figures 7 through 9, plus an analysis of the clustering and closeness coefficients (not provided) implies that the proportion of

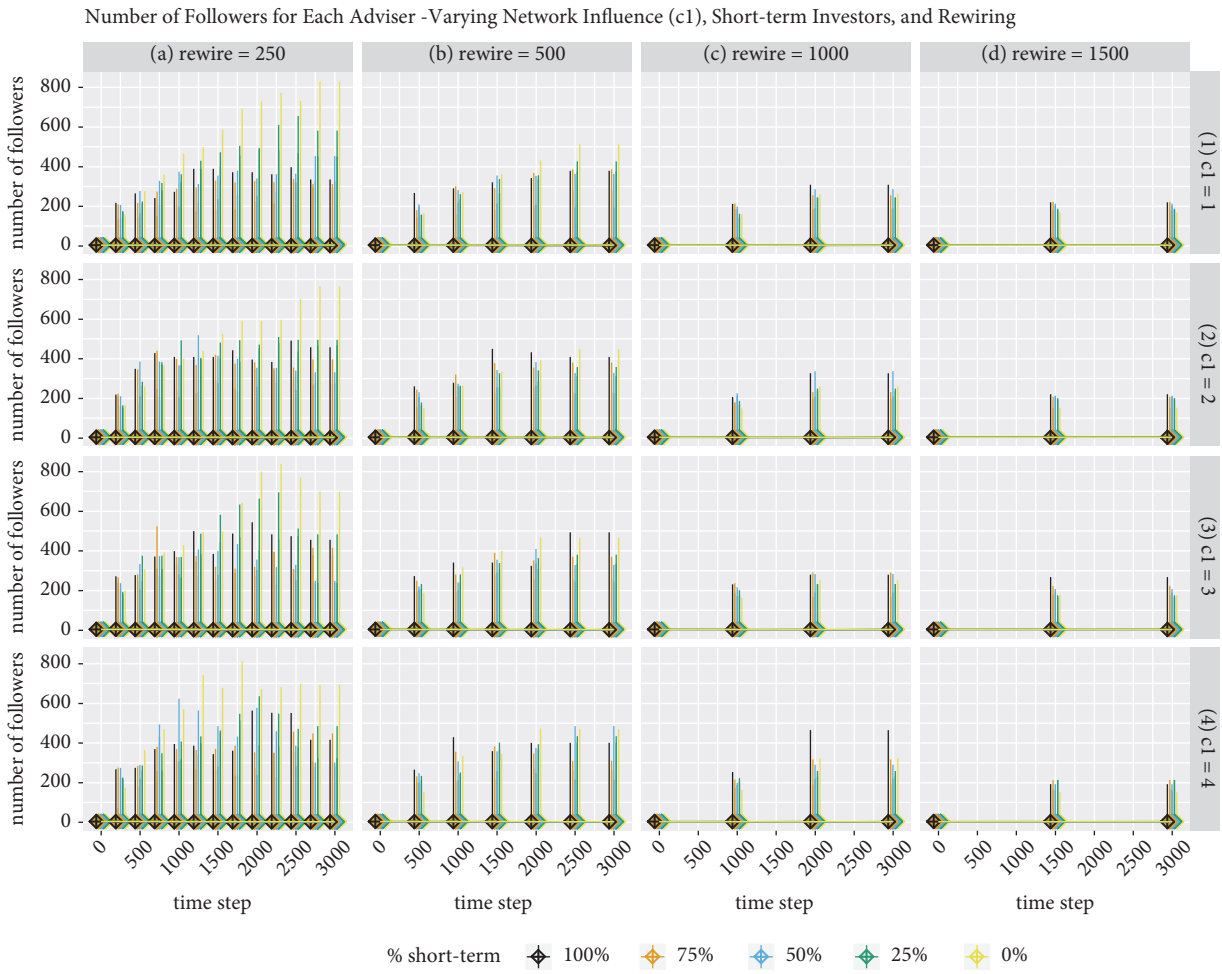

Figure 9: The dynamics for changes in the range of followers per adviser. The lines represent the range while the circles represent the median, noting that the data collection occurs after each rewiring process.

short-term investors in the ecosystem meaningfully affects the topology. That is, the investor network ranges between a scale-free network when there is a lower proportion of short-term investors (and therefore less volatility), to a random network when there is a higher proportion of short-term investors (and hence more volatility). The result implies that in a more volatile market Oracles themselves have trouble maintaining their status, and investors tend to disregard the actions of other investors and focus on public and private information.

(3) The Hunt for Oracles. The previous sections identified the factors that influenced the behavior of the system and how that affected the various investor classes. The findings made it very clear that investors need to be aware of the environment they are engaged in because the system behaves in significantly different ways. Investors need to be particularly mindful of whether short- or long-term investors hold sway in the market and whether investors are predisposed to seek advice from other investors. This section uncovers the attributes of the more successful investors, thus identifying the secrets of investment Oracles.

Figure 10 presents the median portfolio value of the investors and the range of the various portfolio values at each rewiring stage. Therefore, the graph does not capture any wealth that may accumulate and then disappear within a rewiring interval, which would occur as asset bubbles can come and go within a rewiring interval. The most striking result occurs in facet aii4, where the relevant parameters see an asset bubble appear, with the instigation of the boom brought forward by the network rewiring process. What is striking is the extreme skewness in the wealth distribution when the ecosystem is comprised entirely of long-term investors. The extreme result occurs because a given investor starts the positive feedback loop, most likely because the investor has a relatively low threshold, and as more investors follow that investor's action the bubble inflates, and long-term investors build higher and sustainable trust in the original Oracle. The investor is then the first to leave the buying herd while the other long-term investors slowly adjust and start selling well after the original Oracle, thus providing the Oracle ample opportunity to sell at the top of the market. Therefore, the original Oracle achieves the perfect combination of buying low and selling high. This relationship

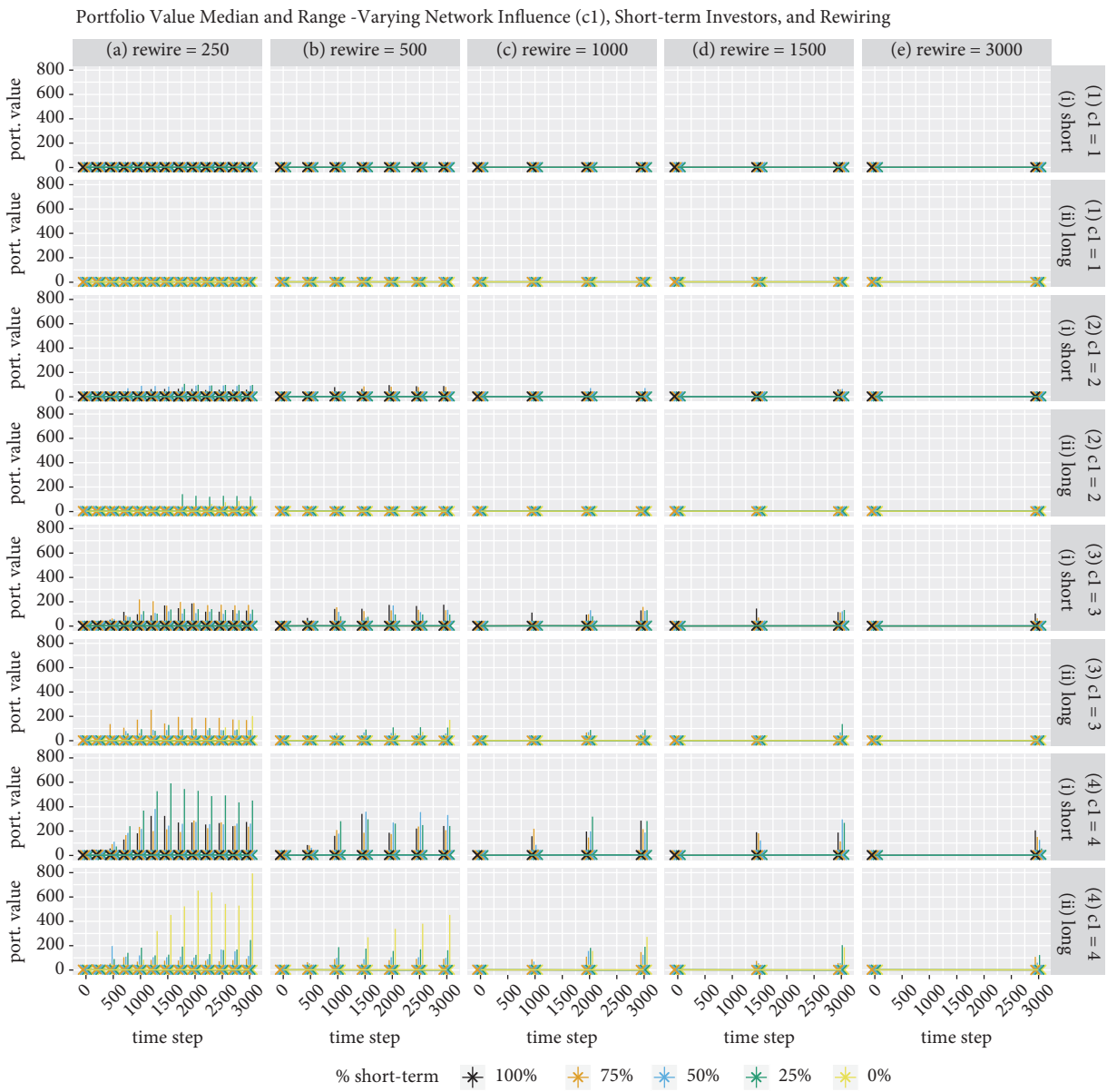

Figure 10: The dynamics of wealth creation. The plot summarizes the distribution of wealth (the agent's portfolio value), per the y-axis, labelled port. value. The vertical lines represent the range of wealth, while the stars represent the median. The range updating occurs after each rewiring step.

is most pronounced with shorter rewiring intervals but does hold with longer intervals.

The previously identified situation of short-term investors gaining wealth at the expense of long-term investors is also evident. Again, in the lower facet rows, the outperformance of at least one short-term investor over the highest performing long-term investor is clear. The gap also increases as the percentage of short-term investor decreases, which is indicative of the advantage short-term investors have in being able to adjust more quickly to the market. The final point of note is that material inequality only occurs when the network influence variable is greater than 2. Under this scenario, it is again short-term investors interacting with a more substantial proportion of long-term investors that produces the outcome.

A principal component analysis (PCA) was conducted on the agent level data to identify the primary influence on wealth creation. The first component showed the significant effect of the dynamics of the network, with the rewire setting making the highest contribution to explaining wealth variation. This result was anticipated given the finding that by allowing agents to rewire affects the dynamics of the market. This dynamic was seen in Figure 4, where decreasing the rewiring interval increased the activity of the system, ceteris paribus. The second component identified the investment decision-making process of the investors, especially their

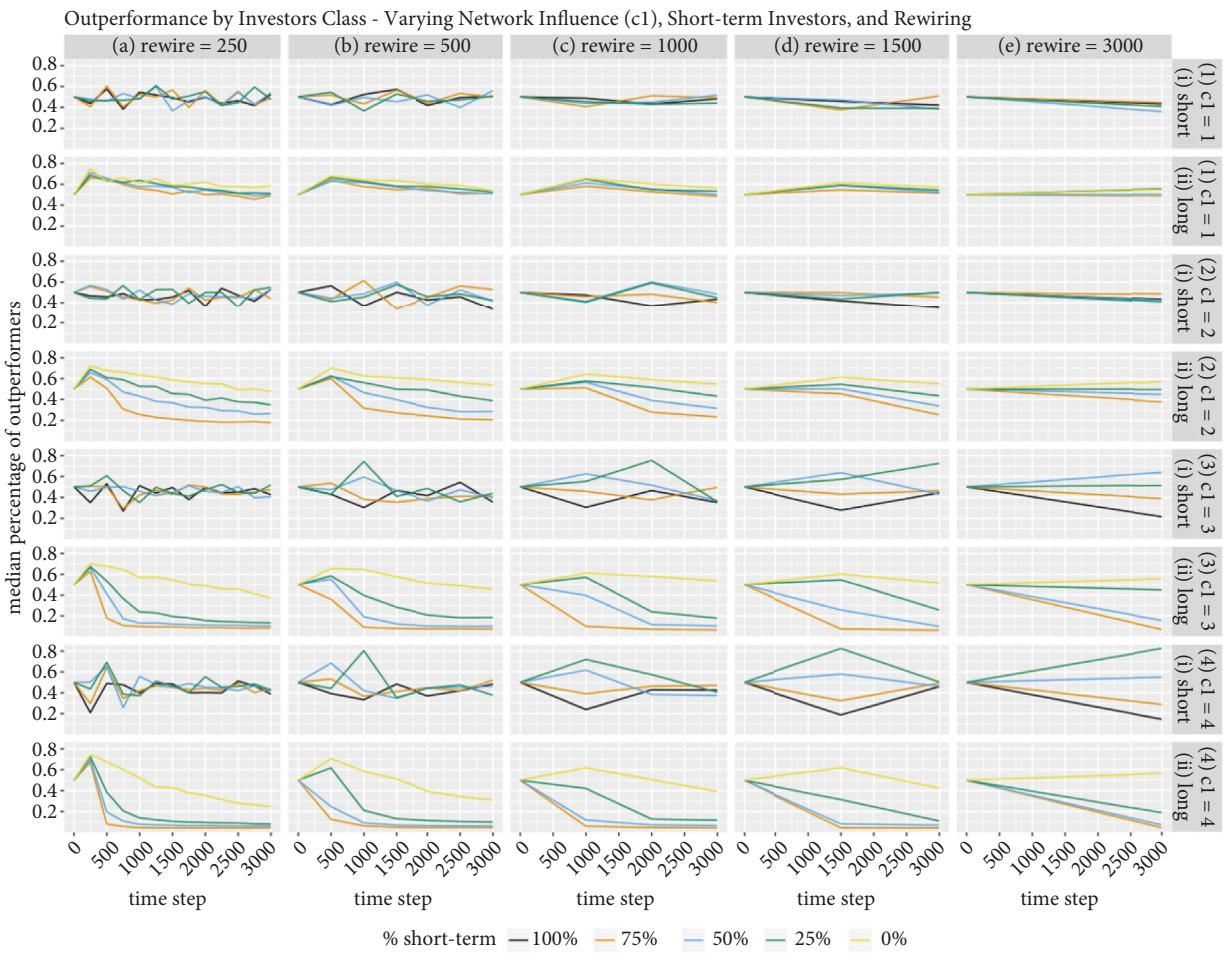

Figure 11: Proportion of outperformers within each investor subclass. Facets now differentiate for the rewiring and c_1 variables and the investor subclasses. The lines represent the temporal evolution of the proportion of outperformers for the various combination of short- and long-term investors. Short-term investors appear to exhibit superior performance.

decision threshold (with a lower threshold being beneficial) and the structure of the population, thereby confirming the previously inferred importance of the investment horizon of investors and the composition of the ecosystem.

4. Discussion

This paper combined research from a variety of fields including agent-based artificial stock markets ([13, 22, 37]), behavioral finance ([11, 49, 50]), evolving social networks ([31, 51]), and empirical research into investor networks ([25, 26, 52]) and financial markets ([17, 53]). By successfully combining these fields the paper delivers meaningful insights into the dynamics responsible for enhanced volatility in financial markets, divergent wealth accumulation by investors, and the detrimental effects of short-term behavior. In addressing these topics, the model added to the developing research of how investor network may evolve, and the effects that the network's evolution has on the behavior of the market. Regarding the detrimental consequence of short-termism, the model demonstrated how short-term traders benefit by exploiting long-term investors, who take longer to adjust to the changing market conditions. However, this trait is only relevant when investors disregard their other information sources and blindly follow the herd, an environment that generates higher volatility. Under such conditions, investors should be more reactive, a result consistent with LeBaron [13]. In contrast, when markets do not experience excessive price movements, short-term investors trade excessively in the futile attempt to find nonexistent profits, a result in line with the work of Barber and Odean [11].

The benefit of pursuing a greater understanding of how a social network, of any description, evolves was demonstrated through the model identifying the conditions under which the investors tended to form and maintain a network of intermediate connectedness. Understanding this process was vital based on the empirical results suggesting that an investor network of intermediate connectedness produces higher volatility ([25, 26]) and scale-free topologies are associated with fragile markets ([28, 54]). An agent-based modeling approach was appropriate for this purpose because it can simulate the effects of heterogeneous interacting agents within a CAS,

thereby uncovering the mechanisms responsible for not only scale-free networks but also extreme market behavior [55]. More specifically this paper uncovered the process by which a benign environment becomes volatile as investors rewire their adviser network. Critically, rewiring at more regular intervals accelerates the arrival of the elevated volatility. The findings also suggest that a higher prevalence of short-term investors, which ceteris paribus produces higher volatility, was responsible for the network becoming relatively unstable as long-term investors disengaged from their advisers.

While this paper provides meaningful insights, it should be considered an interim step in the pursuit of gaining a greater understanding of investors and how their social interaction affects financial markets. To enhance the model's usefulness, the model should look to enhance the decision-making process of the investors, reduce the general level of abstractions, and improve the use of empirical data to inform and calibrate the model. Regarding the investors, a possible enhancement would be to allow the investors to learn (a significant benefit of ABMs [56]) and therefore recognize the conditions that feed the positive feedback loop and adjust their investment approach. Concerning the abstractions, the processes by which investors identify and follow Oracles and modify trust levels are areas of realistic improvements. While allowing investors to search the entire population to identify the leading investors is feasible given the availability of past performance data over more extended periods, the search could be adjusted to allow some agents to obtain time-sensitive trading and investment data. Regarding quantifying investor trust, Gruber [57] and Sirri & Tufano [58] established that the flow into and out of mutual funds is highly dependent on manager performance; thus, flows provide an ex-post proxy of trust. Additionally, the recommendations of stock analysts have been found to influence stock prices positively [59], thereby providing possible insight into what is required for investors to build (and lose) trust in their Oracles.

Efforts to better inform the model with real-world network and trading behavior data are essential. While there has been promising work in the area (see [26, 52]), capturing sufficiently detailed data in a time-sensitive manner remains a challenging pursuit. A crucial issue relates to the confidentiality requirements of investors. Therefore, advances in this area of research will only come from specific companies undertaking assessments of their share registry or making that data available [52]. The benefit of conducting this analysis is that firms would gain a greater appreciation of who their owners are (especially short-term versus long-term investors), thereby improving their ability to interpret signals from the market. Alternatively, share registry services and custodians maintain the necessary shareholder data but accessing this data is extremely difficult due to privacy issues and the need for investors to protect their intellectual property.

5. Conclusion

By leveraging the advantages of agent-based modeling, this paper produces important insights into how investors can prosper and identifies tell-tale signs that policymakers should consider if they aim to reduce market volatility. For investors, they must be vigilant to the environment in which they find themselves, and if there is an overabundance of short-term investors, they can either try and remain just ahead of the market, something many have tried and failed, or, as proposed by the likes of Warren Buffett, find a sustainable investment strategy and stick to it. This finding correlates with Lo's [9] Adaptive Market Hypothesis, which suggests that subgroups of investors can survive and prosper in the market and, more important, can influence the market, even though their strategy is not optimal over the long-term. Without the implementation of a bottom-up modeling process, this insight could not be achieved.

For policymakers, the principal consideration is the appearance of a negative externality in that it may be optimal for any one investor to rewire an information network. However, when the entire population does so, it leads to a homogeneous investment approach appearing, with predictable excessive price movements resulting. Critically, the relevance of the investor network is not consistent, as the results indicated that, in more volatile environments, investors tended to disregard following their advisers. The rise of passive investing in the real world is a comparable phenomenon to these implications; that is, in the aftermath of the Global Financial Crisis (GFC), investors lost faith in active management and were prepared to sacrifice upside gains for the benefit of lower risk and matching the market. It is also apparent that researcher focuses their efforts on understanding how investors form and evolve their information needs, a process that is reliant on simulation to provide the initial insights.

The last conclusion to be drawn from this paper is the pressing need to access detailed empirical data. However, data alone will not provide all the necessary answers as it is essential to identify why data forms in a given way, which in turn allows practitioners to determine if and why a step-change will occur and what effects it may produce and assess whether the economy is moving toward a dangerous state. Therefore, researchers utilizing ABMs must continue to balance the need to integrate more data while also demonstrating their primary advantage of being capable of considering a richer set of specifications, which allows for the assessment of complex phenomena [60]. A practical solution is for those using ABMs to accelerate the process of incorporating data into their modeling process and deliver outputs that can be verified against stylized facts, thereby providing more holistic solutions.

Appendix

See Figure 11.

Data Availability

The CSV file and R scripts used to support the findings of this study are available from the corresponding author upon request. Additionally, the model, with the experiments preloaded, can be found at http://tidy.ws/28jdyT.

Disclosure

No specific funding was allocated to the production of this paper. However, the generous support of George Mason University (GMU), via their Presidential Scholarship, facilitated the production of this paper.

Conflicts of Interest

The author declares that there are no conflicts of interest regarding the publication of this paper.

Acknowledgments

I would also like to thank George Mason University for providing funding to me through the Presidential Scholarship program and my dissertation committee members, including Prof. Rob Axtell, Dr. Rick Bookstaber, Prof. Andrew Crooks, and Prof. Eduardo Lopez, for providing their insights and guidance in the preparation of this paper.

References

[1] P. A. Samuelson, "Proof that properly anticipated prices fluctuate randomly," *Industrial Management Review*, vol. 6, no. 2, pp. 25–38, 1965.

[2] M. F. M. Osborne, "Brownian motion in the stock market," *Operations Research*, vol. 7, no. 2, pp. 145–173, 1959.

[3] E. F. Fama, "Efficient capital markets: a review of theory and empirical work," *The Journal of Finance*, vol. 25, no. 2, p. 383, 1970.

[4] A. Kirou, B. Ruszczycki, M. Walser, and N. F. Johnson, "Computational modeling of collective human behavior: the example of financial markets," in *Computational Science – ICCS 2008*, vol. 5101 of *Lecture Notes in Computer Science*, pp. 33–41, Springer Berlin Heidelberg, Berlin, Heidelberg, 2008.

[5] N. Barberis and R. Thaler, *A Survey of Behavioral Finance*, National Bureau of Economic Research, Cambridge, MA, USA, 2002.

[6] K. Cuthbertson, D. Nitzsche, and N. O'Sullivan, "UK mutual fund performance: skill or luck?" *Journal of Empirical Finance*, vol. 15, no. 4, pp. 613–634, 2008.

[7] B. G. Malkiel, *A Random Walk Down Wall Street: Including a Life-cycle Guide to Personal Investing*, WW Norton & Company, New York, NY, USA, 1999.

[8] M. M. Carhart, "On persistence in mutual fund performance," *Journal of Finance*, vol. 52, no. 1, pp. 57–82, 1997.

[9] A. W. Lo, *Adaptive Markets: Financial Evolution at the Speed of Thought*, Princeton University Press, Princeton, NJ, USA, 2017.

[10] J. O. Weatherall, *The Physics of Wall Street: A Brief History of Predicting the Unpredictable*, Mariner Books, Boston, MA, 2014.

[11] B. M. Barber and T. Odean, "Trading is hazardous to your wealth: the common stock investment performance of individual investors," *Journal of Finance*, vol. 55, no. 2, pp. 773–806, 2000.

[12] J. Kay, *The Kay Review of Equity Markets and Long-term Decision Making*, 2012.

[13] B. LeBaron, "Heterogeneous gain learning and long swings in asset prices," in *Rethinking Expectations: The Way Forward for Macroeconomics*, pp. 169–206, Princeton University Press, Princeton, NJ, USA, 2013.

[14] N. Kaldor, "Capital accumulation and economic growth," in *The Theory of Capital*, F. A. Lutz and D. C. Hague, Eds., pp. 177–222, Macmillan, London, UK, 1961.

[15] B.-O. Heine, M. Meyer, and O. Strangfled, "Stylised facts and the contribution of simulation to the economic analysis of budgeting," *Journal of Artificial Societies and Social Simulation*, vol. 8, no. 4, 2005.

[16] R. Cont, "Volatility clustering in financial markets: empirical facts and agent-based models," in *Long Memory in Economics*, pp. 289–309, Springer, Berlin, Germany, 2007.

[17] N. F. Johnson, P. Jefferies, and P. M. Hui, *Financial Market Complexity*, Oxford University Press, New York, NY, USA, 2003.

[18] F. Botta, H. S. Moat, H. E. Stanley, T. Preis, and Y. Chen, "Quantifying stock return distributions in financial markets," *PLoS ONE*, vol. 10, no. 9, Article ID e0135600, 2015.

[19] J. D. Farmer, M. Gallegati, C. Hommes et al., "A complex systems approach to constructing better models for managing financial markets and the economy," *The European Physical Journal C*, vol. 214, no. 1, pp. 295–324, 2012.

[20] D. Sornette, *Why Stock Markets Crash: Critical Events in Complex Financial Systems*, Princeton University Press, Princeton, NJ, USA, Princeton science library edition edition, 2017.

[21] S. Begušić, Z. Kostanjčar, D. Kovač, H. E. Stanley, and B. Podobnik, "Information feedback in temporal networks as a predictor of market crashes," *Complexity*, vol. 2018, Article ID 2834680, 13 pages, 2018.

[22] V. Panchenko, S. Gerasymchuk, and O. V. Pavlov, "Asset price dynamics with heterogeneous beliefs and local network interactions," *Journal of Economic Dynamics and Control (JEDC)*, vol. 37, no. 12, pp. 2623–2642, 2013.

[23] M. Oldham, "Market fluctuations explained by dividends and investor networks," *Advances in Complex Systems (ACS)*, vol. 20, no. 8, Article ID 1750007, 2017.

[24] Y. Tang, J. J. Xiong, Z. Jia, and Y. Zhang, "Complexities in financial network topological dynamics: modeling of emerging and developed stock markets," *Complexity*, vol. 2018, Article ID 4680140, 31 pages, 2018.

[25] H. N. Ozsoylev and J. Walden, "Asset pricing in large information networks," *Journal of Economic Theory*, vol. 146, no. 6, pp. 2252–2280, 2011.

[26] H. N. Ozsoylev, J. Walden, M. D. Yavuz, and R. Bildik, "Investor networks in the stock market," *Review of Financial Studies*, vol. 27, no. 5, pp. 1323–1366, 2014.

[27] M. Oldham, "Introducing a multi-asset stock market to test the power of investor networks," *Journal of Artificial Societies and Social Simulation*, vol. 20, no. 4, 2017.

[28] K. Khashanah and T. Alsulaiman, "Connectivity, information jumps, and market stability: an agent-based approach," *Complexity*, vol. 2017, Article ID 6752086, 16 pages, 2017.

[29] J. D. Farmer and D. Foley, "The economy needs agent-based modelling," *Nature*, vol. 460, no. 7256, pp. 685-686, 2009.

[30] J. Epstein, "Why Model?" *Journal of Artificial Societies and Social Simulation*, vol. 11, no. 4, 2008.

[31] G. Tedeschi, G. Iori, and M. Gallegati, "Herding effects in order driven markets: The rise and fall of gurus," *Journal of Economic Behavior & Organization*, vol. 81, no. 1, pp. 82–96, 2012.

[32] L. Tesfatsion and K. L. Judd, Eds., *Handbook of Computational Economics*, Elsevier, Amsterdam Boston, 2006.

[33] D. Sornette, "Physics and financial economics (1776–2014): puzzles, ising and agent-based models," *Reports on Progress in Physics*, vol. 77, no. 6, Article ID 062001, 2014.

[34] S. Alfarano, M. Milakovic, and M. Milaković, "Should network structure matter in agent-based finance?" *Economics Working Papers 2008-04, Christian-Albrechts-University of Kiel, Department of Economics*, 2008.

[35] L. Ponta and S. Cincotti, "Traders' networks of interactions and structural properties of financial markets: an agent-based approach," *Complexity*, vol. 2018, Article ID 9072948, 9 pages, 2018.

[36] A. O. I. Hoffman, W. Jager, and J. H. Von Eije, "Social simulation of stock markets: taking it to the next level," *Journal of Artificial Societies and Social Simulation*, vol. 10, no. 2, p. 7, 2007.

[37] G. Harras and D. Sornette, "How to grow a bubble: a model of myopic adapting agents," *Journal of Economic Behavior & Organization*, vol. 80, no. 1, pp. 137–152, 2011.

[38] R. De Caux, C. Smith, D. Kniveton, R. Black, and A. Philippides, "Dynamic, small-world social network generation through local agent interactions," *Complexity*, vol. 19, no. 6, pp. 44–53, 2014.

[39] S. Markose, A. Alentorn, and A. Krause, "Dynamic Learning, Herding and Guru Effects in Network," Working Paper 582, University of Essex, Economics Department, 2004.

[40] V. Grimm, U. Berger, D. L. DeAngelis, J. G. Polhill, J. Giske, and S. F. Railsback, "The ODD protocol: a review and first update," *Ecological Modelling*, vol. 221, no. 23, pp. 2760–2768, 2010.

[41] U. Wilensky, *Netlogo. Northernwestern University. Evanston, IL: Center for Connected Learning and Computer-Based Modeling*, 1999.

[42] A. Oyedale, "How Warren Buffett's annual Q&A meetings exploded to become a must-go extravaganza for Berkshire Hathaway shareholders around the world, 2018".

[43] O. Gergaud and W. T. Ziemba, "Great investors: their methods, results and evaluation," *SSRN Electronic Journal*, 2012.

[44] D. J. Watts and S. H. Strogatz, "Collective dynamics of 'small-world' networks," *Nature*, vol. 393, no. 6684, pp. 440–442, 1998.

[45] M. Mitchell, "Complex systems: network thinking," *Artificial Intelligence*, vol. 170, no. 18, pp. 1194–1212, 2006.

[46] R. Cont and J. Bouchaud, "Herd behavior and aggregate fluctuations in financial markets," *Macroeconomic Dynamics*, vol. 4, no. 2, pp. 170–196, 2000.

[47] J. D. Farmer, "Market force, ecology and evolution," *Industrial and Corporate Change*, vol. 11, no. 5, pp. 895–953, 2002.

[48] J.-S. Lee et al., "The complexities of agent-based modeling output analysis," *Journal of Artificial Societies and Social Simulation*, vol. 18, no. 4, 2015.

[49] R. J. Shiller, "Conversation, information, and herd behavior," *The American Economic Review*, vol. 85, no. 2, pp. 181–185, 1995.

[50] R. J. Shiller, S. Fischer, and B. M. Friedman, "Stock Prices and Social Dynamics," *Brookings Papers on Economic Activity*, vol. 1984, no. 2, pp. 457–498, 1984.

[51] G. Tedeschi, G. Iori, and M. Gallegati, "The role of communication and imitation in limit order markets," *The European Physical Journal B*, vol. 71, no. 4, pp. 489–497, 2009.

[52] F. Musciotto, L. Marotta, J. Piilo, and R. N. Mantegna, "Long-term ecology of investors in a financial market," *Palgrave Communications*, vol. 4, no. 1, 2018.

[53] R. Cont, "Empirical properties of asset returns: stylized facts and statistical issues," *Quantitative Finance*, vol. 1, no. 2, pp. 223–236, 2001.

[54] G. Caldarelli, S. Battiston, D. Garlaschelli, and M. Catanzaro, "Emergence of complexity in financial networks," in *Complex Networks*, E. Ben-Naim, H. Frauenfelder, and Z. Toroczkai, Eds., vol. 650, pp. 399–423, Springer Berlin Heidelberg, Berlin, Germany, 2004.

[55] D. D. Gatti, C. Di Guilmi, E. Gaffeo, G. Giulioni, M. Gallegati, and A. Palestrini, "A new approach to business fluctuations: Heterogeneous interacting agents, scaling laws and financial fragility," *Journal of Economic Behavior & Organization*, vol. 56, no. 4, pp. 489–512, 2005.

[56] C. M. MacAl and M. J. North, "Tutorial on agent-based modelling and simulation," *Journal of Simulation*, vol. 4, no. 3, pp. 151–162, 2010.

[57] M. J. Gruber, "Another puzzle: the growth in actively managed mutual funds," *Journal of Finance*, vol. 51, no. 3, pp. 783–810, 1996.

[58] E. R. Sirri and P. Tufano, "Costly search and mutual fund flows," *The Journal of Finance*, vol. 53, no. 5, pp. 1589–1622, 1998.

[59] B. Barber, R. Lehavy, M. McNichols, and B. Trueman, "Can investors profit from the prophets? security analyst recommendations and stock returns," *Journal of Finance*, vol. 56, no. 2, pp. 531–563, 2001.

[60] R. Leombruni and M. Richiardi, "Why are economists sceptical about agent-based simulations?" *Physica A: Statistical Mechanics and its Applications*, vol. 355, no. 1, pp. 103–109, 2005.

Hindawi
Complexity
Volume 2019, Article ID 1565698, 20 pages
https://doi.org/10.1155/2019/1565698

Research Article

Modeling Overlapped Mutual Funds' Portfolios: A Bipartite Network Approach

Jaime F. Lavin,[1] **Mauricio A. Valle**,[2] **and Nicolás S. Magner**[2]

[1]*Escuela de Negocios, Universidad Adolfo Ibáñez, Diagonal Las Torres 2640, Peñalolén, Santiago, Postal Code 7941169, Chile*
[2]*Facultad de Economia y Negocios, Universidad Finis Terrae, Pedro de Valdivia 1509, Providencia, Santiago, Postal Code 7501015, Chile*

Correspondence should be addressed to Jaime F. Lavin; jaime.lavin@uai.cl

Received 12 February 2019; Accepted 3 June 2019; Published 1 July 2019

Guest Editor: Benjamin M. Tabak

This paper studies the topology of the Chilean mutual fund industry using networks methods. With the physical positions of the local equity portfolios managed during 2003.01-2017.4, we analyze their connectivity structure in both the mutual funds' bipartite network and their one-mode projection. We estimate network measures to examine the potential effects on the topology arising from changes in the industrial environment and changes in the mutual funds' investment strategies in their overlapped portfolios. Our main results show that changes in the bipartite network and its one-mode projection are correlated with variables related to funds' investment strategies and with industry-specific variables. In consequence, these elements are a new potential of disturbance in the financial network conformed by stocks and mutual funds. We contribute to the existing literature, improving the understanding of the aggregate behavior of a financial sector which despite its economic importance has attracted little attention from a systemic risk perspective.

1. Introduction

This paper studies the topology of networks in the mutual fund industry by analyzing the composition of their investment portfolios. Application of a network analysis makes it possible to identify and analyze the interrelation existing between mutual funds that share investments in similar financial assets, using bipartite networks and its one-mode projection. This phenomenon, called overlapping, is a financial network of assets and funds. Understanding the topology of this network is critical, because the assets that each fund allocates affect its financial performance, as the financial literature indicates, and impact the structure of the industry. Consequently, it influences the stability and propagation of financial contagions, such as *firesales* of assets and runs on mutual funds. As a result, this affects risk and industry development.

During the subprime crisis, investors favored liquid assets (*liquidity hoarding)* and those free of risk (*flight to quality)* at the cost of stocks and bonds, significantly affecting the price of financial assets [1]; stocks and bonds suffered drops in their prices that negatively affected the performance of stockbrokers and fund managers, such as mutual funds, commercial banks, pension funds, and hedge funds. As a result, this behavior is recognized as a contagion for the rest of the financial system [2, 3].

The losses inflicted by the crisis highlighted for policymakers, regulators, and academics the importance of assessing the systemic risk and understanding the propagation mechanisms of financial shocks. The crisis made the complexity, instability, and fragility of the existing network structures in the capital markets a tangible reality [4, 5]. As a result, the financial system, particularly the banking system, garnered the attention of the networks literature to study its structure and how changes to it affect the probability of occurrence and spread of financial contagions.

The financial literature identifies two channels of financial crisis contagion. The first, related to direct exposure between two agents, is produced by bilateral asset transactions or contracts, such as credit operations and credit default swaps [2]. The second, called portfolio overlaps, is linked to indirect exposure generated between two or more investors such as

pension funds, hedge funds, and mutual funds that have exposures in the same financial asset [6]. However, despite the size of these investors in the financial system, the literature pays little attention to the second channel[1]. The present study focuses on studying the complexity of the phenomenon of portfolio overlaps through network analysis.

The study of the phenomenon of systemic risk through overlapping portfolios is novel [4, 7]; however, there is a lack of studies applied to the mutual fund industry, despite its importance and size[2]. Delpini and others [8] analyze the bipartite network of US mutual funds during the financial crisis, studying how the systemic fragility of the system depends on the overlap between portfolios. Their results indicate that diversification and similarity in financial investment strategies are factors that increase distress propagation and systemic fragility. The authors confirm that diversification increases systemic risk when the funds use the same investment strategies and diversify using similar assets.

The relation between diversification and systemic risk is important due to the effect of both factors on investment portfolio management. Markowitz [9] argues that diversification, achieved by increasing the number of assets in a portfolio, reduces the unsystematic risk. This definition, however, does not consider the contribution of the overlapping of assets to systemic risk and the propagation of shocks at the aggregate level. In this sense, the network methodology can complement the study of financial risk, analyzing the composition and diversification of portfolios from the same group of investors, as well as of the degree of similarity of the assets that make up their portfolios and of the investment strategies used.

The above reveals the tension existing within portfolio management and the influence of diversification as a tool for risk management. Although diversification reduces the systematic risk of the assets when this occurs in the presence of high similarity in the portfolios, as in the mutual fund industry, for example, diversification becomes a generator of systemic risk. This occurs because by holding diversified portfolios but comprised of the same assets, the funds return to the system as a more vulnerable whole because the interconnections and channels of contagion are increased [3, 10].

An understanding of the risks generated by a portfolio manager that seeks to minimize them through diversification increases the interdependencies on the portfolio overlap networks of mutual and pension fund managers. This phenomenon acquires significance as an amplifier and generator of financial shocks, even more so in small economies with little diversity of assets to invest as is the case in emerging countries.

Nevertheless and contrary to expectations, there is still little attention paid in the literature to the study of financial risks in this intermediary segment [8] and, to our best of knowledge, even nonexistent in a context of emerging markets. The segment of institutional investors includes mutual funds, hedge funds, and pension funds; it is one of the primary investment vehicles globally. They reached a size of USD 46.17 trillion equivalent to 61% of global GDP in the first quarter of 2017. Mutual funds reached a size of USD 42.77 trillion, the most important group in this industry. 65% of the managed assets correspond to stocks and debt instruments, with 43% of total participation being equity funds. These numbers underscore the relevance of these investors, and the need to deepen understanding of the effects of these intermediaries' investment strategies on financial risk in this industry.

The use of networks has made it possible to study mainly the structures of control chains in financial systems, systemic risk, the evolution of commerce between nations, and interbank transactions between banks [11]. These papers consider similarity-based networks, in which the weights of a network represent a measurement of similarity (or distance) between assets; this measurement is a linear correlation between the returns on the assets. The correlation then becomes a distance associated with a Euclidian distance, which is why hierarchical clustering methods can be applied to understand the industry-specific structure and clusters. Also, using the network approach, it is possible to detect the relations between different market agents to discover the underlying control chains [12, 13]. Finally, in the study of transactions between two agents, the links represent the transactions, whereas the nodes represent the agents in the financial market. For example Boss and others [14], study the formation of community structures and other topological elements of the networks that show free scale and small world properties. However, there is a gap in the literature respect to the relation between topological elements of the financial network, the variables of asset management, and industry variables. For example, in the case of mutual funds, how does the path length of the network vary when portfolios managers begin increasing the sale of assets to buy others, or when they decide to increase or reduce the diversification of their portfolios?

Given the logical evolution of the literature on financial networks analysis and to contribute to a deeper understanding of the portfolio overlaps phenomenon in a mutual fund industry context, this study aims to examine how financial management variables in conjunction with specific variables from the mutual fund industry, mold, and shape financial networks between funds and financial assets.

Accordingly, in this work we study the following hypotheses:

(1) the topology of the mutual funds network changes due to variations in the investment strategies selected by the industry actors.

(2) the topology of the mutual funds network changes due to variations in industry-specific variables.

Our research contributes to the literature by improving the understanding of the phenomenon of overlapping from three perspectives. First, we analyze the topology of the mutual funds network using a bipartite network method (similar to Delpini and others [8]), and we complement it with an analysis of its bipartite one-mode network projection (for a summary see Zhou and others [15] and Straka et al. [5]). Second, we study the effect of economic and financial shocks that affect the equity market as a whole on the topological properties of the funds network. And third, we consider studying the impact of changes in the mutual fund's

investment strategies[3] on the basic characteristics of the topology of the network of funds from an emerging market like Chile.

Additionally, we add more depth to the analysis by including network parameters such as diversity, modularity, path length, and assortativity. This is important because the financial phenomenon that involves managing mutual fund assets consists in studying the effect of changes on industry variables, understanding how these intermediaries manage their investments in the event of fluctuations in the financial context, the degree to which they use similar investment strategies, and how much they increase or reduce the diversification of their portfolios.

We study the mutual fund industry because it is the most important financial intermediary in terms of volume of managed assets, invest in the same class of assets and markets, and there is high similarity in their investment strategies and composition; factors that increase the systemic risk of the phenomenon of portfolio overlaps. Finally, our study makes a methodological variation by using bipartite network projections to analyze the extent to which asset overlapping determines the level of interdependence between mutual funds in the same market, in the event of changes in their investment strategies, and fluctuations in industry conditions.

The main results show that the structures of the bipartite mutual fund network and its one-mode projection change over time and are affected by variables related to the fund investment strategies and industry-specific variables. By studying the phenomenon of portfolio overlapping in a segment of investors who invest in the same asset class in the same country, we have found that their behavior affects the structure of the financial network comprised of their funds and the stocks where these invest. This endogenous element is derived from the financial strategies that funds use when they are fulfilling their role as third-party fund managers. This is an additional factor of changes in the structures of the financial networks which has effects on financial stability and risk.

The rest of the paper is structured as follows: in Section 2, we explain the bipartite network and its one mode projection. In Section 3, we describe our data and explain our focus on the Chilean mutual fund industry. In Section 4, we characterize the mutual fund industry using bipartite networks and their one-mode projection. In Section 5, we present the methodology, econometric results, and robustness analysis. Finally, in Section 6, we conclude and provide future research extensions.

2. Model

This section describes how to model the interdependencies between mutual fund managers using a network approach. The network approach offers us the possibility of analyzing the structure and temporal dynamics of these interdependencies, created as a product of decisions about investing in stocks. These purchase and sale decisions are those that ultimately impact the topology of the mutual funds network.

An appropriate network to model the interdependencies between funds and stocks is through a bipartite network. We begin with this description, which gives us the input to project this network in a one-mode. That is a network that represents only the interdependencies between mutual funds.

The bipartite networks are useful for studying situations where financial institutions possess overlapping exposures to different asset classes. The bipartite network has two types of nodes: mutual funds—entities that manage investments—and stocks, denoted by U and V, respectively. We denote with E the links that join the two types of nodes, which are disjointed between them. Each node is linked to a weight w_{ij} that represents the level of exposure of the mutual fund i on the asset j. Then G(U,V,E) is a weighted bipartite network since each element of E connects a vertex of U and V such that there are no edges that connect elements of U and V between them. The links that go from funds to stocks represent diversification, whereas the weights of the bipartite network are equivalent to the exposure of the funds in stocks.

Figure 4(a) shows an example of a bipartite network between mutual funds and stocks. It shows three different cases with different exposures (different weights), but always with the same level of diversification. We analyze the bipartite network using three properties. The first is the degree of the set of nodes corresponding to the mutual funds, which measures the level of diversification of the funds in the stocks. The second is the strength, which measures the level of exposure of the fund to the stocks. Finally, we calculate the diversity, which measures the complexity of a mutual fund given by its diversification and exposure.

The bipartite network tells us how mutual funds and stocks are connected between them. But how do mutual funds relate to each other? The answer is given by the stock portfolios they share. Thus, we propose to compress the bipartite network by one-mode projection to understand how mutual funds relate to each other.

There are different methods to project a bipartite network to a one-mode projection. In particular, for a weighted bipartite network, the resulting weighted adjacent matrix $\{w_{km}\}$ will always be symmetrical, i.e., $w_{km} = w_{mk}$. Nevertheless, the dependency of a fund k on a fund m may be different from the influence that m has on k, because the funds have different levels of exposure among all the different alternatives of assets available to invest. Therefore, a more natural projection alternative is the one that allows for an asymmetrical weighting method. Consequently, we use a network resource-allocation method [15].

The result of this projection is a network in which we only observe links between nodes of the set U of mutual funds, and the weights represent the degree of dependence/influence between them and not a measure of investment amounts as occurs in the bipartite network. These weights are the result of the resource-allocation method determined by [15] applied on the mutual funds that comes from the fund-by-fund connection matrix, which indicates the level of reciprocal interdependence among them, generated by the shared property of the stocks. For any mutual fund i, it will have a weight w_{ki}^{in} that denotes the influence this fund has on fund

k, while at the same time it has a weight of w_{ik}^{out} that denotes that fund i is also influenced by fund k. Therefore, to study the degree of influence and dependency of mutual funds, we focus on the strength of the projected funds network [16]. According to this methodology, the investors (mutual funds) act as retainers of resources that flow through the bipartite network. The appendix shows a simple example with two mutual funds and three stocks with different exposures and their respective one-mode projections. In this way, it is possible to understand better the relationships of dependence and influence between the funds changes.

3. The Data

3.1. Main Data Source. To analyze the bipartite network of mutual funds and stocks and its projection, we constructed a database with the portfolios of each mutual fund for the period January 2003 to April 2016. This study stands on the level and accuracy of the financial and industry data. For this, we obtain information from three sources, the first from the CMF (www.cmf.cl; is the Chilean equivalent of the U.S. Securities and Exchange Commission), the second from the Santiago Stock Exchange (www.sebra.cl), and the third from the Bloomberg platform (www.bloomberg.com). The dataset, free of survivorship bias, includes precise information about the price and number of portfolio stocks, the number of participants, share values, and assets under management for each mutual fund. Additionally, each stock is described by the closing price, market capitalization, trading volume, and book-to-market ratio. Thus, we can construct variables that represent the characteristics of each fund, such as the average size of the investors of the fund, return, and number of stocks where the fund invests, along with variables that according to the financial literature describe their financial strategy over time: size, liquidity, book-to-market, market capitalization, turnover, active share, and others [17–21].

Consequently, we can construct the monthly bipartite network for the Chilean mutual fund industry. To describe its topology, we calculate the degree, strength, and diversity parameters and their probability distributions for the shares on the bipartite network. Then, to extend our analysis, we estimate the bipartite network projection and calculate parameters that help us analyze the mutual fund industry in terms of its interdependencies. These variables are strength, modularity, path-length, and assortativity index.

3.2. The Chilean Mutual Fund Industry. The equity mutual fund network in Chile is interesting for many reasons. First, having accurate monthly data regarding the number of shares in each fund portfolio allows us to study in a dynamic context the networks formed by a segment of institutional investors that have not yet been studied in depth in the literature on financial networks. Second, mutual funds have enjoyed outstanding development, obtaining managed assets of MMUSD 53,887 in 2017 and reaching a penetration of 22% of GDP. This performance places them as the most dynamic investors in the Chilean delegated portfolio management industry. This figure, equivalent to 50% of the mean penetration of developed countries, is higher than the mean growth of developing countries [22]. For example, compared to 2002, when the managed amounts represented a number close to 9% of GDP, this penetration has grown to a mean rate of 5.5% annually. This growth makes mutual funds the third actor in the delegated portfolio management industry in Chile behind pension fund administrators and insurance companies. Third, according to the World Economic Forum, the country has a medium level of financial development, since it ranks 29th out of 62 countries. Consequently, the apprenticeships gained from this industry are useful for other emerging markets on the road to more significant economic and financial development. Finally, equity markets in Chile have a high size in terms of percentage of GDP compared with other OECD markets or other emerging markets.

4. Network Characterization of Chilean Equity Mutual Funds

4.1. The Bipartite Network of Mutual Funds and Stocks. Financial intermediaries, such as mutual funds, fulfill three fundamental roles in providing the delegated portfolio management service. First, activities associated with economies of scale and scope enable them to reduce transaction costs; second, they invest in less liquid but more profitable assets; and, finally, they engage in delegated investment monitoring of the investments (for a survey, see Stracca [23]). Thus, in this delegated portfolio management process, every fund manager must choose from among a wide range of financial assets (equity, bonds, and deposits, mainly) to make up an investment portfolio. The main goal is to achieve the best risk-return combination for their clients.

4.1.1. Degree. The degree distribution of the mutual funds describes the typical scale-free property of the bipartite network. Figure 1 (left) represents the degree distribution of the mutual funds in the bipartite network (k_a) in three different periods: before, during, and after the crisis of 2008. Regardless of the time, we observe that few funds tend to be connected to many stocks, and the majority of the funds tend to be connected to fewer stocks. In other words, there are a few mutual funds that are highly diversified, whereas most funds are less so.

The evolution of this variable over time is in Figure 2(a). Note that there was a change in the degree of mutual funds before and after the financial crisis. Specifically, after the crisis, the mutual funds adjusted their diversification strategy to the downside and, as a result, the degree of the funds falls and increases the concentration of the funds' equity portfolios as a consequence.

4.1.2. Strength. The strength for a mutual fund i is the sum of all weights of the links incident to it, indicating the exposure of the mutual fund. The weights w_{ij} of a fund i on an asset j are related to the amounts of money in local currency that the fund i has on the asset j determined by the composition of its portfolio in a particular month. It is usual for these weights w_{ij} to change from one month to the next reflecting the reassignment of positions (or exposures) in the mutual funds

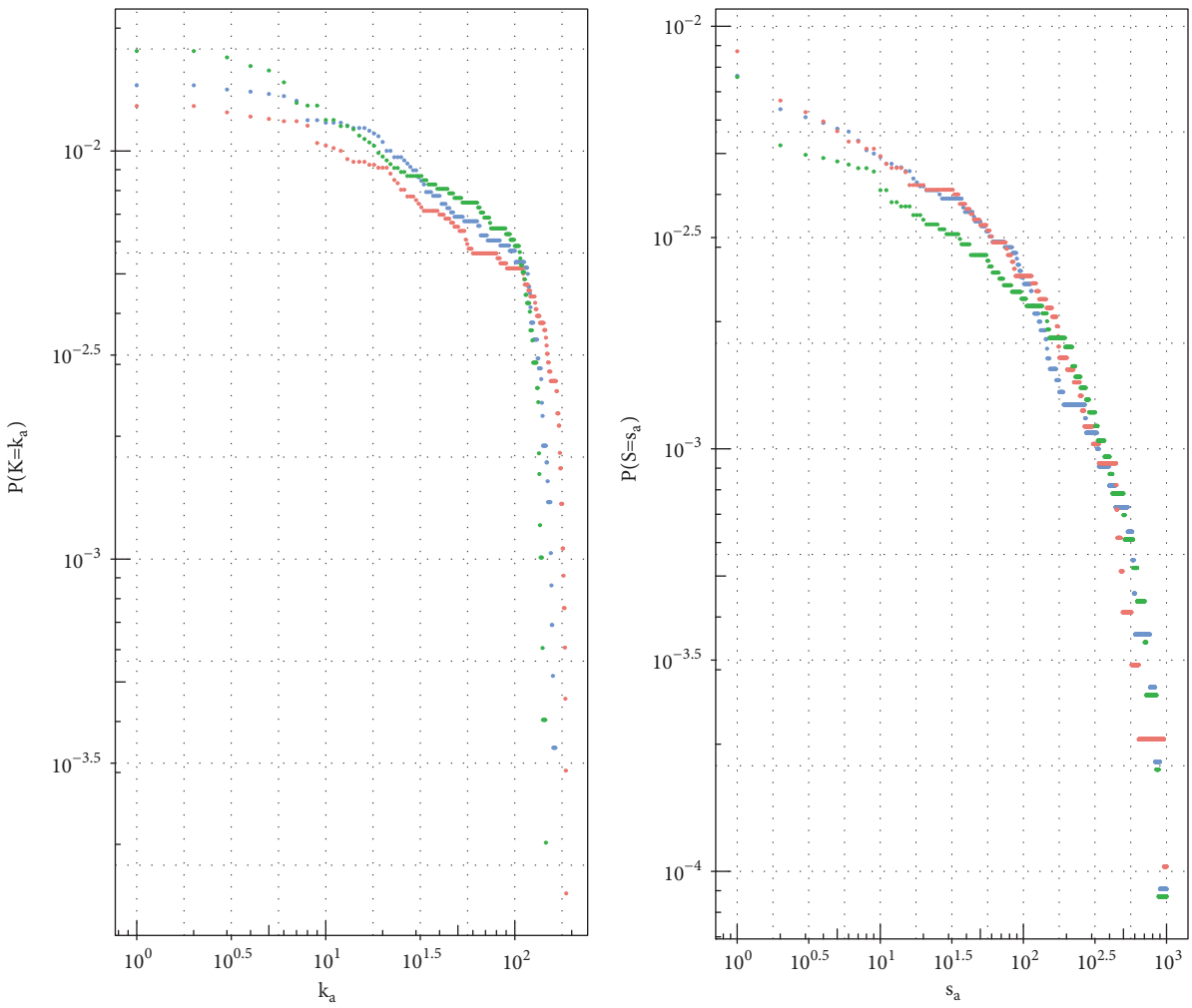

FIGURE 1: Degree (k_a) and Strength (s_a) densities for stocks in the bipartite networks. Different colors for each period. In blue, precrisis period from January to June 2008. In red, crisis period from June 2008 to January 2009. In green, postcrisis period from February to June 2009.

portfolio carried out as part of their particular diversification strategy.

Figure 1 (right) describes the distribution of the strength of the mutual funds in the bipartite network (s_a). Regardless of the analysis period, this distribution also follows a similar behavior. A few mutual funds seem to have very high exposure in assets, whereas the vast majority have less exposure.

The evolution of this variable over time is in Figure 2(a). We observe that, during the crisis, the drop in stock prices negatively affected the strength of the network. However, contrary to expectations, the exposure did not recover during the postcrisis period despite the improvement in stock market prices. This evidence (added with the results of the degree) indicates that there was a change in the portfolios that could not be explained solely by changes in the values of the financial assets, but also by changes in the exposure of the portfolios and fluctuations in the economic and financial conditions of the equity market.

4.1.3. Diversity. If at a given moment, a mutual fund F has a larger number of stocks than another mutual fund F', then fund F has greater diversification than fund F'. Similarly, if fund F has a larger amount invested in stocks than another fund F', then fund F is more exposed than fund F'. In the first case, fund F has a more diversified portfolio, whereas in the second, it is more exposed. To capture the combined property of the level of diversification and exposure, we used the Shannon entropy index [24]. This representation of diversity has been used to describe quantitatively the flow of biomass between different species in ecology literature [25]. For our purposes, the Shannon or entropy index for mutual fund i would be

$$H_i = -\sum_{j=1}^{N} \frac{w_{ij}}{w_{i*}} \log_2 \frac{w_{ij}}{w_{i*}} \tag{1}$$

where w_{ij} represents, as indicated previously, the amount of money that fund i has in stock j. The value w_{i*} is the sum of all the money that fund i has in its portfolio. Shannon entropy is between 0 (minimum) and 1 (maximum). In consequence, H_i is maximum when a mutual fund invests in all the assets in its portfolio in equal proportion, that is when all w_{ij} are equal for each fund and each stock.

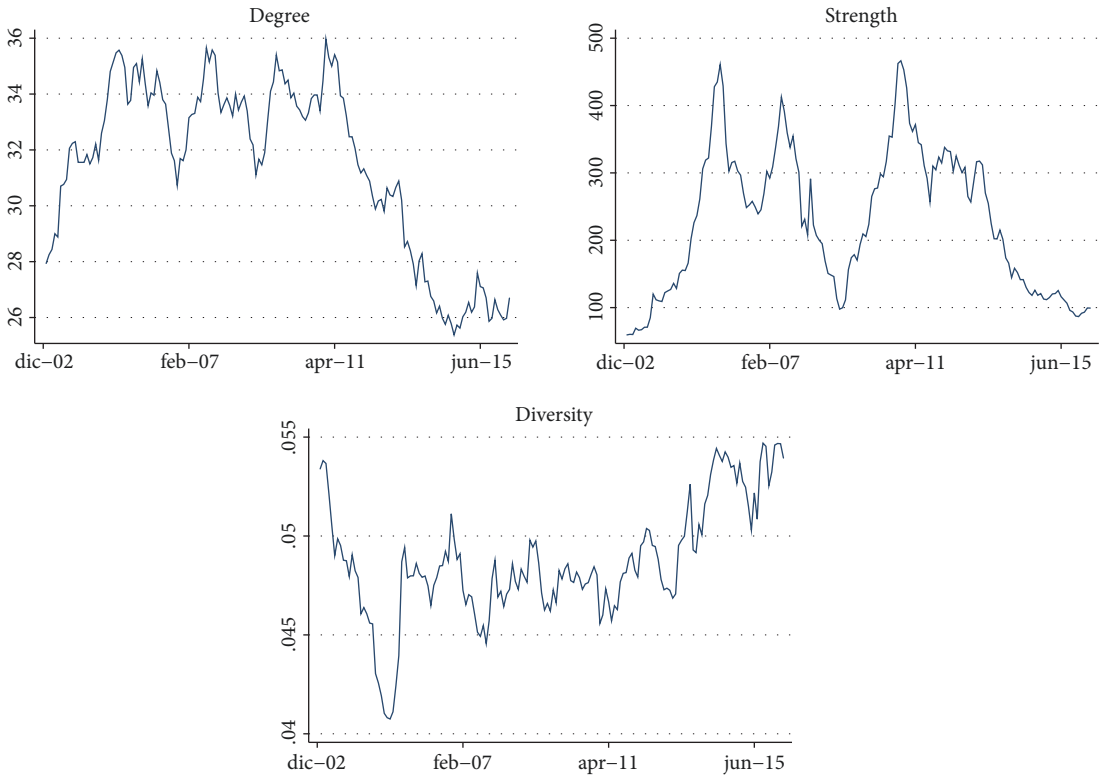

(a) Time series of bipartite networks variables

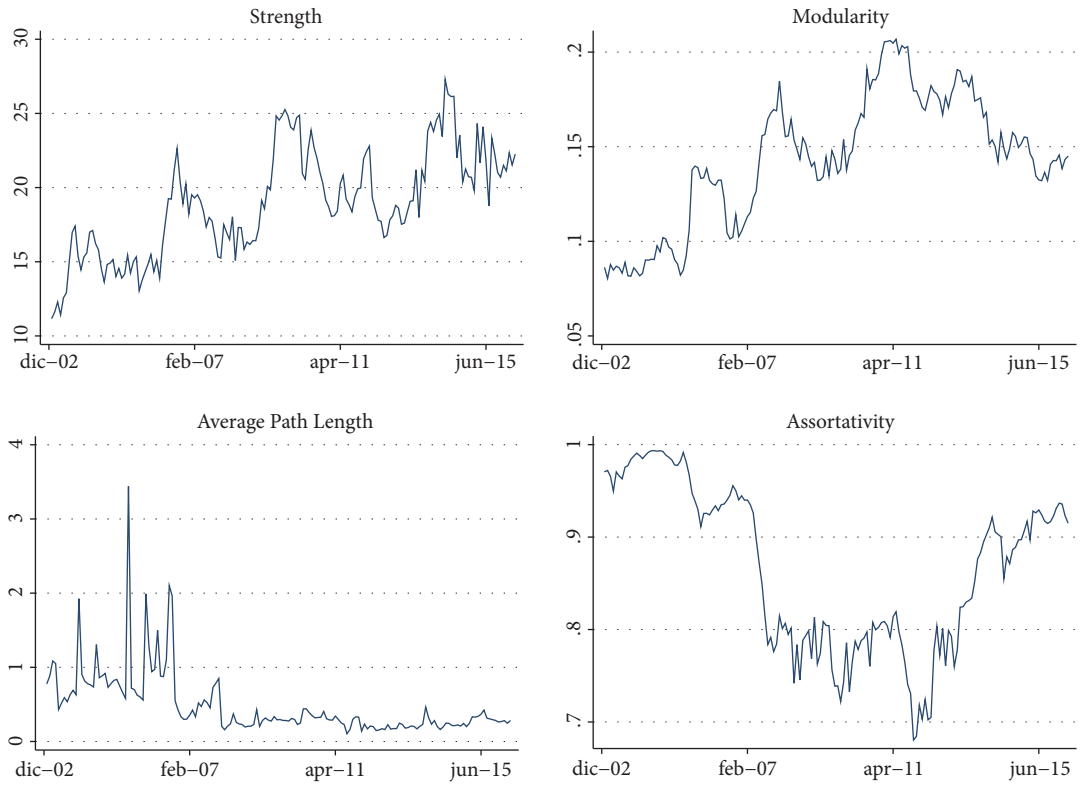

(b) Time series of bipartite network projection variables

Figure 2

As the index is calculated with a logarithm in base 2, we calculate the reciprocal of H_i and n_i where $n_i = 2^{H_i}$, which we will call general diversity. We take the average of the diversity indices of all existing mutual fund for every periods. This way, the higher the value of n_i is, the higher the level of entropy in the industry is.

This measurement fits well to calculate the global diversity of the bipartite network from the fund managers' point of view and therefore to be able to understand how the level of industry diversification and exposure behaves in different periods. Its evolution over time is in Figure 2(a). It is possible to observe a permanent upward trend in general diversity from period April 2011 onwards. In other words, there seems to be a more focused investment in resources by funds over fewer assets (or low diversification). This could be explained by the decrease in the average degree of the system in Figure 2(a) (Degree). On the other hand, investment amounts also have a downward trend (Strength). The combined effect of these elements produces an increase in the Entropy of the industry, which suggests an effect of less exposure and diversification taken by fund managers.

4.2. The One-Mode Projection of the Bipartite Network. From the bipartite network of stocks and mutual funds, it is possible to construct a one-mode projected mutual funds network to build a network in which the funds are related only to each other. We use the one-mode projection proposed by [15] because when choosing stocks to comprise their portfolios, they share the property of some of them, and consequently overlapped portfolios are formed in the mutual fund industry, thus making it possible to study the interdependence among them.

4.2.1. Strength. The strength is the sum of the weights of the incident links to the node. As the one-mode projected network is directed, each node may have links that enter the node and others that leave it. The sum of the weights of the links that enter the node, the in-strength, measures the influence that the fund has on the others. The out-strength, the sum of the weights of the links leaving the node, measures the dependence that the fund has from the others. In this way, we have a way to measure the degree of mutual influence and dependence between the different participants in the fund industry.

As we are dealing with averages over different periods, the mean of the in-strength is equal to the mean of the out-strength, simply because in the one-mode projection process in each period, all the primary resources of the system remain intact. Thus, we speak of strength without making a difference between one and the other[5].

The results indicate that the interconnection (or degree of influence of each fund on the others) of Chilean equity mutual funds is variable over time and increase during the crisis. Figure 3 shows a comparison between strengths for 12 months (a) and 24 months (b), before and after March 2009[6]. We observe that there is variability in the strength of the projected network. In the case of in-strength, note that, before and after the crisis, the variability stays steady, because the median and interquartile ranges are similar. However, in the crisis, we observe an increase in variability, although with values similar to the precrisis period. This is evidence of an increase in the dispersion of the dependency of the funds on each other; i.e., in the crisis the dependence of each fund increases concerning the industry, or in other words the topology of the network projection is variable over time. Similarly, the out-strength shows an increase in the median, which is not accompanied by an increase in its variability.

4.2.2. Modularity. To describe the structure of the one-mode projected network, we perform a calculation of the modularity or cluster quality measure [26], considering all possible community structures based on edge-betweenness edge removals. The edge-betweenness of an edge measures the number of shortest paths that pass through it. The idea of using this measurement to detect communities within a network is that edges with a high edge-betweenness create the bridges between different communities in the network. Thus, if these edges are removed, it would clearly show areas of the network isolated one from the other, revealing the community structure.

The calculation of the modularity Q is done iteratively, finding the number of communities that maximize the value of the modularity. The modularity allows us to know the degree to which specific modules in the network are more or less densely or sparsely connected to other modules [27]. Thus, modularity values close to Q = 0 indicate a low or null level of community structure; by contrast, values close to Q = 1, which is the maximum, indicate a strong presence of community structure. In the case of the projected network, high modularity values suggest that there are structures or modules inside the network that tend to be influenced internally, but not mutually.

In practice, we observe over time that there are increases and decreases of the level of modularity of the network, but they are always between values of 0.1 and 0.2 (see Figure 2(b)), indicating low level of community structure and, consequently, a high level of influence of "all with all", without seeing structures inside the network. However, over time variability is noted, which suggests that certain factors seem to influence the network structure.

4.2.3. Average Path-Length. The average path length < d > is the average of the shortest distances between all the pairs of nodes in the network; for this, we estimate the value for the projection of the bipartite network monthly [28]. As this is a directed network, we have that

$$< d >= \frac{1}{N(N-1)} \sum_{i,j=1..N, i \neq j} d_{i,j} \tag{2}$$

where N is the number of vertices in the network (number of funds in the industry).

Given that the strength of the projection indicates the influence-dependency level on other funds, this value symbolizes the average degree of influence between the funds existing in the market at a given moment. Thus, for example, if at some point in time d_{ik} is low about another period, then it

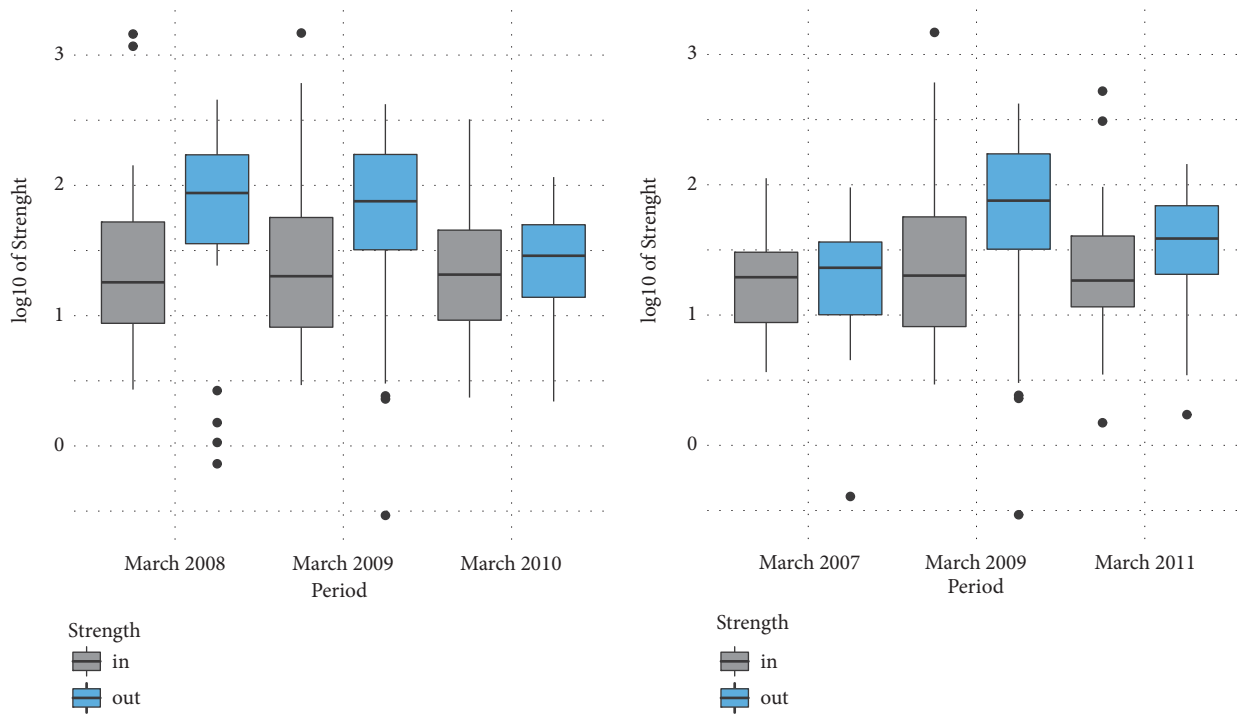

(a) Boxplots of logarithms of strengths-in and strengths-out of the bipartite network projection of mutual funds, 12 months before and after the crisis (March 2008, 2009, and 2010)

(b) Boxplots of logarithms of strengths-in and strengths-out of the bipartite network projection of mutual funds, 24 months before and after the crisis (March 2007, 2009, and 2011)

Figure 3

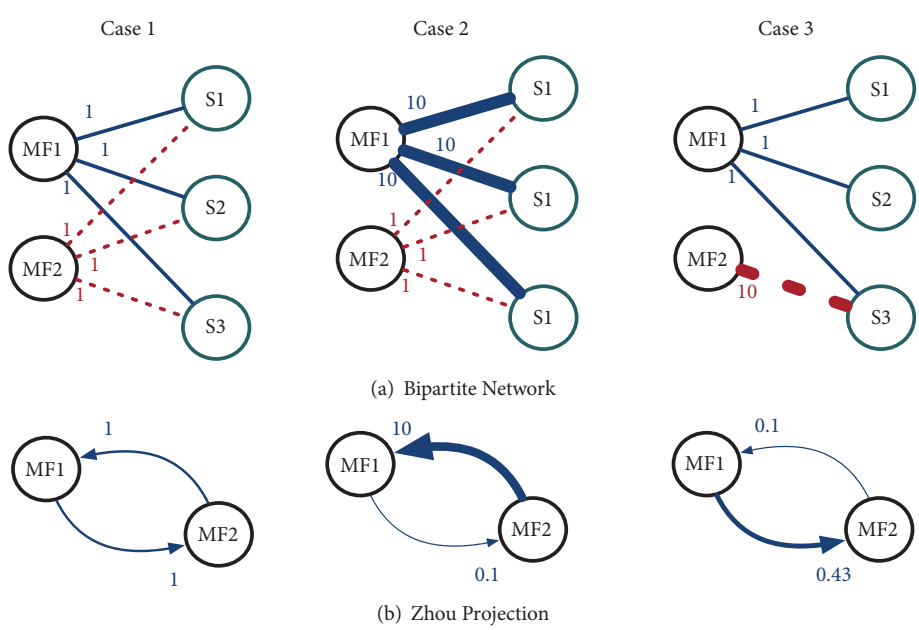

(a) Bipartite Network

(b) Zhou Projection

Figure 4

can be interpreted that the level of interdependence between funds i and k are lower than at the beginning. As a result, a small $< d >$ value indicates little interdependence between the funds in the industry at a specific time, whereas higher values indicate a greater interdependence level. Their evolution over time is in Figure 2(b).

4.2.4. Assortativity. Assortativity measures the tendency of nodes to connect with other nodes of the same degree. Thus, nodes with high degrees tend to be connected to each other, and, in the opposite direction, a disassortative network indicates that nodes with high degrees tend to be connected with low-degree nodes [29].

In our case, as we are dealing with weighted bipartite networks, we wished to find the degree of assortative mixing in terms of the weights w_{ij} of a fund i on an asset j. For this we calculated Pearson's correlation coefficient between the strengths of mutual funds and the shares in the bipartite network for each period [30]. Thus, assortativity levels close to 1 indicate that the mutual funds with high levels of invested capital tend to invest in stocks that are also heavily present in the portfolios of other mutual funds. Otherwise, assortativity values close to -1 indicate that mutual funds with high levels of investment tend to invest in stocks that are little represented in the portfolios of other funds in the industry.

In practice, it is observed that these values are close to 0.9 (see Figure 2(b)), which indicates that the Chilean mutual fund industry tends to exhibit a kind of elevated preferential attachment, in which the funds' portfolios conform to the level of capital they have and the presence of the stocks in the market. This behavior may be the result of investment strategies that managers follow in a high level of portfolio overlap. These values are similar to that found in [31] in the percentage of shares that firms share with each other and in the Italian bank industry [32].

An explanation of the high levels of assortativity found could be based on the phenomena of herding in the management of investments [33] and the reduced diversity and liquidity of shares available in emerging markets. On the other hand, compensation and career development motivate mutual fund managers to invest in shares in which everyone invests, thus eliminating the possibility of losing money when everyone wins, a very negative event for their remuneration and career development. A second explanation is the limited availability of investment options and liquidity problems. This explains why the funds invest a large amount of money in a few shares, as they manage liquidity risk.

5. Econometric Analysis

5.1. Specification of the Model. In this study we focus on the dynamic analysis of the topological behavior of the bipartite network and its projection using elements specific to the mutual fund industry as well as variables related to mutual fund investment management strategies. However, the context in which these investors act is related to the general economic and financial environment, which affects the behavior of the stock market as a whole. Eberhard and others [34] find that the network structure of equity market transactions changes together with variables from the local and international financial environment. Specifically, for the case of the Chilean equity market, the network structure of stock exchange transactions fluctuates with the S&P 500 index, the blue-chip Chilean index (IPSA), the Chicago Board Options Exchange Market Volatility Index (VIX), the exchange rate between the Chilean peso and the USD dollar (CLP), the emerging market index (MSCI), the oil price (Pe), and the copper price (Cu).

For the case of the factors of the mutual fund industry, we use variables that characterize the industry at aggregate level and at financial level. In the first group, the total number of investors or participants in the industry, the total number of stocks in the portfolios under delegated management, and the total number of mutual funds existing in the market are included. In the second group, variables studied by the literature are incorporated to measure the financial performance and investment abilities of the mutual funds. The size of the funds is incorporated, measured by the market capitalization (*ln_mcap*) and the book-to-market ratio (*ln_book*) [17] the momentum of the performance of the funds, measured by the one-month delayed return (*L.performance*), and the rotation of the portfolios, measured by turnover (*ln_to*) [18]; active management of the funds, measured by the active share (*ln_as*) [19, 20]; and the liquidity of the assets of the funds, measured by liquidity of the portfolios (*ln_liq*) [21].

As previously mentioned, our hypothesis studies the impact on the topology of the mutual funds bipartite network and its projection of fluctuations in the economic and financial conditions of the capital market, as well as changes in the investment management decisions made by the funds as a result of their role as third-party portfolio managers. According to this, as we indicate in Sections 3.1 and 3.2, the topological variables that study the bipartite network are the variation in degree (*vdegfon*), the variation in strength (*vstrengthb*), and the variation in the diversity of the funds (*vdiversity*). Likewise, for the case of the projected network, we study the variation in strength (*vstrengthp*), the variation in modularity (*vmodularity*), the variation in path-length (*vpathlenth*), and the variation in assortativity (*vassortativity*).

According to the above, to study the effects of variations on the financial strategies deployed by the mutual funds as a whole and by changes in the mutual funds' industry aggregate variables, we estimate the following econometric model for the bipartite network and its projection:

$$Y_t = \alpha + \beta * X_t + \gamma * C_t + m_t + \varepsilon_t \quad (3)$$

The dependent variable is Y_t and represents the variation in the topological variables of the bipartite and the projected networks. X_t corresponds to the independent variables associated with the investment decisions of the whole funds and aggregate variables of the industry. C_t corresponds to the control variables associated with the economic and financial environment. m_t are monthly fixed effects to control for seasonality. All models are estimated with robust standard errors.

5.2. Main Results. To test our hypotheses, the econometric study that is reported next is based on the analysis of the statistical significance between restricted and unrestricted models in order to evaluate whether the changes in the topological variables of the bipartite networks and the projected one are explained by changes in variables related to the financial management of the funds and/or by changes in the variables specific to the mutual fund industry.

5.2.1. Econometric Models of the Bipartite Network

(1) Degree. Table 1, column (1), shows that changes in the average diversification of the industry (*vdegfon*) are jointly associated by changes related to industry-specific variables

Table 1: Bipartite Network Models. This table summarizes the results of the following model: $Y_t = \alpha + \beta_* X_t + \gamma_* C_t + m_t + \varepsilon_t$. The dependent variable is Y_t and represent the variation in the topological variables of the bipartite networks. X_t corresponds to the independent variables. C_t corresponds to the control variables. m_t are monthly fixed effects to control for seasonality. All models are estimated with robust standard errors.

	(1)	(2)	(3)	(4)	(5)	(6)	(7)	(8)	(9)
		vdegfon			vstrengthb			vdiversity	
ln_mcap	0.0104		-0.000299	-0.0372		-0.0217	0.00857		-0.00878
	(0.248)		(0.964)	(0.356)		(0.444)	(0.378)		(0.266)
ln_liq	**-0.0127***		-0.00336	**-0.0573****		**-0.0559****	-0.00455		0.00477
	(0.072)		(0.616)	**(0.033)**		**(0.023)**	(0.561)		(0.496)
ln_book	0.0212		0.00632	**-0.249****		**-0.144*****	**0.0551****		0.0134
	(0.382)		(0.641)	**(0.019)**		**(0.002)**	**(0.041)**		(0.369)
ln_to	**0.0198*****		0.00509	-0.0583		**-0.0752****	**0.0210****		0.00636
	(0.003)		(0.488)	(0.144)		**(0.033)**	**(0.012)**		(0.412)
ln_as	0.0185		-0.0158	0.0159		0.0186	**0.0483****		0.00522
	(0.327)		(0.293)	(0.813)		(0.745)	**(0.015)**		(0.737)
ln_stocks	**0.155*****	**0.101*****		0.172	0.169		**0.120****	0.0380	
	(0.000)	**(0.000)**		(0.320)	(0.176)		**(0.021)**	(0.314)	
ln_funds	-0.0344	0.0102		-0.0199	-0.0289		**-0.0459***	0.000722	
	(0.135)	(0.333)		(0.837)	(0.583)		**(0.058)**	(0.958)	
ln_investor	**-0.0314****	**-0.0323*****		**-0.109****	-0.0457		-0.00678	-0.0153	
	(0.019)	**(0.001)**		**(0.045)**	(0.193)		(0.648)	(0.154)	
L.performance	**0.166*****	**0.124*****		0.129	0.210		**0.166*****	**0.103*****	
	(0.000)	**(0.000)**		(0.571)	(0.370)		**(0.000)**	**(0.006)**	
ipsa_ret	**0.0829***	0.0327	**0.0893***	**1.075*****	**1.190*****	**1.200*****	0.0638	-0.0175	0.0367
	(0.095)	(0.425)	**(0.065)**	**(0.000)**	**(0.000)**	**(0.000)**	(0.306)	(0.735)	(0.567)
varvix	0.0139	0.0144	0.0173	0.00385	-0.000578	0.00691	-0.00301	-0.00342	-0.00150
	(0.235)	(0.164)	(0.156)	(0.908)	(0.987)	(0.841)	(0.847)	(0.811)	(0.923)
varcu	0.0132	0.00151	-0.0131	-0.0239	0.0148	-0.0426	0.0232	0.00314	0.00393
	(0.544)	(0.946)	(0.623)	(0.818)	(0.895)	(0.680)	(0.438)	(0.912)	(0.893)
varclp	0.0394	0.0326	-0.0255	0.292	0.297	0.287	0.0813	0.0586	0.0291
	(0.395)	(0.478)	(0.640)	(0.409)	(0.404)	(0.404)	(0.175)	(0.286)	(0.611)
varmsci	0.0155	0.0255	0.00213	0.179	0.0846	0.183	**0.111****	**0.113****	**0.101****
	(0.690)	(0.500)	(0.962)	(0.373)	(0.687)	(0.363)	**(0.021)**	**(0.022)**	**(0.043)**
varpe	0.00272	0.00612	0.0195	0.0549	0.0811	0.0716	-0.0224	-0.0129	-0.0111
	(0.883)	(0.719)	(0.329)	(0.549)	(0.403)	(0.439)	(0.318)	(0.531)	(0.612)
spx_ret	0.0931	**0.104***	0.0917	0.0661	0.200	0.0194	-0.0317	-0.0124	-0.0254
	(0.134)	**(0.096)**	(0.249)	(0.841)	(0.539)	(0.952)	(0.708)	(0.886)	(0.781)
L.vdegfon	**-0.133***	-0.120	0.0435						
	(0.071)	(0.133)	(0.609)						
L.vstrengthb				0.0447	0.0524	0.105			
				(0.742)	(0.712)	(0.313)			
L.vherfindahl									
L.ventropy							-0.0483	-0.0207	0.0411
							(0.556)	(0.800)	(0.627)
_cons	-0.293	**-0.141****	-0.00470	0.159	-0.179	-0.286	-0.212	-0.0221	0.160
	(0.139)	**(0.049)**	(0.957)	(0.837)	(0.622)	(0.443)	(0.378)	(0.814)	(0.156)

Table 1: Continued.

	(1)	(2) vdegfon	(3)	(4)	(5) vstrengthb	(6)	(7)	(8) vdiversity	(9)
N	**158**	**158**	**158**	**158**	**158**	**158**	**158**	**158**	**158**
R^2	**0.364**	**0.289**	**0.142**	**0.521**	**0.466**	**0.504**	**0.254**	**0.160**	**0.122**
adj. R^2	**0.226**	**0.167**	**-0.013**	**0.417**	**0.374**	**0.415**	**0.092**	**0.016**	**-0.037**
P-value	**0.00**	**0.00**	**0.58**	**0.00**	**0.00**	**0.00**	**0.05**	**0.34**	**0.77**
F	**3.522**	**3.172**	**1.394**	**9.500**	**6.630**	**9.581**	**1.935**	**1.813**	**1.099**
LR-Chi2		**17.77**	**47.38**		**17.13**	**5.45**		**18.73**	**25.73**
Prob>Chi2		**0.00**	**0.00**		**0.00**	**0.24**		**0.00**	**0.00**

Nonstandardized coefficients. p-values in parentheses. $^{*}p < 0.1$, $^{**}p < 0.05$, and $^{***}p < 0.01$.

and changes in the mutual funds' investment strategies. Within the first group of variables with statistical significance, highlighted by the magnitude of its effect is the variable average number of stocks within the funds (*ln_stocks*); a one standard deviation increase in *ln_stocks* would yield a .79 standard deviation increase in the predicted *vdegfon* (β = 0.79, normalized coefficient). It is also observed that when the past return of the industry increases (*L.perfomance*), diversification also does so. The intuition of these results indicates that when the return of the previous month increases, the industry tends to increase the diversification within the funds, this being consistent with an increase in the number of stocks bought by each fund.

Nevertheless, an inverse effect is noted between the number of investors in the industry (*ln_investors*) and the diversification of the funds (*vdegfon*). In order of magnitude, a one standard deviation increase in *ln_investors* would yield a .53 standard deviation decrease in the predicted *vdegfon* (β = -0.53, normalized coefficient). This result indicates that, in the event of an increase in investors and probably also an increase in the amounts of money managed, mutual funds tend to concentrate the investment in popular or glamour stocks [35], causing the diversification to decrease.

As far as the variables related to the financial management of the funds is concerned, a positive relation can be seen with turnover (*ln_to*) and a negative one with liquidity (*ln_liq*), with the former being the one that presents the greatest magnitude of impact on the diversification of the industry. Indeed, an increase in a one standard deviation in the turnover causes an increase of 0.4 times in the standard deviation of the diversification (β = 0.4, normalized coefficient). The intuition of this phenomenon is based on a relevant objective of investment management, materialized through the rotation of its assets [21], which consists of managing the diversification of the mutual funds. On the other hand, by increasing the liquidity of the assets bought by the funds, these reduce the diversification of their portfolios, concentrating their investments on fewer assets (β = -0.25, normalized coefficient).

(2) Strength. In relation to the level of exposure of the mutual funds (*vstrengthb*), column (6) shows that the changes in the funds' exposure depend exclusively on changes related to investment management variables. Indeed, when the significance test is applied, it is demonstrated that the industry-specific variables do not affect the exposure of the mutual funds (p_{value} = 0.24). Also, it is observed that when they increase the liquidity (*ln_liq*), book-to-market ratio (*ln_book*) and turnover (*ln_to*), the exposure of the funds decreases. When the liquidity of the portfolio assets increases, the funds respond by investing less in these assets, because their expected return is lower [36]. On the other hand, when the book-to-market ratio of the portfolio stocks increases, the funds reduce their exposure, because the prices of the assets are falling, discouraging their appeal [17]. Finally, by increasing the rotation of the portfolios of the funds, the exposure decreases, because the funds reduce the average exposure in each asset. This means, by rotating the portfolio, their investments reassign among a greater number of assets. These three variables have similar magnitudes, with the book-to-market ratio being the most relevant (β = -0.28, normalized coefficient).

(3) Diversity. The complexity of the mutual funds network, measured by the diversity index (*vdiversity*), as in the case of diversification, is dependent on industry-specific variables and the funds' investment management variables. Column (7) shows that there is a positive relation between diversity, the book-to-market ratio (*ln_book*), turnover (*ln_to*), and the active share (*ln_as*) of the mutual funds. Of these three variables related to the financial management of the funds, the one that has the greatest impact is the book-to-market ratio (β = 0.51, normalized coefficient).

In relation to the effect of the industry-specific variables, it is observed that the numbers of stocks per fund (*ln_stocks*) and past performance (*L.performance*) are significant. The importance of the first is highlighted, as its coefficient is similar to the one of the book-to-market ratio (β = 0.53, normalized coefficient). We see that as the number of stocks and past performance increase, the diversity also does, which makes sense, because the greater the availability of stocks to invest, the greater the diversity in terms of portfolio diversification and exposure. On the other hand, a better performance attracts a larger number of participants to the funds [37], causing the funds to invest more [38], and as a result the exposure also increases, increasing the diversity. Interestingly, as the number of funds in the industry increases, the diversity falls. This could be explained because having more funds, the stock of money invested in the industry is distributed among more agents, and therefore the weights w_{ij} tend to decrease.

5.2.2. Econometric Models of the One-Mode Projection. Remembering that the purpose of the projected network is the analysis of the mutual dependency between funds in the industry, the links in this network indicate the degree of dependency that exists between one fund manager and another, unlike the bipartite network, whose links and weights show levels of asset diversification and exposure, respectively. In general terms, the results in Table 2 indicate that changes in the strength, modularity, and assortativity of the projected network depend on both variations in industry variables as well as changes in the funds' financial management variables. However, these variables do not affect the case of path length.

(1) Strength. Table 2, column (1) directly studies the average interdependence level that exists in the industry in a certain period. The significant variables are book-to-market (*ln_book*) and number of funds (*ln_funds*); both are negative magnitudes (β = -0.56 and β = -0.55 respectively, normalized coefficients). This would imply that, by increasing the number of funds in the industry, the interdependence decreases, which could be explained by the fact that, by keeping the exposure constant, by increasing the number of participants in the industry, the average exposure level between them falls, negatively affecting the mutual interdependence. In the case of the book-to-market ratio, the results show that when this falls, it increases the interdependence between

Table 2: Projected Bipartite Network Models. This table summarizes the results of the following model: $Y_t = \alpha + \beta_* X_t + \gamma_* C_t + m_t + \varepsilon_t$. The dependent variable is Y_t and represent the variation in the topological variables of the bipartite networks. X_t corresponds to the independent variables. C_t corresponds to the control variables. m_t are monthly fixed effects to control for seasonality. All models are estimated with robust standard errors.

	(1)	(2)	(3)	(4)	(5)	(6)	(7)	(8)	(9)	(10)	(11)	(12)
		vstrenghtp			vmodularity			vpathlength			vassortativity	
ln_mcap	0.0571		-0.000637	**-0.0855****		-0.0132	0.0522		0.0420	0.000921		-0.00711
	(0.140)		(0.981)	**(0.014)**		(0.495)	(0.862)		(0.792)	(0.950)		(0.490)
ln_liq	0.00252		-0.00607	-0.0221		-0.0225	0.0199		0.0550	**-0.0257*****		**-0.0202*****
	(0.914)		(0.778)	(0.269)		(0.216)	(0.896)		(0.720)	**(0.002)**		**(0.009)**
ln_book	**-0.209****		**-0.0937****	-0.0119		0.0139	-0.405		0.128	-0.0208		**-0.0448*****
	(0.046)		**(0.039)**	(0.894)		(0.663)	(0.618)		(0.640)	(0.512)		**(0.004)**
ln_to	-0.0156		-0.0295	0.0148		**0.0313***	0.213		0.0320	0.0105		0.000331
	(0.586)		(0.239)	(0.417)		**(0.098)**	(0.398)		(0.876)	(0.211)		(0.965)
ln_as	0.0923		0.0367	**-0.123****		-0.0333	0.527		0.413	-0.0130		**-0.0347****
	(0.179)		(0.433)	**(0.041)**		(0.415)	(0.358)		(0.343)	(0.498)		**(0.017)**
ln_stocks	-0.228	-0.0991		0.177	0.103		0.708	0.374		0.0647	0.0272	
	(0.106)	(0.408)		(0.128)	(0.316)		(0.532)	(0.509)		(0.225)	(0.565)	
ln_funds	**-0.256*****	-0.0294		**0.234*****	0.0537		-0.447	0.480		-0.0215	-0.00462	
	(0.005)	(0.473)		**(0.003)**	(0.133)		(0.426)	(0.218)		(0.482)	(0.743)	
ln_investor	-0.0319	0.0564		-0.0441	-0.0484		-0.558	-0.211		-0.00331	0.00136	
	(0.579)	(0.106)		(0.432)	(0.117)		(0.227)	(0.307)		(0.852)	(0.916)	
L.performance	-0.0632	0.0683		-0.171	**-0.202****		1.990	**1.940***		**0.144****	**0.124****	
	(0.717)	(0.623)		(0.117)	**(0.043)**		(0.125)	**(0.072)**		**(0.020)**	**(0.021)**	
ipsa_ret	**-0.402***	-0.197	**-0.282**$*$	0.0888	0.00502	0.0927	-0.177	-0.133	0.650	-0.00888	-0.0356	-0.0188
	(0.051)	(0.219)	**(0.097)**	(0.616)	(0.973)	(0.509)	(0.897)	(0.904)	(0.670)	(0.905)	(0.591)	(0.785)
varvix	**-0.0568***	-0.0591	**-0.0568***	-0.0348	-0.0357	**-0.0405***	-0.147	-0.133	-0.0512	-0.00662	-0.00717	-0.00220
	(0.077)	(0.103)	**(0.097)**	(0.162)	(0.150)	**(0.083)**	(0.380)	(0.428)	(0.771)	(0.560)	(0.538)	(0.853)
varcu	-0.134	-0.157	-0.164	0.0546	0.0855	0.0949	1.014	0.671	0.641	0.0125	0.0177	-0.00388
	(0.219)	(0.162)	(0.145)	(0.419)	(0.158)	(0.129)	(0.254)	(0.374)	(0.456)	(0.732)	(0.603)	(0.916)
varclp	-0.0335	-0.0213	-0.0199	0.184	0.185	0.218	1.292	1.108	0.653	**0.180***	**0.188***	0.138
	(0.887)	(0.928)	(0.933)	(0.335)	(0.335)	(0.234)	(0.355)	(0.401)	(0.566)	**(0.054)**	**(0.054)**	(0.140)
varmsci	-0.0423	-0.0263	0.0207	0.0226	0.00263	-0.00847	-0.225	-0.202	-0.404	0.0899	0.0928	0.0790
	(0.806)	(0.885)	(0.908)	(0.872)	(0.985)	(0.953)	(0.829)	(0.849)	(0.693)	(0.210)	(0.212)	(0.277)
varpe	-0.0436	-0.0497	-0.0626	-0.0682	-0.0490	-0.0573	-0.139	0.0226	0.0186	0.00614	0.00710	0.0154
	(0.589)	(0.543)	(0.450)	(0.197)	(0.304)	(0.274)	(0.800)	(0.963)	(0.971)	(0.834)	(0.804)	(0.619)
spx_ret	0.417	0.393	0.377	-0.284	-0.258	**-0.327***	-2.162	-1.906	-1.753	-0.170	-0.152	-0.145
	(0.102)	(0.129)	(0.139)	(0.119)	(0.128)	**(0.058)**	(0.231)	(0.259)	(0.331)	(0.106)	(0.164)	(0.193)
L.vstrenghtp	**-0.274*****	**-0.226****	**-0.241*****									
	(0.003)	**(0.011)**	**(0.008)**									
L.vmodularity				-0.0472	0.00823	0.0123						
				(0.663)	(0.940)	(0.914)						
L.vpathlength							**-0.186*****	**-0.179*****	**-0.192*****			
							(0.000)	**(0.000)**	**(0.000)**			
L.vassortativity										**-0.225****	**-0.209****	**-0.239****
										(0.028)	**(0.049)**	**(0.022)**
_cons	0.952	0.000335	-0.151	-0.0679	-0.161	0.147	3.411	-1.035	0.339	-0.252	-0.0969	-0.0615
	(0.196)	(0.999)	(0.679)	(0.921)	(0.522)	(0.578)	(0.503)	(0.580)	(0.889)	(0.326)	(0.409)	(0.659)

Table 2: Continued.

	(1)	(2)	(3)	(4)	(5)	(6)	(7)	(8)	(9)	(10)	(11)	(12)
		vstrenghtp			vmodularity			vpathlength			vassortativity	
N	**158**	**158**	**158**	**158**	**158**	**158**	**158**	**158**	**158**	**158**	**158**	**158**
R^2	**0.299**	**0.233**	**0.251**	**0.237**	**0.174**	**0.158**	**0.195**	**0.169**	**0.149**	**0.271**	**0.215**	**0.216**
adj. R^2	**0.147**	**0.101**	**0.115**	**0.071**	**0.032**	**0.006**	**0.020**	**0.026**	**-0.004**	**0.113**	**0.081**	**0.074**
P-value	**0.00**	**0.00**	**0.02**	**0.09**	**0.23**	**0.42**	**0.33**	**0.27**	**0.51**	**0.02**	**0.05**	**0.07**
F	**3.612**	**2.229**	**2.320**	**1.766**	**1.603**	**1.684**	**1.672**	**2.271**	**2.625**	**1.930**	**1.610**	**1.734**
LR-Chi^2		**14.28**	**10.55**		**12.49**	**15.54**		**5.03**	**8.72**		**11.64**	**11.58**
Prob>Chi^2		**0.01**	**0.03**		**0.03**	**0.00**		**0.41**	**0.07**		**0.04**	**0.02**

Nonstandardized coefficients. p-values in parentheses. $^{*}p < 0.1$, $^{**}p < 0.05$, and $^{***}p < 0.001$.

the funds, because the assets are increasing in value, with which the exposure increases and as a result the mutual interdependence increases.

(2) Modularity. In relation to the modularity of the projected network, column (4) shows that the investment management variables of market cap (*ln_mcap*) and active share (*ln_as*) negatively affect this network characteristic (β = -0.44 and β = -0.40, respectively, normalized coefficients). The inverse relation between market cap and modularity could be understood by the fact that when the funds begin to buy stocks with low market capitalization (uncommon assets), inevitably their investment portfolios tend to be different from the rest of the industry, and consequently groups of funds appear in the network that have greater similarity to one another. In the first group are those that invest in assets with low market-cap, and, in the second, those that orient their portfolios to assets with high market-cap, with the mutual interdependence between these groups being low.

The inverse relation between active share (*ln_as*) and modularity can be understood similarly to the previous case. As the active share increases, there are funds whose portfolios begin to be different from those of other investors because they move away from the benchmark when allocating assets into their portfolios, thereby generating a grouping of funds of greater modularity.

The positive relation between number of funds (*ln_funds*) and modularity (β = 0.68 normalized coefficients) has the opposite effect, indicating that when new funds enter the industry, these tend to invest in assets unlike those that funds in the industry already have. Thus, it is observed that the introduction of new funds increases the level of modularity of the projected network, because there are funds with different assets, making it so that mutual funds' clusters that within have the same kind of assets but between them do not.

(3) Assortativity. A high level of assortativity implies that funds with high dependency (high level of strength) are also connected with other funds of high influence (and vice versa). A negative or low assortativity indicates that funds with high dependency are connected with funds of low influence (low level of strength).

Table 2-Column (10) shows that changes in assortativity in the network is negatively affected by changes in the liquidity level (*ln_liq*) and positively by past performance (*L.performance*) (β = -0.37 and β = 0.25, respectively, normalized coefficients). This implies that, in months where the industry increases the liquidity of its mutual funds, they tend to do so by choosing similar stocks (the most liquid), whereas in periods where the industry uses lower liquidity levels, they tend to spread their investments across a larger number of stocks. This aggregate behavior is related to the herding phenomenon that mutual funds exhibit [37, 39], a situation where they buy and they sell the same stocks.

On the other hand, when the past performance is positive (*L.performance*), we observe that assortativity increases. This is due to a good performance being associated with a good decision; as a result, the investment increase in the better stocks amplifies the assortativity between those funds that employ the same investment strategies. By contrast, when the performance is negative, it is natural to observe that the funds change their investment strategies and consequently reduce their interdependence on those funds that had similar strategies.

5.3. Robustness. We provide additional econometrics analyses to provide further insights and to test the robustness of our main results. According to the literature, during the financial crisis of 2008, investors' behavior changed in both the developing and developed financial markets. For example, we observed the liquidity hoarding effect with its resulting impact on prices, returns and assets valuation; and the flight-to-quality effect with its direct impact on risky assets and their valuations [1]. Emerging markets were not immune to this phenomenon and suffered more than developed markets.

Accordingly, Table 3 shows models that evaluate the consistency of the previous results, controlling for the possible effects of the financial crisis of 2008. All models include a dummy variable (*dum_crisis*) that takes the value of 1 for each month in the period from Oct-07 to Oct-09 and zero otherwise[7]. The idea is to corroborate that our results are not the result of the financial turmoil that occurred during that time. As we can see in Table 3 the main results hold when we control for the possible effects of the financial crisis. In other words, the changes in the bipartite network and its projection are driven by variations in the financial decisions of the mutual funds' portfolio managers and changes in the structural characteristics of the mutual fund industry.

6. Conclusions

The network literature states that, in context of financial stress, the interconnectedness among financial institutions play a key role in terms of the systemic risk of the market. In these situations, a shock on a node of the system could trigger a collapse of the entire financial network [40]. Usually these shocks have an exogenous origin. For example, a currency devaluation, a sudden hike in interest rates, a sudden fall in the stock markets, or even an unexpected central bank intervention could turn on the alarms of the entire financial market and, in consequence, generate changes in the structure of the financial network. Depending on the topology of the network is how the propagation of the shocks alter the stability and resiliency of the system [41].

Although, the above is a first-order reaction of the market to external conditions, an external shock generates a second-order reaction from the entities that conform the financial network. Depending on the nature, magnitude, and duration of the financial shock, financial institutions react to maintain their financial viability, preserve clients, minimize exposure, take advantage of price selloffs, or simply hedge financial risks. This reaction modifies their investment strategies and, in consequence, provokes a change in their financial behavior. In turn this response generate a certain kind of chain reaction among the actors of the market that modify the structure of the whole network.

In the above context, the phenomenon of overlapping portfolios among institutional investors takes relevance. In

Table 3: Robustness Models. This table summarizes the results of the following model: $Y_t = \alpha + \beta_* X_t + \gamma_* C_t + m_t + \varepsilon_t$. The dependent variable is Y_t and represent the variation in the topological variables of the bipartite networks. X_t corresponds to the independent variables. C_t corresponds to the control variables. m_t are monthly fixed effects to control for seasonality. All models are estimated with robust standard errors.

	Bipartite Networks			Projected Bipartite Networks		
	(1)	(2)	(3)	(4)	(5)	(6)
	vdegfon	vstrengthb	vdiversity	vstrenghtp	vmodularity	vassortativity
ln_mcap	0.0127	-0.0202	0.00989	0.0565	**-0.0917*****	0.000292
	(0.181)	(0.557)	(0.344)	(0.175)	**(0.007)**	(0.984)
ln_liq	**-0.0119**$*$	**-0.0544****	-0.00409	0.00225	-0.0240	**-0.0260*****
	(0.091)	**(0.037)**	(0.602)	(0.925)	(0.235)	**(0.003)**
ln_book	0.0239	**-0.141*****	**0.0568****	**-0.209****	-0.0188	-0.0216
	(0.323)	**(0.005)**	**(0.039)**	**(0.048)**	(0.829)	(0.493)
ln_to	**0.0207*****	**-0.0750****	**0.0215****	-0.0159	0.0127	0.0102
	(0.002)	**(0.033)**	**(0.010)**	(0.590)	(0.491)	(0.236)
ln_as	0.0204	0.0180	**0.0494****	0.0918	**-0.129****	-0.0135
	(0.273)	(0.756)	**(0.013)**	(0.189)	**(0.031)**	(0.487)
ln_stocks	**0.165*****		**0.126****	-0.231	0.154	0.0620
	(0.000)		**(0.019)**	(0.121)	(0.191)	(0.262)
ln_funds	-0.0372		**-0.0475***	**-0.255*****	**0.243*****	-0.0208
	(0.106)		**(0.051)**	**(0.007)**	**(0.002)**	(0.501)
ln_investor	**-0.0336****		-0.00801	-0.0312	-0.0394	-0.00273
	(0.016)		(0.593)	(0.602)	(0.499)	(0.881)
L.performance	**0.159*****		**0.162*****	-0.0609	-0.154	**0.146****
	(0.000)		**(0.001)**	(0.728)	(0.180)	**(0.022)**
dum_crisis	-0.00531	-0.00630	-0.00314	0.00171	0.0130	0.00152
	(0.195)	(0.899)	(0.602)	(0.947)	(0.355)	(0.833)
ipsa_ret	0.0793	**1.196*****	0.0618	**-0.401***	0.0979	-0.00789
	(0.115)	**(0.000)**	(0.324)	**(0.053)**	(0.587)	(0.915)
varvix	0.0122	0.00476	-0.00406	**-0.0562***	-0.0306	-0.00607
	(0.307)	(0.858)	(0.799)	**(0.083)**	(0.232)	(0.607)
varcu	0.0126	-0.0449	0.0227	-0.134	0.0566	0.0127
	(0.564)	(0.672)	(0.447)	(0.220)	(0.400)	(0.726)
varclp	0.0348	0.278	0.0783	-0.0319	0.197	**0.181***
	(0.448)	(0.482)	(0.190)	(0.895)	(0.292)	**(0.051)**
varmsci	0.0148	0.182	**0.111****	-0.0421	0.0244	0.0901
	(0.704)	(0.377)	**(0.022)**	(0.808)	(0.860)	(0.210)
varpe	0.00451	0.0742	-0.0213	-0.0441	-0.0738	0.00561
	(0.807)	(0.409)	(0.347)	(0.583)	(0.163)	(0.850)
spx_ret	0.0742	-0.00386	-0.0431	0.424	-0.235	-0.164
	(0.245)	(0.990)	(0.620)	(0.114)	(0.206)	(0.122)
L.vdegfon	**-0.140***					
	(0.062)					
L.vstrengthb		0.100				
		(0.406)				
L.vdiversity			-0.0492			
			(0.551)			
L.vstrenghtp				**-0.275*****		
				(0.004)		
L.vmodularity					-0.0589	
					(0.594)	
L.vassortativity						**-0.227****
						(0.027)
_cons	-0.322	-0.297	-0.228	0.961	0.00294	-0.244
	(0.110)	(0.475)	(0.353)	(0.197)	(0.996)	(0.338)

Table 3: Continued.

	Bipartite Networks			Projected Bipartite Networks		
	(1) vdegfon	(2) vstrengthb	(3) vdiversity	(4) vstrenghtp	(5) vmodularity	(6) vassortativity
N	**158**	**158**	**158**	**158**	**158**	**158**
R^2	**0.369**	**0.504**	**0.255**	**0.299**	**0.240**	**0.271**
adj. R^2	**0.226**	**0.410**	**0.086**	**0.140**	**0.068**	**0.106**
P-value	**0.00**	**0.00**	**0.01**	**0.00**	**0.01**	**0.01**
F	**3.520**	**9.374**	**1.938**	**3.443**	**1.877**	**1.840**

Nonstandardized coefficients. p-values in parentheses. $^{*}p < 0.1$, $^{**}p < 0.05$, and $^{***}p < 0.01$.

these circumstances, when two or more investors share the same financial assets and allocate their investments applying similar financial strategies and invest in the same market, the second-order effect of an external shock, as described earlier, could be a source of disturbance that affects the stability of a financial network.

Following the aforementioned, this study dynamically analyzes the phenomenon of overlapped portfolios by studying the aggregate behavior of the equity mutual funds industry in an emerging market context. These markets are characterized for having well-developed physical financial infrastructure such as central banks, commercial banks and stock exchanges, but at the same time, compared to developed markets, for having less well-developed processes and systems of accounting, governance, and regulation, and mainly less efficient markets with less liquidity [42]. Additionally, they possess a high level of property and control concentration of the firms [43], that becomes them sensible to this phenomenon, and their economic effects, especially during economic and financial downturns.

The main conclusion of this work is that in a developing economies context, the structure of the mutual fund network changes as consequence of external financial and economic factors, and as result of changes in the investment behavior of the entities of the network. Specifically, the topology of the bipartite network of funds and its one-mode projection, is dynamic over time and is correlated with variations in the investment strategies of mutual funds (hypothesis 1) and with industry-specific variables (hypothesis 2). From this perspective, changes in macroeconomic and financial conditions, in conjunction with changes in the mutual fund's industry context, promote changes in the funds' investment strategies, that trigger modifications in the fund's network structure.

On the other hand, we believe that there is an interesting vein of study that consists of studying the richness of the information contained in the directed network from the resulting one-mode projection. An analysis of the structural diversity of the network of interdependencies between funds using the assortative or dissassortative nature of the edges that compose it [44], would reveal interesting information on changes in dependence and influence between components of the industry.

Our results evidence new factors that alter the stability and the systemic risk of financial systems that have not yet been studied by the literature in this segment of institutional investors in an emerging market. These results are interesting because the equity portfolios we analyzed in this study fall within the characteristic of overlapped portfolios, confirming the existence of a channel of contagion generated by the aggregate investment behavior of the entities belonging to the network. Similar results are showed by the network literature that study the effects of the interconnectedness of financial institutions and the propagation of shocks over the systemic risk of the financial market [40, 41, 45]. From a policy and regulator point of view, this evidence highlights that improving the knowledge of overlapping portfolios in emerging markets, is a fundamental element to a better understanding of the risks and magnitudes of financial and economic contagions with respect to the likelihood of their occurrence and extension, and their relation to the number and density of the connections within the financial system.

From a financial perspective, our research is related to the study of herding among investors. As this literature states, this phenomenon can exacerbate the volatility levels in the market, destabilizing it, increase the fragility of the financial system, and eventually, generate assets bubbles [46]. This line of research indicates that under certain financial and market conditions, investors exhibit herd behavior in which they do not only apply the same investment strategies of their peers, but they also copy their same buy and sell decisions of financial assets [33, 47, 48]. To our best understanding, the channel evidenced in this study has not yet been linked to the herd behavior literature, despite having similarities. For example, the level of herd behavior among mutual funds increases during high periods of volatility and price downturns [39], precisely when financial shocks disturb the markets. An alternative to study the problem of herding could consider a more detailed analysis of the assortativity of the bipartite network of funds and stocks when considering higher order assortativity measures that could describe new topological characteristics of the network [49].

Gaining a deeper knowledge of how herding could influence the structure of the mutual funds networks will facilitate a better comprehension of the channels for transmission of the systemic risk associate with this financial behavior. However, the financial literature has studied mutual funds extensively for both their size and importance in the delegated portfolio management industry, we believe that this venue of research in conjunction with the perspective of network analysis, has much to contribute to the preservation of the financial stability, especially in developing markets.

Appendix

Relationship between the Bipartite Network and Its Projection in the Mutual Funds Domain

This appendix shows the relationship between a bipartite network of mutual funds and stocks, and their corresponding projection using the Zhou et. al. [15] method. For this, we take as an example three simple bipartite networks, in which there are two mutual funds, MF1 and MF2, which invest in three possible stocks, namely S1, S2 and S3.

Figure 4(a), shows the three bipartite networks and their respective projections in the mutual funds domain in Figure 4(b). For clarity of notation, we will distinguish w_{ij} as the weight of the bipartite network between the mutual fund i and stock j, while w^p_{ik} is the weight of the directed network, resulting from the projection of the bipartite network, indicating the influence that the mutual fund k has on the mutual fund i (or that it is the same, the mutual fund i dependence of the mutual fund k).

In case 1, we have that mutual funds are equally exposed since they invest the same amount of money on all the three stocks. In this case, there is a symmetrical weighted bipartite network. Thus, the weights $w_{ij} = 1$ of the bipartite network for funds $i = 1, 2$ and for stocks $j = 1, 2, 3$. It is not surprising that the corresponding projection indicates that $w^p_{12} = w^p_{21}$. That is, the influence that the MF1 fund has on the MF2 fund (given by w^p_{21}) is the same as the influence that MF2 has on MF1 (given by w^p_{12}).

In case 2, MF1 invests an equal sum of money in the three stocks, so that $w_{ij} = 10$ for $j = 1, 2, 3$. However, MF2 also invests in the three stocks equitably, but one tenth of what MF1 does, so $w_{2j} = 1$ for $j = 1, 2, 3$. In this case, mutual funds invest their money in the same assets, but in asymmetrical way. The result of the projection is such that $w^p_{21} = 10$, while $w^p_{12} = 0.1$. In other words, the influence that MF1 has on MF2 is 100 times greater than the influence that MF2 has on MF1. This indicates that a highly exposed mutual fund with a high investment and diversification in assets in relation to another well diversified mutual fund, but not so exposed in terms of money in the same assets, produces in the projection a high value of strength, indicating the strong effect of the influence of the first mutual fund over the rest.

Case 3 is different, MF1 is more diversified than MF2, but less exposed in their allocations. That is to say, the weights of the bipartite network are asymmetrical as well as the connections, because the degree of MF2 is different from the degree of MF1. Thus, in this case, $w_{1j} = 1$ for all $j = 1, 2, 3$, and $w_{23} = 10$ while $w_{21} = w_{22} = 0$. MF1 is less exposed, but it is well diversified, while MF2 is highly exposed but poorly diversified. The projection result indicates that $w^p_{21} = 0.1$ and $w^p_{12} = 0.43$. In this case, the influence that MF2 has on MF1 is 4.3 times stronger than the influence that MF1 has on MF2. This is because, even when MF2 is not very diversified, it has a high amount of investment in S3. As we increase the exposure values of MF1 but keeping its diversification, the influence of MF2 in relation to MF1 will decrease, until MF1 becomes more influential than MF2.

Data Availability

The data used to support the findings of this study are available from the corresponding author upon request.

Conflicts of Interest

The authors declare that they have no conflicts of interest regarding the publication of this paper.

Acknowledgments

The authors would like to thank CONICYT-Chile under grant Fondecyt 11160072 (Mauricio A. Valle), for financially supporting this research.

Endnotes

1. The impact of financial assets on the propagation of shocks is a significant subject in risk analysis. Although most of the literature on financial networks concentrates on the analysis of interbank loans networks and its response to shocks at assets level, for example, fire-sales; the propagation of shocks through more densely connected networks, such as the networks established through financial assets is greater. Delpini and others [8] indicated that as a consequence of a more diversified pattern of investment – like in pension funds and mutual funds – a more densely connected network serves as a mechanism of propagation of shocks, increasing systemic risk as a result.

2. ICI Fact Book 2017 (www.icifactbook.org).

3. For example, by analyzing the degree distribution and strength of the stocks in a portfolio, it may be determined whether the classic characteristic of free scale property is fulfilled, in which most of the stocks are in the hands of a few funds and where many funds have a few stocks.

4. Using exact positions of each stock over time allows us to avoid their inference from the financial reports of each mutual fund, thereby avoiding unrealistically dense networks and biased underestimation of systemic risk [5].

5. For any period of time of the bipartite network, the sum of all the strengths of the funds must be equal to the sum of the strengths of the stocks. That is equivalent to saying that the amount of money invested by the funds must be the same as the amount of money that is invested in the stocks. For the projection of the bipartite network in mutual funds, the mean of the in-strength is the same as the mean of the out-strength, since the direction in which an edge enters a node is equivalent to the direction in which another node exits, which is why the all the resources are retained in the system.

6. We use March 2009 as a reference point because the S&P 500 Index reached 666.79 points, being this value the minimum during the financial crisis.
7. During this period, the stocks markets experienced the worst performance in terms of return and volatility.

References

[1] A. G. Haldane, "Rethinking the financial network," in *Fragile Stabilität – stabile Fragilität*, pp. 243–278, 2013.

[2] R. Greenwood, A. Landier, and D. Thesmar, "Vulnerable banks," *Journal of Financial Economics*, vol. 115, no. 3, pp. 471–485, 2015.

[3] P. Glasserman and H. P. Young, "Contagion in financial networks," *Journal of Economic Literature*, vol. 54, no. 3, pp. 779–831, 2016.

[4] M. Pollak and Y. Guan, "Partially overlapping ownership and contagion in financial networks," *Complexity*, vol. 2017, Article ID 9895632, 16 pages, 2017.

[5] M. J. Straka, G. Caldarelli, T. Squartini, and F. Saracco, "From ecology to finance (and back?): recent advancements in the analysis of bipartite networks," *Journal of Statistical Physics*, vol. 173, no. 3-4, pp. 1252–1285, 2018.

[6] M. Elliott, B. Golub, and M. O. Jackson, "Financial networks and contagion," *American Economic Review*, vol. 104, no. 10, pp. 3115–3153, 2014.

[7] F. Caccioli, P. Barucca, and T. Kobayashi, "Network models of financial systemic risk: a review," *Journal of Computational Social Science*, vol. 1, no. 1, pp. 81–114, 2017.

[8] D. Delpini, S. Battiston, G. Caldarelli, and M. Riccaboni, "The Network of US Mutual Fund Investments: Diversification, Similarity and Fragility throughout the Global Financial Crisis," 2018, https://arxiv.org/abs/1801.02205.

[9] H. Markowitz, "Portfolio selection," *The Journal of Finance*, vol. 7, no. 1, pp. 77–91, 1952.

[10] P. Glasserman and H. P. Young, "How likely is contagion in financial networks?" *Journal of Banking & Finance*, vol. 50, pp. 383–399, 2015.

[11] S. Battiston, J. B. Glattfelder, D. Garlaschelli, F. Lillo, and G. Caldarelli, "The structure of financial networks," in *Network Science*, pp. 131–163, Springer, London, UK, 2010.

[12] S. Battiston and M. Catanzaro, "Statistical properties of corporate board and director networks," *The European Physical Journal B*, vol. 38, no. 2, pp. 345–352, 2004.

[13] S. Battiston, J. F. Rodrigues, and H. Zeytinoglu, "The network of inter-regional direct investment stocks across Europe," *Advances in Complex Systems (ACS)*, vol. 10, no. 1, pp. 29–51, 2007.

[14] M. Boss, H. Elsinger, M. Summer, and S. Thurner, "Network topology of the interbank market," *Quantitative Finance*, vol. 4, no. 6, pp. 677–684, 2004.

[15] T. Zhou, J. Ren, M. Medo, and Y. C. Zhang, "Bipartite network projection and personal recommendation," *Physical Review E: Statistical, Nonlinear, and Soft Matter Physics*, vol. 76, no. 4, Article ID 046115, 2007.

[16] A. Barrat, M. Barthélemy, R. Pastor-Satorras, and A. Vespignani, "The architecture of complex weighted networks," *Proceedings of the National Acadamy of Sciences of the United States of America*, vol. 101, no. 11, pp. 3747–3752, 2004.

[17] E. F. Fama and K. R. French, "The cross-section of expected stock returns," *The Journal of Finance*, vol. 47, no. 2, pp. 427–465, 1992.

[18] M. M. Carhart, "On persistence in mutual fund performance," *Journal of Finance*, vol. 52, no. 1, pp. 57–82, 1997.

[19] K. J. M. Cremers and A. Petajisto, "How active is your fund manager a new measure that predicts performance," *Review of Financial Studies*, vol. 22, no. 9, pp. 3329–3365, 2009.

[20] A. Petajisto, "Active share and mutual fund performance," *Financial Analysts Journal*, vol. 69, no. 4, pp. 73–93, 2013.

[21] J. Lavin and N. Magner, "Reversing the question: on what does the turnover of mutual funds depend? evidence from equity mutual funds in Chile," *Emerging Markets Finance & Trade*, vol. 50, no. 5, pp. 110–129, 2014.

[22] A. Khorana, H. Servaes, and P. Tufano, "Explaining the size of the mutual fund industry around the world," *Journal of Financial Economics*, vol. 78, no. 1, pp. 145–185, 2005.

[23] L. Stracca, "Delegated portfolio management: A survey of the theoretical literature," *Journal of Economic Surveys*, vol. 20, no. 5, pp. 823–848, 2006.

[24] C. E. Shannon, "A mathematical theory of communication," *Bell Labs Technical Journal*, vol. 27, pp. 379–423, 1948.

[25] L.-F. Bersier, C. Banašek-Richter, and M.-F. Cattin, "Quantitative descriptors of food-web matrices," *Ecology*, vol. 83, no. 9, pp. 2394–2407, 2002.

[26] M. Newman and M. Girvan, "Finding and evaluating community structure in networks," *Physical Review E*, vol. 69, no. 2, pp. 1–16, 2004.

[27] M. E. Newman, "Mixing patterns in networks," *Physical Review E: Statistical, Nonlinear, and Soft Matter Physics*, vol. 67, no. 2, Article ID 026126, 2003.

[28] R. Albert and A. Barabási, "Statistical mechanics of complex networks," *Reviews of Modern Physics*, vol. 74, no. 1, pp. 47–97, 2002.

[29] E. Estrada and P. Knight, *A First Course in Network Theory*, Oxford University Press, USA, 2015.

[30] M. Newman, "Assortative mixing in networks," *Physical Review Letters*, vol. 89, no. 20, Article ID 208701, 2002.

[31] G. Rotundo and A. M. D'Arcangelis, "Ownership and control in shareholding networks," *Journal of Economic Interaction and Coordination*, vol. 5, no. 2, pp. 191–219, 2010.

[32] G. De Masi, G. Iori, and G. Caldarelli, "Fitness model for the Italian interbank money market," *Physical Review E: Statistical, Nonlinear, and Soft Matter Physics*, vol. 74, no. 6, Article ID 066112, 2006.

[33] M. Grinblatt, S. Titman, and R. Wermers, "Momentum investment strategies, portfolio performance, and herding: A study of mutual fund behavior," *The American Economic Review*, pp. 1088–1105, 1995.

[34] J. Eberhard, J. F. Lavin, and A. Montecinos-Pearce, "A network-based dynamic analysis in an equity stock market," *Complexity*, vol. 2017, Article ID 3979836, 16 pages, 2017.

[35] J. Y. Campbell, C. Polk, and T. Vuolteenaho, "Growth or glamour? Fundamentals and systematic risk in stock returns," *Review of Financial Studies* , vol. 23, no. 1, pp. 305–344, 2010.

[36] Ľ. Pástor and R. F. Stambaugh, "Liquidity risk and expected stock returns," *Journal of Political Economy*, vol. 111, no. 3, pp. 642–685, 2003.

[37] V. A. Warther, "Aggregate mutual fund flows and security returns," *Journal of Financial Economics*, vol. 39, no. 2-3, pp. 209–235, 1995.

[38] M. Grinblatt, S. Titman, and R. Wermers, "Momentum investment strategies, portfolio performance, and herding: a study of

mutual fund behavior," *American Economic Review*, vol. 85, no. 5, pp. 1088–1105, 1995.

[39] J. F. Lavin and N. S. Magner, "Herding in the mutual fund industry: evidence from Chile," *Academia Revista Latinoamericana de Administracion*, vol. 27, no. 1, pp. 10–29, 2014.

[40] R. Cerqueti, G. P. Clemente, and R. Grassi, "Systemic risk assessment through high order clustering coefficient," 2018, https://arxiv.org/abs/1810.13250.

[41] M. D'Errico, D. Felletti, and R. Grassi, "Shock propagation and the topology of complex networks," Tech. Rep., Dipartimento di Metodi Quantitativi per le Scienze Economiche ed Aziendali, Università degli studi di Milano Bicocca Working Papers, 2010.

[42] C. Kearney, "Emerging markets research: Trends, issues and future directions," *Emerging Markets Review*, vol. 13, no. 2, pp. 159–183, 2012.

[43] M. P. Abreu, R. Grassi, and R. R. Del-Vecchio, "Structure of control in financial networks: An application to the Brazilian stock market," *Physica A: Statistical Mechanics and Its Applications*, vol. 522, pp. 302–314, 2019.

[44] J. G. Foster, D. V. Foster, P. Grassberger, and M. Paczuski, "Edge direction and the structure of networks," *Proceedings of the National Acadamy of Sciences of the United States of America*, vol. 107, no. 24, pp. 10815–10820, 2010.

[45] G. P. Clemente, R. Grassi, and C. Pederzoli, "Networks and market-based measures of systemic risk: the European banking system in the aftermath of the financial crisis," *Journal of Economic Interaction and Coordination*, pp. 1–23, 2019.

[46] S. Bikhchandani and S. Sharma, "Herd behavior in financial markets," *IMF Staff Papers*, vol. 47, no. 3, pp. 279–310, 2000.

[47] J. Lakonishok, A. Shleifer, and R. W. Vishny, "The impact of institutional trading on stock prices," *Journal of Financial Economics*, vol. 32, no. 1, pp. 23–43, 1992.

[48] R. Wermers, "Mutual fund herding and the impact on stock prices," *The Journal of Finance*, vol. 54, no. 2, pp. 581–622, 1999.

[49] A. Arcagni, R. Grassi, S. Stefani, and A. Torriero, "Higher order assortativity in complex networks," *European Journal of Operational Research*, vol. 262, no. 2, pp. 708–719, 2017.

Hindawi
Complexity
Volume 2019, Article ID 2946018, 12 pages
https://doi.org/10.1155/2019/2946018

Research Article

Nonlinear Dynamics Characteristic of Risk Contagion in Financial Market Based on Agent Modeling and Complex Network

Binghui Wu [1] **and Tingting Duan** [2]

[1] *International Business School, Shaanxi Normal University, Xi'an 710119, China*
[2] *School of Marxism, Northwestern Polytechnical University, Xi'an 710072, China*

Correspondence should be addressed to Binghui Wu; vcmd@163.com

Received 20 February 2019; Accepted 28 May 2019; Published 11 June 2019

Guest Editor: Thiago C. Silva

Risk contagion is becoming a research hotspot in the field of econophysics with the rise of interdisciplinary studies and gains more and more attention from theoretical circles and practical departments. This paper proposes a new research frame to discuss the microscopic mechanism of risk contagion based on agent modeling technology and complex network theory and reveals nonlinear dynamics characteristic of risk contagion from the perspective of market participants in financial market. Based on the proposed SICM model, financial risk can transmit from susceptible agents to infected agents, to contagious agents, or to immune agents. With the increases of contagious probabilities, the simulation experiments show that (1) the amount of susceptible agents continuously decreases; (2) the amount of infected agents increases first and then decreases; (3) the amount of contagious agents increases first and then decreases with a lower speed, relative to the amount of infected agents; and (4) the amount of immune agents continuously increases. The major contribution of this paper is a new method for studying nonlinear dynamics characteristic of risk contagion, which can be used as a theoretic basis for further researches on the behavioral features of microcosmic subject and the inner mechanisms of risk contagion.

1. Introduction

With the rapid development of society, the financial industry has gotten more attention and support from governments. Because the financial development can obviously promote the economy development in theory and practice, governments around the world have always committed to developing domestic finances, especially in financial markets and financial institutions. Many world economic centers can lead the development direction of globe economy because they also serve as world financial centers, such as New York, London, and Hong Kong. But due to the influence of financial risks, the development of finance has not been smooth. Many famous financial crises are still remembered by market participants, for example, Asian financial crisis in 1997, American subprime crisis in 2008, and European debt crisis in 2009. These serious international financial crises brought many destructive impacts on the world economy in the past. In essence, the outbreaks of financial crises are always the results of risk transmission and risk accumulation in financial markets. Therefore, the research of risk contagion not only has significant theoretical values to reveal the interaction mechanisms of participants in financial markets, but also great practical values for the prevention of financial risks for governments.

In the existing literature, a part of researchers mainly focus on the fluctuation of asset prices, which causes the transmission of financial risk from one market to another. Although these researches often adopt empirical analysis method, the behavioral features of microcosmic subject are not well revealed. And another part of researchers depend on complex network theory and agent modeling technology to analyze risk contagion in financial markets. These findings

are more focused on the design of network structure and the construction of artificial financial market.

The contributions of this paper are twofold. First, we propose a new model of risk contagion based on agent modeling and complex network, which can explain the nonlinear dynamics characteristics of risk contagion from the aspect of microcosmic subject in financial market, compared with the existing literature. In simulation experiments, we discuss the interaction process of investor behavior and the dynamic evolution mechanism of risk contagion. The second contribution of this paper is a theoretic expansion of risk contagion. The contagious model built in this paper is a basic theory model, which can explain risk contagion caused by interaction behaviors of market participants. For different types of financial markets, this theoretic model can be used as a basis for discussing the investor behavior and the resulting risk contagion. The remainder of this paper is organized as follows. Section 2 gives a brief review about the existing literature of risk contagion in financial market. Subsequently, Section 3 presents the theoretical model of risk contagion. Next, Section 4 conducts a series of simulation experiments that discusses the evolution characteristics of risk contagion. Finally, Section 5 concludes the work and points out the direction for future researches.

2. Literature Review

The underlying mechanism of risk contagion can hardly be explained from traditional finance theories because risk contagion shows some characteristics, such as global influences, systematic influences, and interactive influences [1]. Global influences indicate that financial risk may well transmit to neighbor region from original region and ultimately to spread from one country to another. And systematic influences emphasize that risk contagion probably causes multiple crises in many financial markets, such as debt crisis, liquidity crisis, and credit crisis. At last, interactive influences involve two parts: the interaction between commodity market and financial market and the interaction among different participants. For the researches on risk contagion in financial markets based on agent modeling and complex network, the literature reviews are shown from the following three aspects.

2.1. The Researches of Risk Contagion in Financial Markets. The early scholars often explained risk contagion in financial markets from the perspective of international trades, economic fundamentals, and international capital flows [2–8]. In international trades, a country could increase its international competitiveness of goods and services through a devaluation. And the successive devaluations of different currencies caused the international transmission of financial risks in international scenes [9, 10]. For example, it was easy to be found that financial risks transmitted among the countries having closer trade ties, after analyzing three decades of panel data coming from industrialized nations [11]. And the worse economic fundamentals easily led to risk contagion from economic fields to financial fields [12]. When a financial crisis broke out in a country, the economic fundamentals of neighbor countries began deteriorating generally. The process of risk contagion involved three effects: monsoonal effects, spillovers effects, and pure contagion effects [13]. However, international capital inflows could not always promote economic growth. When the domestic economy was overheating, international capital inflows would increase the appreciation pressure of domestic currency and then realize risk contagion among different countries [14]. Besides, more scholars increasingly focused on the behaviors of market participants to explain the inner mechanism of risk contagion. They gave up the hypothesis of rational economic man and insisted that the investor had the bounded rationality [15–18]. In the framework of bounded rationality, investors were mainly divided into two kinds: rational traders and noise traders [19–22]. Essentially, noise was a signal caused by the shortcomings of market mechanisms or the decision-making mistakes of market subjects [23]. A small-scale noise trader could increase market liquidity, but a large-scale noise trader was likely to cause excessive price fluctuations in financial markets [24–26]. Moreover, rational traders and noise traders were not unchangeable. And in some cases, rational traders likely turned into noise traders [27]. On the basis of the hypothesis of bounded rationality, the more researches explained risk contagion in financial markets from the perspective of investor behavior bias, such as equity premium puzzle [28–30], idiosyncratic volatility puzzle [31–33], closed-end fund puzzle [34–36], and dividend puzzle [37–39]. In addition, the cognitive bias and irrational behavior of investors were often associated with overconfidence theory. But the studies found that the irrational behaviors of overconfident investors did not generate excess returns in the long term [40, 41]. Furthermore, the behaviors of institutional investors could make a dramatic impact on risk contagion. As institutional investors had larger amounts of money and professional investment strategies, the herd behaviors of institutional investors were easily observed in financial markets [42, 43].

2.2. The Application of Agent Modeling in Financial Markets. The study of risk contagion was always based on efficient market hypothesis and rational expectation theory since long times ago. But in reality, the investor showed the obvious heterogeneity due to the differences of knowledge structure, analytical ability, and risk preference. And investor behavior became more complicated under the influence of interaction effects. It was difficult to reveal the dynamic characteristics of risk contagion for traditional analysis methods, such as theoretical analysis and empirical analysis [44–46]. However, agent modeling technology could solve this dilemma very well [47]. For example, a stochastic multiagent model was built to analyze risk contagion based on investors' mood fluctuations, and the results indicated that the return series showed the characteristics of heavy-tail distributions [48]. A key reason for heavy-tail distributions in financial markets was sheep-flock effect. After analyzing the relationship of peek distribution of return series, market transaction order, and investor imitation, the findings showed that the group decision was a common strategy among agents and the return series followed a power-law distribution [49, 50]. Chen and

Yeh modified the learning mechanism of SFI-ASM model and constructed an agent-based model of "school" in order to analyze the interaction mechanism of agents [51]. Based on [49], Iori paid more attention to individual decisions and found that agents tended to adjust their investment strategies according to an information set received at every time point [52]. Pascual et al. discussed the risk contagion and the heterogeneity of agents after adding psychological factors and emotive factors into artificial stock market model [53]. In addition, artificial stock market model was a common method to study risk contagion caused by the interactive behaviors of agents. For example, agents could be divided into three types: fundamental analysts, optimistic analysts, and pessimistic analysts, which transformed into any of types according to the changes of returns rates in financial markets [54]. Bertella constructed an artificial stock market including fundamental investors and technical investors and found that the volatility of stock price increased with the increasing heterogeneity of agents [55]. Besides, the high-frequency transaction data were usually used to build an artificial stock market in order to reveal the characteristics of risk contagion. By studying the relation between price restraint and risk contagion, the simulation experiment showed that both price ceiling and price floor led to the spillover effect of financial risks [56]. Based on SFI-ASM model, Liu and Han constructed a multiagent stock market model and found that the volatility of stock returns was decreasing with the increasing of simulation period [57].

2.3. The Application of Complex Network in Financial Markets. Complex network theory originated from the study on Seven Bridges of Königsberg [58]. Along with the increasing development of complex network theory, more and more scholars tried to apply this theory to financial markets and studied the inner mechanism of risk contagion [59–61]. Taking stock market as an example, a stock can be abstracted as an agent in a complex network, and the correlation coefficient between two stocks can be seen as an edge in this network. Thus, both agents and edges together form a complex network. Mantegna built a complex network model through the minimum spanning tree algorithm and analyzed risk contagion in stock market [62]. On the basis of [62], the results from Bonanno et al. indicated that the network structure of stock market followed a power-law distribution after analyzing the difference between the minimum spanning tree model and the real stock market model [63]. On a scale-free network, the network structure was changing with the adjustment of threshold value [64]. In addition, the closing price in financial market was often used for studying risk contagion. Emmertstreib and Dehmer used the daily closing price data to investigate the formation of network structure and the dynamic evolutionary process of financial network [65]. Some researchers found that financial market probably had the small-world feature. For example, after analyzing the correlation coefficients between different stocks in Chinese stock market, Li and Li found the obvious small-world feature in Chinese stock market and discussed the interaction effect among different stocks and the risk contagion caused by stock price variation [66]. The similar conclusions could be found from [67], which found the small-world feature of Chinese stock market by building a complex network model based on multiagent modeling. Besides, the changing investor attention could cause the fluctuation of asset price and the intensity of herd behavior in a small-world network [68]. Under the background of global financial crisis, financial risk was easier to transmit from one investor to another. By using stock prices in the Korean stock, Nobi discussed the characteristics of risk contagion, during and after 2008 global financial crisis, based on the hierarchical network and the minimum spanning tree algorithm [69]. Network linkage played a major role in the process of formatting network structure. The dynamic conditional correlations method could be used to study network linkage effects of financial market, especially in stock market. By using the GMM model, Qiao discussed the influences of inner nodes in different positions on stock returns and found that financial risks were easier to transmit from the central area to the marginal area of network [70].

3. Theoretical Model

The researches on transmission dynamics are always the focuses and forefront projects in the academic world. By means of complex network theory, many scholars explain microscopic mechanisms and dynamic characteristics of some practical issues in society. For example, complex network can be used to reveal the transmission mechanism of computer viruses [70–72], the spread process of epidemics [73, 74], and the diffusion intensity of rumor [72, 75]. For the researches on dynamics of complex network, many research achievements are based on the traditional model of virus spread, such as epidemic models. This part introduces the classic infection models at first and then constructs the new risk contagious model in financial market based on agent modeling and complex network.

3.1. The Basis Theoretical Model. In order to reveal the transmission mechanism of complex networks, some theoretical models are gradually developed on the basis of the theory of epidemics, such as SI model, SIS model, SIRS model, SEIR model, and so on. In above models, every agent is probably in a different state in different time points. The main states can be classified into susceptible states, infected states, exposed states, resistant states, etc. Concretely speaking, susceptible states indicate that agents are not infected yet in a model, but they are probably infected by viruses in subsequently time. Infected states show that agents are infected by viruses, and they tend to spread the viruses to others. Exposed states emphasize that agents may keep latent states instead of becoming the infected states, after contacting with viruses. Resistant states contain two types of situations: (1) agents gain the immunity to viruses owing to vaccine injection or rehabilitation and (2) agents are removed from a model owing to the death. No matter which type of situations, agents are no longer able to continue to spread the viruses.

In SI model, all agents are assumed not to be immune to viruses. Thus, they are in susceptible states or infected

states. Without immunity, an agent is likely to immediately transform into infected state from susceptible state, after virus exposure. Considering all agents are impossible to be infected at the same time in the practical studies, the SI model is only applicable for the early stages of virus outbreak. Suppose that the total of agents is invariant, written as N. The percentage of agents in susceptible states is s(t), and the percentage of agents in infected states is i(t). The contagious probability of agents from susceptible states to infected states is assumed as α. That means the agents in infected states will increase $\alpha \cdot s(t) \cdot Ni(t)$. The relationship of above variables is shown in expression (1), which can be further simplified as expression (2):

$$\frac{dNi(t)}{dt} = \alpha \cdot s(t) \cdot Ni(t) \tag{1}$$

$$\frac{di(t)}{dt} = \alpha \cdot s(t) \cdot i(t) \tag{2}$$

Although SI model reflects the basic process of virus spread, it does not take into account the immunity to viruses for an agent. In SIS model, an infected agent is probably cured under a certain probability and returns to the susceptible state from infected state. In addition, an agent who is cured after catching a viral influenza is likely to be infected again in daily life. Let us suppose that β is the transformation probability of agents from cured states to susceptible states. In comparison with SI model, the agents in infected states decrease $\beta \cdot Ni(t)$ in every moment in SIS model. So, the amount of agents in infected states can be expressed as follows:

$$\frac{dNi(t)}{dt} = \alpha \cdot s(t) \cdot Ni(t) - \beta \cdot Ni(t) \tag{3}$$

Obviously, expression (3) can be simplified and written as

$$\frac{di(t)}{dt} = \alpha \cdot i(t)[1 - i(t)] - \beta i(t) \tag{4}$$

Compared with SIS model, SIR model considers the problem of virus immune. A cured agent in infected state will gain immunity to virus and stop spreading virus to other agents. Let us suppose that γ is the transformation probability of agents from infected states to resistant states, and $r(t)$ is the percentage of agents in resistant states. The dynamic characteristics of SIR model can be described as follows:

$$\begin{aligned} \frac{ds(t)}{dt} &= -\alpha i(t) s(t) \\ \frac{di(t)}{dt} &= \alpha i(t) s(t) - \gamma i(t) \\ \frac{dr(t)}{dt} &= \gamma i(t) \end{aligned} \tag{5}$$

However, agents in resistant states may lose their immunity with a probability and enter into susceptible states again. This probability is assumed as p in SIRS model, where the agents in susceptible states increase $pr(t)N$ relative to SIR model. Conversely, the agents in resistant states decrease $pr(t)N$. So, it is not difficult to find that SIRS model is an extension of SIR model. The dynamic characteristics of SIRS model can be described as follows:

$$\begin{aligned} \frac{ds(t)}{dt} &= -\alpha i(t) s(t) + pr(t) \\ \frac{di(t)}{dt} &= \alpha i(t) s(t) - \gamma i(t) \\ \frac{dr(t)}{dt} &= \gamma i(t) - pr(t) \end{aligned} \tag{6}$$

In addition, agents in susceptible states are probably not immediately infected after contacting with viruses. In other words, agents may enter into exposed states. In SEIR model, there are two probability parameters, ε and θ. To be specific, agents enter into exposed states from susceptible states with probability ε, and then they enter into infected states from exposed states with probability θ. Finally, they enter into resistant states with probability γ. Similarly, we assume the percentage of agents in exposed states is $e(t)$. The dynamic characteristics of SEIR model can be described as follows:

$$\begin{aligned} \frac{ds(t)}{dt} &= -\varepsilon i(t) s(t) \\ \frac{de(t)}{dt} &= \varepsilon i(t) s(t) - \theta e(t) \\ \frac{di(t)}{dt} &= \theta i(t) s(t) - \gamma i(t) \\ \frac{dr(t)}{dt} &= \gamma i(t) \end{aligned} \tag{7}$$

3.2. The Risk Contagious Model. Based on the above models, this paper assumes there are four kinds of agents in financial market: susceptible agents, infected agents, contagious agents, and immune agents. These four kinds of agents are abbreviated to S, I, C, and M. In a complex network structure, S, I, C, and M can also be seen as network nodes. S, as a susceptible agent, who is likely to receive some grapevine in market, has not yet received it. And I, as an infected agent, has received a grapevine, but has not made a decision about whether or not to spread this grapevine. If the final decision is spread, infected agent (I) will transform into contagious agent (C). If not, infected agent (I) will transform into immune agent (M). According to the relationship of different network nodes, the risk contagious model is constructed and written as SICM model. The process of risk contagion is shown in Figure 1.

In Figure 1, an agent is presumed to have an unofficial grapevine at the initial moment. This grapevine can be seen as a risk event in financial market. Other agents around this agent have an opportunity to get this grapevine and become susceptible agents. Then susceptible agents will transform into infected agents with probability x_1. If infected agents accept this grapevine, they will become contagious agents with probability x_2. And if not, they will become immune agents with probability x_3. After a while, contagious agents will lose interest in this grapevine and decide not to continue spreading it to other agents. At this time, contagious agents probably become immune agents with probability x_4.

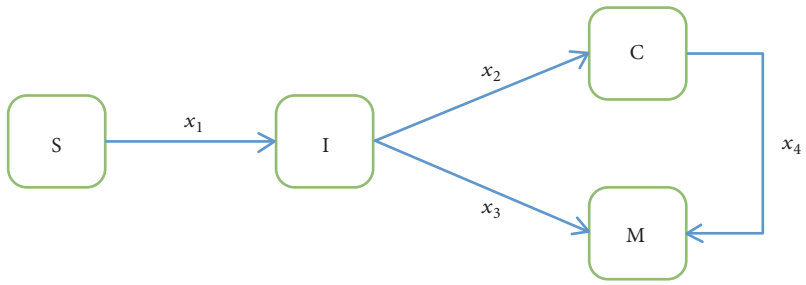

Figure 1: The process of risk contagion based on SICM model.

In our model, the sum total of market participants is assumed to be invariable at any time and written as N. The amount of each type of agents is expressed as S(t), I(t), C(t), and M(t) at time t, respectively. Similarly, the percentages of each type of agents are represented as s(t), i(t), c(t), and m(t) at time t, respectively. The above relationship can be described as follows:

$$S(t) + I(t) + C(t) + M(t) = N \tag{8}$$

$$s(t) + i(t) + c(t) + m(t) = 1 \tag{9}$$

According to the contagious mechanism of SICM model, the dynamic characteristics are shown as follows:

$$\begin{aligned} \frac{ds(t)}{dt} &= -x_1 s(t) c(t) \\ \frac{di(t)}{dt} &= x_1 s(t) c(t) - x_2 i(t) - x_3 i(t) \\ \frac{dc(t)}{dt} &= x_2 i(t) - x_4 c(t) \\ \frac{dm(t)}{dt} &= x_3 i(t) + x_4 c(t) \end{aligned} \tag{10}$$

Expression (10) actually includes four differential equations, which, respectively, represent the rate of change of s(t), i(t), c(t), and m(t) with time t. In order to reflect the microcosmic mechanism of risk contagion in financial market based on SICM model, we try to design the simulation experiments in the next section.

4. The Simulation Experiments

In our simulation experiments, there is only one agent in contagious state; the rest of agents are in susceptible states at initial time. On the basis of the risk contagious model, two basic conclusions can be drawn before the simulation experiments [76]. The first conclusion is that the number of susceptible agents has a decreasing trend. And the second conclusion is that the number of contagious agents has an increasing trend. As for the changing characters of infected agents and immune agents in risk contagion, the conclusions will be drawn after the simulation experiments. Thus, the contagious probabilities of agents are set at first. And then the dynamic characteristics of different types of agents are simulated in the experiments. The baseline configuration is S(0)=N-1, I(0)=0, C(0)=1, M(0)=0, N=3000, x_1=0.005, x_2=0.10, x_3=0.20, and x_4=0.15. In the simulation process, once the number of agents no matter in whatever state is less than 0.0005, the experiment will be set to automatically stop. In this case, we assume that some kind of agent has all become other kinds. In Figure 2, the curve of I(t) and the curve of C(t) have the similar trends increasing first and then decreasing. When the number of I(t) is equal to 0.0004906, the experiment stops at time step 150.

In order to better reveal the influences of contagious probabilities on the process of risk contagion, we change the value of x_1, x_2, x_3, and x_4 in sequence and keep other parameters constant at the same time. The evolutionary characteristics of risk contagion are shown in Figures 3, 4, 5, and 6. The simulation experiments contain 5 cases in Table 1. And each case relates to each figure. For example, cases 1, 2, 3, 4 and 5 correspond to Figures 2, 3, 4, 5, and 6, respectively.

Firstly, x_1 is increased to 0.0010 from 0.0005 and other parameters remain unchanged, as described in Table 1. Likewise, the four curves of agents can be drawn and shown in Figure 3. The curve of S(t) has a similar feature in both Figures 2 and 3. In brief, the two curves of S(t) show a decreasing trend with a higher rate first and then a lower rate. But the other three curves have an obvious difference. In Figure 3, the amount of I(t) reaches a maximum with a faster speed at time step 25, and the curve of I(t) has a steeper trend. And the similar features are seen from the curve of C(t), which has a higher crest relative to Figure 2. For the curve of M(t), the amount of agents in infected states is greater than that in immune states before time step 22. Because of the increase of x_1, a grapevine can be spread to susceptible agents around a contagious agent with a higher probability. Considering that the grapevine is contacted by more agents in susceptible states, the running time of SICM model is shorted to time step 89 from time step 150 in Figure 3.

Secondly, x_2 is increased to 0.60 from 0.10, and other parameters are the same as the parameters in Figure 2. The change of x_2 directly affects the contagious effects from infected agents to contagious agents. More specifically, with a larger value of x_2, agents in infected states are likely to enter into contagious states with a higher probability. Thus, the curve of C(t) has a higher crest than the curve of I(t) in Figure 4, and the curve of C(t) in Figure 2. There are two intersections among the curve of M(t), the curve of I(t) and the curve of C(t). One is between the curve of M(t) and the

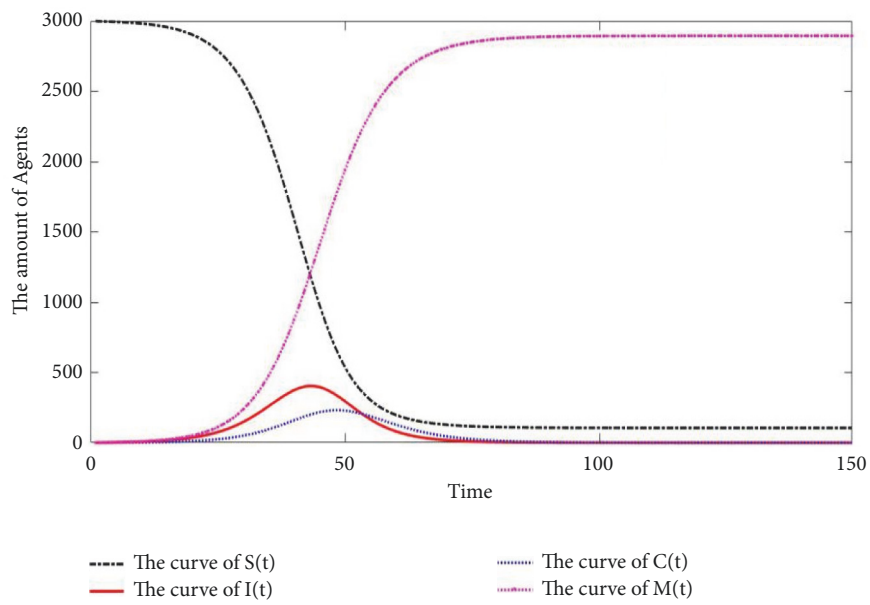

Figure 2: The evolutionary characteristics of risk contagion based on SICM model (Case 1).

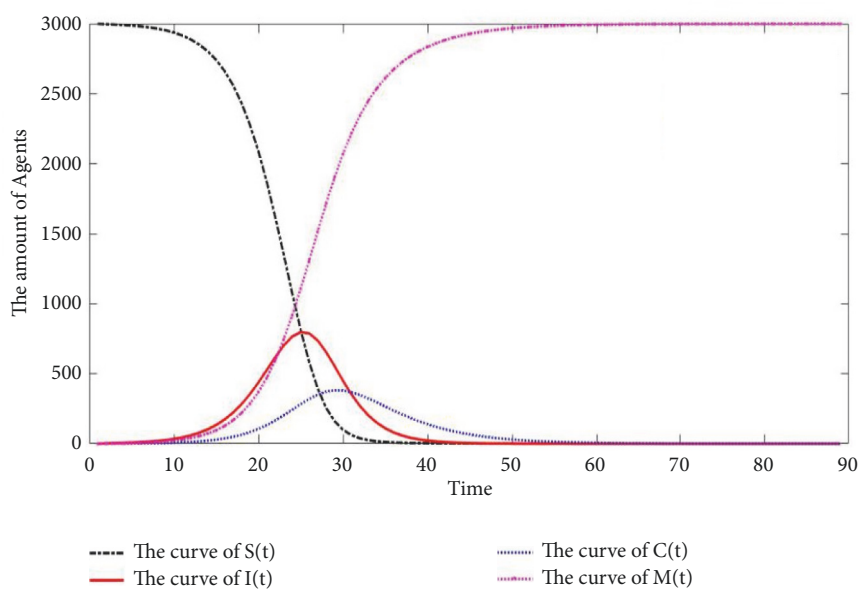

Figure 3: The evolutionary characteristics of risk contagion after increasing x_1 (Case 2).

curve of I(t), and the other intersection is between the curve of M(t) and the curve of C(t). To be specific, the amount of infected agents is larger than the amount of immune agents before time step 17 (including time step 17). And before time step 21 (including time step 21), the amount of contagious agents is larger than the amount of immune agents. But in general, the curve of M(t) shows an increasing trend and the curve of S(t) shows a decreasing trend. As an increasing x_2, the curve of I(t) decreases faster after time step 19, and the model comes to a stop at time step 60.

Thirdly, x_3 is increased to 0.20 from 0.30, and other contagious probabilities, x_1, x_2, and x_4, maintain the initial values of baseline configuration in Table 1. The obvious differences in Figure 5 manifest the curve of S(t) and the curve of M(t) compared with Figure 2. These two curves can be divided into two parts according to the trend characteristics in Figure 5. The two curves show a dramatic decrease or increase in the first stage ($0 \leq$ time step ≤ 90), and a very slow decrease or increase in the second stage ($90 \leq$ time step ≤ 179). For the curve of I(t), there is not a significant change in Figure 5, compared with that in Figure 2. And a similar conclusion can be drawn after analyzing the curve of C(t). As the increase of x_3 implies that susceptible agents become immune agents with a higher probability, the increasing

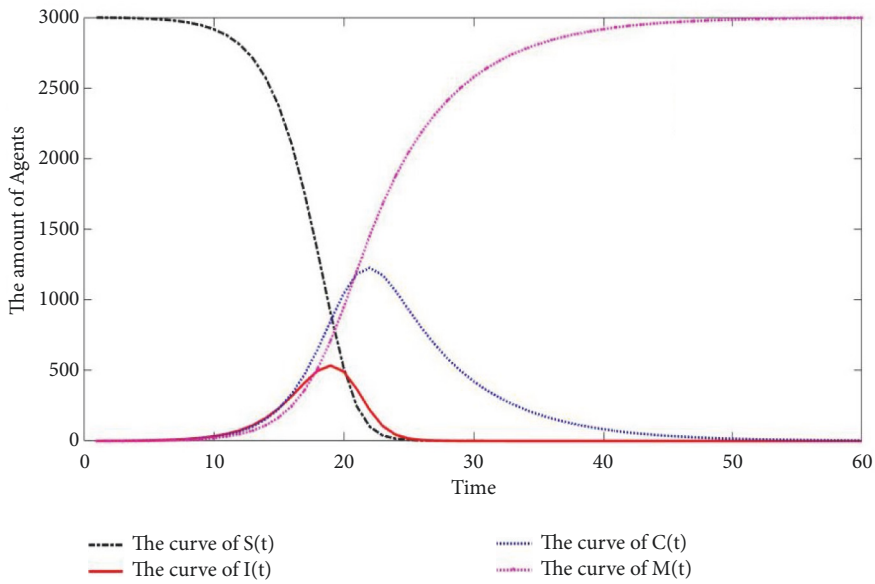

Figure 4: The evolutionary characteristics of risk contagion after increasing x_2 (Case 3).

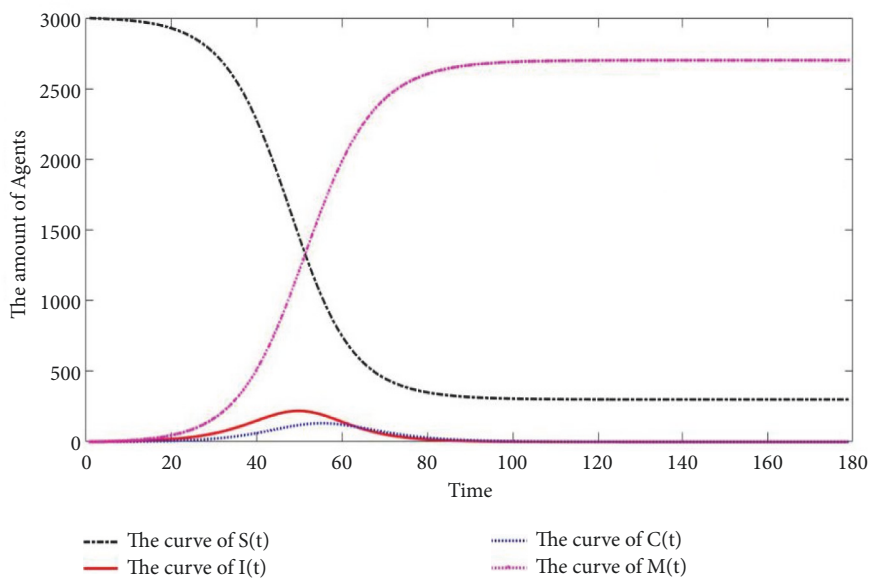

Figure 5: The evolutionary characteristics of risk contagion after increasing x_3 (Case 4).

Table 1: The features of parameters in different simulation environments.

Case	Parameters features	Initial parameters	
		(x_1, x_2, x_3, x_4)	$(S(0), I(0), C(0), M(0))$
Case 1	To keep all parameter values constant	(0.0005, 0.10, 0.20, 0.15)	$S(0) = 2999$; $I(0) = 0$; $C(0) = 1$; $M(0) = 0$.
Case 2	To increase the parameter value of x_1	(0.0010, 0.10, 0.20, 0.15)	
Case 3	To increase the parameter value of x_2	(0.0005, 0.60, 0.20, 0.15)	
Case 4	To increase the parameter value of x_3	(0.0005, 0.10, 0.30, 0.15)	
Case 5	To increase the parameter value of x_4	(0.0005, 0.10, 0.20, 0.25)	

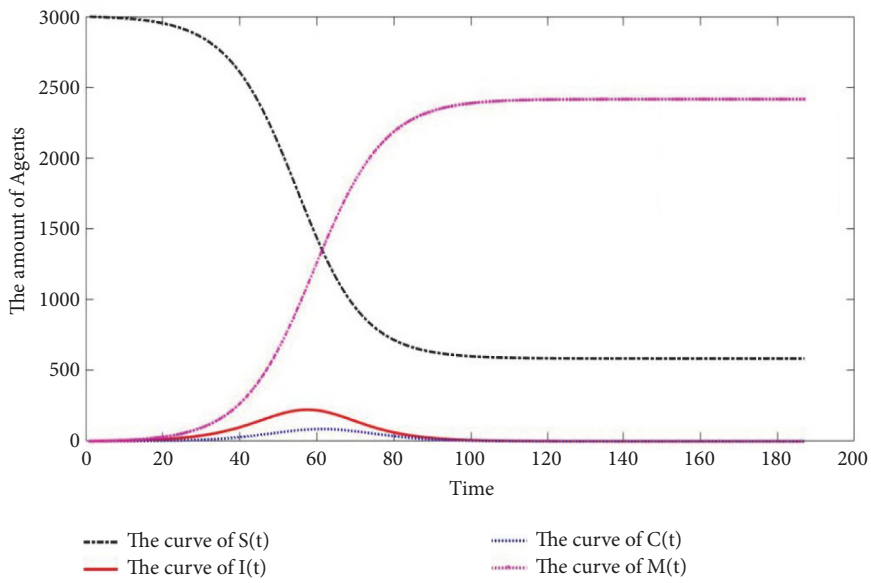

Figure 6: The evolutionary characteristics of risk contagion after increasing x_4 (Case 5).

Table 2: The evolutionary characteristics of agents after finishing simulation processes.

Case	Parameters feature	Running time step	The amount of agents			
			S(t)	I(t)	C(t)	M(t)
Case 1	To keep all parameter values constant	150	105.1358	0.0004906	0.0017	2894.8621
Case 2	To increase the parameter value of x_1	89	1.3262	0.0004985	0.0566	2998.6168
Case 3	To increase the parameter value of x_2	60	0.1921	0.0004809	3.2472	2996.5603
Case 4	To increase the parameter value of x_3	179	299.5044	0.0004789	0.0000959	2700.4942
Case 5	To increase the parameter value of x_4	187	584.3215	0.0006814	0.0004612	2415.6774

quantity of immune agents is slow in the second stage. Simultaneously, the decreasing quantity of susceptible agents is also slow in this stage. In Figure 5, the evolution process of risk contagion finally stops at time step 179.

Fourthly, x_4 is increased to 0.25, and other parameters are unchanged. The evolutionary characteristics of risk contagion are still displayed by the curves of agents, including the curve of S(t), the curve of I(t), the curve of C(t), and the curve of M(t). It is easy to be seen that both Figures 5 and 6 are similar in the trends of the corresponding curves. Because no matter which contagious probability is increased, x_3 or x_4, the final result is the increasing quantity of immune agents. According to Figure 1, there are two ways to make infected agents become immune agents: (1) I⟶M and (2) I⟶C⟶M. As the second way includes two processes: I⟶C and C⟶M, x_4 has less impact on M(t) relative to x_3. Therefore, the final quantity of immune agents is smaller in Figure 6 than that in Figure 5 at the stop time. The curve of S(t) and the curve of M(t) are divided into two parts based on the trend of curves. The first part is the rapid change phase ($0 \leq$ time step ≤ 100), and the second part is the slow change phase ($100 \leq$ time step ≤ 187). During the whole simulation process, the amount of infected agents has little change, and the maximum is 222.7187 at time step 58. However, the amount of contagious agents has less change relative to infected agents, and the maximum is 86.3355, appearing at time step 61.

After the comparative analyses of Figures 2–6, the evolutionary characteristics of agents in SICM model are summarized in Table 2. The running time step indicates that the increase of x_1 or x_2 directly reinforces the effect of risk contagion, but the increase of x_3 or x_4 reduces this effect. In consequence, the running time step is shortened in cases 2 and 3, relative to case 1. Conversely, cases 4 and 5 have a longer running time step compared with that in case 1. When the simulation process automatically stops, the quantitative structures of different kinds of agents are displayed in Table 2. As the amount of I(t) decreases at the highest speed in the second part of simulation processes, the amount of I(t) is lower than the threshold in the shortest time, which is supposed in the baseline configuration of SICM model. In addition, the amount of M(t) is largest at stop time for each case, because most of other agents have been immune to a grapevine after the behavioral interactions of agents again and again.

Considering that the curve of I(t) and the curve of C(t) having similar fluctuation characteristics in SICM model, the amount of agents has a maximum for two curves. Table 3 shows the maximum values of I(t) and C(t) and the

Table 3: The maximum of infected agents and contagious agents in simulation processes.

Case	Parameters feature	The amount of I(t)		The amount of C(t)	
		Maximum	Time step	Maximum	Time step
Case 1	To keep all parameter values constant	403.3906	43	231.3881	48
Case 2	To increase the parameter value of x_1	796.9925	25	382.0501	29
Case 3	To increase the parameter value of x_2	534.3893	19	1181.6496	21
Case 4	To increase the parameter value of x_3	219.2371	50	131.4064	55
Case 5	To increase the parameter value of x_4	222.7187	58	86.3355	61

corresponding time steps. It is easy to be seen that time steps are less in the curve of I(t), rather than the curve of C(I). Namely, the curve of I(t) reaches a peak first; then the curve of C(t) reaches another peak. Only in Figure 4, the curve of C(t) has a higher peak. However, the curve of C(t) has a lower peak in other figures in Table 3. Owing to a grapevine spreading to contagious agents from infected agents, the maximum value of I(t) is often larger than that of C(t) in cases 1, 2, 4, and 5. But an exception appears in case 3. To be specific, more contagious agents become infected agents when the contagious probability x_2 is increased in case 3.

5. Conclusions

In this paper, we employ agent modeling technology and complex network theory to build a new contagious model to analyze the nonlinear dynamics characteristic of risk contagion in financial market. In the model, market participants are divided into four types: susceptible agents, infected agents, contagious agents, and immune agents. Based on the proposed SICM model, a grapevine can spread in four kinds of agents with the different probabilities. According to different configuration parameters, the simulation experiments are conducted. The results show that the same type of curves has similar volatility characteristics without changing any of contagious probabilities. For example, the curve of S(t) has a decreasing trend and the curve of M(t) has an increasing trend in the model. However, the curves of I(t) and C(t) show an ascending trend first and then descending trend. In addition, the results also indicate that the running time of model is shortened after increasing x_1 or x_2. But if x_3 or x_4 is increased, the model needs more running time. From cases 1 to 4, the curves of I(t) reach a peak first, compared with the curve of C(t). In all cases, the amount of M(t) is the most at the stop time, and the amount of I(t) is the least below the stop threshold. In short, the simulation experiments are automatically finished because the amount of I(t) declines rapidly.

Different from other researches, this paper designs the SICM model of risk contagion in financial market and reveals the interaction features of agents under the influences of different contagious probabilities. The conclusions of this paper can offer a theoretical foundation for future studies about the behavioral features of market participants and the contagious mechanisms of financial risks. As an agent-based model, SICM model can also be developed further in future studies. On the one hand, each agent may have a heterogeneous probability of infection. It means that the contagious probability probably is not a constant. For example, each agent has different risk preferences, different understandings of market information, and irrational investment motivations. Because different agents in the same class may have different probabilities of infection, the function of contagious probability should be built in the future. On the other hand, the transmission speed of the grapevine is probably changeable in different network topologies, considering that degree distribution and average path length are not invariable in financial markets. As the transmission speed of the grapevine can affect the available information of agents in unit time, agents may make decisions to buy or sell financial assets more quickly or slowly. And the price of financial asset is likely to be changed, because of the change of the market demand and supply. Based on the above two parts, we will further extend the SICM model in future studies, by building the function of contagious probability, affected by the price of financial asset. In addition, financial data has important significance for the research of risk contagion in a real financial market. In our future works, we will try to import the market data into the model and analyze risk contagion in the real financial market.

Data Availability

The data used to support the findings of this study are available from the corresponding author upon request.

Conflicts of Interest

All authors declare that they have no conflicts of interest regarding the publication of this paper.

Acknowledgments

This work was financially supported by the Program of Humanities and Social Science Youth Foundation of the Ministry of Education of China (Grant No. 19XJC790014), the Research Project of Major Theoretical and Practical Issues in Social Science Circles in Shaanxi Province of China (Grant No. 2019C025), Industry-University Cooperative Education Project of Ministry of Education of China (Grant No. 201801091012), the Fundamental Research Fund for the Central Universities of China (Grant No. GK201803093), and the Program of Social Science Planning Fund in Xi'an City of China (Grant No. 19Z16).

References

[1] B. Wu and J. He, "Review of financial contagion in countries under opening economy conditions," *Comparative Economic Social Systems*, vol. 172, no. 2, pp. 87–96, 2014.

[2] M. L. Schulman, C. E. May, B. Keys, and A. J. Guthrie, "Contagious equine metritis: Artificial reproduction changes the epidemiologic paradigm," *Veterinary Microbiology*, vol. 167, no. 1-2, pp. 2–8, 2013.

[3] A. K. Rose and M. M. Spiegel, "Cross-Country causes and consequences of the 2008 crisis: international linkages and american exposure," *Pacific Economic Review*, vol. 15, no. 3, pp. 340–363, 2010.

[4] M. Baker, J. Wurgler, and Y. Yuan, "Global, local, and contagious investor sentiment," *Journal of Financial Economics*, vol. 104, no. 2, pp. 272–287, 2012.

[5] A. K. Karmakar, *Contagious fInancial Crises in the rEcent past and Their Implications for India*, Analytical issues in trade, development and finance, Springer, New Delhi, India, 2014.

[6] M. Förster, M. Jorra, and P. Tillmann, "The dynamics of international capital flows: Results from a dynamic hierarchical factor model," *Journal of International Money and Finance*, vol. 48, pp. 101–124, 2014.

[7] T. Janus and D. Riera-Crichton, "International gross capital flows: New uses of balance of payments data and application to financial crises," *Journal of Policy Modeling*, vol. 35, no. 1, pp. 16–28, 2013.

[8] J. Helwege, "Financial firm bankruptcy and systemic risk," *Journal of International Financial Markets, Institutions & Money*, vol. 20, no. 1, pp. 1–12, 2010.

[9] Z. Meng, K. Yin, Y. Zhang, and X. Dong, "The risk contagion effect of return volatility between china's offshore and onshore foreign exchange market," *Romanian Journal of Economic Forecasting*, vol. 20, no. 4, pp. 5–21, 2017.

[10] M. Obstfeld and A. M. Taylor, "International monetary relations: taking finance seriously," *Journal of Economic Perspectives*, vol. 31, no. 3, pp. 3–28, 2017.

[11] B. Eichengreen and A. K. Rose, *Contagious currency crises: Channels of conveyance*, Changes in exchange rates in rapidly developing countries: Theory, practice, and policy issues (NBER-EASE volume 7), University of Chicago Press, 1999.

[12] G. A. Calvo, L. Leiderman, and C. M. Reinhart, "Inflows of capital to developing countries in the 1990s," *Journal of Economic Perspectives (JEP)*, vol. 10, no. 2, pp. 123–139, 1996.

[13] P. Masson, "Contagion: Macroeconomic models with multiple equilibria," *Journal of International Money and Finance*, vol. 18, no. 4, pp. 587–602, 1999.

[14] R. Dornbusch, Y. C. Park, and S. Claessens, "Contagion: understanding how it spreads," *The World Bank Research Observer*, vol. 15, no. 2, pp. 177–197, 2000.

[15] B. D. Jones and E. McDaniel, *Bounded Rationality*, he Wiley Blackwell Encyclopedia of Race, Ethnicity, and Nationalism, 2015.

[16] H. A. Simon, *Rationality, bounded*, The new Palgrave dictionary of economics, 2017.

[17] C. A. Robb, P. Babiarz, A. Woodyard, and M. C. Seay, "Bounded rationality and use of alternative financial services," *Journal of Consumer Affairs*, vol. 49, no. 2, pp. 407–435, 2015.

[18] J. Tuyon and Z. Ahmad, "Behavioural finance perspectives on Malaysian stock market efficiency," *Borsa Istanbul Review*, vol. 16, no. 1, pp. 43–61, 2016.

[19] J. B. De Long, A. Shleifer, L. H. Summers, and R. J. Waldmann, "Noise trader risk in financial markets," *Journal of Political Economy*, vol. 98, no. 4, pp. 703–738, 1990.

[20] B. Mendel and A. Shleifer, "Chasing noise," *Journal of Financial Economics*, vol. 104, no. 2, pp. 303–320, 2012.

[21] V. Ramiah, X. Xu, and I. A. Moosa, "Neoclassical finance, behavioral finance and noise traders: A review and assessment of the literature," *International Review of Financial Analysis*, vol. 41, pp. 89–100, 2015.

[22] B. Wu, T. Duan, and J. He, "Dynamics evolution of trading strategies of investors in financial market," *Computational Economics*, vol. 51, no. 4, pp. 743–760, 2018.

[23] A. S. Kyle, "Continuous auctions and insider trading," *Econometrica*, vol. 53, no. 6, pp. 1315–1335, 1985.

[24] R. K. Chou, G. H. K. Wang, and Y.-Y. Wang, "The impacts of individual day trading strategies on market liquidity and volatility: evidence from the taiwan index futures market," *Journal of Futures Markets*, vol. 35, no. 5, pp. 399–425, 2015.

[25] R. Bloomfield, M. O'Hara, and G. Saar, "Hidden liquidity: some new light on dark trading," *Journal of Finance*, vol. 70, no. 5, pp. 2227–2274, 2015.

[26] N. Schmitt and F. Westerhoff, "Heterogeneity, spontaneous coordination and extreme events within large-scale and small-scale agent-based financial market models," *Journal of Evolutionary Economics*, vol. 27, no. 5, pp. 1041–1070, 2017.

[27] J. Sedunov, "What is the systemic risk exposure of financial institutions?" *Journal of Financial Stability*, vol. 24, pp. 71–87, 2016.

[28] M. A. Bellelah, M. O. Bellelah, H. Ben Ameur, and R. Ben Hafsia, "Does the equity premium puzzle persist during financial crisis? The case of the French equity market," *Research in International Business and Finance*, vol. 39, pp. 851–866, 2017.

[29] E. Zervoudi and S. Spyrou, "The equity premium puzzle: new evidence on the optimal holding period and optimal asset allocation," *Review of Behavioral Finance*, vol. 8, no. 1, pp. 39–57, 2016.

[30] S. Rachev, S. Stoyanov, S. Mittnik, and F. J. Fabozzi, *Behavioral Finance–Asset Prices Predictability, Equity Premium Puzzle, Volatility Puzzle: The Rational Finance Approach*, Cornell University, 1710.03211, 2017, https://arxiv.org/abs/1710.03211.

[31] R. F. Stambaugh, J. Yu, and Y. Yuan, "Arbitrage asymmetry and the idiosyncratic volatility puzzle," *Journal of Finance*, vol. 70, no. 5, pp. 1903–1948, 2015.

[32] K. Hou and R. K. Loh, "Have we solved the idiosyncratic volatility puzzle?" *Journal of Financial Economics*, vol. 121, no. 1, pp. 167–194, 2016.

[33] N. Aslanidis, C. Christiansen, N. Lambertides, and C. S. Savva, "Idiosyncratic volatility puzzle: influence of macro-finance factors," *Review of Quantitative Finance and Accounting*, pp. 1–21, 2018.

[34] S. L. Lenkey, "The closed-end fund puzzle: Management fees and private information," *Journal of Financial Intermediation*, vol. 24, no. 1, pp. 112–129, 2015.

[35] S. Anderson, T. R. Beard, H. Kim, and L. V. Stern, "Fear and Closed-End Fund discounts," *Applied Economics Letters*, vol. 20, no. 10, pp. 956–959, 2013.

[36] C. P. Cullinan and X. Zheng, "Valuation scepticism, liquidity benefits and closed-end fund premiums/discounts: Evidence from fair value disclosures," *Accounting & Finance*, vol. 54, no. 3, pp. 729–751, 2014.

[37] D. Shapiro and A. Zhuang, "Dividends as a signaling device and the disappearing dividend puzzle," *Journal of Economics and Business*, vol. 79, pp. 62–81, 2015.

[38] X. Chen, L. Tang, and H. Hu, "Heterogeneous dividend preferences of chinese individual and institutional investors: evidence from categorized daily share holding data," *China Finance Review International*, vol. 4, no. 4, pp. 326–342, 2014.

[39] R. Pan, X. Tang, Y. Tan, and Q. Zhu, "The Chinese stock dividend puzzle," *Emerging Markets Finance and Trade*, vol. 50, no. 3, pp. 178–185, 2014.

[40] K. Daniel and D. Hirshleifer, "Overconfident investors, predictable returns, and excessive trading," *Journal of Economic Perspectives (JEP)*, vol. 29, no. 4, pp. 61–88, 2015.

[41] D. Hirshleifer, "Behavioral Finance," *Annual Review of Financial Economics*, vol. 7, pp. 133–159, 2015.

[42] S. Kremer and D. Nautz, "Causes and consequences of short-term institutional herding," *Journal of Banking & Finance*, vol. 37, no. 5, pp. 1676–1686, 2013.

[43] N. Choi and H. Skiba, "Institutional herding in international markets," *Journal of Banking & Finance*, vol. 55, pp. 246–259, 2015.

[44] Z. Paruk, I. Petersen, A. Bhana, C. Bell, and M. McKay, "Containment and contagion: How to strengthen families to support youth HIV prevention in South Africa," *African Journal of AIDS Research*, vol. 4, no. 1, pp. 57–63, 2005.

[45] W. Chen, Y. Wei, Q. Lang, Y. Lin, and M. Liu, "Financial market volatility and contagion effect: a copula-multifractal volatility approach," *Physica A: Statistical Mechanics and Its Applications*, vol. 398, pp. 289–300, 2014.

[46] C.-Q. Luo, C. Xie, C. Yu, and Y. Xu, "Measuring financial market risk contagion using dynamic MRS-Copula models: the case of Chinese and other international stock markets," *Economic Modelling*, vol. 51, no. 12, pp. 657–671, 2015.

[47] R. Bookstaber, M. Paddrik, and B. Tivnan, "An agent-based model for financial vulnerability," *Journal of Economic Interaction and Coordination*, vol. 13, no. 2, pp. 433–466, 2018.

[48] T. Lux and M. Marchesi, "Scaling and criticality in a stochastic multi-agent model of a financial market," *Nature*, vol. 397, no. 6719, pp. 498–500, 1999.

[49] R. Cont and J.-P. Bouchaud, "Herd behavior and aggregate fluctuations in financial markets," *Macroeconomic Dynamics*, vol. 4, no. 2, pp. 170–196, 2000.

[50] L. Ponta, M. Trinh, M. Raberto, E. Scalas, and S. Cincotti, "Modeling non-stationarities in high-frequency financial time series," *Physica A: Statistical Mechanics and its Applications*, vol. 521, pp. 173–196, 2019.

[51] S.-H. Chen and C.-H. Yeh, "Evolving traders and the business school with genetic programming: a new architecture of the agent-based artificial stock market," *Journal of Economic Dynamics and Control (JEDC)*, vol. 25, no. 3-4, pp. 363–393, 2001.

[52] G. Iori, "A microsimulation of traders activity in the stock market: The role of heterogeneity, agent's interactions and trade frictions," *Journal of Economic Behavior & Organization*, vol. 49, no. 2, pp. 269–285, 2002.

[53] R. Pascual, B. Pascual-Fuster, and F. Climent, "Cross-listing, price discovery and the informativeness of the trading process," *Journal of Financial Markets*, vol. 9, no. 2, pp. 144–161, 2006.

[54] K. Yim, G. Oh, and S. Kim, "The effect of heterogeneous interactions among traders in an artificial stock market," *SSRN Electronic Journal*, 2015.

[55] M. A. Bertella, F. R. Pires, L. Feng, and H. E. Stanley, "Confidence and the stock market: an agent-based approach," *PLoS ONE*, vol. 9, no. 1, Article ID e83488, 2014.

[56] X. Zhang, J. Ping, T. Zhu, Y. Li, X. Xiong, and W. Zhou, "Are price limits effective? an examination of an artificial stock market," *PLoS ONE*, vol. 11, no. 8, p. e0160406, 2016.

[57] M. S. H. Pour, "Malignant melanoma of the oral cavity," *Journal of Dentistry of Tehran University of Medical Sciences*, vol. 4, no. 1, pp. 44–51, 2007.

[58] P. S. Sarpotdar and A. D. Yadav, "Independent verification of Euler's formula in graph theory for n identical circles," *Bulletin of Pure Applied Sciences-Mathematics and Statistics*, vol. 37, no. 1, p. 14, 2018.

[59] Z. Zhao, D. Chen, L. Wang, and C. Han, "Credit risk diffusion in supply chain finance: a complex networks perspective," *Sustainability*, vol. 10, no. 12, Article ID 4608, 20 pages, 2018.

[60] Y. Zhu, F. Yang, and W. Ye, "Financial contagion behavior analysis based on complex network approach," *Annals of Operations Research*, vol. 268, no. 1-2, pp. 93–111, 2018.

[61] C. Liu and N. Arunkumar, "Risk prediction and evaluation of transnational transmission of financial crisis based on complex network," *Cluster Computing*, pp. 1–7, 2018.

[62] R. N. Mantegna, "Hierarchical structure in financial markets," *The European Physical Journal B—Condensed Matter and Complex Systems*, vol. 11, no. 1, pp. 193–197, 1999.

[63] G. Bonanno, G. Caldarelli, F. Lillo, and R. N. Mantegna, "Topology of correlation-based minimal spanning trees in real and model markets," *Physical Review E: Statistical, Nonlinear, and Soft Matter Physics*, vol. 68, no. 4, Article ID 046130, 4 pages, 2003.

[64] B. Lee, L. Rosenthal, C. Veld, and Y. Veld-Merkoulova, "Stock market expectations and risk aversion of individual investors," *International Review of Financial Analysis*, vol. 40, pp. 122–131, 2015.

[65] F. Emmert-Streib, M. Dehmer, and E. Scalas, "Influence of the time scale on the construction of financial networks," *PLoS ONE*, vol. 5, no. 9, Article ID e12884, 9 pages, 2010.

[66] B. Li and Y. Li, "Network dynamics of the Chinese stock market," in *Proceedings of the 2014 2nd International Conference on Systems and Informatics (ICSAI)*, pp. 959–963, Shanghai, China, November 2014.

[67] Z. Liang and Q. Han, "Coherent artificial stock market model based on small world networks," *Complex Systems and Complexity Science*, vol. 6, no. 2, pp. 70–76, 2009.

[68] H. Nie, Y. B. Zhang, J. R. Chen et al., "Research of chinese stock market complex network structure," *International Journal of Economics & Finance*, vol. 7, no. 5, 2015.

[69] A. Nobi, S. E. Maeng, and G. G. Ha, "Structural changes in the minimal spanning tree and the hierarchical network in the Korean stock market around the global financial crisis," *Journal of the Korean Physical Society*, vol. 66, no. 8, pp. 1153–1159, 2015.

[70] H. Qiao, Y. Xia, Y. Li, and W. Zhou, "Can network linkage effects determine return? evidence from chinese stock market," *PLoS ONE*, vol. 11, no. 6, Article ID e0156784, 25 pages, 2016.

[71] L.-X. Yang, X. Yang, J. Liu, Q. Zhu, and C. Gan, "Epidemics of computer viruses: a complex-network approach," *Applied Mathematics and Computation*, vol. 219, no. 16, pp. 8705–8717, 2013.

[72] D. Li, J. Ma, Z. Tian, and H. Zhu, "An evolutionary game for the diffusion of rumor in complex networks," *Physica A: Statistical Mechanics and its Applications*, vol. 433, pp. 51–58, 2015.

[73] R. Pastor-Satorras, C. Castellano, P. Van Mieghem, and A. Vespignani, "Epidemic processes in complex networks," *Reviews of Modern Physics*, vol. 87, no. 3, pp. 925–979, 2015.

[74] S. Hong, H. Yang, T. Zhao, and X. Ma, "Epidemic spreading model of complex dynamical network with the heterogeneity of nodes," *International Journal of Systems Science*, vol. 47, no. 11, pp. 2745–2752, 2016.

[75] C. Wan, T. Li, Y. Wang, and X. Liu, "Rumor spreading of a SICS model on complex social networks with counter mechanism," *Open Access Library Journal*, vol. 3, no. 7, pp. 1–11, 2016.

[76] B. Wu and T. Duan, "Agent-based analysis of risk contagion in stock market from perspective of econophysics," *Journal of Physics: Conference Series*, vol. 1053, p. 012109, 2018.

Hindawi
Complexity
Volume 2019, Article ID 2989204, 14 pages
https://doi.org/10.1155/2019/2989204

Research Article

PD^9 Control Strategy for a Fractional-Order Chaotic Financial Model

Changjin Xu,[1] **Maoxin Liao**,[2] **Peiluan Li**,[3] **Qimei Xiao**,[4] **and Shuai Yuan**[5]

[1] *Guizhou Key Laboratory of Economics System Simulation, Guizhou University of Finance and Economics, Guiyang 550004, China*
[2] *School of Mathematics and Physics, University of South China, Hengyang 421001, China*
[3] *School of Mathematics and Statistics, Henan University of Science and Technology, Luoyang 471023, China*
[4] *Hunan Provincial Key Laboratory of Mathematical Modeling and Analysis in Engineering, Changsha University of Science and Technology, Changsha 410114, China*
[5] *School of Mathematics and Statistics, Central South University, Changsha 410083, China*

Correspondence should be addressed to Changjin Xu; xcj403@126.com

Received 22 January 2019; Revised 6 March 2019; Accepted 8 April 2019; Published 22 April 2019

Guest Editor: Benjamin M. Tabak

In this article, based on the previous works, a new fractional-order financial model is put up. The chaotic behavior of the fractional-order financial model is suppressed by designing an appropriate PD^9 controller. By choosing the delay as the bifurcation parameter, we establish the sufficient condition to guarantee the stability and the existence of Hopf bifurcation of fractional-order financial model. Also, the influence of the delay and the fractional order on the stability and the existence of Hopf bifurcation of fractional-order financial model is revealed. An example is given to confirm the effectiveness of the analysis results. The main findings of this article play an important role in maintaining economic stability.

1. Introduction

Establishing financial models to investigate the complex dynamical behavior of economic society has attracted more attention of scholars in numerous areas. To grasp the law of operation accurately, various financial models have been established to reveal the inherent characteristics of economic development and numerous fruitful results are achieved. For instance, Zhang et al. [1] discussed the stability of a financial hyperchaotic model, Serletic [2] investigated the chaos in economic system, Lin et al. [3] made an detailed analysis on chaotic behavior of a financial complex model, and Gao and Ma [4] studied the chaotic phenomenon and bifurcation of a finance model. For more information on financial models, one can see [5–9].

In many cases, chaotic behavior often happens in financial models. Chaotic phenomenon will have a serious effect on man's everyday life. Thus the research on chaos control of financial models becomes a hot issue in financial community. The appearance of chaotic phenomenon in economic system implies that the macroeconomic operation has its inherent indefiniteness and complexity. Of course, government departments can take measures for control or interference, but the effect is very limited [10]. Thus, it is worthwhile to deal with the control of chaos in financial systems by theoretical analysis.

In 2001, Ma and Chen [11, 12] studied the following financial model:

$$\begin{aligned} \frac{du_1}{dt} &= u_3 + (u_2 - p_1)\, u_1, \\ \frac{du_2}{dt} &= 1 - p_2 u_2 - u_1^2, \\ \frac{du_3}{dt} &= -u_1 - p_3 u_3, \end{aligned} \tag{1}$$

where $p_1 \geq 0$ denotes the saving amount, $p_2 \geq 0$ denotes the cost per investment, $p_3 \geq 0$ denotes the elasticity of demand of commercial markets, u_1 represents interest rate, u_2 represents investment demand, and u_3 represents price index. In 2008, Chen [13] designed a suitable time delayed

feedback controller to control the chaotic phenomena of model (1); computer simulations are presented to illustrate the effectiveness of designed controller. In 2011, Son and Park [14] further dealt with the chaos control issue of model (1) by applying delayed feedback method. Detailed theoretical analysis and numerical simulations are carried out to check the correctness of the controller. In 2009, Gao and Ma [4] discussed the chaos control of model (1) by adding a time delay feedback term to the second equation of system (1). Also the sufficient condition to guarantee the stability and the existence of Hopf bifurcation of involved controlled financial model is established. Considering the effect of time delay on the financial phenomena, Zhang and Zhu [15], Chen et al. [16], Mircea et al. [17], and Zhang [18] established different delayed financial models and analyzed their Hopf bifurcation or chaos control issue. In 2014, Zhao et al. [19] investigated the the anticontrol of Hopf bifurcation and chaos control of model (1) by applying delayed washout filters. For details, one can see [5–7, 20–30].

Here we would like to point out that all the above works are only concerned with the integer-order differential systems. Nowadays, numerous scholars have found that fractional calculus, which is a generalization of ordinary differentiation and integration, has potential applications in numerous fields such as economics, physics, heat transfer, and chemical engineer [31–38]. Many researchers argued that it is more reasonable to describe the object natural phenomena by fractional-order differential equations than integer-order differential equations, since fractional-order differential equations can better describe the memory characteristics and historical dependence. Noticing that financial coefficients possess very long memory and the variation of financial coefficients has close connection with previous and current time, we think that it is important for us to establish fractional-order financial systems. In recent years, there are numerous articles that investigate the fractional-order financial systems. One can see [11, 12, 39–47].

In view of the above analysis and based on system (1), we modify system (1) as the following fractional-order financial model:

$$\begin{aligned} \frac{d^{\vartheta}u_1}{dt^{\vartheta}} &= u_3 + (u_2 - p_1)u_1, \\ \frac{d^{\vartheta}u_2}{dt^{\vartheta}} &= 1 - p_2u_2 - u_1^2, \\ \frac{d^{\vartheta}u_3}{dt^{\vartheta}} &= -u_1 - p_3u_3, \end{aligned} \tag{2}$$

where $0 < \vartheta < 1$ stands for the fractional order. The study reveals that chaotic phenomenon will appear if $\vartheta = 0.73$ and $p_1 = 3$, $p_2 = 0.1$, $p_3 = 1$. The results can be shown in Figures 1–10.

Our key task is concerned with two topics: (i) designing a suitable PD^{ϑ} controller to suppress the chaotic behavior of system (2) and (2) seeking the influence of delay and fractional order on the stability and bifurcation phenomenon of controlled system.

The superiority of this article is stated as follows:

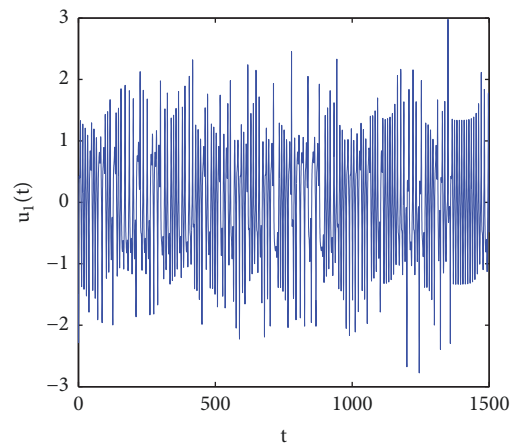

Figure 1: The relation of t and u_1 in model (2) when $\vartheta = 0.73$, $p_1 = 3$, $p_2 = 0.1$, and $p_3 = 1$.

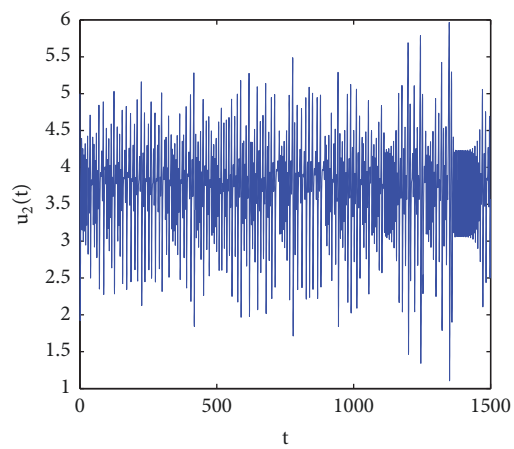

Figure 2: The relation of t and u_2 in model (2) when $\vartheta = 0.73$, $p_1 = 3$, $p_2 = 0.1$, and $p_3 = 1$.

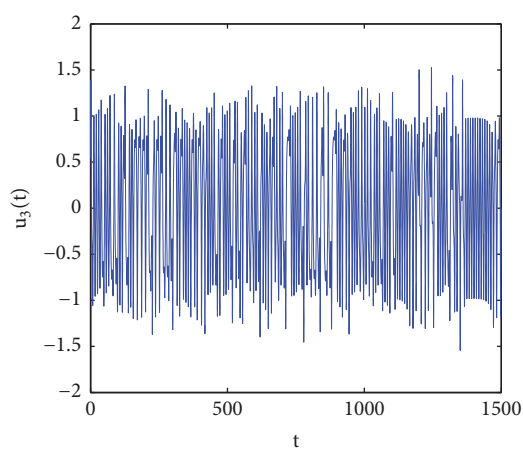

Figure 3: The relation of t and u_3 in model (2) when $\vartheta = 0.73$, $p_1 = 3$, $p_2 = 0.1$, and $p_3 = 1$.

(I) A new fractional-order financial model is established.

(II) A PD^{ϑ} controller is designed to suppress the chaos of the fractional-order financial model. Also, a set of

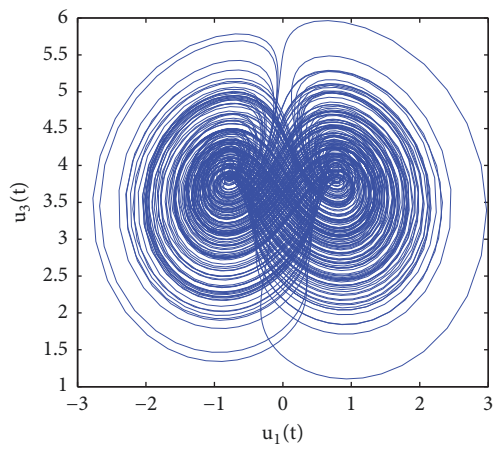

FIGURE 4: The relation of u_1 and u_2 in model (2) when $\vartheta = 0.73$, $p_1 = 3$, $p_2 = 0.1$, and $p_3 = 1$.

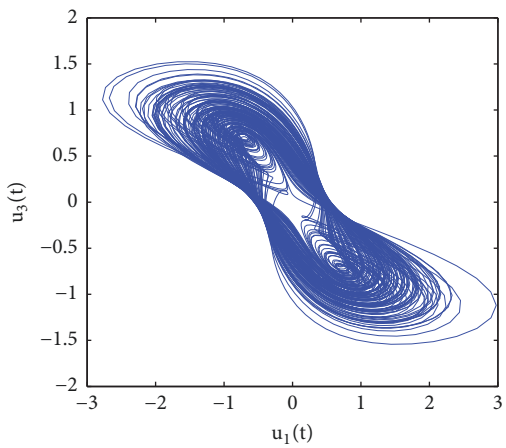

FIGURE 5: The relation of u_1 and u_3 in model (2) when $\vartheta = 0.73$, $p_1 = 3$, $p_2 = 0.1$, and $p_3 = 1$.

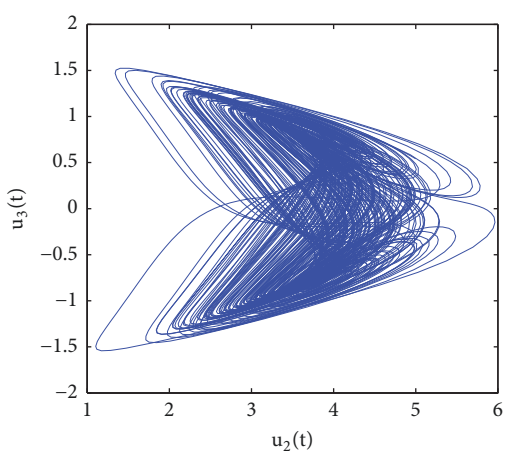

FIGURE 6: The relation of u_2 and u_3 in model (2) when $\vartheta = 0.73$, $p_1 = 3$, $p_2 = 0.1$, and $p_3 = 1$.

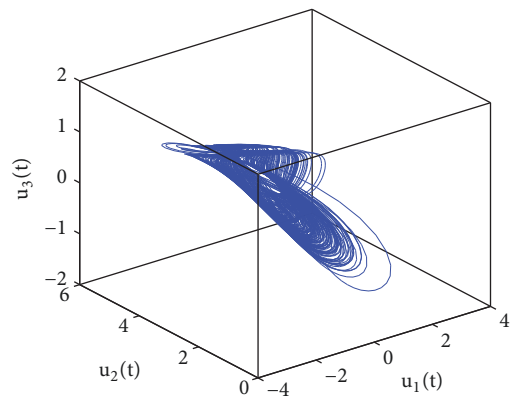

FIGURE 7: The relation of u_1, u_2, and u_3 in model (2) when $\vartheta = 0.73$, $p_1 = 3$, $p_2 = 0.1$, and $p_3 = 1$.

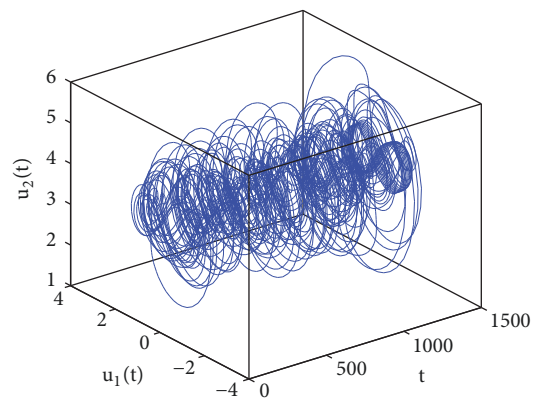

FIGURE 8: The relation of t, u_1, and u_2 in model (2) when $\vartheta = 0.73$, $p_1 = 3$, $p_2 = 0.1$, and $p_3 = 1$.

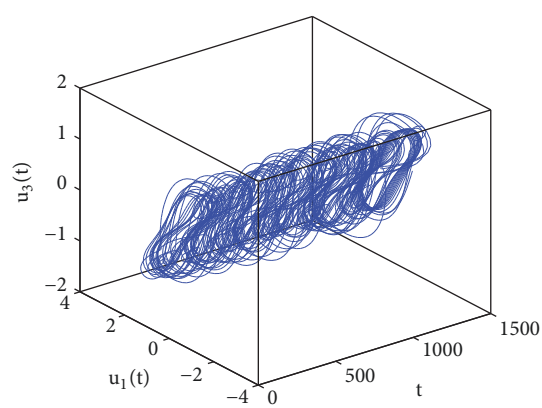

FIGURE 9: The relation of t, u_2, and u_3 in model (2) when $\vartheta = 0.73$, $p_1 = 3$, $p_2 = 0.1$, and $p_3 = 1$.

new sufficient conditions to guarantee the stability and the existence of Hopf bifurcation of fractional-order financial model are obtained. In addition, the effect of the delay and fractional order on the dynamics of fractional-order financial model is displayed.

(III) To the best of our knowledge, it is the first time to control chaos of fractional-order financial model by applying PD^{ϑ} controller.

We organize this article as follows. In Section 2, some basic knowledge on fractional calculus is presented. In Section 3,

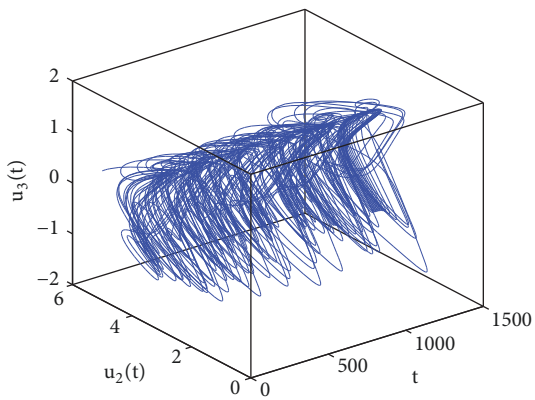

FIGURE 10: The relation of t, u_2, and u_3 in model (2) when $\vartheta = 0.73$, $p_1 = 3$, $p_2 = 0.1$, and $p_3 = 1$.

PD^{ϑ} controller is designed to control chaos of fractional-order financial model. In Section 4, an example is given to show the effectiveness of the main findings. A conclusion is presented in Section 5.

2. Basic Results

In this section, we give some basic results on fractional calculus.

Definition 1 (see [48]). Define Caputo fractional-order derivative as follows:

$$\mathbf{D}^{\vartheta} p(\iota) = \frac{1}{\Gamma(n-\vartheta)} \int_{\iota_0}^{\iota} \frac{p^{(m)}(s)}{(\iota - s)^{\vartheta - m + 1}} ds, \tag{3}$$

where $p(\iota) \in ([\iota_0, \infty), R)$, $\Gamma(s) = \int_0^{\infty} \iota^{s-1} e^{-\iota} d\iota$. $\iota \geq \iota_0$ and m is a positive integer such that $m - 1 \leq \vartheta < m$. If $0 < \vartheta < 1$, then

$$\mathbf{D}^{\vartheta} p(\iota) = \frac{1}{\Gamma(1-\vartheta)} \int_{\iota_0}^{\iota} \frac{p'(s)}{(\iota - s)^{\vartheta}} ds. \tag{4}$$

Definition 2 (see [49]). The point (u_1^*, u_2^*, u_3^*) is called an equilibrium point if the equations

$$\begin{aligned} u_3^* + (u_2^* - p_1) u_1^* &= 0, \\ 1 - p_2 u_2^* - (u_1^*)^2 &= 0, \\ -u_1^* - p_3 u_3^* &= 0 \end{aligned} \tag{5}$$

hold.

Lemma 3 (see [50]). *Let λ_i $(i = 1, 2, \ldots, n)$ be the root of the characteristic equation of the autonomous system $\mathbf{D}^{\vartheta} u = \mathbf{B} u$, $u(0) = u_0$, where $0 < \vartheta < 1$, $u \in R^n$, $\mathbf{B} \in R^{n \times n}$. Then system $\mathbf{D}^{\vartheta} u = \mathbf{B} u$ is asymptotically stable if and only if $|\arg(\lambda_i)| > \vartheta\pi/2$ $(i = 1, 2, \ldots, n)$. The system $\mathbf{D}^{\vartheta} u = \mathbf{B} u$ is stable if and only if $|\arg(\lambda_i)| > \vartheta\pi/2$ $(i = 1, 2, \ldots, n)$ and those critical eigenvalues that satisfy $|\arg(\lambda_i)| = \vartheta\pi/2$ $(i = 1, 2, \ldots, n)$ have geometric multiplicity one.*

Lemma 4 (see [51]). *The system $\mathbf{D}^{\vartheta} v(t) = \mathbf{A}_1 v(t) + \mathbf{A}_2 v(t - \rho)$, where $v(t) = \phi(t)$, $t \in [-\rho, 0]$, $\vartheta \in (0, 1]$, $v \in R^n$, $\mathbf{A}_1, \mathbf{A}_2 \in R^{n \times n}$, $\vartheta \in R^{+(n \times n)}$. Then the characteristic equation of the system is $\det |s^{\vartheta} I - \mathbf{A}_1 - \mathbf{A}_2 e^{-s\rho}| = 0$. If all the roots of the characteristic equation of the system have negative real roots, then the zero solution of the system is asymptotically stable.*

3. Chaos Control by PD^{ϑ} Controller

If $p_2 + p_1 p_2 p_3 - p_3 > 0$, then system (2) has a unique equilibrium point:

$$(u_{10}, u_{20}, u_{30}) = \left(0, \frac{1}{p_2}, 0\right). \tag{6}$$

If $p_2 + p_1 p_2 p_3 - p_3 < 0$, then model (2) has three equilibrium points:

$$\begin{aligned} (u_{10}, u_{20}, u_{30}) &= \left(0, \frac{1}{p_2}, 0\right), \\ (u_1^*, u_2^*, u_3^*) &= \left(\frac{\sqrt{p_3 - p_2 - p_1 p_2 p_3}}{\sqrt{p_3}}, \frac{1 + p_1 p_3}{p_3}, \right. \\ &\quad \left. - \frac{\sqrt{p_3 - p_2 - p_1 p_2 p_3}}{\sqrt[3]{p_3^2}} \right), \\ (u_1^{**}, u_2^{**}, u_3^{**}) &= \left(-\frac{\sqrt{p_3 - p_2 - p_1 p_2 p_3}}{\sqrt{p_3}}, \frac{1 + p_1 p_3}{p_3}, \right. \\ &\quad \left. \frac{\sqrt{p_3 - p_2 - p_1 p_2 p_3}}{\sqrt[3]{p_3^2}} \right). \end{aligned} \tag{7}$$

During the past several decades, many different control strategies have been applied to control the chaos and bifurcation behavior. But they only involve the integer-order differential systems. Applying PD^{ϑ} control strategy to control the chaotic behavior of fractional-order chaotic system is rare. To make up for the deficiency, we try to design a PD^{ϑ} feedback controller to suppress the chaotic phenomenon of model (2). In this paper, we only consider the equilibrium point (u_1^*, u_2^*, u_3^*). The other equilibrium points can be discussed in the same way. Here we omit it. Throughout this paper, we always assume that $p_2 + p_1 p_2 p_3 - p_3 < 0$.

Add the following PD^{ϑ} feedback controller to the first equation of system (2):

$$\varrho(t) = \kappa_p (u_1(t - \rho) - u_1^*) + \kappa_d \frac{d^{\vartheta}}{dt^{\vartheta}} (u_1(t) - u_1^*), \tag{8}$$

where κ_p and κ_d are the proportional control parameter and the derivative control parameter, respectively, and ρ is time delay; then system (2) becomes

$$\begin{aligned} \frac{d^{\vartheta}u_1}{dt^{\vartheta}} &= u_3 + (u_2 - p_1)u_1 + \varrho(t), \\ \frac{d^{\vartheta}u_2}{dt^{\vartheta}} &= 1 - p_2u_2 - u_1^2, \\ \frac{d^{\vartheta}u_3}{dt^{\vartheta}} &= -u_1 - p_3u_3. \end{aligned} \tag{9}$$

That is,

$$\begin{aligned} \frac{d^{\vartheta}u_1}{dt^{\vartheta}} &= u_3 + (u_2 - p_1)u_1 + \kappa_p(u_1(t-\rho) - u_1^*) \\ &\quad + \kappa_d \frac{d^{\vartheta}}{dt^{\vartheta}}(u_1(t) - u_1^*), \\ \frac{d^{\vartheta}u_2}{dt^{\vartheta}} &= 1 - p_2u_2 - u_1^2, \\ \frac{d^{\vartheta}u_3}{dt^{\vartheta}} &= -u_1 - p_3u_3. \end{aligned} \tag{10}$$

Let $v_i(t) = u_i(t) - u_i(t)$ $(i = 1, 2, 3)$; then linear system of system (10) takes the form

$$\begin{aligned} &\frac{d^{\vartheta}v_1}{dt^{\vartheta}} \\ &\quad = \frac{1}{1-\kappa_d}\left[(u_2^* - p_1)v_1 + v_2 + u_1^*v_3 + \kappa_p v_1(t-\rho)\right], \\ &\frac{d^{\vartheta}v_2}{dt^{\vartheta}} = 2u_1^*v_1 - p_2v_2, \\ &\frac{d^{\vartheta}v_3}{dt^{\vartheta}} = -v_1 - p_3v_3. \end{aligned} \tag{11}$$

The corresponding characteristic equation of (11) is given by

$$\det\begin{bmatrix} s^{\vartheta} - \frac{u_2^* - p_1}{1-\kappa_d} - \frac{\kappa_p}{1-\kappa_d}e^{-s\rho} & -\frac{1}{1-\kappa_d} & -\frac{u_1^*}{1-\kappa_d} \\ 2u_1^* & s^{\vartheta} + p_2 & 0 \\ 1 & 0 & s^{\vartheta} + p_3 \end{bmatrix}. \tag{12}$$

Then

$$\mathcal{Q}_1(s) + \mathcal{Q}_2(s)e^{-s\rho} = 0, \tag{13}$$

where

$$\begin{aligned} \mathcal{Q}_1(s) &= s^{3\vartheta} + \left(p_2 + p_3 - \frac{u_2^* - p_1}{1-\kappa_d}\right)s^{2\vartheta} \\ &\quad + \left[p_2p_3 - \frac{(u_2^* - p_1)(p_2 + p_3)}{1-\kappa_d}\right]s^{\vartheta} \\ &\quad - \frac{(u_2^* - p_1)(p_2 + p_3)}{1-\kappa_d}, \\ \mathcal{Q}_2(s) &= -\frac{\kappa_p}{1-\kappa_d}\left(s^{2\vartheta} + (p_2 + p_3)s^{\vartheta} + p_2p_3\right). \end{aligned} \tag{14}$$

Assume that $s = i\zeta = \zeta(\cos(\pi/2) + i\sin(\pi/2))$ is a root of (13); then one has

$$\begin{aligned} \mathcal{Q}_{2R}(\zeta)\cos\zeta\rho + \mathcal{Q}_{2I}(\phi)\sin\zeta\rho &= -\mathcal{Q}_{1R}(\zeta), \\ \mathcal{Q}_{2I}(\zeta)\cos\zeta\rho - \mathcal{Q}_{2R}(\phi)\sin\zeta\rho &= -\mathcal{Q}_{1I}(\zeta), \end{aligned} \tag{15}$$

where

$$\begin{aligned} \mathcal{Q}_{1R}(\zeta) &= \zeta^{3\vartheta}\cos\frac{3\vartheta\pi}{2} + \left(p_2 + p_3 - \frac{u_2^* - p_1}{1-\kappa_d}\right)\zeta^{2\vartheta} \\ &\quad \cdot \cos\vartheta\pi + \left[p_2p_3 - \frac{(u_2^* - p_1)(p_2 + p_3)}{1-\kappa_d}\right]\zeta^{\vartheta}\cos\frac{\vartheta\pi}{2} \\ &\quad - \frac{(u_2^* - p_1)(p_2 + p_3)}{1-\kappa_d}, \\ \mathcal{Q}_{1I}(\zeta) &= \zeta^{3\vartheta}\sin\frac{3\vartheta\pi}{2} + \left(p_2 + p_3 - \frac{u_2^* - p_1}{1-\kappa_d}\right)\zeta^{2\vartheta} \\ &\quad \cdot \sin\vartheta\pi + \left[p_2p_3 - \frac{(u_2^* - p_1)(p_2 + p_3)}{1-\kappa_d}\right]\zeta^{\vartheta}\sin\frac{\vartheta\pi}{2}, \\ \mathcal{Q}_{2R}(\zeta) &= -\frac{\kappa_p}{1-\kappa_d}\left(\vartheta^{2\vartheta}\cos\vartheta\pi + (p_2 + p_3)\zeta^{\vartheta}\cos\frac{\vartheta\pi}{2}\right. \\ &\quad \left. + p_2p_3\right), \\ \mathcal{Q}_{2I}(\zeta) &= -\frac{\kappa_p}{1-\kappa_d}\left(\vartheta^{2\vartheta}\sin\vartheta\pi + (p_2 + p_3)\zeta^{\vartheta}\sin\frac{\vartheta\pi}{2}\right). \end{aligned} \tag{16}$$

By (15), one has

$$\begin{aligned} \cos\zeta\rho &= -\frac{\mathcal{Q}_{1R}(\zeta)\mathcal{Q}_{2R}(\zeta) + \mathcal{Q}_{1I}(\zeta)\mathcal{Q}_{2I}(\zeta)}{\mathcal{Q}_{2R}^2(\zeta) + \mathcal{Q}_{2I}^2(\zeta)}, \\ \sin\zeta\rho &= -\frac{\mathcal{Q}_{1R}(\zeta)\mathcal{Q}_{2I}(\zeta) - \mathcal{Q}_{1I}(\zeta)\mathcal{Q}_{2R}(\zeta)}{\mathcal{Q}_{2R}^2(\zeta) + \mathcal{Q}_{2I}^2(\zeta)}. \end{aligned} \tag{17}$$

Let

$$\begin{aligned} a_1 &= \cos\frac{3\vartheta\pi}{2}, \\ a_2 &= \left(p_2 + p_3 - \frac{u_2^* - p_1}{1-\kappa_d}\right)\cos\vartheta\pi, \end{aligned}$$

$$
\begin{aligned}
a_3 &= \left[p_2p_3 - \frac{(u_2^* - p_1)(p_2+p_3)}{1-\kappa_d}\right]\cos\frac{\vartheta\pi}{2},\\
a_4 &= -\frac{(u_2^* - p_1)(p_2+p_3)}{1-\kappa_d},\\
a_5 &= \sin\frac{3\vartheta\pi}{2},\\
a_6 &= \left(p_2+p_3-\frac{u_2^*-p_1}{1-\kappa_d}\right)\sin\vartheta\pi,\\
a_7 &= \left[p_2p_3 - \frac{(u_2^* - p_1)(p_2+p_3)}{1-\kappa_d}\right]\sin\frac{\vartheta\pi}{2},\\
a_8 &= -\frac{\kappa_p\cos\vartheta\pi}{1-\kappa_d},\\
a_9 &= -\frac{\kappa_p(p_2+p_3)}{1-\kappa_d},\\
a_{10} &= -\frac{\kappa_p p_2p_3}{1-\kappa_d},\\
a_{11} &= -\frac{\kappa_p\sin\vartheta\pi}{1-\kappa_d},\\
a_{12} &= -\frac{\kappa_p(p_2+p_3)\sin(\vartheta\pi/2)}{1-\kappa_d}.
\end{aligned}
\tag{18}
$$

Then

$$
\begin{aligned}
\mathcal{Q}_{1R}(\zeta) &= a_1\zeta^{3\vartheta} + a_2\zeta^{2\vartheta} + a_3\zeta^{\vartheta} + a_4,\\
\mathcal{Q}_{1I}(\zeta) &= a_5\zeta^{3\vartheta} + a_6\zeta^{2\vartheta} + a_7\zeta^{\vartheta},\\
\mathcal{Q}_{2R}(\zeta) &= a_8\zeta^{2\vartheta} + a_9\zeta^{\vartheta} + a_{10},\\
\mathcal{Q}_{2I}(\zeta) &= a_{11}\zeta^{2\vartheta} + a_{12}\zeta^{\vartheta}.
\end{aligned}
\tag{19}
$$

It follows from (17) that

$$
\begin{aligned}
&\left[\mathcal{Q}_{1R}\mathcal{Q}_{2R} + \mathcal{Q}_{1I}\mathcal{Q}_{2I}\right]^2 + \left[\mathcal{Q}_{1R}\mathcal{Q}_{2I} - \mathcal{Q}_{1I}\mathcal{Q}_{2R}\right]^2\\
&\quad = \left[\mathcal{Q}_{2R}^2(\phi) + \mathcal{Q}_{2I}^2(\phi)\right]^2.
\end{aligned}
\tag{20}
$$

Notice that

$$
\begin{aligned}
&\left[\mathcal{Q}_{1R}(\zeta)\mathcal{Q}_{2R}(\zeta) + \mathcal{Q}_{1I}(\zeta)\mathcal{Q}_{2I}(\zeta)\right]^2\\
&\quad = \left(b_1\phi^{5\vartheta} + b_2\phi^{4\vartheta} + b_3\zeta^{3\vartheta} + b_4\zeta^{2\vartheta} + b_5\zeta^{\vartheta} + b_6\right)^2,\\
&\left[\mathcal{Q}_{1R}(\zeta)\mathcal{Q}_{2I}(\zeta) - \mathcal{Q}_{1I}(\zeta)\mathcal{Q}_{2R}(\zeta)\right]^2\\
&\quad = \left(b_7\phi^{5\vartheta} + b_8\phi^{4\vartheta} + b_9\phi^{3\vartheta} + b_{10}\zeta^{2\vartheta} + b_{11}\zeta^{\vartheta}\right)^2,\\
&\left[\mathcal{Q}_{2R}^2(\zeta) + \mathcal{Q}_{2I}^2(\zeta)\right]^2\\
&\quad = \left(b_{12}\zeta^{4q} + b_{13}\zeta^{3\vartheta} + b_{14}\zeta^{2\vartheta} + b_{15}\zeta^{\vartheta}\right)^2,
\end{aligned}
\tag{21}
$$

where

$$
\begin{aligned}
b_1 &= a_1a_8 + a_5a_{11},\\
b_2 &= a_2a_8 + a_1a_9 + a_6a_{11} + a_5a_{12},\\
b_3 &= a_3a_8 + a_2a_9 + a_1a_{10} + a_7a_{11} + a_6a_{12},\\
b_4 &= a_4a_8 + a_3a_9 + a_2a_{10} + a_7a_{12},\\
b_5 &= a_4a_9 + a_3a_{10},\\
b_6 &= a_4a_{10},\\
b_7 &= a_1a_{11} - a_5a_8,\\
b_8 &= a_2a_{11} + a_1a_{12} - a_5a_9 - a_6a_8,\\
b_9 &= la_3a_{11} + a_2a_{12} - a_5a_{10} - a_6a_9 - a_7a_8,\\
b_{10} &= a_4a_{11} + a_3a_{12} - a_6a_{10} - a_7a_9,\\
b_{11} &= a_4a_{12} - a_7a_{10},\\
b_{12} &= a_8^2 + a_{11}^2,\\
b_{13} &= 2(a_8a_9 + a_{11}a_{12}),\\
b_{14} &= 2a_8a_{10} + a_{12}^2,\\
b_{15} &= 2a_9a_{10}.
\end{aligned}
\tag{22}
$$

By (20), one has

$$
\begin{aligned}
&\varrho_1\zeta^{10\vartheta} + \varrho_2\zeta^{9\vartheta} + \varrho_3\zeta^{8\vartheta} + \varrho_4\zeta^{7\vartheta} + \varrho_5\zeta^{6\vartheta} + \varrho_6\zeta^{5\vartheta} + \varrho_7\zeta^{4\vartheta}\\
&\quad + \varrho_8\zeta^{3\vartheta} + \varrho_9\zeta^{2\vartheta} + \varrho_{10}\zeta^{\vartheta} + \varrho_{11} = 0,
\end{aligned}
\tag{23}
$$

where

$$
\begin{aligned}
\varrho_1 &= b_1^2 + b_7^2,\\
\varrho_2 &= 2b_1b_2 + 2b_7b_8,\\
\varrho_3 &= b_2^2 + b_8^2 - b_{12}^2 + 2b_1b_3 + 2b_7b_9,\\
\varrho_4 &= 2(b_2b_3 + b_1b_2 + b_7b_{10} + b_8b_9 - b_{12}b_{13}),\\
\varrho_5 &= b_3^2 + 2b_1b_5 + 2b_2b_4 + b_9^2 + 2b_7b_{11} + 2b_8b_{10} - b_{13}^2\\
&\quad - 2b_{12}b_{14},\\
\varrho_6 &= 2b_1b_6 + 2b_2b_5 + 2b_3b_4 + 2b_9b_{10} - 2b_{12}b_{15}\\
&\quad - 2b_{13}b_{14},\\
\varrho_7 &= b_4^2 + 2b_3b_5 + b_{10}^2 + 2b_8b_{11} + 2b_9b_{11} - b_{14}^2\\
&\quad - 2b_{13}b_{15},\\
\varrho_8 &= 2b_3b_6 + 2b_4b_5 + 2b_{10}b_{11} - 2b_{14}b_{15},\\
\varrho_9 &= b_5^2 + 2b_4b_6 + b_{11}^2 - b_{15}^2,\\
\varrho_{10} &= 2b_5b_6,\\
\varrho_{11} &= b_6^2.
\end{aligned}
\tag{24}
$$

Let

$$\Phi(\zeta) = \varrho_1\zeta^{10\vartheta} + \varrho_2\zeta^{9\vartheta} + \varrho_3\zeta^{8\vartheta} + \varrho_4\zeta^{7\vartheta} + \varrho_5\zeta^{6\vartheta} + \varrho_6\zeta^{5\vartheta} + \varrho_7\zeta^{4\vartheta} + \varrho_8\zeta^{3\vartheta} + \varrho_9\zeta^{2\vartheta} + \varrho_{10}\zeta^{\vartheta} + \varrho_{11} \tag{25}$$

and

$$\gamma(\nu) = \varrho_1\nu^{10} + \varrho_2\nu^{9} + \varrho_3\nu^{8} + \varrho_4\nu^{7} + \varrho_5\nu^{6} + \varrho_6\nu^{5} + \varrho_7\nu^{4} + \varrho_8\nu^{3} + \varrho_9\nu^{2} + \varrho_{10}\nu + \varrho_{11}. \tag{26}$$

Lemma 5. *(a) If $\varrho_i > 0$ $(i = 1, 2, 3, \ldots, 11)$, then (13) has no root with zero real parts; (b) if $\varrho_{11} > 0$ and there exists a constant $\nu_0 > 0$ such that $\gamma(\nu_0) < 0$, then (13) has at least two pairs of purely imaginary roots.*

Proof. (a) It follows from (25) that

$$\begin{aligned}\frac{d\Phi(\zeta)}{d\zeta} &= 10\vartheta\varrho_1\zeta^{10\vartheta-1} + 9\vartheta\varrho_2\zeta^{9\vartheta-1} + 8\vartheta\varrho_3\zeta^{8\vartheta-1} \\ &\quad + 7\vartheta\varrho_4\zeta^{7\vartheta-1} + 6\vartheta\varrho_5\zeta^{6\vartheta-1} + 5\vartheta\varrho_6\zeta^{5\vartheta-1} \\ &\quad + 4\vartheta\varrho_7\zeta^{4\vartheta-1} + 3\vartheta\varrho_8\zeta^{3\vartheta-1} + 2\vartheta\varrho_9\zeta^{2\vartheta-1} \\ &\quad + \vartheta\varrho_{10}\zeta^{\vartheta-1}.\end{aligned} \tag{27}$$

Notice that $\varrho_i > 0$ $(i = 1, 2, 3, \ldots, 10)$; then $d\Phi(\zeta)/d\zeta > 0$, $\forall\zeta > 0$. By $\Phi(0) = \varrho_{11} > 0$, one knows that (26) has no positive real root. In addition, $s = 0$ is not the root of (13). We complete the proof of (a).

(b) Notice that $\gamma(0) = \varrho_{11} > 0$, $\gamma(\eta_0) < 0$ $(\eta_0 > 0)$ and $\lim_{\mu\longrightarrow+\infty}(\gamma(\mu)/d\mu) = +\infty$; then $\exists\eta_{01} \in (0, \eta_0)$ and $\varepsilon_{02} \in (\eta_0, +\infty)$ such that $\gamma(\eta_{01}) = \gamma(\eta_{02}) = 0$, and then (25) has at least two positive real roots. Thus (13) has at least two pairs of purely imaginary roots. We complete the proof of (b). □

Without loss of generality, one can assume that (23) has ten positive real roots ζ_j $(j = 1, 2, \ldots, 10)$. By (13), we obtain

$$\rho_j^l = \frac{1}{\zeta_j}\left[\arccos\left(-\frac{\mathcal{Q}_{1R}(\zeta_j)\mathcal{Q}_{2R}(\zeta_j) + \mathcal{Q}_{1I}(\zeta_j)\mathcal{Q}_{2I}(\zeta_j)}{\mathcal{Q}_{2R}^2(\zeta_j) + \mathcal{Q}_{2I}^2(\zeta_j)}\right) + 2l\pi\right], \tag{28}$$

where $l = 0, 1, 2, \ldots,$ $j = 1, 2, \ldots, 10$. Then $\pm i\zeta_j$ is a pair of purely imaginary roots of (10) when $\rho = \rho_j^l$. Let

$$\rho_0 = \min_{j=1,2,\ldots,11}\left\{\rho_j^0\right\}, \qquad \zeta_0 = \zeta|_{\rho=\rho_0}. \tag{29}$$

Now we give the following assumption:

$(\mathcal{A}1)$ $\mathcal{U}_1\mathcal{V}_1 + \mathcal{U}_2\mathcal{V}_2 > 0$, where

$$\begin{aligned}\mathcal{U}_1 &= 3\vartheta\zeta_0^{3\vartheta-1}\cos\frac{(3\vartheta-1)\pi}{2} + 2\vartheta\left(p_2 + p_3 - \frac{u_2^* - p_1}{1-\kappa_d}\right)\zeta_0^{2\vartheta-1}\cos\frac{(2\vartheta-1)\pi}{2} + \vartheta\left[p_2p_3 - \frac{(u_2^* - p_1)(p_2+p_3)}{1-\kappa_d}\right]\zeta_0^{\vartheta-1}\cos\frac{(\vartheta-1)\pi}{2} \\ &\quad - \frac{\kappa_p}{1-\kappa_d}\left[2\vartheta\zeta_0^{2\vartheta-1}\cos\frac{(2\vartheta-1)\pi}{2} + \vartheta(p_2+p_3)\zeta_0^{\vartheta-1}\cos\frac{(\vartheta-1)\pi}{2}\right]\cos\zeta_0\rho_0 \\ &\quad - \frac{\kappa_p}{1-\kappa_d}\left[2\vartheta\zeta_0^{2\vartheta-1}\sin\frac{(2\vartheta-1)\pi}{2} + \vartheta(p_2+p_3)\zeta_0^{\vartheta-1}\sin\frac{(\vartheta-1)\pi}{2}\right]\sin\zeta_0\rho_0, \\ \mathcal{U}_2 &= 3\vartheta\zeta_0^{3\vartheta-1}\sin\frac{(3\vartheta-1)\pi}{2} + 2\vartheta\left(p_2 + p_3 - \frac{u_2^* - p_1}{1-\kappa_d}\right)\zeta_0^{2\vartheta-1}\sin\frac{(2\vartheta-1)\pi}{2} + \vartheta\left[p_2p_3 - \frac{(u_2^* - p_1)(p_2+p_3)}{1-\kappa_d}\right]\zeta_0^{\vartheta-1}\sin\frac{(\vartheta-1)\pi}{2} \\ &\quad + \frac{\kappa_p}{1-\kappa_d}\left[2\vartheta\zeta_0^{2\vartheta-1}\cos\frac{(2\vartheta-1)\pi}{2} + \vartheta(p_2+p_3)\zeta_0^{\vartheta-1}\cos\frac{(\vartheta-1)\pi}{2}\right]\sin\zeta_0\rho_0 \\ &\quad - \frac{\kappa_p}{1-\kappa_d}\left[2\vartheta\zeta_0^{2\vartheta-1}\sin\frac{(2\vartheta-1)\pi}{2} + \vartheta(p_2+p_3)\zeta_0^{\vartheta-1}\sin\frac{(\vartheta-1)\pi}{2}\right]\cos\zeta_0\rho_0, \\ \mathcal{V}_1 &= -\frac{\kappa_p}{1-\kappa_d}\left[\zeta_0^{2\vartheta}\cos\vartheta\pi + (p_2+p_3)\zeta_0^{\vartheta}\cos\frac{\vartheta\pi}{2} + p_2p_3\right]\zeta_0\sin\zeta_0\rho_0 + \frac{\kappa_p}{1-\kappa_d}\left[\zeta_0^{2\vartheta}\sin\vartheta\pi + (p_2+p_3)\zeta_0^{\vartheta}\sin\frac{\vartheta\pi}{2} + p_2p_3\right]\zeta_0\cos\zeta_0\rho_0, \\ \mathcal{V}_2 &= -\frac{\kappa_p}{1-\kappa_d}\left[\zeta_0^{2\vartheta}\cos\vartheta\pi + (p_2+p_3)\zeta_0^{\vartheta}\cos\frac{\vartheta\pi}{2} + p_2p_3\right]\zeta_0\cos\zeta_0\rho_0 - \frac{\kappa_p}{1-\kappa_d}\left[\zeta_0^{2\vartheta}\sin\vartheta\pi + (p_2+p_3)\zeta_0^{\vartheta}\sin\frac{\vartheta\pi}{2} + p_2p_3\right]\zeta_0\sin\zeta_0\rho_0.\end{aligned} \tag{30}$$

Lemma 6. *If $s(\rho) = \xi(\rho) + i\psi(\rho)$ is the root of (13) near $\rho = \rho_0$ which satisfies $\xi(\rho_0) = 0$, $\psi(\rho_0) = \psi_0$, then* $\operatorname{Re}[ds/d\rho]|_{\rho=\rho_0,\psi=\psi_0} > 0$.

Proof. By (13), one has

$$\frac{\mathcal{Q}_1(s)}{d\rho} + \frac{\mathcal{Q}_2(s)}{d\rho}e^{-s\rho} - e^{-s\rho}\left(\frac{ds}{d\rho}\rho + s\right)\mathcal{Q}_2(s) = 0. \tag{31}$$

Notice that

$$\begin{aligned}\frac{\mathcal{Q}_1(s)}{d\rho} &= 3\vartheta s^{3\vartheta-1}\frac{ds}{d\rho} + 2\vartheta\left(p_2 + p_3 - \frac{u_2^* - p_1}{1-\kappa_d}\right)\\ &\quad\cdot s^{2\vartheta-1}\frac{ds}{d\rho} + \vartheta\left[p_2p_3 - \frac{(u_2^* - p_1)(p_2+p_3)}{1-\kappa_d}\right]\\ &\quad\cdot s^{\vartheta-1}\frac{ds}{d\rho} = \left\{3\vartheta s^{3\vartheta-1}\right.\\ &\quad + 2\vartheta\left(p_2 + p_3 - \frac{u_2^* - p_1}{1-\kappa_d}\right)s^{2\vartheta-1}\\ &\quad\left. + \vartheta\left[p_2p_3 - \frac{(u_2^* - p_1)(p_2+p_3)}{1-\kappa_d}\right]s^{\vartheta-1}\right\}\frac{ds}{d\rho},\\ \frac{\mathcal{Q}_2(s)}{d\rho} &= -\frac{\kappa_p}{1-\kappa_d}\left[2\vartheta s^{2\vartheta-1} + \vartheta(p_2+p_3)s^{\vartheta-1}\right]\frac{ds}{d\rho},\end{aligned} \tag{32}$$

and then one has

$$\left[\frac{ds}{d\rho}\right]^{-1} = \frac{\mathcal{F}_1(\rho)}{\mathcal{F}_2(\rho)} - \frac{\rho}{s}, \tag{33}$$

where

$$\begin{aligned}\mathcal{F}_1(s) &= 3\vartheta s^{3\vartheta-1} + 2\vartheta\left(p_2 + p_3 - \frac{u_2^* - p_1}{1-\kappa_d}\right)s^{2\vartheta-1}\\ &\quad + \vartheta\left[p_2p_3 - \frac{(u_2^* - p_1)(p_2+p_3)}{1-\kappa_d}\right]s^{\vartheta-1}\\ &\quad - \frac{\kappa_p}{1-\kappa_d}\left[2\vartheta s^{2\vartheta-1} + \vartheta(p_2+p_3)s^{\vartheta-1}\right]e^{-s\rho},\\ \mathcal{F}_2(s) &= \mathcal{Q}_2(s)\,se^{-s\rho}.\end{aligned} \tag{34}$$

Then

$$\operatorname{Re}\left\{\left[\frac{ds}{d\rho}\right]^{-1}\right\} = \operatorname{Re}\left\{\frac{\mathcal{F}_1(\rho)}{\mathcal{F}_2(\rho)}\right\}. \tag{35}$$

Thus

$$\begin{aligned}\operatorname{Re}\left\{\frac{ds}{d\rho}\right\}\Big|_{\rho=\rho_0,\psi=\psi_0} &= \operatorname{Re}\left\{\frac{F_1(\rho)}{F_2(\rho)}\right\}\Big|_{\rho=\rho_0,\psi=\psi_0}\\ &= \frac{\mathcal{U}_1\mathcal{V}_1 + \mathcal{U}_2\mathcal{V}_2}{\mathcal{V}_1^2 + \mathcal{V}_2^2}.\end{aligned} \tag{36}$$

It follows from $(\mathcal{A}1)$ that

$$\operatorname{Re}\left\{\left[\frac{ds}{d\rho}\right]^{-1}\right\}\Big|_{\rho=\rho_0,\psi=\psi_0} > 0. \tag{37}$$

Th proof of Lemma 6 is completed. □

Let

$$\begin{aligned}\epsilon_1 &= \left(p_2 + p_3 - \frac{u_2^* - p_1}{1-\kappa_d}\right) - \frac{\kappa_p}{1-\kappa_d},\\ \epsilon_2 &= p_2p_3 - \frac{(u_2^* - p_1 - \kappa_p)(p_2+p_3)}{1-\kappa_d},\\ \epsilon_3 &= -\frac{\kappa_p p_2 p_3 + (u_2^* - p_1)(p_2+p_3)}{1-\kappa_d}.\end{aligned} \tag{38}$$

Next we give an assumption as follows:

$(\mathcal{A}2)$ $\epsilon_1 > 0$, $\epsilon_1\epsilon_2 > 2\epsilon_3$, $\epsilon_3 > 0$.

Lemma 7. *If $\rho = 0$ and $(\mathcal{A}2)$ holds true, then system (9) is locally asymptotically stable.*

Proof. If $\rho = 0$, then (13) takes the form

$$\lambda^3 + \epsilon_1\lambda^2 + \epsilon_2\lambda + \epsilon_3 = 0. \tag{39}$$

By $(\mathcal{A}2)$, all roots λ_i of (39) satisfy $|\arg(\lambda_i)| > \vartheta\pi/2$ ($i = 1, 2, 3$). By Lemma 3, we know that the conclusion of Lemma 4.3 holds. The proof of Lemma 3.4 is completed. □

According to the analysis above, we have the following conclusion.

Theorem 8. *In addition to condition (b) of Lemma 6. If $(\mathcal{A}1)$ and $(\mathcal{A}2)$ are fulfilled, then the equilibrium point (u_1^*, u_2^*, u_3^*) of system (9) is locally asymptotically stable when $\rho \in [0, \rho_0)$ and a Hopf bifurcation will appear around the equilibrium point E_1 when $\rho = \rho_0$.*

Remark 9. In [4–7, 13–20], the authors studied the various dynamics of integer-order financial models. They did not involve the fractional-order forms. In [39], Bhalekar and Gejji considered the chaos of fractional-order financial model by predictor-corrector method. In this article, we control the chaos of fractional-order financial model by applying PD^{ϑ} control strategy. All the derived results and analysis ways of [4–7, 13–20, 39] can not be transferred to (2) to control the chaotic behavior. Based on these viewpoints, the fruits of this paper are entirely innovative and supplement the previous publications.

4. An Example

We give the following controlled financial system:

$$\begin{aligned}\frac{d^{\vartheta}u_1}{dt^{\vartheta}} &= u_3 + (u_2 - 3)u_1 + \kappa_p(u_1(t-\rho) - u_1^*)\\ &\quad + \kappa_d\frac{d^{\vartheta}}{dt^{\vartheta}}(u_1(t) - u_1^*),\\ \frac{d^{\vartheta}u_2}{dt^{\vartheta}} &= 1 - 0.1u_2 - u_1^2,\\ \frac{d^{\vartheta}u_3}{dt^{\vartheta}} &= -u_1 - u_3.\end{aligned} \tag{40}$$

Table 1: The relation of parameters ϑ and ρ_0 of model (40).

ϑ	ρ_0
0.195	0.1968
0.267	0.2569
0.384	0.3450
0.558	0.4593
0.672	0.5262
0.736	0.5615
0.829	0.6104

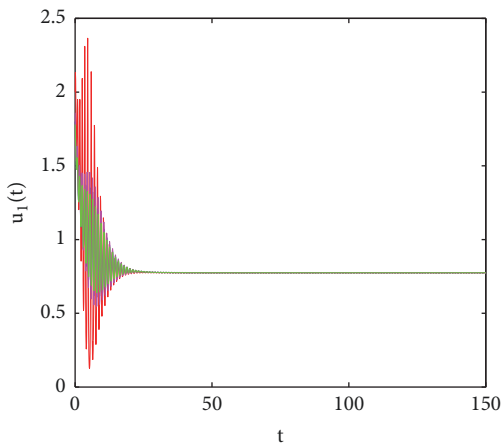

Figure 11: The relation of t and u_1 in model (40) when $\rho = 0.4237 < \rho_0 = 0.5262$.

Clearly, system (40) has an equilibrium point (0.6831, 2.6667, −0.4554). Let $\kappa_p = 0.07$, $\kappa_p = 0.32$, $\vartheta = 0.672$. Then the critical frequency $\zeta_0 = 0.8653$ and the bifurcation point $\rho_0 = 0.5262$. We can check that the assumptions in Theorem 8 hold true. Figures 11–20 indicate that when $\rho \in [0, 0.5262)$, the equilibrium point (0.6831, 2.6667, −0.4554) of model (40) is locally asymptotically stable. From the financial point of view, it means that as time goes on, the interest rate will tend to the constant 0.6831, investment demand will tend to the constant 2.6667, and price index will tend to the constant -0.4554. Figures 21–30 indicate that $\rho \in [0.5262, +\infty)$, system (40) becomes unstable, and a Hopf bifurcation emerges. From the financial point of view, it means that as time goes on, the interest rate, investment demand, and price index will keep a periodic cycle. In addition, we show the relation of parameters ϑ and ρ_0 of (40) with Table 1.

5. Conclusions

In this paper, we propose a new fractional-order financial system. To control the chaotic behavior of the fractional-order financial system, we successfully design a PD^{ϑ} controller to achieve our goal. By adjusting the proportional and derivative parameters, we can change the stability and Hopf bifurcation character of the considered fractional-order financial system. By regarding the time delay as bifurcation parameter, we have established a new sufficient condition to ensure the stability

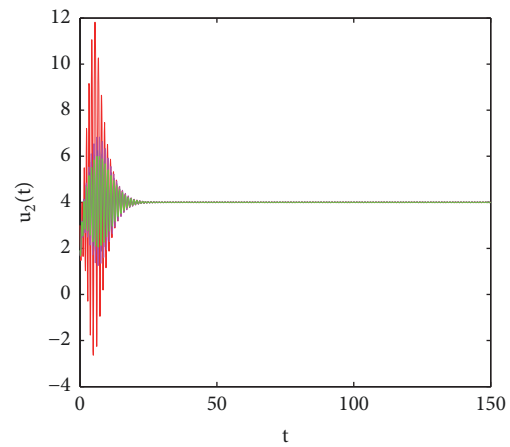

Figure 12: The relation of t and u_2 in model (40) when $\rho = 0.4237 < \rho_0 = 0.5262$.

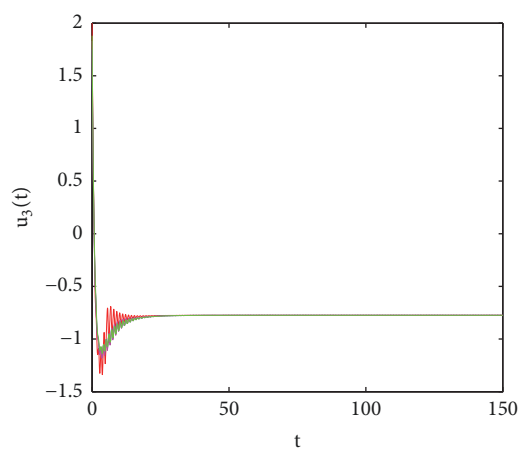

Figure 13: The relation of t and u_3 in model (40) when $\rho = 0.4237 < \rho_0 = 0.5262$.

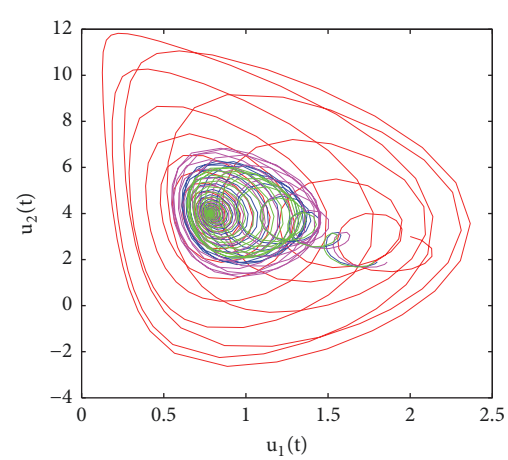

Figure 14: The relation of u_1 and u_2 in model (40) when $\rho = 0.4237 < \rho_0 = 0.5262$.

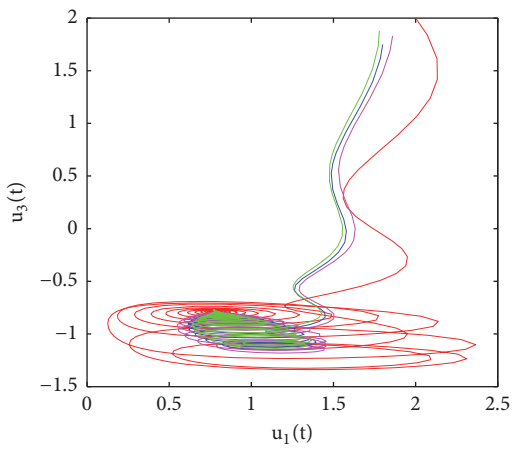

Figure 15: The relation of u_1 and u_3 in model (40) when $\rho = 0.4237 < \rho_0 = 0.5262$.

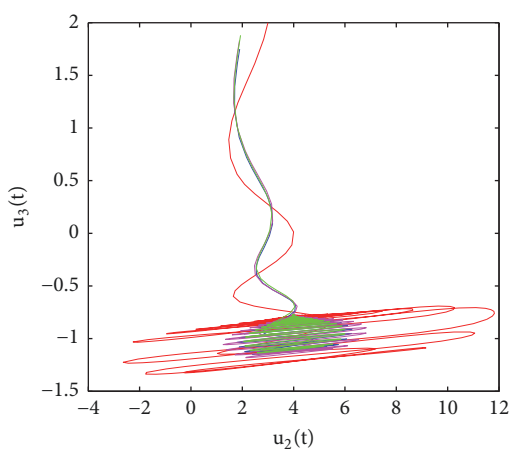

Figure 16: The relation of u_2 and u_3 in model (40) when $\rho = 0.4237 < \rho_0 = 0.5262$.

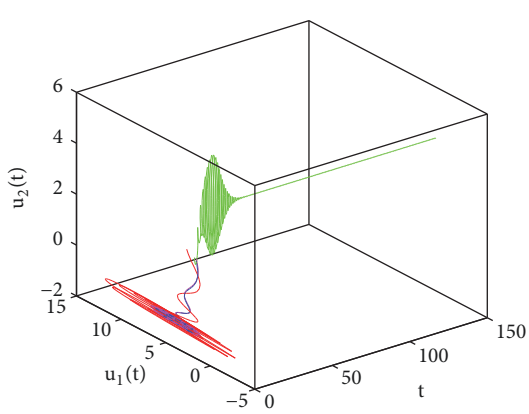

Figure 17: The relation of u_1, u_2, and u_3 in model (40) when $\rho = 0.4237 < \rho_0 = 0.5262$.

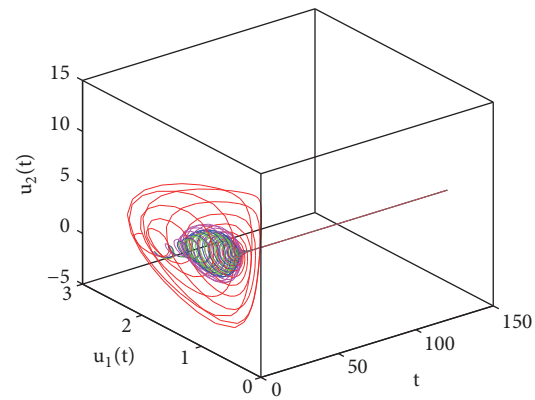

Figure 18: The relation of t, u_1, and $u2$ in model (40) when $\rho = 0.4237 < \rho_0 = 0.5262$.

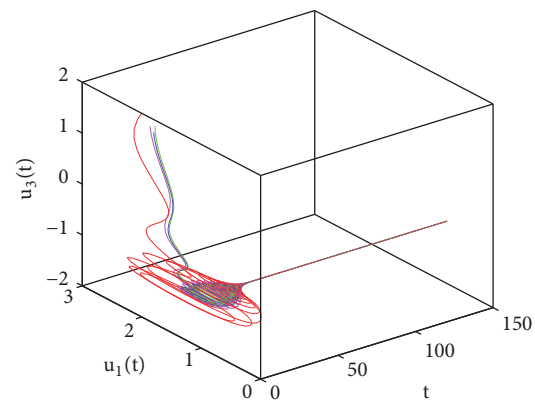

Figure 19: The relation of t, u_2, and u_3 in model (40) when $\rho = 0.4237 < \rho_0 = 0.5262$.

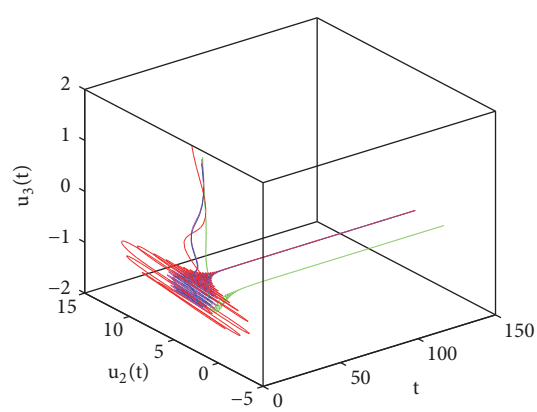

Figure 20: The relation of t, u_2, and u_3 in model (40) when $\rho = 0.4237 < \rho_0 = 0.5262$.

and the existence of Hopf bifurcation of the fractional-order financial model. Also, the effect of the fractional order and delay on the stability and Hopf bifurcation is revealed. The research idea and the obtained theoretical

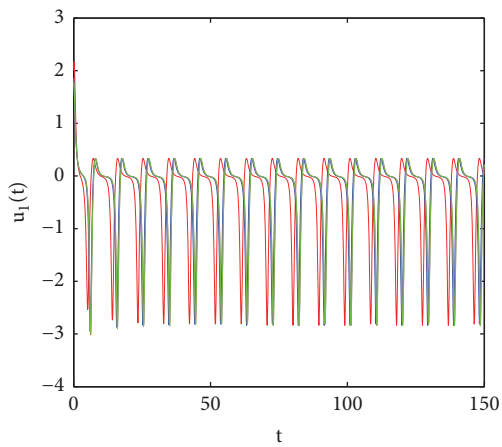

FIGURE 21: The relation of t and u_1 in model (40) when $\rho = 0.8345 > \rho_0 = 0.5262$.

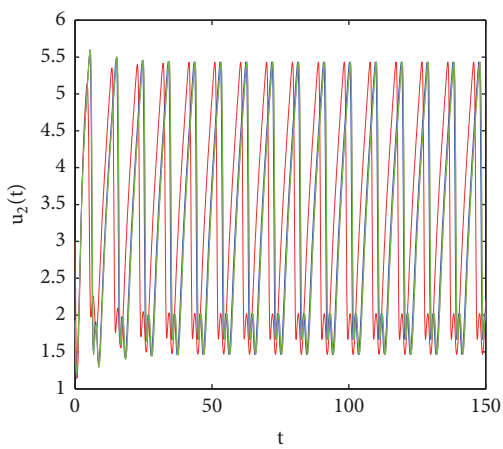

FIGURE 22: The relation of t and u_2 in model (40) when $\rho = 0.8345 > \rho_0 = 0.5262$.

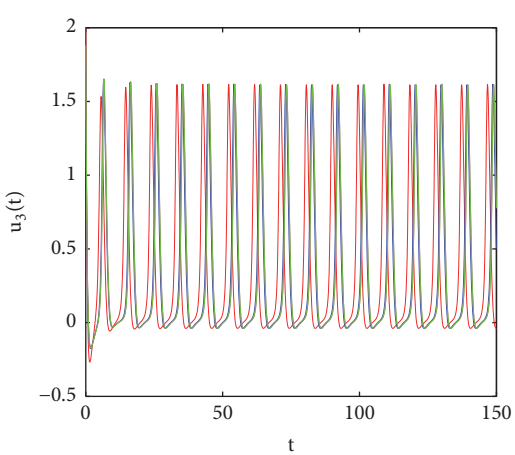

FIGURE 23: The relation of t and u_3 in model (40) when $\rho = 0.8345 > \rho_0 = 0.5262$.

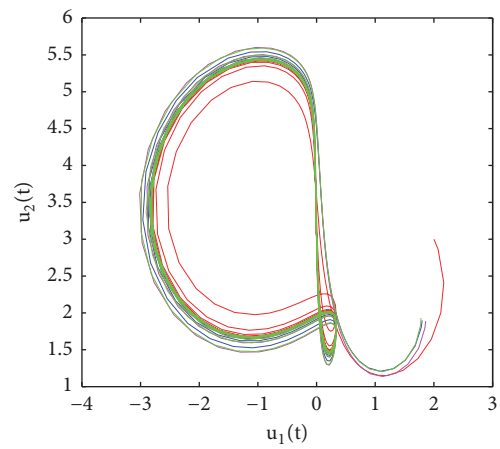

FIGURE 24: The relation of u_1 and u_2 in model (40) when $\rho = 0.8345 > \rho_0 = 0.5262$.

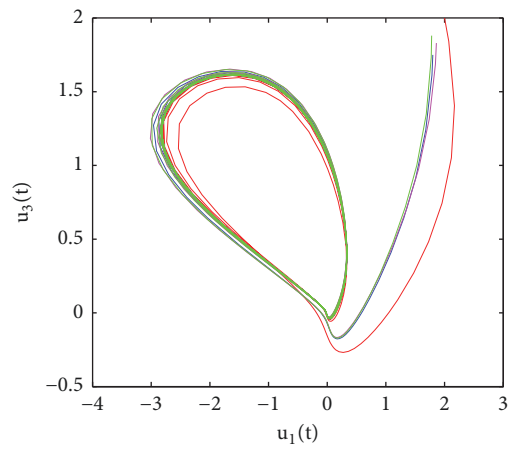

FIGURE 25: The relation of u_1 and u_3 in model (40) when $\rho = 0.8345 > \rho_0 = 0.5262$.

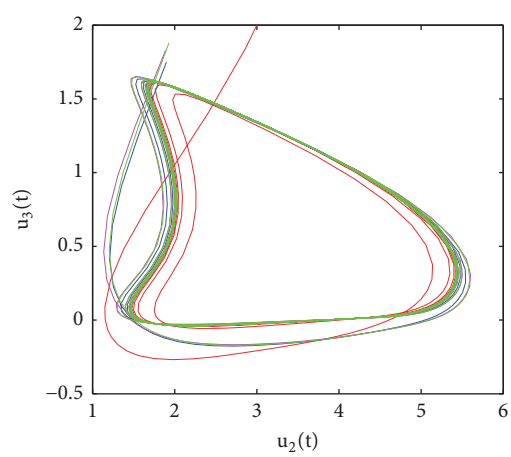

FIGURE 26: The relation of u_2 and u_3 in model (40) when $\rho = 0.8345 > \rho_0 = 0.5262$.

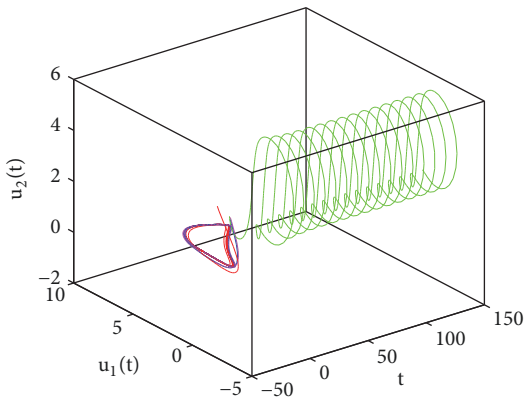

Figure 27: The relation of u_1, u_2, and u_3 in model (40) when $\rho = 0.8345 > \rho_0 = 0.5262$.

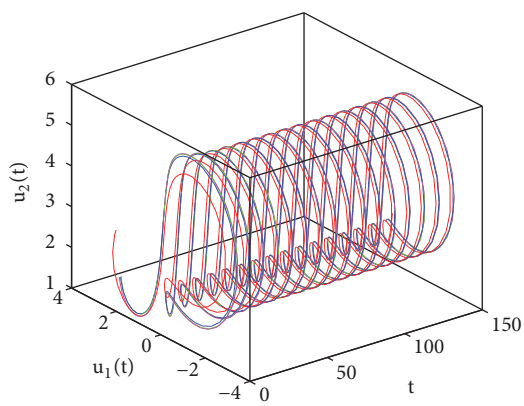

Figure 28: The relation of t, u_1, and u_2 in model (40) when $\rho = 0.8345 > \rho_0 = 0.5262$.

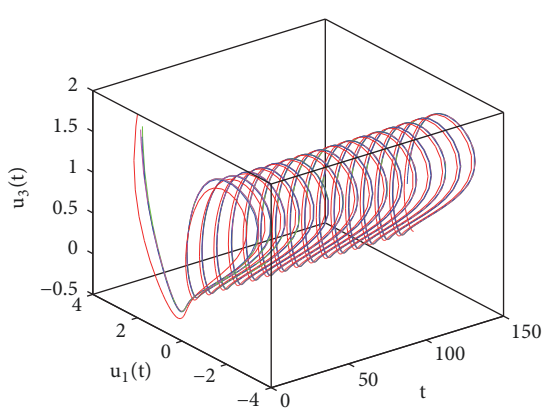

Figure 29: The relation of t, u_2, and u_3 in model (40) when $\rho = 0.8345 > \rho_0 = 0.5262$.

results of this article enrich and develop the bifurcation and control theory of fractional-order differential equations. The obtained results can provide useful guidance to people in financial community. We can properly adjust the parameter of the PD^{ϑ} controller to apply the suggested fractional-order financial models to deal with financially chaotic problems. In

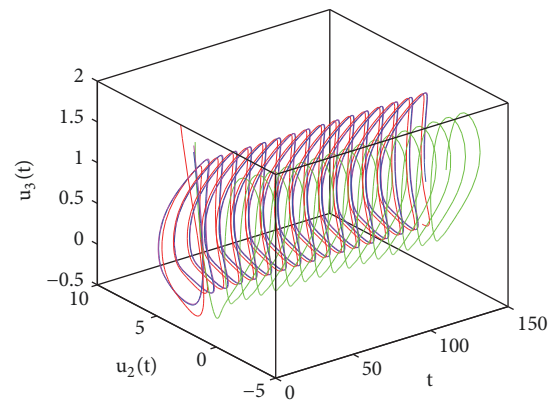

Figure 30: The relation of t, u_2, and u_3 in model (40) when $\rho = 0.8345 > \rho_0 = 0.5262$.

addition, we point out that although the PD^{ϑ} controller can effectively control the chaos of the fractional-order financial model, it involves multiple parameters: proportional control parameter κ_p, the derivative control parameter κ_d, time delay ρ, and fractional order ϑ. In the future, we will seek some more simple controllers with less parameters to suppress the chaotic behavior.

Data Availability

No data were used to support this study.

Conflicts of Interest

The authors declare that they have no conflicts of interest.

Acknowledgments

The authors were supported by the National Natural Science Foundation of China (no. 61673008), Project of High-Level Innovative Talents of Guizhou Province ([2016]5651), Major Research Project of the Innovation Group of the Education Department of Guizhou Province ([2017]039), Project of Key Laboratory of Guizhou Province with Financial and Physical Features ([2017]004), Foundation of Science and Technology of Guizhou Province ([2018]1025 and [2018]1020), and Hunan Provincial Key Laboratory of Mathematical Modeling and Analysis in Engineering (Changsha University of Science & Technology) (2018MMAEZD21).

References

[1] L. L. Zhang, G. L. Cai, and X. L. Fang, "Stability for a novel time-delay financial hyperchaotic system by adaptive periodically intermittent linear control," *Journal of Applied Analysis and Computation*, vol. 7, no. 1, pp. 79–91, 2017.

[2] A. Serletis, "Is there chaos in economic time series?" *Canadian Journal of Economics*, vol. 29, pp. S210–S212, 1996.

[3] Y. Lin, Y. Chen, and Q. Cao, "Nonliear and chaotic analysis of a financial complex system," *Applied Mathematics and Mechnics*, vol. 31, no. 10, pp. 1305–1316, 2010.

[4] Q. Gao and J. Ma, "Chaos and Hopf bifurcation of a finance system," *Nonlinear Dynamics*, vol. 58, no. 1-2, pp. 209–216, 2009.

[5] J. Zhang, J. Nan, Y. Chu, W. Du, and X. An, "Stochastic Hopf bifurcation of a novel finance chaotic system," *Journal of Nonlinear Sciences and Applications. JNSA*, vol. 9, no. 5, pp. 2727–2739, 2016.

[6] G. L. Cai, L. Yao, P. Hu, and X. L. Fang, "Adaptive full state hybrid function projective synchronization of financial hyperchaotic systems with uncertain parameters," *Discrete and Continuous Dynamical Systems - Series B*, vol. 18, no. 8, pp. 2019–2028, 2013.

[7] J. H. Ma and H. I. Bangura, "Complexity analysis research of financial and economic system under the condition of three parameters' change circumstances," *Nonlinear Dynamics*, vol. 70, no. 4, pp. 2313–2326, 2012.

[8] J. H. Ma and Y. S. Chen, "Study for the bifurcation topological structure and the global complicated character of a kind of nonlinear finance system," *Applied Mathematics and Mechanics*, vol. 22, no. 11, pp. 1240–1251, 2001.

[9] J. H. Ma and Y. S. Chen, "Study for the bifurcation topological structure and the global complicated character of a kind of nonlinear finance system (II)," *Applied Mathematics and Mechanics*, vol. 22, no. 12, pp. 1375–1382, 2001.

[10] M. S. Abd-Elouahab, N. E. Hamri, and J. W. Wang, "Chaos control of a fractional-order financial system," *Mathematical Problems in Engineering*, vol. 2010, Article ID 270646, 18 pages, 2010.

[11] A. Hajipour and H. Tavakoli, "Analysis and circuit simulation of a novel nonlinear fractional incommensurate order financial system," *Optik - International Journal for Light and Electron Optics*, vol. 127, no. 22, pp. 10643–10652, 2016.

[12] C. Huang, L. Cai, and J. Cao, "Linear control for synchronization of a fractional-order time-delayed chaotic financial system," *Chaos, Solitons & Fractals*, vol. 113, pp. 326–332, 2018.

[13] W.-C. Chen, "Dynamics and control of a financial system with time-delayed feedbacks," *Chaos, Solitons & Fractals*, vol. 37, no. 4, pp. 1198–1207, 2008.

[14] W.-S. Son and Y.-J. Park, "Delayed feedback on the dynamical model of a financial system," *Chaos, Solitons & Fractals*, vol. 44, no. 4, pp. 208–217, 2011.

[15] X. Zhang and H. Zhu, "Hopf bifurcation and chaos of a delayed finance system," *Complexity*, vol. 2019, Article ID 6715036, 18 pages, 2019.

[16] X. Chen, H. Liu, and C. Xu, "The new result on delayed finance system," *Nonlinear Dynamics*, vol. 78, no. 3, pp. 1989–1998, 2014.

[17] G. Mircea, M. Neamtu, O. Bundau, and D. Opris, "Uncertain and stochastic financial models with multiple delays," *International Journal of Bifurcation and Chaos*, vol. 22, no. 6, Article ID 1250131, 19 pages, 2012.

[18] R. Y. Zhang, "Bifurcation analysis for a kind of nonlinear finance system with delayed feedback and its application to control of chaos," *Journal of Applied Mathematics*, vol. 2012, Article ID 316390, 18 pages, 2012.

[19] Y. T. Ding and J. Cao, "Bifurcation analysis and chaos switchover phenomenon in a nonlinear financial system with delay feedback," *International Journal of Bifurcation and Chaos*, vol. 25, no. 12, Article ID 1550165, 21 pages, 2015.

[20] X. L. Chai, Z. H. Gan, and C. X. Shi, "Impulsive synchronization and adaptive-impulsive synchronization of a novel financial hyperchaotic system," *Mathematical Problems in Engineering*, vol. 2013, Article ID 751616, 10 pages, 2013.

[21] Z. Wang, X. H. Wang, Y. X. Li, and X. Huang, "Stability and hopf bifurcation of fractional-order complex-valued single neuron model with time delay," *International Journal of Bifurcation and Chaos*, vol. 27, no. 13, Article ID 1750209, 2017.

[22] Z. Wang, L. Li, Y. X. Li, and Z. S. Cheng, "Stability and hopf bifurcation of a three-neuron network with multiple discrete and distributed delays," *Neural Processing Letters*, vol. 48, no. 3, pp. 1481–1502, 2018.

[23] X. Li and S. Song, "Stabilization of delay systems: delay-dependent impulsive control," *IEEE Transactions on Automatic Control*, vol. 62, no. 1, pp. 406–411, 2017.

[24] X. Li and J. Cao, "An impulsive delay inequality involving unbounded time-varying delay and applications," *Institute of Electrical and Electronics Engineers Transactions on Automatic Control*, vol. 62, no. 7, pp. 3618–3625, 2017.

[25] X. H. Tang and S. Chen, "Ground state solutions of Nehari-Pohozaev type for Kirchhoff-type problems with general potentials," *Calculus of Variations and Partial Differential Equations*, vol. 56, no. 4, pp. 1–25, 2017.

[26] S. Chen and X. Tang, "Improved results for klein-gordon-maxwell systems with general nonlinearity," *Discrete and Continuous Dynamical Systems- Series A*, vol. 38, no. 5, pp. 2333–2348, 2018.

[27] S. Chen and X. Tang, "Geometrically distinct solutions for Klein-Gordon-Maxwell systems with super-linear nonlinearities," *Applied Mathematics Letters*, vol. 90, pp. 188–193, 2019.

[28] X. H. Tang and X. Y. Lin, "Existence of ground state solutions of Nehari-Pankov type to Schrödinger systems," *Science China Mathematics*, vol. 62, 2019.

[29] Y. Bai and Y. Li, "Stability and Hopf bifurcation for a stage-structured predator-prey model incorporating refuge for prey and additional food for predator," *Advances in Difference Equations*, vol. 2019, article no 42, 2019.

[30] W. Zhu, Y. Xia, B. Zhang, and Y. Bai, "Exact traveling wave solutions and bifurcations of the time-fractional differential equations with applications," *International Journal of Bifurcation and Chaos*, vol. 29, no. 3, Article ID 1950041, 2019.

[31] J. Zhang, Z. Lou, Y. Ji, and W. Shao, "Ground state of Kirchhoff type fractional Schrödinger equations with critical growth," *Journal of Mathematical Analysis and Applications*, vol. 462, no. 1, pp. 57–83, 2018.

[32] X. Zhang, L. Liu, Y. Wu, and B. Wiwatanapataphee, "Nontrivial solutions for a fractional advection dispersion equation in anomalous diffusion," *Applied Mathematics Letters*, vol. 66, pp. 1–8, 2017.

[33] Y. Q. Wang and L. S. Liu, "Positive solutions for a class of fractional 3-point boundary value problems at resonance," *Advances in Difference Equations*, vol. 7, pp. 1–13, 2017.

[34] M. Zuo, X. Hao, L. Liu, and Y. Cui, "Existence results for impulsive fractional integro-differential equation of mixed type with constant coefficient and antiperiodic boundary conditions," *Boundary Value Problems*, vol. 161, 15 pages, 2017.

[35] Y. Wang and J. Q. Jiang, "Existence and nonexistence of positive solutions for the fractional coupled system involving generalized p-Laplacian," *Advances in Difference Equations*, vol. 337, pp. 1–19, 2017.

[36] Q. H. Feng and F. W. Meng, "Traveling wave solutions for fractional partial differential equations arising in mathematical physics by an improved fractional Jacobi elliptic equation method," *Mathematical Methods in the Applied Sciences*, vol. 40, no. 10, pp. 3676–3686, 2017.

[37] B. Zhu, L. S. Liu, and Y. H. Wu, "Existence and uniqueness of global mild solutions for a class of nonlinear fractional reaction-diffusion equations with delay," *Computers & Mathematics with Applications*, in press, 2016.

[38] M. M. Li and J. R. Wang, "Exploring delayed Mittag-Leffler type matrix functions to study finite time stability of fractional delay differential equations," *Applied Mathematics and Computation*, vol. 324, pp. 254–265, 2018.

[39] V. D. Gejji and S. Bhalekar, "Chaos in fractional order financial delay system," *Computers & Mathematics with Applications*, vol. 59, no. 3, pp. 1117–1127, 2010.

[40] Z. Wang, X. Huang, and G. Shi, "Analysis of nonlinear dynamics and chaos in a fractional order financial system with time delay," *Computers & Mathematics with Applications*, vol. 62, no. 3, pp. 1531–1539, 2011.

[41] X. B. Gui, C. Tong, and L. Y. Qin, "Complexity evolvement of a chaotic fractional-order financial system," *Acta Physica Sinica*, vol. 60, no. 4, Article ID 048901, 6 pages, 2011.

[42] J. H. Luo, G. J. Li, and H. Liu, "Linear control of fractional-order financial chaotic system with input saturation," *Discrete Dynamics in Nature and Society*, vol. 2014, Article ID 802429, 8 pages, 2014.

[43] B. G. Xin and Y. T. Li, "0-1 Test for chaos in a fractional order financial system with investment incentive," *Abstract and Applied Analysis*, vol. 2013, Article ID 876298, 10 pages, 2013.

[44] Y. D. Yue, L. He, and G. C. Liu, "Modeling and application of a new nonlinear fractional financial model," *Journal of Applied Mathematics*, vol. 2013, Article ID 325050, 9 pages, 2013.

[45] B. G. Xin and T. Chen, "Projective synchronization of N-dimensional chaotic fractional-order systems via linear state error feedback control," *Discrete Dynamics in Nature and Society*, vol. 2012, Article ID 191063, 10 pages, 2012.

[46] W. W. Zhang, J. D. Cao, A. Alsaedi, and F. E. S. Alsaadi, "Synchronization of time delayed fractional order chaotic financial system," *Discrete Dynamics in Nature and Society*, vol. 2017, Article ID 1230396, 5 pages, 2017.

[47] L. P. Chen, Y. Chai, and R. C. Wu, "Control and synchronization of fractional-order financial system based on linear control," *Discrete Dynamics in Nature and Society*, vol. 2011, Article ID 958393, 21 pages, 2011.

[48] I. Podlubny, *Fractional Differential Equations*, Mathematics in Science and Engineering, Academic Press, New York, NY, USA, 1999.

[49] B. Bandyopadhyay and S. Kamal, *Stabliization and Control of Fractional Order Systems: A Sliding Mode Approach*, vol. 317, Springer, Heidelberg, Germany, 2015.

[50] D. Matignon, "Stability results for fractional differential equations with applications to control processing," in *Proceedings of the Computational engineering in systems and application multiconference, IMACS. In: IEEE-SMC Proceedings*, vol. 2, pp. 963–968, France, 1996.

[51] W. H. Deng, C. P. Li, and J. H. Lu, "Stability analysis of linear fractional differential system with multiple time delays," *Nonlinear Dynamics*, vol. 48, no. 4, pp. 409–416, 2007.

Hindawi
Complexity
Volume 2019, Article ID 1817248, 11 pages
https://doi.org/10.1155/2019/1817248

Research Article

Thermodynamic Entropy in Quantum Statistics for Stock Market Networks

Jianjia Wang [1], Chenyue Lin [2], and Yilei Wang [3]

[1] *Department of Computer Science, Shanghai University, 200444, China*
[2] *Department of Mathematics and Statistics, Queen's University, Canada K7L 3N6*
[3] *State Grid Nanjing Power Supply Company, State Grid Corporation of China, Nanjing 210019, China*

Correspondence should be addressed to Jianjia Wang; jianjiawang@shu.edu.cn

Received 20 February 2019; Accepted 9 April 2019; Published 21 April 2019

Guest Editor: Thiago Christiano Silva

The stock market is a dynamical system composed of intricate relationships between financial entities, such as banks, corporations, and institutions. Such a complex interactive system can be represented by the network structure. The underlying mechanism of stock exchange establishes a time-evolving network among companies and individuals, which characterise the correlations of stock prices in the time sequential trades. Here, we develop a novel technique in quantum statistics to analyse the financial market evolution. We commence from heat bath analogy where the normalised Laplacian matrix plays the role of the Hamiltonian operator of the network. The eigenvalues of the Hamiltonian specify energy states of the network. These states are occupied by either indistinguishable bosons or fermions with corresponding Bose-Einstein and Fermi-Dirac statistics. Using the relevant partition functions, we develop the thermodynamic entropy to explore dynamic network characterisations. We conduct the experiments to apply this novel method to identify the significant variance in network structure during the financial crisis. The thermodynamic entropy provides an excellent framework to represent the variations taking place in the stock market.

1. Introduction

The stock price is usually regarded as one of the chief representatives of economic activity in the financial market [1, 2]. It reflects the interaction among each individual and company [3]. The correlation between different financial entities is a complex system that evolves with time. Exploring the dynamic evolution of such a complex system reveals the intrinsic mechanism of the financial market and attracts scientists from different fields [1–5].

To quantify such a dynamic system, tools from complex networks have been applied to study the time sequential stock market prices [1, 5, 6]. Generally, most available network approaches map time series into the network domain so that it presents the topological and structural properties of the system [6, 7]. For example, the hierarchical structure of a minimal spanning tree provides a topological space in correlation coefficients of economic taxonomy [8]. The community structure of stock market networks represents the structural variations during the financial crisis [6].

However, most of the available work mainly focuses on the topological structure of the financial networks. They only introduce the global information of a specific period. Since the strong correlation in the time evolution of the stock market, it is significant to study the statistical properties of dynamic networks, especially during the financial crisis [4, 9, 10]. Recently, a robust method introduces the entropic measurement to quantify the network characterisation [9, 11, 12]. For example, the von Neumann entropy gives a qualitative expression for the entropy associated with the degree combinations of nodes forming edges [11–13].

To embark on this type of analysis, this paper is motivated by establishing effective and efficient methods for measuring the thermodynamic entropy in time-evolving networks. In particular, we analyse the stock market networks from the New York Stock Exchange (NYSE) [6]. We show that the financial crashes are characterised by the presence of well-defined changes to the thermodynamic entropy [13, 14], whereas outside these critical periods this characterisation remains stable for long periods. To do this, we make use of

some recent framework in quantum statistics concerning the normalised Laplacian matrix for the construction of partition functions in Bose-Einstein and Fermi-Dirac statistics [15, 16].

1.1. Related Literature. The study of correlation of financial equities plays a vital role in improving the ability to model financial entities, such as stock portfolios and fragility. The underlying principle is the use of financial time series, from which a correlation (or covariance) matrix is estimated, to construct networks [3, 17]. Then, the network characterisations shed new light on their underlying structure and dynamics.

There are different approaches to address this problem [1–5, 7]. The most common one is the principal component analysis of the correlation matrix of the time sequential financial data [18]. But this method only considers the global and linear information between pairs of financial entities. More and more research finds that the intermediate connections and collective dynamics are also crucial in analysing the financial system, especially in describing the cascade effect of the crisis [6, 13, 17]. In such a case, the occurrence of extreme events is inferred from the detection of anomalies in the time series originating from the network evolution.

Recently, an investigation of the thermodynamic properties has been performed by physicists by using the perspective and theoretical results of the network theory [5, 7, 10]. Network entropy has been extensively used to characterise the salient features of the structure in the network dynamics [9]. For example, the von Neumann entropy can be used as an effective characterisation of network structure, commencing from a quantum analogue in which the Laplacian matrix plays the role of the density matrix [11, 12]. Since the eigenvalues of the density matrix reflect the energy states of a network, this approach is closely related to the heat bath analogy in thermal physics. This provides a convenient route to use entropy to analyse network characterisations.

The heat bath analogy provides the framework of energy states in the network. It applies the matrix representation using the eigenvalues of network structure. These energy states are in the situation of thermal equilibrium, which are occupied by particles with the heat reservoir [19, 20]. Due to the thermal effect of this analogy, the particle occupation follows the quantum statistical distribution in these energy states. This specifies the microstates of the network structure and provides deep insights into network behaviour [15].

Two kinds of quantum statistical distribution are described in this thermodynamic picture, i.e., Bose-Einstein statistics and Fermi-Dirac statistics [21–23]. The relevant partition functions in each case provide the thermodynamic characterisations in network structure, such as entropy [19]. Here, in order to apply this heat bath analogy, we commence the Hamiltonian representation using the Laplacian matrix in the networks. Then, the eigenvalues of Laplacian matrix are regarded as the energy states populated by particles following Bose-Einstein and Fermi-Dirac statistics, respectively [20]. Two kinds of partition function in each quantum case provide different occupation statistics for the energy levels. This gives different thermodynamic entropy for each statistical distribution [16]. The qualitative description is that particles in Fermi-Dirac statistics obey the Pauli exclusion principle with only one particle for each energy state. This population is less dense than Bose-Einstein statistics since particles can aggregate in the same energy state [24].

The quantum representation of Bose-Einstein and Fermi-Dirac statistics also manifests differently in thermodynamic framework [24]. For instance, particles in Bose-Einstein statistics tend to condense in the lowest energy states at low temperature [21], compared to Fermi-Dirac statistics, there is only one particle per energy state [22, 23]. This is because there is little thermal disruption dictated by the Pauli exclusion principle [21, 22]. Therefore, the entropy derived from this thermodynamic perspective conveys different aspects of network structure. Since the particle samples the spectrum of Laplacian energy states, at low temperature in Bose-Einstein statistics, it is likely to respond more strongly to the spectral gap (the difference between the zero and first nonzero normalised Laplacian eigenvalues) and are thus sensitive to cluster or community structure [24, 25]. On the other hand, particles in Fermi-Dirac statistics occupy a broader spectrum of energy states. It is more sensitive to the details of spectrum density and thus convey more information about the Laplacian structural spectrum, such as the path length and cycle length distributions [26, 27].

1.2. Paper Outline. The aim of this paper is to explore the behaviour of the thermodynamic entropy from quantum statistics in stock market networks. In particular, we validate our framework by analysing time-evolving networks constructed through correlation coefficients between stocks traded at the New York Stock Exchange (NYSE). We show that the financial crashes are characterised by the presence of salient fluctuation in thermodynamic entropy. To do this, we make use of some recent results from spectral graph theory concerning the construction of the normalised Laplacian matrix for partition function in quantum statistics.

This paper is organised as follows. In Section 2 we specify how the time-evolving network of the financial market is constructed and describe some basic concepts in network representation. In Section 3 we present the methodology used to derive thermodynamic entropy using the network Hamiltonian and partition function. We highlight the relevance of quantum statistics, i.e., Bose-Einstein and Fermi-Dirac statistics, for the financial market characterisation. In Section 4, we provide our experimental results and evaluation. Finally, in Section 5 we present the conclusions of the study.

2. The Time-Evolving Stock Market Networks

2.1. Stock Market Dataset. The New York Stock Exchange dataset contains the daily prices of 3,799 stocks which had been traded continuously on the New York Stock Exchange for over 6005 trading days. The stock prices were obtained from the Yahoo! financial database (http://finance.yahoo.com). A total of 347 stocks were selected from this set, all of which listed the historical stock prices from January 1986 to February 2011 [6]. For these stocks, we apply the logarithm of return R in (1) to describes the closure price of stocks over the trading period [1, 3].

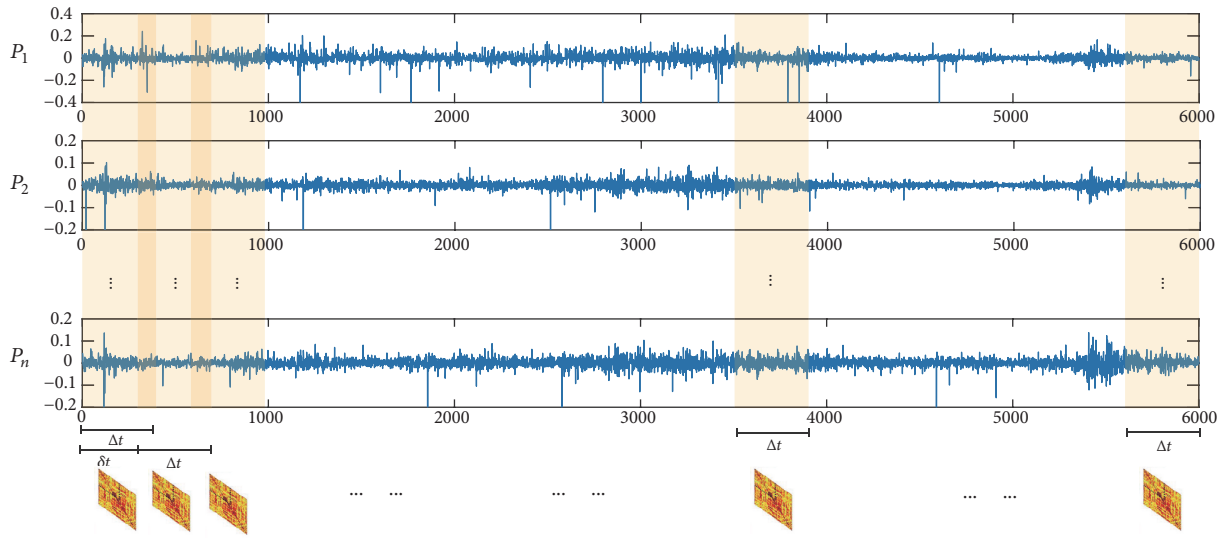

Figure 1: The illustration of the method to construct stock market networks. The network is constructed by calculating the correlations between the stocks return prices Pi (i = 1, 2, . . . , N) inside a time window of length Δt. Next, by shifting this time window by amounts δt until the end of the database is reached, we obtain the network evolution.

$$R_i(t) = \log P_i(t) - \log P_i(t-1) \tag{1}$$

where $P_i(t)$ is the ith stock price at day t. The advantage of using the logarithm of return price, instead of the stock price directly, is that it is independent of inflation and discount factors and does not require the nonlinear or stochastic transformations to correct some common trends [28, 29]. Thus, the stock market dataset contains the closure prices of 347 stocks over the period of 6004 days.

2.2. Stock Market Networks. In our network representation, the nodes correspond to various stocks and the edges indicate that there is a statistical similarity between the time series associated with the stock closing prices. In particular, to determine the edge structure of the network, we apply the Pearson correlation coefficient in (2) to quantify the similarity between two time sequential stock prices.

$$\rho_{ij} = \frac{\langle R_i R_j \rangle - \langle R_i \rangle \langle R_j \rangle}{\sqrt{\left(\langle R_i^2 \rangle - \langle R_i \rangle^2\right)\left(\langle R_j^2 \rangle - \langle R_j \rangle^2\right)}} \tag{2}$$

where R_i is the logarithm of return. Therefore, we obtain a fully weighted matrix of correlation coefficients which represents the weight of edges by ρ_{ij}.

However, the correlation coefficient matrix cannot straightly represent the topology structure of financial networks, since it does not fulfill the definition of axioms of a metric. In order to analyse the network structure using the adjacency matrix, we set a threshold ϵ to get a strong connection matrix for the edges. This leads to the definition of stock market networks by

$$A_{ij} = \Theta\left(\rho_{ij} - \epsilon\right) - \delta_{ij} \tag{3}$$

where $\Theta(\bullet)$ is the Heaviside function [30] and δ_{ij} is the Kronecker delta [31].

To analyse the time evolution of the stock market networks, we use a time window to compute the correlation coefficients between the time series for each stock pair [6]. Specifically, as shown in Figure 1, we set the length of time window $\Delta t = 30$ days inside which the network is constructed by the correlations. Connections are created between a stock pair if the correlation exceeds a determined threshold. In our experiments, we set the correlation coefficient threshold to the value to $\epsilon = 0.85$ so that $\eta = 10\%$ of all possible $N(N-1)/2$ edges remained at each time. The empirical results show that there are no significant changes for the network entropy if η belongs to the range [5%, 25%]. Then, we sequentially slide the window by $\delta t = 1$ to generate a sequence of networks according to the stock market time [6]. This yields a time-varying stock market network with a fixed number of 347 nodes and varying edge structure for each of the 6,000 trading days. The edges of the network, therefore, represent how the closing prices of the stock follow each other.

2.3. Network Representation. Let $G(V, E)$ be an undirected network with node set V and edge set $E \subseteq V \times V$, and let $|V|$ represent the total number of nodes on network $G(V, E)$. The adjacency matrix A of a network is defined as

$$A = \begin{cases} 1, & if \ (u, v) \in E \\ 0, & otherwise \end{cases} \tag{4}$$

Then the degree of node u is $d_u = \sum_{v \in V} A_{uv}$.

The normalised Laplacian matrix $\widetilde{L}$ of the network G is defined as $\widetilde{L} = D^{-1/2} L D^{1/2}$, where $L = D - A$ is the Laplacian matrix and D denotes the degree diagonal matrix whose elements are given by $D(u, u) = d_u$ and zeros elsewhere. The element-wise expression of $\widetilde{L}$ is

$$\widetilde{L}_{uv} = \begin{cases} 1, & if\ u = v\ and\ d_u \neq 0 \\ -\dfrac{1}{\sqrt{d_u d_v}}, & if\ u \neq v\ and\ (u,v) \in E \\ 0, & otherwise. \end{cases} \tag{5}$$

3. Quantum Statistics in Networks

In order to characterise network properties, we apply the methods in quantum statistics to analyse the network structure. Commencing from the network Hamiltonian, the network is regarded as a system of grand canonical ensemble [20]. The corresponding partition function is then developed to derive the thermal quantities, such as energy and entropy [24].

3.1. Network Hamiltonian. The Hamiltonian operator is usually used to describe the system energy in quantum mechanics. It involves two terms of the particles, namely, the kinetic energy and potential energy [32]. The standard definition of Hamiltonian is

$$\widehat{H} = -\nabla^2 + U(r,t) \tag{6}$$

In terms of the network description, we apply the heat bath analogy to describe the network behaviour. The network energy states can be regarded as the eigenvalues of the Laplacian matrix which determines the Hamiltonian operator [14]. Since the particle occupation in the energy state subject to thermal agitation, the Hamiltonian operator governs the particles in the networks by the heat bath. The temperature of thermal reservoir determines the particle occupation statistics and the relevant chemical potential plays a vital rule in the number of particles of the network system [15, 19].

Here, in the network thermal analogy, we regard the kinetic energy operator $-\nabla^2$ as the negative of the adjacency matrix, i.e., -A, and the potential energy *U(r, t)* as the degree matrix D. Thus, the Hamiltonian operator is identical to the network Laplacian matrix [33]. Similarly, the normalised form of the network Laplacian is regarded as the Hamiltonian operator

$$\widehat{H} = \widetilde{L} \tag{7}$$

In this case, the eigenvalues of the Hamiltonian are the energy states of the network $\{\varepsilon_i\}$. These eigenvalues all greater than or equal to zero, and the multiplicity of the zero eigenvalues is the number of connected components within the network.

3.2. Thermodynamic Quantities. To describe the network using the thermodynamic quantities, we consider the network system with N particles. The corresponding Hamiltonian operator governs the network energy states which is immersed in a thermal reservoir of temperature T. The relevant partition function *Z(β, N)* represents the thermodynamic characterisations in the network, where β is inverse of temperature [20]. When specified in this way, we can derive the thermodynamic quantities. For example, the average energy is given by

$$\begin{aligned} \mathrm{U} &= \left[-\frac{\partial}{\partial\beta}\log Z(\beta,N)\right]_N \\ &= k_B T^2 \left[\frac{\partial}{\partial T}\log Z(T,N)\right]_N \end{aligned} \tag{8}$$

the thermodynamic entropy by

$$S = \log Z + \beta U = k_B \left[\frac{\partial}{\partial T} T \log Z(T,N)\right]_N \tag{9}$$

and the chemical potential by

$$\mu = -k_B T \left[\frac{\partial}{\partial N}\log Z(T,N)\right]_\beta \tag{10}$$

In terms of the particle distribution in the energy states, the statistical properties of particles describe the thermodynamic quantities associated with the partition function for the different occupation statistics [34]. Therefore, the network characterisations, including the entropy, energy, and temperature, can be computed from the related partition function.

3.3. Bose-Einstein Statistics. Particles in Bose-Einstein statistics are indistinguishable so that they accommodate each energy state with an unlimited number [21]. The network Hamiltonian specifies the energy states to make bosons aggregate in the same energy state without obeying Pauli exclusion principle [21].

Thus, in the network system, it contains a varying number of particles N with a control parameter chemical potential μ. The corresponding partition function is given by

$$\begin{aligned} Z_{BE} &= \det\left[I - \exp\left(\beta\left(\mu - \widetilde{L}\right)\right)\right]^{-1} \\ &= \prod_{i=1}^{V}\left(\frac{1}{1 - e^{\beta(\mu-\varepsilon_i)}}\right) \end{aligned} \tag{11}$$

Then, the related entropy can be achieved from (9),

$$\begin{aligned} S_{BE} &= \log Z - \beta\frac{\partial \log Z}{\partial\beta} \\ &= \sum_{i=1}^{V}\log\left(1 - e^{\beta(\mu-\varepsilon_i)}\right) - \beta\sum_{i=1}^{V}\frac{(\mu-\varepsilon_i)\,e^{\beta(\mu-\varepsilon_i)}}{1 - e^{\beta(\mu-\varepsilon_i)}} \end{aligned} \tag{12}$$

This kind of thermodynamic entropy depends on the chemical potential. It closely relates to the number of particles with the partition function. As the temperature β controls the thermal occupation in each energy state, the corresponding number of particles in the level i with energy ε_i is

$$n_i = \frac{1}{\exp\left[\beta(\varepsilon_i - \mu)\right] - 1} \tag{13}$$

As a result, the total number of particles in the system is

$$\begin{aligned} \mathrm{N} &= \sum_{i=1}^{V} n_i = \sum_{i=1}^{V}\frac{1}{\exp\left[\beta(\varepsilon_i - \mu)\right] - 1} \\ &= Tr\left[\frac{1}{\exp\left[\beta\left(\widetilde{L} - \mu\right)\right] - I}\right] \end{aligned} \tag{14}$$

Due to the nonnegative number of particles in each energy state, the control parameter, i.e., chemical potential μ should be less than the minimum energy state, i.e., $\mu < \min \varepsilon_i$.

As the particles in Bose-Einstein statistics tend to congregate in the lower energy state at the low temperature, the relevant thermodynamic entropy strongly reflects the smaller Laplacian eigenvalues. Therefore, this kind of network characterisation closely relates to the spectral gap (the degree of bipartiality in a graph) and the number of connected components (the multiplicity of the zero eigenvalues) [24].

3.4. Fermi-Dirac Statistics. Particles in Fermi-Dirac statistics are indistinguishable fermions so that they obey the Pauli exclusion principle [22, 23]. Each energy state has a maximum number of occupation that only one particle can accommodate at the state [22, 23].

The network Hamiltonian determines the behaviour of these particles, where the free fermions follow Fermi-Dirac statistics. The corresponding partition function provides the statistical properties of the networks, which is given by

$$Z_{FD} = \det\left[I + \exp\left(\beta\left(\mu - \widetilde{L}\right)\right)\right] = \prod_{i=1}^{V} 1 + e^{\beta(\mu-\varepsilon_i)} \tag{15}$$

The associated entropy is achieved by

$$\begin{aligned} S_{FD} &= \log Z - \beta\frac{\partial \log Z}{\partial \beta} \\ &= \sum_{i=1}^{V} \log\left(1 + e^{\beta(\mu-\varepsilon_i)}\right) - \beta\sum_{i=1}^{V}\frac{\left(\mu - \varepsilon_i\right)e^{\beta(\mu-\varepsilon_i)}}{1 + e^{\beta(\mu-\varepsilon_i)}} \end{aligned} \tag{16}$$

In accordance with the Pauli exclusion principle, the number of particles accommodating the ith energy state is

$$n_i = \frac{1}{\exp\left[\beta\left(\varepsilon_i - \mu\right)\right] + 1} \tag{17}$$

and the total number of particles in the network is

$$\begin{aligned} \mathrm{N} &= \sum_{i=1}^{V} n_i = \sum_{i=1}^{V}\frac{1}{\exp\left[\beta\left(\varepsilon_i - \mu\right)\right] + 1} \\ &= Tr\left[\frac{1}{\exp\left[\beta\left(\widetilde{L} - \mu\right)\right] + I}\right] \end{aligned} \tag{18}$$

In order for a single particle per energy state, the chemical potential is the nth energy level, and so $\mu = \varepsilon_n$.

Since Fermi-Dirac statistics exclude multiple occupations at the same state, this kind of thermodynamic entropy does not strongly represent the properties of the Laplacian spectrum. But it samples a broader distribution of Laplacian eigenvalues which is sensitive to a greater portion of network spectrum. Therefore, this thermodynamic characterisation might expect to reflect subtle differences within a network structure.

4. Experiments and Evaluations

4.1. Experimental Results. We now conduct the experiments on the thermodynamic entropy to the stock market network evolutions. This provides a useful characterisation for analysing the stock market fluctuation. We first investigate whether this kind of entropy is effective to detect the network structural variance in time series.

Figure 2 shows New York Stock Exchange in the thermodynamic entropy from Bose-Einstein and Fermi-Dirac statistics. The sharp peaks in the time sequential data indicate the positions of significant financial events, such as Black Monday, Friday the 13th mini-crash, Early 1990s Recession, 1997 Asian Crisis, 9.11 Attacks, Downturn of 2002-2003, 2007 Financial Crisis, the Bankruptcy of Lehman Brothers, and the European Debt Crisis [9, 10]. Each financial crisis indicates the significant variance in entropy associated with dramatic network structural changes. We take the downturn of 2002-2003 as an example. After the 9.11 attacks, the investors lost trust in the United States economy due to the terrorism. Many Internet companies collapsed subsequently. This forced numerous large corporations to restate earnings and reestablished investors' confidence [7]. This considerably altered the interrelationships among stocks and resulted in a significant fluctuation in the structure of the entire market [16].

In order to better understand the relationship between network structure and thermodynamic entropy, we take the 1997 Asian financial crisis as an example to further visualise how the network structure organised with entropy near a critical time point. This works as a reference for the effect of financial instabilities in the network structure [7, 35, 36]. During July to November in 1997, as shown in Figure 3, the thermodynamic entropy describes the instability of the network structure in the stock market. We note that the community structure or the connected components of the network always correspond to the fluctuation of thermodynamic entropy. Here, we select four different instants of time, using node colour to represent the density of degree connections. To correctly observe the thermodynamic evolution, the parameters of temperature and particle numbers are kept fixed for the four instant times in the visualisation of networks A, B, C, and D.

In Figure 3, we note that before the crisis the network structure is mainly composed of two predominant communities and the thermodynamic entropy remain stable at the low-value area. As the network approaches the crisis, the network structure changes drastically. Only a highly connected cluster at the centre of the network remains. The two community structures substantially vanish and the value of entropy tends to climb up. During the crisis, the network structure exhibits a more homogeneous connection, as represented by the higher values of entropy. At this epoch, most stocks are disconnected, meaning that the prices evolve without strong correlations. Similar patterns of the 1997 Asian Crisis can be found in temporal network analysis. This result also agrees with other findings on the structural organisation of financial market networks [7, 18, 35, 36]. Throughout the crisis period, the connected compositions preserve most of

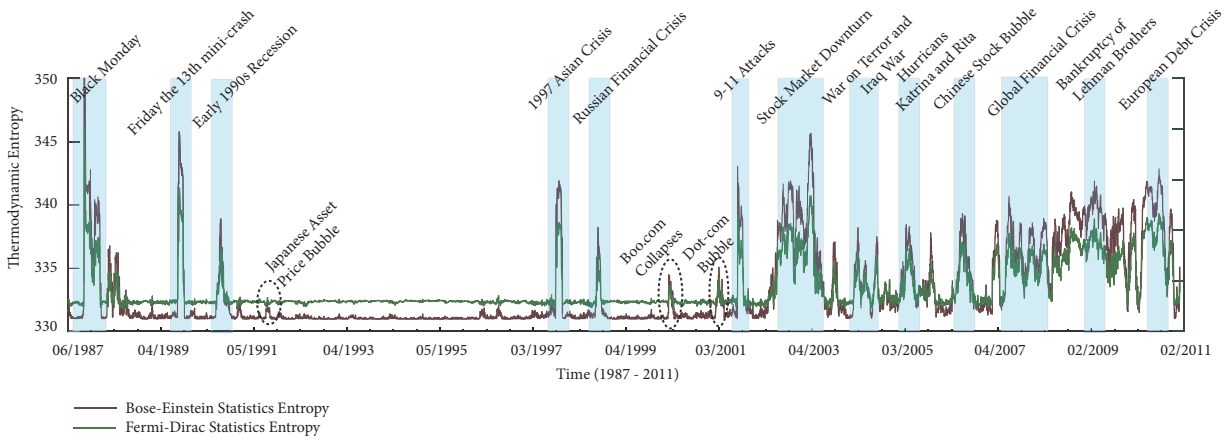

Figure 2: Entropy in NYSE (1987-2011) derived from Bose-Einstein and Fermi-Dirac statistics. Critical financial events, i.e., Black Monday, Friday the 13th mini-crash, Early 1990s Recession, 1997 Asian Crisis, 9.11 Attacks, Downturn of 2002-2003, 2007 Financial Crisis, the Bankruptcy of Lehman Brothers, the European Debt Crisis, etc. It is efficient to use thermodynamic entropy to identify critical events in NYSE.

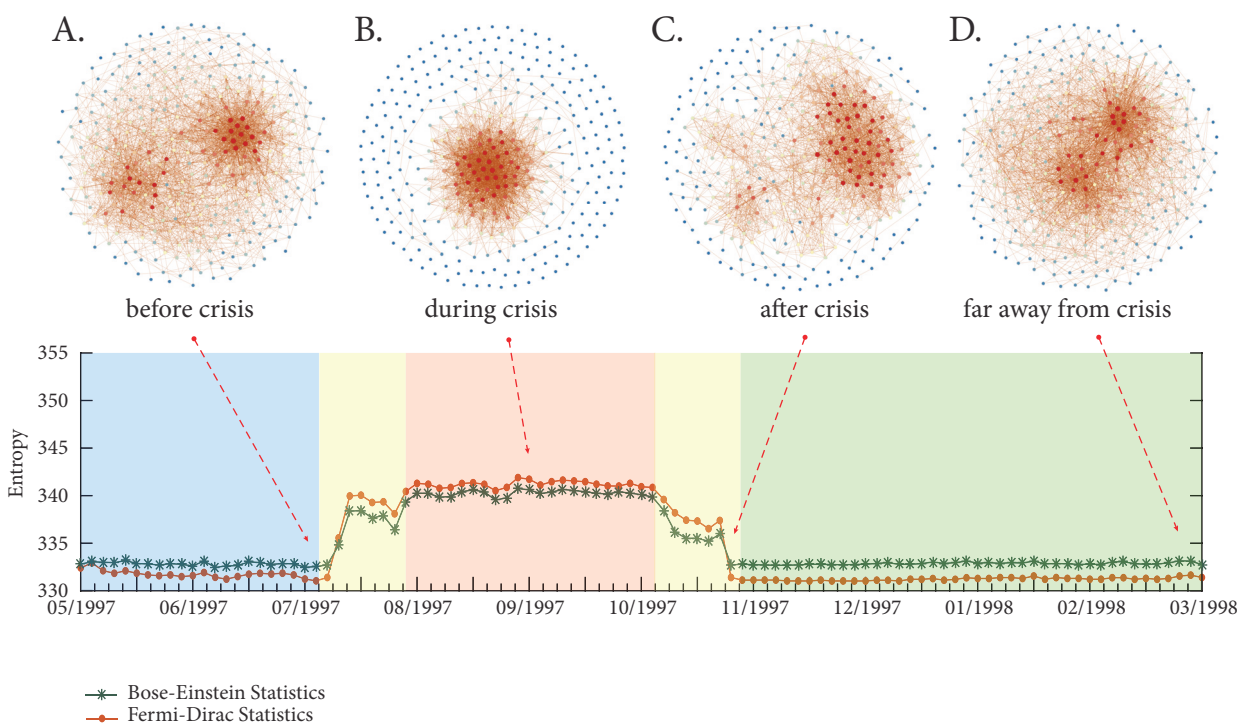

Figure 3: Thermodynamic entropy of the NYSE networks in distinct times during and around the 1997 Asian financial crisis. We show a visualisation of the network at four specific days. Node colours correspond to the degree found for the network. We note that the average degrees of networks A, B, C, and D are the same.

their communities, and the entropy becomes to decrease to the low value. After the crash in a long period, the network recovers to connect again.

To better quantitatively investigate the relationship between a financial crisis and thermodynamic entropy, we present a set of critical crisis periods in Figure 4. These periods are marked alongside the curve of the thermodynamic entropy in Bose-Einstein statistics, which exhibits a similar tendency in Fermi-Dirac statistics. As shown in Figure 4, the most striking observation is that almost all of the largest peaks and troughs can find their realistic financial crisis correspondences, which show the thermodynamic entropy is sensitive to network structural changes.

In addition, for each considered crisis, we observe different detailed behaviours around the time span of the crisis. For example, both Friday 13th the mini-crash and 1997 Asian Crisis present a sharp trough and peak in the corresponding time series, which dramatically change the network structure in a short time. On the other hand, Bankruptcy of Lehman Brothers and European Debt Crisis

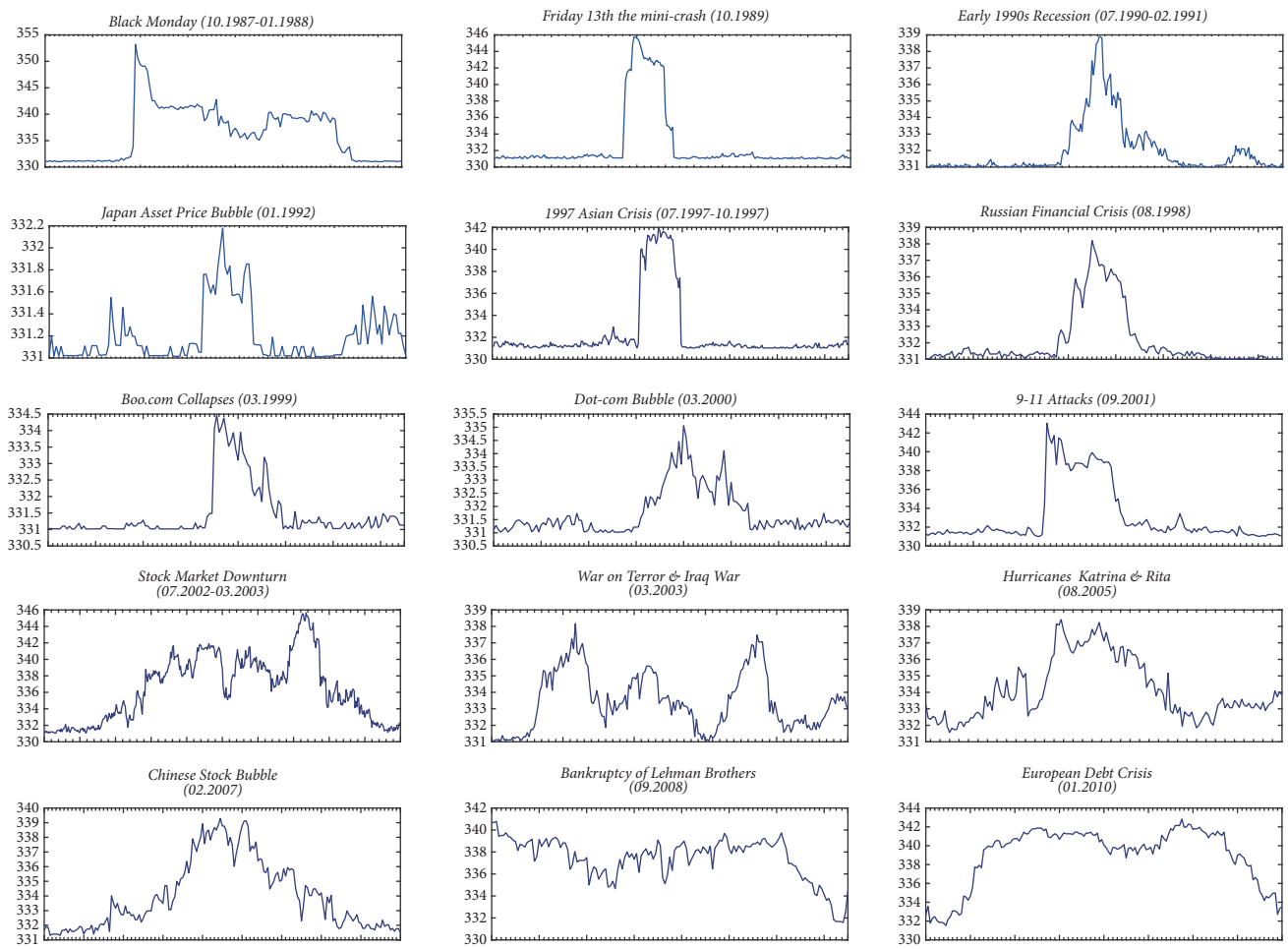

Figure 4: The individual time series of the stock market network. The thermodynamic entropy for all the different global events that have been identified.

exhibit a persistent influence on the stock market with a broad entropic fluctuation in those periods. Therefore, this indicates that the thermodynamic entropy can capture network characterisations related to the financial crisis at different times.

4.2. Evaluations. The correlation coefficient is computed between all the possible pairs of the stock price. Here, to validate the thermodynamic network entropy, we build the financial networks with another form of network construction, i.e., mutual information [37]. Figure 5 shows the entropy fluctuation in both traditional pairwise correlation and mutual information. Both diagrams contain time series for all of our stock market price. In each case, the entropy undergoes a sharp increase corresponding to the financial crises, which are associated with dramatic structural changes in the networks. Similarly, in Figure 2, the alternative form of network construction is also effective in indicating the critical events. The different feature is that, compared to other network construction method, the thermodynamic quantities show the greatest variation during the crises, suggesting that changes in cluster-structure (modularity) are important during these episodes.

We then compare our thermodynamic entropy with other thermodynamic characterisations, namely, the heat kernel signature [38] and the wave kernel signature [39], to analyse the dynamic financial networks. Figure 6 shows three-dimensional scatter plots obtained from the principal component analysis (PCA) of network representations, respectively. Both plots show a compact manifold structure. However, the smooth and compact manifold trajectory does not identify the critical points, such as Black Monday, 1997 Asian Crisis, and Stock Market Downturn. This indicates that although thermodynamic characterisation is effective to analyse financial network evolution, other thermal representation methods preserve information concerning significant changes in network evolution compared to the thermodynamic entropy [6, 19].

Next, we analyse the network similarity at different time steps. We compare the financial crisis of the same nature happened at two different time periods, i.e., 1929 and 2008. Figure 7 shows the network topologies at the global stock market crisis in 1929 and in 2008 [40]. These two events have a similar in magnitude. They both lead to the recessions in the world trade and unemployment [40]. As shown in Figure 7, both of two global crises have a similar entropy

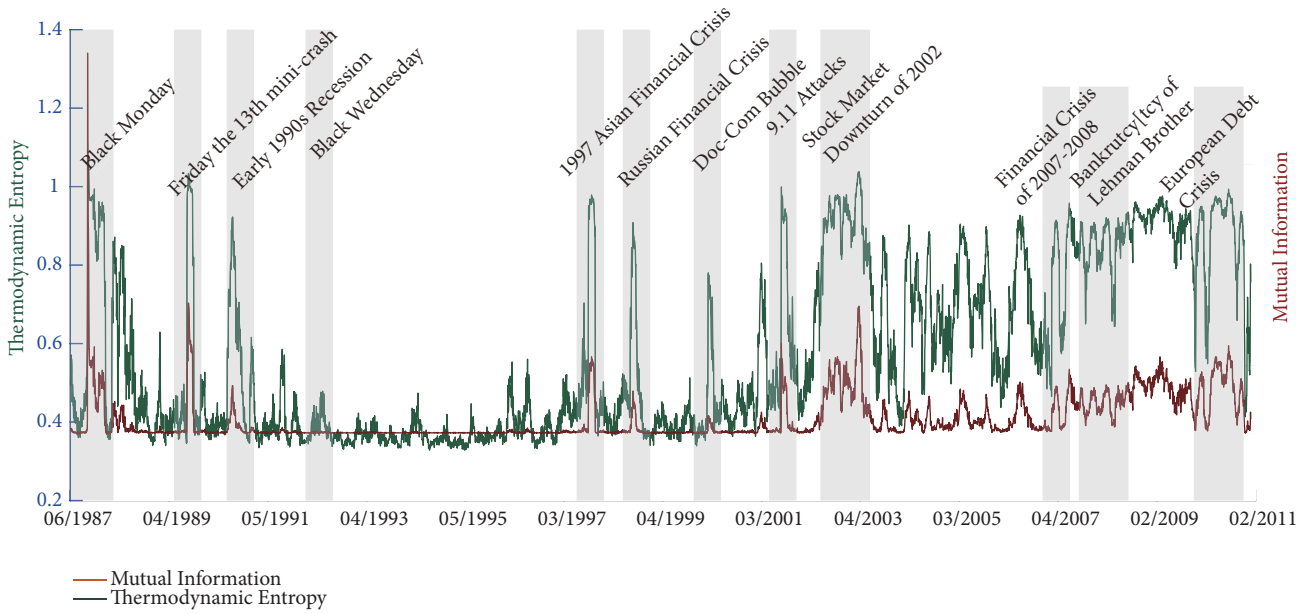

Figure 5: Entropy fluctuation in NYSE (1987-2011). The network structure is derived from traditional pairwise correlation and mutual information. (a) Green line, correlation coefficient; (b) brown line, mutual information.

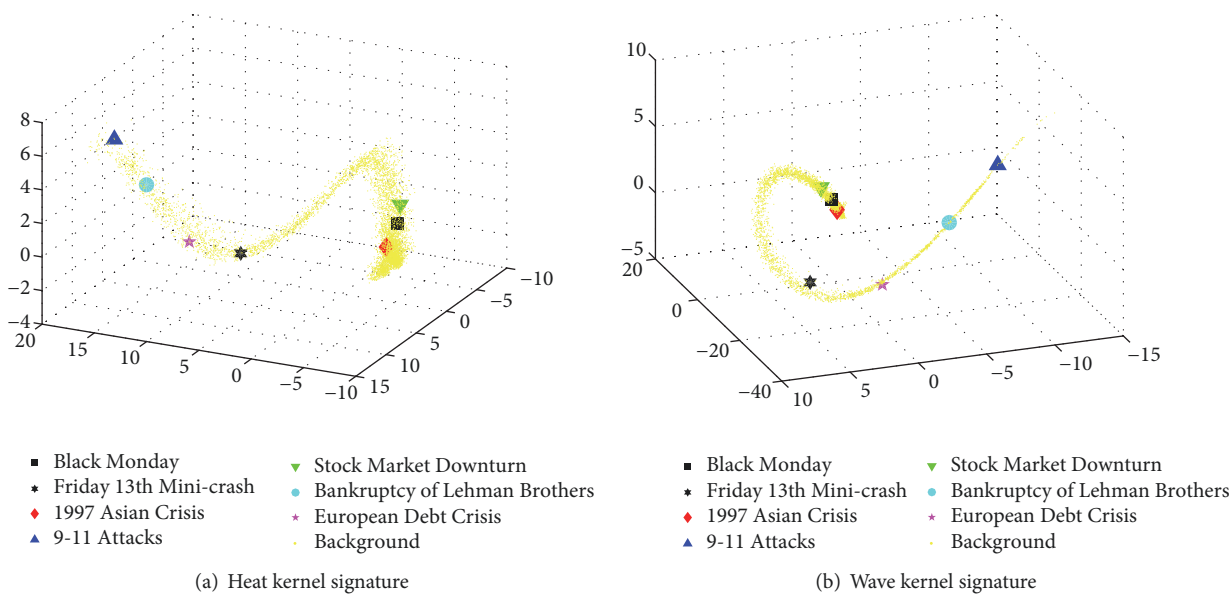

(a) Heat kernel signature (b) Wave kernel signature

Figure 6: The 3D visualisation of PCA plots in the dynamic stock correlation networks described by other thermodynamic characterisation methods. (a) Heat kernel signature; (b) wave kernel signature.

trajectory and the network topology also exhibit a similar pattern. During the crisis, the network structure exhibits a more homogeneous connection, with remaining only a highly connected cluster at the centre of the network.

Finally, we focus in detail on a critical financial event, namely, the 1997 Asian Crisis, to explore the dynamic structural difference with the entropic variance. We decompose the edge entropy by using the eigenvector of the Laplacian matrix and replacing its eigenvalues with the thermodynamic entropy elements. As shown before in Figure 3, the network structure has a dense cluster before the crisis and the number of connections decreases significantly during the financial crash. After that, the stocks begin to recover connections with another and a few stocks tend to form some clusters in the network structure. This phenomenon also reflects on the edge of entropy decomposition. Figure 8 shows the edge entropy distribution around the crisis for two quantum statistics. There is a narrow distribution during the 1997 Asian Crisis, compared with a broader edge entropy distribution before and after the crash.

Moreover, an interesting observation is the difference of edge entropy distribution between Bose-Einstein and

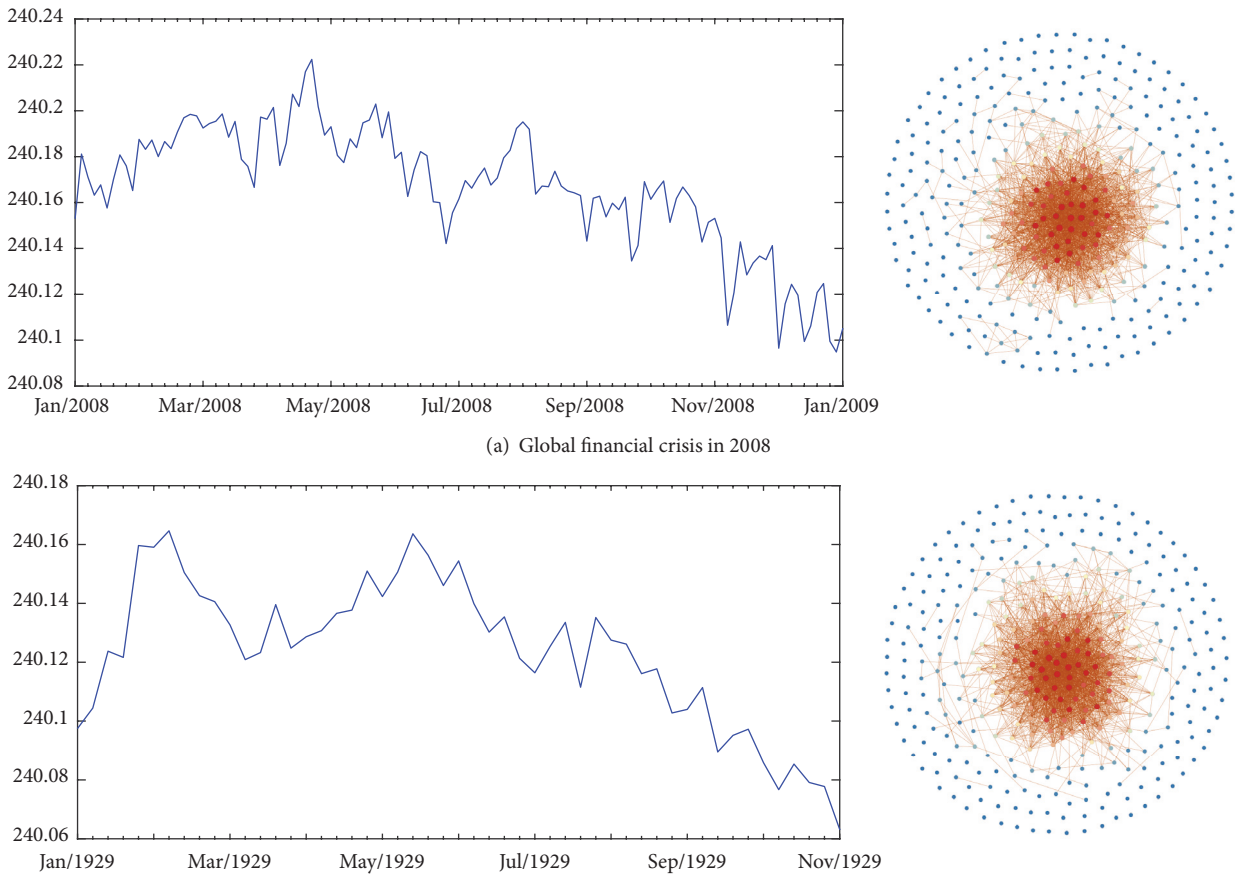

(a) Global financial crisis in 2008

(b) Global financial crisis in 1929

Figure 7: The comparison of network topology at two different global financial crises in 1929 and in 2008.

Fermi-Dirac statistics after the Asian Crisis. This is because the networks make some clusters with community structure. Since Bose-Einstein statistics preferentially sample the lower energy levels with the network eigenvalue spectrum, it is more suitable to detect networks with strong community edge connection [34], while Fermi-Dirac statistics may be more sensitive to the mean and variance of the eigenvalue distribution since they probe a wider range of energy levels [15].

In conclusion, the thermodynamic entropy from quantum statistics can provide an effective tool to represent the dynamic structure of network evolution. To explore a more detail, Bose-Einstein statistics is more sensitive to reflect strong community edge connection, while Fermi-Dirac edge entropy is more suitable to represent high degree variations.

5. Conclusions

The study of stock market networks not only improves the decisions related to the industrial entities but also provides a reliable indicator for an imminent widespread stock value decline, which refers to a financial crisis. This description of the network evolution tends to convey the dynamic financial market which infers the underlying financial activities and partnerships.

The goal of this paper is to show that thermodynamic entropy can be used to describe the dynamics of stock market networks. Here, we explore the thermodynamic framework from quantum statistics, i.e., Bose-Einstein statistics and Fermi-Dirac statistics. By considering the heat bath analogy, we derive the Hamiltonian operator as the normalised Laplacian matrix of the network. Derived by different choices of partition functions, we compute the thermodynamic entropy based on the particle distribution with energy level occupation statistics.

The results indicate that it is suitable to use the thermodynamic entropy to attest the statistical significance of experimental observations on stock market networks. Entropy in quantum statistics can provide an indicator to identify the financial crisis during the network evolution. Furthermore, the thermodynamic characterisations in both quantum statistics are effective in representing dynamic network structure. The difference between two cases is that particles in Bose-Einstein statistics tend to condense into a low energy state, which preferentially samples the small value eigenvalues of network spectrum. The corresponding entropy is more suitable to detect networks with strong community edge connection. Particles in Fermi-Dirac statistics, on the other hand, follow the Puli exclusion principle with only one particle per energy state. It probes a wider range of network

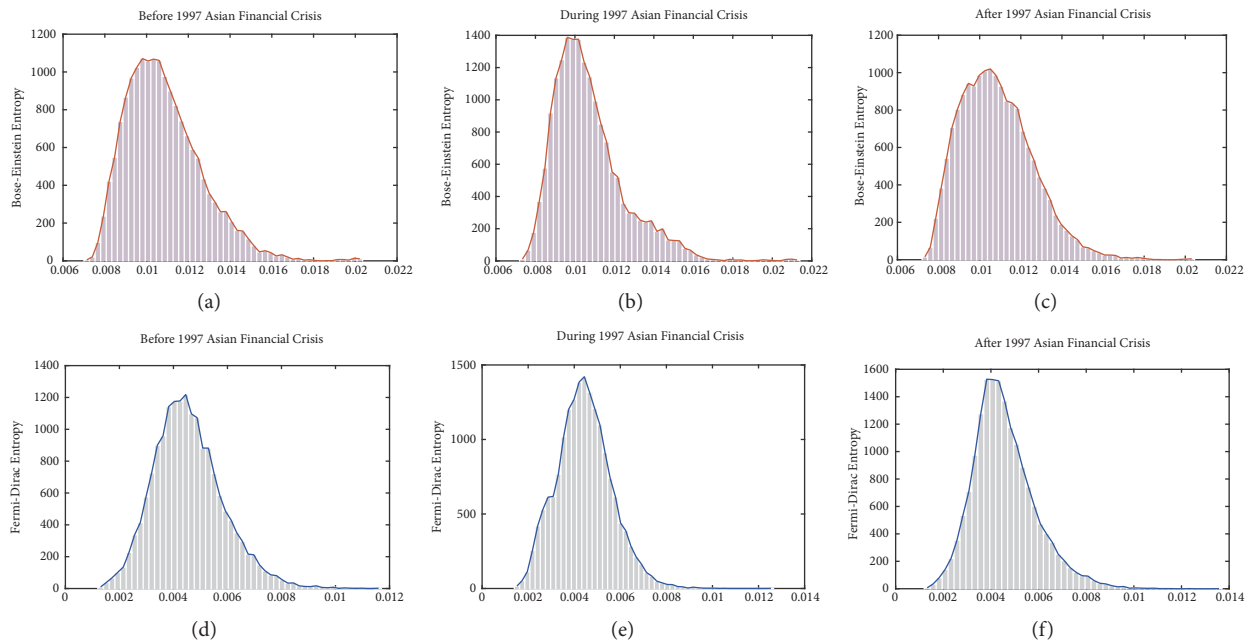

Figure 8: Edge entropy distribution of network structure before, during, and after the 1997 Asian financial crisis. (a)-(e) Bose-Einstein statistics. (d)-(f) Fermi-Dirac statistics.

spectrum which is more sensitive to the mean and variance of the eigenvalue distribution.

In addition, a more interesting study would be remained to explore different pruning techniques which can be used to transform a correlation matrix into the adjacency matrix. Novel network construction method would provide new insights about the structural characterisations. Furthermore, other datasets related to the financial market, such as interbank ownership, could provide additional developments about the relevance of thermodynamic characterisations during pronounced market crises.

Data Availability

The New York Stock Exchange date is available at http://finance.yahoo.com. The corresponding code is freely available upon request.

Disclosure

This research received no specific grant from any funding agency in the public, commercial, or not-for-profit sectors.

Conflicts of Interest

The authors declare that they have no conflicts of interest.

Acknowledgments

The authors would like to thank Weimin Li and Bing Wang for useful supports and comments. The authors acknowledge simulating discussions and help with Edwin R. Hancock and Richard C. Wilson.

References

[1] G. Bonanno, G. Caldarelli, F. Lillo, S. Micciché, N. Vandewalle, and R. N. Mantegna, "Networks of equities in financial markets," *The European Physical Journal B - Condensed Matter and Complex Systems*, vol. 38, no. 2, pp. 363–371, 2004.

[2] Y.-C. Gao, Z.-W. Wei, and B.-H. Wang, "Dynamic evolution of financial network and its relation to economic crises," *International Journal of Modern Physics C*, vol. 24, no. 2, 1350005, 10 pages, 2013.

[3] J. Eberhard, J. F. Lavin, and A. Montecinos-Pearce, "A network-based dynamic analysis in an equity stock market," *Complexity*, vol. 2017, Article ID 3979836, 16 pages, 2017.

[4] I. Anagnostou, S. Sourabh, and D. Kandhai, "Incorporating contagion in portfolio credit risk models using network theory," *Complexity*, vol. 2018, Article ID 6076173, 15 pages, 2018.

[5] D. Y. Kenett and S. Havlin, "Network science: a useful tool in economics and finance," *Mind & Society*, vol. 14, no. 2, pp. 155–167, 2015.

[6] F. N. Silva, C. H. Comin, T. K. D. Peron et al., "Modular dynamics of financial market networks," 2015, https://arxiv.org/abs/1501.05040.

[7] A. Sheng, "Financial crisis and global governance: a network analysis," in *Globalization and Growth Implications for a Post-Crisis World*, pp. 69–93, 2010.

[8] D.-M. Song, M. Tumminello, W.-X. Zhou, and R. N. Mantegna, "Evolution of worldwide stock markets, correlation structure, and correlation-based graphs," *Physical Review E: Statistical, Nonlinear, and Soft Matter Physics*, vol. 84, no. 2, Article ID 026108, 2011.

[9] L. He and S. Li, "Network entropy and systemic risk in dynamic banking systems," *Complexity*, vol. 2017, Article ID 1852897, 7 pages, 2017.

[10] T. Squartini, A. Gabrielli, D. Garlaschelli, T. Gili, A. Bifone, and F. Caccioli, "Complexity in neural and financial systems:

from time-series to networks," *Complexity*, vol. 2018, Article ID 3132940, 2 pages, 2018.

[11] F. Passerini and S. Severini, "The von Neumann entropy of networks," *International Journal of Agent Technologies*, pp. 58–67, 2008.

[12] L. Han, F. Escolano, E. R. Hancock, and R. C. Wilson, "Graph characterizations from von Neumann entropy," *Pattern Recognition Letters*, vol. 33, no. 15, pp. 1958–1967, 2012.

[13] J. Wang, R. C. Wilson, and E. R. Hancock, "Directed and undirected network evolution from Euler–Lagrange dynamics," *Pattern Recognition Letters*, 2018.

[14] E. Schrödinger, "An undulatory theory of the mechanics of atoms and molecules," *Physical Review A: Atomic, Molecular and Optical Physics*, vol. 28, no. 6, pp. 1049–1070, 1926.

[15] J. Wang, R. C. Wilson, and E. R. Hancock, "Thermodynamic network analysis with quantum spin statistics," in *Structural, syntactic, and statistical pattern recognition*, vol. 10029 of *Lecture Notes in Computer Science*, pp. 153–162, Springer, Cham, Switzerland, 2016.

[16] J. Wang, R. C. Wilson, and E. R. Hancock, "Network edge entropy from Maxwell-Boltzmann statistics," in *Image analysis and processing—ICIAP*, vol. 10484, Part I of *Lecture Notes in Computer Science*, pp. 254–264, Springer, Cham, Switzerland, 2017.

[17] Y. Zhang, S. Chen, and J. Ge, "Noise removal in Shackhartamnn wavefront sensor based on nonconvex weighted adaptively regularization," *Optik - International Journal for Light and Electron Optics*, vol. 144, pp. 199–206, 2017.

[18] E. J. Elton and M. J. Gruber, "Risk reduction and portfolio size: an analytical solution," *The Journal of Business*, vol. 50, no. 4, pp. 415–437, 1977.

[19] C. Ye, C. H. Comin, T. K. Peron et al., "Thermodynamic characterization of networks using graph polynomials," *Physical Review E: Statistical, Nonlinear, and Soft Matter Physics*, vol. 92, no. 3, Article ID 032810, 2015.

[20] D. Petz, *Quantum Information Theory and Quantum Statistics*, Springer Science & Business Media, 2007.

[21] Bose, "Plancks Gesetz und Lichtquantenhypothese," *Zeitschrift für Physik*, vol. 26, no. 1, pp. 178–181, 1924.

[22] E. Fermi, "Sulla quantizzazione del gas perfetto monoatomico," *Rendiconti Lincei*, vol. 3, pp. 145–149, 1926 (Italian).

[23] P. Dirac, "On the theory of quantum mechanics," *Proceedings of the Royal Society A Mathematical, Physical and Engineering Sciences*, vol. 112, no. 762, p. 661, 1926.

[24] J. Wang, *Statistical Mechanics for Network Structure and Evolution [Ph.D. thesis]*, University of York, 2018.

[25] G. Bianconi and A.-L. Barabási, "Bose-Einstein condensation in complex networks," *Physical Review Letters*, vol. 86, no. 24, pp. 5632–5635, 2001.

[26] A. P. de Moura, "Fermi-Dirac statistics and traffic in complex networks," *Physical Review E: Statistical, Nonlinear, and Soft Matter Physics*, vol. 71, no. 6, Article ID 066114, 2005.

[27] Y. Shen, D.-L. Zhu, and W.-M. Liu, "Fermi-dirac statistics of complex networks," *Chinese Physics Letters*, vol. 22, no. 5, pp. 1281–1284, 2005.

[28] Z. Griliches, "Estimating the returns to schooling: some econometric problems," *Econometrica*, vol. 45, no. 1, pp. 1–22, 1977.

[29] R. N. Mantegna and H. E. Stanley, *An Introduction to Econophysics: Correlations and Complexity in Finance*, Cambridge University Press, Cambridge, UK, 2000.

[30] A. N. Varchenko and I. M. Gel'fand, "Heaviside functions of a configuration of hyperplanes," *Functional Analysis and its Applications*, vol. 21, no. 4, pp. 255–270, 1987.

[31] J. H. Trowbridge, "On a technique for measurement of turbulent shear stress in the presence of surface waves," *Journal of Atmospheric and Oceanic Technology*, vol. 15, no. 1, pp. 290–298, 1998.

[32] O. Shanker, "Defining dimension of a complex network," *Modern Physics Letters B*, vol. 21, no. 6, pp. 321–326, 2007.

[33] F. R. Chung and F. C. Graham, *Spectral Graph Theory*, CBMS Regional Conference Series in Mathematics, no. 92, American Mathematical Society, 1997.

[34] J. Wang, R. C. Wilson, and E. R. Hancock, "Spin statistics, partition functions and network entropy," *Journal of Complex Networks*, vol. 5, no. 6, pp. 858–883, 2017.

[35] K. A. Erturk, "Overcapacity and the East Asian crisis," *Journal of Post Keynesian Economics*, vol. 24, no. 2, pp. 253–275, 2001.

[36] S. Radelet and J. D. Sachs, "The East Asian financial crisis: Diagnosis, remedies, prospects," *Brookings Papers on Economic Activity*, no. 1, pp. 1–90, 1998.

[37] X. Zhou, X. Wang, and E. R. Dougherty, "Construction of genomic networks using mutual-information clustering and reversible-jump Markov-chain-Monte-Carlo predictor design," *Signal Processing*, vol. 83, no. 4, pp. 745–761, 2003.

[38] M. M. Bronstein and I. Kokkinos, "Scale-invariant heat kernel signatures for non-rigid shape recognition," in *Proceedings of the 2010 IEEE Computer Society Conference on Computer Vision and Pattern Recognition, CVPR 2010*, pp. 1704–1711, June 2010.

[39] M. Aubry, U. Schlickewei, and D. Cremers, "The wave kernel signature: A quantum mechanical approach to shape analysis," in *Proceedings of the 2011 IEEE International Conference on Computer Vision Workshops, ICCV Workshops 2011*, pp. 1626–1633, Spain, November 2011.

[40] B. Bernanke and H. James, "The gold standard, deflation, and financial crisis in the great depression: an international comparison," in *Financial markets and financial crises*, pp. 33–68, University of Chicago Press, 1990.

Hindawi
Complexity
Volume 2019, Article ID 5317819, 12 pages
https://doi.org/10.1155/2019/5317819

Research Article

Systemic Risk in the Interbank Market with Overlapping Portfolios

Shanshan Jiang and Hong Fan

Glorious Sun School of Business and Management, Donghua University, Shanghai 200051, China

Correspondence should be addressed to Hong Fan; hongfan@dhu.edu.cn

Received 14 December 2018; Revised 22 February 2019; Accepted 24 March 2019; Published 16 April 2019

Guest Editor: Ahmet Sensoy

The increasing frequency and scope of the financial crisis have attracted more attention in the research of the systemic risk of banking system. A new model for the interbank market with overlapping portfolios is proposed to simulate a banking system in this work. The proposed model uses a bipartite network of banks and their assets to analyze the impact of bank investment on the stability of the banking system. In addition, this model introduces investment risk and allows banks to make up for liquidity by selling devaluated assets, which reflects the operating rules of the banking system more realistically. The results show that allowing banks to sell devaluated assets to make up for liquidity can improve the stability of the banking system and the interbank market can also improve the stability of the banking system. For the investment of banks, the investment risk is an uncertain factor that affects the stability of the banking system. The proposed model further analyzes the impact of average investment interest rate, savings interest rate, deposit reserve ratio, and investment asset diversity on the stability of the banking system. The model provides a tool for policy-makers and supervision agencies to prevent the systemic risk of banking system.

1. Introduction

The increasing frequency and scope of the financial crisis have attracted more attention in the research of the systemic risk of banking system [1, 2]. Most of the current research on the systemic risk of banking system analyzed the risk of financial systems from the perspective of interbank lending [3, 4]. The interbank market provides convenience for banks making up for liquidity and also provides an infectious channel for the spread of the crisis [5]. The network formed by interbank lending relations plays an important role in the systemic risk of banking system [6, 7]. Kaufman and Scott [8] believed that systemic risk referred to the risk or possibility of the collapse of the entire system by the interbank network. Mistrulli's empirical research [9] showed that the interbank market was able to handle liquidity shocks but also acted as a risk communication channel for bank failures through interbank lending. Allen and Gale [10] studied the risk contagion of banking systems under different static network structure. It was found that the possibility of financial contagion in the interbank market largely depended on the market structure and the complete market structure was more robust than the incomplete market structure. Freixas et al. [11] found that the higher the connection among banks, the faster recovery of single banks in crisis. The shortcoming was not to eliminate inefficient banks, which was similar to the results of Allen and Gale [10]. Leitner [12] studied the optimal structure of banking network, which showed that the optimal banking network structure should be trade-off between risk sharing and potential "Domino collapse." Vivier-Lirimont [13] studied the optimal network structure from the perspective of improving the depositors' utility. He found that the sparse network structure accorded with the Pareto optimal assignment. Iori et al. [14] and Lenzu and Tedeschi [15] studied the stability of bank network systems in the case of heterogeneous or homogeneous bank nodes. They found that banking networks were more stable when banks were homogenous. When banks were heterogeneous, the stability of the banking network system had a nonmonotonic relationship with the connectivity. Nier et al. [16] found that the impact of the connectivity among banks on systemic risk was not monotonous. At the initial time, a slight increase in connectivity increased the infection. When the connectivity was increased to a certain value, the connectivity increased

the ability of the banking system to absorb the shock and thus increased the stability of the banking system. Caccioli et al. [17] studied the impact of the network topology on systemic risk when nodes in a banking network were subjected to random shocks and selective shocks. They found that when a node in the banking network was subjected to a random shock, the scale-free network structure had less systemic risk than the random network structure. When a node with high connectivity was chosen, the systemic risk of a scale-free network structure was larger than that of a random network structure. Lenzu and Tedeschi [15] studies had shown that there was a critical connection value between banks with scale-free network structure, which was more likely to be contagious exceeding the critical connection value. Smerlak et al. [18] analyzed the characteristics of single bank's risk contagion in systemic risk contagion from the section dimension and found that large and low capital banks could increase systemic risk. Georg [19] studied different interbank network structures and the results showed that money-centre networks were more stable than random networks. Kok [20] proposed a sequential network formation mechanism to investigate how key parameters may affect interbank network structures. Han and Cao [21] found that liquidity hoarding behaviors mitigated systemic risk contagion at early stage and the composition of risk-averse behaviors exacerbated the systemic risk contagion. Steinbacher et al. [22] proposed a network-based structural model of credit risk to demonstrate how idiosyncratic and systemic shocks propagate across the banking system and evaluate the costs. Yao's work [23] found that contagion effect was most significant if the originating shocked bank was leveraged highly or had high network connectivity.

The above researches mainly analyzed systemic risk from the perspective of interbank market, while there was little consideration for the devaluation of portfolios caused by systemic risk. Lagunoff's study [24] found that overlap portfolios between banks were an important reason of financial risk. Based on overlap portfolios, Uhlig [25] had studied two types of financial crises. One type was that a bank was redistributing its portfolio because of the external shocks. In this case, the loss of assets had gradually expanded, making more banks' assets in crisis and leading to the financial crisis. Another type was due to the fact that some banks had shifted their assets to safer portfolios, leading to a decline in some asset prices, causing some banks to fall into crisis. Vries [26] did a similar research of Uhlig's work. Due to the correlation of bank assets, the fat tail nature of bank asset distribution caused the risk of bankruptcy for banks. Cifuentes et al. [27] and Greenwood et al. [28] found that, in a network with overlap portfolios, the risk of infection mainly came from the decline in asset prices. Huang et al. [29] built a bank asset bilateral network model and used the 2007 US commercial bank balance sheet data to carry out an empirical study of the risk contagion. Caccioli et al. [30, 31] built a multiasset model of investment and discussed the probability and degree of financial contagion under the condition of leverage, market congestion, asset diversification, and market impact. The above researches mainly analyzed systemic risk from the perspective of overlap portfolio; the evolution law of the interbank network with overlap portfolios could not be fully analyzed.

In summary, there are still some problems in above works: (i) the above models consider either the role of interbank lending or overlap portfolios in the systemic risk, instead of considering both overlap portfolios and interbank lending; (ii) in the above interbank network models, the rate of return on investment assets is set to a fixed value, but, in fact, investment is risky, and the return rate of investment should be dynamic. Zhou and Li [32] proposed a complex network system from the obligation links among banks and links created by portfolio overlaps, which considered interbank lending and overlap portfolios. But in Zhou's work, the ratio of the interbank loan was certain, the ratio of capital asset was certain, and the strategy of investment and borrowing was still unclear. Based on the above analysis, inspired by the work of Iori et al. [14], this paper constructs a systemic risk contagion model based on the interbank network with overlapping portfolios. In Iori's work, only interbank lending is considered, the rate of return on investment is fixed, and the model does not allow banks to replenish liquidity by selling assets. In the proposed model, we consider the impact of both overlap portfolios and interbank lending on systemic risk and then analyze the evolution rule of overlap portfolios and interbank network when systemic risk occurs. In the proposed model, there are multiple channels to improve liquidity, including interbank loans and asset sales when banks are in low liquidity, and asset depreciation is also considered when assets are sold. In the proposed model, the return rate of assets is dynamic, and the return rate of different assets is different. This hypothesis is more in line with the actual economic laws.

2. The Model

In a banking system, a bank failure often results from lack of liquidity. The liquidity of a bank is closely related to savings, investment, and interbank lending. This paper proposed a systemic risk contagion model based on the interbank network with overlapping portfolios as shown in Figure 1, which can well reflect the reality of banking systems. Unlike the traditional bank systemic risk model based on interbank lending [14], the proposed model considers both interbank lending and overlapping portfolios and establishes the relationship rules of overlapping portfolios. Compared with the traditional model based on interbank lending, the model proposed in this paper is more in line with the actual operation rules of the banking system.

2.1. A Dynamic Banking Network System. When banks are short of liquidity, they will borrow from each other in the interbank market, which is shown in Figure 1. In a random interbank network, nodes are randomly connected and the connection matrix is expressed as J, in which J_{ij} is either one or zero. $J_{ij} = 1$ indicates a possible credit linkage between bank i and bank j, while $J_{ij} = 0$ indicates no relationship between bank i and bank j. Bank i and bank j are connected by probability p_{ij}.

N_t is the number of banks in the network at time t; N_t is a bounded integer. The system operates in discrete time $t = 1, 2, 3, \ldots, T$. The liquidity of bank i at time t can be described as [14]

$$L_i(t) = \widehat{L}_i(t) - D_i(t) - I_i(t) + \sum_{j=1}^{N_t} c_{ij}(t) B_{ij}(t), \quad (1)$$

where $\widehat{L}_i(t)$ is a liquidity asset before banks invest, dividend, and borrow; $D_i(t)$ is the dividend of bank i at time t; $I_i(t)$ is the investment of bank i at time t; c_{ij} describes the connection relationship between bank i and bank j; if there is a loan relationship between bank i and bank j, $c_{ij}(t) = 1$; otherwise $c_{ij}(t) = 0$ (note that $c(t)$ is not equal to J and $c_{ij}(t)$ represents a real loan relationship between bank i and bank j, while J_{ij} indicates a possible credit linkage between bank i and bank j); $B_{ij}(t) > 0$ indicates the amount of bank i borrowed from bank j, and $B_{ij}(t) < 0$ indicates that bank i loans to bank j.

At time t, the liquidity of every bank will change, including the interest paid to the depositors, the income from the investment, the expiry investment income, and the fluctuation of the deposit. At time t, the liquidity before banks invest, dividend, and borrow can be described:

$$\begin{aligned}\widehat{L}_i(t) = {} & L_i(t-1) + A_i(t) - A_i(t-1) - r_a A_i(t-1) \\ & + U_i(t),\end{aligned} \quad (2)$$

where $A_i(t)$ denotes deposits held by the general public in bank i at time t, r_a is the bank deposit rate, and $U_i(t)$ is a realized investment and profit in each time step. In the absence of investment, all investment assets held by the bank i before the investment recovery are as follows:

$$Y_i(t) = \sum_{j=1}^{M} Q_{ij}(t-1) g_j(t), \quad (3)$$

where $Q_{ij}(t-1)$ is the number of shares of asset j held by bank i at time $t-1$. $Q_{ij}(t)$ is a dynamic change value, because bank i is likely to make new investments at each time step and the liquidation of assets can also be realized in each time step. $g_j(t)$ is the price of asset j at time t, which can be described as follows:

$$g_j(t) = g_j(t-1)\left(1 + \delta_j(t)\right), \quad (4)$$

where $\delta_j(t)$ is the rate of return on investment j at time t, which obeys the normal distribution based on the mean of τ; that is, $\delta_j(t) \in N(\tau, \theta)$. τ can be considered as the average rate of return for all investments, θ is the asset price volatility. In Iori's model, investment risk is not taken into account; rate of return on investment is fixed. In reality, the real rate return on investment of different assets is different, and the different return on investment of banks directly reflects the different investment strategies. Different from Iori's model, the rate of return on investment of different assets is different, and the rate of return on investment of all assets obeys normal distribution in this work. At time step t, bank i will recover a part of its investment assets randomly in this work; that is, $U_i(t) = p \times Y_i(t)$, where p is the proportion of investment recovery. After investment recovery, all investment assets held by the bank i before investment is $\widehat{Y}_i(t) = \sum_{j=1}^{M} \overline{Q}_{ij}(t) g_j(t)$, where $\overline{Q}_{ij}(t)$ is the number of shares of asset j held by bank i after investment recovery.

Thus, the owner's equity of bank i at time t before dividend and investment is

$$\widehat{V}_i(t) = \widehat{L}_i(t) + \widehat{Y}_i(t) - A_i(t) - \left(1 + r_b\right) B_i(t-1), \quad (5)$$

where $B_i(t-1)$ is the total loan of bank i at time $t-1$; r_b is the interbank lending rate. In (1), the dividend $D_i(t)$ of bank i at the time t is calculated as follows:

$$\begin{aligned}D_i(t) = \max\{0, \min\big[&U_i(t) - r_a A_i(t-1), \\ &\widehat{L}_i(t) - \beta A_i(t), \widehat{L}_i(t) + \widehat{Y}_i(t) - (1+\chi) A_i(t)\big]\},\end{aligned} \quad (6)$$

where χ is the capital savings ratio and β is the deposit reserve ratio. The condition of the bank's dividend is $\widehat{V}_i(t)/A_i(t) \geq \chi$. In practice, depositories $A_i(t)$ for bank i are decided by the following equation:

$$A_i(t) = \left(1 + \sigma_A \eta_t\right) \overline{A}, \quad (7)$$

where σ_A is the standard deviation of all bank's random deposits, $\overline{A}$ is the mean of all bank's deposits, and $\eta_t \in N(0,1)$. The investment $I_i(t)$ of bank i at time t can be decided by

$$\begin{aligned}&I_i(t) \\ &\quad = \min\left\{\max\left[0, \widehat{L}_i(t) - \beta A_i(t) - D_i(t)\right], w_i(t)\right\},\end{aligned} \quad (8)$$

where $w_i(t)$ is the investment opportunity of bank i at time t, which is defined as follows:

$$w_i(t) = \overline{w}\left(1 + \sigma_w \mu\right), \quad (9)$$

where $\overline{w}$ is the mean value of all banks' investment opportunities, σ_w is the standard deviation of all banks' investment opportunities, and μ obeys normal distribution $N(0,1)$. It is assumed that the quantity of assets j invested by the bank i is $\Delta Q_{ij}(t)$ at time t, which satisfies $I_i(t) = \sum_{j=1}^{M} \Delta Q_{ij}(t) g_j(t)$. Thus, the value of $Y_i(t)$ after investment is updated as $Y_i(t) = \sum_{j=1}^{M} Q_{ij}(t) g_j(t)$, where $Q_{ij}(t) = \overline{Q}_{ij}(t) + \Delta Q_{ij}(t)$.

In the above banking system, a bank appears to bankrupt in the following situations: lack of liquidity, being unable to settle the expired depositor's deposit, or debt maturity. For a bank with its equity more than 0, if there is a surplus of liquidity after dividends and investment, then the bank is a potential creditor bank, which can provide funds in the interbank market. In order to maintain the normal operation, a debt bank needs to borrow money from the interbank market. For debt banks, repayments are made if the borrowing from the interbank market is sufficient to repay the borrowing of the previous period. At the same time, the liquidity of the debt banks has changed to 0. If the borrowing is not available or the borrowing will not be paid enough to repay the last loan and deposits, debt banks will sell the

investment assets until they can repay the previous loan and deposits. If the sale of assets is not enough to reimburse the previous dismantling, then the debt bank fails and carries out the liquidation of the assets; the assets must be used to pay back the deposits firstly and the resting will be paid back to the creditor bank in proportion. The operation process of banking network in this paper is different from Iori's model [14]. Iori's model does not allow banks to replenish liquidity by selling assets, which is inconsistent with the actual operation of the banking system, making Iori's model overestimate the systemic risk of banking system.

2.2. Investment Constraints in Interbank Lending. In the process of interbank lending, interbank lending funds are strictly limited to make up for the shortage of short-term funds rather than for investment. For a bank with liquidity surplus, (8) clearly limits the amount of its investment and cannot exceed its existing liquidity funds. For banks with insufficient liquidity, only through the interbank market to borrow their lack of liquidity $\sum_{j=1}^{N_{t-1}}(1+r_b)c_{ij}(t-1)B_{ij}(t-1)-\widehat{L}_i(t)$, r_b is the interbank market interest rate. The dynamic interbank lending process is described in Figure 2. The interbank lending process with investment constraints can be described as follows.

Step 1. Calculate the liquidity $\widehat{L}_i(t)$ of bank i at time t according to (2). If the liquidity $\widehat{L}_i(t)$ of bank i is positive, but the debt $B_i(t-1)$ of bank i at time $t-1$ is negative, then bank i is temporary potential creditor bank. If the liquidity $\widehat{L}_i(t)$ and liability $B_i(t-1)$ are positive at the same time and there is $\widehat{L}_i(t) > (1+r_b)B_i(t-1)$, then all the debts are repaid and the liquidity is updated to $\widehat{L}_i(t) = \widehat{L}_i(t) - (1+r_b)B_i(t-1)$. At the same time, bank i becomes a temporary potential creditor bank. If liquidity is not able to repay the loan, that is, $\widehat{L}_i(t) < (1+r_b)B_i(t-1)$, then bank i is a potential debt bank.

Step 2. For each temporary potential creditor bank, the dividends and investment are operated according to (6) and (8), and the liquidity is updated to $\widehat{L}_i(t) - D_i(t) - I_i(t)$.

Step 3. For a temporary potential creditor bank i, if $\widehat{L}_i(t) - \beta A_i(t) > 0$, then bank i is a potential creditor bank, and it can lend its liquidity to other banks. The largest loan amount is $\widehat{L}_i(t) - \beta A_i(t)$.

Step 4. For time t, the debt bank i keeps borrowing from the potential creditor banks in a random order, with a total amount of B_{ij} (B_{ij} is the maximum amount that the potential creditor bank j can offer the loan), until bank i borrowed money from other potential creditor banks enough to repay the previous interbank loan $(1+r_b)B_i(t-1)$. At this time, the debt Bank i's loan amount is $(1+r_b)B_i(t-1) - \widehat{L}_i(t)$; the debt bank's liquidity is set as $\widehat{L}_i(t) = 0$. After the repayment of the debt bank i, the liquidity of the creditor bank j is updated to $\widehat{L}_j(t) = \widehat{L}_j(t) + (1+r_b)B_{ij}(t-1)$. If bank i has already made loans to all potential creditor banks but still cannot borrow enough loans to repay $(1+r_b)B_i(t-1)$, then the bank sells assets Q_{ij} randomly until it meets the repayment requirements. If the sale of the asset S_Q^i is still unable to repay the loan, the bank is bankrupt and liquidated (the assets must be used to pay back the deposits firstly, and all the remaining assets are returned to all creditor banks in proportion).

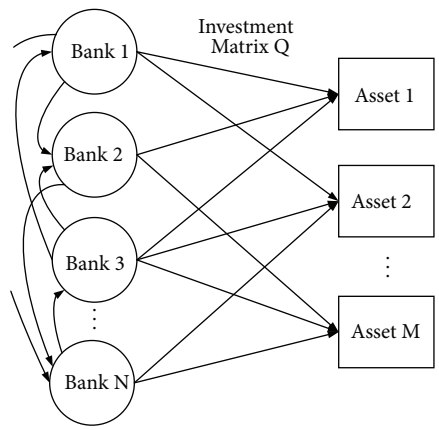

Figure 1: The structure of interbank market with overlapping portfolios.

2.3. Dynamic Evolution of Assets Prices with Overlapping Portfolios. From Section 2.2, it can be seen that when a bank has insufficient liquidity to repay its debt, it needs to sell assets for repayment. If the sale of the assets is still not able to repay the debt, the bank will go bankrupt and liquidate. In the above process, the selling of bank assets will lead to a fall in asset prices. A network of financial institutions holding the different assets is a bipartite graph shown as in Figure 1. Assuming that there are N financial institutions and M assets in the network, the market density is defined as $MD = M/N$. Each bank makes an investment according to (8), the asset portfolio of the bank i is $\{H_{i1}, H_{i2}, \ldots, H_{iM}\}$ ($H_{ij} = Q_{ij}(t)g_j(t)$), and the total investment assets are $H_i = H_{i1} + H_{i2} + \cdots + H_{iM}$. It is obvious that many financial institutions will invest in the same asset at the same time. There is an indirect connection between different financial institutions through the overlapping portfolios. The change in asset prices also affects multiple holding agencies. The changes in assets of a bank will affect other banks through overlapping portfolios. Assuming that the number of assets holds by the bank i is d_i, the average asset diversity of all banks in the interbank network system is

$$\overline{d} = \frac{1}{NM}\sum_{i=1}^{N} d_i. \tag{10}$$

The average asset diversity represents the indirect intensity of interbank. Banks should sell assets to make up for liquidity when they are short of liquidity and cannot make loans. In addition, if bank fails, the bankrupt banks will sell their asset portfolios due to asset liquidation. The assets sold will depreciate. Banks holding the same assets will be affected by the depreciation of assets, resulting in loss of all owners' rights and interests, which may lead to insolvency, thus

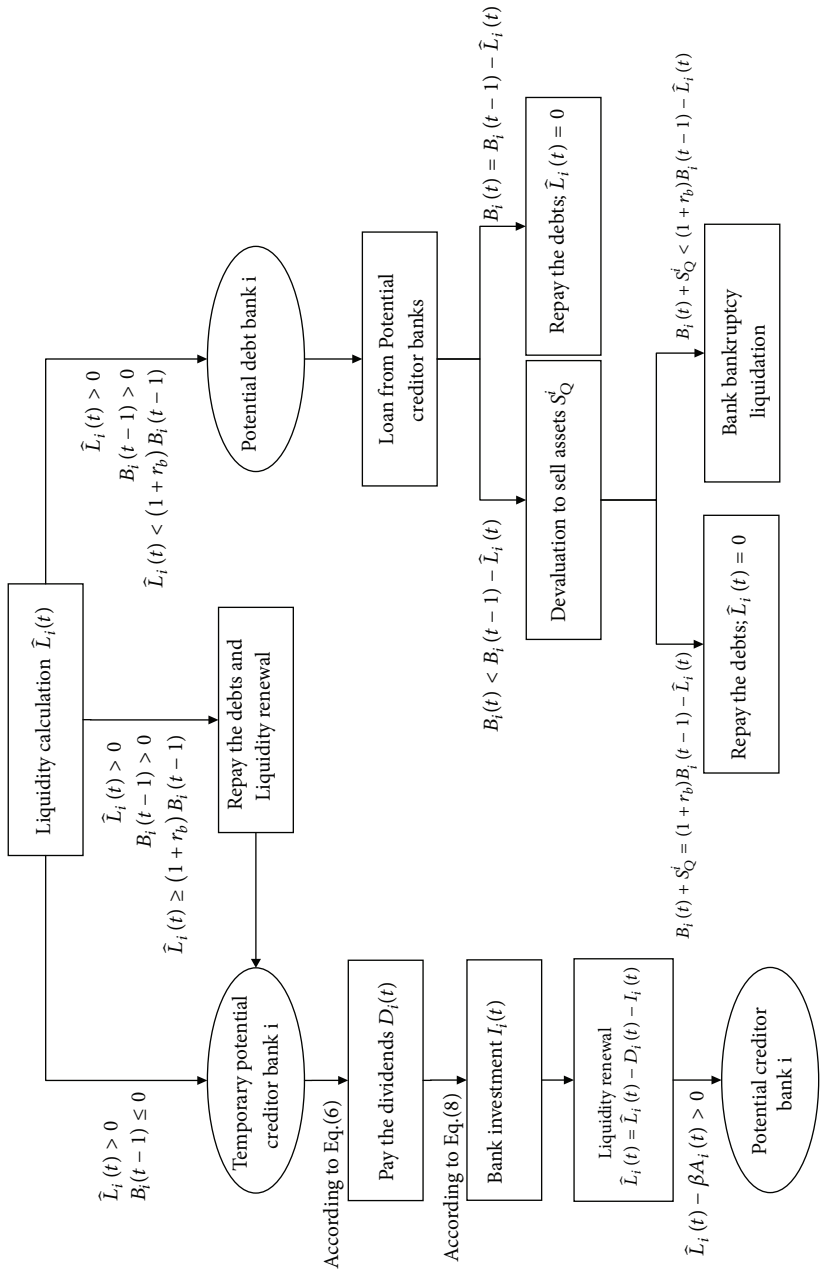

Figure 2: The dynamic process of bank i.

resulting in bank bankruptcy, which will further damage the assets of creditor banks. Through this evolutionary process, the initial shock of the interbank network is constantly propagated in the system. At time t, $Q_{ij}(t)$ is the quantity of shares of asset j held by bank i and $g_j(t)$ is the price of asset j. When banks sell their assets due to lack of liquidity or a bank is liquidated because of bankruptcy, assets will be sold in devaluation [33, 34]. Here, the market impact function is introduced to reflect the change of asset prices [30]:

$$f\left(x_j^t\right) = e^{-\alpha x_j^t}, \tag{11}$$

where x_j^t is the fraction of asset j liquidated up to time t. α represents the sensitivity of asset prices, that is, the degree of price volatility produced by the selling of assets. Thus, the price of asset j at time t is

$$g_j(t) = g_j(t)\, f\left(x_j^t\right). \tag{12}$$

In this paper, we refer to Caccioli's study [30] to take $\alpha = 1.0536$; that is, when 10% of the asset is sold, the price of the asset is also reduced by 10%, which corresponds to linear market impact for log-prices [35]. All prices are set to $g_j(0) = 1$ at time 0.

3. Simulation and Analysis

The whole banking network system evolves with time t. For a bank, its liquidity assets, owner's equity, and rate of return on investment (ROI) vary with time t. In the evolution of the bank network system, banks in the bank network system will fail due to the different operating conditions and operation strategies of the banks. One or several banks failures will lead to cascading failures of other banks in the system, which is due to the systemic risk of the banking system. The systemic risk of banking network system at time t is determined by the internal state and internal parameters of network system rather than the external factors of bank network system, such as savings interest rate and ROI. External factors affect the bank network systemic risk by influencing the internal variables of the bank's network system. The network evolves with external factors such as savings interest rate r_a, lending interest rate r_b, capital reserve ratio β, and average investment return rate δ. The failure of the banking system can reflect current systemic risk. To effectively characterize the systemic risk of banks, we calculate the normalized value $Risk(t)$ of the average number of bankrupt banks in $[t+1, t+T]$. $Risk(t)$ is the calculated value of systemic risk, which can be expressed as follows:

$$Risk(t) = \frac{1}{TN_e}\sum_{i=1}^{N_e}\sum_{j=t+1}^{t+T}\frac{M_j^i}{N_j^i}, \tag{13}$$

where N_e is the number of repeated simulations, N_j^i the number of surviving banks in the network at time j, and M_j^i is number of banks that fail during the ith simulation. T is the time scale, which is set as $T = 200$ in this work.

In order to further verify the effectiveness of the proposed model in characterizing the credit risk contagion, this paper simulates the model from different angles: (i) evolution process of systemic risk under different ROI; (ii) the impact of asset price volatility on the stability of the banking system; (iii) the impact of asset diversity on the stability of the banking system; (iv) the effect of banks' reserve ratio on the liquidity and stability of the banking system; and (v) the dynamic process of banks suffering asset depreciation in the financial crisis.

Establishing this model needs a certain theoretical background and needs to understand the practical operation rules and supervision rules of the banking system. In fact, the setting of parameters in this paper corresponds well with the parameters in the actual banking network system. Different parameter values will lead to different evolution results of the banking network system, which is also consistent with the operation process of the actual banking system. Our model is able to analyze the risk of the banking system under different parameters, which is conducive to our analysis of the systemic risk of the banking system and can also provide relevant reference for decision-makers.

In this work, 200 banks are used for simulations (more banks can be selected for simulation, but the 200 are already sufficiently responsive to the characteristics of banking network). The maximum simulation time step is 2000 (within 2000 time steps, the dynamic characteristics of the banking network can be fully embodied). There are 150 types of assets that banks can invest. At each time, each bank will recover 35% of its investment assets randomly. In this work, the initial owner's equities are subject to a standard normal distribution with a mean of 200. The average rate of return on investment is greater than the interest rate of deposit, that is, $\delta > r_a$, which ensures that the banking system has a profit margin. The profit margin will affect the stability of the banking system [36]. The greater the profit margin is, the more profits in the banking system are and the more stable the operation of the bank is. The capital saving ratio χ is set as 30% in this work; that is say, the dividends must satisfy the condition that the bank's liquidity is more than 30% of the savings. The condition guarantees that only a profitable bank can pay dividends. We only consider constraint behavior for banks; that is, the banks' loan cannot be used for investment and can only be used to repay the loan.

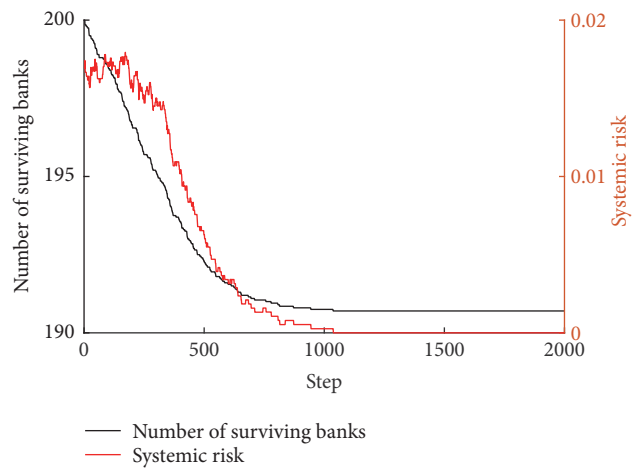

Figure 3: Changes in the number of surviving banks in the bank network as well as the corresponding systemic risks. The parameters are set as $\overline{d} = 0.1067$, $\theta = 0.02$, $\delta_{ave} = 0.009$, $p = 0.05$, $C = 0.03$, $\sigma_A = 0.15$, $\sigma_w = 0.25$, $\overline{A} = 1000$, $\overline{w} = 500$, $\chi = 0.3$, $\beta = 0.25$, $N = 200$, $M = 150$, $r_a = 0.004$, and $r_b = 0.008$.

Figure 3 shows the changes in the number of surviving banks in a banking network as well as the corresponding systemic risks. Figure 3 indicates that there may be banks collapsing from the first step, until the banking system is stable around 1000 steps. Systemic risk is the largest in the beginning of the network evolution, which is caused by the different initial state of the banks in the banking system. The initial net assets of banks are in the normal distribution with mean value of 200. The initial liquidity, the initial investment value, and the investment strategy of each bank are different. In the real financial market, investment is risky, so the return rate of investment in this work is in the normal distribution. For banks with low net assets and less liquidity, if the investment strategy is not good enough, then the investment income is not enough to pay the savings interest and loan; it is easy to go bankrupt. The bankrupt bank will be wound up, which devaluates the assets. On one hand, the bankrupt bank may not be able to fully repay the interbank borrowing. On the other hand, these bankrupt banks will devalue the

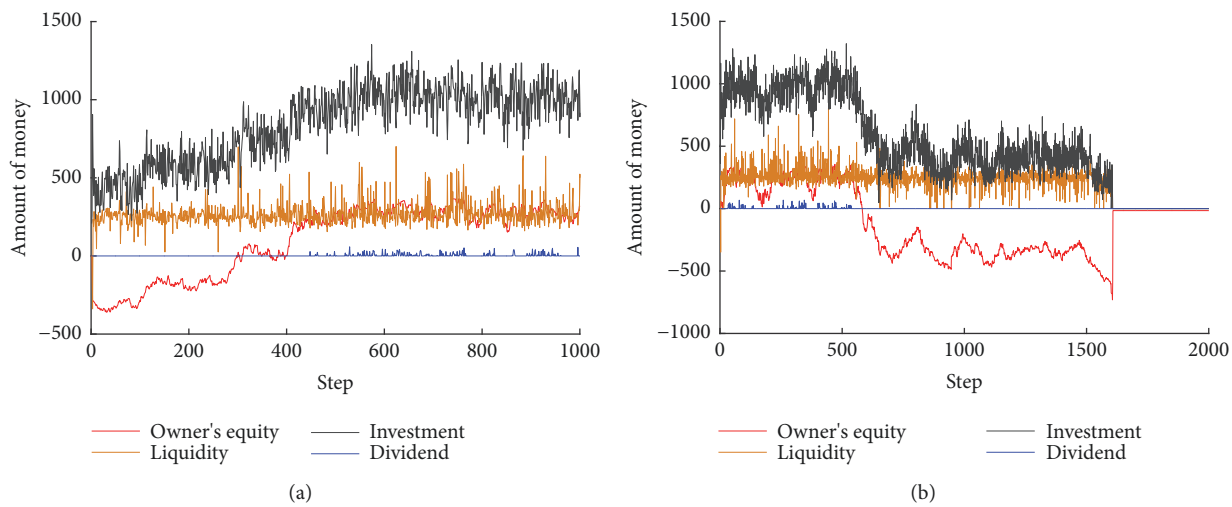

FIGURE 4: (a) The evolutionary process of a bank with negative initial value of ownership, but it eventually can run a stable operation. (b) The evolutionary process of a bank with positive initial value of ownership, and it finally goes bankrupt. The parameters are set as $\overline{d} = 0.0533$, $\delta_{ave} = 0.009$, $\theta = 0.06$, $p = 0.05$, $C = 0.03$, $\sigma_A = 0.15$, $\sigma_w = 0.25$, $\overline{A} = 1000$, $\overline{w} = 500$, $\chi = 0.3$, $\beta = 0.25$, $BankNo = 200$, $AssetNo = 150$, $r_a = 0.004$, and $r_b = 0.008$.

assets of other banks because of the overlapping portfolios. These two reasons will lead to the "domino effect" of bank bankruptcy and form the contagion of bank credit risk. Of course, for a bank with good initial state (high net assets and liquidity), if the investment strategy is not good, it will also lead to a decline in profit or even loss and finally bankruptcy. After 1000 steps, the banking system will be stable and no bank will fail. This is because the banking system has digested the risk in the system. Without external shocks, the banking system has enough capacity to resist the fluctuation of asset prices.

Figure 4 shows the dynamic evolution of two banks with different initial states. The net initial net value of one bank is negative, as shown in Figure 4(a). The net assets of another bank are positive, as shown in Figure 4(b). From Figure 4(a), it can be seen that the bank has gradually increased its net assets through continuous investment income and then further increases the total amount of investment and expands revenue, which has transformed the bank from a unhealthy state to a well-run bank. However, the initial state of the bank shown in Figure 4(b) is good, but at about 500 steps, the investment strategy is not good enough, resulting in the loss of assets, resulting in the gradual decline of net assets and the lack of liquidity, which eventually leads to bankruptcy. As can be seen from Figure 4, the state of a bank is not only related to the initial state, but also related to the investment strategy of the bank in the evolution process.

In real financial networks, the average rate of ROI represents the overall situation of the current financial market. Therefore, in order to reflect the impact of ROI on the stability of banking system, the average ROI is used to analyze the evolution of banking network. Figure 5 shows the changes in the banking system under different average ROI. Figure 5 shows that the higher the average ROI is set, the more stable the banking system can be achieved. When the average ROI

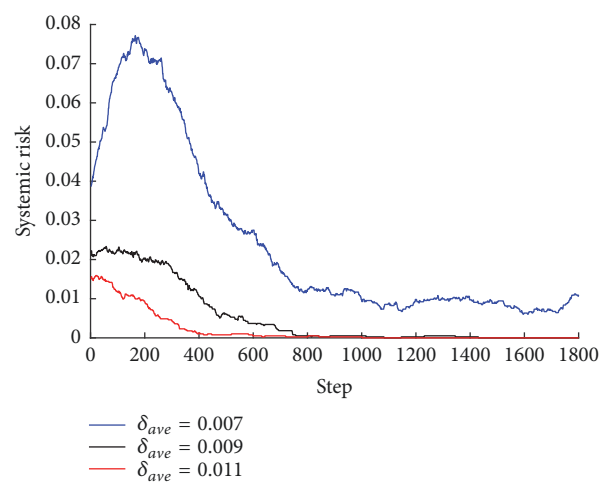

FIGURE 5: Systemic risk under different values of δ_{ave}. The parameters are set as $\overline{d} = 0.0533$, $\theta = 0.04$, $p = 0.05$, $C = 0.03$, $\sigma_A = 0.15$, $\sigma_w = 0.25$, $\overline{A} = 1000$, $\overline{w} = 500$ $\chi = 0.3$, $\beta = 0.25$, $N = 200$, $M = 150$, $r_a = 0.004$, and $r_b = 0.008$.

is 0.011 and 0.009, the banking system is able to quickly reach a stable state. When the average ROI is 0.07, the probability of banks failure in the banking system is greater than zero. From Figure 5, it can be seen that when the average ROI is 0.011 and 0.009, the risk of the system can be changed to 0 within 800 steps, while the average ROI is 0.007; the systemic risk always exists in the banking network. This is because the average ROI is too small to generate enough margin between deposit rate and investment income, which leads to the decline of banks' profitability, resulting in the weak ability to resist risk. Therefore, the low average ROI makes the banking network always have systemic risk.

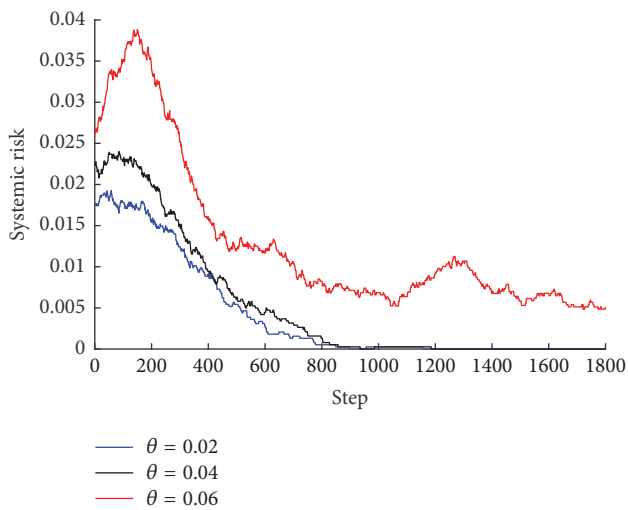

Figure 6: Systemic risk under different values of θ. The parameters are set as $\overline{d} = 0.0533$, $\delta_{ave} = 0.009$, $p = 0.05$, $C = 0.03$, $\sigma_A = 0.15$, $\sigma_w = 0.25$, $\overline{A} = 1000$, $\overline{w} = 500$, $\chi = 0.3$, $\beta = 0.25$, $BankNo = 200$, $AssetNo = 150$, $r_a = 0.004$, and $r_b = 0.008$.

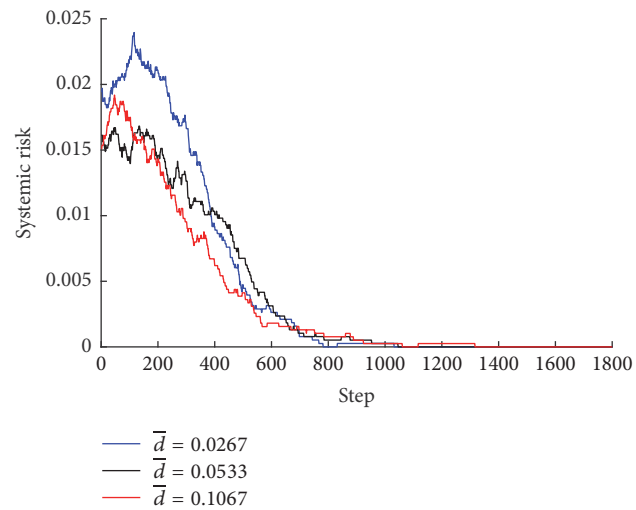

Figure 7: Systemic risk under different values of $\overline{d}$. The parameters are set as $\theta = 0.02$, $\delta_{ave} = 0.009$, $\theta = 0.02$, $C = 0.03$, $\sigma_A = 0.15$, $\sigma_w = 0.25$, $\overline{A} = 1000$, $\overline{w} = 500$, $\chi = 0.3$, $\beta = 0.25$, $BankNo = 200$, $AssetNo = 150$, and $r_b = 0.008$.

The choice of the investment strategy of banks has an important influence on the stability of the banking system. In addition to the average ROI, the objective description of the financial market should also take into account the volatility of the ROI θ. The greater θ is, the greater difference of ROI between different investment products at the same time step is and the greater the difference of ROI for the same investment product at different time steps is, which puts forward higher requirements for banks' asset selection. Figure 6 shows the results of the evolution of the banking system under different θ values. The more volatility of ROI is seen in Figure 6, the more banks that fail in the banking network. When the values of θ are 0.02 and 0.04, the network can evolve into a stable state. But when the value of θ is 0.06, that is, when the ROI is very volatile, the network will always have the probability of banks failure. From Figure 6, we can see that when the ROI of the network fluctuates greatly, the risk of the system increases sharply, reaching the maximum value at about 200 steps, and then the systemic risk is gradually released, but the systemic risk is consistent. Before the 200th step, banks that have low net assets and poor liquidity will have a certain probability of excessive investment losses, which leads to the bankruptcy. This phenomenon is caused by the following reasons: when the fluctuation of return on investment is very small, the probability of excessive loss of investment products is small. Banks can make up for the loss through borrowing and other investments. When the volatility of ROI is too large, the probability of excessive loss of investment products will increase. If the current state of a bank is not good enough, it is easy to see that the overall investment income is not enough to pay interest on savings and loans. In the financial crisis of 2008, many financial institutions were heavily invested in high-risk investment products, leading to bankruptcy.

The average asset density can reflect the distribution of bank investment. The greater the average asset density, the more decentralized the bank investment. The smaller the average asset density, the more centralized the bank investment. Figure 7 shows that the evolution of the banking network under the different average asset density. The values 0.02, 0.05, and 0.1 for $\overline{d}$ represented the average invest numbers 4, 8, and 16, respectively. Figure 7 shows that the banking network can all tend to be stable under different density of assets. But more banks will fail in the network with greater average asset density. This result indicated that the more decentralized a bank's investment is, the more stable the bank is. When the average ROI and the volatility of the ROI are fixed, all investment products suffer losses with same probability in the model. If there are too few investment types, every investment product is heavily loaded. Once an investment product has a big loss, the loss of the bank will become large, which will lead to the weakening of net assets and liquidity of the bank. In addition, once s asset is heavily loaded by a bank, if the bank fails, the price of the asset will depreciate substantially. On the contrary, if the investment is relatively scattered, even if an investment product suffers large losses, the impact on the overall investment income will not be too big. This model can be a good reflection of the fact of the real financial market, which is contrary to the existing model with overlapping portfolios [30]. The existing models based on overlapping portfolios only consider the degree of coupling between assets. If the investment is more dispersed, the asset coupling is greater, and the indirect association among the banks becomes stronger, which will increase the spread of the credit risk among the banks. In addition, the overlapping-portfolios-based model does not take into account the interbank market, while interbank market can provide support for the stability of the banking system (refer

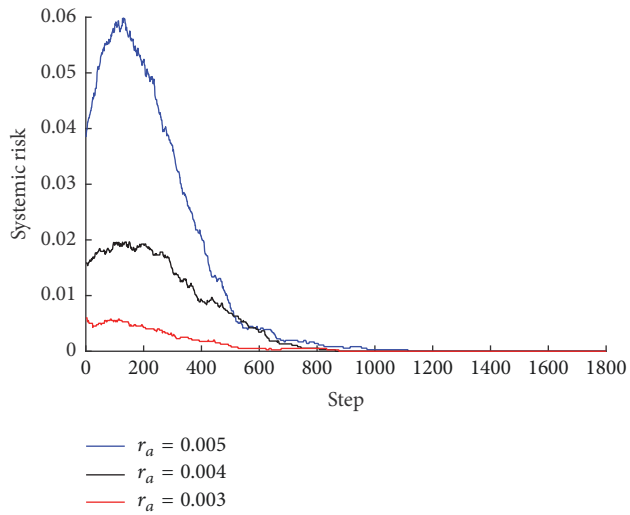

Figure 8: Systemic risk under different values of r_a. The parameters are set as $\overline{d} = 0.0533$, $\delta_{ave} = 0.009$, $p = 0.05$, $\theta = 0.02$, $C = 0.03$, $\sigma_A = 0.15$, $\sigma_w = 0.25$, $\overline{A} = 1000$, $\overline{w} = 500$, $\chi = 0.3$, $\beta = 0.25$, $BankNo = 200$, $AssetNo = 150$, and $r_b = 0.008$.

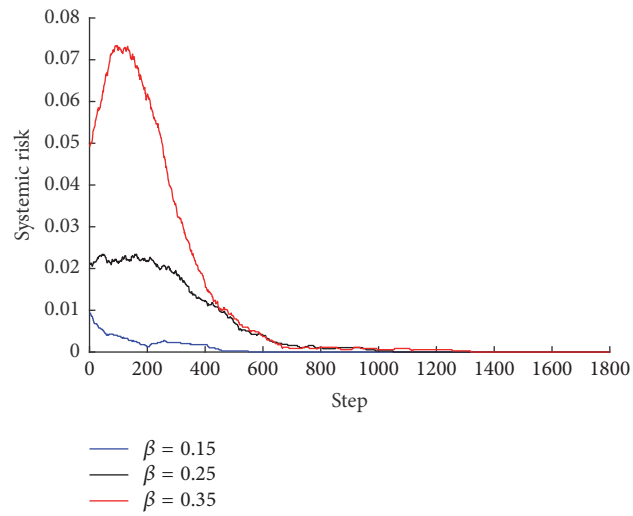

Figure 9: Systemic risk under different values of β. The parameters are set as $\overline{d} = 0.0533$, $\delta_{ave} = 0.009$, $\theta = 0.04$, $p = 0.05$, $C = 0.03$, $\sigma_A = 0.15$, $\sigma_w = 0.25$, $\overline{A} = 1000$, $\overline{w} = 500$, $\chi = 0.3$, $BankNo = 200$, $AssetNo = 150$, $r_a = 0.004$, and $r_a = 0.008$.

to the simulation in Figure 11), which can offset the risk of the coupling increase.

The margin of the investment and deposit is the main source of the banks' profit; the banks' profit level is affected by the deposit rate. Figure 8 shows the evolutionary results of an interbank network with different deposit rates. Figure 8 shows that the deposit rate has a greater impact on the stability of the banking system, and the higher the deposit rate, the more banks that eventually fail. In Figure 8, when the deposit rate is 0.005, the risk of the banking system increases sharply. The results show that the stability of the bank is sensitive to the deposit rate, and the change of the deposit rate will have a greater impact on the banking system. This is because, in the banking system, banks' liquidity is mainly provided by the savings, and the savings account for a large proportion of the funds in the bank. A slight increase of deposit rate will lead to the expansion of the deposit rate expenditure, thus causing a sharp shrinkage of banks' profits, which eventually leads to the failure of some banks with low net assets and liquidity.

The deposit reserve ratio can restrict the use of banks' funds and have an important impact on the stability of the banking system. Figure 9 shows the changes in the banking system under three different bank reserve ratios. From Figure 9, it can be seen that the lower the deposit reserve rate is, the less banks have to go bankrupt. When the deposit reserve is raised, the amount of money that can be used for investment is decreased; that is, the income of the investment is decreased, but the savings interest has not been reduced. Therefore, the increase of the deposit reserve ratio reduces the margin difference between investment and deposit, which will lead to a weaker bank's ability to deal with risks and increase the probability of a credit default.

During the financial crisis, many investment products will inevitably suffer huge losses, which will cause great damage to the banking system, for example, the global financial crisis in 2008. Here, we analyze the changes in the banking system when the price of the assets has fallen. One of the important manifestations of the financial crisis is the substantial fall in the price of assets. Figure 10 shows the evolution of the banking network when the assets fell at the 750th step. Figure 10(a) shows that when the average asset price fell by 15% and 30%, the number of bankrupted banks was not increased and the banking system remained stable. But when the average asset price falls by 45%, there will be a lot of credit default. This conclusion gives us an inspiration: there is a threshold. When the average asset price falls beyond this threshold, banks will have systemic risk. When the average asset price falls less than this threshold, the banking system can absorb the impact of asset shrinkage. Through our model simulation, the threshold is about 38% when the parameter setting is shown in Figure 10.

Interbank lending can make up for the lack of temporary liquidity and play an important role in the stability of banking system. At present, the research on the bank-assets bipartite network does not take into account the role of interbank lending. Figure 11 shows the evolution of banking system in the case of interbank lending compared with that without interbank lending. As can be seen from Figure 11, if there is no interbank loan, the banking network will accumulate lots of risks in the initial stage, and the number of bankrupt banks is large. In the absence of interbank lending, banks with insufficient liquidity can only sell assets to make up for liquidity, which can lead to a decline in the profitability of the banks, resulting in further reduction and even negative interest rates between investment and deposits, which further leads to the tension of the banks' liquidity, resulting in breach of contract. Figure 11 indicates that interbank lending can improve the stability of banking network.

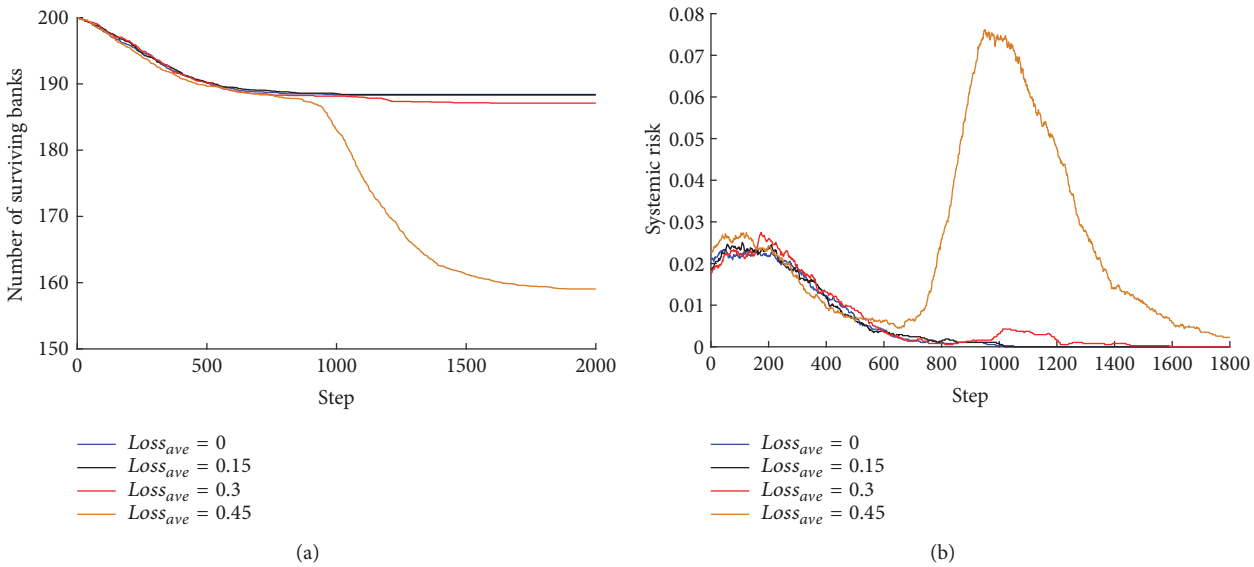

Figure 10: (a) The evolution process when the investment suffer a loss at step 750. (b) Systemic risk when the investment suffers a loss at step 750. The parameters are set as $\overline{d} = 0.0533$, $\delta_{ave} = 0.009$, $\theta = 0.04$, $p = 0.05$, $\sigma_A = 0.15$, $\sigma_w = 0.25$, $C = 0.03\ \overline{A} = 1000$, $\overline{w} = 500$, $\chi = 0.3$, $\beta = 0.25$, $BankNo = 200$, $AssetNo = 150$, $r_a = 0.004$, and $r_a = 0.008$.

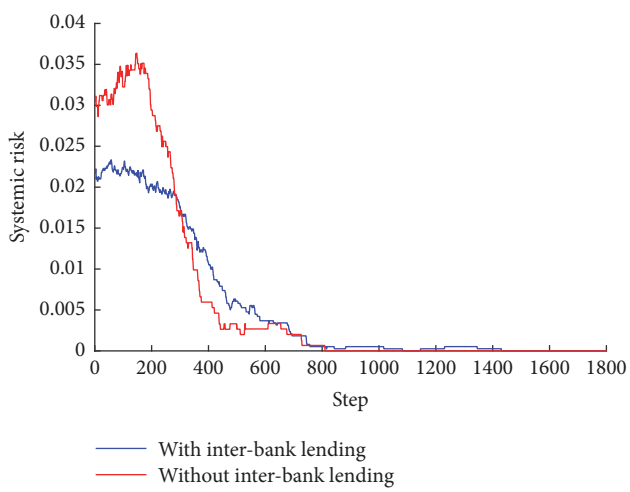

Figure 11: The evolution process of the system with interbank lending and without interbank lending. The parameters are set as $\overline{d} = 0.0533$, $\delta_{ave} = 0.009$, $\theta = 0.04$, $p = 0.05$, $\sigma_A = 0.15$, $\sigma_w = 0.25$, $\overline{A} = 1000$, $\overline{w} = 500$, $\chi = 0.3$, $\beta = 0.25$, $BankNo = 200$, $AssetNo = 150$, $r_a = 0.004$, and $r_a = 0.008$.

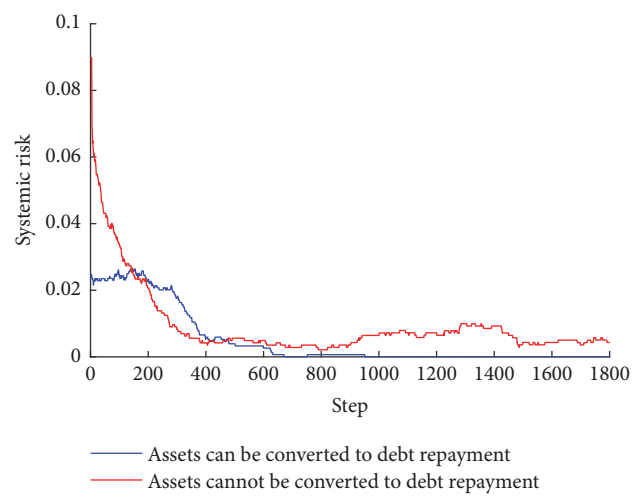

Figure 12: The evolution process of the system when the assets cannot be converted to debt repayment. The parameters are set as $\overline{d} = 0.0533$, $\delta_{ave} = 0.009$, $\theta = 0.04$, $p = 0.05$, $\sigma_A = 0.15$, $\sigma_w = 0.25$, $C = 0.03\ \overline{A} = 1000$, $\overline{w} = 500$, $\chi = 0.3$, $\beta = 0.25$, $BankNo = 200$, $AssetNo = 150$, $r_a = 0.004$, and $r_a = 0.008$.

In the existing models of bank investment, when a bank lacks liquidity, it only considers the interbank loan but does not consider the liquidation of assets as well as asset devaluation when assets are realizable. Therefore, there are too many banks failures in the existing models, which is not in line with the reality. In fact, when banks encounter insufficient liquidity, they can sell some investment assets to supplement liquidity. Figure 12 shows the evolution process of banking network when banks cannot sell assets to supplement liquidity. From Figure 12, it can be seen that when banks cannot add liquidity by selling assets, the banking system will have a large systemic risk, and the systemic risk will always exist. When bank liquidity is insufficient and banks' borrowing is insufficient to meet the repayment of savings and loans, banks will fail if they are not able to make liquidity by selling assets. The result shows that the selling of assets plays an important role in the stability of the banking system. It can supplement the shortage of liquidity in time and solve the problem of the shortage of sudden liquidity in the banking system.

4. Conclusions and Discussion

Financial contagion is one of the most important forms for financial system to spread financial crisis. The financial system is a complex network system composed of a series of financial institutions and the interconnections between them. The connection relationship not only has the direct relation of the interbank market but also the indirect relation between the investment of the same assets among the financial institutions. Existing studies either focus on interbank market or pay attention to the overlapping portfolios of bank investment, which cannot accurately model the banking system. In addition, some hypothesis of current research is not practical. For example, the investment interest rate is fixed; liquidity cannot be complemented by devaluation to sell assets. Because of the one-sided and unrealistic assumptions of the research, the previous model cannot effectively respond to the real situation of a banking system, which leads to the banking system being too fragile reflected by the existing model. In order to better reflect the evolution of banking system, a new model for interbank market with overlapping portfolios is proposed in this work. In the proposed model, interbank lending and overlapping portfolios are both considered. The investment risk is also considered in this work, which plays an important role in the stability of the banking system. The proposed model allows banks to make up liquidity by devaluation to sell assets, with more realistic responses to the operating rules of the banking system. Through numerical simulation, this paper gets a series of conclusions which have important theoretical value and management significance. The main points are as follows:

(i) The bigger the average ROI, the more stable the banking system. If the average ROI is too small, the margin between deposit rate and investment income becomes small or negative, which leads to the decline of bank profitability, resulting in the weak ability to resist risk, making the banking network always have systemic risk.

(ii) If the volatility of ROI is increased, the probability of excessive loss of investment products will increase. If the current state of a bank is not good enough, there's not enough money to invest; the overall investment income may be not enough to pay interest on savings and loans, which leads to more systemic risk.

(iii) The model reveals that the more decentralized the bank's investment is (i.e., bigger average asset density), the more stable the bank is. The average asset density can reflect the distribution of bank investment.

(iv) The stability of the bank is sensitive to the deposit rate; the change of the deposit rate has a greater impact on the banking system. The higher the deposit rate, the greater the systemic risk.

(v) The increase of the deposit reserve ratio reduces the margin between investment income and deposit rate, which will lead to a weaker bank's ability to deal with risks and increase the systemic risk.

(vi) There exists a threshold for asset prices shrink. When the average asset price falls beyond this threshold, banks will have systemic risk. When the average asset price falls less than this threshold, the banking system can absorb the impact of asset shrinkage.

(vii) Interbank lending can make up for the lack of temporary liquidity and play an important role in the stability of banking system. The model presents that interbank lending can improve the stability of banking network.

(viii) Devaluation to sell assets plays an important role in the stability of the bank, which can supplement the shortage of liquidity in time and solve the problem of the shortage of sudden liquidity in the banking system.

These conclusions have important theoretical value and practical significance for systemic risk management practice. This work is of great theoretical and practical significance to the formulation of an effective, reasonable, and scientific systemic risk management strategy. The banking system is very complex; there are many points that can continue to be discussed. For example, the banking network structure is not a random network; relevant studies show that banking networks have significant scale-free network characteristics [37]. The investment of banks is not completely random, and there may be herd effect [38]. However, the model in this paper can well reflect the risk of the banking system. Above points can be empirically studied on the basis of the proposed model in the future.

At present, there are two main ways to model the banking system. The first way is the physical mechanism model for the operation process of the banking network system [14, 31]. Physical mechanism model can clearly describe the operation process of the banking network and can effectively model the banking behavior. The second way is a macroscopic dynamic equation model [39]. The second method is based on dynamic equation, which can get a series of conclusions through strict theoretical proof. However, the detailed description of the actual operation of the banking system is not clear enough, and it is difficult to model the banking behavior in the banking network. The physical mechanism model is adopted in this paper. The proposed method in this paper has not been proven and analyzed theoretically. At present, it is difficult to theoretically deduce the mechanism modeling of banking system. The model proposed in this paper is a dynamic process physical model with practical basis. It is very complex, highly nonlinear, and discontinuous, so it is difficult to get a conclusion through theoretical proof. Therefore, a series of meaningful conclusions are obtained through various simulations in this paper. However, theoretical derivation based on such models is an important research direction in the future.

Data Availability

The data used to support the findings of this study are available from the corresponding author upon request.

Conflicts of Interest

The authors declare that there are no conflicts of interest regarding the publication of this paper.

Acknowledgments

This work is supported by the National Natural Science Foundation of China (71371046) and the Fundamental Research Funds for the Central Universities (nos. CUSF-DH-D-2019101 and 19D110803).

References

[1] A. R. Neveu, "A survey of network-based analysis and systemic risk measurement," *Journal of Economic Interaction and Coordination*, vol. 1, pp. 1–41, 2016.

[2] M. Pollak and Y. Guan, "Partially overlapping ownership and contagion in financial networks," *Complexity*, vol. 2017, Article ID 9895632, 16 pages, 2017.

[3] W. Silva, H. Kimura, and V. A. Sobreiro, "An analysis of the literature on systemic financial risk: A survey," *Journal of Financial Stability*, vol. 28, pp. 91–114, 2016.

[4] R. Grilli, G. Tedeschi, and M. Gallegati, "Markets connectivity and financial contagion," *Journal of Economic Interaction and Coordination*, vol. 10, no. 2, pp. 287–304, 2015.

[5] A. Hryckiewicz and L. Kozlowski, "The consequences of liquidity imbalance: When net lenders leave interbank markets," *Journal of Financial Stability*, vol. 36, pp. 82–97, 2018.

[6] M. Kanno, "Assessing systemic risk using interbank exposures in the global banking system," *Journal of Financial Stability*, vol. 20, pp. 105–130, 2015.

[7] T. Schuler and L. Corrado, "Interbank market failure and macro-prudential policies," *Journal of Financial Stability*, vol. 33, pp. 133–149, 2017.

[8] G. G. Kaufman and K. E. Scott, "What is systemic risk, and do bank regulators retard or contribute to it?" *Independent Review*, vol. 7, no. 3, pp. 371–391, 2003.

[9] P. E. Mistrulli, "Assessing financial contagion in the interbank market: maximum entropy versus observed interbank lending patterns," *Journal of Banking & Finance*, vol. 35, no. 5, pp. 1114–1127, 2011.

[10] F. Allen and D. Gale, "Financial contagion," *Journal of Political Economy*, vol. 108, no. 1, pp. 1–33, 2000.

[11] X. Freixas, B. M. Parigi, and J.-C. Rochet, "Systemic risk, interbank relations, and liquidity provision by the Central Bank," *Journal of Money, Credit and Banking*, vol. 32, no. 4, pp. 611–638, 2000.

[12] Y. Leitner, "Financial networks: contagion, commitment, and private sector bailouts," *Journal of Finance*, vol. 60, no. 6, pp. 2925–2953, 2005.

[13] S. Vivier-Lirimont, *Interbanking Networks: Towards a Small Financial World*, Cahiers De La Maison Des Sciences Economiques, 2004.

[14] G. Iori, S. Jafarey, and F. G. Padilla, "Systemic risk on the interbank market," *Journal of Economic Behavior & Organization*, vol. 61, no. 4, pp. 525–542, 2006.

[15] S. Lenzu and G. Tedeschi, "Systemic risk on different interbank network topologies," *Physica A: Statistical Mechanics and its Applications*, vol. 391, no. 18, pp. 4331–4341, 2012.

[16] E. Nier, J. Yang, T. Yorulmazer, and A. Alentorn, "Network models and financial stability," *Journal of Economic Dynamics and Control (JEDC)*, vol. 31, no. 6, pp. 2033–2060, 2007.

[17] F. Caccioli, T. A. Catanach, and J. D. Farmer, "Heterogeneity, correlations and financial contagion," *Advances in Complex Systems (ACS)*, vol. 15, Article ID 1250058, 2012.

[18] M. Smerlak, B. Stoll, A. Gupta, and J. S. Magdanz, "Mapping systemic risk: Critical degree and failures distribution in financial networks," *PLoS ONE*, vol. 10, no. 7, Article ID e0130948, 2015.

[19] C.-P. Georg, "The effect of the interbank network structure on contagion and common shocks," *Journal of Banking & Finance*, vol. 37, no. 7, pp. 2216–2228, 2013.

[20] C. Kok, "Modelling the emergence of the interbank networks," *Quantitative Finance*, vol. 15, no. 4, pp. 653–671, 2015.

[21] J. Han and Y. Cao, "Systemic risk contagion of interbank network based on risk-averse behaviors," *Complex Systems and Complexity Science*, vol. 14, no. 1, pp. 75–80, 2017.

[22] M. Steinbacher, M. Steinbacher, and M. Steinbacher, "Robustness of banking networks to idiosyncratic and systemic shocks: a network-based approach," *Journal of Economic Interaction and Coordination*, vol. 11, no. 1, pp. 95–117, 2016.

[23] D. Yao, X. Liu, and X. Zhang, "Financial contagion in interbank network," *International Journal of Monetary Economics and Finance*, vol. 9, no. 2, pp. 132–148, 2016.

[24] R. Lagunoff and S. L. Schreft, "A model of financial fragility," *Journal of Economic Theory*, vol. 99, no. 1-2, pp. 220–264, 2001.

[25] H. Uhlig, "A model of a systemic bank run," *Journal of Monetary Economics*, vol. 57, no. 1, pp. 78–96, 2010.

[26] C. G. De Vries, "The simple economics of bank fragility," *Journal of Banking & Finance*, vol. 29, no. 4, pp. 803–825, 2005.

[27] R. Cifuentes, G. Ferrucci, and H. S. Shin, "Liquidity risk and contagion," *Journal of the European Economic Association*, vol. 3, no. 2-3, pp. 556–566, 2005.

[28] R. Greenwood, A. Landier, and D. Thesmar, "Vulnerable banks," *Journal of Financial Economics*, vol. 115, no. 3, pp. 471–485, 2015.

[29] X. Huang, I. Vodenska, S. Havlin, and H. E. Stanley, "Cascading failures in Bi-partite graphs: model for systemic risk propagation," *Scientific Reports*, vol. 3, no. 2, pp. 1219-1219, 2013.

[30] F. Caccioli, M. Shrestha, C. Moore, and J. D. Farmer, "Stability analysis of financial contagion due to overlapping portfolios," *Journal of Banking & Finance*, vol. 46, no. 1, pp. 233–245, 2014.

[31] F. Caccioli, J. D. Farmer, N. Foti, and D. Rockmore, "Overlapping portfolios, contagion, and financial stability," *Journal of Economic Dynamics and Control*, vol. 51, pp. 50–63, 2015.

[32] Y. Zhou and H. Li, "Asset diversification and systemic risk in the financial system," *Journal of Economic Interaction and Coordination*, vol. 1, pp. 1–26, 2017.

[33] K. Fink, U. Krüger, B. Meller, and L.-H. Wong, "The credit quality channel: Modeling contagion in the interbank market," *Journal of Financial Stability*, vol. 25, pp. 83–97, 2016.

[34] M. Bluhm and J. P. Krahnen, "Systemic risk in an interconnected banking system with endogenous asset markets," *Journal of Financial Stability*, vol. 13, pp. 75–94, 2014.

[35] J. D. Farmer, "Market force, ecology and evolution," *Industrial and Corporate Change*, vol. 11, no. 5, pp. 895–953, 2002.

[36] E. Yoldas and Z. Senyuz, "Financial stress and equilibrium dynamics in term interbank funding markets," *Journal of Financial Stability*, vol. 34, pp. 136–149, 2018.

[37] S. Gabrieli, "The microstructure of the money market before and after the financial crisis: a network perspective," *SSRN Electronic Journal*, vol. 9, no. 181, pp. 1–40, 2011.

[38] A. Bensa, M. Jlassi, and H. Litimi, "Volume-herding interaction in the American market," *American Journal of Finance and Accounting*, vol. 4, no. 1, pp. 50–69, 2015.

[39] A. Dassios and H. Zhao, "A generalised contagion process with an application to credit risk," *International Journal of Theoretical and Applied Finance*, vol. 20, no. 1, Article ID 1750003, 2017.

Hindawi
Complexity
Volume 2019, Article ID 4727868, 21 pages
https://doi.org/10.1155/2019/4727868

Research Article

Price Linkage Rumors in the Stock Market and Investor Risk Contagion on Bilayer-Coupled Networks

Yue Dong,[1] Jiepeng Wang,[2] and Tingqiang Chen [2]

[1] *School of Economics, Renmin University of China, Beijing, China*
[2] *School of Economics and Management, Nanjing Tech University, Nanjing, China*

Correspondence should be addressed to Tingqiang Chen; tingqiang88888888@163.com

Received 28 November 2018; Revised 7 March 2019; Accepted 21 March 2019; Published 10 April 2019

Guest Editor: Thiago C. Silva

Investor heterogeneities include investor risk preference, investor risk cognitive level, information value, and investor influence. From the perspective of the stock price linkage, this article constructs an SCIR contagion model of investor risk on a single-layer network. It digs out the investor risk caused by rumors in the stock market under the stock price linkage and its contagion mechanism. The function and influence of different mechanism probabilities and investor heterogeneities on the effects of risk contagion in the stock market are explored through computer simulation. Based on the SCIR contagion model of investor risk on single-layer network, we construct an SCI_1I_2R contagion model of investor risk on bilayer-coupled networks. Initially, the evolution mechanisms of investor risk contagion in the stock market are compared in single-layer and bilayer-coupled networks. Thereafter, the evolution characteristics and rules of investor risk contagion under different connection modes and heterogeneous mechanism probabilities are compared on bilayer-coupled networks. The results corroborate the following. (1) In the SCIR contagion model of investor risk on a single-layer network, immune failure probability and immune probability have the "global effect". (2) Investor heterogeneities both have "global effect" and "local effect" on investor risk contagion. (3) Compared with the investor risk contagion on a single-layer network, bilayer-coupled networks can expand the investor risk contagion and have a "global enhancement" effect. (4) Among the three interlayer connection modes of the SCI_1I_2R model of investor risk contagion on bilayer-coupled networks, the assortative link has the effect of "local enhancement", while the disassortative link has the effect of "local inhibition". (5) In the SCI_1I_2R model of investor risk contagion on bilayer-coupled networks, heterogeneous mechanism probabilities have "global effect" and "local effect". The research conclusion provides a theoretical basis for regulators to prevent financial risks from spreading among different investors, which is of high theoretical value and practical significance.

1. Introduction

The price linkage can be considered a "barometer" for the stock market [1, 2]. When the price linkage exceeds the investors' expectations, it leads to changes in investors' decision-making behavior. The uncertainty of information in the financial market easily triggers stock market rumors. Stock market rumors refer to special information that begins to circulate in the stock market without confirmation [3]. Stock market rumors turn into investor risk through their contagion and diffusion on investors' networks, which affects the status of investors toward rumors in the stock market in turn and the trading behavior of investors, thereby bringing the stock price linkage. Therefore, clarifying the formation and contagion mechanism of the investor risk caused by rumors in the stock market is important for understanding the actual process of investor stock trading influenced by information including stock market rumors, effective management of stock market rumors, and the management and control of investor risk.

Figure 1 shows that stock price linkage exceeds investors' expectations, thereby affecting investors' investment behavior on the one hand. On the other hand, information advantage investors make use of information asymmetry to spread stock market rumors driven by interests to obtain higher returns in the stock market. In the stock market, investors not only have cognitive and behavioral biases [4], but also have significant herd effects [5–7]. Egan et al. [7] corroborated that, if most investors choose to buy, they are also willing to buy and that, if most investors choose to sell, they are also willing to sell.

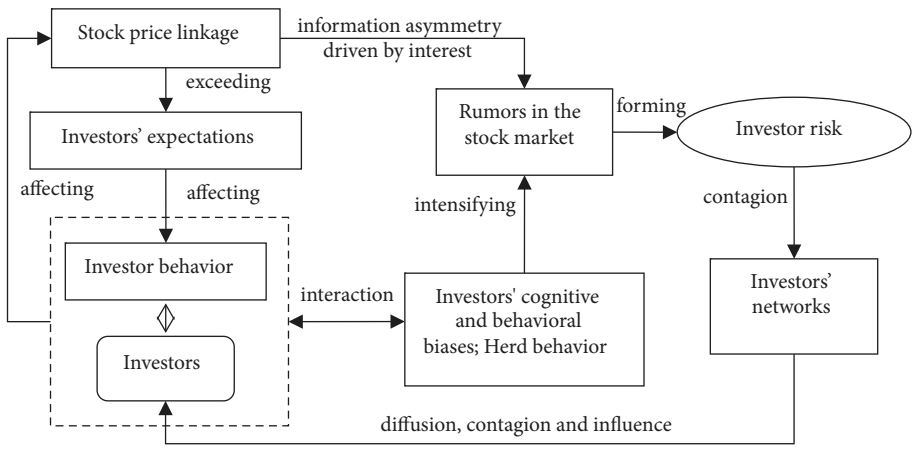

Figure 1: Mechanism analysis of investor risk formed by stock market rumors under the influence of price linkage.

As a result of these factors and influences, the formation of the stock market rumors accelerates. Market rumors can be regarded as "infected market information", which is highly contagious; the essence of investor risk formed by rumors is the interaction and diffusion of information among investors who carry "infected market information". Most investors who receive rumors think that they are in the middle of the rumor transmission sequence and that the stock price moves while rumors intersect with other investors' opinions and behaviors [8]. Therefore, investor risk spreads and diffuses in the investors' networks, such as social networks, kinship networks, friend networks, and work networks [9], thereby affecting investor behavior and decision-making and stock price linkage [10, 11].

In recent years, the impact of stock market rumors on price linkage in the stock market has become increasingly prominent. The investor risk and its evolution brought by stock market rumors under the influence of price linkage have an important impact on the health and stability of the stock market, which has been widely concerned by academic circles and financial regulators. Considerable literature has demonstrated the impact of market rumors on stock market linkage [10, 12, 13], Chen et al. 2010, [11]. For instance, Pound and Zeckhauser [10] contended that the stock price of the takeover target company generally has a significant increase before the takeover rumors published in the Wall Street journal. Clarkson et al. [13] and Gao and Oler [11] affirmed the significant increase in the trading activity of target securities before the announcement of merger rumors. Given the difficult issues of investor psychology and trading data availability, some studies have combined experimental and investigation methods. For instance, using college students in conducting simulated investment experiments, Schinlder [8] deduced that participants who receive rumors would conduct transactions, leading to the linkage of asset prices. Kosfeld [14] and Andrei and Cujean [15] introduced other ways of modeling and analysis. From the perspective of the exchange of information among traders, they believed that the more the exchanges among traders, the more the possible transactions that will be conducted, which will lead to price linkage. Existing literature analysis shows that empirical studies mainly discuss the effect of rumors, while theoretical modeling studies focus on the evolution of investor behavior.

The innovation of this paper focuses on a new perspective, stock price linkage, which considers the investor risk contagion caused by stock market rumors and concentrates on the investor risk contagion path and change rules. We use epidemic models to measure the investor risk. Based on that, we use a broad set of investor heterogeneities to modify the classic models. We use computer simulation to depict investor risk contagion because of the challenge of getting real data.

The structure of this article is as follows. In the second section, on the basis of the definition of investor risk, the research on the diffusion model of rumors is organized and summarized, and the adaptability of the epidemic model is analyzed. In the third section, an investor risk contagion model in the stock market on single-layer networks under the price linkage is constructed. Concurrently, the investor risk contagion probability model in the stock market on single-layer networks is constructed by considering the heterogeneity of investors, and the computer simulation analysis is conducted. In the fourth section, an investor risk contagion model in the stock market on bilayer-coupled networks is constructed, and the computer simulation analysis is implemented. The last section summarizes and concludes the research.

2. Investor Risk and Adaptability of the Epidemic Model

To better analyze the effects and influence factors of investor risk contagion, as well as look for the effective risk control strategy, this section initially defines the concept of investor risk. Studies of the rumor diffusion model, complex network theory, and related research are reviewed, while the adaptability of epidemic model is analyzed.

2.1. Investor Risk. Market rumors, regarded as "infected market information", are highly contagious. In this paper, investor risk is defined as follows: under the diffusion of rumors in the stock market, the investor's risk is formed by the change of his status toward rumors; its essence is the

interaction and diffusion of information between investors carrying "infected market information".

From the idea of the SIR model of infectious disease, Daley and Kendall [16] first proposed the random model of rumor diffusion (DK model). Maki and Thompson [17] further proposed an improved model (MK model). Thereafter, Nokovee et al. [18] combined the MK model and the SIR model and proposed a rumor diffusion model on complex networks. Through theoretical analysis and numerical simulation, the steady state and the evolution of the diffusion process over time in homogeneous networks, ER stochastic maps, and scale-free networks are analyzed comprehensively. Xiong et al. [19] proposed an SCIR diffusion model to describe the diffusion of rumors. In Zhao et al. [20] and Zan et al. [21], the individual is divided into the following categories, respectively: SIHR (ignorant-Spreader-Hibernator-stifler) and SCIR (Susceptible-infective-counter-refractory). These papers considered forgetting and counter mechanism. Jia and Wu [22] proposed a rumor transmission model with incubation period and constant recruitment in social networks. Moreover, the current research on complex network theory is mostly limited to a single network, while a single network is only a subset of a larger complex network, and complex systems are coupled from many networks with different structures and functions [23], Wu et al. 2018, [24]. Wu et al. (2018) found the double transition for information spreading on layered networks. Wang et al. [24] found that the information spreading is suppressed on multirelational networks especially when the average degree of hostile network is large through extensive numerical simulations. Therefore, the social networks are always multirelational, which can be described by using the multilayer network [25–32].

In sum, to make the model closer to the stock market based on the SCIR model, [19], Jia and Wu [22], and consider the heterogeneity of investors and bilayer-coupled structure of investors' networks, this study constructs an investor risk contagion model on bilayer-coupled networks on the basis of establishing an investor risk contagion model on single-layer network in the stock market to explore the path and change rules of investor risk contagion.

2.2. Adaptability of the Epidemic Model. Epidemic models are widely used in the study of diffusion problems, such as the spread and diffusion of public opinions, rumors, and knowledge, and many results have been achieved [24, 33, 34]. The contagion of investor risk in the investors' networks is similar to that of infectious diseases in the population. Specific performances are as follows.

2.2.1. Contagion Environment. Infectious diseases are mainly spread in social networks composed of individuals, and they infect the nodes (people) in social networks through the edges (connections established between people). The contagion of investor risk is spread in the investors' networks, which are composed of shareholding investors. Investor risk infects the nodes (investors) in the investors' networks through the edges (the relationship between investors) in the investors' networks. Therefore, in terms of the contagion environment, the contagion of investor risk is similar to the viral contagion.

2.2.2. Contagion Process. In the transmission of infectious diseases, viruses generally can only spread from infected individuals to those whom they have contact with. Similarly, in the contagion process of investor risk, after a certain node investor is infected with the risk, the associated investor is affected by the risk first, which then impacts the entire investors' network. Therefore, in terms of the contagion process, the contagion of investor risk is similar to the viral contagion.

2.2.3. Contagion Objects. In the transmission process of infectious diseases, the infected object is the individual in the social network. As an independent individual, it has a high degree of autonomy, and its resistance to the virus varies with its immunity. Similarly, given the heterogeneity of investors, investors in the investors' networks have different response levels and tolerance to risk contagion. Therefore, investor risk is similar to infectious disease in terms of contagion objects.

2.2.4. Contagion Direction. The spread of infectious virus in social networks is radiation, not directional. Similarly in the contagion process of investor risk, once a node investor is infected with the risk, the associated investors will be affected, and the contagion is not directional. Therefore, in terms of the contagion direction, investor risk and infectious diseases are similar.

3. Construction and Analysis of Investor Risk Contagion Model on Single-Layer Network in the Stock Market under the Price Linkage

3.1. Investor Risk Contagion Mechanism on Single-Layer Network in the Stock Market. In the stock market, to maximize capital appreciation, investors commonly exchange information and discuss investment strategies together. Therefore, a few informed investors spread market rumors among investors through various interactions of close investors (such as relatives, friends, neighbors, and colleagues) and manipulate the market to increase their trading profits. Concurrently, different investors explain and distinguish the rumors in the market on the basis of their own knowledge of the stock market and investment skills, among which experienced investors become "immune" when they think the rumors cannot be trusted and do not further spread them. That is, investors only believe the market rumors with certain probability and then spread the market rumors. Meanwhile, some investors who spread market rumors find that the news is outdated or untrue in the process of spreading; thus, the market rumors have lost their value, and investors will not continue to spread them.

Suppose that four different types of investors are in the stock market: trusting investors (S), transforming investors (C), infecting investors (I), and immune investors (R). Specifically, trusting investors are those who are likely to receive rumors from other investors but have not received rumors yet. Transforming investors are those who have received

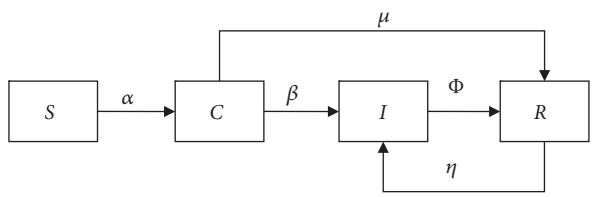

Figure 2: Investor risk contagion mechanism in the stock market.

rumors and have not decided whether to spread them. When transforming investors decide to spread rumors, they become infecting investors who are considered contagious. On the contrary, if transforming investors are immune to the rumors and do not spread them, then transforming investors will turn into immune investors. And if rumors are destructive enough, immune investors will turn into infecting investors. For example, an investor believes that a piece of information in the stock market is a rumor and is immune from it. However, the surrounding relationships of him are believing the information is true (or some top companies in the stock market announced the wrong information). According to the herd effect of investors, he would change his mind and becomes an infecting investor. On the basis of the interaction between different types of investors, this study has constructed an SCIR investor risk contagion model in the stock market, and the contagion process is shown in Figure 2.

Specific contagion process of investor risk is as follows. Assume that there is an investor in the initial time with some unofficial information. The surrounding trusting investors (S) have the opportunity to know this information and become transforming investors (C) in transformation probability α. Transforming investors (C) will learn the information to choose to receive this information and become infecting investors (I) in contagion probability β. These investors also may choose not to believe or reject the information and become immune investors (R) in direct immune probability μ. For infecting investors (I), they choose to believe the information and spread it outward, but after a period of contagion, the infecting investors (I) may gradually lose interest in the information and no longer spread it outward. At this point, the infecting investors (I) may turn into immune investors (R) in immune probability ϕ. Immune investors (R) will not be immune forever; they will potentially be infecting investors (I) in immune failure probability η.

The idea of the SCIR virus epidemic model [19, 22] assumes that there are total Ninvestors in the stock market and that the market size remains unchanged. The sum of different types of investors at any time should be equal to the total number of investors N; that is, the relationship formula is expressed as follows.

$$S(t) + C(t) + I(t) + R(t) = N \tag{1}$$

Accordingly, the ratio of the number of different investors in the total amount $s(t)$, $c(t)$, $i(t)$, $r(t)$ is summed.

$$s(t) + c(t) + i(t) + r(t) = 1 \tag{2}$$

On the basis of the risk contagion mechanism of the SCIR model, the system dynamics characteristics can be described by the following differential equations.

$$\begin{aligned} \frac{dS(t)}{dt} &= -\alpha S(t) I(t) \\ \frac{dC(t)}{dt} &= \alpha S(t) I(t) - (\beta + \mu) C(t) \\ \frac{dI(t)}{dt} &= \beta C(t) - \phi I(t) + \eta R(t) \\ \frac{dR(t)}{dt} &= \mu C(t) + \phi I(t) - \eta R(t) \end{aligned} \tag{3}$$

3.2. Analysis of Transformation Probability of Investor Risk by Considering the Heterogeneity of Investors and Information Function. The heterogeneity of investors can be divided into four aspects: heterogeneous belief, heterogeneous constraint, heterogeneous income, and heterogeneous preference [35–37]. From the point of view of information function, considering the heterogeneity of investors, the transformation probability model of investor risk is constructed.

3.2.1. Investor Risk Preference θ, $0 < \theta < 1$. Combined with the latest research results of behavioral finance, the degree of investor risk preference is an important factor influencing the transformation rate of investor risk [37]. The degree of investor preference promotes and inhibits risk contagion. That is, risk-averse investors help curb the spread and contagion of risk, while risk-appetite investors play a role in promoting risk contagion. The expression $0 < \theta < 0.5$ means that investors are risk-averse; $\theta = 0.5$ means that investors are risk-neutral; and $0.5 < \theta < 1$ means that investors are risk-appetite.

3.2.2. Investor Risk Cognitive Level τ, $0 < \tau < 1$. Investor risk cognitive level includes their own knowledge and skills of stock investment and decision-making ability to face risks [38–40]. The greater the τ, the more analytical and responsive the investors are to stock market rumors. Investors with high risk cognitive level can adopt more prudent and appropriate decision-making behavior through their own stock investment knowledge and analysis of the stock market.

3.2.3. Information Value v_0, $0 \le v_0 \le 1$ [41]. This expression shows the difficulty investors have in obtaining information, where 0 means information is easy to obtain and 1 means information is hard to acquire.

High information value arouses information asymmetry and information distortion, which intensifies investor risk. Information asymmetry influences investor behavior indirectly. As show in Figure 3, when information asymmetry and distortion happens, some investors with low cognitive level of investor risk, poor psychological quality, and poor information decision-making ability cannot recognize or tell rumors. They cause behavior biases, panic, and scare. And in the meantime, investors carrying "investor risk" spread this low-quality information via media channels and

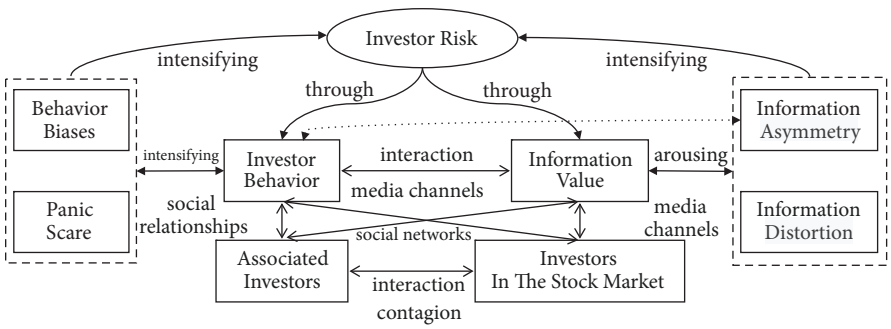

FIGURE 3: Information value, information asymmetry, and investor risk.

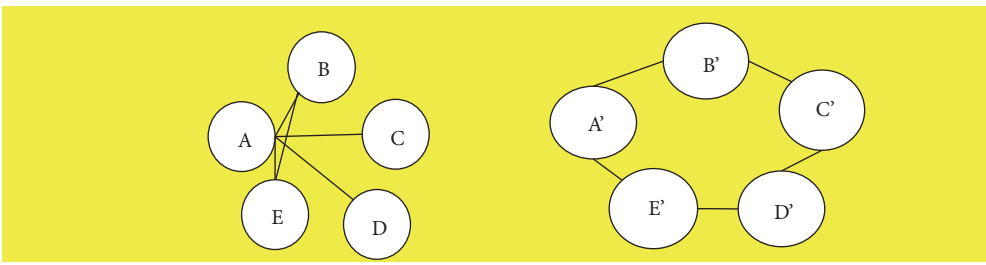

FIGURE 4: A simple example of measuring investor influence.

social networks (relationships). Under the situation, investor risk is enhanced through "investor behavior" and "information value". The information asymmetry phenomenon helps trusting investors to become transforming investors.

3.2.4. Investor Influence λ_i. The influence of investors is related to the topological structure of the investors' networks [34, 42, 43]. In this paper, the investor influence is measured by the edge weight w and the investor's degree K, which represents the weighted average of the edge weight between the investor and the connected K investors:

$$\lambda_i = \frac{\sum w_i}{K_i} \tag{4}$$

where $\sum w_i$ represents the sum of the edge weight associated with investor i; K_i represents the degree of investor i. The edge weight is defined as the interaction frequency between investors, that is, the one-way diffusion times between investors in recent time. The degree of the investor is also called the connectivity, which refers to the number of edges connected between the associated investor and the investor.

Figure 4 shows the way to measure investor influence. Let the left side of the picture be network P and the right side be network P'. Let $\sum w_A = 0.06$, $\sum w_{A'} = 0.04$. Then. In network P, $\lambda_A = 0.015$. In network P', $\lambda_{A'} = 0.02$. For easy analysis, when evaluating λ_i, firstly we settle the investors' network, then we know K_i is a fixed value, and then we assume the $\sum w_i$ is a fixed value. Thus Investor influence λ_i is a fixed value.

The investor risk transformation probability model on single-layer network in the stock market is summarized as follows.

$$\alpha = (v_0 \times \lambda_i)^{(1-\theta)\tau} \tag{5}$$

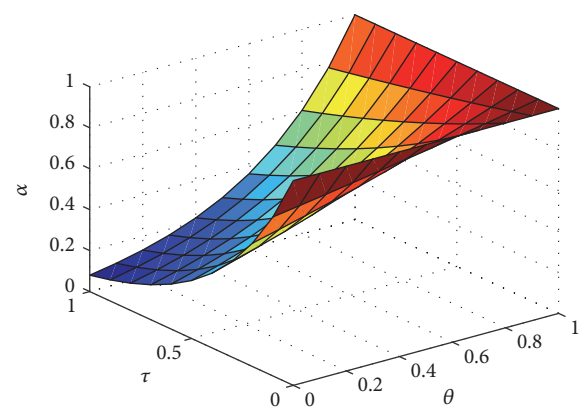

FIGURE 5: Effects of investor risk preference θ and investor risk cognitive level τ on investor transformation probability α when $v_0 = 0.4$ $\lambda_i = 0.2$.

Figure 5 presents the impact of investor risk preference θ and investor risk cognitive level τ on investor risk transformation probability when information value $v_0 = 0.4$ and investor influence $\lambda_i = 0.2$. With the increase of risk preference or the decrease of investor risk cognitive level, the transformation probability of investor risk increases nonlinearly. Combined with the sensitivity analysis in Table 1, the risk preference of investors shows an increasing marginal feature for the transformation probability of investor risk. The risk cognitive level of investors shows a decreasing feature for the transformation probability of investor risk, which is consistent with the actual financial market. Therefore, constructing the investor risk transformation probability model on single-layer network in the stock market is reasonable.

Table 1: Sensitivity analysis of investor risk preference θ and investor risk cognitive level τ to investor transformation probability α.

τ	θ									Expectation	Variance
	0.1	0.2	0.3	0.4	0.5	0.6	0.7	0.8	0.9		
0.1	0.796669	0.817047	0.837947	0.859380	0.881362	0.903907	0.927028	0.950740	0.975059	0.883238	0.003729
0.2	0.634682	0.667566	0.702154	0.738535	0.776800	0.817047	0.859380	0.903907	0.950740	0.783423	0.011703
0.3	0.505632	0.545433	0.588368	0.634682	0.684642	0.738535	0.796669	0.859380	0.927028	0.697819	0.020796
0.4	0.402821	0.445645	0.493021	0.545433	0.603418	0.667566	0.738535	0.817047	0.903907	0.624155	0.029389
0.5	0.320915	0.364113	0.413125	0.468735	0.531830	0.603418	0.684642	0.776800	0.881362	0.560549	0.036740
0.6	0.255663	0.297497	0.346177	0.402821	0.468735	0.545433	0.634682	0.738535	0.859380	0.505436	0.042598
0.7	0.203679	0.243069	0.290078	0.346177	0.413125	0.493021	0.588368	0.702154	0.837947	0.457513	0.046973
0.8	0.162265	0.198599	0.243069	0.297497	0.364113	0.445645	0.545433	0.667566	0.817047	0.415693	0.050005
0.9	0.129272	0.162265	0.203679	0.255663	0.320915	0.402821	0.505632	0.634682	0.796669	0.379067	0.051886

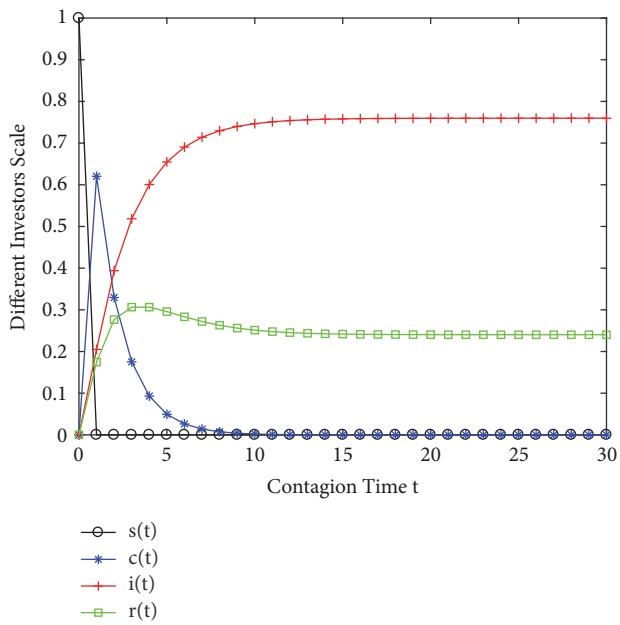

Figure 6: Change of trend of investors' scale in different states in SCIR risk contagion model in the stock market.

3.3. Mechanism Probability. According to Sections 3.1 and 3.2, taking investor heterogeneities into account, mechanism probabilities of SCIR are as in Table 2.

3.4. Computer Simulation Analysis. Suppose that there are N investors in the stock market. Only 1 investor is infected in the initial stage (I), and the rest $N - 1$ investors are all trusting investors (S). $N = 10000$. In the meantime, there are no transforming investors (C) or immune investors (R) in the initial stage. That is, $S(0) = N - 1$, $C(0) = 0$, $I(0) = 1$, $R(0) = 0$. At the moment, the only investor in a contagious state (I) in the system begins to spread rumors to the $N - 1$ trusting investors around.

From the simple analysis above, a basic conclusion can be drawn: the number of trusting investors (S) decreases, while the number of infecting investors (I) increases. However, drawing conclusions directly from the analysis above about the change features of transforming investors (C) and immune investors (R) is impossible. Therefore, by setting the values of different probabilities, the curve of the scale of different types of investors changes with contagion time can be obtained to reveal the characteristics of the scale change of transforming investors (C) and immune investors (R).

Given the absence of a large number of empirical tests of time series data, simulation analysis is relatively the most effective test method. Suppose that the initial parameters of the SCIR model in the stock market are as follows: $\theta = 0.5$, $\tau = 0.5$, $v_0 = 0.5$, $\lambda_i = 0.001$, $\beta' = 0.1$, $\mu' = 0.1$, $\eta' = 0.1$, and $\phi' = 0.01$. The simulation is conducted by Matlab2016b, and Figure 6 shows the graph obtained.

Figure 6 depicts the evolution characteristics of the scale of the different types of investors with the contagion time. In Figure 6, the scale of transforming investors and immune investors shows an increasing trend and then decreases. Additionally, it is consistent with the previous analysis that the scale of trusting investors tends to decrease while the scale of infecting investors tends to increase. When the contagion time reaches a certain value, the scale of all types of investors in the investor network is in a stable state in the stock market, which indicates that the investor network has reached a stable state. We also contend that trusting investors and infecting investors will eventually go to zero and diminish.

Different parameters are changed for simulation to better reveal the impact of different factors on the investor risk contagion mechanism on single-layer network in the stock market. Without changing the value of the transformation probability α, the change trend of the scale of different states of investors in the SCIR investor risk contagion model in the stock market is studied by changing different contagion probability β', direct immune probability μ', immune probability ϕ', and immune failure probability η'. Table 3 shows the original value of SCIR investor risk contagion model in the stock market under different mechanism probability environments.

Figure 7 shows the investor scale trends in different states of the SCIR investor risk contagion model in the stock market under different probability mechanism environments. Table 4 shows infecting investors and immune investors scale changes of SCIR investor risk contagion model in the stock market under different mechanism probability environments. After the contagion time reaches a certain value, that is, when the investor network reaches the steady state of the network, the scales of different types of investors basically remain unchanged.

In Figure 7(a), contagion probability β' increases, while the values of other parameters remain unchanged. Compared with those in Figure 6, combined with Table 4, the scales of investors in each state reach a stable state faster. But there is no obvious change in the scales of the different types of investors in the steady state of the investor network. Moreover, during the risk contagion process of investors, the peak of the scale of transforming investors is lower. This trend shows that the increased contagion probability β' not only enables the investor network to reach the steady state faster, but also plays a significant role in changing investors from transforming to infecting.

In Figure 7(b), direct immunity probability μ' increases, while the values of other parameters remain unchanged. Compared with those in Figure 6, combined with Table 4, there is no obvious change in the contagion time when the scales of the different types of investors reach the steady state of the investor network. However, in the process of investor risk contagion, the peak value of transforming investors is lower than that in Figure 6, while the peak value of the scale of immune investors is higher than that in Figure 6. The increasing to decreasing trend is more evident, thereby indicating that the increase of immune probability μ' not only enables the investor network to reach the steady state faster, but has a significant effect on the transformation from transforming investors to immune investors.

In Figure 7(c), the immune probability ϕ' increases, while the values of other parameters remain unchanged. Compared with those in Figure 6, combined with Table 4,

Table 2: Relationship of mechanism probability and heterogeneous mechanism probability in SCIR.

contagion probability β'	heterogeneous contagion probability β	$\beta = (\beta')^{\sqrt[3]{(1-\theta)\tau(1-\nu_0)}}$
direct immune probability μ'	heterogeneous direct immune probability μ	$\mu = (\mu')^{\sqrt[3]{\theta(1-\tau)\nu_0}}$
immune probability ϕ'	heterogeneous immune probability ϕ	$\phi = (\phi')^{\sqrt[3]{\theta(1-\tau)\nu_0}}$
immune failure probability η'	heterogeneous immune failure probability η	$\eta = (\eta')^{\sqrt[3]{(1-\theta)\tau(1-\nu_0)}}$

Table 3: Numerical changes of SCIR investor risk contagion model in the stock market under different mechanism probability environments.

Tendency chart	Variation of parameters	β'	μ'	η'	ϕ'	$(s(0), c(0), i(0), r(0))$
Figure 6	None	0.1	0.1	0.1	0.01	(0.999,0,0.001,0)
Figure 7(a)	Increased contagion probability β	0.5	0.1	0.1	0.01	(0.999,0,0.001,0)
Figure 7(b)	Increased direct immune probability μ	0.1	0.5	0.1	0.01	(0.999,0,0.001,0)
Figure 7(c)	Increased immune probability ϕ	0.1	0.1	0.1	0.05	(0.999,0,0.001,0)
Figure 7(d)	Increased immune failure probability η	0.1	0.1	0.6	0.01	(0.999,0,0.001,0)

Table 4: Infecting investors and immune investors scale changes of SCIR investor risk contagion model in the stock market under different mechanism probability environments.

	$s(\infty)$	Δ	$i(\infty)$	Δ
Figure 6	0.7597	-	0.2403	-
Figure 7(a)	0.7597	0	0.2403	0
Figure 7(b)	0.7597	0	0.2403	0
Figure 7(c)	0.5858	-0.1739	0.4142	+0.1739
Figure 7(d)	0.8857	+0.126	0.1143	-0.126

the scales of investors in each state reached a stable state faster. When the investor network reaches steady state, the scale of immune investors is larger and the scale of infecting investors is smaller. This trend shows that the increasing immune probability ϕ' not only enables the investor network to reach the steady state faster, but also plays a significant role in the transformation from infecting investors to immune investors.

In Figure 7(d), the immune failure probability η' increases, while the values of other parameters remain unchanged. Compared with Figure 6, combined with Table 4, the scales of investors in each state reached a stable state faster. In the process of investor risk contagion, the peak of the scale of transforming investors is larger. Immune state investors have smaller peaks. When the investor networks reach steady state, the immune investors are smaller and the infecting investors are larger. This trend shows that the increasing immune failure probability η not only enables the investor network to reach the steady state faster, but also plays a significant role in the transformation of immune investors to infecting investors.

In Figure 7, the transformation probability α and the change trend of the scale of trusting investors remain unchanged. Subsequently, we try to change investor risk preference θ, investor risk cognitive level τ, information value v_0, and investor influence λ_i, to explore the evolution rule of investor risk contagion with the contagion time under the change of different factors.

Figures 8–10 show the variation rules of the scale of infecting investors and immune investors with the contagion time when investor risk preference θ, investor risk cognitive level τ, and information value v_0 are different while the other initial conditions remain unchanged. After reaching a certain contagion time, the scale of the infecting investors and immune investors will tend to a fixed value, at which time the investors' network reaches a steady state. In the process of credit risk contagion, the steady state scale of the infecting investors will increase (or the immune investors will decrease); as the investor risk preference θ and information value v_0 increase, the investor risk cognitive level τ decreases. Moreover, they reduce the contagion time t when the investors' network reaches steady state. Therefore, investor risk preference θ and information value v_0 have "global enhancement" effects on investor risk contagion. Investor risk cognitive level τ has a "global inhibition" effect on investor risk contagion.

Figure 11 shows the variation rules of the scale of infecting investors and immune investors with the contagion time when investor influence λ_i is different while the other initial conditions remain unchanged. Figure 11(a) shows that in the investor risk contagion process, the increase of investor influence λ_i increases the scale of the infecting investors. When the investor network reaches steady state, the scale of infecting investors tends to be fixed under different values of investor influence λ_i. It shows that the increase of investor influence λ_i promotes investor risk contagion and has the "local enhancement" effect. Figure 11(b) shows that in the process of investor risk contagion, the increase of investor influence λ_i shortens the contagion time for immune investors to reach the stable state of the network.

4. Construction and Analysis of Investor Risk Contagion Model on Bilayer-Coupled Networks in the Stock Market under the Price Linkage

4.1. Model Construction. Using multilayer coupling network theory and the propagation dynamics theory for [44], an investor risk contagion model on bilayer-coupled networks in the stock market is constructed based on the SCIR investor risk contagion model. Figure 12 presents the investor risk contagion mechanism on bilayer-coupled networks in the stock market. Figure 12(a) shows the layer process of investor risk contagion on bilayer-coupled networks in the stock market, while Figure 12(b) shows the process of investor risk contagion between layers on bilayer-coupled networks in the stock market.

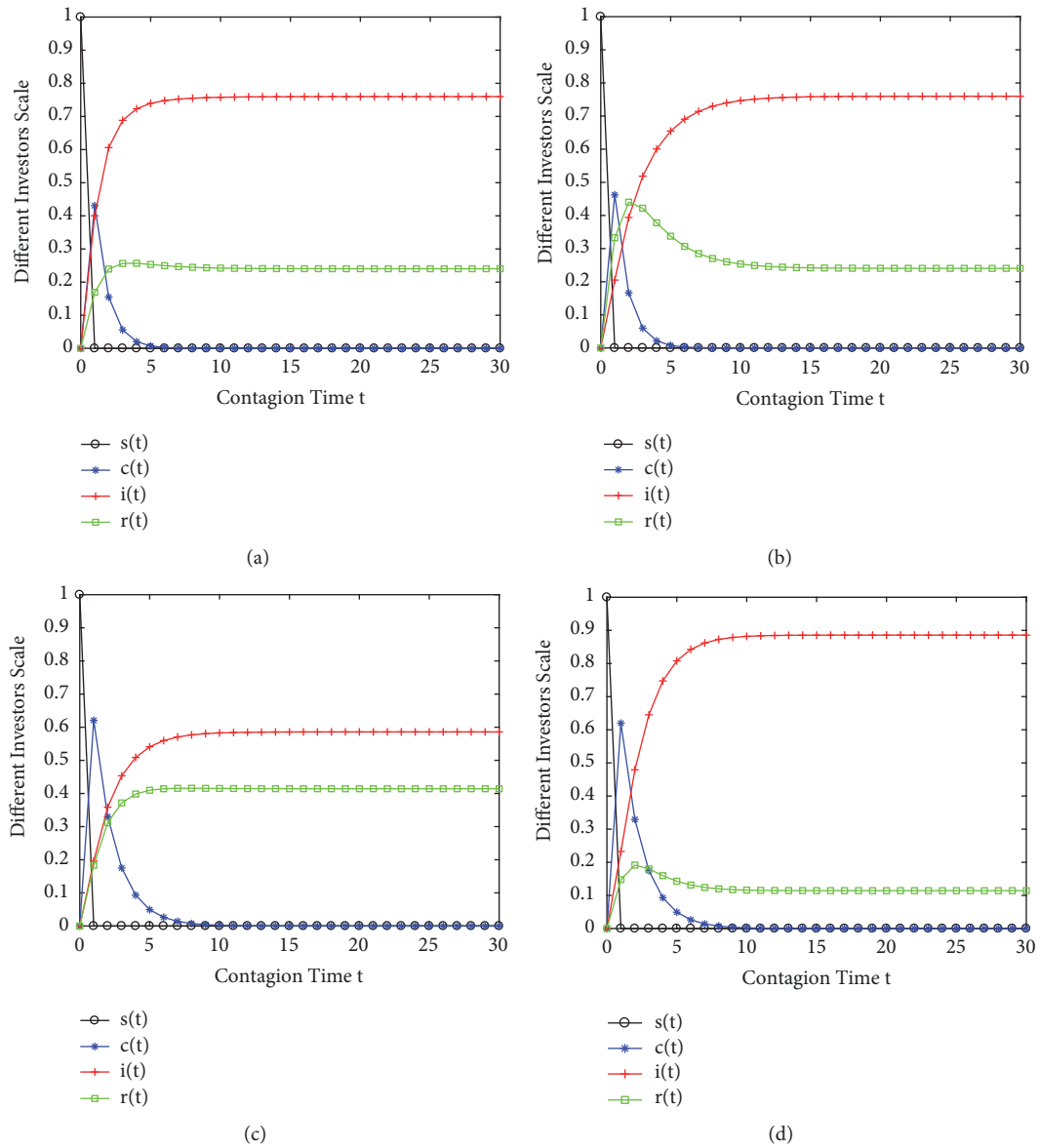

Figure 7: Investor scale trends in different states of SCIR investor risk contagion model in the stock market under different mechanism probability environments.

Suppose there are five different types of investors in the stock market: trusting investors (S), transforming investors (C), intralayer infecting investors (I_1), interlayer infecting investors (I_2), and immune investors (R), and the rumors in the stock market are released in the A-share stock market investor network W. The specific risk contagion process is as follows:

Trusting investors (S) in network W turn to transforming investors (C) with the transformation probability α'. Transforming investors (C) spread stock market rumors to the local network with the intralayer contagion probability β_1 and become intralayer infecting investors (I_1), or spread stock market rumors to the B-share stock market investor network M with the interlayer contagion probability β_2 and become interlayer infecting investors (I_2), or do not spread stock market rumors and become immune investors (R) with the immune probability μ. Intralayer infecting investors (I_1) and interlayer infecting investors (I_2) take the intralayer and interlayer immune probability ϕ_1, ϕ_2, respectively, and change into immune investors (R). Immune investors (R) transform into intralayer infecting investors (I_1) and interlayer infecting investors (I_2) by the intralayer and interlayer immune failure probability η_1, η_2.

Given that there are N investors in the stock market at the initial time and the market size remains unchanged. The sum of different types of investors at any given time should be equal to the total number of investors N; that is, the relationship is expressed as

$$S(t) + C(t) + I_1(t) + I_2(t) + R(t) = N. \quad (6)$$

The system dynamics modeling idea is used to establish the investor risk contagion model on bilayer-coupled

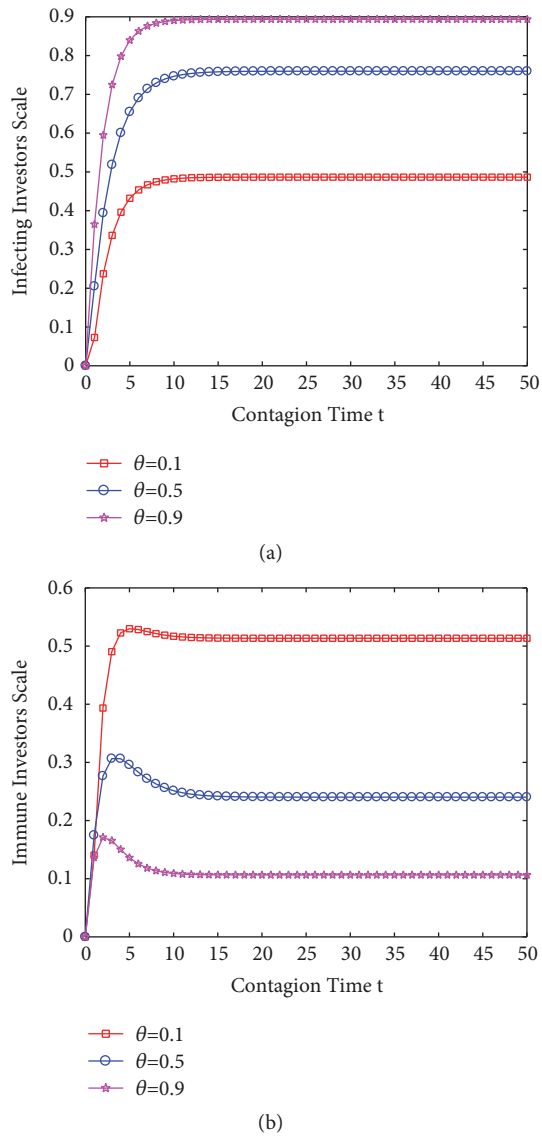

FIGURE 8: Changes in the scale of infecting investors and immune investors with the contagion time under different investor risk preference θ.

networks in the stock market through the differential equations. The corresponding differential equation of this model is as follows.

$$\begin{aligned}
\frac{dS(t)}{dt} &= -\alpha S(t)\left(I_1(t)+I_2(t)\right)\\
\frac{dC(t)}{dt} &= \alpha S(t)\left(I_1(t)+I_2(t)\right)-\left(\beta_1+\beta_2+\mu\right)C(t)\\
\frac{dI_1(t)}{dt} &= \beta_1 C(t)+\eta_1 R(t)-\phi_1 I_1(t)\\
\frac{dI_2(t)}{dt} &= \beta_2 C(t)+\eta_2 R(t)-\phi_2 I_2(t)\\
\frac{dR(t)}{dt} &= \mu C(t)-\left(\eta_1+\eta_2\right)R(t)+\phi_1 I_1(t)+\phi_2 I_2(t)
\end{aligned} \tag{7}$$

4.2. Connection Modes of Bilayer-Coupled Networks. According to the degree correlation of the relational investor nodes between the coupling networks, in the construction of the coupled network structure model of investor risk contagion on bilayer-coupled networks in the stock market, this paper mainly adopts three different coupling connection modes, namely, degree-degree positive correlation, degree-degree negative correlation, and random connection [44]. To simplify the implementation process of the bilayer-coupled networks model analysis, the following provisions are given:

(1) Suppose the A-share stock market investor network and B-share stock market investor network have the same scale and size, and the investors between different networks are one-to-one corresponding connections.

(2) During the construction, all coupling investor nodes are sorted according to the size of degree in their respective investor networks, and then different coupling networks are created according to three different connection modes, namely, interlayer assortative link, interlayer disassortative link, and interlayer random link.

(a) As for interlayer assortative link (AL), investors of A-share stock market investor network W and investors of B-share stock market investor network M are connecting according to the size of the degree of investor nodes. Specifically, large degree of investors of A-share stock market investor network W is connecting with large degree of investors of B-share stock market investor network M, while small degree of investors of A-share stock market investor network W is connecting with small degree of investors of B-share stock market investor network M; this is also called positive correlation link. When the investors' node degrees are the same, investors are randomly selected to set up bilayer-coupled networks in one-to-one node connection mode according to $W_i \longleftrightarrow M_j$.

(b) Interlayer disassortative link (DL) is opposite to AL. Large degree of investors of A-share stock market investor network W is connecting with small degree of investors of B-share stock market investor network M, and small degree of investors of A-share stock market investor network W is connecting with large degree of investors of B-share stock market investor network M; this is also called negative correlation link. The equation $W_i \longleftrightarrow M_j$ $(j = N - i + 1)$ establishes a one-to-one connection mode between the coupling networks.

(c) For interlayer random link (RL), investors of A-share stock market investor network W are randomly connecting with investors of B-share stock market investor network M, which indicates that the nodes connection mode is one-to-one in investor networks in the stock market.

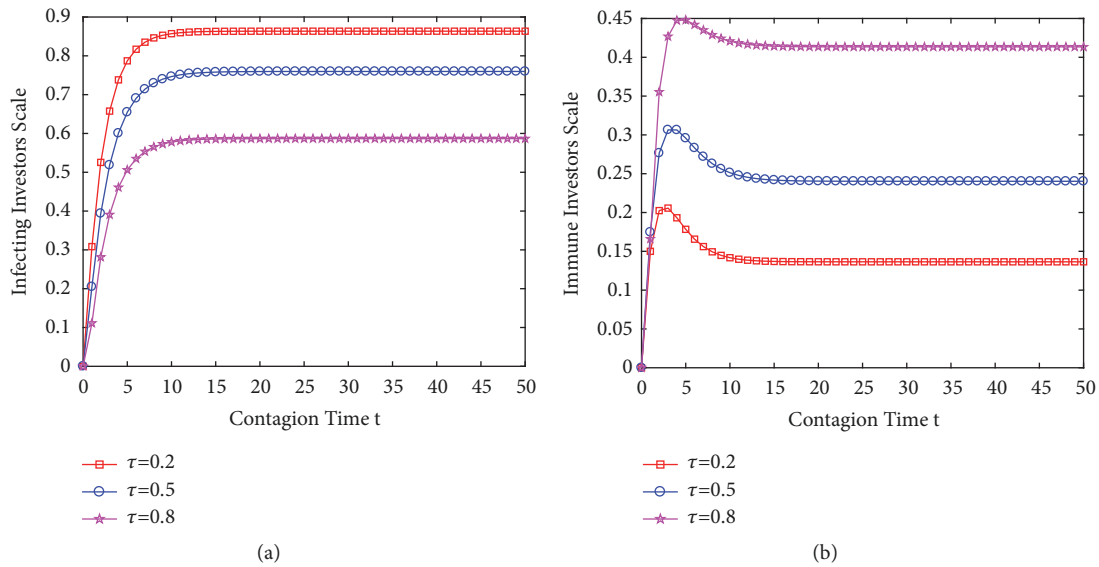

Figure 9: Changes in the scale of infecting investors and immune investors with the contagion time under different investor risk cognitive level τ.

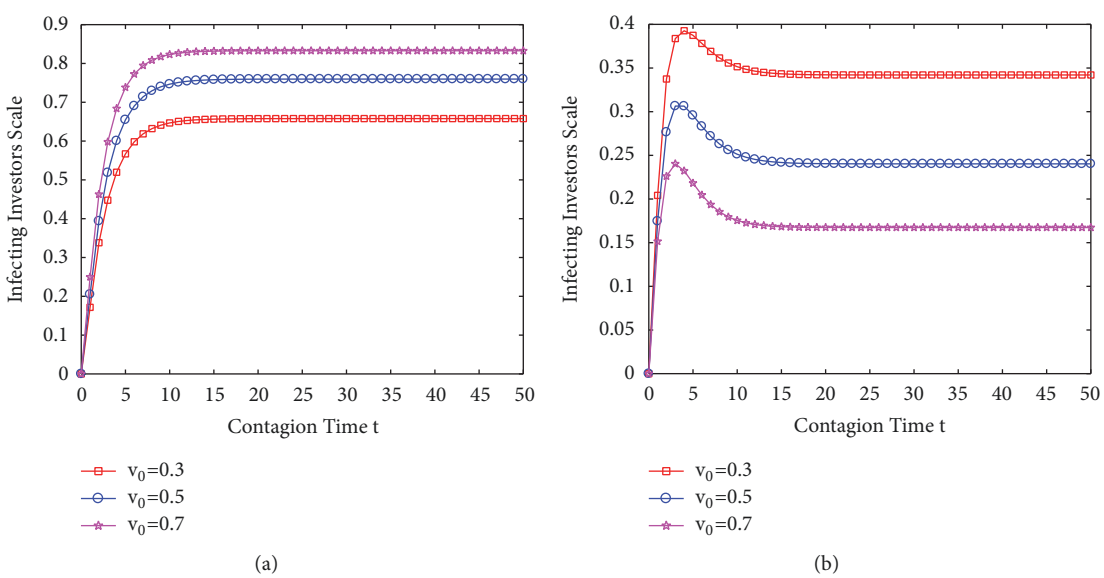

Figure 10: Changes in the scale of infecting investors and immune investors with the contagion time under different information value v_0.

4.3. Transformation Probability of Investor Risk on Bilayer-Coupled Networks. (1) On bilayer-coupled networks, the edge weight of the investor is expressed as the weight of the internal network w_{ij-in} and the weight of the external network w_{ij-out}, representing the edge weight between the investor and the neighboring node investor in this layer and outer layer, respectively.

(2) On bilayer-coupled networks, the degree of investor i is divided into K_{i-in} and K_{i-out}, which represents the number of interactions between investors in local network and outer network, respectively.

(3) Matching coefficient:

Newman [45] proposed the concept of matching coefficient to quantify the degree correlation between nodes in a complex network:

$$\rho = \frac{\sum_{K_x K_y} K_x K_y \left(e_{K_x K_y} - a_{K_x} b_{K_y}\right)}{\sigma_{K_x} \sigma_{K_y}} \tag{8}$$

where $e_{K_x K_y}$ represents the proportion of all edges in the network whose connection degree is K_x and K_y; a_{K_x}, b_{K_x} denote the proportion of the edge whose degree is K_x, K_y; $\sigma_{K_x} = \sqrt{\mathrm{var}[K_x]}$ is the variance of the random variable K_x.

In $-1 \le \rho \le 1$, $\rho > 0$ denotes AL; that is, large degree nodes tend to connect with other large degree nodes and the larger $|\rho|$ has positive correlation; $\rho < 0$ denotes DL; that is, large degree nodes tend to connect with small degree nodes, and the larger $|\rho|$ has negative correlation. By calculating the extreme value of matching coefficients $\rho_{\max}$ and $\rho_{\min}$ of many real world networks, it is found that the matching coefficient

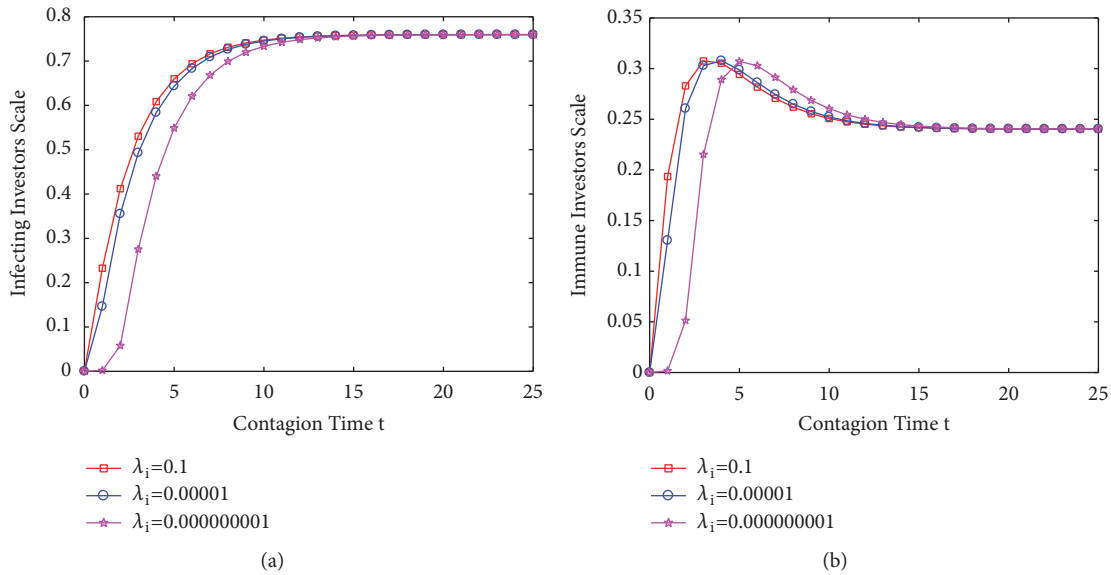

Figure 11: Changes in the scale of infecting investors and immune investors with the contagion time under different investor influence λ_i.

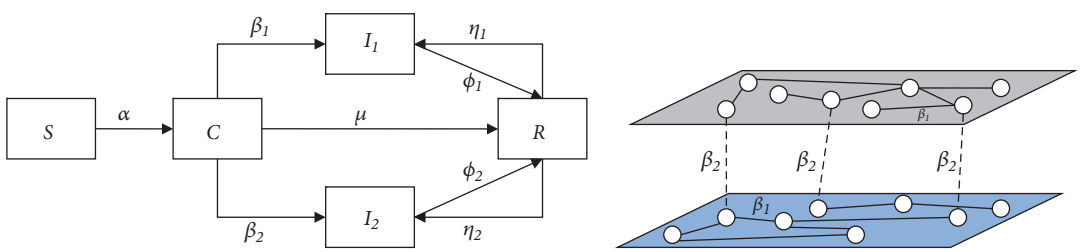

(a) Layer process of investor risk contagion on bilayer-coupled networks in the stock market

(b) Process of investor risk contagion between layers on bilayer-coupled networks in the stock market

Figure 12: Investor risk contagion mechanism on bilayer-coupled networks in the stock market.

of general networks satisfies $-1 < \rho_{\min} < \rho_{\max} < 1$, where $\rho = 1$ when it is completely AL, $\rho = -1$ when it is completely DL, and $\rho = 0$ when it indicates that the network structure has random and irrelevant characteristics (RL).

(4) Investor influence in the stock market on bilayer-coupled networks:

In this paper, the investor influence is expressed as the weighted average of all K edge weights that interact with the investor. The investor influence on bilayer-coupled networks is divided into internal influence λ_{i-in} and external influence λ_{i-out}. The internal influence λ_{i-in} of investor i refers to the influence of investor i in the same layer network, represented by K_{i-in} and w_{ij-in} as follows.

$$\lambda_{i-in} = \frac{\sum_{j=1}^{K_{i-in}} w_{ij-in}}{K_{i-in}} \tag{9}$$

The external influence of investor i represents the influence of investor i in other layer networks, represented by K_{i-out} and w_{ij-out} as follows.

$$\lambda_{i-out} = \frac{\sum_{j=1}^{K_{i-out}} w_{ij-out}}{K_{i-out}} \tag{10}$$

On the basis of the indicator KSCC [46] and the internal and external influences of investors in the stock market on bilayer-coupled networks, this study measures the influence of node investors on bilayer-coupled networks as follows:

$$KSCC\,(i) = x\left[\lambda_{i-in}\right] + y\rho^{|WM|}\left[\lambda_{i-out}\right], \tag{11}$$

where $\rho^{|WM|}$ is the index of degree-degree correlation between network W and M. x, y are internal and external influencing factors, satisfying $x > 0$, $y > 0$, $x + y = 1$.

Combined with the analysis in Section 3.2, transformation probability of investor risk on bilayer-coupled networks is defined as follows.

$$\alpha' = \left(v_0 \times KSCC\,(i)\right)^{(1-\theta)\tau} \times KSCC(i)^{(1-\theta)\tau\rho^{|WM|}} \tag{12}$$

4.4. Mechanism Probability. According to Sections 3.1 and 3.2, taking investor heterogeneities into account, mechanism probabilities of SCI_1I_2R are as in Table 5.

4.5. Computer Simulation Analysis. Simulation analysis is relatively the most effective test method because of the

Table 5: Relationship of mechanism probability and heterogeneous mechanism probability in SCI_1I_2R.

intra-layer contagion probability β_1'	heterogeneous intra-layer contagion probability β_1	$\beta_1 = (\beta_1')^{\sqrt[3]{(1-\theta)\tau(1-\nu_0)}}$
inter-layer contagion probability β_2'	heterogeneous inter-layer contagion probability β_2	$\beta_2 = (\beta_2')^{\sqrt[3]{(1-\theta)\tau(1-\nu_0)}}$
intra-layer immune failure probability η_1'	heterogeneous intra-layer immune failure probability η_1	$\eta_1 = (\eta_1')^{\sqrt[3]{(1-\theta)\tau(1-\nu_0)}}$
inter-layer immune failure probability η_2'	heterogeneous inter-layer immune failure probability η_2	$\eta_2 = (\eta_2')^{\sqrt[3]{(1-\theta)\tau(1-\nu_0)}}$
intra-layer immune probability ϕ_1'	heterogeneous intra-layer immune probability ϕ_1	$\phi_1 = (\phi_1')^{\sqrt[3]{\theta(1-\tau)\nu_0}}$
inter-layer immune probability ϕ_2'	heterogeneous inter-layer immune probability ϕ_2	$\phi_2 = (\phi_2')^{\sqrt[3]{\theta(1-\tau)\nu_0}}$

Table 6: Comparison of initial parameters between single-layer network and bilayer-coupled networks.

Single-layer Network	Bilayer-coupled Networks
$N = 10000$, When $t = 0$, there are: $S(0) = N - 1, C(0) = 0, I(0) = 1, R(0) = 0$	$N_W = N_M = 10000$, When $t = 0$, there are: $S(0) = N - 2, C(0) = 0, I_1(0) = 1, I_2(0) = 1, R(0) = 0$
$\theta = 0.5, \tau = 0.5, v_0 = 0.2, \beta' = 0.07, \mu' = 0.03, \phi' = 0.01, \eta' = 0.03, \lambda_i = 0.02$	$\theta = 0.5, \tau = 0.5, v_0 = 0.2, \beta_1' = 0.07, \beta_2' = 0.07, \mu' = 0.03, \phi_1' = 0.01, \phi_2' = 0.01, \eta_1' = 0.03, \eta_2' = 0.03, x = 0.5, y = 0.5, \rho^{\lvert WM \rvert} = 0$

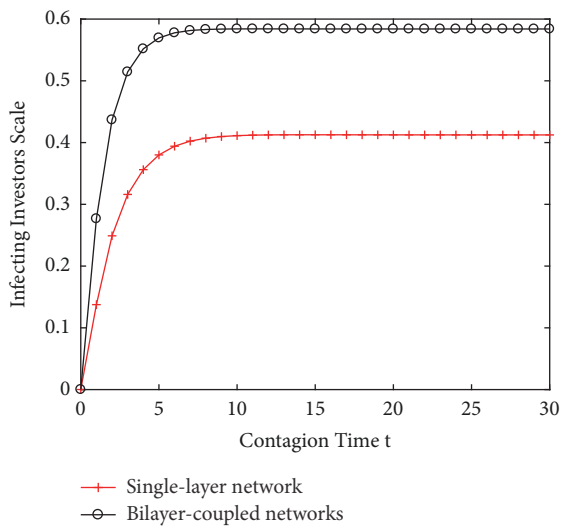

Figure 13: Comparison of investor risk contagion on single-layer network and bilayer-coupled networks in the stock market.

absence of a large number of empirical tests of time series data.

4.5.1. Effect of Single-Layer Network and Bilayer-Coupled Networks on Investor Risk Contagion in the Stock Market. To explore the impact of different network structures on investor risk contagion effect in the stock market, the single-layer network with an average degree $< K_i >= 5$ of investor nodes is simulated numerically on the SCIR investor risk contagion model in this section. For the convenience of comparison, the bilayer-coupled networks with an average degree $< K_i >= 5$ of the investor nodes are also simulated on the SCI_1I_2R investor risk contagion model. The risk contagion effect of investor risk in the stock market is measured by the scale of infecting investors (including intralayer infecting investors (I_1) and interlayer infecting investors (I_2) on bilayer-coupled networks). The greater the $s(i)$ is, the greater the scale of risk contagion is, and the more noticeable the contagion effect is. Table 6 shows the initial parameters of the two models.

Using Matlab2016b, the SCIR investor risk contagion model and the SCI_1I_2R investor risk contagion model on bilayer-coupled networks are simulated. The results are shown in Figure 13.

Figure 13 depicts the change rule of the scale of infecting investors with contagion time under the different network structures of the single-layer network and the bilayer-coupled networks. From the simulation results, it is found that the scale of infecting investors increases with the increase of the contagion time whether it is single-layer network or bilayer-coupled networks. After a certain contagion time, the scale of infecting investors on investor networks remains constant, indicating that the investor networks have reached a stable state at this time. We also confirmed the following:

(a) Under the condition that the parameters are all the same, the scale of infecting investors on the bilayer-coupled networks is significantly larger than that of the single-layer network, which indicates that the bilayer-coupled networks expand the investor risk contagion and have the "global enhancement" effect.

(b) For the scale of investor risk contagion of the two network structures, the bilayer-coupled networks structure is not twice as large as the single-layer network, simply. It is a nonlinear positive correlation.

4.5.2. Effect of Interlayer Connection Modes on Investor Risk Contagion in the Stock Market. To eliminate other impacts, the remaining parameters are kept in the initial state of Table 3. The SCI_1I_2R investor risk contagion model on bilayer-coupled networks is simulated by setting $\rho^{\lvert WM \rvert}$ as -0.2,-0.1, 0, 0.5, and 0.9. The simulation results are shown in Figure 14.

Figure 14 depicts the change rule of the scale of infecting investors with contagion time under different connection modes of bilayer-coupled networks. The scale of infecting investors is increasing with the rise of the contagion time no matter what connection modes the bilayer-coupled networks have. Moreover, after a certain contagion time, the scale of infecting investors in the investor networks remains unchanged and tends to have constant value. We also affirmed the following results:

(a) In case that all parameters are the same, in the process of investor risk contagion, the scale of infecting investors is the largest under the AL mode of bilayer-coupled networks, followed by the RL mode. Finally, the scale of infecting investors is the smallest under the mode of DL. Among the three modes of interlayer connection of bilayer-coupled networks, the AL mode has the effect of "local enhancement", while the DL mode has the effect of "local inhibition". In other words, the AL mode is most conducive to the investor risk contagion, while the DL mode is most unfavorable to the investor risk contagion.

(b) In the AL mode, during the contagion process, $|\rho^{\lvert WM \rvert}|$ increases, the positive correlation of the bilayer-coupled networks increases, and the scale of the infecting investors also increases. Under the mode of AL, the increase of $|\rho^{\lvert WM \rvert}|$

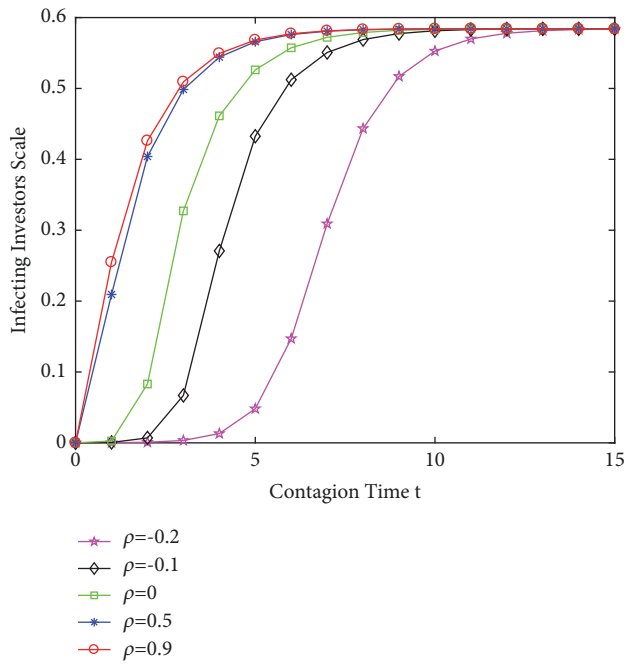

Figure 14: Comparison of investor risk contagion in the stock market under different connection modes of bilayer-coupled networks.

is conducive to the investor risk contagion and has the effect of "local enhancement".

(c) Under the DL mode, during the contagion process, $|\rho^{|WM|}|$ increases and the negative correlation of bilayer-coupled networks increases, while the scale of infecting investors decreases. In the DL mode, the increase of $|\rho^{|WM|}|$ is not conducive to the investor risk contagion and has a "local inhibition" effect.

4.5.3. Effect of Different Heterogeneous Mechanism Probabilities on Investor Risk Contagion in the Stock Market. To better reveal the influence of different factors on investor risk contagion effect on bilayer-coupled networks in the stock market, different heterogeneous mechanism probabilities with fixing transformation probability α' are used to simulate the SCI_1I_2R risk contagion model on the bilayer-coupled networks. Table 7 shows numerical changes of SCI_1I_2R investor risk contagion model under different heterogeneous mechanism probabilities. The simulation results are shown in Figure 15.

Figure 15 depicts the different trends of the investor scale of different states in SCI_1I_2R investor risk contagion model on the bilayer-coupled networks in the stock market under different heterogeneous mechanism probabilities over contagion time. Figure 15(a) shows the variation trend of the investor scale in different states with contagion time in Table 7, while Figures 15(b)–15(f) show the variation trend of the investor scale in different states with changing different mechanism probabilities of Table 7. Given that the transformation probability α' is not changed, the change trend of the scale of trusting investors in Figure 15 also does not change and tends to become zero in a very short contagion time. In Figure 15, the change trend of the scale of transforming investors increases first and then decreases. Compared with Figure 15(a) , except the decreasing peak values of the scale of transforming investors in Figures 15(b), 15(c), and 15(d) , there is little change in the rest of the figures. We focus on the evolution of the scale of intralayer infecting investors, interlayer infecting investors, and immune investors over contagion time t.

Comparing Figures 15(a) and 15(b) , we found an increase in the heterogeneous intralayer contagion probability β_1, an increase in the scale of intralayer infecting investors, and a decrease in the scale of interlayer infecting investors. Comparing Figures 15(a) and 15(c) , we found an increase in the heterogeneous interlayer contagion probability β_2, an increase in the scale of interlayer infecting investors, and an decrease in the scale of intralayer infecting investors. With Figures 15(a) and 15(d) , it is found that the scale of immune investors fluctuates more clearly in the process of investor risk contagion, and the scale of immune investors increases when the network reaches steady state. Comparisons between Figures 15(a), 15(b), 15(c), and 15(d) show that when the heterogeneous intralayer contagion probability β_1 is equal to the heterogeneous interlayer contagion probability β_2, the scale of intralayer infecting investors and the scale of interlayer infecting investors will be consistent on bilayer-coupled networks when the network reaches steady state. However, any change of the heterogeneous intralayer contagion probability β_1 or the heterogeneous interlayer contagion probability β_2 will not change the scale of immune investors when the network reaches steady state, thus indicating that the scale of infecting investors does not change when the network reaches steady state. The only change is the scale of the intralayer or interlayer infecting investors, but their sum does not change.

By comparing Figures 15(a) and 15(e) , it is found that there is an increase in heterogeneous intralayer immune failure probability η_1 and the scale of intralayer infecting investors and a noticeable decrease of the scale of interlayer infecting investors. The scale of immune investors has also decreased significantly. Comparing Figures 15(a) and 15(f) , we can find that there is an increase in heterogeneous interlayer immune failure probability η_2, a noticeable increase of the scale of interlayer infecting investors, and apparent decrease of the scale of intralayer infecting investors. The scale of immune investors has also decreased significantly. Comparing Figures 15(a) and 15(g) , it is found that there is an increase in heterogeneous intralayer immune probability ϕ_1, a noticeable increase of the scale of interlayer infecting investors, and apparent decrease of the scale of intralayer infecting investors. The scale of immune investors has increased significantly. By comparing Figures 15(a) and 15(h) , we can find that there is an increase in heterogeneous interlayer immune probability ϕ_2, noticeable increase of the scale of intralayer infecting investors, and apparent decrease of the scale of interlayer infecting investors. Moreover, the scale of immune investors has increased significantly. Comparisons between Figures 15(a), 15(e), 15(f), 15(g), and 15(h) show that even when the heterogeneous intralayer contagion probability

Table 7: Numerical changes of SCI_1I_2R investor risk contagion model under different heterogeneous mechanism probabilities.

Tendency chart	Variation of parameters	β_1	β_2	μ	η_1	η_2	ϕ_1	ϕ_2	$(s(0), c(0), i_1(0), i_2(0), r(0))$
Figure 15(a)	None	0.07	0.07	0.03	0.03	0.03	0.01	0.01	(0.9999,0,0.00005.0.00005,0)
Figure 15(b)	Increased intra-layer contagion probability β_1	0.2	0.07	0.03	0.03	0.03	0.01	0.01	(0.9999,0,0.00005.0.00005,0)
Figure 15(c)	Increased inter-layer contagion probability β_2	0.07	0.1	0.03	0.03	0.03	0.01	0.01	(0.9999,0,0.00005.0.00005,0)
Figure 15(d)	Increased direct immune probability μ	0.07	0.07	0.1	0.03	0.03	0.01	0.01	(0.9999,0,0.00005.0.00005,0)
Figure 15(e)	Increased intra-layer immune failure probability η_1	0.07	0.07	0.03	0.2	0.03	0.01	0.01	(0.9999,0,0.00005.0.00005,0)
Figure 15(f)	Increased inter-layer immune failure probability η_2	0.07	0.07	0.03	0.03	0.1	0.01	0.01	(0.9999,0,0.00005.0.00005,0)
Figure 15(g)	Increased intra-layer immune probability ϕ_1	0.07	0.07	0.03	0.03	0.03	0.05	0.01	(0.9999,0,0.00005.0.00005,0)
Figure 15(h)	Increased inter-layer immune probability ϕ_2	0.07	0.07	0.03	0.03	0.03	0.01	0.1	(0.9999,0,0.00005.0.00005,0)

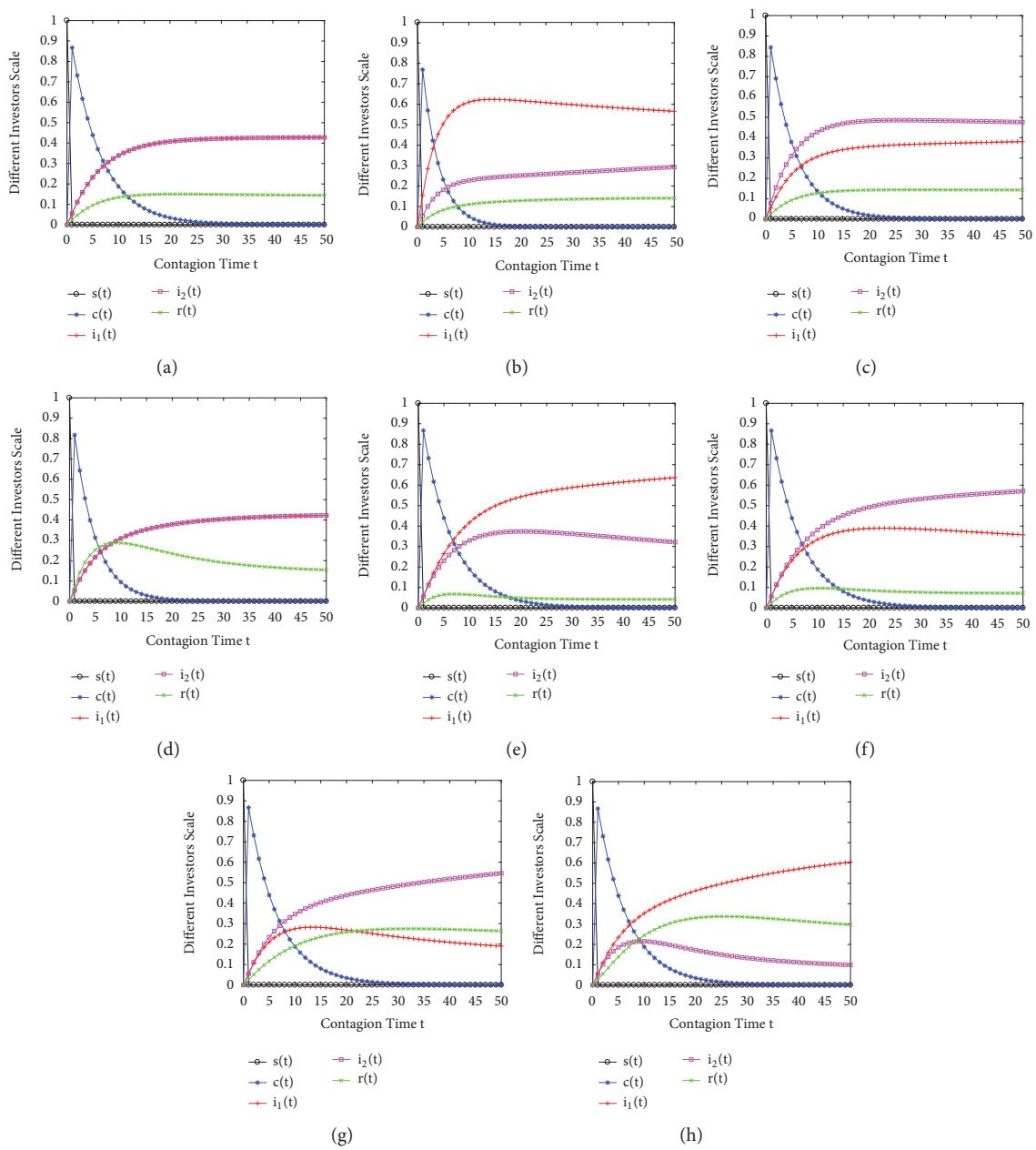

Figure 15: Investor scale trends of different states in SCI_1I_2R investor risk contagion model on bilayer-coupled networks in the stock market under different heterogeneous mechanism probability environments.

β_1 is equal to the heterogeneous interlayer contagion probability β_2, any change in the heterogeneous intralayer immune failure probability η_1, heterogeneous interlayer immune failure probability η_2, heterogeneous intralayer immune probability ϕ_1, or heterogeneous interlayer immune probability ϕ_2 will change the scale of intralayer or interlayer infecting investors. Additionally, increasing heterogeneous immune failure probability reduces the scale of immune investors, and increasing heterogeneous immune probability increases the scale of immune investors.

To sum up, heterogeneous intralayer contagion probability β_1 and heterogeneous interlayer contagion probability β_2 have "local regulation" effect, while the heterogeneous direct immune probability μ, heterogeneous immune failure probability η_1, η_2, and heterogeneous immune probability ϕ_1, ϕ_2 have "global regulation" effect.

5. Conclusion

From the perspective of the stock price linkage, considering the heterogeneities of investors, including investor risk preference, investor risk cognitive level, information value, and investor influence, this article constructs an SCIR contagion model of investor risk on single-layer network to remove investor risk caused by rumors in the stock market under the stock price linkage and its contagion mechanism. Through

computer simulation, this study explores the function and influence of different mechanism probabilities and investor heterogeneity on the effects of risk contagion in the stock market. On the basis of the SCIR contagion model of investor risk on single-layer networks, we construct a SCI_1I_2R contagion model of investor risk on bilayer-coupled networks. Initially, the evolution mechanism of investor risk contagion in the stock market is compared between single-layer and bilayer-coupled networks. Thereafter, the evolution characteristics and rules of investor risk contagion under different connection modes and different mechanism probabilities are compared on bilayer-coupled networks. The conclusions of this paper are as follows:

(1) In the SCIR contagion model of investor risk on single-layer network, some mechanism probabilities have "global effect"; immune failure probability η' has a "global enhancement" effect; and immune probability ϕ' has a "global inhibition" effect. The increase of contagion probability β' not only enables the investor network to reach the steady state faster, but also plays a significant role in the change from transforming investor to infecting investors. The increase of direct immune probability μ' has an evident effect on the transformation from transforming investors to immune investors. The increase of immune probability ϕ' not only enables the investor network to reach the steady state faster, but also plays a significant role in the transformation from infecting investors to immune investors. The increase of immune failure probability η' plays a significant role in the transformation from immune investors to infecting investors.

(2) Investor heterogeneities have "global effect" and "local effect" on investor risk contagion. The increase of investor risk preference θ and information value v_0 can promote the investor risk contagion and has the effect of "global enhancement". Investor risk cognitive level τ can inhibit the investor risk contagion and has the effect of "global inhibition". The increase of investor influence λ_i can promote the investor risk contagion and has the effect of "local enhancement".

(3) Compared with the investor risk contagion on single-layer network, bilayer-coupled networks can expand the investor risk contagion and have the "global enhancement" effect; it is not twice as large as the single-layer network, simply. It is a nonlinear positive correlation.

(4) Among the three interlayer connection modes of the SCI_1I_2R model of investor risk contagion on bilayer-coupled networks, the assortative link has the effect of "local enhancement", while the disassortative link has the effect of "local inhibition". In AL connection mode, the increase of $|\rho^{|WM|}|$ promotes investor risk contagion and has "local enhancement" effect. In DL connection mode, the increase of $|\rho^{|WM|}|$ is not conducive to investor risk contagion and has "local inhibition" effect.

(5) In the SCI_1I_2R model of investor risk contagion on bilayer-coupled networks, heterogeneous mechanism probabilities have "global effect" and "local effect". There is an increase of heterogeneous intralayer contagion probability β_1, heterogeneous intralayer immune failure probability η_1, and heterogeneous interlayer immunity probability ϕ_2; a noticeable increase of the scale of intralayer infecting investors; and a decrease of interlayer infecting investors. Similarly, there is an increase of heterogeneous interlayer contagion probability β_2, heterogeneous interlayer immune failure probability η_2, and heterogeneous intralayer immunity probability ϕ_1; a noticeable increase of the scale of interlayer infecting investors; and a decrease of intralayer infecting investors. Heterogeneous intralayer contagion probability β_1 and heterogeneous interlayer contagion probability β_2 have "local regulation" effect on investor risk contagion, while the heterogeneous direct immune probability μ, heterogeneous immune failure probability η_1, η_2, and heterogeneous immune probability ϕ_1, ϕ_2 have "global regulation" effect on investor risk contagion.

To a certain extent, the research conclusions have expounded the key factors and contagion path of investor risk contagion evolution, have revealed the changing rules of investor risk, and have provided a certain theoretical support for the financial management department to formulate macro policies.

Data Availability

The method in this article is computer mathematical simulation. Numerical simulation analysis is the most effective way to test real-time dynamic data without a large number of empirical validations. The authors use simulation to explore the evolution mechanisms and characteristics of investor risk contagion in the stock market, compared in single-layer and bilayer-coupled networks by using Matlab2016b software. This paper does not have the data that can be obtained because they directly use the plot function of Matlab2016b software to make the images.

Conflicts of Interest

The authors declare that they have no conflicts of interest.

Authors' Contributions

Yue Dong, Jiepeng Wang, and Tingqiang Chen contributed equally to this work. They are co-first authors.

Acknowledgments

This work was supported by the National Natural Science Foundation of China (Nos. 71871115, 71501094, 71501131), the Natural Science Foundation of Jiangsu Province of China (Nos. BK20150961), the Key Project of Philosophy and Social Science Research in Colleges and Universities in Jiangsu Province (No. 2017ZDIXM074), Postgraduate Research & Practice Innovation Program of Jiangsu Province (No. SJCX17-0275), and the Innovation Team Project of Philosophy and Social Sciences in Colleges and Universities in Jiangsu Province (No. 2017ZSTD005).

References

[1] M. Grinblatt and M. Keloharju, "What makes investors trade?" *Journal of Finance*, vol. 56, no. 2, pp. 589–616, 2001.

[2] J. M. Griffin, F. Nardari, and R. M. Stulz, "Do investors trade more when stocks have performed well? evidence from 46 countries," *Review of Financial Studies* , vol. 20, no. 3, pp. 905–951, 2007.

[3] N. DiFonzo and P. Bordia, *Rumor Psychology: Social and Organizational Approaches*, American Psychological Association, Washington, DC, USA, 2007.

[4] M. Zouaoui, G. Nouyrigat, and F. Beer, "How does investor sentiment affect stock market crises? Evidence from panel data," *Financial Review*, vol. 46, no. 4, pp. 723–747, 2011.

[5] J. R. Nofsinger and R. W. Sias, "Herding and feedback trading by institutional and individual investors," *Journal of Finance*, vol. 54, no. 6, pp. 2263–2295, 1999.

[6] F. Villatoro, "The delegated portfolio management problem: Reputation and herding," *Journal of Banking & Finance*, vol. 33, no. 11, pp. 2062–2069, 2009.

[7] D. Egan, C. Merkle, and M. Weber, "Second-order beliefs and the individual investor," *Journal of Economic Behavior & Organization*, vol. 107, pp. 652–666, 2014.

[8] M. Schindler, *Rumors in Financial Markets*, John Wiley& Sons, Ltd., New Jersey, NJ, USA, 2007.

[9] A. Johansen and D. Sornette, "Bubbles and anti-bubbles in latin-american, asian and western stock markets: An Empirical Study," *International Journal of Theoretical and Applied Finance*, vol. 4, no. 6, pp. 853–920, 2001.

[10] J. Pound and R. Zeckhauser, "Clearly heard on the street: the effect of takeover rumors on stock prices," *The Journal of Business*, vol. 63, no. 3, pp. 291–308, 1990.

[11] Y. Gao and D. Oler, "Rumors and pre-announcement trading: Why sell target stocks before acquisition announcements?" *Review of Quantitative Finance and Accounting*, vol. 39, no. 4, pp. 485–508, 2012.

[12] H. Kiymaz, "The stock market rumours and stock prices: A test of price pressure and size effect in an emerging market," *Applied Financial Economics*, vol. 12, no. 7, pp. 469–474, 2002.

[13] P. M. Clarkson, D. Joyce, and I. Tutticci, "Market reaction to takeover rumour in Internet Discussion Sites," *Accounting & Finance*, vol. 46, no. 1, pp. 31–52, 2006.

[14] M. Kosfeld, "Rumours and markets," *Journal of Mathematical Economics*, vol. 41, no. 6, pp. 646–664, 2005.

[15] D. Andrei and J. Cujean, "Information percolation, momentum and reversal," *Journal of Financial Economics*, vol. 123, no. 3, pp. 617–645, 2017.

[16] D. J. Daley and D. G. Kendall, "Stochastic rumours," *Journal of the Institute of Mathematics and Its Applications*, vol. 1, no. 1, pp. 42–55, 1965.

[17] D. Maki and M. Thomson, *Mathematical Models and Applications*, Prentice-Hall, Englewood Cliffs, 1973.

[18] M. Nekovee, Y. Moreno, G. Bianconi, and M. Marsili, "Theory of rumour spreading in complex social networks," *Physica A: Statistical Mechanics and Its Applications*, vol. 374, no. 1, pp. 457–470, 2007.

[19] F. Xiong, Y. Liu, Z. Zhang, J. Zhu, and Y. Zhang, "An information diffusion model based on retweeting mechanism for online social media," *Physics Letters A*, vol. 376, no. 30-31, pp. 2103–2108, 2012.

[20] L. J. Zhao, J. J. Wang, Y. C. Chen, Q. Wang, J. Cheng, and H. Cui, "SIHR rumor spreading model in social networks," *Physica A: Statistical Mechanics and Its Applications*, vol. 391, no. 7, pp. 2444–2453, 2012.

[21] Y. Zan, J. Wu, P. Li, and Q. Yu, "SICR rumor spreading model in complex networks: counterattack and self-resistance," *Physica A: Statistical Mechanics and Its Applications*, vol. 405, pp. 159–170, 2014.

[22] J. Jia and W. Wu, "A rumor transmission model with incubation in social networks," *Physica A: Statistical Mechanics and Its Applications*, vol. 491, pp. 453–462, 2018.

[23] S. V. Buldyrev, R. Parshani, G. Paul, H. E. Stanley, and S. Havlin, "Catastrophic cascade of failures in interdependent networks," *Nature*, vol. 464, no. 7291, pp. 1025–1028, 2010.

[24] J. Wang, B. Zhou, and W. Wang, "Information spreading on multirelational networks," *Physica A: Statistical Mechanics and Its Applications*, vol. 517, pp. 21–28, 2019.

[25] J. Gao, S. V. Buldyrev, H. E. Stanley, and S. Havlin, "Networks formed from interdependent networks," *Nature Physics*, vol. 8, no. 1, pp. 40–48, 2012.

[26] E. Cozzo, R. A. Baños, S. Meloni, and Y. Moreno, "Contact-based social contagion in multiplex networks," *Physical Review E: Statistical, Nonlinear, and Soft Matter Physics*, vol. 88, no. 5, Article ID 050801, 2013.

[27] C. Granell, S. Gómez, and A. Arenas, "Dynamical interplay between awareness and epidemic spreading in multiplex networks," *Physical Review Letters*, vol. 111, no. 12, Article ID 128701, 2013.

[28] S. Gómez, A. Díaz-Guilera, J. Gómez-Gardeñes, C. J. Pérez-Vicente, Y. Moreno, and A. Arenas, "Diffusion dynamics on multiplex networks," *Physical Review Letters*, vol. 110, no. 2, Article ID 028701, 2013.

[29] S. Boccaletti, G. Bianconi, and R. Criado, "The structure and dynamics of multilayer networks," *Physics Reports*, vol. 544, no. 1, pp. 1–122, 2014.

[30] M. Kivelä, A. Arenas, M. Barthelemy, J. P. Gleeson, Y. Moreno, and M. A. Porter, "Multilayer networks," *Journal of Complex Networks*, vol. 2, no. 3, pp. 203–271, 2014.

[31] X. Zhang, S. Boccaletti, S. Guan, and Z. Liu, "Explosive synchronization in adaptive and multilayer networks," *Physical Review Letters*, vol. 114, no. 3, Article ID 038701, 2015.

[32] A. Solé-Ribalta, S. Gómez, and A. Arenas, "Congestion induced by the structure of multiplex networks," *Physical Review Letters*, vol. 116, no. 10, Article ID 108701, 2016.

[33] T. Chen, L. Wang, J. Wang, and Q. Yang, "A network diffusion model of food safety scare behavior considering information transparency," *Complexity*, vol. 2017, Article ID 5724925, 16 pages, 2017.

[34] T. Chen, J. Wang, H. Liu, and Y. He, "Contagion model on counterparty credit risk in the CRT market by considering the heterogeneity of counterparties and preferential-random mixing attachment," *Physica A: Statistical Mechanics and Its Applications*, vol. 520, pp. 458–480, 2019.

[35] E. M. Miller, "Risk, uncertainty, and divergence of opinion," *The Journal of Finance*, vol. 32, no. 4, pp. 1151–1168, 1977.

[36] J. Y. Campbell, "Asset pricing at the millennium," *Journal of Finance*, vol. 55, no. 4, pp. 1515–1567, 2000.

[37] Tingqiang Chen, Binqing Xiao, and Haife Liu I, "Credit risk contagion in an evolving network model integrating spillover effects and behavioral interventions," *Complexity*, vol. 2018, Article ID 1843792, 16 pages, 2018.

[38] D. Kahneman and A. Tversky, "Prospect theory: an a nalysis of decision under risk," *Econometrica*, vol. 47, no. 2, pp. 263–292, 1979.

[39] M. Baker and J. C. Stein, "Market liquidity as a sentiment indicator," *Journal of Financial Markets*, vol. 7, no. 3, pp. 271–299, 2004.

[40] N. Linciano, C. Lucarelli, M. Gentile, and P. Soccorso, "How financial information disclosure affects risk perception. Evidence from Italian investors' behaviour," *European Journal of Finance*, vol. 3, no. 15, pp. 1–22, 2018.

[41] R. Z. Xu, H. L. Li, and C. M. Xing, "Research on information dissemination model for social networking services," *International of Computer Science and Application*, vol. 2, no. 1, pp. 1–6, 2013.

[42] A. V. Felbert, "Network structure and counterparty credit risk," *Quantitative Finance*, vol. 5, pp. 1–21, 2015.

[43] G. A. Meissner, D. Mesarch, and A. Olkov, "The valuation of credit default swaps including investor-counterparty-reference entity default correlation," *The Journal of Risk*, vol. 16, no. 2, pp. 1–19, 2016.

[44] J. Wang, C. Jiang, and J. Qian, "Robustness of interdependent networks with different link patterns against cascading failures," *Physica A: Statistical Mechanics and its Applications*, vol. 393, pp. 535–541, 2014.

[45] M. E. J. Newman, "Spread of epidemic disease on networks," *Physical Review E: Statistical, Nonlinear, and Soft Matter Physics*, vol. 66, no. 1, Article ID 016128, 11 pages, 2002.

[46] K. Yu and L. Rong, "A new attack on scale-free networks based on cascading failures," *Modern Physics Letters B*, vol. 23, no. 20-21, pp. 2497–2505, 2009.

Hindawi
Complexity
Volume 2019, Article ID 6543590, 8 pages
https://doi.org/10.1155/2019/6543590

Research Article

EC-Structure: Establishing Consumption Structure through Mining E-Commerce Data to Discover Consumption Upgrade

Lin Guo [1] and Dongliang Zhang [2]

[1] *School of Economics and Management, Changchun University of Science and Technology, Jilin 130022, China*
[2] *Institution of technical science, Fudan University, Shanghai 200000, China*

Correspondence should be addressed to Lin Guo; guolin@cust.edu.cn

Received 24 December 2018; Accepted 26 February 2019; Published 12 March 2019

Guest Editor: Thiago C. Silva

The traditional methods of analyzing consumption structure have many limitations, and data acquisition is difficult, so it is hard to scientifically verify the accuracy of algorithms. With the development of Internet economy, many scientific researchers focus on mining knowledge of consumer behavior using big data analysis technology. Because consumption decisions are influenced by not only personal characteristics but also social trends and environment, it is one-sided to analyze the impact of one single factor on the phenomenon of consumption. The authors of this paper combine the consumption structure analysis method and data processing technology using data from an e-commerce platform to extract the consumption structure of cities, compare the structural differences between different periods, and then discover consumption upgrading according to swarm intelligence. The experiments prove the efficacy of the algorithm proposed in this paper compared to other similar algorithms using several different datasets, which illustrates the algorithm's efficacy and stable performance in consumption structure analysis.

1. Introduction

With the continuous expansion of consumption scale, consumers' personalized demands are becoming increasingly obvious. Consumer behaviors, such as purchasing decisions, are influenced by not only personal characteristics but also interpersonal relationships, social environments, network culture, and so on. Therefore, the analysis of consumption just from the individual perspective is one-sided and unscientific.

At present, most research on consumption upgrading is carried out from the macroperspective and is realized based on national statistical yearbook data. The analysis of consumption upgrading from a macroperspective is relatively simple. However, it is difficult to find individual consumption structures at the microlevel from the perspective of consumers. From the perspective of management and economics, consumption upgrading is difficult to measure, and there is no strict boundary with which to distinguish between consumption upgrading and nonupgrading, and relevant experimental data is also difficult to obtain. The authors of this paper can fully quantify the judgment process of consumption upgrading, propose a set of evaluation criteria, and use big data with comprehensive coverage of user features for mining. Therefore, the algorithm proposed in this paper is scientific and accurate.

This paper combines the consumption structure analysis method and data processing technology to extract collective wisdom to construct an economic map that describes urban economic hotspots. The algorithm involves studying consumer consumption structures to realize consumption upgrading mechanism research and building a consumption upgrading model to analyze whether consumption upgrading occurred. The results obtained from the multiangle and multidimensional research will be comprehensive and reasonable.

2. Related Work

The research on consumption function theory is mainly focused on Persistent Income Theory (PIH) and Life Cycle Theory (LCH). The only difference between PIH and LCH is

that the former usually uses an indefinite limitation while the latter uses a definite limitation, so they are generally called LC-PIH when combined. Many researchers [1–4] use LC-PIH to study the consumption problems of Western residents, but their conclusions are inconsistent.

With the development of the Internet economy, an increasing number of researchers focus on the impact of Internet technology. Electronic commerce (e-commerce) is any type of business or commercial transaction that involves information transfer across the Internet [5]. A user's behaviors on a website can reflect their interests and purchase intentions. Therefore, consumption structure can be analyzed by studying the data of e-commerce platforms, which is difficult to realize using to traditional research methods.

When analyzing the characteristics of a network, the distribution of user activity is investigated and a network of bidders that is connected by common interest in individual articles is constructed [6, 7]. The network's cluster structure corresponds with the main user groups according to common interests, exhibiting hierarchy and overlap.

Regarding the characteristics of uses, Curme [5], Chattopadhyay [8], and Guo [9] analyze user behaviors from the perspective of complex systems and extract implicit semantic information from large-scale semistructured data. Glass [10], Singh [11], and Aviano [12] find personal characteristics through the feature extraction of original website data, mine important features of users using to feature selection methods, and finally extract a user profile model. Kim [13], Ouaftouh [14], and Diao [15] classify customers into different groups according to their similarities that are calculated through demographic features and psychological features or features such as customer value, customer consumption, and lifetime value.

3. Classification of Consumption Data

The rapid development of social networking resulted in the explosive growth of data that contains large amounts of high-quality information, such as information about user interests and interpersonal relationships. Therefore, social data processing and knowledge mining are intricate and indispensable. Consumption data contains much redundant or nonrepresentative data. We adopt the matrix analysis method to quickly classify consumption data into negative data, positive data, insufficient evidence data, and disputed data.

Definition 1 (negative data). The normalized value of negative comment times is greater than 0, and the normalized value of positive comment times is less than 0.

Definition 2 (positive data). The normalized value of positive comment times is greater than 0, and the normalized value of negative comment times is less than 0.

Definition 3 (insufficient data). The number of positive and negative comments is relatively small, so there is no authoritative data based on which to measure the nature of the data.

Definition 4 (controversial data). The number of positive and negative comments is relatively large, so there is no way to find absolute, salient features based on which to measure the nature of the data.

Because socialized data can reflect the characteristics and interpersonal relationship information about real society, the knowledge of regional and overall consumption structure (the coverage of analysis results are determined by data capture granularity) can be acquired by analyzing the data of <user, comment> that is gathered from websites. After word segmentation and semantic analysis, we can obtain the <consumption object, comment times, positive times, negative times> data. Due to large differences in the evaluation data about different consumption objects, we use standardized data to control data to within a range to measure the popularity of different consumption objects. The formula for data normalization is shown as follows:

$$(x, y) = \left(\frac{x_i - \overline{x}}{s_x}, \frac{y_i - \overline{y}}{s_y} \right) \tag{1}$$

$$\overline{x} = \frac{1}{n} \sum_{p=1}^{n} x_p \tag{2}$$

$$\overline{y} = \frac{1}{n} \sum_{p=1}^{n} y_p \tag{3}$$

$$s_x = \sqrt{\frac{1}{n-1} \sum_{p=1}^{n} \left(x_p - \overline{x} \right)^2} \tag{4}$$

$$s_y = \sqrt{\frac{1}{n-1} \sum_{p=1}^{n} \left(y_p - \overline{y} \right)^2} \tag{5}$$

(x, y) is the calculated result after standardization. Its mean value is 0, the variance is 1, and it is dimensionless. (x, y) can be mapped to a two-dimensional coordinate interval [-1, +1]. The standardized variable value fluctuates around 0. A value greater than 0 indicates that (x, y) is higher than the average level, and a value less than 0 indicates that (x, y) is lower than the average level.

The authors of this paper use nodes to describe consumption objects. Therefore, the locations of nodes in the matrix can describe status of consumption objects. In the consumption matrix, X and Y coordinates, respectively, represent the standardized data of positive data and negative data. In the four interval matrixes, the consumption data is divided into four categories.

The consumption matrix is divided into four regions, as shown in Figure 1.

It can be seen from Figure 1 that the X-coordinate value of the node in the negative partition is less than 0 and the Y-coordinate value is greater than 0, which indicates that the nodes in the negative partition have more negative data than the average. The nodes in the positive partition are just the opposite. The other two types of nodes are controversial and insufficient nodes. Among them, the controversial node

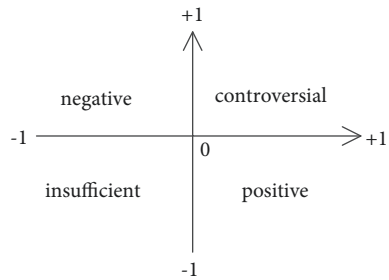

Figure 1: Coordinate distribution of four types of nodes.

has much positive and negative information. The insufficient node has little positive and negative information. Neither of these two types of nodes can be classified into one specific partition. To reduce the impact of invalid or redundant data on the accuracy of the analysis, the authors of this paper only focus on the nodes in positive and negative areas. In addition, by manually analyzing the nodes in positive and negative regions, it is found that the data about these nodes is authoritative and clean. It is enough to describe the information about consumption structure of users and sufficient for the subsequent experiments.

4. Analysis of Consumption Coefficient

By analyzing the data obtained in the above process, the matrix ITEM(x, y) is constructed from positive and negative data. Each node in the matrix describes the situation of the positive and negative comments about a consumption object. By comparing the consumption matrixes from different periods, the consumption trends, changes to the structure, and consumption upgrading can be judged and identified.

With the continuous expansion of consumption scale, consumers' personalized demands are becoming increasingly obvious. Consumer behavior, such as purchase decisions, is affected by multiple factors, so consumption hotspots and structures often change. This change may be strong or weak; of course significant changes in structures are relatively easy to detect, but weak changes are difficult to capture. Therefore, to identify changes in consumption structures, it is necessary to calculate the proportions of different consumption objects in the total consumption field and discover changes of consumption structure in time by analyzing changes in proportion. In this paper, we calculate the consumption coefficient of each consumption object, measure the proportion of different consumption objects in the total consumption field, and then identify changes and trends in the consumption structures of users.

The formula for calculating the consumption coefficient is as follows:

$$coeff = \frac{heat\,(q)}{heat\,(all)} \times 100\% \tag{6}$$

coeff is the consumption coefficient of consumption object q. heat(q) represents the heat of the consumption object q. heat(*all*) represents the heat of all consumption objects. It can be seen from the formula that the consumption coefficient is the proportion of a certain consumption object in the total consumption objects. The consumption coefficient is added to the matrix ITEM(x, y) as an additional parameter, so the expression of the matrix becomes ITEM(x, y, *coeff*). Therefore, the structural characteristics of consumption can be described from three dimensions. By analyzing ITEM(x, y, *coeff*), the implied information about consumption structure, consumption trend, and consumption upgrading can be obtained. The detailed analysis process is described in the next section.

5. Discovery of Individual Consumption Upgrading

To compare the consumption data from different periods, the differing degrees of the matrixes that describe the consumption structures in different periods need to be calculated. If the difference degree exceeds a certain threshold value, then the consumption upgrading phenomenon is considered as happening. Here, the consumption matrix at moment n is denoted as ITEM_n and the consumption matrix at moment n+1 is denoted as ITEM_{n+1}. By comparing ITEM_n and ITEM_{n+1}, the differences of different consumption matrixes can be calculated and structural changes can be detected. The formula for calculating degree of difference is as follows:

$$COR\left(\text{ITEM}_n, \text{ITEM}_{n+1}\right) = \frac{\sum_{i=1}^{n}\left(ITEM_i - \overline{ITEM_n}\right)\sum_{j=1}^{n+1}\left(ITEM_j - \overline{ITEM_{n+1}}\right)}{\sqrt{\sum_{i=1}^{n}\left(ITEM_i - \overline{ITEM_n}\right)^2\sum_{j=1}^{n+1}\left(ITEM_j - \overline{ITEM_{n+1}}\right)^2}} \tag{7}$$

According to the formula, the coefficient *COR* is obtained by dividing the covariance by the standard deviation of two variables. The covariance can reflect the correlation degree between two random variables. When the covariance is greater than 0, it means that the two variables are positively correlated, and when the covariance is less than 0, it means that the two variables are negatively correlated. Note that the coefficient is meaningful when both variables are not zero, and the range of the coefficient is [-1, 1]. When *COR* is 1, ITEM_n and ITEM_{n+1} are completely positively correlated. When *COR* is -1, ITEM_n and ITEM_{n+1} are completely

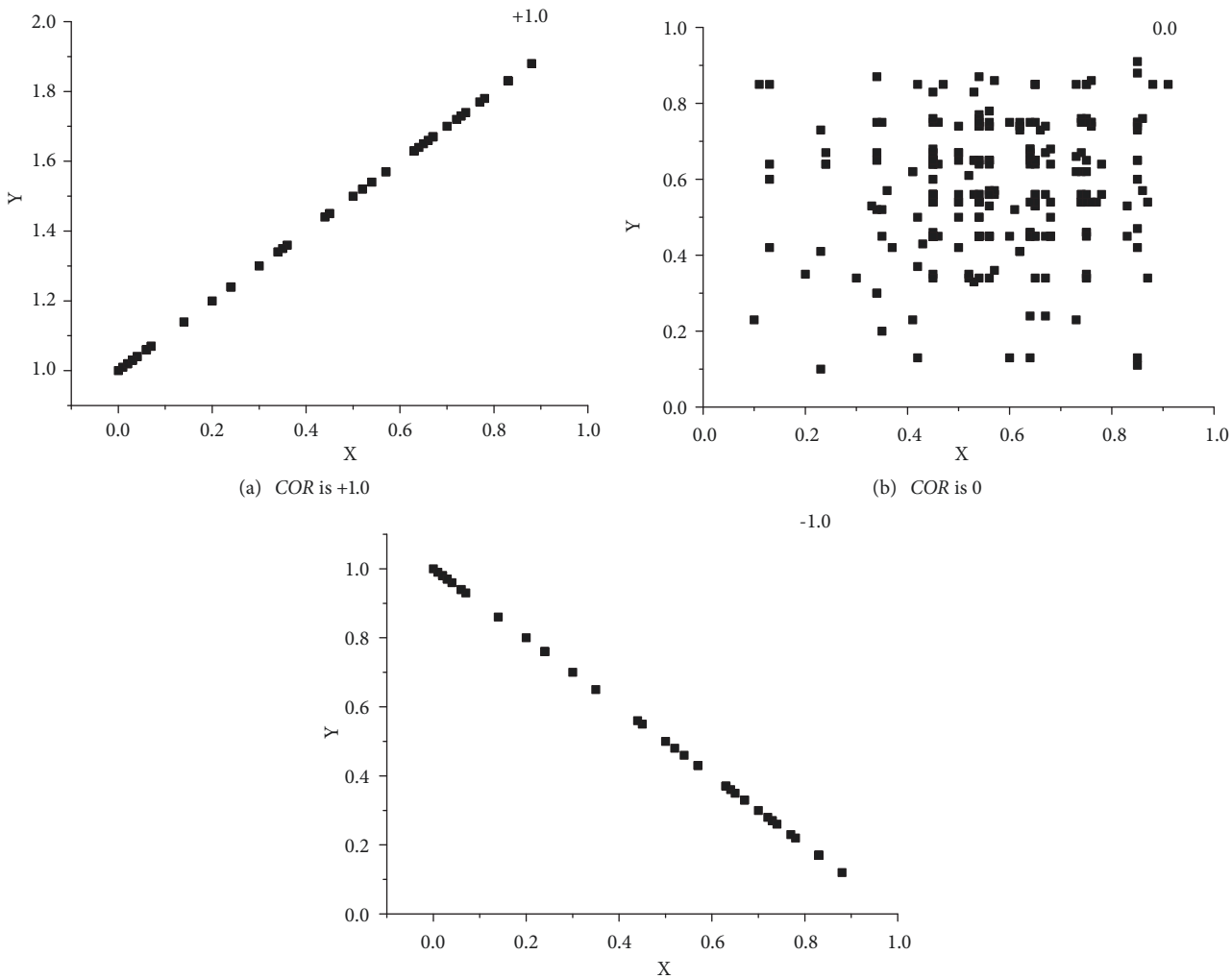

(a) *COR* is +1.0

(c) *COR* is -1.0

Figure 2: The coefficient *COR* of different consumption structure.

negatively correlated. The greater the absolute value of *COR* is, the stronger the correlation degree between ITEM_n and ITEM_{n+1} is. The closer the coefficient *COR* is to 0, the weaker the correlation degree between ITEM_n and ITEM_{n+1} is.

Through the above methods, we can build consumption matrixes for different periods and judge the differences in consumption structure in between periods by calculating the coefficient, *COR*. When *COR* approaches 1 or -1, it means that the consumption structure significantly changed, so it can be considered that consumption upgrading occurred. As shown in Figure 2, the closer the coefficient is 1 or -1, the greater the structural difference is, while a coefficient that is near 0 indicates that the consumption structure changed little and there is no upgrading.

6. Experiment

The datasets used throughout the experiments are Zachary's Karate Club(http://www-personal.umich.edu/~mejn/netdata/), Dolphin's Associations(http://www-personal.umich.edu/~mejn/netdata/), LesMiserables(http://wiki.gephi.org/index.php/Datasets), MovieLens(http://www.datatang.com/datares/detail.aspx?id=44295), and EP dataset(http://www.dianping.com/).

(1) The dataset of Zachary's Karate Club is a social network of friendships between 34 members, so edges in the graph describe the higher frequency of interactions between members.

(2) The dataset of Dolphin's Associations is an undirected social network of frequent associations between 62 dolphins, which has 62 nodes and 159 edges.

(3) The dataset of LesMiserables is a coappearance network of characters in Les Miserables, which contains 77 nodes and 254 edges.

(4) The dataset of MovieLens is a synthesized recommendation system and virtual community, which is commonly used for social computing.

(5) The EP dataset was captured from an e-commerce platform (dianping.com). It contains 15,890,209 pieces of data and was updated in August 2018. The data collection fields are

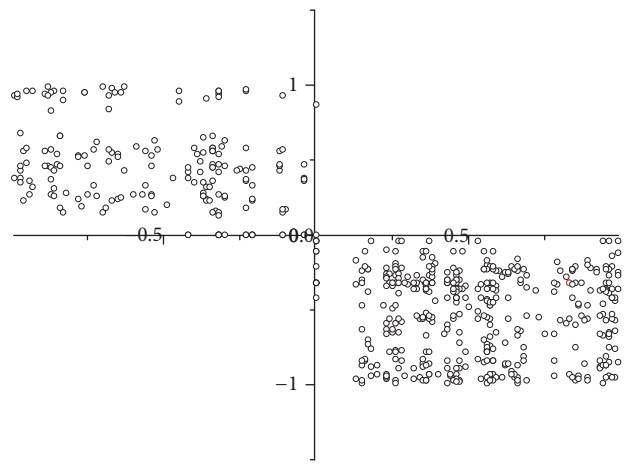

Figure 3: The positive and negative distribution of comments.

shop_id (uniqueness), province, city, city_id, area, big_cate (the primary classification), big_cate_id, small_cate (the secondary classification), small_cate_id, service_rating, all_remarks, very_good_remarks (5-star review), good_remarks (4-star review), common_remarks (3-star review), bad_remarks (2-star review), and very_bad_remarks (1-star review).

Comparison Methods. NMFOSC [16] presents an approach to community detection that utilizes a nonnegative matrix factorization model to divide overlapping communities from networks. RNM [17] is a local expansion method based on rough neighborhood. CPM [18] greedily expands natural communities of seeds until the whole graph is covered by using a local fitness function. EdgeB-Cluster [19] bundles similar edges, adjusts the locations of nodes to optimize the visualized output of the graph and analyzes networks from a community level.

Through the analysis of a consumption object in a certain region in the e-commerce platform, it was found that the number of positive comments is very large. This is because there is a phenomenon of deliberately increasing the number of good comments to improve the store's reputation, which results in the presence of too many good comments. On the contrary, the numbers of neutral and negative comments are relatively reasonable, and few of these comments are intentionally added or deleted, so they are convincing. Based on the above factors, the authors of this paper did not analyze the quantity of positive comments and only considered the quantity of neutral and negative comments. Through experimental verification of the quality of the neutral and negative comments, it was found that the data is authentic and abundant, and enough to describe the object to be tested.

Figure 3 shows the distribution of positive and negative comments. The nodes in the insufficient and controversial areas do not provide valuable information for subsequent analysis, so they were removed. It can be seen that there are more positive nodes than negative ones, and the difference between them is large. It is important to note that although the nodes in the negative area represent that the user's comments are negative, they still provide useful knowledge about consumption trends that cannot be removed.

Figure 3 shows the regional analysis results while Figure 4 shows the overall analysis results. Figure 4 is the visual output of the results generated by the algorithm. Figure 4(a) shows the distribution of nodes, and the colors of nodes indicate the heat of different consumption objects. The darker a node color is, the more attention the node received. Figure 4(b) is a heat map of a center node, and the black node is the center node. Figure 4(b) shows that there is a certain correlation between the central node and a large number of other nodes, indicating that there are many high correlations between different consumer groups. Thus, the characteristics of consumption objects can be further analyzed based on the relationships between consumers and commodities.

Figure 5 depicts the distribution of different consumption objects. In this case, the node with a ratio of more than 0.6 is regarded as a popular consumption node while a node with a ratio of less than or equal to 0.6 is regarded as an unpopular consumption node. Of course, if the ratio threshold is lowered, then additional nodes will be divided into popular consumption areas. It can be seen from Figure 5 that most nodes belong to the nonhot field, which is in-line with the actual situation.

Figure 6(a) depicts the characteristics of nodes that were divided into two categories to describe different consumption heat (some representative nodes are extracted). It can be seen that the characteristics of nodes in different categories vary greatly. Figure 6(b) describes the closeness centrality distribution of the nodes belong to the same category. This shows that the node locations have normal distribution, so the similarity between the nodes in the same category is very high. That is to say, the classification is reasonable.

For the purpose of analyzing the experimental results, the following measurement parameters are used [20]: Multiplicity Precision calculated by $MP = \min(|C(e) \cap C(e')|, |L(e) \cap L(e')|)/|C(e) \cap C(e')|$, Multiplicity Recall by $MR = \min(|C(e) \cap C(e')|, |L(e) \cap L(e')|)/|L(e) \cap L(e')|$. Let $L(e)$ and

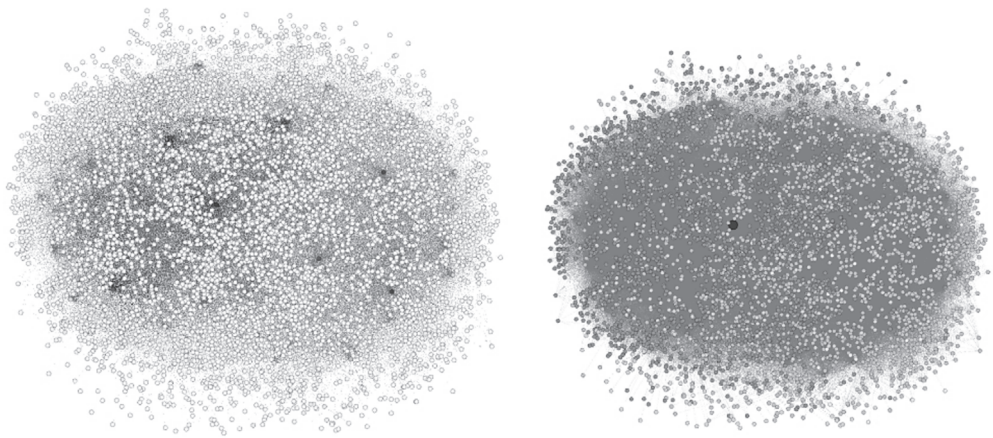

(a) Distribution of nodes (b) The heat map

Figure 4: Visualization of the results generated by the algorithm.

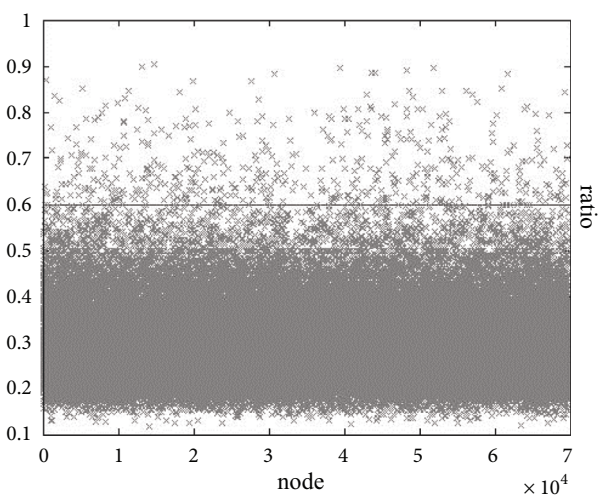

Figure 5: The distribution of different consumption objects.

$C(e)$ denote the category and the cluster of an item e. e is a cluster with n items belonging to the same category and e' is a cluster merging n items from unary categories. FB is a comprehensive measure of MP and MR, and the algorithm is $FB=MP\times MR\times 2/(MP+MR)$.

Table 1 proves the validity and feasibility of the algorithm. The numbers in italic indicate the highest value of the same parameter in each row. Table 1 displays a comparison of the algorithm proposed in this paper to other similar algorithms. The datasets Karate Club, Dolphin, LesMiserables, and MovieLens are used to prove the performance of the algorithms in structural analysis. The EP dataset is used to prove the performance of e-commerce data analysis. It is found that EC-Structure performs better than other algorithms and performs stably with different data sets. The main reasons for which EC-Structure is superior to other algorithms are that (1) it reduces the influence of erroneous e-business platform data on the algorithm, (2) it increases the consumption coefficient as a parameter with which to measure the proportions of different consumption objects, and (3) the coefficient COR can help researchers accurately judge changes in consumption structures. Therefore, the operation effect of this algorithm is effective.

7. Conclusion

Research on consumer behavior can be made by extracting and analyzing useful information from a large amount of incomplete, vague, and random consumer behavior data. The algorithm proposed in this paper builds consumption structures and a consumption upgrading model based on the data from e-commerce platforms to analyze whether consumption upgrading occurred. The results of the experiment verified the implementation efficacy and analysis accuracy of the algorithm. It was found that the algorithm is effective. The implementation efficacy of the proposed algorithm is superior to those of other algorithms, and it runs stably with different datasets.

Data Availability

The data used to support the findings of this study are included within the article.

Conflicts of Interest

The authors declare that there are no conflicts of interest regarding the publication of this paper.

Acknowledgments

This work was supported by Youth Fund of Humanity and Social Science of Ministry of Education of China (Grant no. 18YJCZH041); Project of Education Department of Jilin Province of China (Grant no. JJKH20190612SK).

Table 1: The performance comparisons.

dataset	NMFOSC			RNM			CPM			EdgeB-Cluster			EC-Structure		
	MR	MP	FB	MR	MP	FB	MR	MP	FB	MR	MP	FB	MR	MP	FB
Karate Club	*1.00*	0.92	0.96	0.84	*1.00*	0.91	0.58	0.94	0.71	*1.00*	*1.00*	*1.00*	*1.00*	*1.00*	*1.00*
Dolphin	0.64	0.90	0.75	0.46	0.97	0.62	0.40	0.94	0.56	0.73	*0.98*	0.83	*0.80*	*0.98*	*0.88*
LesMiserables	0.72	0.87	0.79	0.80	0.88	*0.84*	0.48	*0.89*	0.62	*0.81*	0.88	*0.84*	*0.88*	0.83	*0.85*
MovieLens	*0.83*	0.85	0.84	0.56	0.86	0.68	0.81	0.86	0.83	0.81	*0.88*	*0.84*	0.82	*0.88*	*0.85*
EP dataset	*0.85*	0.80	0.82	0.53	0.56	0.54	0.53	0.65	0.58	0.79	*0.83*	0.81	0.85	0.82	*0.83*

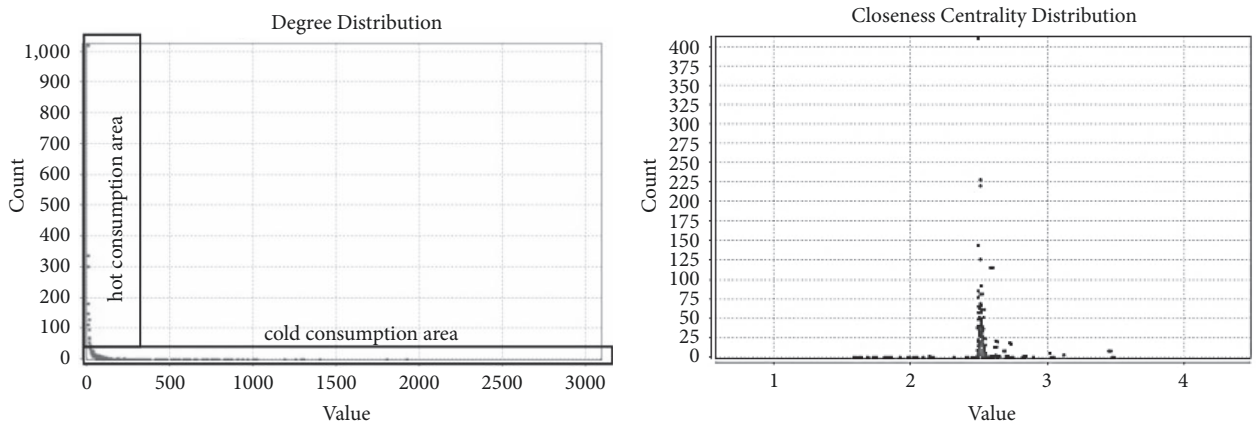

(a) Degree distribution

(b) Closeness centrality distribution

Figure 6: The characteristic distribution of hot consumption and cold consumption nodes.

References

[1] P. N. Ireland, "Using the permanent income hypothesis for forecasting," *Federal Reserve Bank of Richmond Economic Quarterly*, vol. 81, no. 1, pp. 49–63, 1995.

[2] L. A. Fisher and G. Kingston, "Improved forecasts of tax revenue via the permanent income hypothesis," *Australian Economic Review*, vol. 50, no. 1, pp. 21–31, 2017.

[3] L. Zhou, C. Wang, and S. O. Finance, "Household debt and consumption-evidence from micro data," *Soft Science*, vol. 3, pp. 32–43, 2018.

[4] M. Zagler, "Empirical evidence on growth and business cycles," *Empirica*, vol. 44, pp. 1–20, 2017.

[5] C. Curme, T. Preis, and H. E. Stanley, "Quantifying the semantics of search behavior before stock market moves," *Proceedings of the National Academy of Sciences of the United States of America*, vol. 111, no. 32, pp. 11600–11605, 2014.

[6] J. Reichardt and S. Bornholdt, Ebay users from stable groups of common interest, 2005.

[7] H. Halpin, "The semantics of search," in *Social Semantics*, pp. 149–186, Springer US, 2013.

[8] T. Chattopadhyay, S. Maiti, A. Pal et al., "Automatic discovery of emerging trends using cluster name synthesis on user consumption data: extended abstract," in *Proceedings of International Conference Companion on World Wide Web*, pp. 981–983, 2016.

[9] L. Guo, W. Zuo, and T. Peng, "Inference network building and movements prediction based on analysis of induced dependencies," *IET Software*, vol. 11, no. 1, pp. 12–17, 2017.

[10] B. Glass, Z. Benenson, and R. Landwirth, "Look before you leap: improving the users' ability to detect fraud in electronic marketplaces," in *Proceedings of the CHI Conference on Human Factors in Computing Systems*, pp. 3870–3882, ACM, 2016.

[11] P. Singh and M. Singh, "Fraud detection by monitoring customer behavior and activities," *Annals of Regional Science*, vol. 49, no. 1, pp. 1–27, 2012.

[12] D. Aviano, B. L. Putro, and E. P. Nugroho, "Behavioral tracking analysis on learning management system with apriori association rules algorithm," in *Proceedings of the 2017 3rd International Conference on Science in Information Technology (ICSITech)*, Bandung, Indonesia, 2017.

[13] K. Kim, Y. Choi, and J. Park, "Pricing fraud detection in online shopping malls using a finite mixture model," *Electronic Commerce Research and Applications*, vol. 12, no. 3, pp. 195–207, 2013.

[14] S. Ouaftouh, A. Zellou, and A. Idri, "User profile model: a user dimension based classification," in *Proceedings of the 2015 10th International Conference on Intelligent Systems: Theories and Applications (SITA)*, Rabat, Morocco, 2015.

[15] Y. Diao, K. Y. Liu, and L. Hu, "Classification of massive user load characteristics in distribution network based on agglomerative hierarchical algorithm," in *Proceedings of the 2016 International Conference on Cyber-Enabled Distributed Computing and Knowledge Discovery (CyberC)*, Chengdu, China, 2017.

[16] N. Chen, Y. Liu, and H.-C. Chao, "Overlapping community detection using non-negative matrix factorization with orthogonal and sparseness constraints," *IEEE Access*, vol. 6, pp. 21266–21274, 2017.

[17] Z. H. Zhang, D. Q. Miao, and J. Qian, "Detecting overlapping communities with heuristic expansion method based on rough neighborhood," *Chinese Journal of Computer*, vol. 36, no. 10, 2013.

[18] F. Havemann, M. Heinz, and A. Struch, "Identication of overlapping communities and their hierarchy by locally calculating community-changing resolution levels," *Journal of Statistical Mechanics: Theory and Experiment*, vol. 1, 2011.

[19] L. Guo, W. Zuo, T. Peng, and B. K. Adhikari, "Attribute-based edge bundling for visualizing social networks," *Physica A: Statistical Mechanics and Its Applications*, vol. 438, pp. 48–55, 2015.

[20] E. Amigó, J. Gonzalo, J. Artiles, and F. Verdejo, "A comparison of extrinsic clustering evaluation metrics based on formal constraints," *Information Retrieval*, vol. 12, no. 4, pp. 461–486, 2009.